LIMIT AND SHAKEDOWN ANALYSIS OF STRUCTURES BY THE FINITE ELEMENT METHOD

by

Jinhua Shi

Thesis Submitted to the
University of Strathclyde
for the Degree of
Doctor of Philosophy

Department of Mechanical Engineering
University of Strathclyde
Glasgow, UK

March 1996

ABSTRACT

Limit and shakedown analyses are powerful methods in designing pressure vessel components and other engineering structures. With the development of computer technology the use of finite element analysis as an alternative tool for engineering structure design has become ever more increasing. In this thesis the finite element method utilises the novel **elastic compensation** method to carry out the limit and shakedown analyses on variety engineering structures: nozzles in pressure vessels, plates with a central hole and frame structures.

There are two main objectives of the present study. One of them is to conduct limit and shakedown analyses on a series of thick cylinders, nozzle/sphere intersections under internal pressure, plates with a hole and frame structures under multiple loading conditions using the initially developed **elastic compensation** method based on 2-D solid element models. A comparision of the lower, upper bound limit loads and shakedown solutions is made with the results available in literature or with new elasto-plastic analyses. The results obtained using the **elastic compensation** method were found to be of useful accuracy. Another is to further develop the **elastic compensation** method using generalised yield criteria. Then the procedure is implemented to beam and shell finite elements to calculated limit loads for beam and shell structures. A number of 2-D and 3-D frames were examined using a general yield surface. The obtained results were compared with that of theoretical plastic analysis and with the results available in literature and were found to be in good agreement. Parametric studies of nozzle/sphere intersections and nozzle/cylinder intersections under internal pressure were carried out using Ilyushin's and Ivanov's generalised yield criteria. The results calculated were compared with the solutions obtained using the initially **elastic compensation** method and with the solutions available in literature and were found to also be in good agreement. The newly developed **elastic compensation** procedure using generalised yield criteria was found to be more economic

and useful in engineering design.

From this study, some new design methods based on limit and shakedown loads are proposed for nozzle/sphere intersections and for other engineering structures. The newly developed **elastic compensation** procedure using generalised yield criteria is highly recommended in structural design for a quick limit load estimation.

ACKNOWLEDGEMENTS

I would like to express my deep sense of gratitude to my supervisor **Professor James T Boyle** for his advise, constructive suggestion and the guidance he provided to me throughout the project.

I gratefully acknowledge the support and help of **Drs. Donald Mackenzie** and **Robert Hamilton**, Lecturers, whom I worked very closely with during this project. I also would like to express my respectful gratitude to **Professor John Spence**, Vice-Principal Elect and Former Head of Department of Mechanical Engineering, and **Professor Thomas G F Gray**, Head of Department of Mechanical Engineering, for their permission to carry out this research project and to use all facilities in the Department of Mechanical Engineering.

Many thanks are also due to all my **friends** for their help during the work and for their pleasant company throughout the period of this research.

I am thankful to my **parents** for their continuous encouragement.

Many thanks to my beloved wife **Shufen** for fully continuous support and encouragement given to me. I am really sorry for leaving my wife and our son to themselves for two years.

Finally I would like to thank my son **Hao** and I am sorry again for having spent so little spare time with him.

CONTENTS

CHAPTER 1

INTRODUCTION

1.1 Introductory Remarks

The conventional methods of analysis and design of engineering structures are often based on a permissible working stress whose value is well within the elastic limit. The concentrations of stress that occur at sudden changes in cross section are usually disregarded in the elastic analysis. Since the results of the elastic analysis cease to hold when the yield limit is exceeded at the most critical cross section, the elastic design of a structure requires a margin of safety that ensures a fully elastic response. A limitation of structural designs based on the elastic analysis is evident from the fact that minor structural imperfections, which have no effect on the overall strength of the structure, have a marked influence on the elastic behaviour.

The load-carrying capacity of a structure made of a ductile material is rarely exhausted at the onset of plastic yielding, since excessive deflections do not occur before the load is appreciably higher than that at the elastic limit. This effect is more pronounced in statically indeterminate structures, where there is a redistribution of stress beyond the elastic limit, resulting in a marked increase in the carrying capacity. It follows that an economical design of a structure can be based on a suitable safety factor applied to the load for which the overall deflection begins to increase in a more or less unrestricted manner. Such a load is called the *collapse load*, which can be determined by the methods of plastic analysis without having to consider the intervening elastic/plastic range of deformation. The calculations involved in the plastic analysis are much simpler than those required in the corresponding elastic analysis. The influence of work-hardening is usually neglected in the plastic analysis so that the estimated carrying capacity is always conservative.

The strength of a structure is characterized by its collapse load which is obtained on the basis of certain idealizations. Considering a nonhardening elastic/plastic structure, a state of plastic collapse is defined as one for which the deflections, regarded as small, continue to increase under constant external loads. Since the bending moment distribution remains unchanged during the collapse, the change in curvature vanishes everywhere except at certain critical cross sections where the bending moment attains the fully plastic value. Infinitely large curvatures give rise to a link-type mechanism for plastic collapse. The ratio of the collapse load to the working load, known as the *load factor*, represents the margin of safety under service conditions.

According to the *lower bound theorem* of limit analysis, an external load in equilibrium with a distribution of bending moment which nowhere exceeds the fully plastic value is less than or equal to the collapse load. Such a distribution of bending moment is referred to as statically admissible. The *upper bound theorem*, on the other hand, states that the load obtained by equating the external work done by it to the internal work absorbed at the plastic hinges in any assumed collapse mechanism is greater than or equal to the collapse load. The deformation mode represented by a collapse mechanism is said to be kinematically admissible. The two limit theorems can be obtained to form a *uniqueness theorem* which states that if any statically admissible distribution of bending moment can be found in a structure that has sufficient number of yield hinges to produce a mechanism, the corresponding load is equal to the collapse load. When a structure is subjected to a number of loads which may or may not increase in strict proportion to one another, plastic collapse will occur at the first combination of loads for which a statically admissible bending moment distribution that satisfies the mechanism condition can be found. The load-carrying capacity of the structure can therefore be determined for any given ratios of the applied loads in the state of collapse, without any reference to the loading history. It follows that the collapse load is unaffected by initial internal stresses, as well as by any flexibility of support and

imperfect fit of members. If the problem is not statically determined at collapse, the distribution of bending moment will depend, however, on such factors as the history of loading, initial stresses, and settlement of supports.

An important corollary of the lower bound theorem is that the collapse load cannot be decreased by increasing the strength of any part of the structure. Indeed, the bending moment distribution corresponding to the state of collapse will remain statically admissible for the modified structure in which the fully plastic moment is increased at one or more cross sections. The load-carrying capacity of the structure can therefore be determined for any given ratios of the applied loads in the state of collapse, without any reference to the loading history. This conclusion follows from the fact that the mechanism corresponding to the state of collapse will produce in the modified structure an internal work that is less than or equal to that in the unmodified structure. The resulting upper bound obtained for the weakened structure, therefore, cannot exceed the collapse load for the original structure.

It is seen from above description that limit analysis provides an alternative to incremental elastic-plastic analysis for determining a limit load. A knowledge of the limit load enables determination of the reserve strength that exists in structures beyond the initial yield. The key to establishing the limit behaviour of a structure or component is the nature of the collapse mechanisms. These have only really been established for simple generic components and load conditions. An alternative and a simpler resource is to invoke the upper and lower bound theorems and obtain limit bounds on the exact solution. However, this procedure can also be often mathematically intractable and is therefore limited to simple descriptions.

Limit load calculations form the basis for the design of several pressure vessel components and other structures - for example in BS 5500 Appendix A [BSI 1994] it is stated that '...there should be the same theoretical margin against gross

plastic deformation for all design details as that provided against gross plastic deformation in major membrane areas...In establishing conformity with this criterion investigations should take account of plastic behaviour. If the theory of plastic limit analysis is employed, the limit load may be taken as the load producing gross plastic deformation, although this may be a conservative estimate...' (A.3.1.1). A similar adoption of limit analysis can also be found in ASME B&PV Code [1995].

These do not really specify how the limit load should be used as the basis for design. It would be expected that the important primary membrane and bending stresses in pressure vessels would remain limited to yield - then the limit load could be used as the basis for determining the design margin (currently primary membrane stresses are limited to two thirds of yield, with primary membrane plus bending allowed to take values up to yield).

The availability of computers revolutionalised the approach to limit analysis. It has enabled analysts to apply incremental plastic theory to complex components. Analysis models were more realistically simulated in plastic analysis, and the limit solutions obtained were closer to the actual limit loads. With rapid improvement in the speed and memory size of the ordinary desk-top computers, coupled with advancement in the development of finite element software programs. elastic-plastic finite element analysis became more prevalent in limit analysis. However, the elastic-plastic requires much greater computing resource than elastic analysis and requires the definition of materials models and is consequently much more expensive to perform. Direct calculation of limit load, using the upper and lower bound theorems by finite element method, has also proved difficulty. A recent summary by Berak and Gerdeen [1990] demonstrated an effective technique using finite element procedures for simple two-dimensional problems but concluded with the observation that'...this procedure is particularly applicable to the solution of complex problems using parallel processing on a superconputer...'.

In recent years, many researchers have been concentrated on the increased use of elastic finite element analysis as a means of obtaining the limit loads. A new technique - known as **elastic compensation** - which requires only elastic finite element analysis has been shown to give good lower and upper bound estimates for limit loads in a variety of pressure vessel components and other structures [Mackenzie and Boyle 1993]. The writer has been working in the Strathclyde Research Group on elastic compensation while the method was being developed.

In the above we have seen that the concept of a limit load can be used to provide a basis for design against plastic collapse on initial application of load. However, during the operational life of most structures the loading history becomes roughly cyclic. It gives rise to the possibility of low-cycle fatigue in regions of peak stress, but here we are interested in overall structural behaviour due to cycles of load.

Our description of computer behaviour for cyclic loads is mostly limited to the assumption of perfect plasticity. Two concepts are important - that of **shakedown** and that of **ratchetting** (which is what happens if a condition of shakedown is not achieved). In general for cyclic loading we design for shakedown in order to avoid ratchetting which can lead to **incremental collapse**. For cyclic loading shakedown is the condition that after first cycle of load, the component behaviour is purely elastic; some plastic strain does take place in the first cycle but not in the second or subsequent cycles. The highest load for which we can assure shakedown is called **shakedown load.**

The evaluation of shakedown loads is also quite difficult, and these have only been established for simple components. Most shakedown loads which have been published make use of so-called **shakedown theorems.** For example Melan's Theorem states that'...if any distribution of self-equilibrating residual stress can be found which, when taken together with the elastic stress (assuming perfectly plastic behaviour for the load cycles) constitute a system of stress within the yield

limit, then the structure will automatically reach this stress condition or a better one and will shakedown...'.

The design and assessment of complex structures subjected to histories of variable load remains a challenge to the analyst. In design the need for full inelastic analysis is removed in all but extreme cases by the use of simple design Codes, such as ASME B&PV [1995] and BS 5500 [1994], based upon limit load and shakedown concepts. These Codes tend to be conservative, sometimes excessively so, and are particularly difficulty to formulate for non-proportional loading. The ability to generate limit load and shakedown limits by linear finite element analysis can provide some advantages over full inelastic analysis in some circumstances. As described above, a new technique, called elastic compensation, can be used to calculate lower and upper bound limit loads of a structure. It will be shown in this thesis that the procedure can also be used to obtain lower and upper bound shakedown limits.

1.2 Objective and Scope of the Project

The main objectives of the present study were to further develop the elastic compensation method and to conduct limit and shakedown analysis on a series of pressure vessel components under internal pressure, plate with a hole and beam structures under multiple loading conditions. A comparision of the lower and upper bound limit loads and shakedown solutions are made with results available in literature or with new elasto-plastic analyses.

A preview of the scope of the thesis is given in the following:

At the beginning of the study, the author collected many papers on the topic of research. In order to find out a better procedure, a general literature survey on limit and shakedown analysis by finite element method is given in Chapter 2.

Chapter 3 gives a literature survey on the development of the modified elastic modulus method. In this Chapter an introduction to the elastic compensation method is also presented and the implementation of the lower bound, upper bound limit theorems and lower bound shakedown theorem is examined. A few examples, such as thick cylinders and frames, are also given in order to demonstrate how the method is working. The results obtained are then compared with the existing solutions.

In Chapter 4 the elastic compensation method is used in conjunction with elastic finite element analysis to obtain the lower, upper bound limit loads and shakedown limits for a square plate with a hole under various loading conditions. The results calculated are compared with the solutions available in the literature.

In Chapter 5, a design study is conducted to obtain the lower and upper bound limit loads for nozzles in spherical pressure vessels under internal pressure. Again the elastic compensation method is used in conjunction with elastic finite element analysis to obtain these results. For the thinner models, the obtained results are compared with the results available in the literature; for the thicker models, because of lacking available solutions the results calculated are compared with new elasto-plastic results and some comments are made for the purpose of design.

In Chapter 6, a design study is also conducted to calculate the lower and upper bound shakedown limits for all models analysed in Chapter 5. Again the obtained results are compared with the existing solutions and with the ASME B&PV Code [1995] and also some comments are made for the purpose of design.

Generalised yield criteria for beams and thin shells are surveyed in Chapter 7. These criteria are then implemented to structural finite elements using elastic compensation to calculate lower bound limit loads for beam and shell structures.

In Chapter 8, a number of two dimensional beams and frames and a three

dimensional frame are analysed using the procedure proposed in Chapter 7. The obtained results are compared with that of plasticity theory and with the results available in the literature.

In Chapter 9, a parametric study is carried out to obtain lower bound limit loads for nozzles in spherical shells and nozzles in cylindrical shells under internal pressure using the method proposed in Chapter 7. The results calculated are compared with the solutions obtained in Chapter 5 and available in the literature.

Finally, Chapter 10 concludes the thesis with a summary of the findings of the research work and with recommendation to further work.

Before the PhD project the author carried out sixteen months research work which related to the present project in the Research Group. Some research results have been published in the past five years and the published papers are given in Appendix I.

1.3 References

American Society of Mechanical Engineers, (1995), *ASME Boiler and Pressure Vessel Code.*

Berak, E.G. & Gerdeen, J.C., (1990), A finite element technique for limit analysis of structures, *Tran. ASME, J. Pres. Ves. Technol.*, **112**, 138–144.

British Standards Institute, (1994), *BS 5500: Specification for unfired Fusion Welded Pressure Vessels*, London.

Mackenzie, D. & Boyle, J.T., (1993), A method of estimating limit loads by iterative elastic analysis, I-simple examples, *Int. J. Pres. Ves. & Pipings.* **53**, 77–95.

CHAPTER 2

A BRIEF REVIEW OF LIMIT AND SHAKEDOWN ANALYSIS OF STRUCTURES BY FINITE ELEMENT METHOD

2.1 Introduction

Limit analysis is concerned with the determination of the maximum load amplification (or load or safety factor) which can be sustained by a perfectly-plastic structure subjected to given loads. Information regarding the stress-state at collapse and the collapse mechanism may be obtained as a by-product. While the material properties are usually described as being rigid-plastic, the required perfectly-plastic terminal stage need not be preceded by rigidity.

The two essential notions of limit analysis had been developed in full generality and rigour by the early fifties in the form of the static (or safe or lower bound) theorem and the kinematic (or unsafe or upper bound) theorem.

If an elasto-plastic structure is subjected to a program of variable-repeated mechanical or thermal loads, then the structure may fail by incremental collapse (or ratchetting) or by alternating plasticity (or low cycle fatigue). However, for some lower value of the load factor, the structure may, after a number of loading cycles, load and unload elastically; that is to say plastic strains will cease to develop. The structure is said to **shakedown**, and the object of shakedown analysis is to determine the maximum value of the load factor (safety factor) for which this phenomenon applies.

For doing this project, the author has collected many papers on the limit and shakedown analyses of structures. In order to benefit other researchers on the related research projects, in this Chapter, a brief literature review of limit and

shakedown analysis of structures by finite element method will be carried out respectively.

2.2 A Brief Review of Limit Analysis of Structures by Finite Element Method

The application of limit analysis to structures began with the attempt to predict the collapse loads of steel structures. In 1914 Kazinczy concluded from his experiments on clamped steel beams that the theory of elasticity could not provide a realistic estimate of the load-carrying capacity [Kazinczy 1914]. He introduced the concept of *plastic hinges* and developed several principles and methods which even today are valid and used in engineering practice [Kazinczy 1933, 1942]. Kazinczy's early work failed to receive the attention it merited, partly because it was written in Hungarian and partly because of the war. Hence, a few years later Kist [1917] independently presented similar ideas. Taking plastic behaviour of the material into account, Maier-Leibnitz [1928] carried out experiments with continuous steel beams and Ingerslev [1921] and Johansen [1932] investigated the plastic behaviour of reinforced concrete slabs.

The problem of accumulating plastic deformations was first investigated by Grüning [1926]. Girkmann [1931] and Bleich [1932] dealt with the load-carrying capacity of steel frames. This work was continued by Baker [1938] who carried out intensive experimental and theoretical investigations, and published the first book on plastic analysis of steel frames [Baker, Horne and Heyman 1956].

The lower and upper bound theorems of limit analysis were first established - for frames and plates - by Gvozdev [1936]. Like Kazinczy's work Gvozdev's results did not attract attention because of the war. Thus, these theorems were independently derived by Greenberg and Prager [1951] for beam and frames. Drucker, Greenberg and Prager [1951, 1952] for plane and general continuum problem respectively. These theorems have been developed to bracket the limit

load, because they are easier to obtain than exact solutions. The formal proofs of these theorems are well documented and can be found in the texts of Symonds [1962]; Hodge [1963] and Calladine [1965, 1985]. The theoretical limit analysis of engineering structures using these theorem can be found in a large number of books, such as Baker *et al.* [1956], Neal [1956, 1977], Heyman [1957, 1964], Hodge [1959, 1963], Massonnet and Save [1965], Baker and Heyman [1969, 1971], Horne [1971], Save and Massonnet [1972], Martin [1975], Chakrabarty [1987], Kaliszky [1989] and Lubliner [1990].

Mathematical programming methods for solutions of the limit analysis problem were first studied for trusses, beams and frames. The first identifications of the limit analysis of trusses as a linear programming (LP) problem are generally attributed to Charnes and Greenberg and to Prager [Prager 1957]. There are so many references, nowadays, on the limit analysis of structures by mathematical programming methods. The detailed mathematical programming applications to the limit analysis of structures can be found in the review papers of Maier and Munro [1982] and Maier and Lloyd [1986]. This review will only concentrate on the finite element method.

2.2.1 Direct Finite Element Method

The finite element method is a numerical procedure for analysing structures and continua and is well known to be extremely efficacious for the analysis of complex structures, both linear and non-linear. The finite element method can also be used to calculate the limit load of a structure and in this case bounds are obtained by maximising and minimising the load factor. The validity of the approach is dependent upon the limit load theorems of plasticity which imply that load factors calculated on the basis of assumed displacement fields are in excess of the true value, while load factors calculated on the basis of equilibrium stress fields which nowhere violate the yield condition, are less than the true value. In the displacement method the free parameters are chosen to minimise the load

factor while in the stress method the free parameters are chosen to maximise the load factor.

The first finite element method for determining upper bounds on the limit load for perfectly plastic plane stress problems was developed by Hayes and Marcal [1967]. By means of a finite element technique, they constructed a parametric family of kinematically admissible velocity fields and then obtained a best upper bound by minimising the associated load multiplier. Three years later, a complementary method for finding the lower bound on the limit load for plane stress problems was described by Belytschko and Hodge [1970]. In this case, the finite element technique is used to construct a parametric family of equilibrium stress fields. A couple of years later, the finite element method used to determine limit loads for complex structures has been demonstrated by Ranaweera and Leckie [1972]. After giving several examples, they pointed out that the procedures appear to be expensive in computer time.

Up to now the mentioned references above only concern the plane stress problems and plate bending problems. It is Nguyen [1976] who first developed a new hybrid finite element with an arbitrary stress field in the interior and a quadratic displacement field on the boundary to be applied to the direct limit analysis of plates and shells. The results of the analysis were very encouraging.

In the early 1980s, Casciaro and Cascini [1982] proposed a mixed variational principle for the limit analysis of rigid perfect plastic continua and derived a mixed finite element discrete formulation. A number of examples have been presented in both structural and soil mechanics.

Recently, a finite element technique for limit analysis of structures has been demonstrated by Berak and Gerdeen [1990]. The technique is developed for calculating bounds to the limit load multiplier for two-dimensional structures which obey the von Mises yield criterion. They indicated that their 'finite element for-

mulations are more general and more rigorous, resulting in more accurate solutions for the upper and lower bounds of limit load'. After presenting a number of two-dimensional examples, they concluded that: '... Although the upper-bound procedure can give a considerable saving of computer time when simple elements are used, the lower-bound solution process remains expensive, since the usage of building block elements is inevitable. ... Both of the finite element limit analysis procedures, however, are ideally suited for parallel processing on super computers.'

'The variational formulation of the upper and lower-bound problems is completely general and can be extended to more complicated problems such as shells of revolution or nonsymmetric shells. ... Because shell elements have more degrees of freedom, the computational time will be increased significantly. Therefore, parallel processing on a super-computer is recommended if the finite element limit analysis procedures are applied to such elements.'

2.2.2 Elastic Plastic Finite Element Method

Nowadays, elastic-plastic finite element analysis is well developed technique and a number of non-linear programs are commercially available, such as ABAQUS [1995] and ANSYS [1993]. Therefore, the references on this field will not be reviewed here.

2.2.3 Modified Elastic Modulus Finite Element Method

The reduced elastic modulus method was initially developed as a stress categorisation tool for piping systems to determine the nature of elastic follow-up but was later extended to more general pressure vessel applications. The method seeks to classify stresses by comparing the simulated inelastic response of a material with models of ideal primary and secondary stress. The basis of the method was outlined by Jones and Dhalla [1981, 1986] in a procedure for classifying local

clamp induced stresses in Liquid Metal Fast Breeder Reactor pipes.

It is Marriott [1988] who noted that the elastic reduced modulus procedure, which was used to address problems in elastic follow up in piping systems by both Dholla [1984] and Severud [1984], could be used to determine the lower bound limit load of a structure by performing iterative elastic finite element analysis and invoking the lower bound limit load theorem. Marriott's procedure is a truly iterative elastic procedure:

An initial elastic analysis is performed and all elements with stress intensity greater than the (Code allowable) stress S_m are identified. The elastic modulus of these elements are then individually reduced on an element basis, according to the equation:

$$E_R = E_0 \frac{S_m}{SI} \tag{2.1}$$

where

E_0 = Previous elastic modulus

S_m = Code allowable stress

SI = Stress intensity of element

The analysis is then rerun and the next set of results is obtained. Using these results the elastic modulus of those elements which are still greater than S_m are reduced and the analysis is rerun again. This procedure is carried on in an iterative fashion until the maximum element stress intensity is less than S_m or converges to some other values.

As well as defining a methodology for categorising pressure vessel stresses. Marriot also noted that the reduced modulus method in conjunction with the lower bound limit load theorem could be used to define a lower bound limit load for the component. A lower bound limit load solution is one in which a statically admissible stress field exists in which the stress nowhere exceeds the yield stress of the material. In his procedure if the maximum stress after a number of iterations

is less than yield stress then the applied load has satisfied the lower bound limit load criterion. On the other hand, if the converged solution gives a maximum stress which is greater than the yield stress then the applied load does not meet the lower bound limit load criterion.

Seshadri [1991] and Seshadri and Fernando [1991] proposed a method for approximate estimates of limit load using the modified elastic modulus method, referred to as the GLOSS-R-Node (Generalised LOcal Stress Strain Re-distribution Node) method. The basic concept of this method is that when inelasticity occurs and the stresses are redistributed in a component, there are certain locations where the stresses will remain constant. These locations are defined as re-distribution-node or r-nodes. The r-nodes stresses are insensitive to material model and may be considered as reference stress similar to creep analysis reference and skeletal stress [Boyle and Spence, 1983]. The reference stress σ_{ref} at the r-node is related to the yield stress of an elastic perfectly plastic material by the expression.

$$\sigma_{ref} = \mu\sigma_y \tag{2.2}$$

where μ is less than one prior to plastic hinge formation and equal to one when the hinge occurs; when an elastic perfectly plastic material is assumed. By calculating the r-node stress σ_{ref} corresponding to a given load P, the limit load P_L for a statically determinate structure can be obtained from the expression

$$P_L = \frac{\sigma_y}{\sigma_{ref}} P \tag{2.3}$$

The collapse load for the case when two r-nodes form across the thickness, as is the case when direct loads are accompanied by bending action, is given by the expression

$$\{P, M\}_L = \frac{\sigma_y}{\sigma_{ref}} \{P, M\} \tag{2.4}$$

where $\{P, M\}$ is the primary membrane and bending load combination.

The basic procedure to find the GLOSS r-node is as follows: A linear elastic finite element analysis of a mechanical component or structure is carried out for

the prescribed loading and the pseudo-elastic stresses are obtained. The elastic modulus of the model is then locally modified on an element to element basis according to the equation

$$E_m = \frac{\sigma_j}{\sigma} E_0 \tag{2.5}$$

Where E_m is the modified element modulus, E_0 the original modulus, σ the element stress and σ_j is the equivalent stress chosen so that stress redistribution occurs in most of the component. A second linear elastic analysis is then carried out and the position of the r-node or nodes are obtained at which the stresses are unchanged. Using these stress values the limit load then can be calculated by using either equations (2.3) or (2.4).

Although the GLOSS r-node method can be used to calculate limit loads for certain components, the concept of r-node especially in 3D models, is quite difficult both to visualize and calculate. Also fine through thickness finite element meshes are required in order to use the method effectively. This will lead to 3D models with very refined meshes with subsequent problems in computer processing time and memory storage space. In practice, software and computing restrictions generally restrict the number of through thickness meshes in 3-D pressure vessel models to three or four elements.

Based on the modified elastic modulus method, Carter and Ponter [1992] developed a linear elastic finite element method to calculate lower and upper bound limit loads boundaries which has been implemented for planar finite element structures under both plane stress and plane strain conditions. They have also developed a theoretical background, although this has not been published at the time of writing. The procedure is as follows:

1. An elastic analysis of the structure is performed for the applied loads P assuming that the elastic modulus E is initially constant throughout the structure giving the elastic stress distribution $\sigma_1(x, P, E)$ from which von Mises equivalent stress distribution $\phi[\sigma_1(x, P, E)]$ is calculated. This establishes the relationship

of the stresses to the yield surface.

2. The elastic modulus is then modified throughout the structure according to the ratio of the current elastic modulus to the equivalent stress at that point

$$E_1(x) = \sigma_y \frac{E}{\phi[\sigma_1(x, P, E)]} \tag{2.6}$$

3. The limit load is then calculated from

$$P_L^1 = P \frac{\sigma_y}{\phi[\sigma_1(x, P, E)]_{max}} \tag{2.7}$$

Finally this procedure is iterated to a stable solution by returning to step 1. recalculating the elastic stress distribution using the new elastic moduli $E_1(x)$ to give $\sigma_2(x, P, E_1(x))$ and thus the new equivalent stress distribution. This is then applied to step 2 and step 3 to give $E_2(x)$ and P_L^2 respectively. The procedure is convergent in approximately 5 iterations.

The elastic compensation method as first devised by Mackenzie and Boyle [1993a] is based on the modified elastic modulus method; in particular. Marriott's lower bound theorem approach and Seshadri's redistribution technique, to obtain lower and upper bound limit loads by several elastic finite element analyses. This is done by selectively correcting the elastic modulus in finite element in each iteration in order to mimic the form of the limit state stress distribution hence forming the plastic hinges for the collapse mechanism. By invoking the lower bound limit load theorem, conservative limit loads can then be obtained. Then by using the compatible displacement and strain fields from the same element model and substituting them into the upper bound theorem an upper bound solution to the model could be calculated [Mackenzie *et al.*, 1992, 1993], [Nadarajah *et al.*, 1993], [Shi *et al.*, 1993]. The method will be reviewed in more detail in the next Chapter.

2.3 A Brief Review of Shakedown Analysis of Structures by Finite Element Method

The fact that the collapse loads calculated according to limit analysis may fail to provide a proper measure of structural safety in the case of variable repeated loads, was pointed out for the first time by Grüning [1926] as early as 1926 and later by Bleich [1932], who proved the static shakedown theorem for a system of beams of ideal I-cross-section. In 1936 Melan [1936] presented a more general theorem and later extended it to the general case of a continuum [1938a, 1938b]. It is worth realizing that at that stage the shakedown theory was developed quite independently of the limit analysis theory. It is well known that in 1938 Gvozdev [1938] arrived at his fundamental results in the limit analysis of elastic-perfectly plastic structures subjected to single loading.

In 1950 Neal [1950] presented a method of shakedown analysis for frames by analysing possible mechanisms of plastic flow. The first solution to the shakedown problem in continuum media were arrived at in papers of Symonds [1951] and Hodge [1954]. In both papers the shakedown was limited by the alternating (i.e.; of changing sign) yielding; the corresponding magnitudes load factors were compared with those of the limit analysis. It was Koiter [1956], who first recognized the fact that the theorem on plastic collapse should be understood as limiting cases of shakedown theorems corresponding to the coinciding of the upper and lower bounds for each of the contributing external actions. Based on this analogy, Koiter put forward the kinematic shakedown theorem and thus stated and proved the plastic analysis theorems, i.e. the limit analysis and shakedown ones in the form used nowadays [1960].

At present the shakedown theory constitutes a well established branch of plasticity theory. A complete account of it can be found in books of Martin [1975]. Gokhfeld and Chernniavsky [1980], König [1987], Lubliner [1990] and in review paper of König and Maier [1981].

By using discrete finite element approach, Maier [1970] proved all the above shakedown theorems for a very general class of piecewise linear hardening rules [Maier 1969, 1972a]. He also pointed out that shakedown problems can be handled by means of mathematical programming methods and the precise duality of the static and kinematic approaches holds. The detailed mathematical programming applications to shakedown analysis can be found inthe review papers of Maier and Munro [1982] and Maier and Lloyd [1986]. Here only a few papers using an equilibrium finite element technique with nonlinear programming applied directly to the shakedown theorems will be reviewed.

2.3.1 Direct Finite Element Method

A general method has been firstly developed by Belytschko [1972] for the determination of lower bounds on the shakedown load for plane stress problems using finite element method. The method is formulated by means of Melan's shakedown theorem. Two years latter, Corradi and Zavelani [1974] developed a finite element method to calculate shakedown load for two and three dimensional structures by applying Bleich and Melan's theorem. Then a finite element formulation for shakedown problems using a yield criterion of the mean has been derived by Ngnyen and Konig [1979]. They concluded that hybrid stress elements are probably the most suitable type in generating the necessary self-stress state for shakedown problems.

In the early of 1980s, Ngnyen and Palgen [1980-1981] carried out a shakedown analysis by displacement method and equilibrium finite element. Lower bounds of the safety factor of elastic perfectly plastic structures with respect to shakedown were obtained by use of an equilibrium finite element approach and nonlinear programming techniques. Then, the lower bound shakedown finite element analysis of elastic perfectly plastic thin plates and shells with symmetry of revolution has been performed by Ngnyen and Morelle [1982]. The finite element formulation

is based on Melan's theorem. In the analysis a new finite element is developed which allows to discretise the shells into a series of conical shells. A few years later the shakedown analysis of axisymmetric elastic perfectly plastic sandwich shells has been presented by Morelle [1986] using a new upper bound formulation based on a special form of Koiter's theorem concerning piecewise linearised yield surfaces.

In 1988, Genna [1988] presented a nonlinear inequality, finite element approach to the direct computation of shakedown load safety factors. The main features of this computation are the use of local, a posteriori linearisation of the yield surface, which allows the prescription of a maximum violation of the constitutive law, and the use of a physically oriented solution algorithm to the linear complementarity problem to which the shakedown analysis is reduced. Meantime, a general finite element method for shakedown analysis has been performed by Shen [1988] based on Melan's theorem and mathematical programming technique. Recently, a lower bound finite element computational shakedown analysis of axisymmetric shells has been carried out by Lu *et al.* [1991].

2.3.2 Modified Elastic Modulus Finite Element Method

It was mentioned in Section 2 of this Chapter that several modified elastic modulus methods can be used to calculate the limit loads of structures. In this Section, these methods are applied to shakedown analysis of structures.

After developing GLOSS (Generalised LOcal Stress Strain) method for estimating creep damage in pressurised components experiencing multiaxial relation and elastic follow-up type behaviour [Seshadri 1990], in 1992 Seshadri and Gie [1992] presented a simple method for estimating residual stresses and assessing shakedown loads using the GLOSS analysis.

As described in the Section 2 of this Chapter Carter and Ponter [1992] devel-

oped a linear elastic finite element method to calculate lower and upper bound limit load boundaries based on the modified elastic modulus method. In the same paper they also presented a procedure for calculating shakedown load of a structure. The proposed procedure is as follows:

The structure is assumed to be subject to a constant mechanical load and a cyclically varying thermal load. For this the elastic stress distribution can be factorized into mechanical and thermal terms

$$\sigma(x) = \sigma_P(x) + \sigma_T(x) \tag{2.8}$$

where the thermo-elastic stress $\sigma_T(x)$ is calculated in the absence of any mechanical load such that the maximum value over the loading cycle $t = (0 - \tau)$ at any point in the structure is used

$$\sigma_T(x) = Max\{\sigma_T(x,t)\} \tag{2.9}$$

The elastic modulus is then scaled according to the combination of the mechanical and thermal stresses by

$$E_1(x) = \frac{\sigma_y}{\phi[\sigma_P(x) + \sigma_T(x)]} \tag{2.10}$$

This can be shown to work for all values of the thermal stress distribution including inside the plastic shakedown region where $\sigma_T > 2\sigma_y$. The mechanical load at the boundary between shakedown and ratchetting of the structure is now given by

$$P_S^1 = P(\sigma_y / \{\phi[\sigma_P(x) + \sigma_T(x)]\}_{max}) \tag{2.11}$$

Thus the thermo-elastic stress distribution acts as an initial stress field to the procedure.

After developing the *elastic compensation* method for calculating lower and upper bound limit loads of structures, Mackenzie and Boyle [1993b] proposed a method for calculating lower bound shakedown load using the *elastic compensation* method and Melan's theorem. The method will be described in detail in the next Chapter.

2.4 Summary

It has been seen from the above brief review that there are many publications on limit and shakedown analysis of structures by the finite element method but for some problems it is necessary to carry out further research. For example, for the problem of a nozzle in spherical pressure vessels, most of publications in the past have been concentrated on thin shell problems. There are very few parametric studies have been done to obtain the limit and shakedown loads for thick nozzle/sphere problems.

In the era of computer technology, the use of finite element analysis to calculate plastic (limit) loads is one of several options a designer could use. However. the use of non-linear finite element analysis to obtain plastic (limit) loads still requires extensive computing resources and is consequently much more difficult to perform. The use of non-linear finite element analysis is also difficult as it requires the definition of material properties and control of iterative procedures. Even with a load against deflection plot obtained from the finite element analysis. there is still an uncertainty in predicting the plastic (limit) loads as there are so many different techniques proposed by the various authors, for example Gerdeen [1979] and Blachut [1995].

From the design point of view, the lower and upper bound limit loads and shakedown loads will be of great importance. Hence using linear elastic finite element analysis to calculate these loads as an alternative tool to non-linear finite element analysis will be a vital step forward in design. In the next Chapter, the reduced modulus method, modified modulus method and elastic compensation method will be reviewed in more detail.

2.5 Refrences

Baker, J.F. and Roderick, J.W., (1938), An experimental investigation of the strength of seven portal frames, *Trans. Inst. Weld.*, Vol. 1.

Baker, J.F., Horne, M.R. and Heyman, J., (1956), *The Steel Skeleton*, Vol. 2, Cambridge.

Baker, J.F. and Heyman, J., (1969), *Plastic Analysis of Frames*, Cambridge.

Baker, J. and Heyman, J., (1971), *Plastic Design of Frames*, Vols I and II. Cambridge University Press.

Belytschko, T., (1972), Plane stress shakedown analysis by finite elements, *Int. J. Mech. Sci.*, Vol. 14, 619–625.

Belytschko, T., and Hodge, P.G., Jr., (1970), Plane stress limit analysis by finite elements, *J. Engrg. Mech. Div.*, Vol.96, No.EM6, 931–944.

Berak, E.G. and Gerdeen, J.C., (1990), A finite element technique for limit analysis of structures, *J. Pres. Ves. Tech.* **112**, 138–144.

Bleich, H., (1932), Über die bemessung statisch unbestimmter stahlwerke under der berücksichtigung des elastich–plastischen verhaltens des baustoffes, *Bauingenieur*, **13**, 261–267.

Blachut, J., (1995), Plastic loads for internally pressurised torisphers, *Int. J. Pres. Ves. & Piping*, **64**, 91–100.

Boyle, J.T. & Spence, J., (1983), *Stress Analysis for Creep*, Butterworths.

Carter, K.F., and Ponter, A.R.S., (1992), Caculation of limit loads and shakedown boundaries using the modified elastic modulus method, *Computational Plasticity Fundamentals and Applications*, part II, 1597–1608.

Calladine, C.R., (1965), *Plasticity for Engineers*, Ellis Horwood Ltd, Chichester.

Calladine, C.R., (1985), *Plasticity for Engineers*, Ellis Horwood Ltd., Chichester.

Casciaro, R., and Cascini, L., (1982), A mixed formulation and mixed finite elements for limit analysis, *Int. J. Numberical methods in Engrg.*, Vol.18. 211–243.

Chakrabarty, J., (1987), *Theory of Plasticity*, McGraw-Hill Book Co., Singapore.

Corradi, L., and Zavelani, A., (1974), A linear programming approach to shakedown analysis of structures, *Comput. Methods Mech. Eng.*, Vol.3, 37–53.

Dhalla, A.K., (1984), Verification of an elastic procedure to estimate follow-up. *Design of Elevated Temperature Piping*, Eds: R.H. Mallet & R.M. Mello, *PVP-Vol. 86, ASME*, New York, 81–96.

Dhalla, A.K. & Jones, G.L., (1986), ASME Code classification of pipe stresses: a simplified elastic procedure, *Int. J. Press. Ves. & Piping* **26**, 145–166.

Drucker, D.C., Greenberg, H.H. and Prager, W., (1951), The safety factory of an elastic-plastic body in plane strain, *J. Appl. Mech.* **18**, 371.

Drucker, D.C., Greenberg, H.H. and Prager, W., (1952), Extended limit design theorems for continuous media, *Quart. Appl. Math.* **9**, 381.

Genna, F. , (1988), A nonlinear inequality, finite element approach to the direct computation of shakedown load safety factors, *Int. J. Mech. Sci.*, Vol.30, No.10, 769–789.

Gerdeen, J.C., (1979), A critical evaluation of plastic behavior data and a united definition of plastic loads for pressure components, *WRC Bulletin 254.*

Girkmann, K., (1931), Bemessungen von rahmentragwerken unter zugrundelegung eines ideal-plastischen stahles, *Sizungsberichte der Akademie der Wissenschaften in Wien*, Springer Verlag, Vienna.

Gokhfeld, D.A. and Cherniavsky, O.F., (1980), *Limit Analysis of Structures at Thermal Cycling*, Sijthoff and Noorhoff.

Greenberg, H.H. and Prager, W., (1951), Limit design of beams and frames, *Proc. ASCE* **77**, (Separate 59).

Grüning, M., (1926), Die Trafähiggkeit statisch unbestimmter Tragwerke aus stahl bei beliebig häufig wiederhelter belstunh, Springer, Berlin,1926.

Gvozdev, A.A., (1936), Determination of the value of collapse load for statically in determinate systems undergoing plastic deformation (In Russian), *Int. J. Mech. Sci.*, 1960, London, 322–335.

Hayes, D.J., and Marcal, P.V., (1967), Determination of upper bounds for problems in plane stress using finite element techniques, *Int. J. Mech. Sci.*, Vol.9, 245–251.

Heyman, J., (1957), *Plastic Design of Portal Frames*, Cambridge.

Heyman, J., (1964), *Beams and Framed Structures*, Pergamon Press, London.

Hibbitt, Karlsson & Sorensen, Inc. (1995), *ABAQUS User's Manual for Version 5.4*, 1080 Main Street, Pawtucket, RI 02860-4847.

Hodge, P G. Jr., (1954), Shakedown of elastic–plastic structures, In *Residual Stresses in Metal Construction*, edited by W.R. Osgood, Reinhald, New York.

Hodge, P.G. Jr., (1959), *Plastic Analysis of Structures*, McGram-Hill (N.Y.).

Hodge, P.G. Jr., (1963), *Limit Analysis of Rotationally Symmetric Plates and Shells*, Prentice Hall (Englewood Cliffs, N. Y.).

Horne, M.R., (1971), *The Plastic Theory of Structures*, Nelson.

Ingerslev, A., (1921), Om en elementaer beregningsmetode of krydsarmbrede plader. *Ingenioren*, **30**, 507–515.

Johansen, K.W., (1932), Bruchmomente der kranzweise bewehrten platten, Abhandlungen, *Int. Ver. Brucken- und Hochbau*, Zurich, 227–296.

Jones, G.L. and Dhalla, A.K., (1981), Classification of clamp induced stresses in thin-walled pipe, *PVP-Vol. 81, ASME*, New York.

Kaliszky, S., (1989), *Plasticity: Theory and Engineering Applications*, Elsevier Science Publishers.

Kazinczy, G., (1914), Experiments with clamped beams (In Hungarian), *Betinszele*, **2**, No. 4, 5, 6, 68–71, 83–87, 101–104.

Kazinczy, G., (1933), Die Bemessung unvollkommen eingespanner Stahl-I-Deckenträger unter Berücksichtigung der plastischen Rormänderungen, *Int. Ver. Brücken- und Hochbau*, Berlin, Schlussbericht, 56–69.

Kazinczy, G., (1942), The importance of the plastic behaviour of materials from the point of view of the load carrying capacity of structures (In Hungarian), Budapest, *Mernoki Tovabbkepzo Intezet*, Bd. III. H. 13.

Kist, N.C., (1917), Fuhrt eine auf das Hookesch Gesetz gegrundete Spannungsberechnung zu einer befriedigenden bemessung von Stahlbrucken and Gebauden? (In Holland), *De Ingenieur.*

Koiter, W.T., (1956), A new general theorem on shake–down of elastic–plastic structures, *Proc. Kominkl. Ned, Akad, Wed, B59*, 24–34.

Koiter, W. T. , (1960), General theorems for elastic–plastic solids, in *Progress in Solid Mechanics*, (ed. I. N. Sneddon and R. Hill), Vol. 1, North-Holland, Amsterdam, 165–221.

König, J.A., (1987),*Shakedown of Elastic–Plastic Structures*, PWN–Polish Scientific Publishers, Warsaw and Elsevier, Amsterdam.

König, J.A., and Maier, G., (1981), Shakedown analysis of elastoplastic structures: A review of recent developments, *J. Nuclear Engng. Design*, **66**, 81–95.

Lu, M.W., Xue, W.M. and Chen, S.Z., (1991), Computational shakedown analysis of axi-symmetric shells: A lower bound solution, *Computational Mechanics*. Cheung, Lee & Leung (eds), Balkema, Rotterdam, 105–110.

Lubliner, J. , (1990), *Plasticity Theory*, Macmillan Publishing Company, New York.

Mackenzie, D., Shi, J., Nadarajah, C., and Boyle, J.T., (1992), An iterative elastic analysis procedure for estimating lower bound limit loads. *PVP-Vol. 230. ASME*, 129–134.

Mackenzie, D., and Boyle, J.T., (1993a), A method of estimating limit loads by iterative elastic analysis. I–Simple examples. *Int. J. Pres. Ves. & Piping*, Vol. 53, No.1, 77–95.

Mackenzie, D., and Boyle, J.T., (1993b), A simple method of estimating shakedown loads for complex structures, *PVP-Vol. 265, ASME*, 89-94.

Mackenzie, D., Nadarajah, C., Shi, J., and Boyle, J.T., (1993), Simple bounds on limit loads by elastic finite element analysis. *J. Pres. Ves. Technology*, Vol.115, 27–31.

Maier, G., (1969), Shakedown theory in perfect elastoplasticity with associated and nonassociated plow–laws, *Meccanica*, **6**, 250–260.

Maier, G., (1970), A matrix structural theory of piecewise–linear plasticity with interacting yield planes, *Meccanicca*, **7**, 51–66.

Maier, G., (1972), A shakedown matrix theory allowing for workhardening and second–order geometric effects, *Proc. Symp. Foundations of Plasticity*, Warsaw, (ed. A. Sawczuk), 417–433.

Maier, G. and Munro, J., (1982), Mathematical programming application to engineering plastic analysis. *Appl. Mech. Rev.*, **35**, 1631–1643.

Maier, G. and Lloyd, D., (1986), Update to 'Mathematical programming application to engineering plastic analysis'. *ASME Appl. Meah. Update*, 377–383.

Maier-Leibnitz, H., (1828), Beitrag zur frage der tatsachlichen tragfahigkeit einfacher und durchlaufender balkentrager aus St 37 und aus Holz, *Bautechnik*, **6**.

Martin, J.B., (1975), *Plasticity: Fundamentals and General Results*, Cambridge, Mass., MIT Press.

Marriot, D.L., (1988), Evaluation of deformation or load control of stresses under inelastic conditions using elastic finite element stress analysis, *PVP-Vol. 136. ASME*, Pittsburgh.

Massonnet, C. and Save, M., (1965), *Plastic Analysis and Design*, Blaisdell (Boston).

Melan, E., (1936), Theorie statisch unbestimmter systeme, *Proc. Second Congr. IABSE*, Berlin , 43–64.

Melan, E., (1938a), Der spannumngszstand eines Mises–Henckyschen kontinuums bei veräderlicher belastung, *Sitzber. Akad, Wiss. Wien IIa*, **147**, 73–87.

Melan, E., (1938b), Zur plastizität des raumlichen kontinuums, *Ing. Archiv*, 8. 116–126.

Morelle, P., (1986), Numerical shakedown analysis of axisymmetric sandwich shells: an upper bound formulation, *Int. J. Numer. Meth. Engineering*, Vol. 23. 2071–2088.

Nadarajah, C., Mackenzie, D., and Boyle, J.T., (1993), A method of estimating limit loads by iterative elastic analysis. II–Nozzle sphere intersections with internal pressure and radial load. *Int. J. Pres. Ves. & Piping*, Vol. 53, No.1, 97–119.

Neal, B.G., (1950), Plastic collapse and shakedown theorems for structures of strain–hardening material, *J. Aero. Sci.*, **17**, 297–306.

Neal, B.G., (1956), *The Plastic Methods of Structural Analysis*, Chapman and Hall (London).

Neal, B.G., (1977), *The Plastic Methods of Structural Analysis*, 3rd ed., Chapman and Hall.

Nguyen, D.H., (1976), Direct limit analysis via rigid-plastic finite elements,*Comput. Meth. Appl. Mech. Engrn.* **8**, 81–116.

Nguyen, D.H. and König, J.A., (1976), A finite element formulation for shakedown problems using a yield criterion of the mean, *Comput. Meth. Appl. Mech. Engrn.* **8**, 179–192.

Nguyen, D.H., and Palgen, L., (1980), Shakedown analysis by displacement method and equilibrium finite element, *Trans. of the Canadian Society Mechanical Engineers*, Vol.6, 34–40.

Nguyen, D.H., and Morelle, P., (1982), Numerical shakedown analysis of plates and shells of revolution by equilibrium finite element methods, *Proceedings of new and Future Development in Commercial Finite Element Methods Congress*, Los Angeles, USA.

Prager, W., (1957), Linear programming and structural design: I. Limit analysis, Rand Coropration, Report P-1122, 6–26.

Ranawerra, M.P. and Leckie, F.A., (1970), Bound methods in limit analysis. In: *Finite Element Techniques in Structural Mechanics*, edited by H. Tottenham and C. Brebbia. Southampton Univ. Press.

Save, M.A. and Massonnet, C.E., (1972), *Plastic Analysis and Design of Plates. Shells and Disks*, North–Holland, Amsterdam.

Seshadri, R., (1991), The generalised local stress strain (GLOSS) analysis-theory and applications, *J. Press. Vess. Tech.*, 219–227.

Seshadri, R. and Fernando, C.P.D., (1991), Limit loads of mechanical components and structures using the GLOSS R-Node method, *PVP-Vol. 210-2. ASME*, San Diego.

Seshadri, R., and Ge, W., (1992), Residual stress estimation and shakedown evaluation using GLOSS analysis, *PVP–Vol. 230, ASME*, 13–21.

Severud, L.K., (1984), A simplified method of evaluation for piping elastic follow up, Proc. 5th Int. Conf. Pres. Vessel. Tech., ASME, San Francisco, 367–387.

Shen, W., (1988), A general method for shakedown analysis, *Computers & Structures*, **30** (4), 901–903.

Shi, J., Mackenzie, D., and Boyle, J.T., (1993), A method of estimating limit loads by iterative elastic analysis. III–Torispherical heads under internal pressure. *Int. J. Pres. Ves. & Piping*, Vol. 53, No.1, 121–142.

Swanson Analysis Systems, Inc. (1993), *ANSYS User's Manual for Revision 5.0A*, SASI,PO Box 65, Johnson Road, Houston PA 15342-0065.

Symonds, P.S., (1951), Shakedown in continuous media, *J. Appl. Mech.*, **1**.

Symonds, P.S., (1962), *Limit Analysis*, Chapt. 49, Handbook of engineering Mechanics, W. Flügge (Ed), McGraw–Hill, New York.

CHAPTER 3

THE METHOD OF ELASTIC COMPENSATION: AN OVERVIEW

3.1 Introduction

With increasing access to powerful computers and the availability of finite element software, inelastic analyses are no longer prohibitive but do require much greater computing resources than elastic analysis and are consequently much more expensive to perform. However, robust approximate methods, such as the elastic compensation method developed by Mackenzie and Boyle [1993], provide simple and useful ways of obtaining useful design information from limit load analysis.

The elastic compensation method is a unique procedure which uses the results of an elastic finite element analysis, coupled with a reduced modulus scheme. to determine the approximate limit load of a component under single or multiple loadings using the lower and upper bound limit load theorems.

The procedure is simple and straight forward; therefore, it can be easily 'automated' and applied as a batch program, hence relieving the analyst of the tedious task of manual programming. This also reduces human errors.

In this Chapter, a brief survey on the background of the reduced elastic modulus method and the modified elastic modulus method and the concept of elastic compensation method will be discussed. Also a practical approach using this method will be described.

3.2 Reduced Elastic Modulus Methods

The reduced elastic modulus method was initially developed as a stress categorisation tool for piping systems to determine the nature of elastic follow-up but was later extended to more general pressure vessel applications. The method seeks to classify stresses by comparing the simulated inelastic response of a material with models of ideal primary and secondary stress. The basis of the method was outlined by Jones and Dhalla [1981, 1986] in a procedure for classifying local clamp induced stresses in Liquid Metal Fast Breeder Reactor pipes. They found that the clamp induced stresses tend to redistribute due to material or geometric non-linearity, and thus these could be considered as secondary stress and secondary stress limits could be applied. However, what was of more interest is the way in which the effect of local inelasticity was assessed and not in the actual categorisation. It was found that instead of performing an inelastic analysis to find the behaviour of inelastic response, an iterative elastic analysis could be used. In this analysis, the loaded region of the structure was systematically weakened by the reduction of the local modulus of elasticity to simulate the effect of local inelasticity. It was found that this approach was not only less expensive in computing time, but it adequately simulated the inelastic behaviour of the pipe/clamp structure for the purpose of design. Dhalla and Jones called this method the 'elastic secant modulus procedure'.

The reduced modulus method was used by Dhalla [1984] and independently by Severud [1984] to address problems in elastic follow-up in piping systems. Using only elastic piping flexibility programs, the inelastic response and follow up characteristic of the piping system could be simulated by reducing the elastic modulus in highly loaded bends in an iterative elastic analysis. In their publications they examined the conservatism and accuracy of this method by comparing the results with inelastic analyses. Boyle and Nakamura [1987]. Nakamura and Boyle [1987] studied the approach used by Severud/Dhalla amongst others. and concluded that although this method is practical. it is only useful to demon-

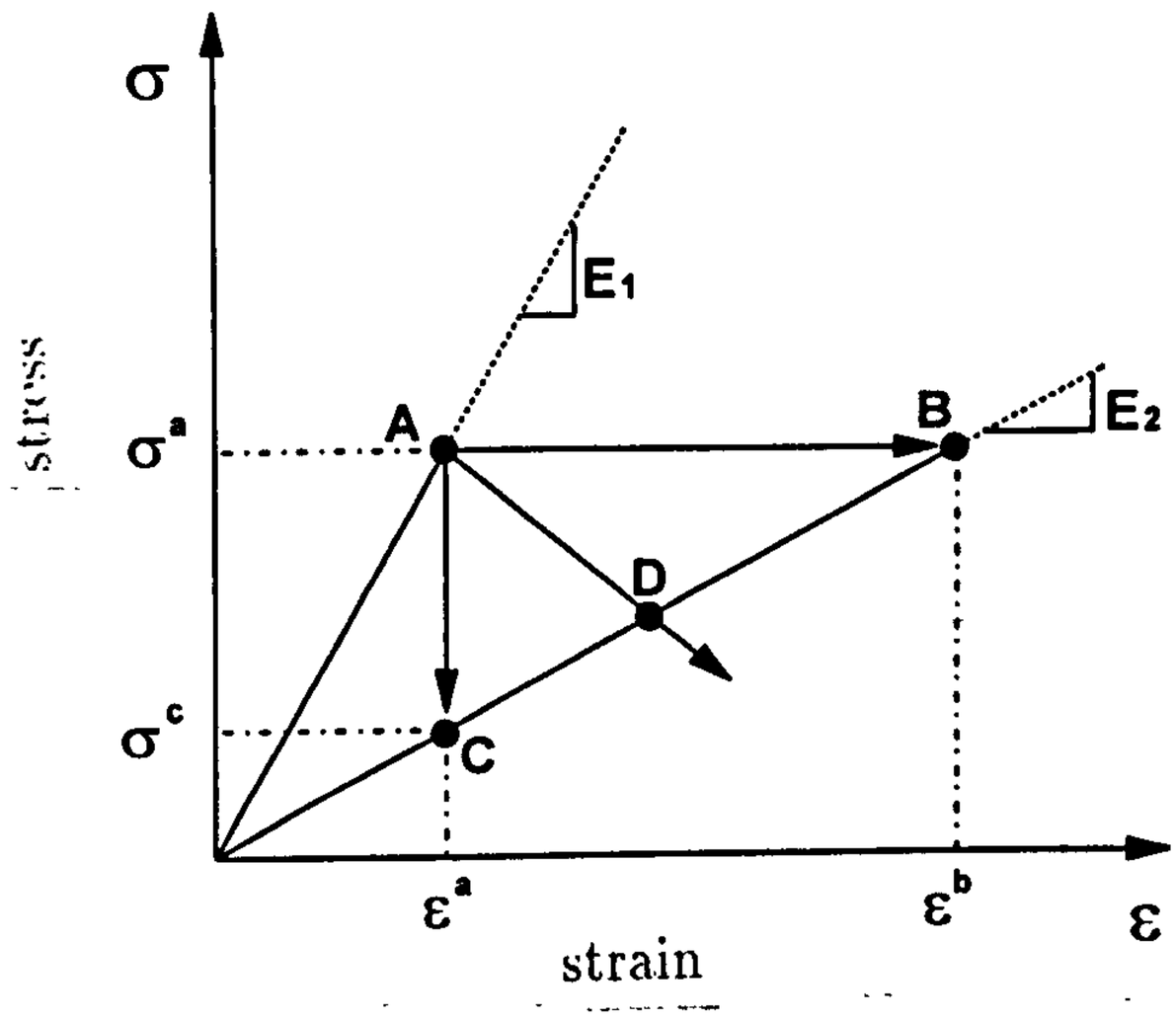

Figure 3.1: Idealised load-controlled and deformation-controlled response

strate that elastic follow up is *not* a problem for a given piping system. They also advised that in this method some care has to be taken especially in the selection of the elements chosen for modulus reduction. Boyle and Spence [1988] presented a method for assessing elastic follow-up in high temperature piping systems based on the Severud/Dhalla modulus reduction method and as a development of Roche's classification procedure [Roche 1986]. Further appraisal of the method was presented by Gambioni *et al.* [1989] the following year.

The success of the reduced modulus method in piping design led to its being applied to stress categorisation problems in pressure vessel components in the late 1980's. In 1987 Dhalla implemented the reduced modulus method for stress categorisation problems in pressure vessel components. The procedure was based on partitioning elastically calculated stresses at highly loaded regions of a pressure vessel component into primary and secondary stresses. These stresses were then applied with appropriate stress limits. The Dhalla reduced modulus procedure for stress categorisation is described below:

The elastic stress (σ^a) generated by an applied mechanical load or thermal deformation is represented by point A in Figure 3.1. If the local region experiences no decrease in stress due to inelastic (plastic or creep) deformation then the

applied pressure loading, and the resulting stress can be classified as primary. That is, the stress (σ^a) would be constant for different elastic moduli E_1 and E_2 used in two elastic analyses; where, E_1 is the elastic modulus E and E_2 simulates the local inelastic response ($E_2 = E_s^i = \sigma^a/\epsilon^b$). Of cource, the calculated strain would increase from ϵ^a to ϵ^b due to the reduced material flexibility. The Line AB, in Figure 3.1 represents a 100% load-controlled response at a constant elastic stress (σ^a). The correponding strain ratio would vary inversly with the elastic modulus ratio

$$\epsilon^a/\epsilon^b = E_2/E_1 \quad when \quad \sigma^a = constant \tag{3.1}$$

In contract, if the appiled loading is deformation-controlled (and without any elastic follow-up effect) then the change in elastic moduli would not affect the predicted elastic local strain, ϵ^a, but the elastic local stress would decrease from (σ^a) to (σ^c). Thus, Line AC in Figure 3.1, represents a 100% deformation-controlled response at a constant elastic strain ϵ^a. The correponding stress ratio (σ^a/σ^b) would vary in direct proportion to the elastic moduli ratio (E_1/E_2)

$$\sigma^a/\sigma^c = E_1/E_2 \quad when \quad \epsilon^a = constant \tag{3.2}$$

In general, it is difficulty to judge a priori the correct ASME Code stress classification at structural discontinuities. For example, the stress generated at structural discontinuities of internally pressurised vessels may result in a mixed response indicated by Line AD, in Figure 3.1. The primary-secondary stress classification procedure for the mixed response is summarised in the following:

1. Perform an elastic analysis and identify the most highly loaded location in the structure.

2. Estimate inelastic (either plastic or creep) strain accumulated at this location. This estimate could be very rough. The strain may be the maximum strain for assumed load-controlled response (point B in Figure 3.1), or a specified limit such as the 1% membrane strain defined in ASME Code case N-47.

3. Calculate the minimum secant modulus E_s^m at a point which corresponds to the initial elastic stress level σ^a and estimated total strain level ϵ^b. Assign this reduced modulus to highly stressed regions in the structure.

4. Perform at least three elastic analyses assuming equivalent elastic moduli varying between the material Young's modulus E to the minimum estimated secont modulus E_s^m for the most highly stressed local regions of the structure. The response is to establish a trend of stress relaxation with respect to the reduction in secant modulus.

5. Plot the equivalent elastic analysis prediction on a generalised stress-strain plot; then relate the local response to either 100% load-controlled or 100% deformation-controlled response as represented by Lines AB and AC, respectively, in Figure 3.1, or a mixed response shown by Line AD.

The effective stresses and strains for the original elastic and the reduced modulus analyses at the high stress region are then plotted on a normalised stress strain plot. The effective stress is taken to be equivalent or von Mises stress. In the elastic and reduced modulus analyses, the corresponding equivalent strain is simply the equivalent stress divided by the elastic or reduced elastic modulus respectively. Figure 3.2 shows the normalised stress strain plot for a single reduced modulus analysis. Lines between elastically calculated point A and the reduced modulus calculated points R on the normalised plot are referred to as mixed response lines. The mixed response line is defined in term of θ in Figure 3.2.

In the procedure used by Dhalla, the pseudo elastic stress σ_A is partitioned into primary and secondary components, depending on the angle θ. If θ is 0^0, the stress component is taken as 100% load control, hence 100% primary stress. For mixed response as above, the amount of primary stress is calculated by

$$PSF = \frac{\theta}{90} \tag{3.3}$$

Where PSF =Primary stress factor.

Marriott [1988] suggested that a modified version of the reduced modulus procedure could be used to perform limit analysis. In his analysis, an initial elastic analysis is performed and all elements with stress intensity greater than

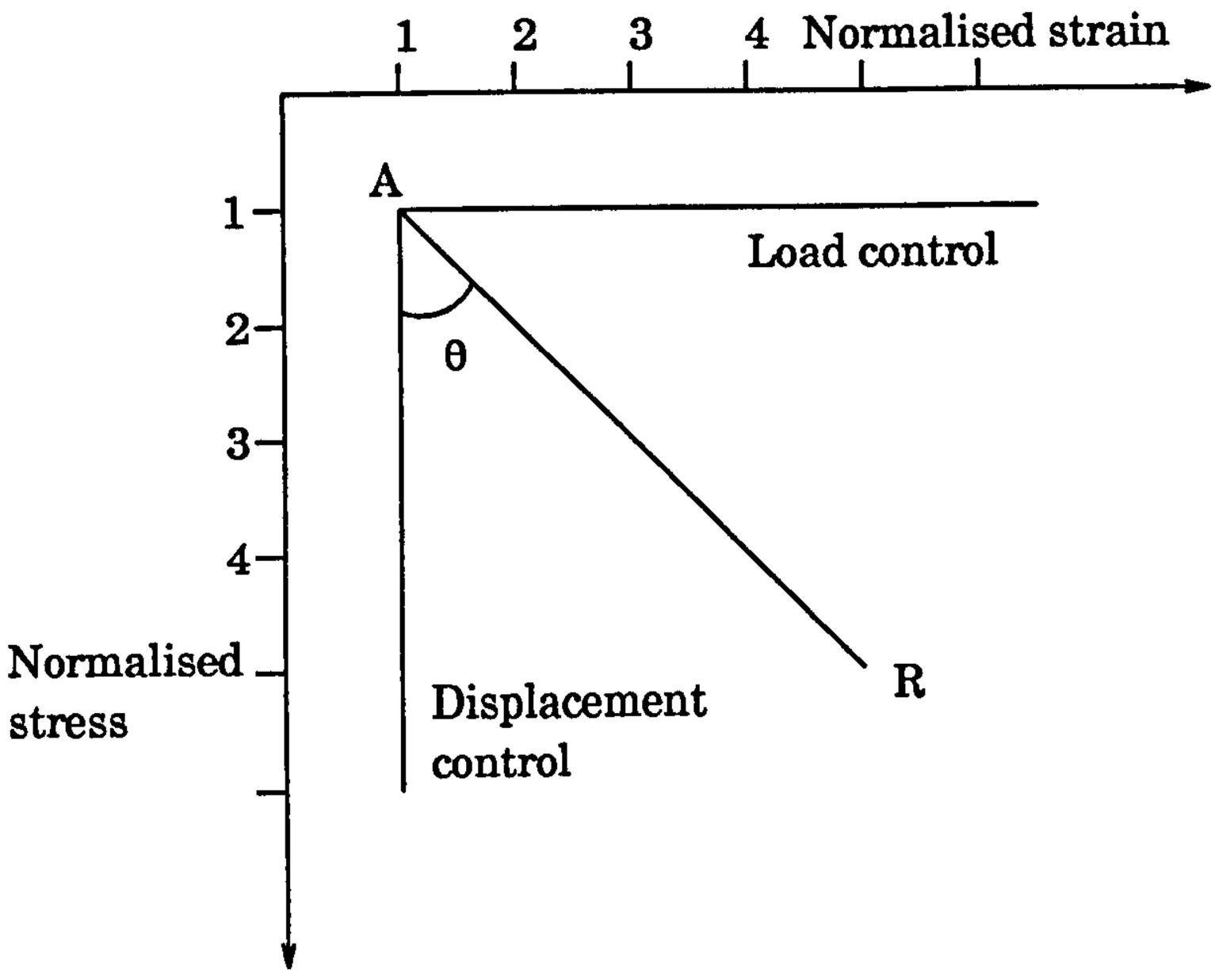

Figure 3.2: Dhalla's normalised stress strain plot [1986]

the (Code allowable) stress S_m are identified. The elastic moduli of these elements are then individually reduced on an element basis, according to the equation:

$$E_R = E_0 \frac{S_m}{SI} \tag{3.4}$$

where

E_0 = Previous elastic modulus

S_m = Code allowable stress

SI = Stress intensity of element

The analysis is then rerun and the next set of results is obtained. Using these results the elastic modulus of those elements which are still greater than S_m are reduced and the analysis is rerun again. This procedure is carried on in an iterative fashion until the maximum element stress intensity is less than S_m or converges to some other values. This procedure is illustrated in Figure 3.3.

As well as defining a methodology for categorising pressure vessel stresses, Marriott also noted that the reduced modulus method in conjunction with the

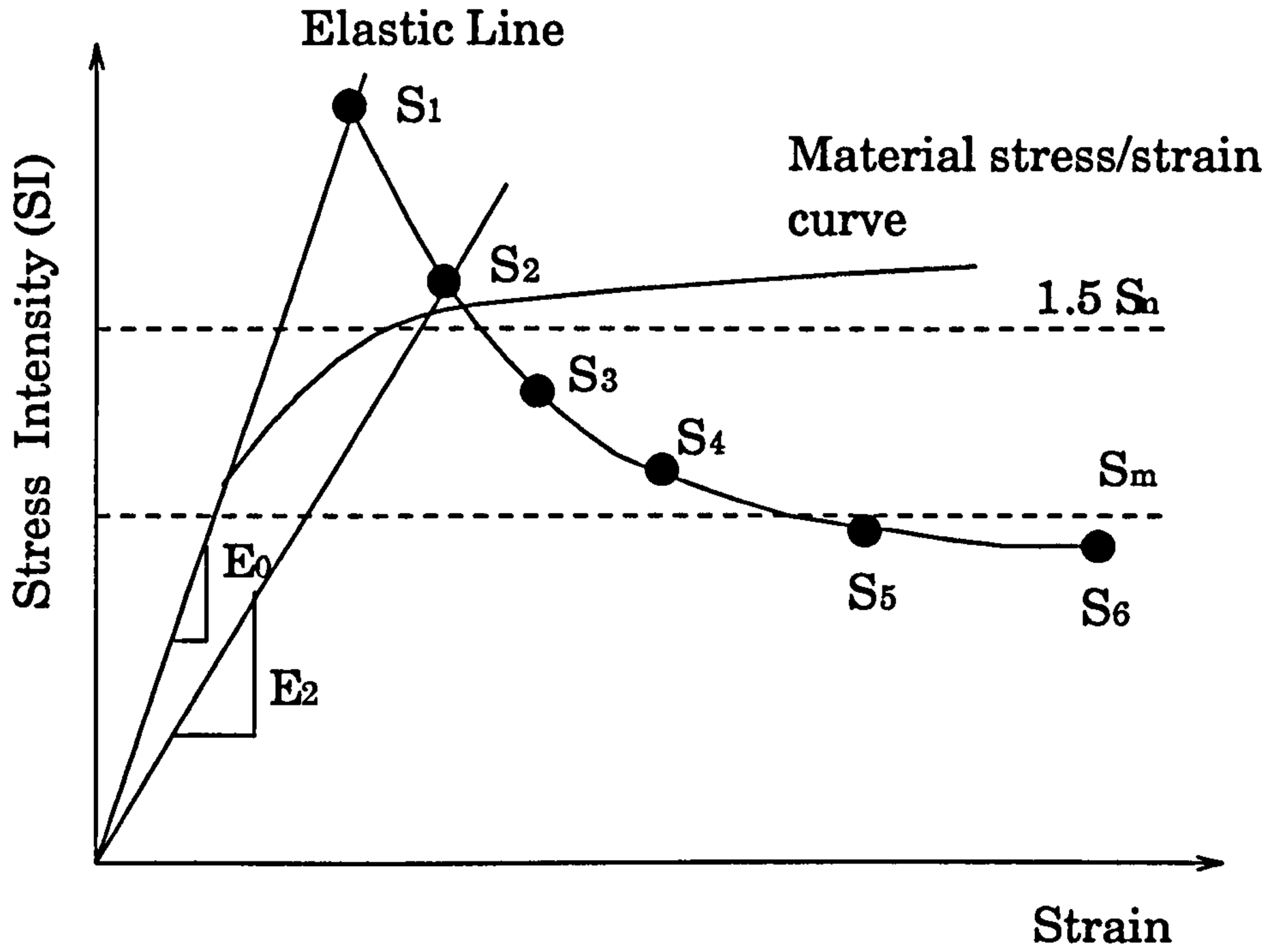

Figure 3.3: Procedure used by Marriott [1988] for modulus reduction

lower bound limit load theorem could be used to define a lower bound limit load for the component. A lower bound limit load solution is one in which a statically admissible stress field exists in which the stress nowhere exceeds the yield stress of the material. In his procedure if the maximum stress after a number of iterations is less than yield stress then the applied load has satisfied the lower bound limit load criterion. On the other hand, if the converged solution gives a maximum stress which is greater than the yield stress then the applied load does not meet the lower bound limit load criterion.

Marriott also proposed a tentative guideline for the classification of stresses from a finite element analysis. If S_n, the stress on the nth iteration, is less than S_m and the slope of the locus of S is greater in magnitude than (1/2) the Young's modulus, then the stresses in excess of S_n are secondary. However, if S_n on the nth iteration is less than S_m, and the slope of the locus of S is less than (1/2) Young's modulus, then the stress is all primary regardless of whether $S_n \leq S_m$ or not.

Roche [1988, 1989] and Boyle [1989] have identified the underlying problem in design by analysis as the categorisation of stress, and suggested that such categorisation could not be based on elastic analysis alone. Both showed that structural behaviour similar to elastic follow-up in piping systems could confer primary characteristics on what was essentially thought to be secondary stress.

Several papers by Seshadri *et al* [1991a, 1991b, 1991c] have applied the reduced elastic modulus procedure in a number of areas. The method used by Seshadri incorporated the aspects of both the Dhalla and Marriot procedures. The modulus reduction is based on equivalent stress in a similar manner to that used by Dhalla. However, the modulus is reduced on an element by element basis as in Marriot's method. An elastic analysis is performed and all elements with equivalent stress greater than the material yield stress are identified. Assuming 100% displacement control and elastic-perfectly plastic material, inelasticity would cause the stress to fall to σ_y whilst strain maintains its original level. The reduced elastic modulus required to give these values of stress and strain in elastic solution is:

$$E_R = E_o \frac{\sigma_y}{\sigma_e}$$

where

E_R = the reduced modulus value

E_o = the original modulus

σ_y = the material yield stress

σ_e = the centriodal equivalent stress of the element

In 1990 and 1991, Seshadri showed that the reduced elastic modulus analysis provided a simplified method for estimating creep damage in pressurised components experiencing multiaxial relaxation and elastic follow-up type behaviour. In his publications he introduced the term GLOSS (Generalised LOcal Stress

Strain) to the reduced modulus vocabulary and used the GLOSS diagram to partition creep damage into load and deformation controlled fractions. Other work [Vaidynathan *et al.* 1989] extended the GLOSS method to elevated temperature component design. Seshadri [1990] also extended the GLOSS analysis procedure to inelastic analyses of pressure vessel components. The GLOSS method was applied to several problems of practical interest involving plastic analysis, multiaxial stress relation and strain concentration factors in notched components and found that this method can be used to simulate inelastic behaviour to good effect. Also this method was used to address the problem of stress classification in pressure components by Seshadri [1990].

The problem of using reduced elastic modulus method procedure to categorise stresses in simple components has been addressed by Boyle and Mackenzie [1991], Mackenzie and Boyle [1992]. In their early work they found that the elastic follow-up type of response used in such a procedure to classify stresses was not only dependent on component geometry but also on load level. This meant that when the load is increased or decreased the value of primary and secondary stresses changed considerably. They also found that the stress categories given by these procedures for simple pressurised components did not coincide with categories defined for these components in the Codes. It was argued that if the procedure could not be verified for simple components, for which categories have been defined, it was unsafe to use these procedures for more complex designs. However, while this work has questioned the viability of the reduced elastic modulus method for stress categorisation, it has opened the door for the method to be used in simplified pseudo-inelastic analysis.

3.3 Modified Elastic Modulus Method

Seshadri [1991] and Seshadri and Fernando [1991] proposed a method for approximate estimates of limit load using the modified elastic modulus method, referred to as the GLOSS-R-Node method. The basic concept of this method is

that when inelasticity occurs and the stresses are redistributed in a component, there are certain locations where the stresses will remain constant. These locations are defined as re-distribution-nodes or r-nodes. The r-nodes stresses are insensitive to material model and may be considered as reference stress similar to creep analysis reference and skeletal stress [Boyle and Spence, 1983]. The reference stress σ_{ref} at the r-node is related to the yield stress of an elastic perfectly plastic material by the expression.

$$\sigma_{ref} = \mu\sigma_y \tag{3.5}$$

where μ is less than one prior to plastic hinge formation and equal to one when the hinge occurs; when an elastic perfectly plastic material is assumed. By calculating the r-node stress σ_{ref} corresponding to a given load P, the limit load P_L for a statically determinate structure can be obtained from the expression

$$P_L = \frac{\sigma_y}{\sigma_{ref}} P \tag{3.6}$$

The collapse load for the case when two r-nodes form across the thickness, as is the case when direct loads are accompanied by bending action, is given by the expression

$$\{P, M\}_L = \frac{\sigma_y}{\sigma_{ref}} \{P, M\} \tag{3.7}$$

where $\{P, M\}$ is the primary membrane and bending load combination.

The basic procedure to find the GLOSS r-node is as follows: A linear elastic finite element analysis of a mechanical component or structure is carried out for the prescribed loading and the pseudo-elastic stresses are obtained. The elastic modulus of the model is then locally modified on an element to element basis according to the equation

$$E_m = \frac{\sigma_j}{\sigma} E_0 \tag{3.8}$$

Where E_m is the modified element modulus, E_0 the original modulus, σ the element stress and σ_j is the equivalent stress chosen so that stress redistribution occurs in most of the component. A second linear elastic analysis is then carried out and the position of the r-node or nodes are obtained at which the stresses

are unchanged. Using these stress values the limit load then can be calculated by using either equations (3.6) or (3.7).

Although the GLOSS r-node method can be used to calculate limit loads for certain components, the concept of r-nodes especially in 3D models, is quite difficult both to visualize and calculate. Also fine through thickness finite element meshes are required in order to use the method effectively. This will lead to 3D models with very refined meshes with subsequent problems in computer processing time and memory storage space. In practice, software and computing restrictions generally restrict the number of through thickness meshes in 3-D pressure vessel models to three or four elements.

Based on the modified elastic modulus method, Carter and Ponter [1992] developed a linear elastic finite element method to calculate lower and upper bound limit loads boundaries which has been implemented for planar finite element structures under both plane stress and plane strain conditions. They have also developed a theoretical background, although this has not been published at the time of writing.

It is seen from the literature review that the concept of modifying the elastic modulus of the elements in a finite element model, has proved to be a useful tool in simplified inelastic analysis. Nonetheless, the GLOSS r-node method introduces several good ideas into the calculation of limit loads by modified modulus analysis, not least the idea of increasing as well as decreasing local modulus. This provided an impetus for a new method of obtaining limit and shakedown loads referred as the *elastic compensation* method. In the next Section the *elastic compensation* method will be reviewed in detail.

3.4 Elastic Compensation Method

The elastic compensation method as first devised by Mackenzie and Boyle

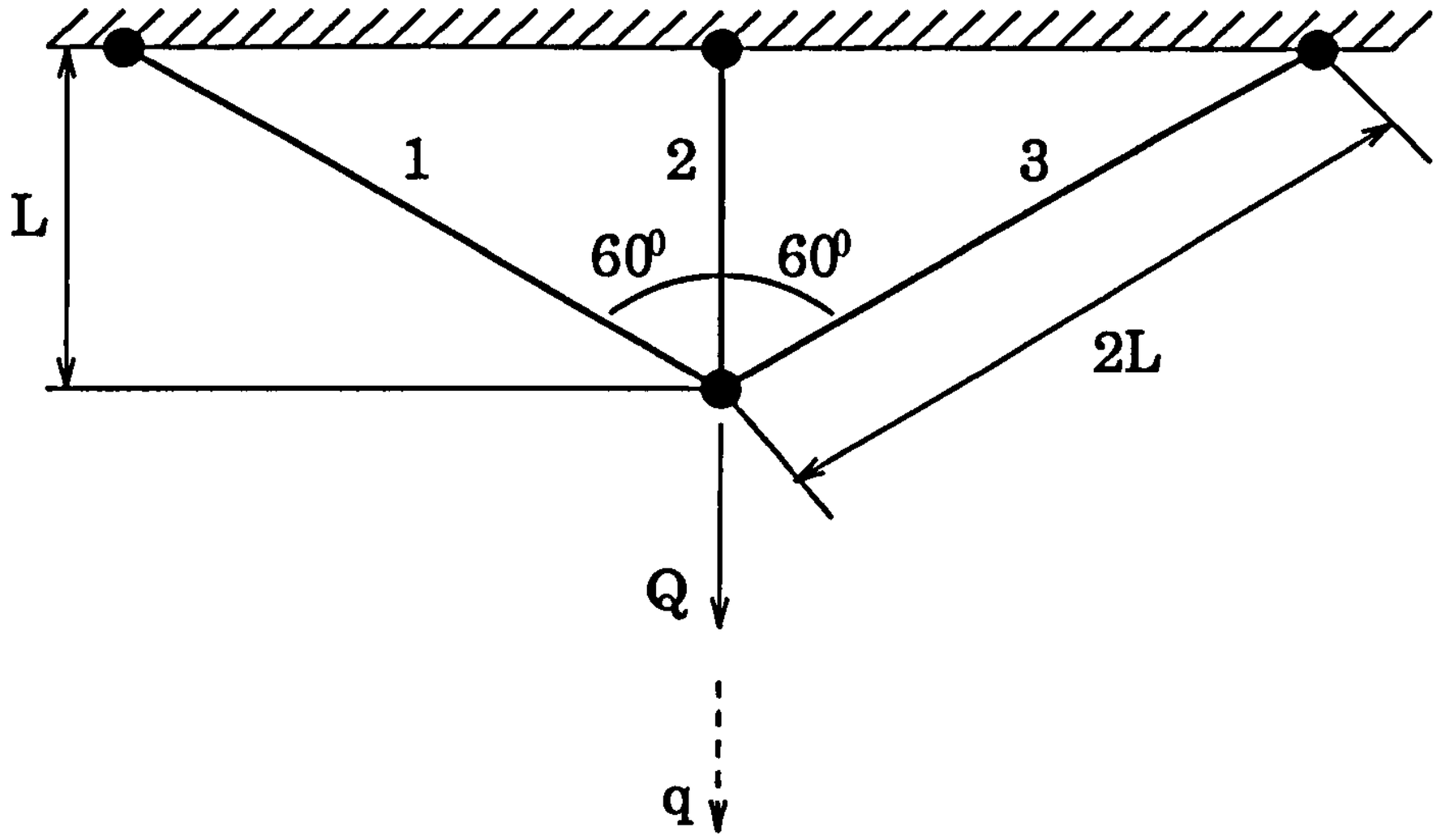

Figure 3.4: Three bar truss with vertical loading

[1993a] is based on the modified elastic modulus method; in particular, Marriott's lower bound theorem approach and Seshadri's redistribution technique, to obtain lower and upper bound limit loads by several elastic finite element analyses. This is done by selectively correcting the elastic modulus in finite element in each iteration in order to mimic the form of the limit state stress distribution hence forming the plastic hinges for the collapse mechanism. By invoking the lower bound limit load theorem, conservative limit loads can then be obtained. Then by using the compatible displacement and strain fields from the same element model and substituting them into the upper bound theorem an upper bound solution to the model could be calculated [Mackenzie *et al.*, 1993].

Before going into the potential of such a procedure simple example problems are considered where exact limit loads are calculated using this method.

3.4.1 Limit Load for a Three Bar Truss Under Vertical Loading

Each bar is uniform and has an area equal to A. If σ_1, σ_2, σ_3 are the stresses in the bars then the equilibriums are:

Vertical equilibrium

$$(\sigma_3 A + \sigma_1 A)\cos 60^0 + \sigma_2 A = Q \tag{3.9}$$

Horizontal equilibrium

$$\sigma_1 A = \sigma_3 A, \quad \sigma_1 = \sigma_3 \tag{3.10}$$

Thus

$$(2\sigma_1)(\frac{1}{2}) + \sigma_2 = \frac{Q}{A} \tag{3.11}$$

$$\sigma_1 + \sigma_2 = \frac{Q}{A} \tag{3.12}$$

Similarly if ϵ_1, ϵ_2, ϵ_3 are the strains in the three bars and q is the vertical displacement at their common joint then the strain or displacement relations are:

$$\epsilon_1 = \epsilon_3 = (\frac{q}{2})\frac{1}{2L} = \frac{q}{4L} \tag{3.13}$$

$$\epsilon_2 = \frac{q}{L} \tag{3.14}$$

The three bar constitutive relations:

$$\sigma = E\epsilon \tag{3.15}$$

Therefore substituting equations (3.13), (3.14) and (3.15) into equation (3.12)

$$\sigma_1 + \sigma_2 = E_1\frac{q}{4L} + E_2\frac{q}{L} = \frac{Q}{A} \tag{3.16}$$

$$q = \frac{4QL}{A}\left(\frac{1}{E_1 + 4E_2}\right) \tag{3.17}$$

Substituting equation (3.17) into equations (3.13) and (3.14)

$$\epsilon_1 = \epsilon_3 = \frac{q}{4L} = \frac{Q}{A(E_1 + 4E_2)} \tag{3.18}$$

$$\epsilon_2 = \frac{q}{L} = \frac{4Q}{A(E_1 + 4E_2)} \tag{3.19}$$

Substituting equations (3.18) and (3.19) into equation (3.15) yields

$$\sigma_1 = \sigma_3 = E_1\epsilon_1 = \frac{QE_1}{A(E_1 + 4E_2)} \tag{3.20}$$

$$\sigma_2 = E_2\epsilon_2 = \frac{4QE_2}{A(E_1 + 4E_2)} \tag{3.21}$$

Elastic solution

Assuming the bars are of the same material, that is, $E_1 = E_2 = E_3$, and substituting into equations (3.20) and (3.21), the bar elastic stresses are

$$\sigma_1 = \sigma_3 = \frac{Q}{5A} \tag{3.22}$$

$$\sigma_2 = \frac{4Q}{5A} \tag{3.23}$$

First yield

By inspection, first yield occurs in bar 2 when $Q = Q_y$. At first yield

$$\sigma_2 = \frac{4Q_y}{5A} = \sigma_y \tag{3.24}$$

Rearranging, the load at first yield and stress in bars 1 and 3 at first yield are given by the equations:

$$Q_y = \frac{5}{4}\sigma_y A \tag{3.25}$$

$$\sigma_{1y} = \sigma_{3y} = \frac{Q_y}{5A} = \frac{\sigma_y}{4} \tag{3.26}$$

Post yield

Assuming perfect plasticity and post yield force increment of ΔQ

$$\Delta F_1 + \Delta F_2 = \Delta Q \tag{3.27}$$

or

$$\Delta\sigma_1 + \Delta\sigma_2 = \frac{\Delta Q}{A} \tag{3.28}$$

For perfect plasticity, $\Delta\sigma_2 = 0$. Therefore

$$\Delta\sigma_1 = \frac{\Delta Q}{A} \tag{3.29}$$

Limit load

The limit load is reached when bar 1 yields. That is:

$$\sigma_1 = \sigma_{1y} + \Delta\sigma_{1L} = \sigma_y \tag{3.30}$$

or

$$\frac{\sigma_y}{4} + \frac{\Delta Q_L}{A} = \sigma_y \tag{3.31}$$

Therefore the post yield load increment to the limit state is

$$\Delta Q_L = A(\sigma_y - \frac{\sigma_y}{4}) = \frac{3}{4}\sigma_y A \tag{3.32}$$

The limit load Q_L is therefore given by the expression:

$$Q_L = Q_y + \Delta Q_L = \frac{5}{4}\sigma_y A + \frac{3}{4}\sigma_y A = 2\sigma_y A \tag{3.33}$$

Modulus modification method

The elastic moduli in the bars are modified based on the results of the initial elastic analysis according to the expression:

$$E_m = E_0\frac{S}{\sigma} \tag{3.34}$$

where E_m is the modified modulus, E_0 is the original modulus, σ the elastically calculated stress in the bar and S arbitrary stress given by

$$S = \alpha\sigma_y \quad where \quad 0 < \alpha < 1 \tag{3.35}$$

Thus the modified moduli are given by the expression

$$E_m = E_0 \frac{\alpha \sigma_y}{\sigma} \tag{3.36}$$

Substituting the bar stresses from equations (3.22) and 3.26) into equation (3.36), the elastic solution for bar 1 will be

$$E_{m1} = E_0 \alpha \frac{4Q_y}{5A} \frac{5A}{Q} = 4E_0 \alpha \frac{Q_y}{Q} \tag{3.37}$$

and similarly for bar 2 substituting equations (3.23) and (3.24) into equation (3.36)

$$E_{m2} = E_0 \alpha \frac{\sigma_y}{\sigma} = E_0 \alpha \frac{Q_y}{Q} \tag{3.38}$$

Substituting the modified moduli into the expression for bar stresses (equations (3.20) and (3.21))

$$\sigma_1 = \sigma_3 = \frac{QE_{m1}}{A(E_{m1} + 4E_{m2})} = \frac{Q}{2A} \tag{3.39}$$

$$\sigma_2 = \frac{4QE_{m2}}{A(E_{m1} + 4E_{m2})} = \frac{Q}{2A} \tag{3.40}$$

The modified modulus solution gives equal stress in all three bars. At limit load the stress in all three bars is equal to σ_y, thus the modified modulus stress distribution is similar to the limit stress distribution.

At the limit load $Q = Q_L$, all three bars yield; that is $\sigma_1 = \sigma_2 = \sigma_3 = \sigma_y$, thus

$$\frac{Q_L}{2A} = \sigma_y, \quad Q_L = 2\sigma_y A \tag{3.41}$$

which agrees <u>exactly</u> with the elastic perfectly plastic solution.

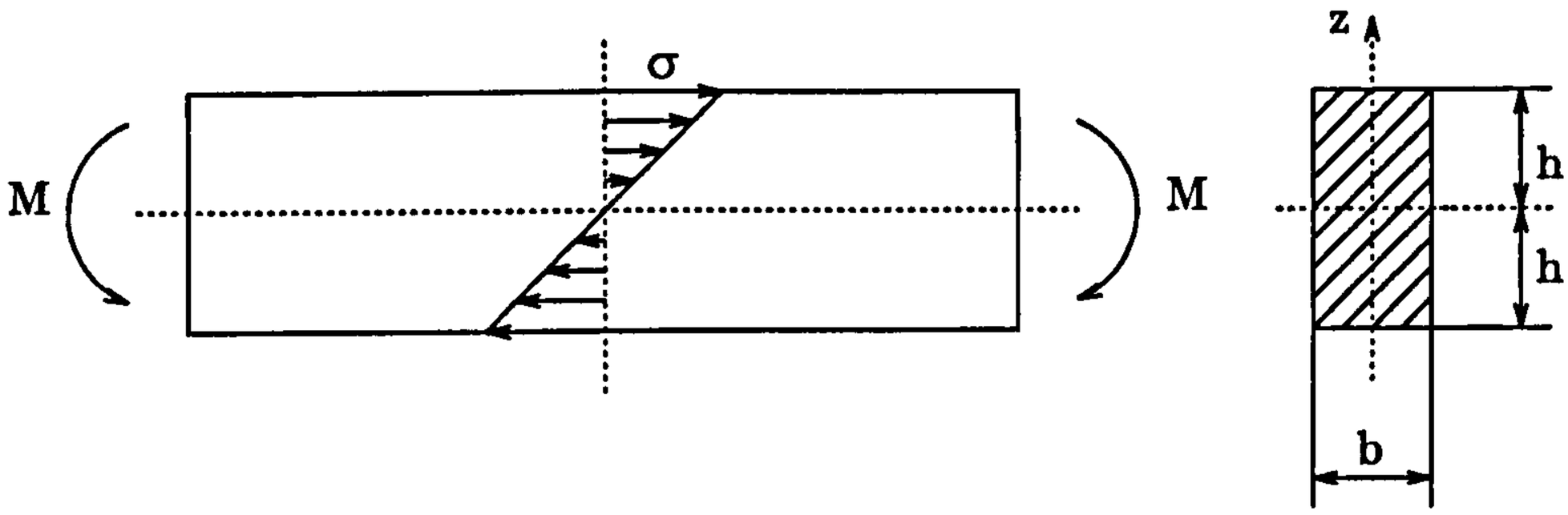

Figure 3.5: Beam under pure bending

3.4.2 Limit Load for a Beam Under Pure Bending

The limit load for rectangular beam under pure moment loading calculated by elastic perfectly plastic analysis is

$$M_L = \frac{3}{2} M_y \tag{3.42}$$

where M_L is the plastic moment and M_y is the moment to cause first yield in the beam and is equal to $\sigma_y bd^2/6$. σ_y is the yield stress of the material.

The limit load can also be established by modified modulus analysis. Applying equilibrium to a section through the beam, noting the symmetric stress distribution:

$$M = 2b \int_0^h \sigma z dz \tag{3.43}$$

The material constitutive equation and assumed strain-displacement relationship are:

$$\sigma = E_{(z)} \epsilon \tag{3.44}$$

$$\epsilon = \kappa z \tag{3.45}$$

where

E = Young's modulus

κ = (1/radius of curvature of a beam in bending)

Substituting into the equilibrium equation:

$$M = 2b\int_0^h E_{(z)}\kappa z^2 dz = \kappa I_1 \tag{3.46}$$

where

$$I_1 = 2b\int_0^h E_{(z)} z^2 dz \tag{3.47}$$

Elastic solution

The well known elastic solution for stress at point z through thickness is

$$\sigma_e = \frac{Mz}{I} \tag{3.48}$$

where I is the second moment of area of the beam

$$I = \frac{2bh^3}{3} \tag{3.49}$$

First yield occurs at $z = h$ for load M_y

$$\sigma_y = \frac{M_y h}{I} \tag{3.50}$$

The elastic modulus at point z through thickness is modified according to the equation

$$E_z = E_0\alpha\frac{\sigma_y}{\sigma_z} \tag{3.51}$$

where α is an arbitrary constant of value $0 < \alpha < 1$.

Substituting equations (3.48) and (3.50) into equation (3.51) gives

$$E_{(z)} = E_0\alpha\frac{M_y}{M}\frac{h}{z} \tag{3.52}$$

Substituting equation (3.52) into equation (3.47)

$$I_1 = 2bE_0\alpha\frac{M_y}{M}h\int_0^h z dz = 2bE_0\alpha\frac{M_y}{M}h(\frac{h^2}{2}) = bE_0\alpha\frac{M_y}{M}h^3 \tag{3.53}$$

Text cut off in original

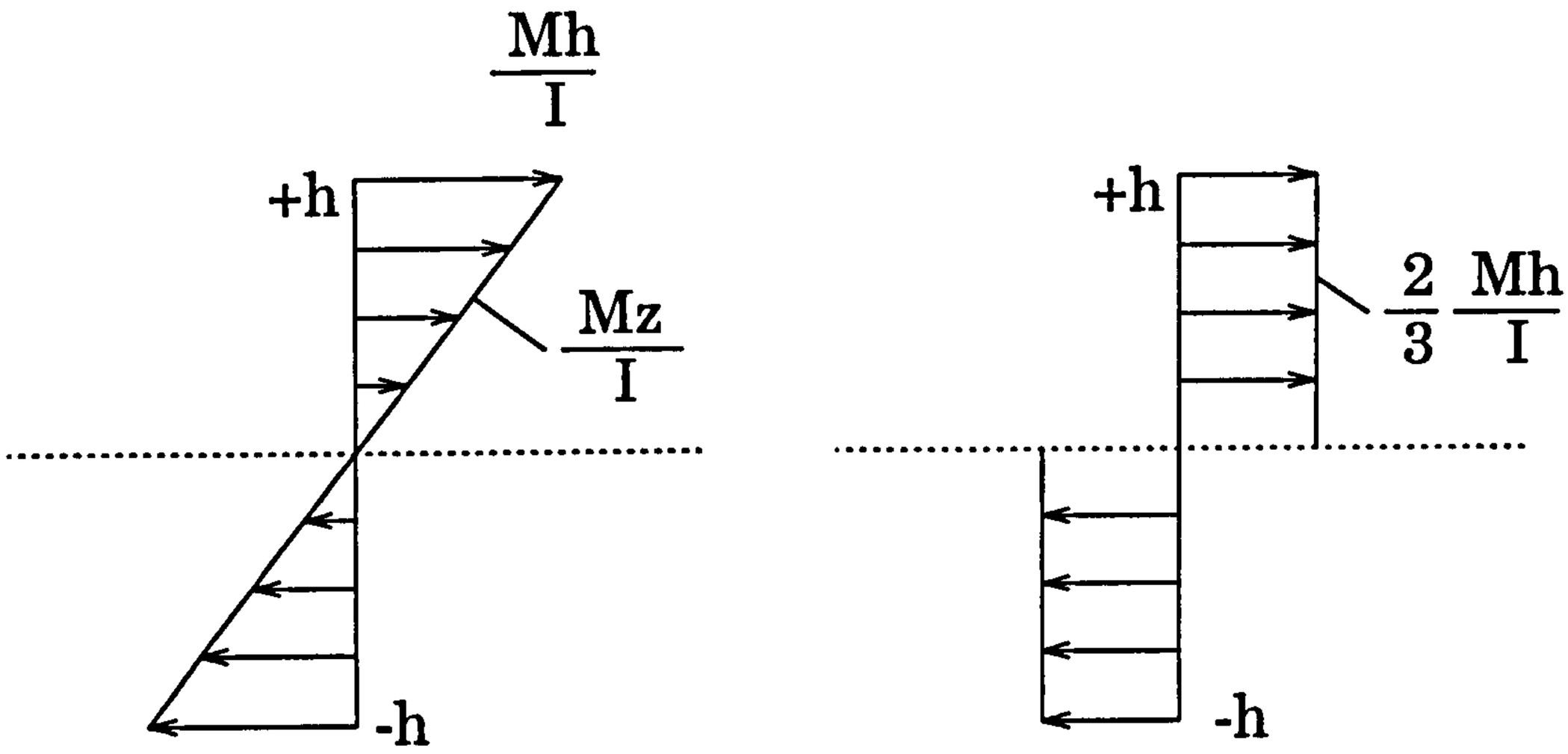

Figure 3.6: Stress distribution through thickness for beam under pure bending

Substituting equation (3.49) into (3.53)

$$I_1 = \frac{3}{2} E_0 \alpha \frac{M_y}{M} I \tag{3.54}$$

From the moment curvature relationship, $M = \kappa I_1$

$$\kappa = \frac{M}{I_1} = \frac{2M^2}{3E_0 \alpha M_y I} \tag{3.55}$$

Substituting equation (3.55) into equation (3.45)

$$\epsilon_z = \kappa z = \frac{2}{3} \frac{M^2 z}{E_0 \alpha M_y I} \tag{3.56}$$

Sustituting equations (3.52) and (3.56) into equation (3.44)

$$\sigma_{(z)} = E_{(z)} \epsilon_z = \frac{2}{3} \frac{Mh}{I} \tag{3.57}$$

Clearly the modified modulus stress is constant through thickness. Thus the form of modified modulus stress distribution is similar to the limit state stress distribution. See Figure 3.6.

At limit load, the stress at all points z through thickness will be σ_y; that is $\sigma_z = \sigma_y$. Therefore

$$\frac{2}{3}\frac{M_L h}{I} = \frac{M_y h}{I} \tag{3.58}$$

Rearranging:

$$M_L = \frac{3}{2} M_y \tag{3.59}$$

which agrees exactly with the inelastic solution.

3.5 Upper Bound Limit Loads by Elastic Compensation

In this section the upper bound theorem is implemented in conjunction with the elastic compensation method to obtain exact limit loads for the two problems examined in the previous sections.

The upper bound limit load theorem states that if, for a given load the rate of dissipation of internal energy in a body is equal to the rate at which external forces do work in any postulated mechanism of deformation, the applied load set will be equal to or greater than the plastic collapse load [Calladine 1985]. Mathematically, a complete plastic collapse requires definition of P and σ, an equilibrium set of loads and stresses respectively, and $\dot{u}$ and $\dot{\epsilon}$, a geometrically compatible set of displacement and strain increments, respectively. An upper-bound solution requires only a *partial* or *incomplete* plastic collapse solution to be defined; specifically, $\dot{u}^*$ and $\dot{\epsilon}^*$, representing any compatible sets of displacement and strain increments, respectively, which define a geometrically possible mode of deformation. The asterisk notation therefore denotes a solution which is incomplete in the sense that the stress field is not defined. Applying virtual work to the problem, it can be shown [Calladine 1985]

$$\sum P\dot{u}^* = \int_V \dot{D}^* dV \tag{3.60}$$

where $\dot{D}^*$ is the increment of dissipation of energy per unit volume calculated for the incomplete solution. The increment of energy dissipation per unit volume for a Tresca perfectly plastic material is given by the expression

$$\dot{D}^* = \sigma_Y |\dot{\epsilon}^*|_{max} \tag{3.61}$$

where $|\dot{\epsilon}^*|$ is the greatest principal strain rate magnitude. In the case of a Mises perfectly plastic material, the more complex expression is given by

$$\dot{D}^* = \sigma_y \frac{2}{3} \sqrt{\dot{\epsilon}_x^2 + \dot{\epsilon}_y^2 + \dot{\epsilon}_z^2 - \dot{\epsilon}_x\dot{\epsilon}_y - \dot{\epsilon}_y\dot{\epsilon}_z - \dot{\epsilon}_z\dot{\epsilon}_x + \frac{3}{4}(\dot{\gamma}_{xy}^2 + \dot{\gamma}_{yz}^2 + \dot{\gamma}_{zx}^2)} \tag{3.62}$$

or

$$\dot{D}^* = \sigma_y \sqrt{\frac{2}{9}[(\dot{\epsilon}_1 - \dot{\epsilon}_2)^2 + (\dot{\epsilon}_2 - \dot{\epsilon}_3)^2 + (\dot{\epsilon}_1 - \dot{\epsilon}_3)^2]} \tag{3.63}$$

where $|\dot{\epsilon}| : i = 1,2,3$ are the principal strain rates and $\dot{\epsilon}_x, \dot{\epsilon}_y, \dot{\epsilon}_z$ are total component strain rates and $\dot{\gamma}_{xy}$, $\dot{\gamma}_{yz}$, $\dot{\gamma}_{zx}$ are engineering shear strain rates.

An upper-bound limit load for a structure can be obtained by substituting the elastic compensation displacement increment field $\dot{u}^*$ and strain increment field $\dot{\epsilon}^*$ into the upper bound theorem as expressed in equation (3.60). However, this approach can lead to practical problems since calculating the work term can be laborious if corresponding load and displacement vectors are not directly accessible in the finite element program, (pressure loads on nonplanar surfaces present particular problems). In practice, it is more convenient to take advantage of the linear elastic nature of the elastic compensation solution: as the solution is elastic, the external work done must equal the elastic strain energy of the structure; thus

$$\sum P\dot{u}^* = \int_V \sigma\dot{\epsilon}^* dV$$

where σ is the elastically calculated stress, and $\dot{\epsilon}^*$ the elasticly calculated strain increment. Thus, the upper bound theorem inequality may be written

$$\int_V \sigma\dot{\epsilon}^* dV \leq \dot{\mathbf{D}}^* dV \tag{3.64}$$

Using this equation the upper bound limit load for a structure can be calculated. This will be demonstrated in the following problems.

3.5.1 Three Bar Truss Under Vertical Loading

Using equation (3.60), for a three bar structure

$$\sum_{i=1}^{3} \sigma_i \epsilon_i v_i = \sum_{i=1}^{3} \sigma_y \epsilon_i v_i \tag{3.65}$$

$$\sigma_1 \epsilon_1 v_1 + \sigma_2 \epsilon_2 v_2 + \sigma_3 \epsilon_3 v_3 = \sigma_y (\epsilon_1 v_1 + \epsilon_2 v_2 + \epsilon_3 v_3) \tag{3.66}$$

$$\sigma_1 = \sigma_3, \quad \epsilon_1 = \epsilon_3, \quad v_1 = v_3 = 2AL, \quad v_2 = AL \tag{3.67}$$

$$2A\sigma_1 \epsilon_1 L + A\sigma_2 \epsilon_2 L + 2A\sigma_1 \epsilon_1 L = \sigma_y (2AL\epsilon_1 + AL\epsilon_2 + 2AL\epsilon_3) \tag{3.68}$$

$$4\sigma_1 \epsilon_1 + \sigma_2 \epsilon_2 = \sigma_y (2\epsilon_1 + \epsilon_2 + 2\epsilon_3) \tag{3.69}$$

After modulus reduction from equations (3.39) and (3.40)

$$\sigma_1 = \sigma_2 = \frac{Q}{2A}$$

Therefore

$$4\frac{Q}{2A}\epsilon_1 + \frac{Q}{2A}\epsilon_2 = \sigma_y (4\epsilon_1 + \epsilon_2) \tag{3.70}$$

$$\frac{Q}{2} A (4\epsilon_1 + \epsilon_2) = \sigma_y (4\epsilon_1 + \epsilon_2) \tag{3.71}$$

$$Q = 2\sigma_y A \tag{3.72}$$

Substituting Q_L for Q

$$Q_L = 2\sigma_y A \tag{3.73}$$

which again agrees with the exact solution.

3.5.2 Beam Under Pure Bending

Using symmetry and applying the upper bound theorem gives

$$2\int_0^h \sigma\epsilon dz = 2\sigma_y \int_0^h \epsilon dz \tag{3.74}$$

Substituting equations (3.56) and (3.57) into equation (3.74)

$$\frac{4}{9}\frac{M^3 h}{E_0 \alpha M_y I^2}\int_0^h z dz = \frac{2}{3}\sigma_y \frac{M^2}{E_0 \alpha M_y I}\int_0^h z dz \tag{3.75}$$

$$\frac{2}{9}\frac{M^3 h^3}{E_0 \alpha M_y I^2} = \frac{1}{3}\sigma_y \frac{M^2 h^2}{E_0 \alpha M_y I} \tag{3.76}$$

$$\frac{2}{9}\frac{Mh}{I} = \frac{1}{3}\sigma_y \tag{3.77}$$

From equation (3.50)

$$\sigma_y = \frac{M_y h}{I}$$

Let $M = M_L$

$$\frac{2}{9}\frac{M_L h}{I} = \frac{M_y h}{3I} \tag{3.78}$$

$$M_L = \frac{3}{2}M_y \tag{3.79}$$

which again is the <u>exact</u> solution.

3.6 Procedures for Estimating Limit Loads by Finite Element Analysis

The elastic compensation method has been further developed by the Strathclyde group as a robust technique for evaluating limit loads for complex structures: see Mackenzie and Boyle [1993b, 1994]; Mackenzie *et al.* [1992, 1993, 1994a, 1994b, 1994c, 1995]; Nadarajah *et al.* [1993]; Shi *et al.* [1993]; Hamilton

et al. [1994,1995].

The elastic compensation method is based on an iterative elastic analysis procedure and application of the lower and upper bound limit load theorems. In the elastic compensation method, limit loads are bounded by modifying the moduli of all the elements in the model. In a series of elastic analysis highly loaded elements have their modulus reduced and lowly loaded elements have their's increased. The resulting stress and strain fields are then substituted into the appropriate bounding theorems to derive the limit loads.

In the elastic compensation method, an initial linear elastic finite element analysis is performed for a nominal design loading P_0 to establish the elastic stress field σ_e. This analysis forms iteration zero in a series linear elastic analysis in which the moduli of elements are systematically modified to redistribute the stress in the component. In each subsequent iteration, the modulus of each element is modified according to an equation of the form:

$$E_i = E_{(i-1)} \frac{\sigma_n}{\sigma_{(i-1)}} \tag{3.80}$$

where subscript i is the iteration number, σ_n a nominal stress value and $\sigma_{(i-1)}$ the maximum (unaveraged) nodal equivalent stress associated with the element from the previous solution. The value chosen for σ_n in Eqn.(3.80) is somewhat arbitrary – usually equal to or two thirds of yield. Care has to be taken. however. to ensure that the divisor of Eqn.(3.80) does not approach zero as this could lead to numerical problems in the finite element solution. This iterative procedure redistributes the stress in the component and over a number of iterations the net effects is to decrease the maximum stress in the model as illustrated in Fig. 3.7.

3.6.1 A Procedure for Estimating Lower Bound Limit Loads

A lower estimate of the limit load is calculated by invoking the lower bound limit theorem, which sates that if a statically admissible stress field in which the stress nowhere exceeds yield exists for a given component under given loading.

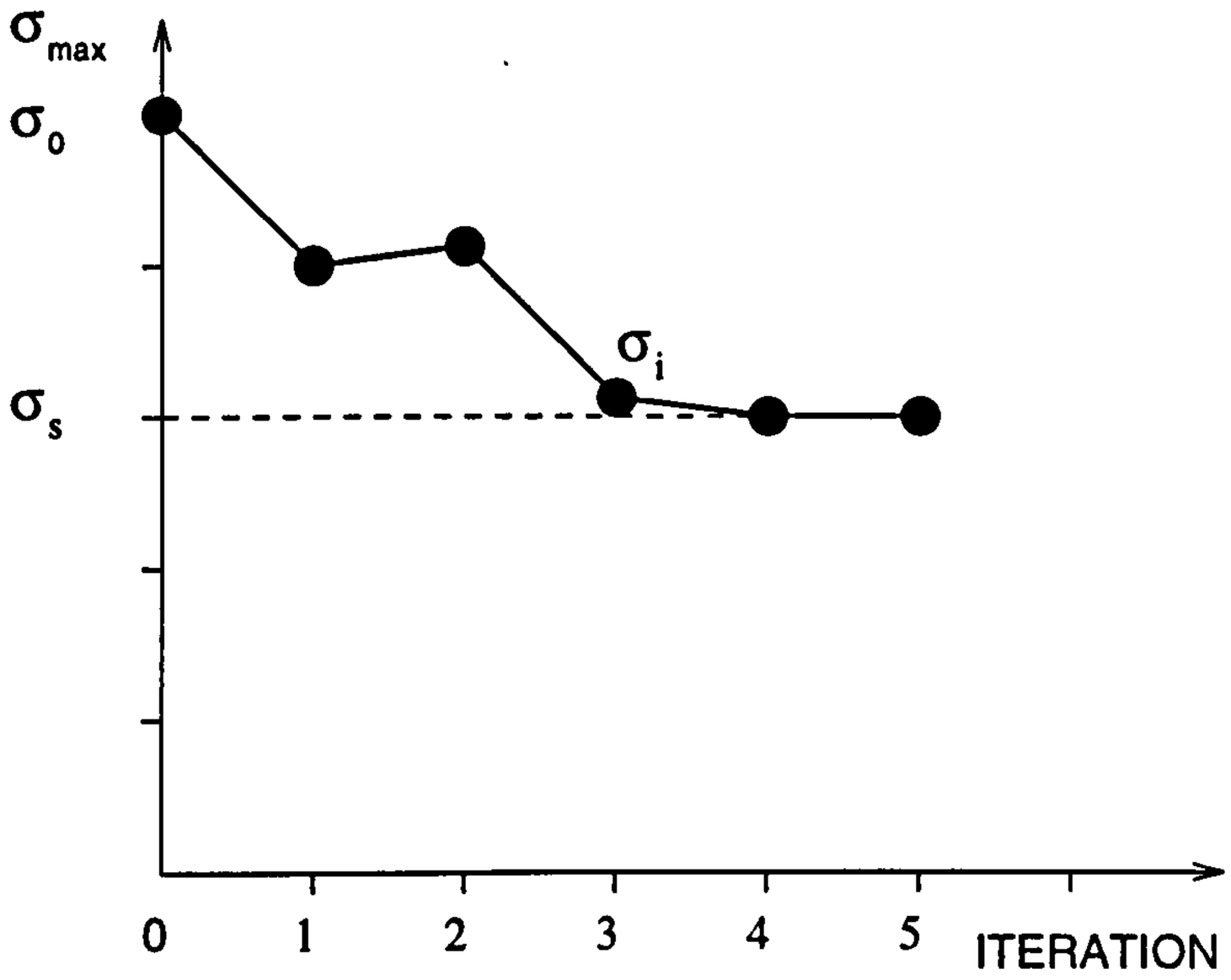

Figure 3.7: **Maximum stress for each iteration.**

the loading is a lower bound on the limit load (Calladine 1985). The elastic compensation solution meets the first requirement of the lower bound theorem in that it is statically admissible (subject to the usual finite element approximations). As the iteration solutions are linear elastic, the stress magnitude is proportional to the applied load. A lower bound limit load can therefore be established by calculating the load required to give a maximum (unaveraged) nodal stress equal to nominal yield strength σ_Y from proportionality. Considering the iteration giving the lowest value of maximum nodal stress σ_s

$$P_L = P_1 \frac{\sigma_Y}{\sigma_s} \tag{3.81}$$

where P_L is the best estimate of lower bound limit load given by the above procedure. The applied load set P_1 is not restricted to single loads and may represent multiple forces, moments, pressures, etc., in the manner of proportional loading in conventional limit analysis.

3.6.2. A Procedure for Estimating Upper Bound Limit Loads

In a linear elastic analysis, the upper bound theorem may be expressed by

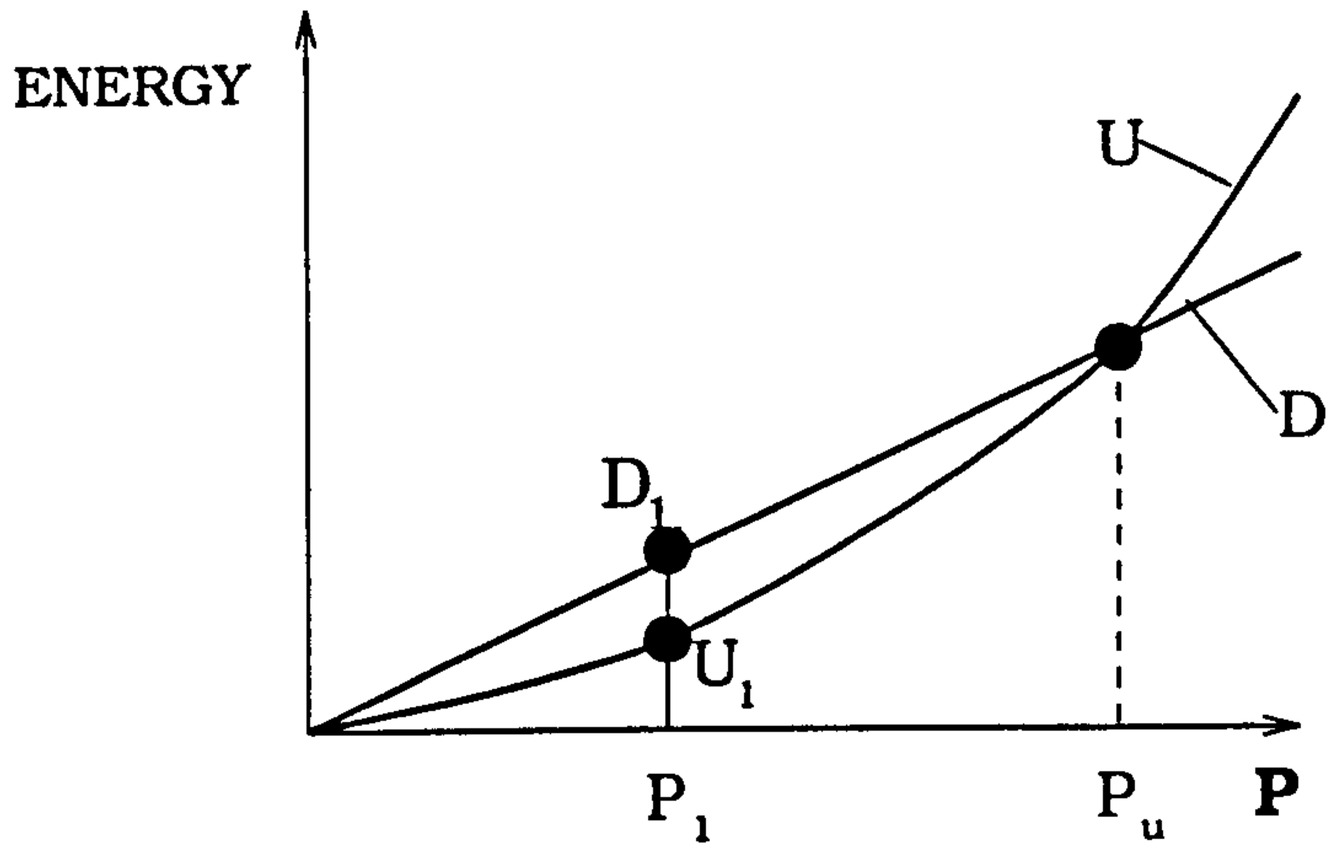

Figure 3.8: Plot of strain energy and energy dissipation against applied external load

inequality (3.64)

$$\int_V \sigma \dot{\epsilon}^* dV \leq \dot{\mathbf{D}}^* dV$$

or

$$U \leq D$$

The strain energy U of a linear elastic body varies with the applied load set squared. The dissipation of internal energy D varies directly with the applied load set. Thus,

$$U = \int_V \sigma \dot{\epsilon}^* dv = AP^2 \tag{3.82}$$

$$D = \int^V \dot{\mathbf{D}}^* dV = BP \tag{3.83}$$

Plotting strain energy and energy dissipation against applied external load gives curves of the form shown in Fig. 3.8. When the strain energy and energy dissipation curves intersect, the equality is satisfied and the (upper bound) limit load is established. The intersection can be calculated by performing a finite element analysis for an arbitrary load set P_1 and evaluating the corresponding

strain energy U_1 and energy dissipation D_1. Substituting the calculated values into Eqs. (82) and (83) gives

$$A = \frac{U_1}{P_1^2}, \quad B = \frac{D_1}{P_1}$$

and the strain energy and energy dissipation may be expressed as

$$U = \frac{U_1}{P_1^2}P^2, \quad D = \frac{D_1}{P_1}P$$

The applied load set P is an upper bound limit P_u load when $U = D$: that is.

$$\frac{U_1}{P_1}P_u^2 = \frac{D_1}{P_1}P_u$$

and, hence, the upper bound limit load is given by the expression

$$P_u = \frac{D_1}{U_1}P_1 \tag{3.84}$$

It is a routine matter to evaluate approximations to U_1 and D_1 from the results of a finite element analysis. Both strain energy and the model strain fields are given as results of the finite element analysis.

3.7 A Procedure for Calculating Lower Bound Shakedown Loads

It has long been known that there is an analogy between the limit load and shakedown bounding theorems in plasticity. Early on the Strathclyde Group decided to investigate the application of elastic compensation finite element procedure to shakedown also.

There have been several attempts to obtain shakedown loads directly using finite element methods; for example, Belytschko [1972] and Corradi and Zavelani [1974] applied linear programming techniques directly to the shakedown theorem. These analyses were typically computationally expensive and only simple two dimensional structures were examined. In this section a simple procedure for

indirectly calculating lower bound shakedown loads by the elastic compensation approach is briefly presented. The details of formulation can be found in Mackenzie and Boyle [1993].

In the elastic compensation procedure the stress and displacement fields generated by iterative elastic analysis procedure are substituted into Melan's lower bound shakedown theorem, which states:

> *For a given load set P, if any distribution of self-equilibriating residual stresses σ_r can be found, (assuming perfect plasticity), which when taken together with elastically calculated stresses σ_e, constitute a system of stresses within the yield limit σ_y then P is a lower bound shakedown load set and the structure will shake down.*

The requirement of Melan's theorem is simply to show that a structure will shake down for a given load and this can be assured by establishing an acceptable residual stress system - it does not necessarily have to be the actual residual stress system in the real structure at that load level. By definition the load level for which this is demonstrated will be a lower bound on the so called shakedown load.

A simplified outline of the proposed approximate procedure is given in the following:

For a given load set P, the lower bound shakedown theorem can be stated as follows. If

$$\sigma_r : |\sigma_r|_{max} \leq \sigma_y \tag{3.85}$$

exits and satisfies the condition:

$$|\sigma_r + \sigma_e|_{max} \leq \sigma_y \tag{3.86}$$

where,

σ_r – The residual stress field.

σ_e – The elastic stress field.

σ_y – The material yield stress.

P – the lower bound shakedown load set.

In the elastic compensation method, an initial elastic finite element analysis is performed for a nominal design loading p^d to establish the elastic stress field σ_e. This analysis forms iteration zero in a series of linear elastic analyses in which the moduli of elements are systematically modified to redistribute the stress in the component. In each subsequent iteration, the modulus of each element is modified according to the eqn. (3.80):

$$E_i = E_{(i-1)} \frac{\sigma_n}{\sigma_{(i-1)}}$$

where subscript i is the iteration number, σ_n a nominal stress value and σ_{i-1} the maximum (unaveraged) nodal equivalent stress associated with the element from the previous solution.

The redistributed stress field calculated for each iteration is designated as a possible shakedown stress field σ_{si}: that is, the stress field in the component under full load after shakedown has occurred. This stress field is taken to be the sum of the initial elastic stress field σ_e and a residual stress field σ_{ri} (for iteration i):

$$\sigma_{si} = \sigma_e + \sigma_{ri} \tag{3.87}$$

Thus, the residual stress field σ_r is defined implicity in the elastic compensation procedure, such that:

$$\sigma_{ri} = \sigma_{si} - \sigma_e \tag{3.88}$$

Shakedown criterion (3.85) may therefore be rewritten as:

$$|\sigma_{si} - \sigma_e| \leq \sigma_y \tag{3.89}$$

As the elastic compensation procedure is linear, the magnitude of the stress field is proportional to the applied load set. Therefore

$$\frac{P}{P^d} = \frac{\sigma}{\sigma^d} \tag{3.90}$$

Where P^d and σ^d are a nominal applied load set and resulting stress field respectively. The elastic and shakedown stress fields can therefore be written:

$$\sigma_e = \sigma_e^d \frac{P}{P^d} \tag{3.91}$$

$$\sigma_{si} = \sigma_{si}^d \frac{P}{P^d} \tag{3.92}$$

Substituting expressions eqns. (3.91) and (3.92) into eqn. (3.88) and invoking the shakedown criterion eqn (3.85) gives:

$$|\sigma_{ri}| = |\sigma_{si}^d - \sigma_e^d|_{max} \frac{P}{P^d} \leq \sigma_y \tag{3.93}$$

Similarly, criterion eqn. (3.86) gives:

$$|\sigma_{si}|_{max} = |\sigma_{si}^d| \frac{P}{P^d} \leq \sigma_y \tag{3.94}$$

At shakedown, either the residual stress is at yield:

$$|\sigma_{si}|_{max} = |\sigma_{si}^d - \sigma_e^d|_{max} \frac{P_{1i}}{P^d} = \sigma_y \tag{3.95}$$

with the maximum shakedown stress less than or equal to yield, or the maximum shakedown stress is at yield:

$$|\sigma_{si}|_{max} = |\sigma_{si}^d|_{max} \frac{P_{2i}}{P^d} = \sigma_y \tag{3.96}$$

with the maximum residual stress less than or equal to yield. Equation (3.95) gives a shakedown load P_{1i} for iteration i, such that

$$P_{1i} = P^d \frac{\sigma_y}{|\sigma_{si}^d - \sigma_e^d|_{max}} \tag{3.97}$$

and eqn. (3.96) gives a shakedown load P_{2i} for iteration i, such that

$$P_{2i} = P^d \frac{\sigma_y}{|\sigma_{si}^d|_{max}} \tag{3.98}$$

Equation (3.98) which is equivalent to the equation for the iteration i lower bound limit load used in elastic compensation limit load calculation.

The lower bound shakedown load P_{si} calculated for iteration i is the smaller of the two calculated loads P_{1i} and P_{2i}, that is;

$$P_{si} = min(P_{1i}, P_{2i}) \tag{3.99}$$

The best lower bound shakedown load calculated by the elastic compensation method is the highest iteration shakedown load P_{si} given by the procedure:

$$P_{si} = max(P_{si}) \tag{3.100}$$

In practice, the best lower bound limit loads and shakedown loads are usually given by different iterations in the elastic compensation procedure.

3.8 Example 1: Limit Analysis of Pressurized Cylinder

The elastic compensation method has been successfully verified by the Strathclyde Group to obtain limit loads for different pressure vessel components. In this section, the elastic compensation method will be demonstrated in the calculation of lower and upper bound limit loads for pressurised thick cylinders.

3.8.1 Cylinder Model Geometry

In the following study, eleven different thick cylinders under internal pressure are analyzed. For the all models the cylinder outer radius was constant at $b = 550mm$ and the inner radius a was varied to give a range of ratios of $b/a = 1.1, 1.25, 1.5, 1.75, 2, 2.25, 2.5, 2.75, 3, 3.25$ and 3.5, with wall thickness verying from 50 mm to 392.9 mm. The detailed model geometries are shown in Table 3.1.

3.8.2 Finite Element Model

It is known from previous studies [Mackenzie, Shi and Boyle 1994] that the accuracy of the elastic compensation method is significantly affected by mesh density and element order. Therefore, in this study the element models of each geometry were generated using eight node isoparametric plane element in ANSYS (PLANE82) [1994]. The element is defined by eight nodes having two degrees of freedom at each node: translations in the nodal x and y directions. The element

Table 3.1: *Cylinder model geometry*

Model	b (mm)	a (mm)	b/a
THICK1	550	500	1.1
THICK2	550	440	1.25
THICK3	550	366.7	1.5
THICK4	550	314.3	1.75
THICK5	550	275	2.0
THICK6	550	244.4	2.25
THICK7	550	220	2.5
THICK8	550	200	2.75
THICK9	550	183.3	3.0
THICK10	550	169.2	3.25
THICK11	550	157.1	3.5

Table 3.2: *Finite element numbers of models*

Model	b (mm)	a (mm)	b/a	Elements Through Thickness	Total Elements
THICK1	550	500	1.1	10	260
THICK2	550	440	1.25	15	390
THICK3	550	366.7	1.5	20	520
THICK4	550	314.3	1.75	20	520
THICK5	550	275	2.0	25	650
THICK6	550	244.4	2.25	25	650
THICK7	550	220	2.5	30	780
THICK8	550	200	2.75	30	780
THICK9	550	183.3	3.0	30	780
THICK10	550	169.2	3.25	40	1040
THICK11	550	157.1	3.5	40	1040

may be used as a biaxial plane element or as an axisymmetric element: further information on PLANE82 can be found in Appendix III. The Tresca yield criterion was used in the elastic compensation analysis.

The finite element meshes were fine enough according to the computing limitation and the elements through thickness were varied from 10 to 40 according to the ratios of b/a, as shown in Table 3.2. The finite element mesh and boundary conditions for THICK8 is illustrated in Figure 3.9. The initial elastic modulus value for all models is equal to $200E3N/mm^2$ with a Poisson's ratio of 0.3. The yield stress of the material is equal to $300N/mm^2$ and the Tresca yield criterion is used in this Chapter.

3.8.3 Lower and Upper Bound Limit Pressures

As the elastic compensation procedure is completely automated it can be programmed with little difficulty. In *ANSYS*, the entire procedure can be implemented as an *ANSYS* Design Parametric Language (ADPL) macro (see Appendix II), as illustrated by the flow diagram in Figure 3.10 for calculating the lower and upper bound limit load. The macro reads stresses from the *ANSYS* results file (file.rst), calculates new Young's modulus values for each element. writes an input file with appropriate material property and element modification commands, reads the modification file into the *ANSYS* pre-processor */PREP7* and repeats the solution procedure. All the user is required to input is the number of iterations i to be performed.

The lower and upper bound limit loads for the thick cylinders were obtained using the elastic compensation method which was carried out using MAC5 and TRIAL1 in Appendix II. Up to 10 iterations were performed for each model in this case and the modulii were modified according to eqn (3.80)

$$E_i = E_{(i-1)} \frac{\sigma_n}{\sigma_{(i-1)}}$$

where subscript i is the iteration number, σ_n a nominal stress value and $\sigma_{(i-1)}$

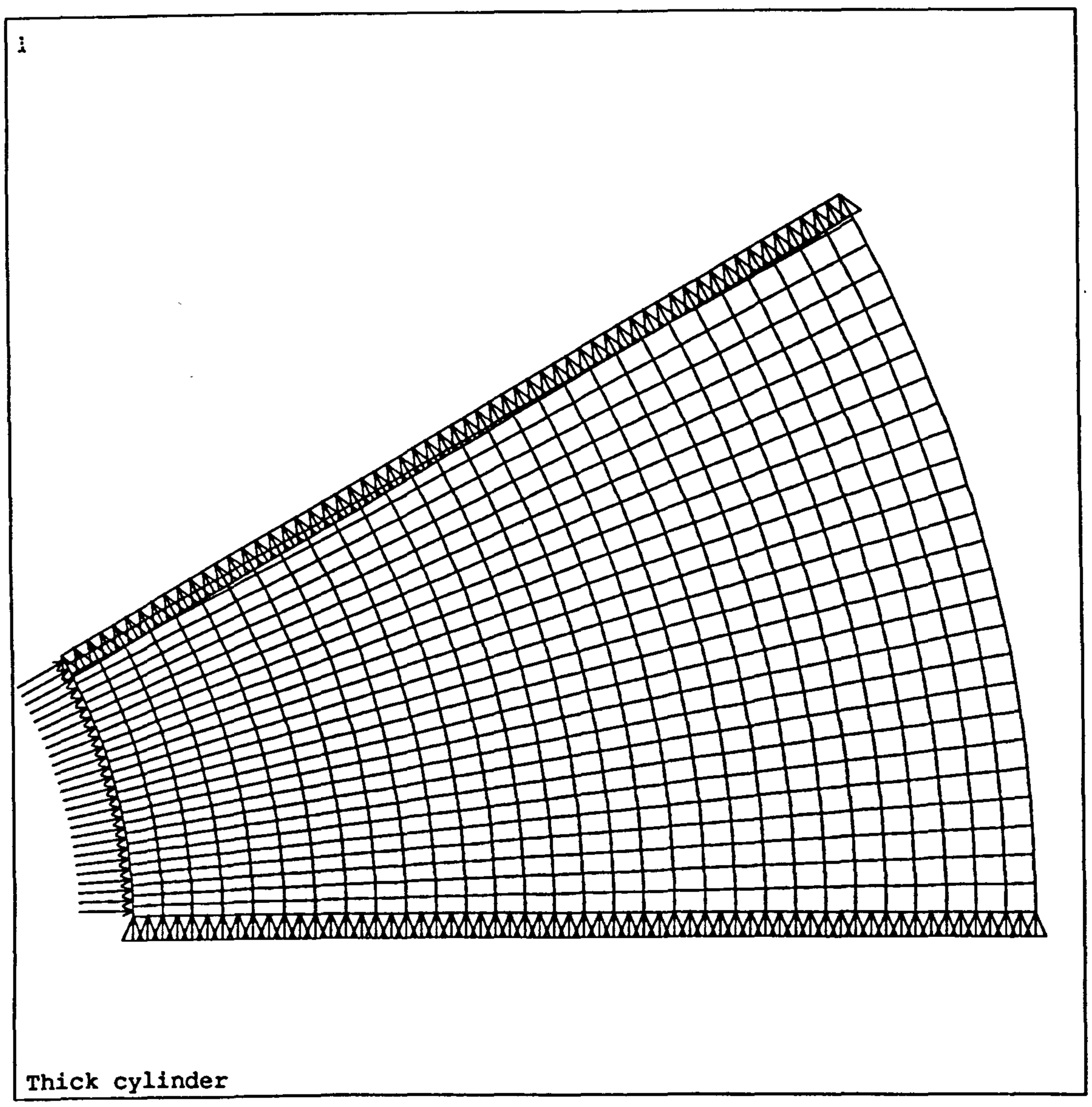

Figure 3.9: Finite element mesh and boundary conditions of THICK8

Table 3.3: *Varision of maximum non-averaged nodal stress with iteration*

Iteration	Maximum non-averaged nodal stress (N/mm^2)
0	92.06
1	55.059
2	47.668
3	44.639
4	43.102
5	42.245
6	41.745
7	41.446
8	41.265
9	41.155
10	41.088

the maximum (unaveraged) nodal equivalent stress associated with the element from the previous solution.

An example of the maximum non-averaged Tressca nodal stresses obtained from the lower bound solution for the model THICK8 is shown in Table 3.3. The model has a applied internal pressure $P_0 = 40 N/mm^2$.

For model THICK8, the lower bound limit pressure can be obtained from eqn 3.81.

$$P_l = \frac{300}{41.088} \times 40 = 292.06 \quad N/mm^2$$

The upper bound limit pressure was then obtained by using the stress and strain fields of the model after final iteration. By running *ANSYS* ADPL macro 'TRIAL1' (see Appendix II), the followings were calculated:

Energy dissipation D = 0.6377875E-05

Strain energy U = 0.8378389E-06

Then, the upper bound limit pressure can be evaluated, eqn.(3.84), as

$$P_u = \frac{D}{U} \times 40 = 304.49 N/mm^2$$

The lower and upper bound limit pressures for all other models were obtained by the similar process as illustrated above. The calculated first yield P_y, lower bound limit P_l and upper bound limit P_u pressures are compared with the theoretical ultimate pressure P_L obtained by the eqn. (3.101), in Table 3.4 and Figure 3.11. It can be seen from Table 3.4 and Figure 3.11 that the results calculated are in very good agreement with theoretical results, especially in the case of upper bound limit pressure which are almost the same as those obtained by the eqn. (3.101).

$$P_L = \frac{\sigma_y}{2} ln(b/a)^2 \qquad (3.101)$$

3.9 Example 2: Lower Bound Shakedown of Pressurized Cylinder

The previous eleven models used for the lower and upper bound limit analyses are also used to obtain the lower bound shakedown pressures in this section. An *ANSYS* ADPL macro for shakedown is an extension to the previous macro used in the calculation of the lower bound limit pressure. The macro is shown in Appendix II and the function of this macro is shown via a flowchart in Figure 3.12. The model's mesh, boundary conditions and applied load condition are the same as before.

The lower bound shakedown pressure for the model THICK8 is illustrated in Table 3.5. Column 4 and 5 in Table 3.5 shows the lower bound shakedown pressure obtained from the maximum shakedown stress (eqn. 1.98) and the maximum residual stress (eqn. 3.97), respectively. Column 6 in the Table 3.5 shows the lower bound shakedown pressure (min (P_1, P_2)) obtained after each iteration. The optimum shakedown pressure of $253.06 N/mm^2$ occurs at iteration 3 is shown in bold. Unaveraged stress intensity contour plots related to the lower bound limit and shakedown pressures calculated for THICK8 are shown in Fig-

ure 3.13 for the elastic stress (iteration 0), Figure 3.14 for the shakedown stress (iteration 1), Figure 3.15 for the residual stress (iteration 1), Figure 3.16 for the shakedown stress (iteration 3), Figure 3.17 for the residual stress (iteration 3). Figure 3.18 for the shakedown stress (iteration 10) and Figure 3.19 for the residual stress (iteration 10), respectively.

For all the other models, the lower bound shakedown pressures were obtained in the similar way as described above. The calculated shakedown pressures are compared with the theoretical results obtained by the equation $P_s = min(P_U, \ 2P_y)$ in Table 3.6 and Figure 3.20. These show that the lower bound shakedown loads calculated are also very close to the theoretical results.

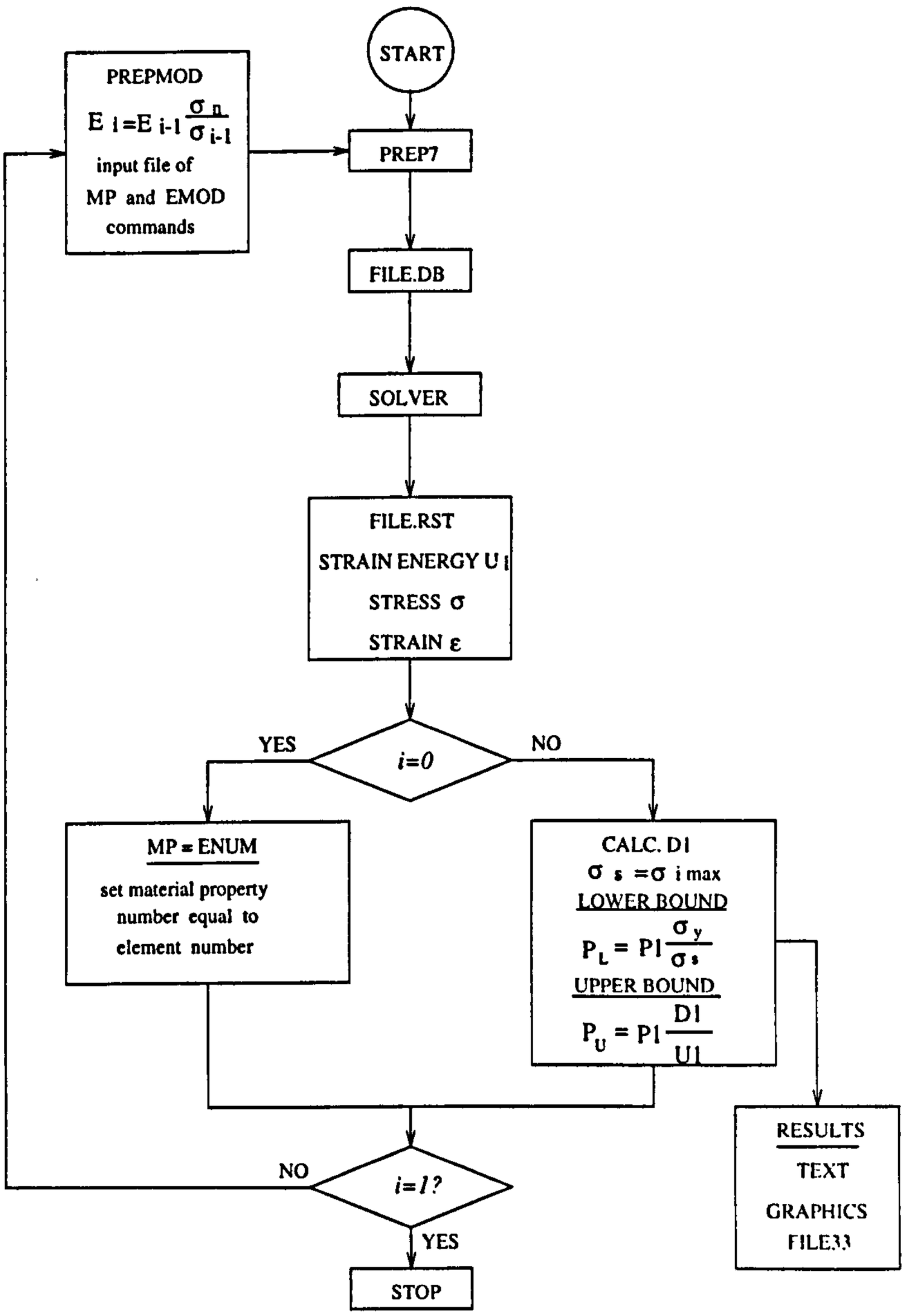

Figure 3.10: Elastic compensation limit load macro flow diagram for i iterations

Table 3.4: *Limit pressures of thick cylinders*

Model	b/a	P_y	P_L	P_l	P_u
THICK1	1.1	26.03	28.59	28.32	28.6
THICK2	1.25	54.00	66.94	65.95	66.95
THICK3	1.5	83.33	121.64	119.15	121.64
THICK4	1.75	101.07	167.88	163.19	167.95
THICK5	2	112.57	207.94	202.11	208.11
THICK6	2.25	120.50	243.28	235.26	243.71
THICK7	2.5	126.13	274.89	265.98	275.48
THICK8	2.75	130.35	303.48	292.06	304.49
THICK9	3.0	133.59	329.58	315.08	331.17
THICK10	3.25	135.98	353.60	338.18	355.05
THICK11	3.5	137.99	375.83	355.24	377.35

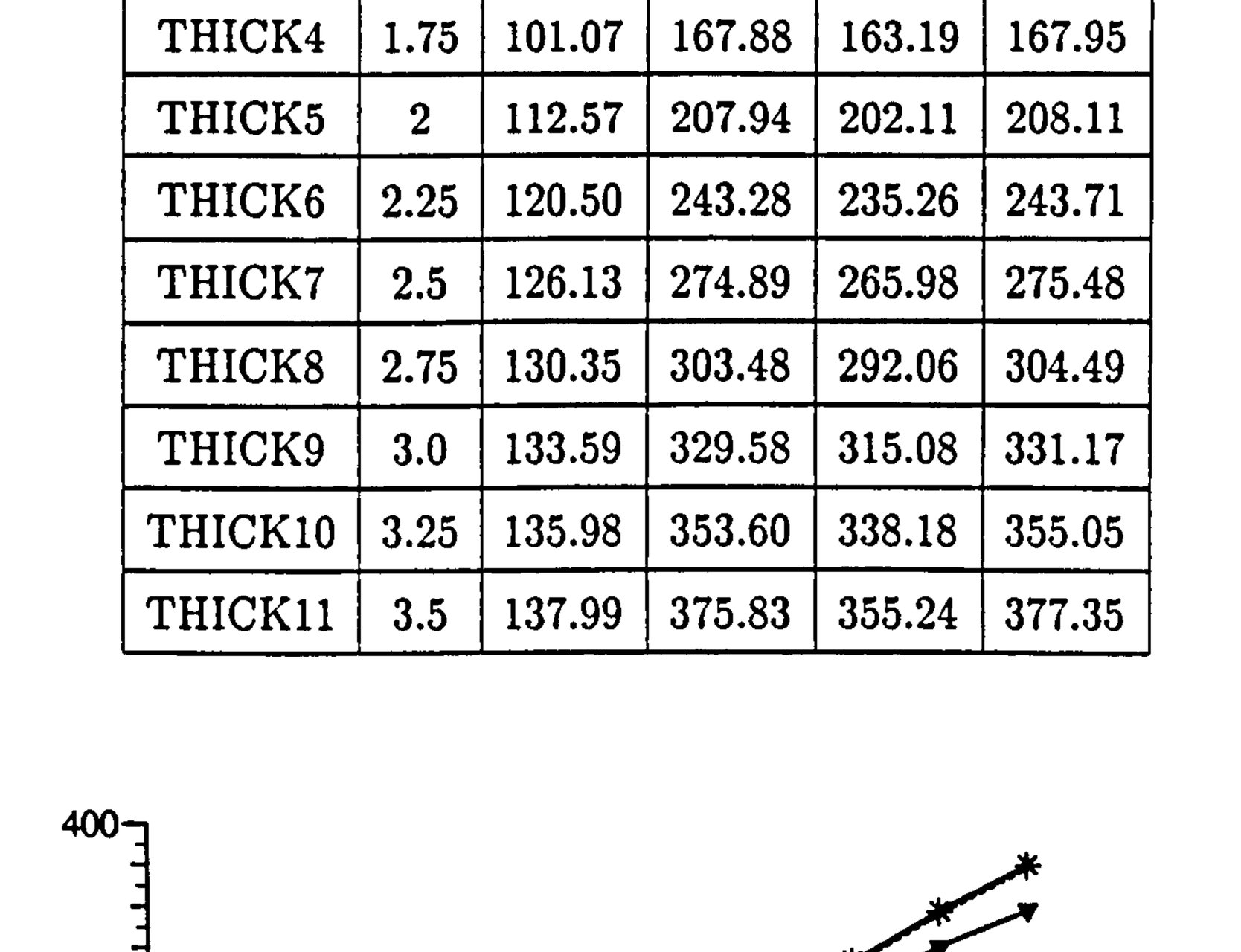

Figure 3.11: Limit pressures of thick cylinders

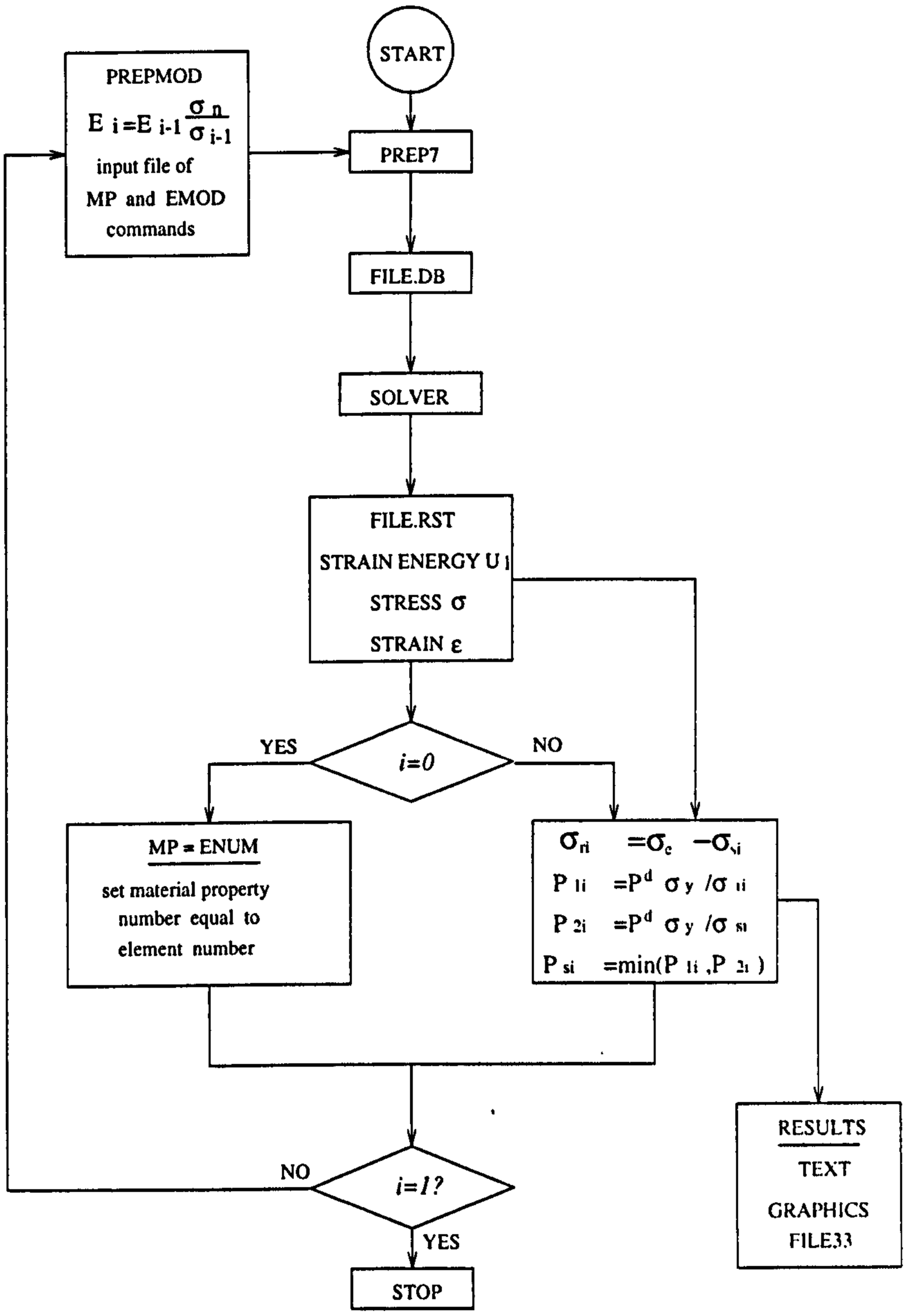

Figure 3.12: Elastic compensation lower bound limit and shakedown macro flow diagram for i iterations

Table 3.5: *Variation of maximum shakedown, residual stress and shakedown pressure with iterations*

Iteration	$\|\sigma_s\|_{max}$ (N/mm^2)	$\|\sigma_r\|_{max}$ (N/mm^2)	$P_2 = P_0 \frac{\sigma_y}{\|\sigma_{si}\|_{max}}$ (N/mm^2)	$P_1 = P_0 \frac{\sigma_y}{\|\sigma_{ri}\|_{max}}$ (N/mm^2)	$P_s = min(P_1, P_2)$ (N/mm^2)
0	92.06				
1	55.06	37.00	217.94	324.32	217.94
2	47.67	44.39	251.73	270.33	251.73
3	44.64	47.42	268.82	253.06	**253.06**
4	43.10	48.96	278.42	245.10	245.10
5	42.24	49.81	284.09	240.92	240.92
6	41.75	50.32	287.43	238.47	238.47
7	41.45	50.62	289.51	237.06	237.06
8	41.27	50.80	290.98	236.22	236.22
9	41.16	50.91	291.55	235.71	235.71
10	41.09	50.97	292.04	235.43	235.43

Figure 3.13: Iteration 0: Tresca (elastic) stress distribution

Figure 3.14: Iteration 1: Tresca stress distribution

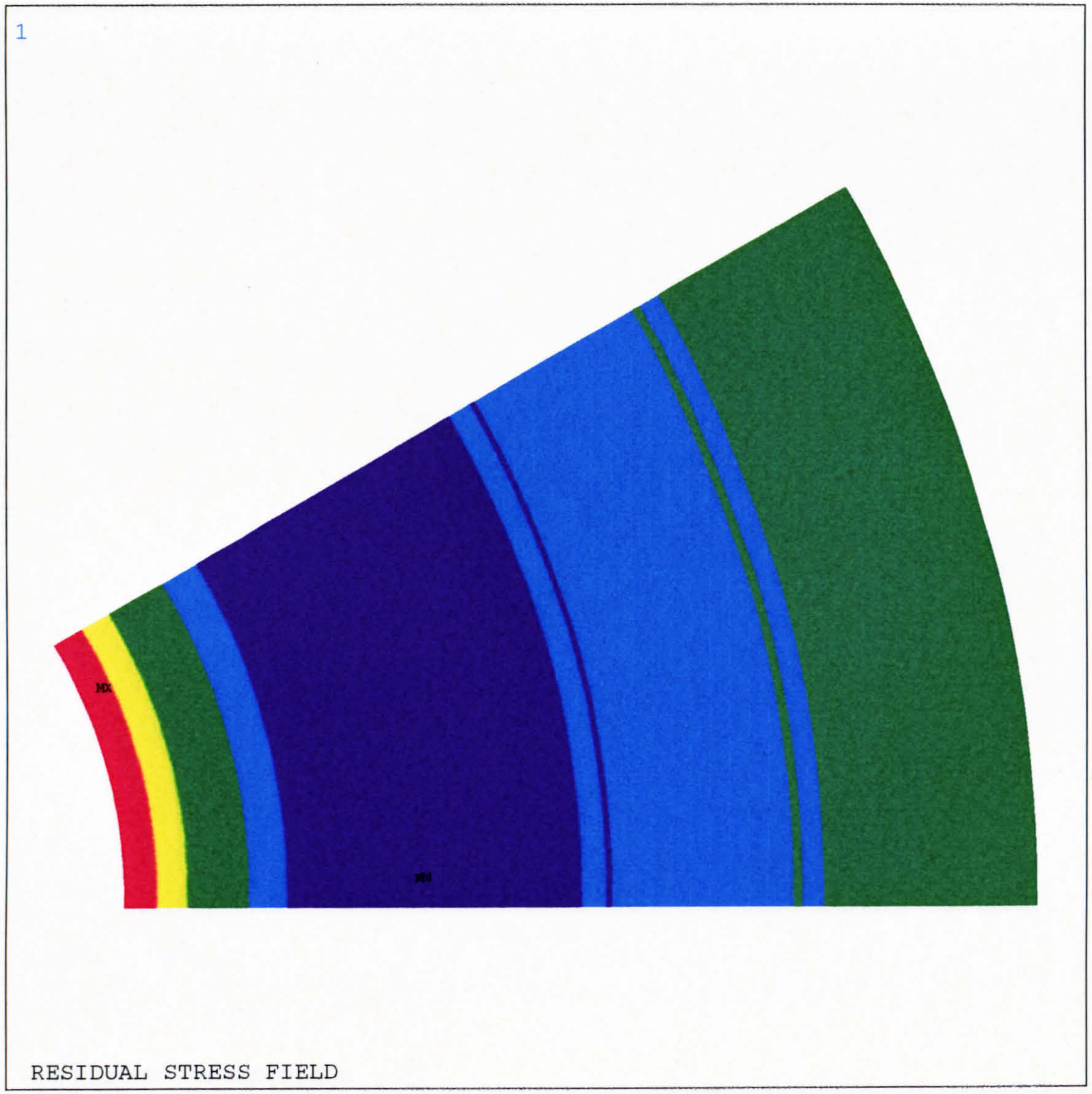

Figure 3.15: Iteration 1: Tresca residual stress distribution

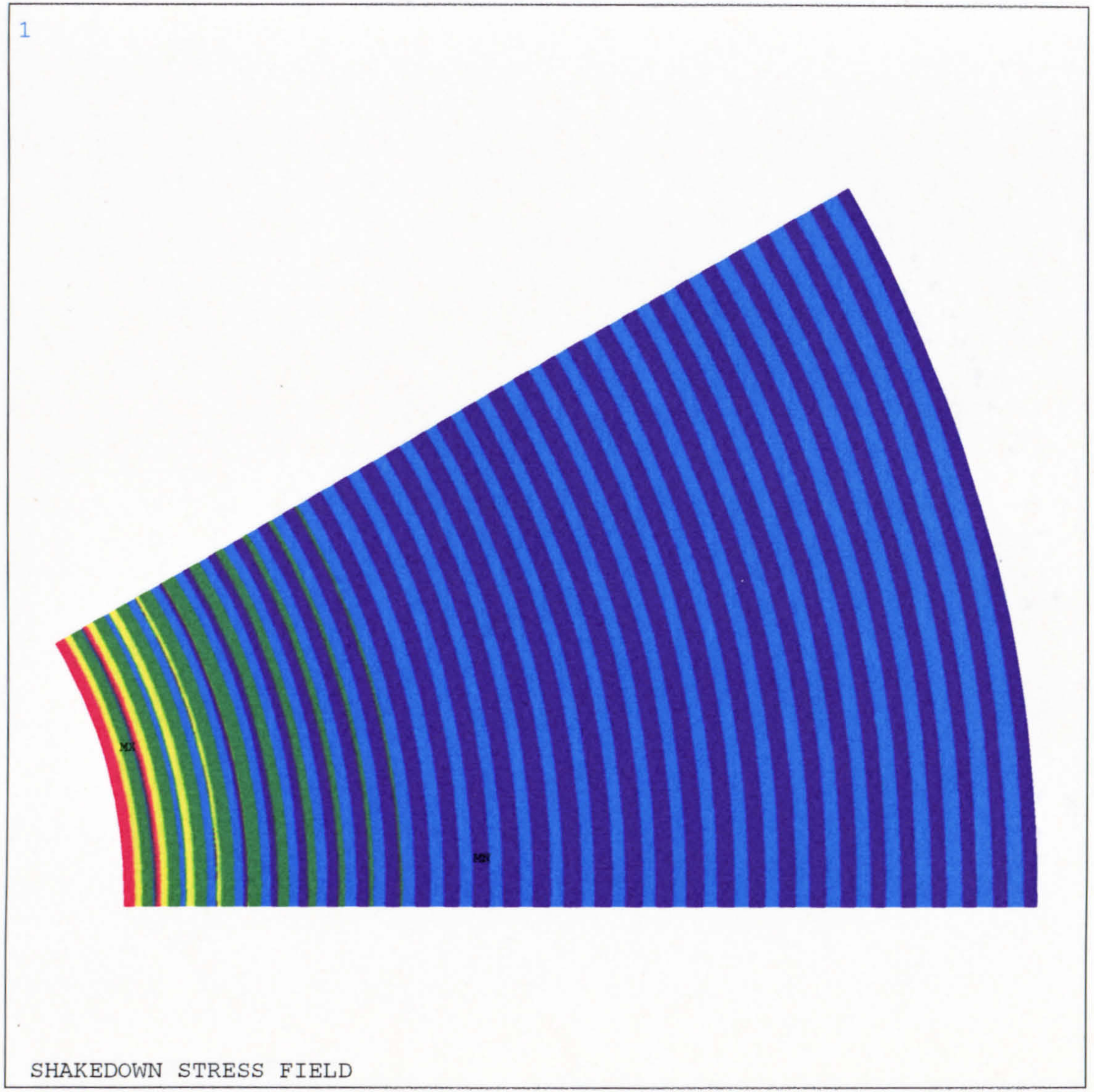

Figure 3.16: Iteration 3: Tresca shakedown stress distribution

Figure 3.17: Iteration 3: Tresca residual stress distribution

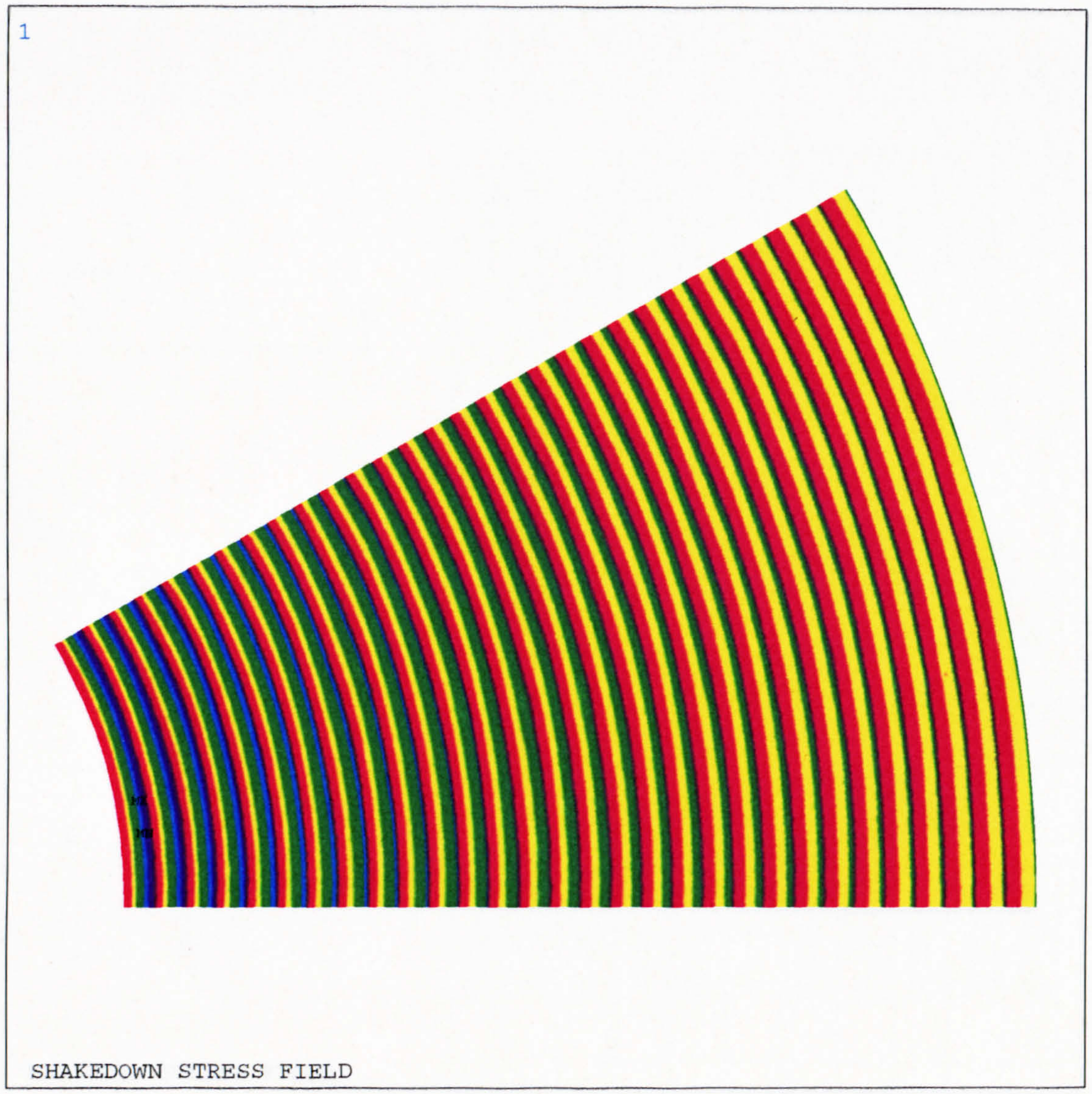

Figure 3.18: Iteration 10: Tresca shakedown stress distribution

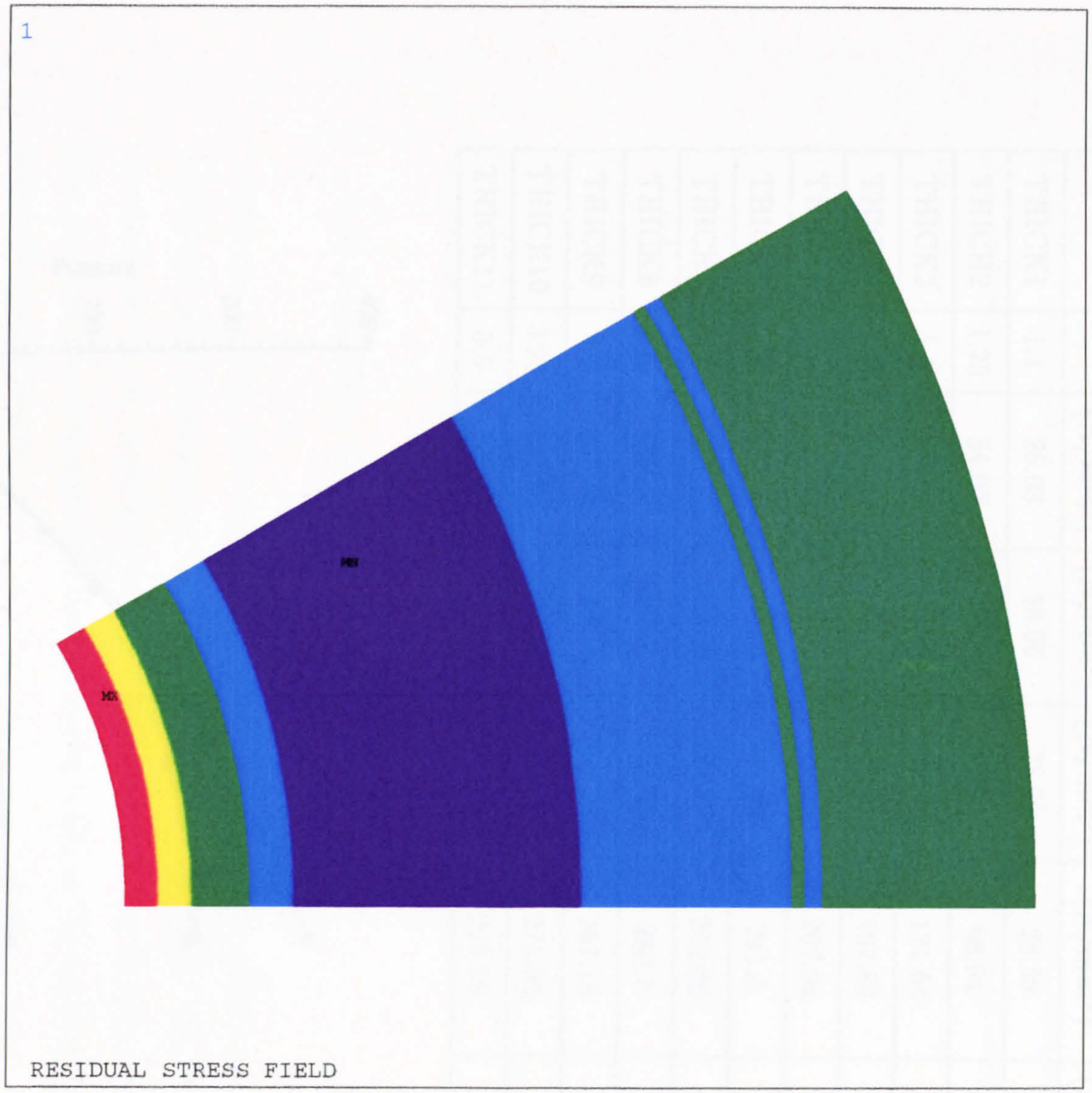

Figure 3.19: Iteration 10: Tresca residual stress distribution

Table 3.6: *Lower bound shakedown pressures of thick cylinders*

Model	b/a	P_y (N/mm^2)	$2P_y$ (N/mm^2)	P_U (N/mm^2)	$\min(P_U, 2P_y)$ (N/mm^2)	P_s (N/mm^2)
THICK1	1.1	26.03	56.06	28.59	28.59	28.32
THICH2	1.25	54.00	108.0	66.94	66.94	65.95
THICK3	1.5	83.33	166.66	121.64	121.64	119.15
THICK4	1.75	101.07	202.14	167.88	167.88	163.19
THICK5	2.0	112.57	225.14	207.94	207.94	202.11
THICK6	2.25	120.50	241.0	243.28	241.0	235.26
THICK7	2.5	126.13	252.26	274.89	252.26	250.57
THICK8	2.75	130.35	260.7	303.48	260.7	253.05
THICK9	3.0	133.59	267.18	329.58	267.18	263.48
THICK10	3.25	135.98	271.96	353.6	271.96	269.25
THICK11	3.5	137.99	275.98	375.83	275.98	270.10

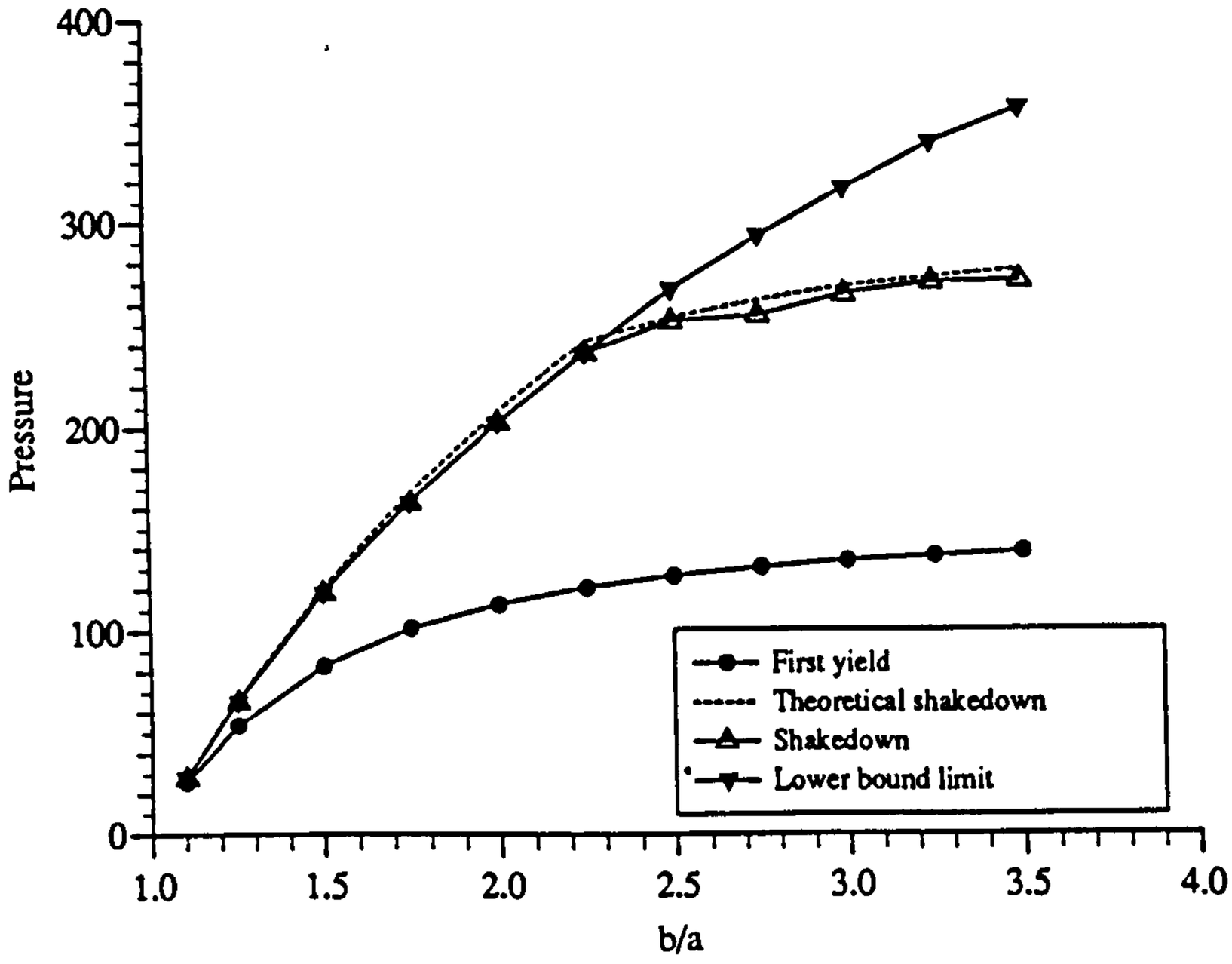

Figure 3.20: Lower bound shakedown pressures of thick cylinders

3.10 Example 3: Limit Analysis of Beam Structures

So far the elastic compensation method has been developed for 'solid' finite elements (as in the thick cylinder problem). One of the main features of this thesis has been to extend to beam and shell elements. Before considering this, it is worthwile examining the computational problems involved in using elastic compensation for frame problems with solid elements.

3.10.1 One-Bay, One-Story Frame

For the one-bay, one-story frame subject to combined loads, shown in Figure 3.21, the finite element model was created using eight node axisymmetric solid element (*ANSYS* PLANE82) and the finite element mesh is shown in Figure 3.22. A total 600 elements were used. The lower and upper bound limit loads calculated using the elastic compensation method are compared with the results of Lubliner [1990] in Figure 3.23. Again the comparison is good.

3.10.2 One-Bay, Two-Story Frame

For the one-bay, two-story frame, shown in Figure 3.24 taken from König [1987], the finite element mesh for $h/L = 1/4$ is shown in Figure 8.25. Element numbers used in this problem were 600. The lower and upper limit load interaction diagrams are compared with those of König [1987] in Figures 3.26 and 3.27 which show good results.

3.11 Summary

The elastic compensation method described above gives solutions to the lower and upper bound limit loads of structures. From a design point of view, the lower and upper bound limit loads and shakedown loads are of great importance. In the next few Chapters the elastic compensation method will be used in conjunc-

tion with elastic finite element analysis to obtain lower and upper limit loads and shakedown loads for structures including pressure vessel components. plate with a central hole and frame structures for design purposes. However this method still needs to be further developed to calculate upper bound shakedown loads of the structures. Due to the high running cost for solid element models. especially for 3D models, lower costing shell element and beam element are needed to implemented to the elastic compensation. These work will be done in this Project.

3.12 References

Belytschko, T., (1972), Plane stress shakedown analysis by finite elements. *Int. J. Mech. Sci.*, Vol. 14, 619–625.

Boyle, J.T., (1989), Elastic follow-up and the categorisation of secondary stress. *PVP-Vol. 161, ASME*, Honolulu, 47–53.

Boyle, J.T. & Mackenzie, D., (1991), An investigation of a simple procedure for stress categorisation, *PVP-Vol. 210-2, ASME*, San Diego, 161–165.

Boyle, J.T. & Nakamura. K., (1987), The assessment of elastic follow up in high temperature piping systems-overall survey and theoretical aspects. *Int. J. Pres. Ves. & Piping* **29**, 167–194.

Boyle, J.T. & Spence, J., (1983), *Stress Analysis for Creep*, Butterworths.

Boyle, J.T. & Spence, J., (1988), A procedure for the assessment of elastic follow-up in high temperature piping systems, *J. Press. Ves. Tech.*, Vol. 110, 197–201.

Calladine, C.R., (1985), *Plasticity for Engineers*, Ellis Horwood Ltd., Chichester.

Carter, K.F., and Ponter, A.R.S., (1992), Caculation of limit loads and shakedown boundaries using the modified elastic modulus method, *Computational Plasticity Fundamentals and Applications*, part II, 1597–1608.

Corradi, L., and Zavelani, A., (1974), A linear programming approach to shakedown analysis of structures, *Comput. Methods Mech. Eng.*, Vol.3, 37–53.

Dhalla, A.K., (1984), Verification of an elastic procedure to estimate follow-up. *Design of Elevated Temperature Piping*, Eds: R.H. Mallet & R.M. Mello. *PVP-Vol. 86, ASME*, New York, 81–96.

Dhalla, A.K., (1987), A simplified procedure to classify stresses for elevated temperature service, *PVP-Vol. 120, ASME*, San Diego, 177–188.

Dhalla, A.K. & Jones, G.L., (1986), ASME Code classification of pipe stresses: a simplified elastic procedure, *Int. J. Press. Ves. & Piping* **26**. 145–166.

Gambioni, S., Ravera, A. & Stretti, G., (1989), Appraisal of elastic follow up for a generic mechanical structure through two simplified methods. *Int. J. Press. Vess. & Piping* **37**, 221–241.

Hamilton, R. , Mackenzie, D., Shi, J. and Boyle, J.T., (1995), Limit load bounds for a plane stress problem by the elastic compensation method. The Fourth Pan American Congress of Applied Mechanics, Bnenos Aires. Argentina. January.

Hamilton, R., Shi, J., Mackenzie, D., and Boyle, J.T., (1994), Approximate limit analysis of pressurised axisymmetric nozzles: a parameter study. *PVP-Vol. 277, ASME*, 121–126.

Jones, G.L. and Dhalla, A.K., (1981), Classification of clamp induced stresses in thin-walled pipe, *PVP-Vol. 81, ASME*, New York.

Kizhatil, R.K. and Seshadri, R., (1991), Inelastic strain concentration factors and low cycle fatigue of pressure components using GLOSS analysis. *PVP-Vol. 210-2, ASME*, 149–154.

König, J.A., (1987), *Shakedown of Elastic–Plastic Structures*, PWN–Polish Scientific Publishers, Warsaw and Elsevier, Amsterdam.

Lubliner, J. , (1990), *Plasticity Theory*, Macmillan Publishing Company. New York.

Mackenzie, D., and Boyle, J.T., (1993a), A method of estimating limit loads by iterative elastic analysis. I–Simple examples. *Int. J. Pres. Ves. & Piping.* Vol. 53, No.1, 77–95.

Mackenzie, D., and Boyle, J.T., (1993b), A simple method of estimating shakedown loads for complex structures, *PVP-Vol. 265. ASME.* 89-94.

Mackenzie, D., and Boyle, J.T., (1994), A computational procedure for calculating primary stress for the ASME B&PV Code, *J. Press. Ves. Tech.*, Vol. 116, 339–344.

Mackenzie, D., and Boyle, J.T. and Spence, J., (1994), Some recent developments in pressure vessel design by analysis, *Proc. Instn Mech. Engrs*, Vol. 208, 23–29.

Mackenzie, D., Hamilton, R. and Boyle, J.T., (1994), Using ANSYS ADPL macros to calculate limit loads by iterative elastic finite element analysis. Proc. 6th Int. ANSYS Conf., Pittsburgh, PA, Vol. 3, 14.31–14.38.

Mackenzie, D., Hamilton, R., Shi, J., and Boyle, J.T., (1995), A finite element method for shakedown analysis, ACME Conference, Oxford, January.

Mackenzie, D., Hamilton, R., Shi, J., and Boyle, J.T., (1995), Secondary stress and shakedown in axisymmetric nozzles, ASME PVP Conference, Honolulu, July.

Mackenzie, D., Nadarajah, C., Shi, J., and Boyle, J.T., (1993). Simple bounds on limit loads by elastic finite element analysis. *J. Pres. Ves. Technology*, Vol.115, 27–31

Mackenzie, D., Shi, J., Nadarajah, C., and Boyle, J.T., (1992). An iterative elastic analysis procedure for estimating lower bound limit loads. *PVP-Vol. 230, ASME*, 129–134.

Mackenzie, D., Shi, J. and Boyle, J. T., (1994), Finite element modeling for limit analysis by the elastic compensation method.*Computer & Structures*, Vol. 51, No. 4, 403–410.

Marriot, D.L., (1988), Evaluation of deformation or load control of stresses under inelastic conditions using elastic finite element stress analysis, *PVP-Vol. 136, ASME*, Pittsburgh.

Nadarajah, C., Mackenzie, D., and Boyle, J.T., (1993), A method of estimating limit loads by iterative elastic analysis. II–Nozzle sphere intersections with

internal pressure and radial load. *Int. J. Pres. Ves. & Piping.* Vol. 53. No.1, 97–119.

Nakamura, K. & Boyle, J.T., (1987), The assessment of elastic follow up in high temperature piping systems-some example problems, *Int. J. Pres. Ves. & Piping* **29**, 249–273.

Roche, R.L., (1986), Estimation of piping elastic follow up by using conventional computations, *Int. J. Pres. Ves. and Piping*, Vol. 26, 53–78.

Roche, R.L., (1988), Modes of failure-primary and secondary stresses. *J. Press. Ves. Tech.*, Vol. 110, 171–176.

Roche, R.L., (1989), Practical procedures for stress classification. *Int. J. Press. Ves. & Piping* **37**, 27–44.

Seshadri, R., (1990), The effect of multiaxiality and follow-up on creep damage. *J. Pres. Vessel Tech.*, Vol. 112, 378–385.

Seshadri, R., (1990), Classification of stresses in pressure components using the 'GLOSS' diagram, *PVP-Vol. 186, ASME*, Nashville, 115–123.

Seshadri, R., (1991), Simplified method for determining multiaxial relaxation and creep damage, *PVP-Vol. 210-2, ASME*, San Diego, 173–180.

Seshadri, R., (1991), The generalised local stress strain (GLOSS) analysis-theory and applications, *J. Press. Vess. Tech.*, 219–227.

Seshadri, R. and Fernando, C.P.D., (1991), Limit loads of mechanical components and structures using the GLOSS R-Node method. *PVP-Vol. 210-2. ASME*, San Diego.

Seshadri, R. and Kizhatil, R.K., (1990), Inelastic analyses of pressure components using the 'GLOSS' diagram, *PVP-Vol. 186. ASME.* Nashville. 105–113.

Severud, L.K., (1984), A simplified method of evaluation for piping elastic follow up, Proc. 5th Int. Conf. Pres. Vessel. Tech., ASME, San Francisco. 367–387.

Shi, J., Mackenzie, D., and Boyle, J.T., (1993), A method of estimating limit loads by iterative elastic analysis. III–Torispherical heads under internal pressure. *Int. J. Pres. Ves. & Piping*, Vol. 53, No.1, 121–142.

Swanson Analysis Systems, Inc. (1993), *ANSYS User's Manual for Revision 5.0A*, SASI,PO Box 65, Johnson Road, Houston PA 15342-0065.

Vaidyanathan, S., Kizhatil, R.K. and Seshadri, R., (1989), GLOSS plot-validation and application to elevated temperature components design, *PVP-Vol. 161. ASME*, Honolulu, 25–31.

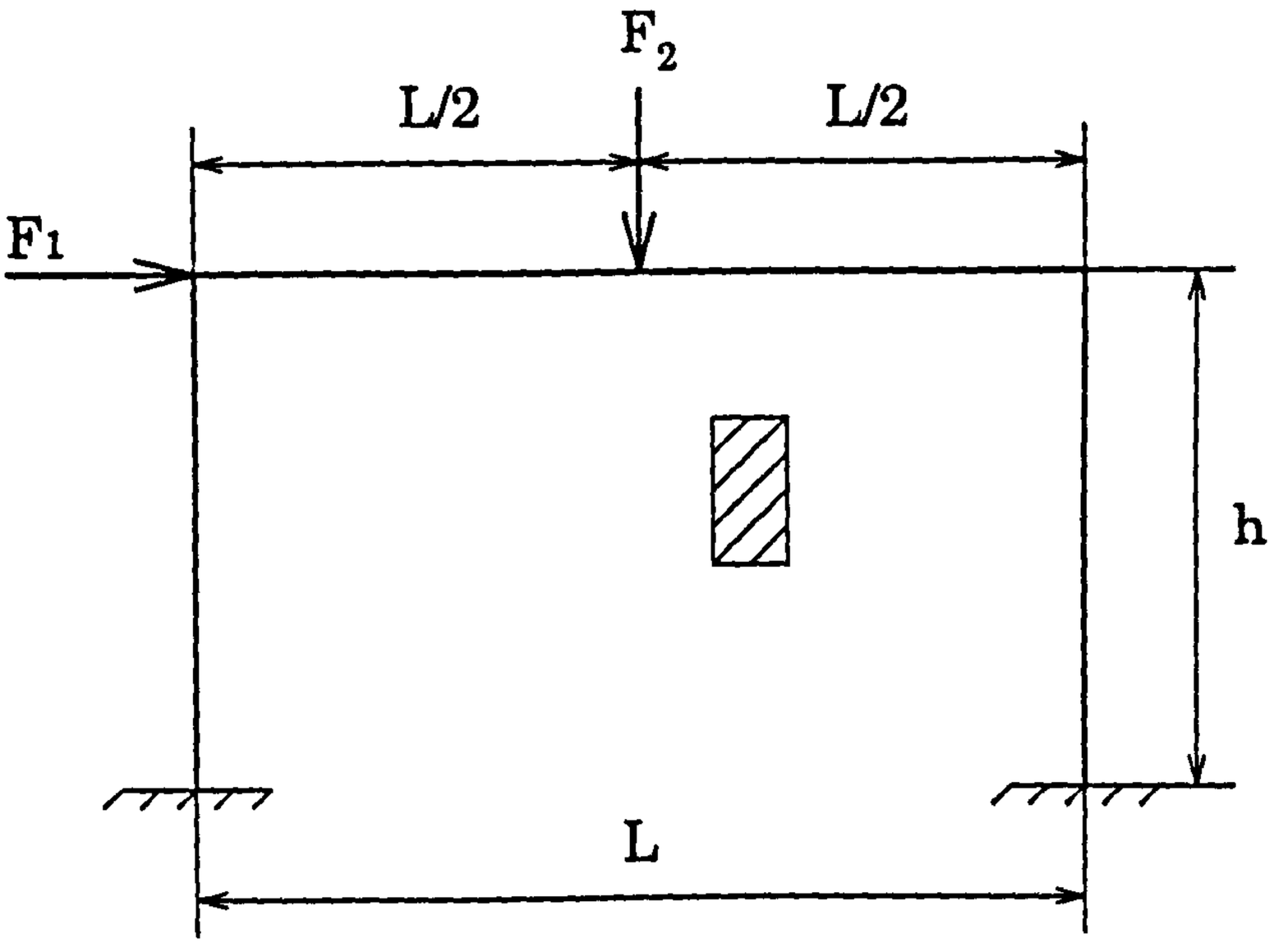

Figure 3.21: One-bay, one-story frame

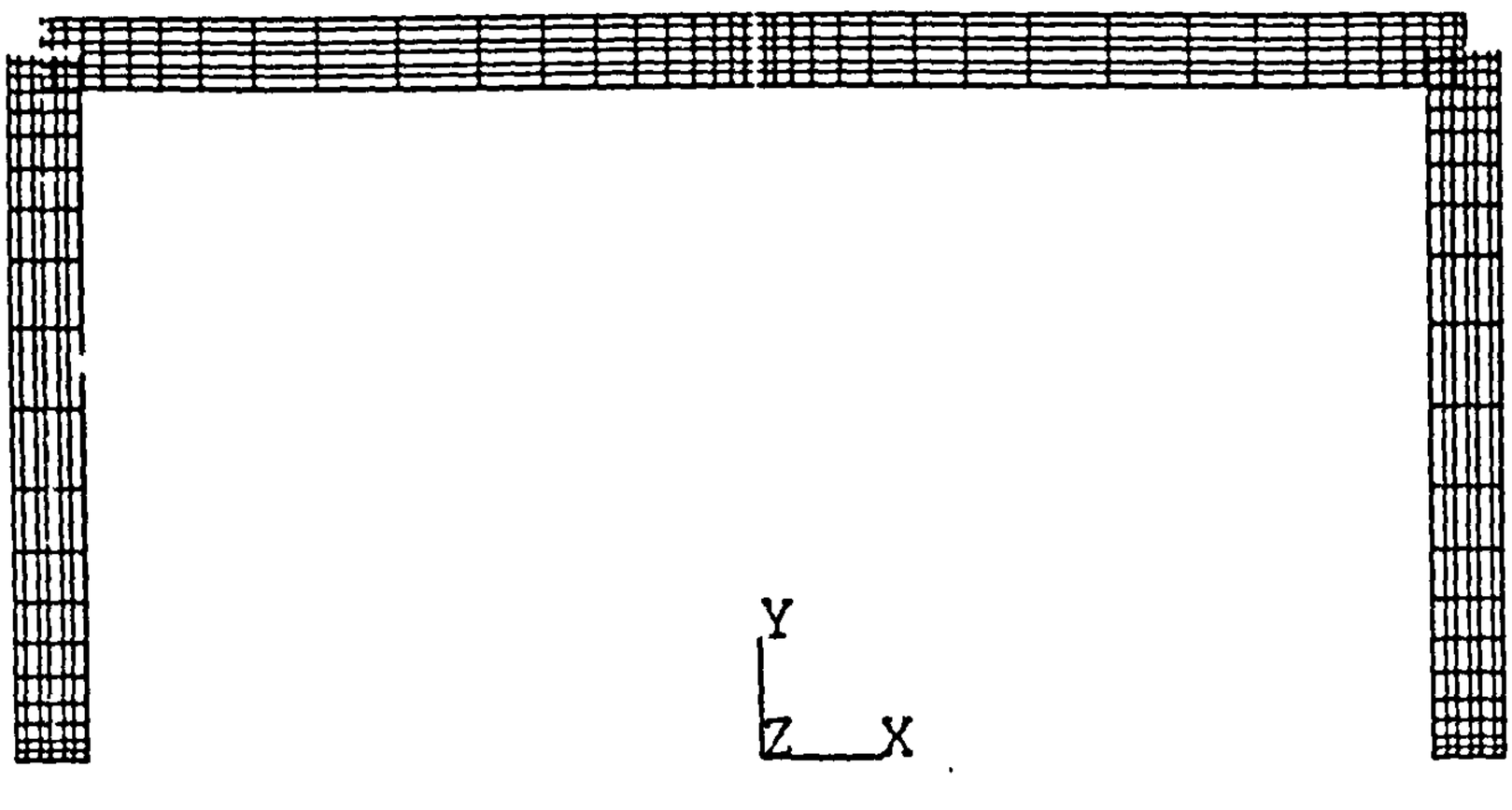

Figure 3.22: Finite element mesh of one-bay. one-story frame

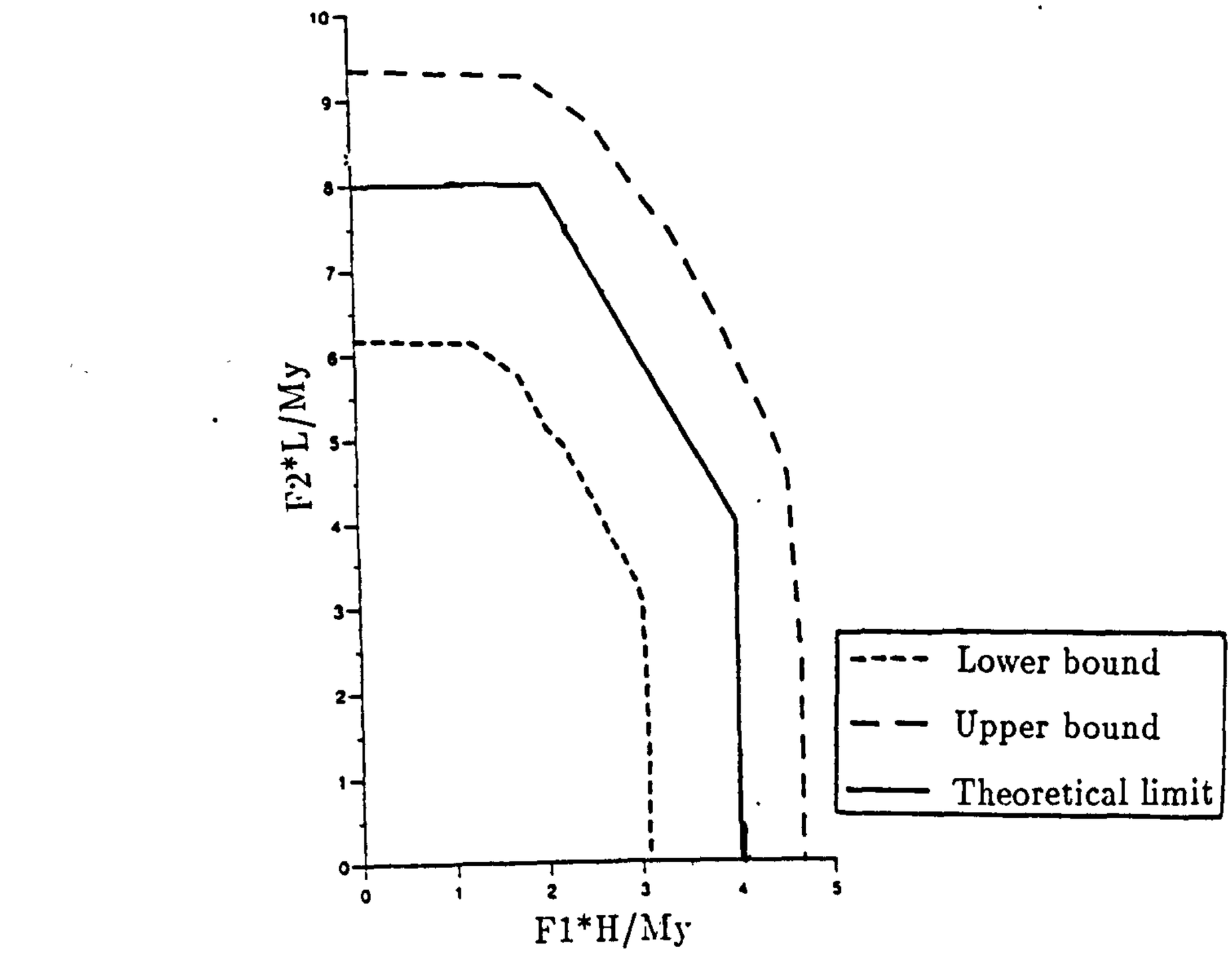

Figure 3.23: Results of one-bay. one-story frame

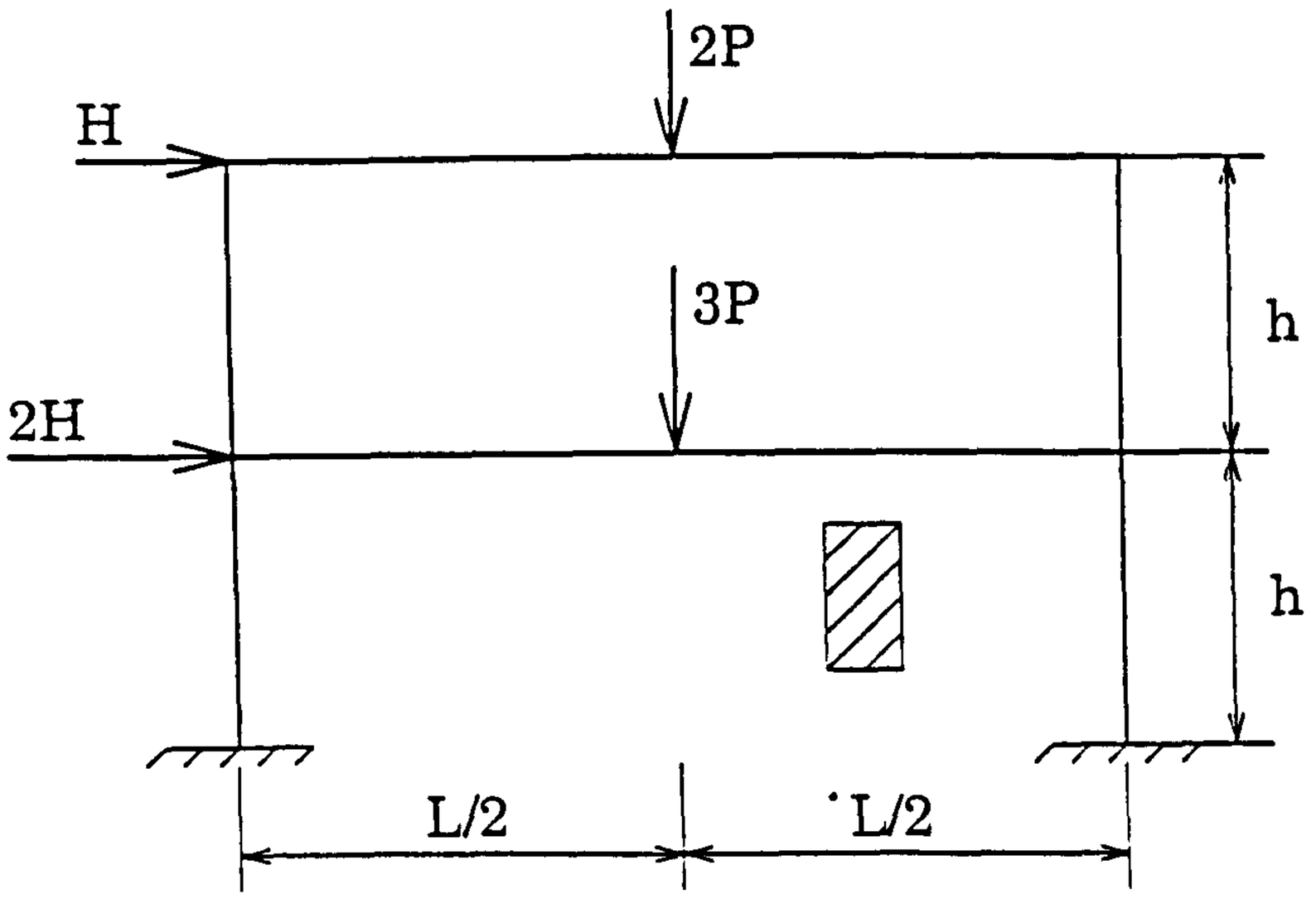

Figure 3.24: One-bay. two-story frame

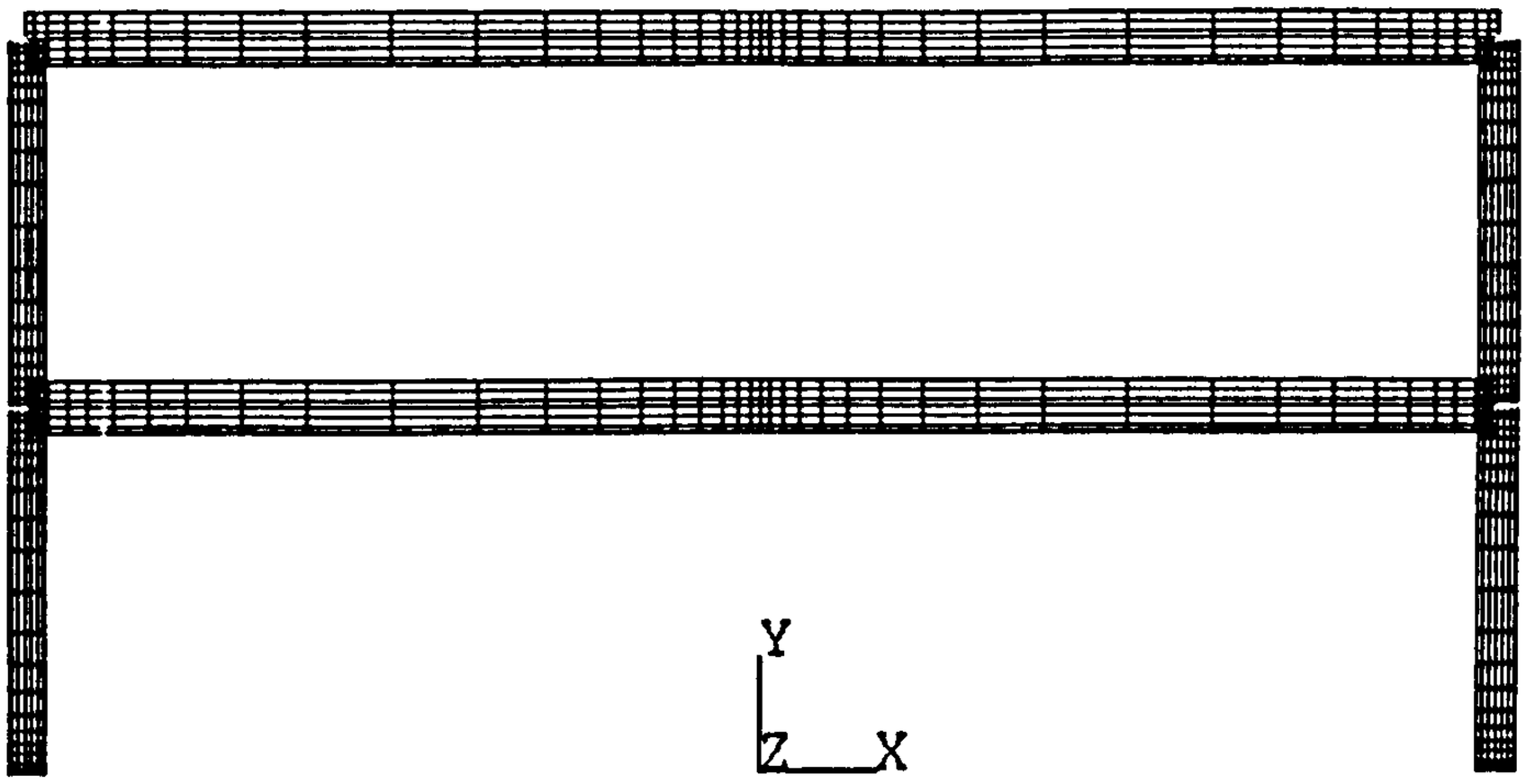

Figure 3.25: Finite element mesh of two-bay, two-story frame

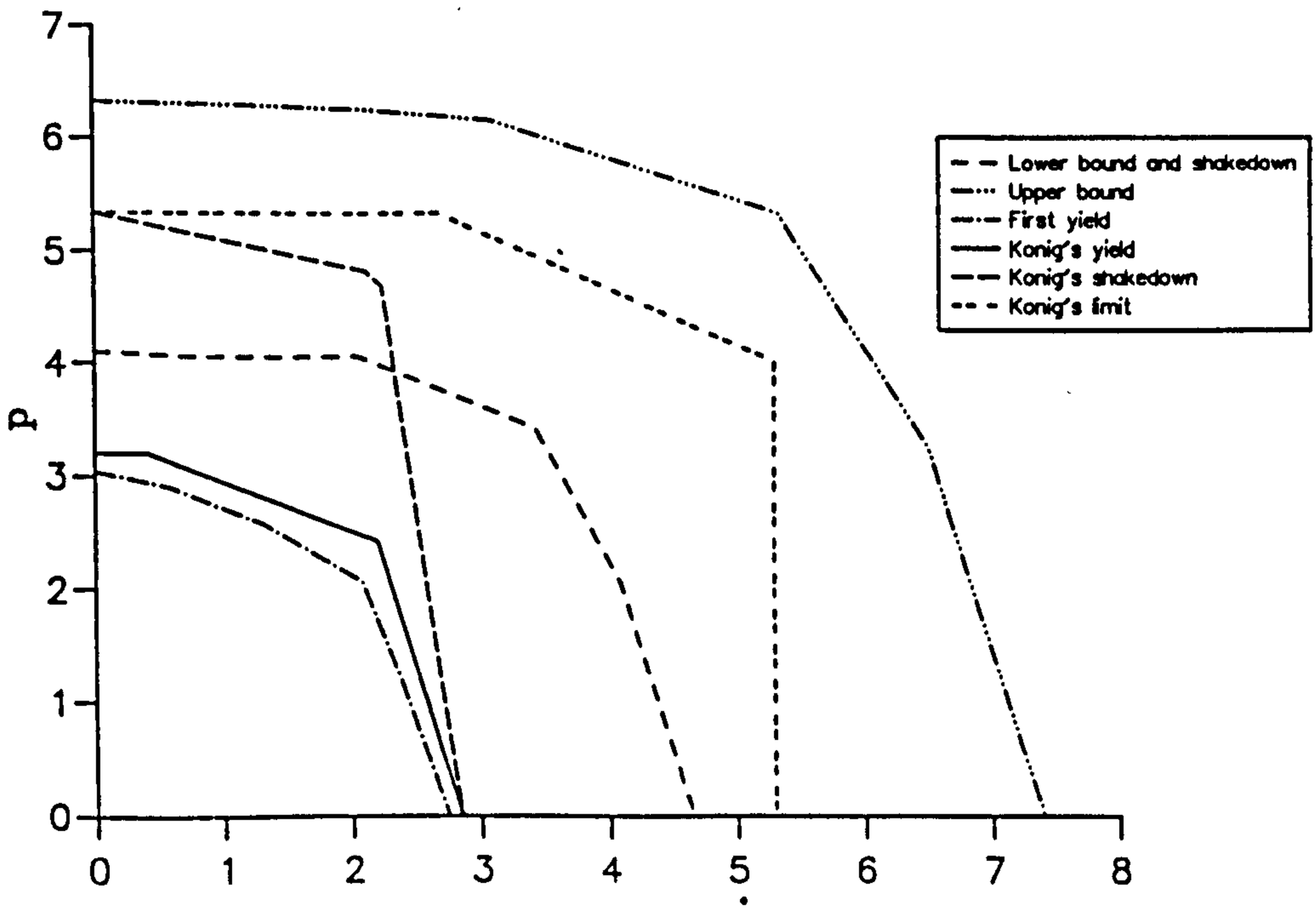

Figure 3.26: Results of one-bay. two-story frame. $h/L = 1/4$

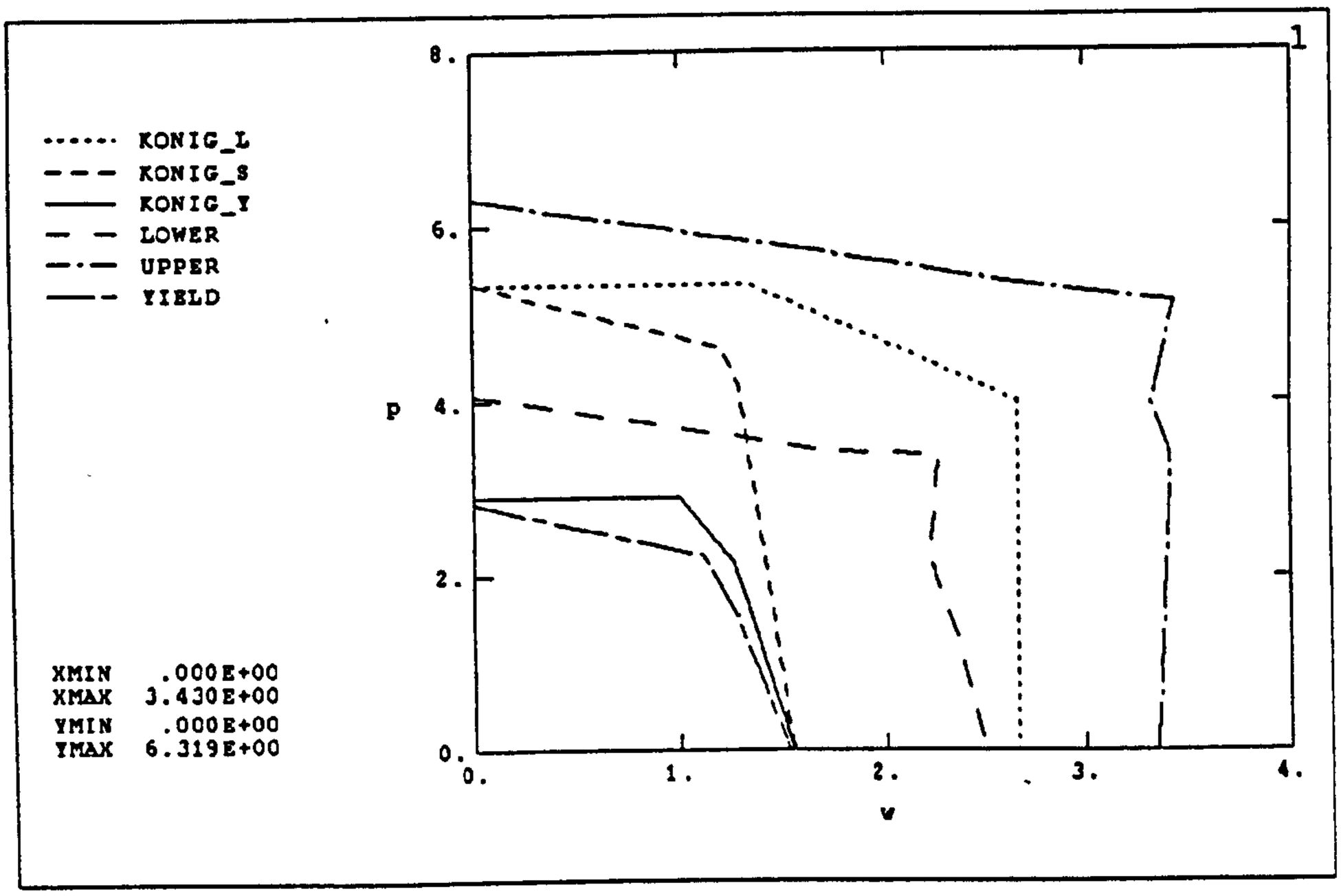

Figure 3.27: Results of one-bay, two-story frame, $h/L = 1/2$

CHAPTER 4

LIMIT AND SHAKEDOWN LOAD INTERACTION DIAGRAMS

4.1 Introduction

In Chapter 3 the elastic compensation method devised by the Strathclyde Group has been reviewed. The method was verified for a few simple problems and it was shown that useful limit and shakedown loads could be found. As pointed out in Chapter 3, the Strathclyde Group has applied the elastic compensation method to a wide range of structural problems. However so far few demonstrations of the method for load interaction have been given. To remedy this in this Chapter the application of elastic compensation to the evaluation of interaction diagrams for limit and shakedown loads is examined for the (simple) problem of a plate with a hole under proportional biaxial load. Before doing this. the problem is reviewed:

A theoretical investigation of the lower and upper bound limit loads of a square plate with central circular hole was carried out firstly by Hodge [1953] using the Tresca yield criterion, and then by Gaydon and McCrum [1954] using the von Mises yield criterion.

Hayes and Marcal [1967] developed a finite element method for determining upper bounds on the limit load for this problem. Three years later. Belytschko and Hodge [1970] proposed a complementary method for finding the lower bound on the limit load for this problem using the finite element technique. A mixed formulation and mixed finite elements for limit analysis of this problem has been discussed by Casciaro and Cascini [1982]. More recently the same problem has been analysed by Hamilton *et al.* [1995] by the elastic compensation method.

For shakedown, this problem is a popular benchmark for calculating shakedown loads using finite element methods and several authors have published solutions over the years. Belytschko [1972] was the first to provide a finite element solution of this problem: he used an equilibrium finite element technique with nonlinear programming applied directly to the lower bound shakedown theorem. Hung and Palgen [1980] used a similar approach, but discussed the results in more detail. Corradi and Zavelani [1974] on the other hand used linear programming and also derived a dual formulation which gave a (pseudo) upper bound. Recently Genna [1988] has demonstrated a finite element technique which is based on a nonlinear inequality formulation with linearization of the yield surface.

Shakedown with nonlinear strain-hardening material using finite element method has been developed by Stein *et al.* [1992]. They investigated the same problem in cases of both elastic-perfectly plastic material and nonlinear strain-hardening material and concluded that for this system under the given loading. the strain-hardening had no influence on the shakedown behaviour, that is. the results for an elastic-perfectly plastic material are the same as for a nonlinear kinematic hardening material. Their results are quite similar as those of Corradi and Zavelani [1974].

In this chapter, the lower and upper bound limit and shakedown loads will be carried out by the elastic compensation method and finite element analysis. then these results will be compared with elasto-plastic analysis and results from the literature .

4.2 Limit Load Interaction Diagram by Elastic Compensation

In this section, the elastic compensation method is applied to the plane stress problem of a plate with a circular hole under uniaxial tension and various combinations of biaxial loads P_1 and P_2. The loads are proportional. Lower and upper bound limit loads are calculated using elastic compensation and compared with

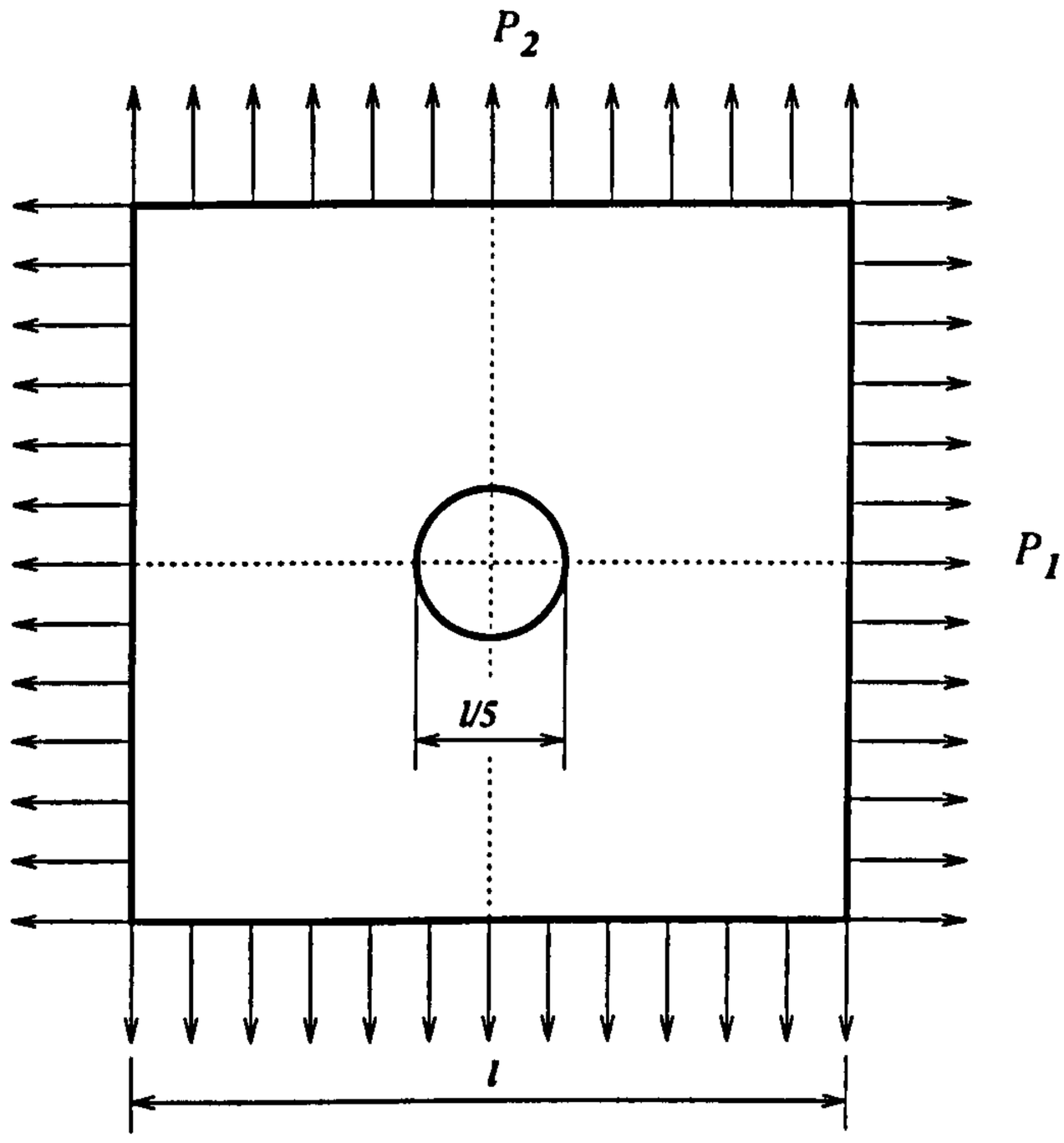

Figure 4.1: Plate with a hole under biaxial loads P_1 and P_2

the results from elasto-plastic finite element analysis and results given in the literature. The problem geometry is shown in Figure 4.1 and the finite element mesh is developed using eight node axisymmetric solid element *PLANS2* in ANSYS as shown in Figure 4.2. For all models, 450 elements were used. Computations were made for a Poisson's ratio of 0.3 and yield stress of 300 N/mm^2.

The lower and upper bound limit loads calculated for various load combinations, (based on 10 analysis iterations), are compared with elastic-plastic analysis limit loads (elastic-perfectly plastic material model) in Table 4.1 and Figure 4.3 and results from the literature in Table 4.2 and are generally in good agreement.

4.3 Shakedown Load Interaction Diagram by Elastic Compensation

In this section, as an illustration the elastic compensation method is applied to the same problem. This problem is a popular benchmark for calculating shakedown loads using finite element methods. A brief review has been given in the beginning of this chapter. All of these formulations are quite complex but more

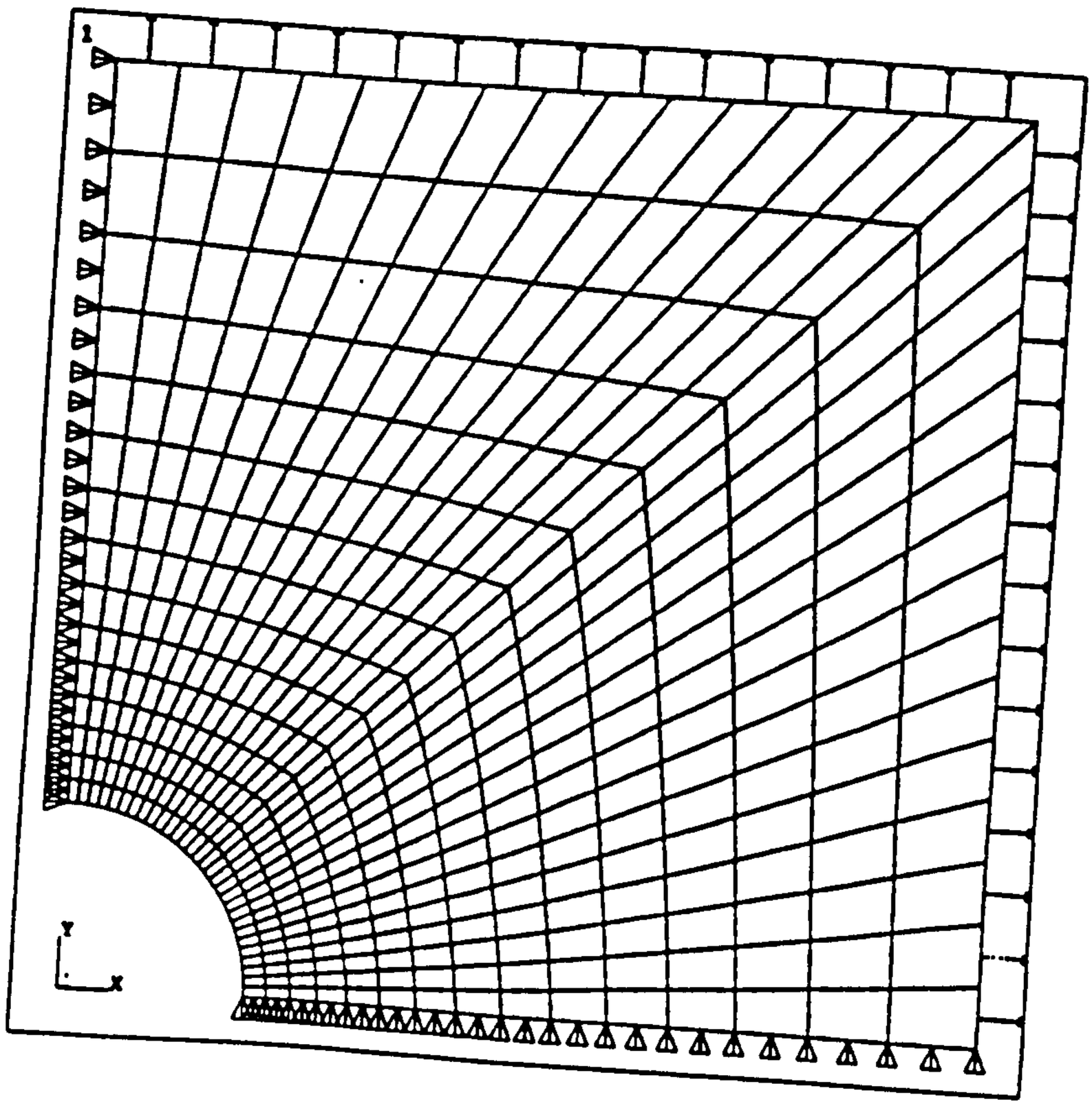

Figure 4.2: Finite element mesh and boundary conditions

Table 4.1: Values of normalised limit loads P_2/σ_y using elastic compensation

P_1/P_2	First yield	Limit load (Lower bound)	Limit load (Upper bound)	Elasto-Plastic Limit load
1.00	0.483	0.853	0.908	0.883
0.90	0.458	0.858	0.940	–
0.75	0.422	0.850	0.965	0.917
0.60	0.391	0.856	0.958	–
0.50	0.373	0.857	0.953	0.900
0.40	0.356	0.838	0.932	–
0.25	0.334	0.815	0.904	0.873
0.10	0.314	0.767	0.859	–
0.00	0.302	0.747	0.830	0.800
-0.5	0.254	0.564	0.645	0.613
-1.0	0.219	0.450	0.494	0.467

importantly require special purpose finite element analysis software. The elastic compensation procedure for calculating lower and upper bound shakedown loads in Chapter 3 will be used here again to obtain the lower and upper bound shakedown loads for the plate with a circular hole under tension and various combinations of proportional biaxial loads. The finite element program ANSYS is used: the writer has automated the elastic compensation procedure using the *ANSYS* ADPL macro language, see Appendix II. The problem geometry, finite element mesh and symmetry boundary conditions are the same as in the previous section. In this case the load set will be taken as

$$P_1 = \mu(P_1^0 + f(t)\Delta P_1)$$
$$P_2 = \mu(P_2^0 + f(t)\Delta P_2)$$

The coefficients P_1^0, ΔP_1, P_2^0, ΔP_2 are *constants* for a given analysis but can be chosen independently to reflect different families of load cycles. Here two specific

Table 4.2: Values of normalised limit loads P_2/σ_y from the literature

Method	P_1/P_2	Limit load (Lower bound)	Limit Load (Upper bound)	Other
Gaydon and McCrum	1.0	0.9	0.929	–
	0	0.8	0.8	-
	-1.0	0.447	0.492	–
Belytschko and Hodge	0	0.793	0.824	–
Hayes and Marcal	0	–	0.885	–
Genna	0	–	–	0.791
Belytschko	1.0	0.8	–	–
	0	0.78	–	–
Rimamawi and Dogan	0	–	–	0.8
Casciaro and Cascini	1.0	–	–	0.892
	0	–	–	0.8035
	-1.0	–	–	0.4678
Corradi and Zavelani	1.0	0.691	0.8	0.767
	0	0.691	0.8	0.691

families will be studied by way of example:

$$Case1 \quad P_1^0 = P_2^0 = 0 \quad \Delta P_1 = \lambda P \quad \Delta P_2 = P$$

$$Case2 \quad \Delta P_1 = P_2^0 = 0 \quad P_1^0 = \lambda P \quad \Delta P_2 = P$$

where the ration λ will take on different values. The results will be normalised with respect to P/σ_y.

Elastic compensation lower and upper bound shakedown loads for these families of load cases are evaluated and the results shown in Table 4.3 and 4.4 for various of λ. Also shown are initial yield and the corresponding lower and upper bound limit loads. In each case 10 iterations were used; the best limit and shakedown loads are usually given by different iterations in the elastic compensation

Table 4.3: Normalised lower bound shakedown and limit loads P/σ_y using elastic compensation

λ	First yield	Limit load	Shakedown Case 1	Shakedown Case 2
1.00	0.483	0.853	0.853	0.423
0.75	0.422	0.850	0.826	0.497
0.50	0.373	0.857	0.739	0.569
0.25	0.334	0.815	0.640	0.589
0.00	0.302	0.747	0.578	0.578
-0.5	0.254	0.564	0.496	0.563
-1.0	0.219	0.450	0.435	0.450

procedure.

It can be seen from Table 4.3 that for $\lambda = 1$, the lower bound shakedown load. for case 1, equals the lower bound limit load. Also it should be noted that in some instances, specifically when the lower bound shakedown load is very close to the lower bound limit load, the upper bound shakedown load value drops below the lower bound shakedown load value. This could be explained by numerical errors in the finite element model and the approximate nature of the bound calculations. However Martin [1975] maintains that where the lower shakedown and limit loads are close then the need to calculate the upper bound shakedown load is nullified. In other words in this situation the failure will be by gross plastic collapse rather than incremental failure in the form of ratcheting and the shakedown bounds are invalid.

The results can now be compared to previously published solutions [Belytschko, 1972], [Corradi and Zavelani, 1974], [Hung and Palgen. 1980]. [Genna. 1988], but some careful interpretation is required:

Shakedown and limit interaction diagrams are shown in Figure 4.4 as a com-

Table 4.4: Normalised upper bound shakedown and limit loads P/σ_y using elastic compensation

λ	First yield	Limit load	Shakedown Case 1	Shakedown Case 2
1.00	0.483	0.908	0.781	0.466
0.75	0.422	0.965	0.779	0.516
0.50	0.373	0.953	0.748	0.571
0.25	0.334	0.904	0.713	0.632
0.00	0.302	0.830	0.667	0.667
-0.5	0.254	0.645	0.545	0.553
-1.0	0.219	0.494	0.425	0.433

posite from Corradi and Zavelani [1974] and Hung and Palgen [1980]: these are typical of the results found using programming techniques. In these diagrams *two* elastic and limit domains are distinguished: here these will be denoted as *safety* and *interaction* domains. For example the elastic safety domain ensures elastic behaviour for any load combination in the specified region; however for proportional loading the derived interaction domain lies adds elastic load combinations which are guaranteed to be safe, while again there are safe load combinations outside the safety domain. The safety *domains* thus ensure either elastic behaviour or avoidance of gross plastic collapse, but ignore any interaction by assuming the load *histories* to be wholly independent. It is important to appreciate that shakedown domain shown in Figure 4.4 by mathematical programming is also a safety domain. Acceptable shakedown load combinations can, and do, lie outside the safety domain. Analysis using programming techniques can only estimate safety domains since load domains are searched for worst possible combinations, without regard to actual load history during the cycle. This can be seen for the two load families considered here: interaction diagrams are shown in Figure 4.5 and 4.6 for lower and upper bound solutions from elastic compensation. It can be seen that load Case 1 does give acceptable shakedown load combinations outside

the safety domain, while load Case 2 lies closer to the safety domain. The effect of including the true load cycle history is evident.

4.4 Conclusions

The development of bounding procedure for limit and shakedown analysis described here has been kept simple so that the major steps can be easily identified. The sample benchmark problem presented in this chapter illustrates the use of the elastic compensation method in limit and shakedown analyses for proportinal loading and the results indicate that the method can be used to calculate lower and upper bound limit and shakedown loads for actual proportional load histories with useful accuracy. The procedure automatically calculates both lower and upper bound limit and shakedown loads and, most significantly, *requires only elastic analysis capability.* Thus a significant amount of valuable design information can be obtained from a single, easily implemented, analysis procedure.

4.5 References

Belytschko, T., (1972), Plane stress shakedown analysis by finite elements. *Int. J. Mech. Sci.*, Vol. 14, 619–625.

Belytschko, T., and Hodge, P.G., Jr., (1970), Plane stress limit analysis by finite elements, *J. Engrg. Mech. Div.*, Vol.96, No.EM6, 931–944.

Casciaro, R., and Cascini, L., (1982), A mixed formulation and mixed finite elements for limit analysis, *Int. J. Numberical methods in Engrg.*, Vol.18. 211–243.

Corradi, L., and Zavelani, A., (1974), A linear programming approach to shakedown analysis of structures, *Comput. Methods Mech. Eng.*, Vol.3. 37–53.

Gaydon, F.A. and McCrum, A.M., (1954), A theoretical investigation of the yield point loading of a square plate with central circular hole. *J. Mech. Phys. Solids*, Vol. 2, 156–169.

Genna, F. , (1988), A nonlinear inequality, finite element approach to the direct computation of shakedown load safety factors, *Int. J. Mech. Sci.*, Vol.30. No.10, 769–789.

Hayes, D.J., and Marcal, P.V., (1967), Determination of upper bounds for problems in plane stress using finite element techniques, *Int. J. Mech. Sci.*, Vol.9, 245–251.

Hodge, P.G. Jr., (1953), Final report on yield loads of slabs with reforced cutouts, *DAM Rept.* B11-22, Brown University, Providence.

Hodge, P.G. Jr., (1959), *Plastic Analysis of Structures*. McGram-Hill (N.Y.).

Hung, N.D., and Palgen, L., (1980), Shakedown analysis by displacement method and equilibrium finite element, *Trans. of the Canadian Society Mechanical Engineers*, Vol.6, 34–40.

Martin, J.B., (1975), *Plasticity: Fundamentals and General Results*. Cambridge. Mass., MIT Press.

Rimamawi, W.H. and Dogan, E., (1970), Experiments on yielding of tension specimens with notches and holes, *Exper. Mech.*, **10**, 427–432.

Stein, E., Zhang, G. and König, J.A., (1992), Shakedown with nonlinear strain-hardening including structural computation using finite element method. *Int. J. Plasticity*, Vol. 8, 1–31.

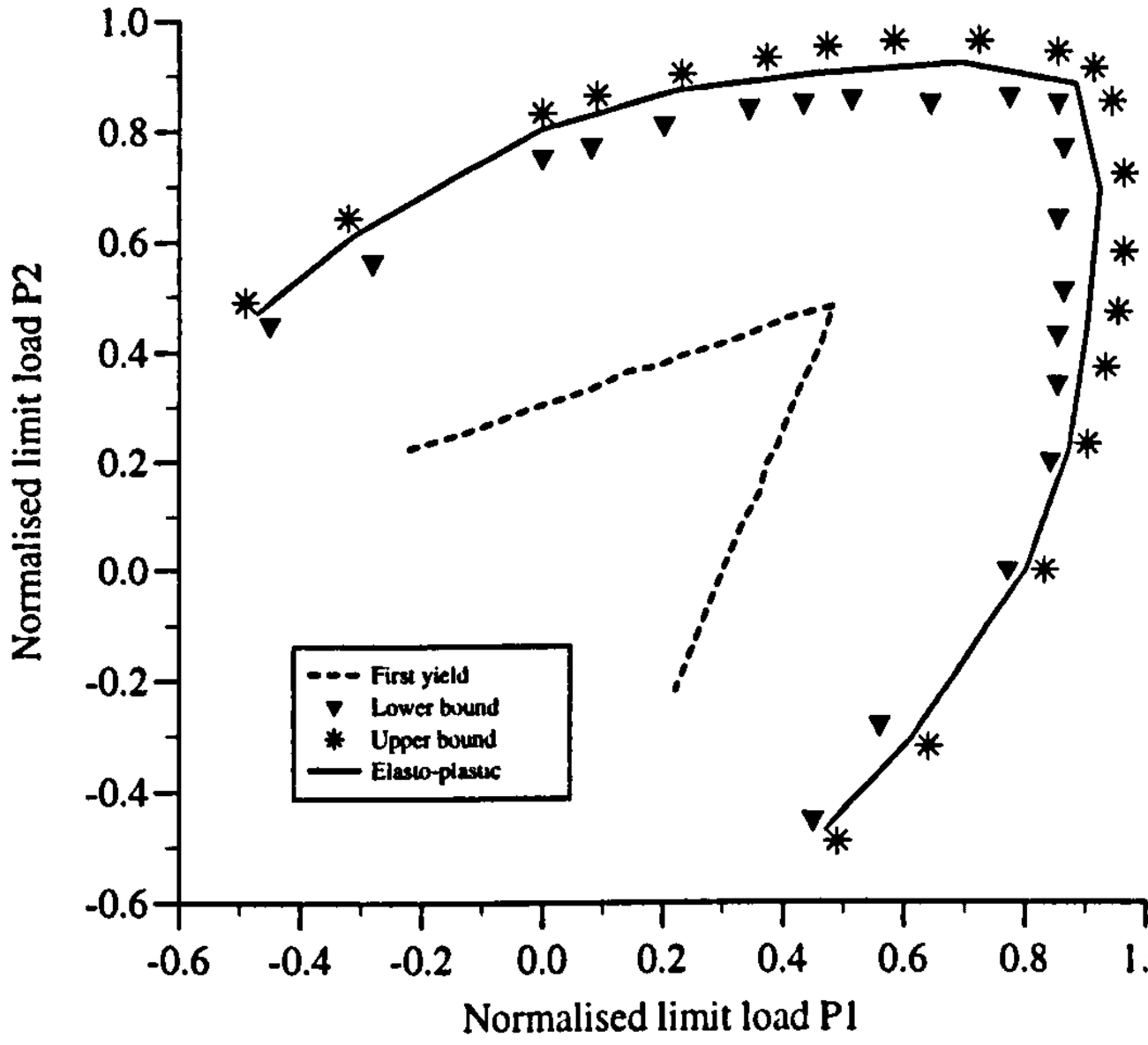

Figure 4.3: Load interaction diagram for a plate with a hole under biaxial loads

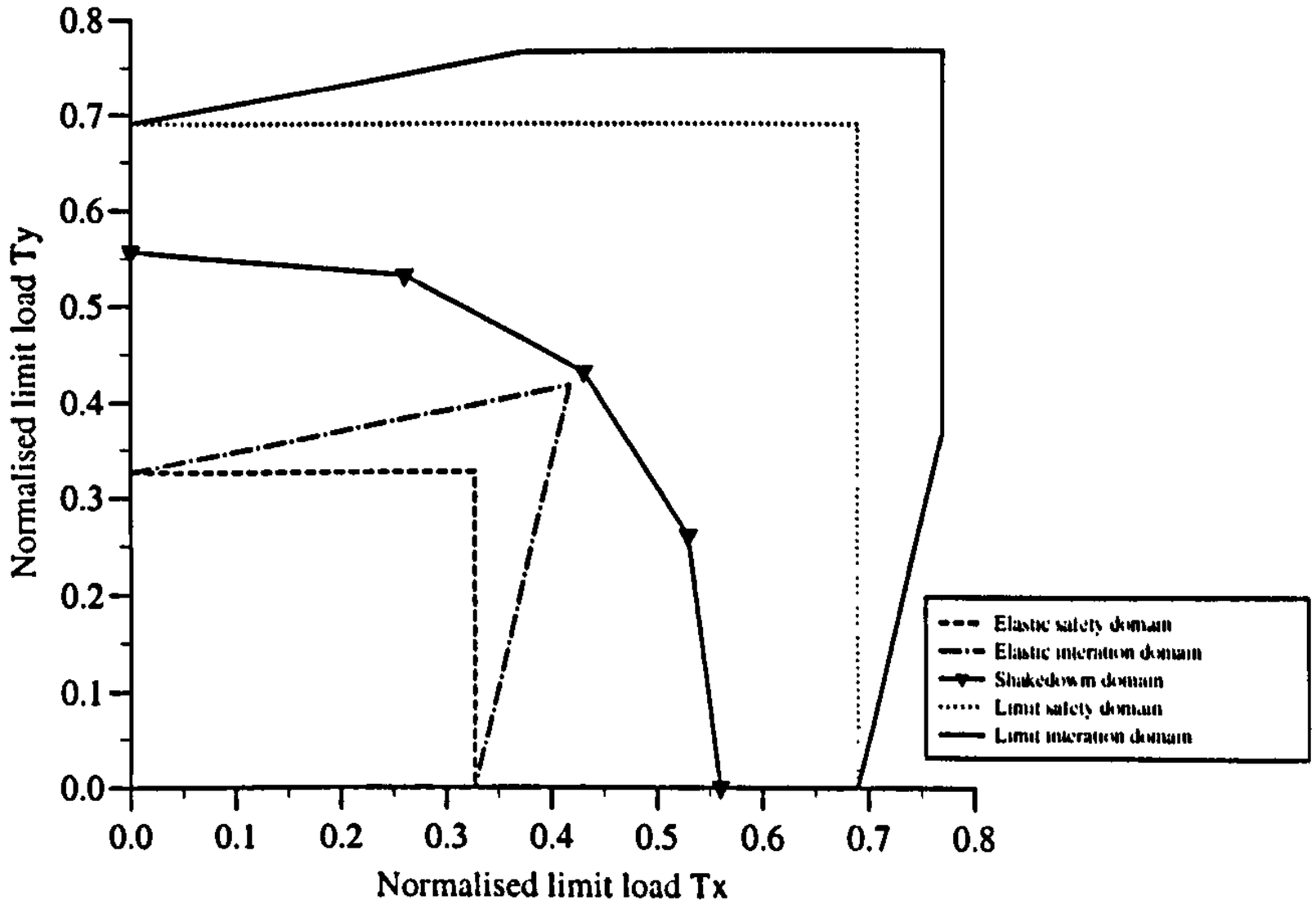

Figure 4.4: Shakedown load interaction diagram, Corradi and Zavelani [1974] and Hung and Palgen [1980]

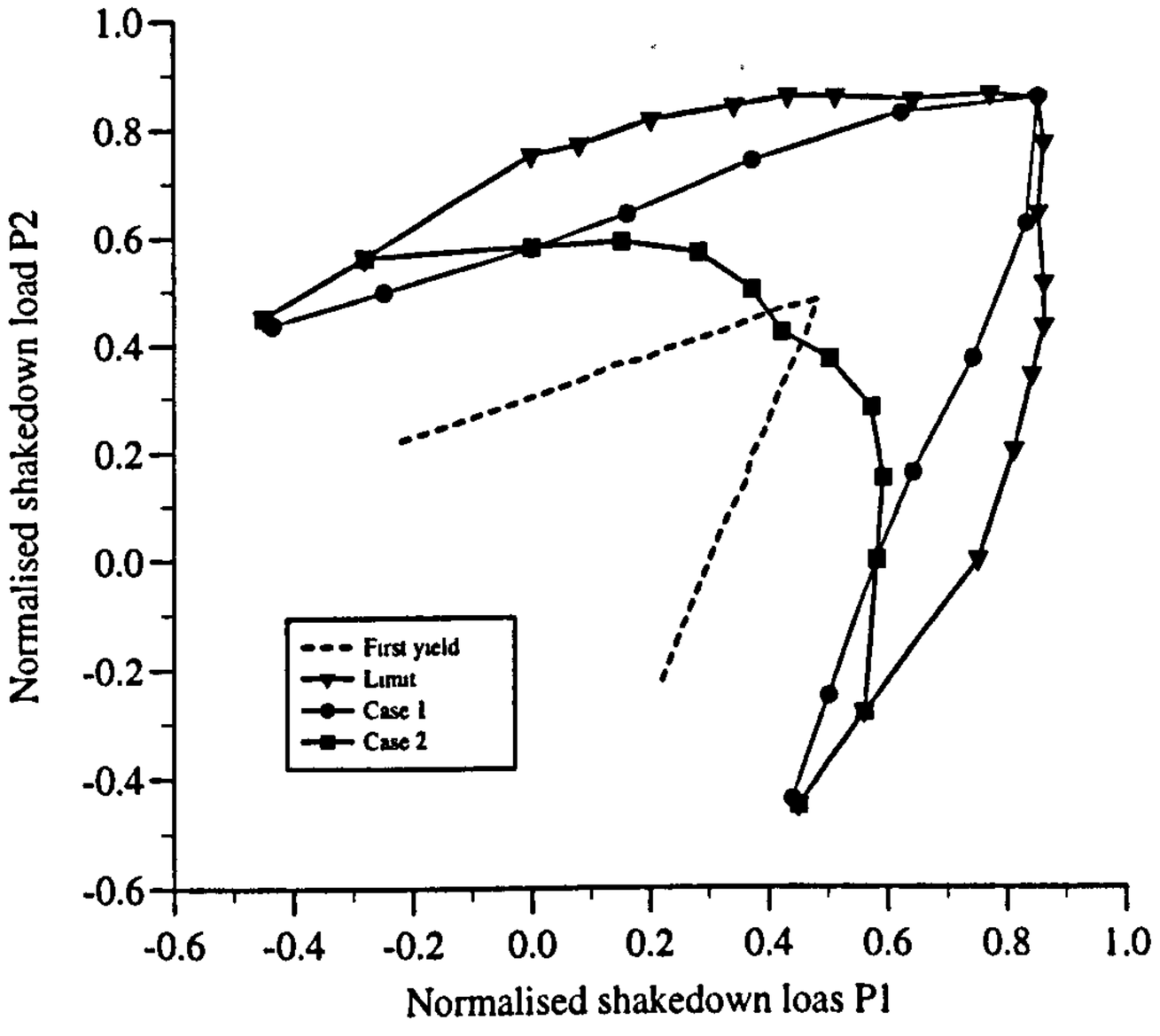

Figure 4.5: Lower bound shakedown load interaction diagram for a plate with a hole

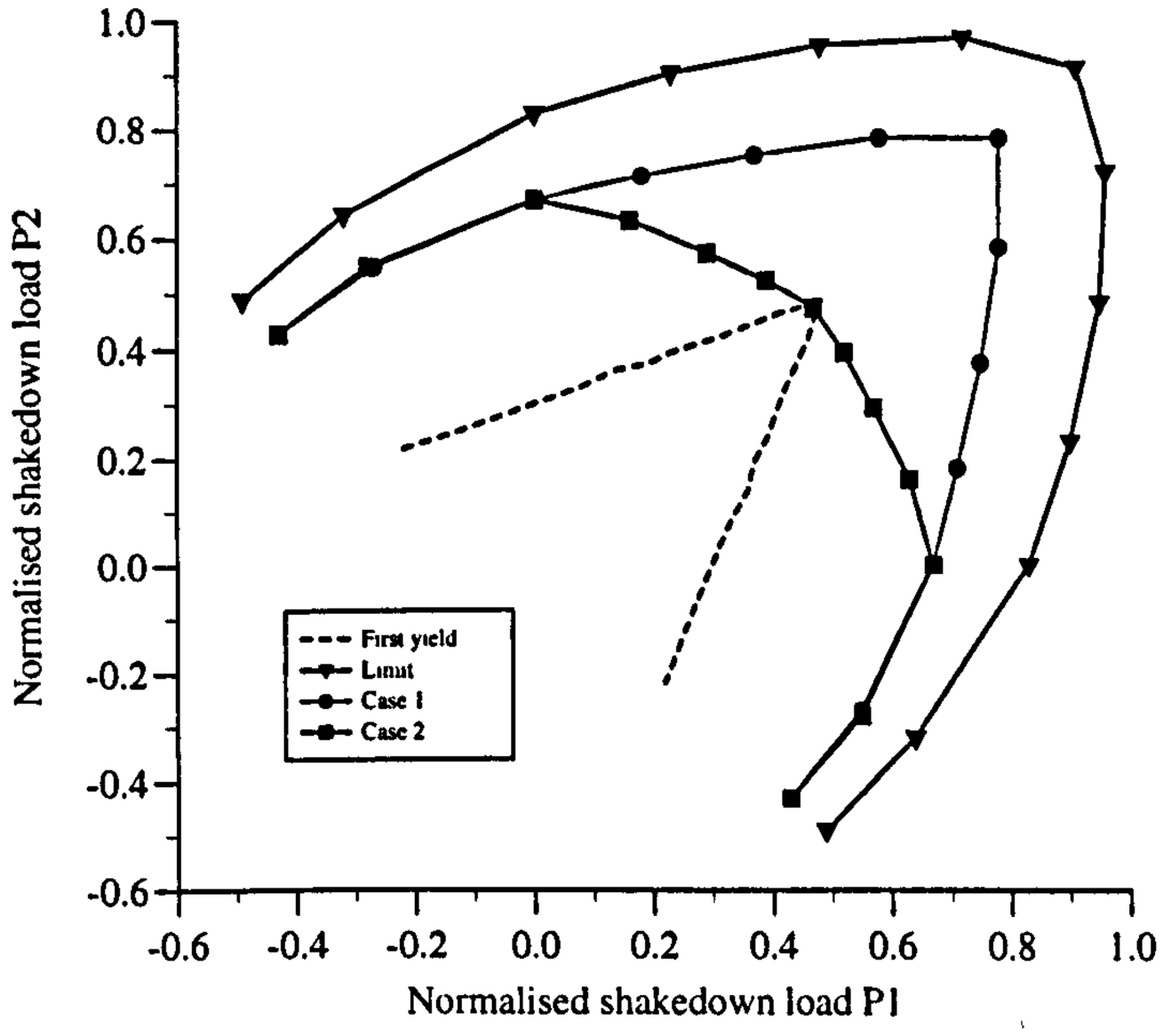

Figure 4.6: Upper bound shakedown load interaction diagram for a plate with a hole

CHAPTER 5

LIMIT ANALYSIS OF NOZZLES IN PRESSURE VESSELS

5.1 Introduction

Limit analysis of nozzles in spherical pressure vessels under internal pressure has been received considerable attention in the past three decades. Consequently, many methods for estimating the limit load have been developed.

In this Chapter, a brief review of limit analysis for nozzles in pressure vessels is given first and then a *parametric* study of the limit loads for nozzles in spherical pressure vessels will be carried out using the elastic compensation method.

5.2 Brief Review of Limit Analysis of Nozzle/Spherical Intersections Under Internal Pressure

The basic principles of the application of limit analysis to shells have been developed since about 1950. The application of these principles to problems of technological significance has occurred since about 1958 and the subject is still developing. By the early sixties researchers have been looking into methods to derive the limit pressure for flush cylindrical nozzle in a spherical pressure vessel. Three papers Lind [1964], Gill [1964] and Cloud [1965] were published at about the same time.

The paper by Lind [1964] considers the shell nozzle junction as shown in Figure 5.1 for a rigid-plastic material obeying the Tresca criterion. The cross-section of Figure 5.1 is basically the intersection of a cylindrical nozzle and spherical shell with fillet radii on the inside and outside at the junction. The limit pressure is calculated corresponding to plastic hinges forming at points 1, 2, 3, with tensile

circumferential yield between 1 and 3. The hinge circle, 2, is at the junction of the cylinder and sphere.

Gill's [1964] paper derives upper and lower bounds to the limit pressure for a flush cylindrical nozzle in a spherical vessel using the one moment limited interaction surface. The analysis is based on the mechanism shown in Figure 5.2 consisting of hinge circles in the branch, sphere and at the junction. Between hinge circles there is a radially outward movement and hence the material in this region is at circumferential yield. The mechanism also implies an outward rigid body displacement of the branch.

The theoretical analysis presented in the paper by Cloud [1965] is very similar to Gill's [1964]. The one-moment limited intersection surface is used and a lower bound is found by putting $M_\theta = M_\phi$ in the sphere equilibrium equations. The paper also considers the effect of different lengths and thicknesses of integral reinforcement of the spherical shell. Cloud [1965] also reports three tests carried out to compare the theory with experimental results.

The more general problem of the limit analysis of the junction of cylindrical and spherical shell is considered in the paper of Dinno and Gill [1965a] which covers a wide range of parameters from the nozzle of [Gill 1964] to the case

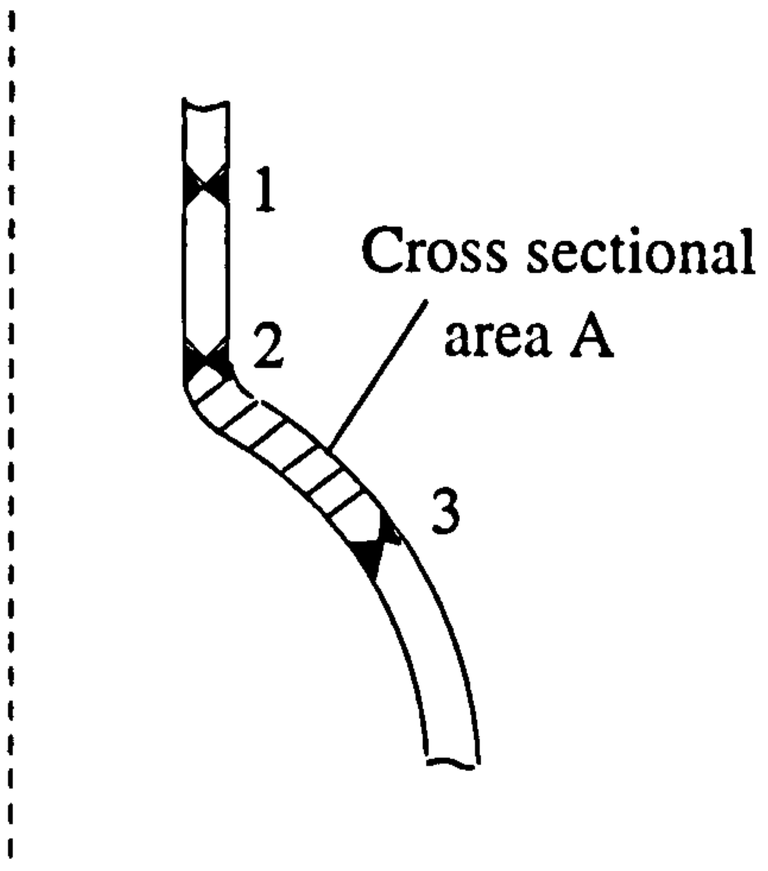

Figure 5.1: Shell nozzle junction

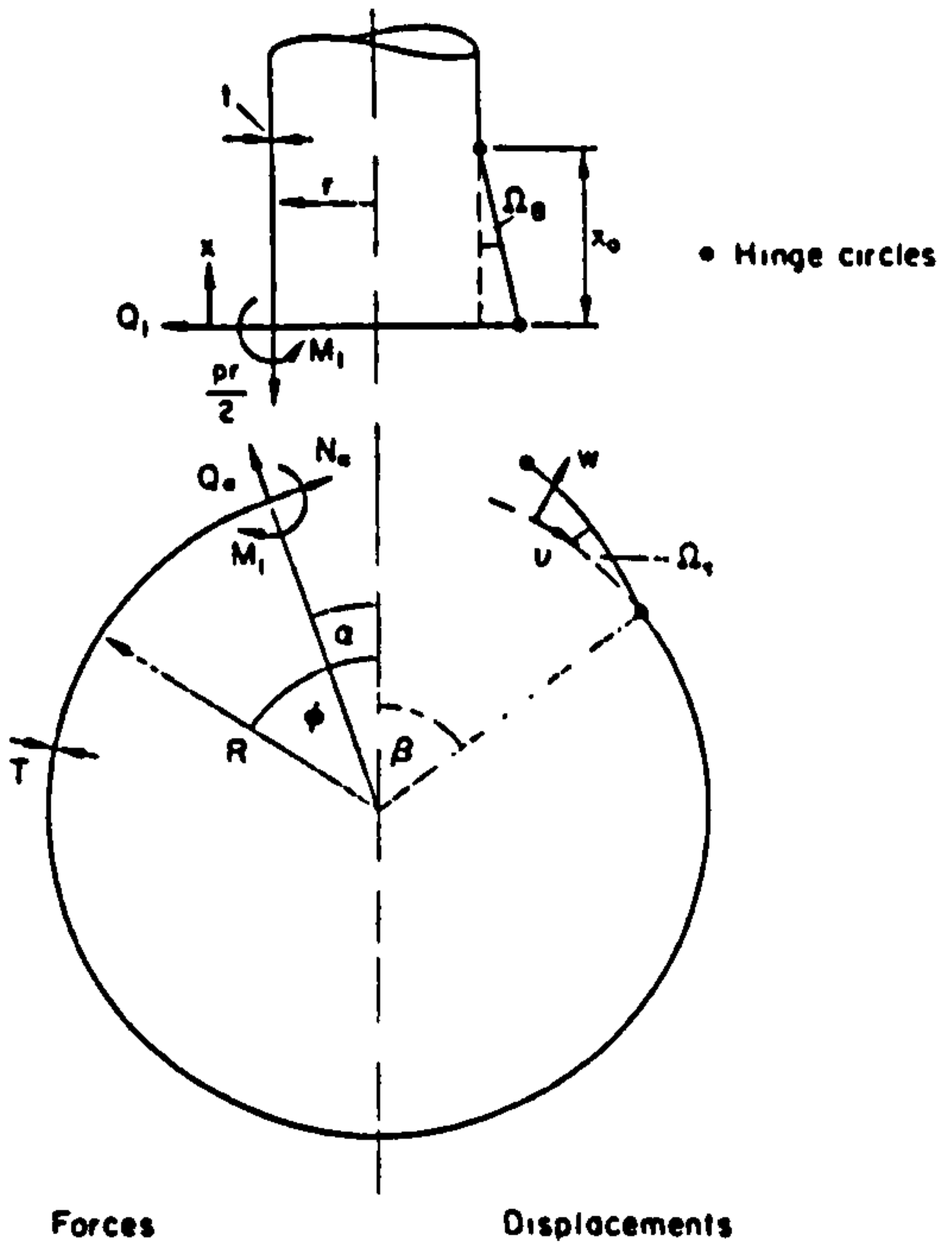

Figure 5.2: Collapse mechanism of a nozzle in a spherical vessel

where the cylinder and sphere have the same diameters, i.e. the cylindrical vessel with hemispherical ends. A full investigation is given of different ratios of branch/sphere thickness which in particular establishes the conditions under which the three-hinge mechanism of [Lind 1964, Gill 1964, Cloud 1965] is valid. Ellyin and Sherbourne [1965a, 1965b] have made similar studies of this problem.

In 1965, Leckie and Payne [1965] represented Gill's [1964] results for limit pressure against a single dimensionless nozzle geometry parameter ρ for various nozzle to shell thickness ratios. Gill [1970] has also presented summarised results in a similar form.

Following the experimental programme carried out by Cloud [1965], some further tests on six nozzles carried out by Dinno and Gill [1965b] with more elaborate instrumentation confirmed that the pattern of stress is similar to that assumed in the theory. The experimental limit pressures were in all cases somewhat higher than the limit pressures as calculated using the one-moment limited interaction surface. However the specimens used by Dinno and Gill had a typical fillet weld at the nozzle sphere junction which would increase the strength of the structure.

One significant feature of the experimental results [Dinno and Gill, 1965b] is

the increase of pressure with deformation after the limit pressure, an effect which appears to be partly due to the effect of change of geometry and partly due to strain hardening of the material. The change of geometry problem has been studied theoretically by Allman and Gill [1968]. The theory only gives the initial rate of change of limit pressure with change of geometry at zero change of geometry for a rigid-plastic material and is based on a development of Gill [1964]. This change of geometry effect, taken in conjunction with the experimental results of Cloud [1965], Dinno and Gill [1965b] suggests that theoretical limit pressures for flush nozzles in spherical vessels predicted by the type of analysis discussed can be used as a design basis where appropriate, and that there is an inherent margin of safety due to the effect of deformation under load.

In the early seventies, Robinson and Gill [1973] proposed a method to calculate a lower bound to the limit pressure of a cylindrical branch in a spherical pressure vessel using non-linear programming techniques. The stress resultants in the branch and vessel were expressed in terms of an independent set of variables and the Ilyushin's yield surface obeying von Mises yield criterion was used. Force/moment equilibrium at the junction of the branch and sphere was satisfied approximately by using one overall inequality constraint and the pressure was then optimised subject to the yield and equilibrium constraints. They obtained results for a wide range of nozzle/sphere parameters which were then presented in graphical form. Recently this problem has been re-examined by Nadarajah *et al.* [1993] and Mackenzie *et al.* [1992] [1993] by elastic compensation.

In this Chapter a detailed parameter study of the limit behaviour of nozzles is presented.

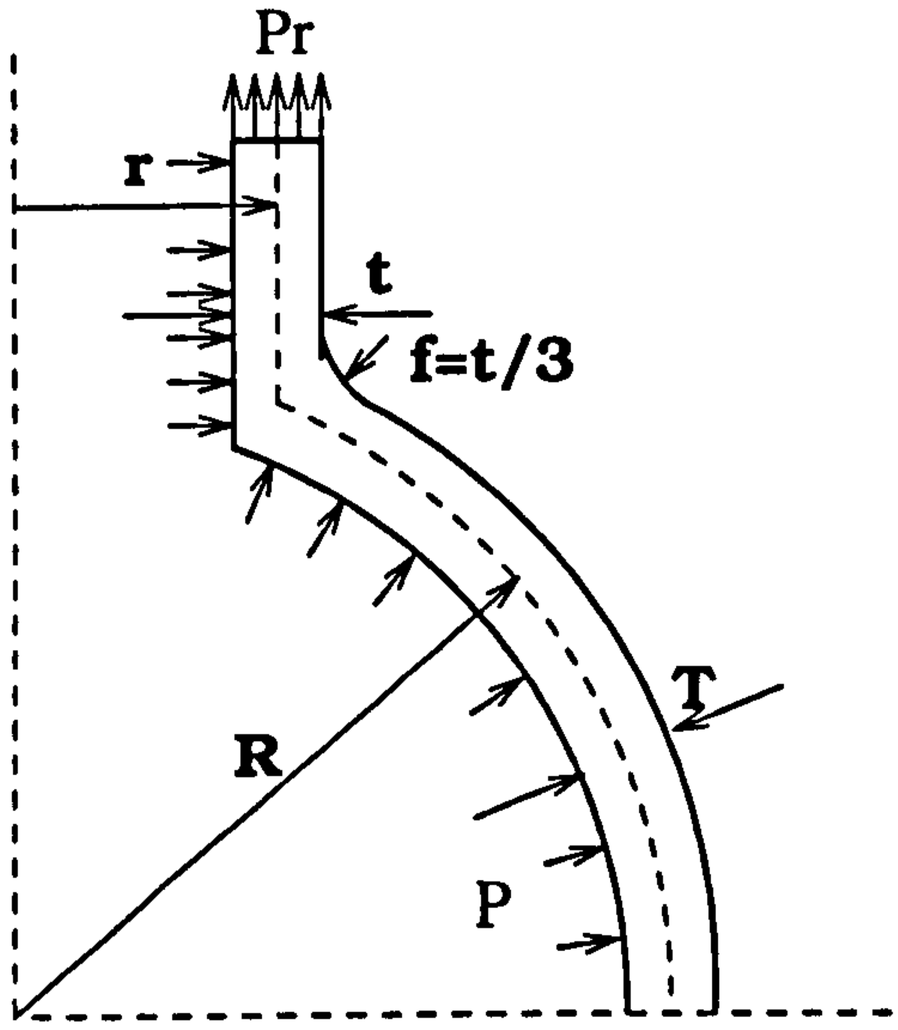

Figure 5.3: The geometry of axisymmetric nozzle in spherical shell

5.3 Approximate Limit Analysis of Nozzle/Spherical Intersections Under Internal Pressure

5.3.1 Model Geometry

The nozzle/spherical shell geometries are shown in Figure 5.3. Here the dimensionless geometry parameter ρ: $\rho = \frac{r}{R}(\frac{R}{T})^{\frac{1}{2}}$ is used as same as that in the paper of Leckie and Payne [1965]. In Figure 5.3, r is the radius to mid-section of the nozzle, R the radius to mid-section of the shell, t the thickness of the nozzle, T the thickness of the sphere, and f the fillet radius at the nozzle/sphere intersection. For the nozzles with $T = 10mm$, $f = 5mm$ and for the remainder $f = t/3$. The fillet of radius f at the nozzle/sphere intersection is modeled in order to counter the problem of singularities at re-entrant corners in elasticity theory. P is the internal pressure and P_r the radial outward pressure as shown.

For first stage of the study the radius ratio was taken constant at $R/r = 5$ ($R = 1000mm$, $r = 200mm$), with thickness $T = t$ varied from 250mm to 23.67mm over 9 models, (this naturally leads to some rather curious nozzle geometries). The detailed geometric parameters are shown in Table 5.1. For all the models examined the modulus of elasticity is taken as $200E3.N/mm^2$ with Poisson's ratio 0.3. The yield stress of the material is taken as $300.N/mm^2$.

Table 5.1: *Nozzle model geometry,* $r = 200mm$

Nozzle	1	2	3	4	5	6	7	8	9
$R(mm)$	1000	1000	1000	1000	1000	1000	1000	1000	1000
$r(mm)$	200	200	200	200	200	200	200	200	200
$T(mm)$	250	160	111.1	81.6	62.5	40	33.06	27.8	23.67
R/T	4	6.25	9	12.25	16	25	30.25	36	42.2
ρ	0.4	0.5	0.6	0.7	0.8	1.0	1.1	1.2	1.3

Further a series of nozzle/spherical models with set sphere radius. sphere thickness and nozzle thickness ($T = t$) were investigated such that R/T and t/T was constant. Nozzle radius r was varied to give a range of values for ρ. R was set at $R = 1000$ and seven wall thicknesses examined ($T = 10, 20, 40, 100. 120. 140. 160$) give seven groups of models with constant shell radius to thickness ratio of $R/T = 100,\ 50,\ 25,\ 10,\ 8.33,\ 7.14$, and 6.25. In this way. the variation in limit load with **two** dimensionless geometry parameters ρ and R/T was investigated. Eighty four models were thus studied!

5.3.2 Finite Element Model

All eighty four models of each geometry were developed using eight node axisymmetric solid element in *ANSYS* (PLANE82). The models were restrained in the meridional direction, but allowed to move radially. at a distance sufficiently far removed from the nozzle. A typical finite element mesh. in this case for model number 67, is shown in Figure 5.4. For the different models with different thickness the element numbers through thickness are different. The detailed elements used through wall thickness for all models are given in Table 5.2.

For the models with internal pressure P, it was necessary to apply a radial outward load (pressure) P_r at the end of the nozzle due to the internal pressure

Table 5.2: *Elements used through wall thickness*

Nozzle	$T(mm)$	R/T	Elements through thickness
1	250.0	4.0	14
2	160.0	6.24	14
3	111.1	9.0	10
4	81.6	12.25	10
5	62.5	16.0	10
6	40.0	25.0	8
7	33.06	30.25	8
8	27.8	36.0	5
9	23.67	42.2	5
10a-10k	10.0	100.0	5
10-20	20.0	50.0	5
21-31	40.0	25.0	5
32-42	100.0	10.0	10
43-53	120.0	8.33	10
54-64	140.0	7.14	10
65-74	160.0	6.26	10

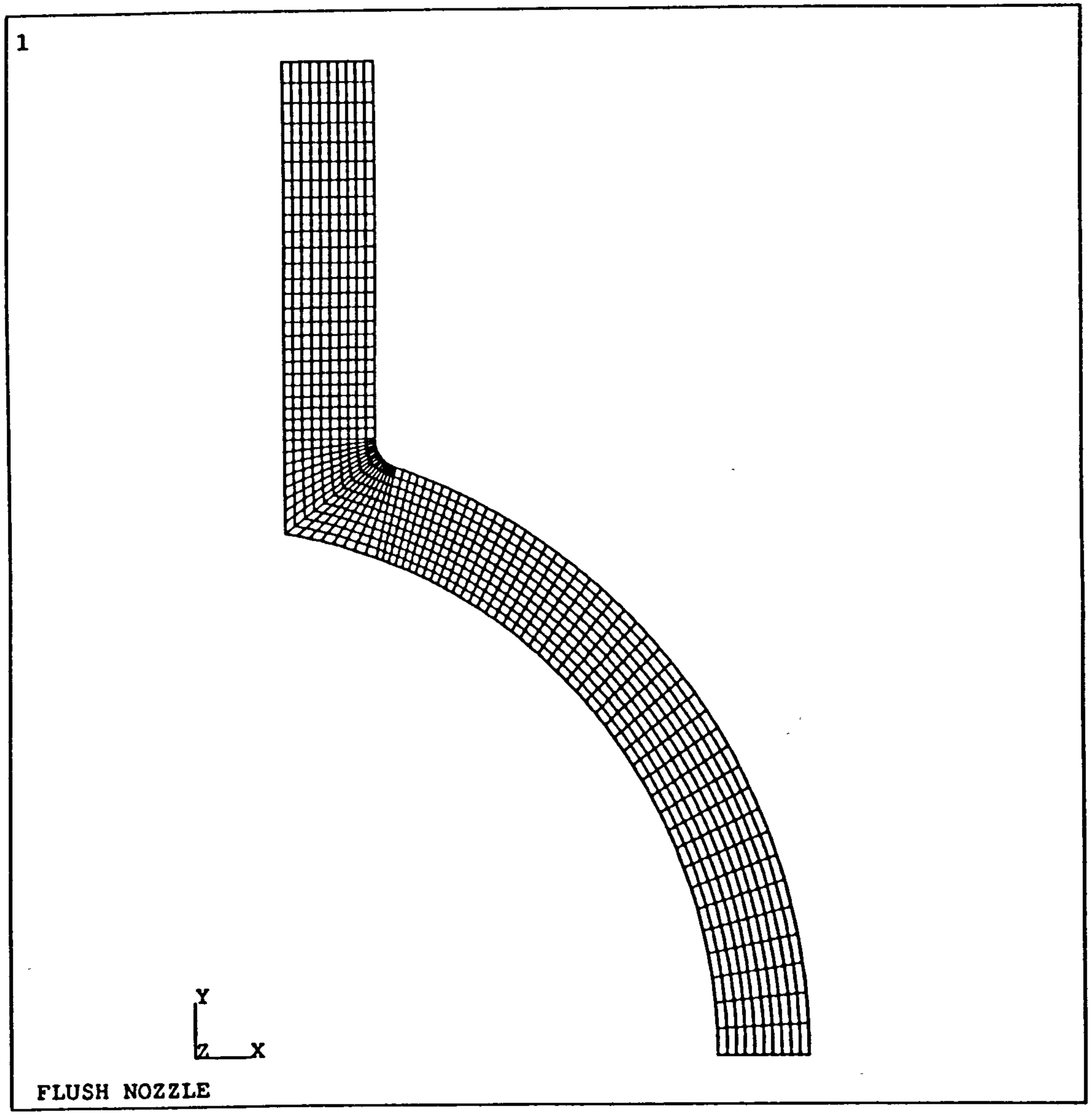

Figure 5.4: Solid finite element mesh for nozzle/spherical intersection

acting on the nozzle; the values of load being calculated as

$$P_r = \frac{Pr_i^2}{r_o^2 - r_i^2}$$

where r_o is outside radius and r_i inside radius of the shell. The boundary conditions of models is shown in Figure 5.5.

5.3.3 Lower and Upper Bound Limit Loads

The lower and upper bound limit pressures, P_l and P_u are obtained by automatically running elastic compensation macros (see Appendix II) which are defined in the *ANSYS* Design Parametric Language (ADPL). In this case ten elastic re-analyses are used during elastic compensation. The results calculated are normalised according to the expression

$$\overline{P} = \frac{R}{2T\sigma_y}P$$

Normalised lower and upper bound limit pressures, $\overline{P_l}$ and $\overline{P_u}$ respectively. normalised pressure to first yield pressure $\overline{P_y}$ and normalised elasto-plastic limit pressures $\overline{P_p}$ (will be demonstrated in next section) for models 1 to 9 are given in Table 5.3 and plotted against the nozzle geometry parameter ρ in Figure 5.9. Lower bound limit loads by Leckie and Payne [1965] are also given in Table 5.3 and Figure 5.9. For other seven groups of models with constant shell radius to thickness ratio of $R/T = 100,\ 50,\ 25,\ 10,\ 8.33,\ 7.14$ and 6.25, the results of the elastic compensation analyses are compared with Robinson and Gill [1973]. $\overline{P_{R+G}}$. for the thiner shells and with new elasto-plastic analysis (will be discussed later). for thicker nozzles, $R/T \leq 10$, where there does not appear to be any comparable results available in the literature (due to the limitations of shell theory). The results are presented in Tables 5.4-5.10 and Figures 5.10-5.16 and summarised and compared with the results of Leckie and Payne [1965] in Figures 5.17-5.18.

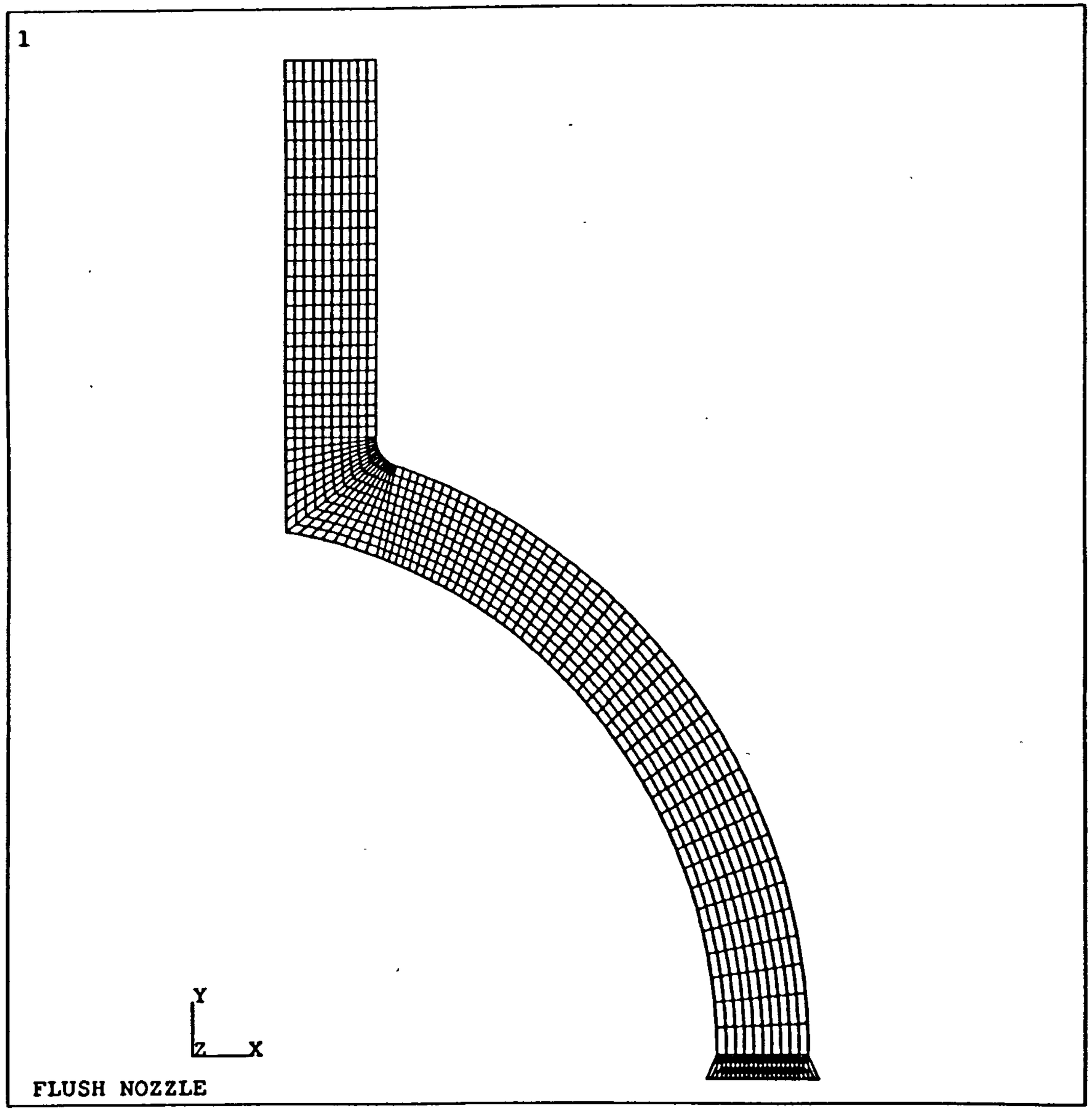

Figure 5.5: Finite element boundary conditions for nozzle/spherical intersection

5.4 Elasto-Plastic Finite Element Analyses

Elasto-plastic analysis is also a useful tool in determining the collapse load of structures but of course more computationally expensive. Here elasto-plastic analysis is used to verify the elastic compensation results. *ANSYS* provides different geometrically non-linear options, such as large strain. large deflection and stress stiffening, to assist in non-linear static analysis. In addition, it also provides for material non-linearities in the structural model. In the elasto-plastic model used in the project, the non-linear options used are large strain, large deflection classical bi-linear kinematic hardening as the material's non-linear property. Each of these options will be discussed in detail. Before doing that let us first review the methods used to indentify the plastic or 'collapse' load as a lower bound on the limit load from elasto-plastic analysis.

Tangent Intersect Load (P_c)

A collapse load has been defined by Save [1972] by drawing tangents to the elastic and plastic parts of the load and displacement curve as shown in Figure 5.6. The load at the intersection of the two tangents is taken as a definition of the collapse load, P_c. The value of the collapse load obtained by this method is sensitive to where the tangent is drawn in the plastic range. If the load and displacement curve exhibits a relatively straight line portion beyond the 'knee' in the curve, the tangent intersect method can give consistent results.

Twice-Elastic-Deformation Load (P_{2y})

The twice-elastic-deformation load defined as the load at which the deflection or strain reachs twice the value of the elastic deflection (δ_y) or elastic strain at the first yield load (P_y) as shown in Figue 5.7. This definition has been used in the ASME Boiler and Pressure Vessel Code. 1974 edition [1974]. This method depends on the yield load, P_y and the elastic deflection. The yield load or elastic deflection can be obtained through the use of strain gauges in experiments or through approximations from the load and displacement curve. Gerdeen in [1979]

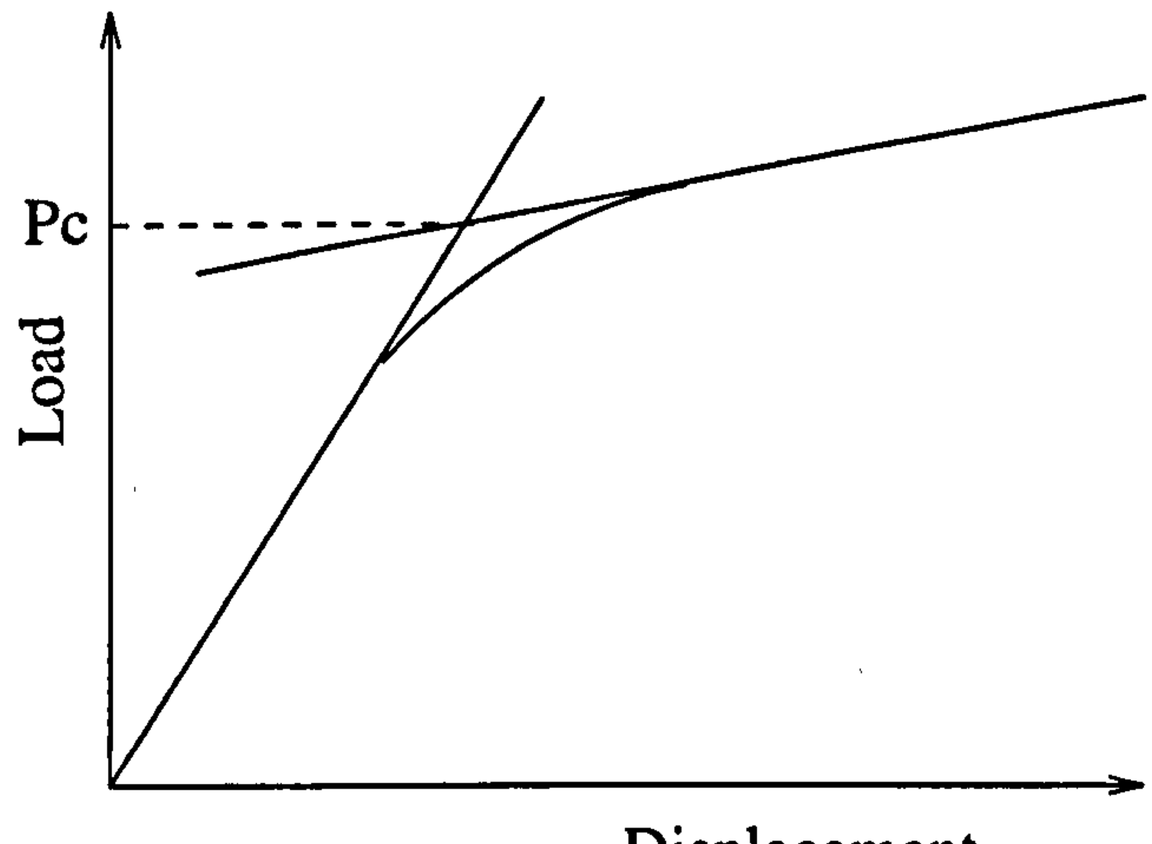

Figure 5.6: Tangent intersect load method

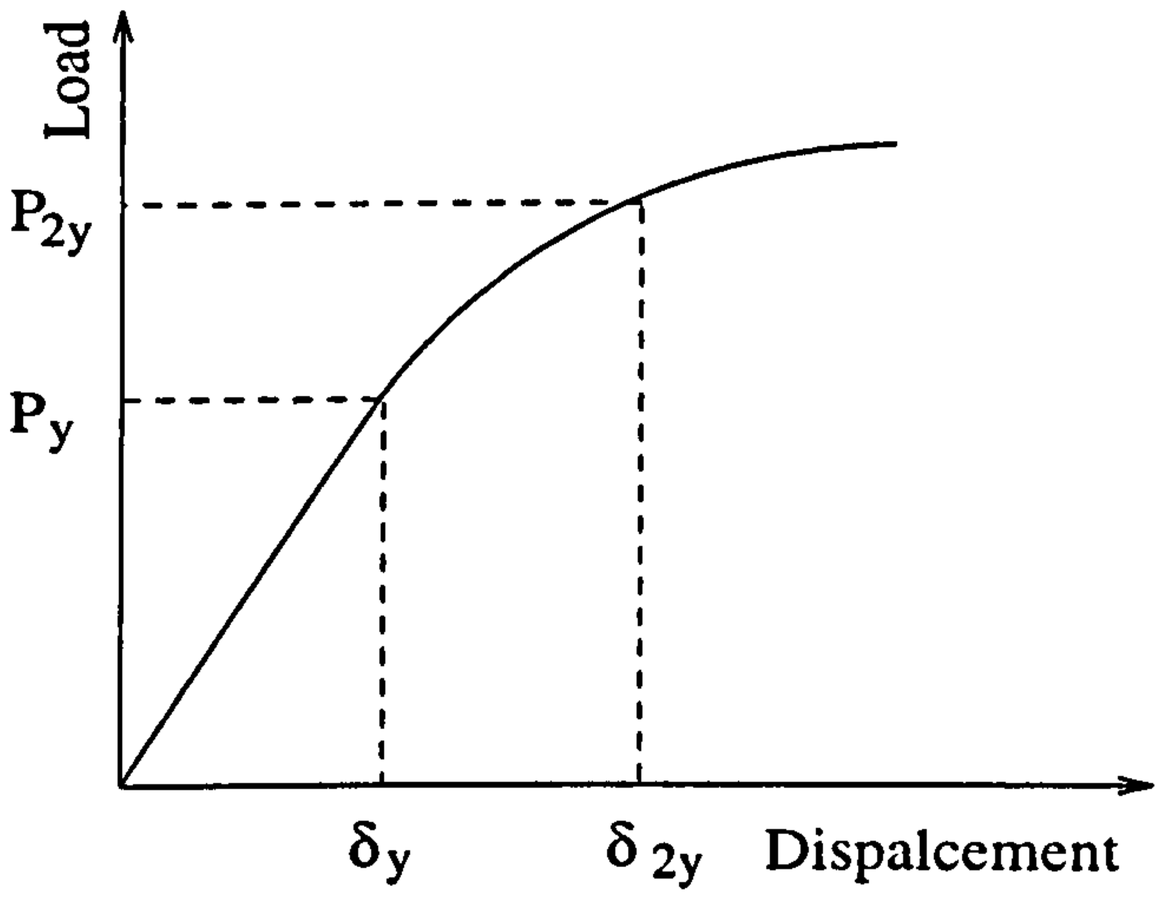

Figure 5.7: Twice-elastic-deformation load method

reported that this method is the most conservative but is subject to error through the approximation of the yield.

Twice-Elastic Slope Load (P_ϕ)

This collapse load is defined to be the value at the intercept of a line drawn from the origin of a load and displacement curve at a slope of twice the value of the slope of the elastic portion of the curve as shown in Figure 5.8. This method has been adopted in Section III [1975] and Section VIII [1977] of the ASME Boiler and Pressure Vessel Code. The definition can be expressed as:

$$P = P_\phi, \quad when \quad \tan\phi = 2\tan\theta$$

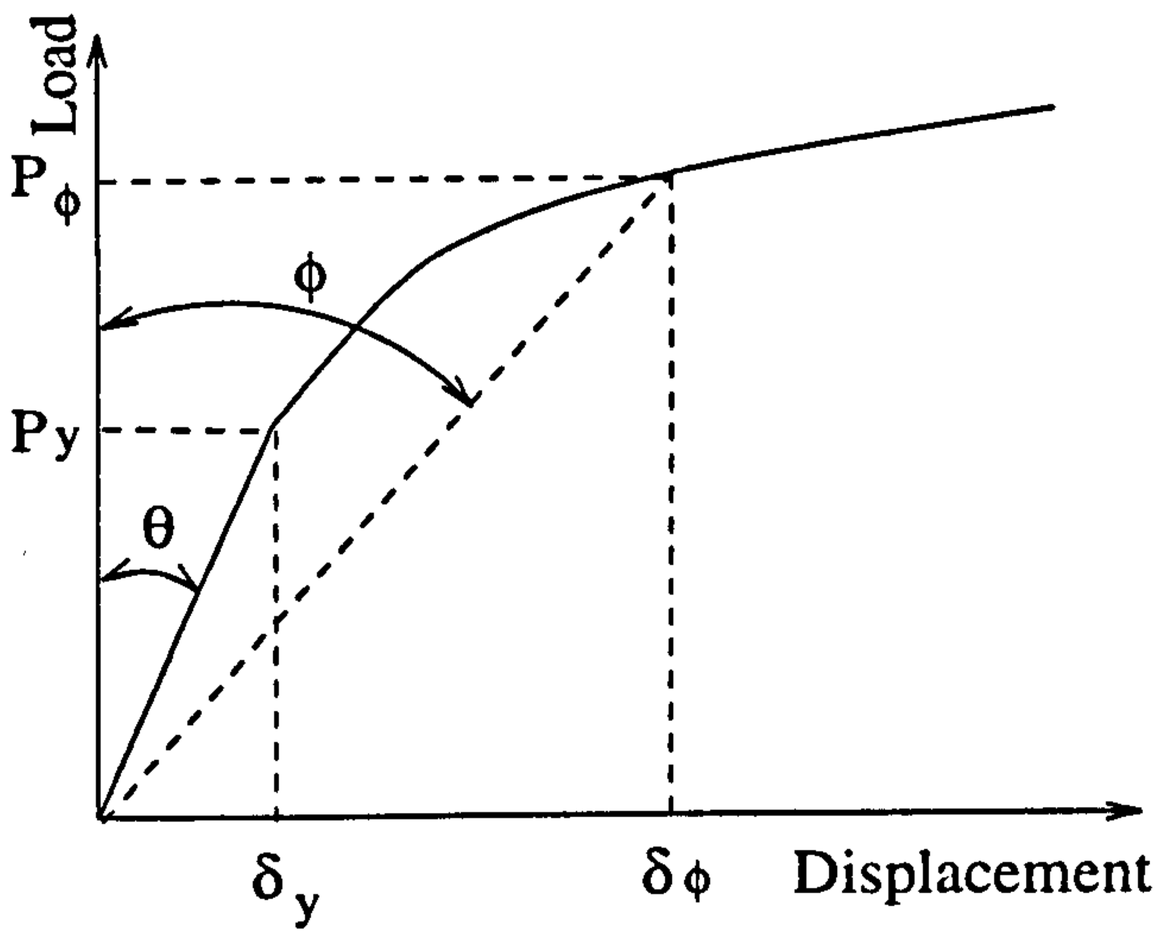

Figure 5.8: Twice-elastic-slope method

where

P_ϕ = the twice-elastic-slope pressure

$\tan\theta$ = slope of the elastic portion of the curve

This method is least subject to error but is impossible to evaluate in some cases.

0.2 Percent Offset Strain Load ($P_{0.2}$)

This is defined as the load causing a permanent strain of 0.2 per cent. This is similar to the 0.2% offset definition used to define yield strength under simple tension. A strain basis for defining a plastic load may be subjected to error in locating the exact location of the maximum strain. Strain is also a load phenomenon, say a bending strain at a yield hinge, and is not indicative of overall plastic collapse as other yield hinges may be present.

5.4.1 Finite Element Model

The finite element models of each geometry were also developed using eight node axisymmetric solid element in *ANSYS* (PLANE82). The element has plasticity, large deformation and large strain capabilities and is well suited for modeling complex structures. The models were restrained in the meridional direction.

but allowed to move radially, at a distance sufficiently far removed from the nozzle. The finite element meshes are the same as used for elastic compensation.

5.4.2 Limit Loads from Elasto-Plastic Analysis

The twice elastic slope method was used as a basis of obtaining the elasto-plastic limit loads. These were obtained from graphs plotting the applied load and the displacement. The results calculated are also normalised according to the expression

$$\overline{P} = \frac{R}{2T\sigma_y} P$$

The elasto-plastic limit loads for all models were tabulated in Table 5.4 to 5.10 and also shown in Figures 5.10 to 5.16.

The normalised elasto-plastic limit pressures, $\overline{P_p}$ are compared with the lower and upper bound limit loads obtained by the elastic compensation method in Tables 5.4-5.10 and Figures 5.10-5.16.

5.5 Discussion of Results

Figure 5.9 shows that the lower bound pressures for the models 1-9 calculated using 2D solid element PLANE82 are slightly lower than Leckie and Payne's plot [1965] except for values of ρ larger than 1 where the obtained results are much lower than values of Leckie and Payne with the value of ρ increasing. The upper bound limit pressures calculated for all nine models are higher than the results of Leckie and Payne. These results form good limit bounds for the models.

For three sets of thinner nozzles, i.e. $R/T = 100,\ 50,\ 25$. it can be seen from Figures 5.10 to 5.12 that the lower bound limit pressures calculated are generally close to the results of Robinson and Gill [1973] and the obtained upper bound limit loads are close to the values of elasto-plastic analyses.

Figures 5.13 to 5.16 show that for thicker models, i.e. $R/T = 10.\ 8.33.\ 7.14.\ 6.25.$ the upper bound limit loads calculated are very close to but slightly higher than the elasto-plastic limit loads, but the lower bound limit loads are much lower.

5.6 Concluding Comments

Comparing the results of the parametric study with results from literature and incremental elastic-plastic analysis (with an elastic-perfectly plastic material model) indicates that the elastic compensation method is a robust method for bounding limit loads without recourse to complex incremental elastic-plastic analysis. The results of the study also indicate that whilst the lower bound limit load is a function of the dimensionless geometry parameter ρ used by Leckie *et al*, Figures 5.17 to 5.18, it cannot be fully characterised by this single parameter. The spread in the results for the lower and upper bound limit pressure for the various R/T ratios indicates that this parameter also has an influence.

5.7 References

Allman, D. and Gill, S.S., (1968), The effects of change of geometry on the limit pressure of flush nozzles in spherical pressure vessels, *Int. J. Mech. Sci.*, **7**. 21–42.

ASME Boiler and Pressure Vessel Code, (1974), Section III, Division 1. Par. 1430, Appendix II.

ASME Boiler and Pressure Vessel Code, (1975), Section III, Division 1. Par. 1430, 1975 Winter Addendum.

ASME Boiler and Pressure Vessel Code, (1977), Section VIII, Division 2. Appendix 4, Par. 4-136.3 and Appendix 6, Par. 6-153.

Cloud, R. L., (1965), Limit pressure of radial nozzles in spherical shells. *Nuclear Struct. Engrg.*, **1**, 403–413.

Dinno, L.S., and Gill, S.S., (1965a), The limit analysis of a pressure vessel consisting of the junction of a cylindrical and spherical shell, *Int. J. Mech. Sci.*, **7**, 21–42.

Dinno, L.S., and Gill, S.S., (1965b), Experimental investigation into plastic behaviour of flush nozzles in spherical pressure vessels, *Int. J. Mech. Sci.*. **7**, 817.

Drucker , D.C., and Shield, R.T., (1959), Limit analysis of symmetrically loaded thin shells of revolution, *Trans. ASME*, Vol.81, Ser. E, 61–68.

Ellyin, F., and Sherbourne, A.N., (1965a), Limit analysis of axisymmetric intersecting shells of revolution, *Nucl. Struct. Engng.*, **2**, 86.

Ellyin, F., and Sherbourne, A.N., (1965b), The collapse of cylinder/sphere intersection pressure vessel, *Nucl. Struct. Engng.*, **2**, 169–180.

Gerdeen, J.C., (1982), *Limit Analysis and Plasticity*, Pressure Vessel and Piping Design Technology, A decade of progress, ASME.

Gill, S.S., (1964), The limit pressure for a flush cylindrical nozzle in spherical pressure vessel, *Int. J. Mech. Sci.*, 6, 105–115.

Gill, S.S., (1970), *The Stress Analysis of Pressure Vessles & Pressure Vessle Componemts*, Pergamon.

Leckie, F.A. and Payne, D.J., (1965-1966), Some observations on the design of spherical pressure vessels with flush cylindrical nozzles, *Proc. Inst. Mech. Engineers*, Vol. 180, Part I, No. 20, 497–501.

Lind, N.C., (1964), Plastic analysis of radial outlets from spherical pressure vessels, *ASME J. Eng. Industry* 86, Ser. B, 193–198.

Mackenzie, D., Shi, J., Nadarajah, C. and Boyle, J.T., (1992). An iterative elastic analysis procedure for estimating lower bound limit loads, *PVP-Vol. 230*, ASME, 129–134.

Mackenzie, D., Nadarajah, C., Shi, J., and Boyle, J.T., (1993). Simple bounds on limit loads by elastic finite element analysis, *J. Pres. Ves. Technology*. Vol.115, 27–31.

Nakamura, T., (1963), in *I.A.S.S. Symposium*, Warsaw, 768.

Nadarajah, C., (1993), *A Design Study of Nozzles and Attachments in Pressure Vessels*, Doctoral Thesis, University of Strathclyde, Glasgow.

Nadarajah, C., Mackenzie, D., and Boyle, J.T., (1993), A method of estimating limit loads by iterative elastic analysis: II-Nozzle sphere intersections with internal pressure and radial load, *Int. J. Pres. Ves. Piping*. Vol. 53. No. 1, 77–95.

Nadarajah, C., Mackenzie, D., and Boyle, J.T., (1995), Approximate limit and shakedown analysis of nozzle-cylinder intersections under internal pressure and in-plane moment loading, *Int. J. Pres. Ves. Piping*. under review.

Robinson, M., and Gill, S. S., (1973), Limit analysis of flush radial and oblique cylindrical nozzles in spherical pressure vessels. Part 1: A parametric survey of results, *Int. J. of Pressure Vessel and Piping*, Vol. 1. No. 3. July. 199-231.

Table 5.3: *Normalised lower and upper bound limit pressure of nozzles versus* ρ. $r = 200mm, \quad R = 1000mm$

Nozzle	$T(mm)$	ρ	$\bar{P}_y$	$\bar{P}_l$	$\bar{P}_u$	L+P
1	250	0.4	0.361	0.923	1.000	0.969
2	160	0.5	0.414	0.898	0.990	0.944
3	111.1	0.6	0.446	0.862	0.974	0.911
4	81.6	0.7	0.463	0.818	0.952	0.876
5	62.5	0.8	0.468	0.777	0.923	0.841
6	40	1.0	0.435	0.696	0.850	0.775
7	33.06	1.1	0.399	0.659	0.812	0.747
8	27.8	1.2	0.393	0.615	0.770	0.725
9	23.67	1.3	0.366	0.577	0.741	0.700

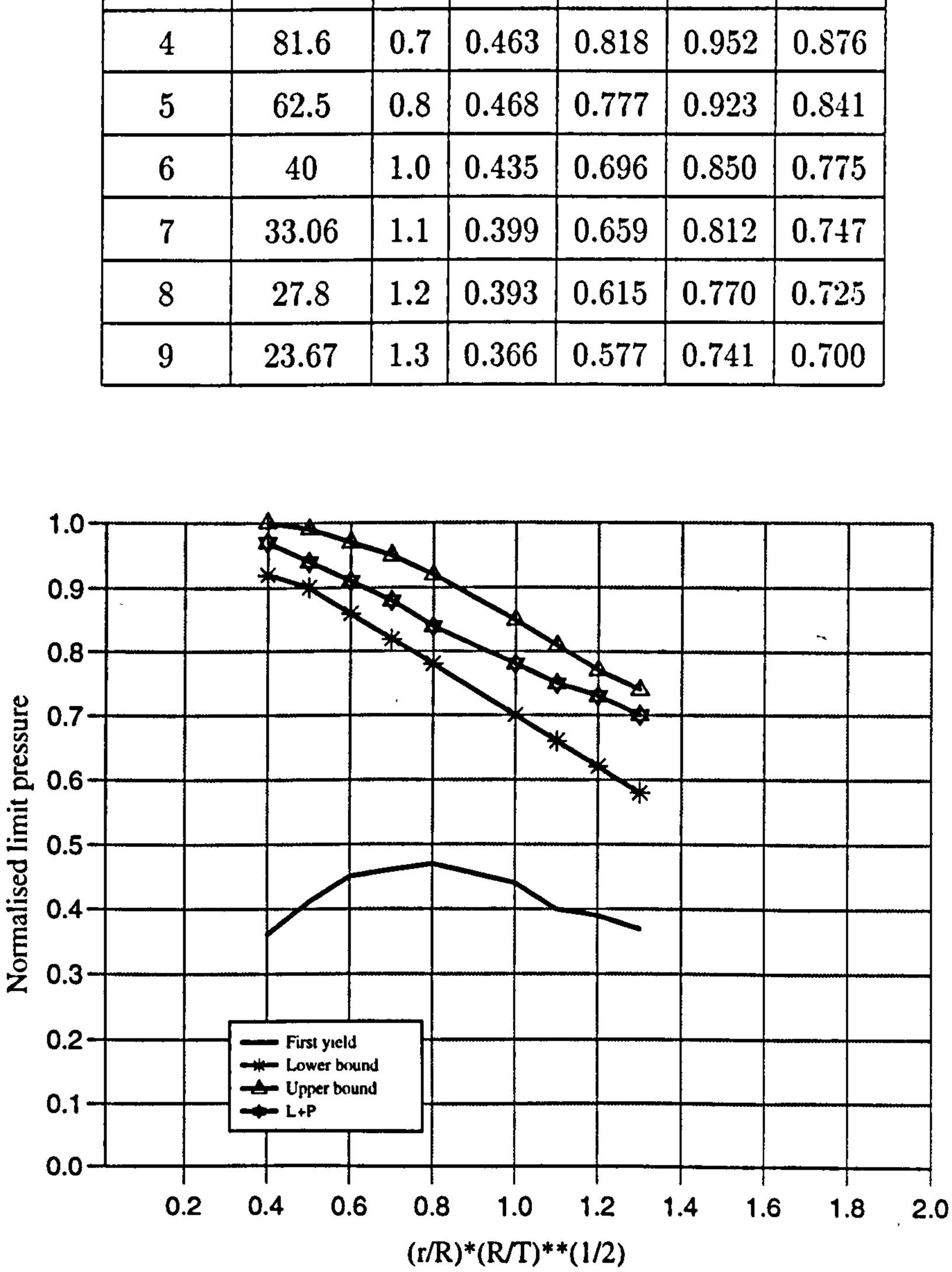

Figure 5.9: Normalised lower and upper bound limit pressure of nozzles versus ρ. $r = 200mm, \quad R = 1000mm$

Table 5.4: *Normalised lower and upper bound limit pressure of nozzles.* $T = 10mm$, $R/T = 100$

Nozzle	$r(mm)$	ρ	$\bar{P}_y$	$\bar{P}_l$	$\bar{P}_u$	P_{R+G}	P_P
10a	10	0.1	0.429	0.953	1.0	—	0.992
10b	20	0.2	0.442	0.904	1.0	—	0.992
10c	30	0.3	0.459	0.885	1.0	—	0.975
10e	50	0.5	0.47	0.85	0.993	0.876	0.958
10f	60	0.6	0.469	0.799	0.993	0.836	0.917
10g	70	0.7	0.465	0.769	0.968	0.80	0.883
10h	80	0.8	0.459	0.709	0.918	0.744	0.85
10i	90	0.9	0.44	0.698	0.901	0.71	0.817
10j	100	1.0	0.412	0.651	0.817	0.68	0.792
10k	200	2.0	0.257	0.455	0.561	0.472	0.542

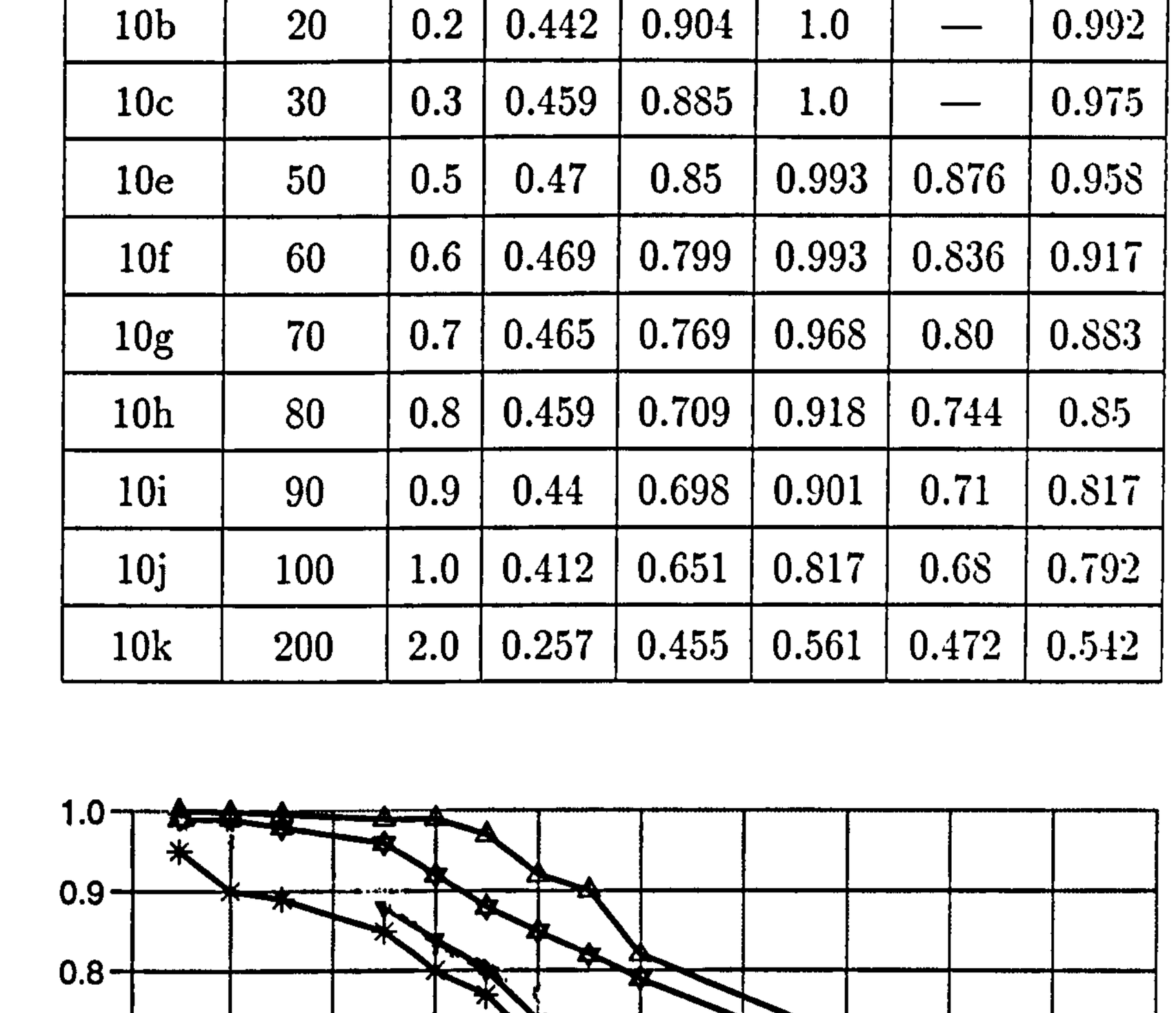

Figure 5.10: Normalised lower and upper bound limit pressure of nozzles. $T = 10mm$, $R/T = 100$

Table 5.5: *Normalised lower and upper bound limit pressure of nozzles,* $T = 20mm$, $R/T = 50$

Nozzle	$r(mm)$	ρ	$\bar{P}_y$	$\bar{P}_l$	$\bar{P}_u$	P_{R+G}	P_P
10	14.14	0.1	0.469	0.955	1.0	—	0.992
11	28.28	0.2	0.436	0.9	1.0	—	0.992
12	56.57	0.4	0.464	0.833	0.997	0.928	0.967
13	70.71	0.5	0.471	0.803	0.99	0.888	0.933
14	84.85	0.6	0.473	0.776	0.977	0.846	0.90
15	98.99	0.7	0.471	0.745	0.955	0.81	0.867
16	113.1	0.8	0.467	0.715	0.923	0.774	0.833
17	127.3	0.9	0.448	0.685	0.884	0.736	0.817
18	141.2	1.0	0.419	0.657	0.843	0.704	0.783
19	212.1	1.5	0.32	0.541	0.683	0.583	0.658
20	282.8	2.0	0.264	0.463	0.584	0.496	0.55

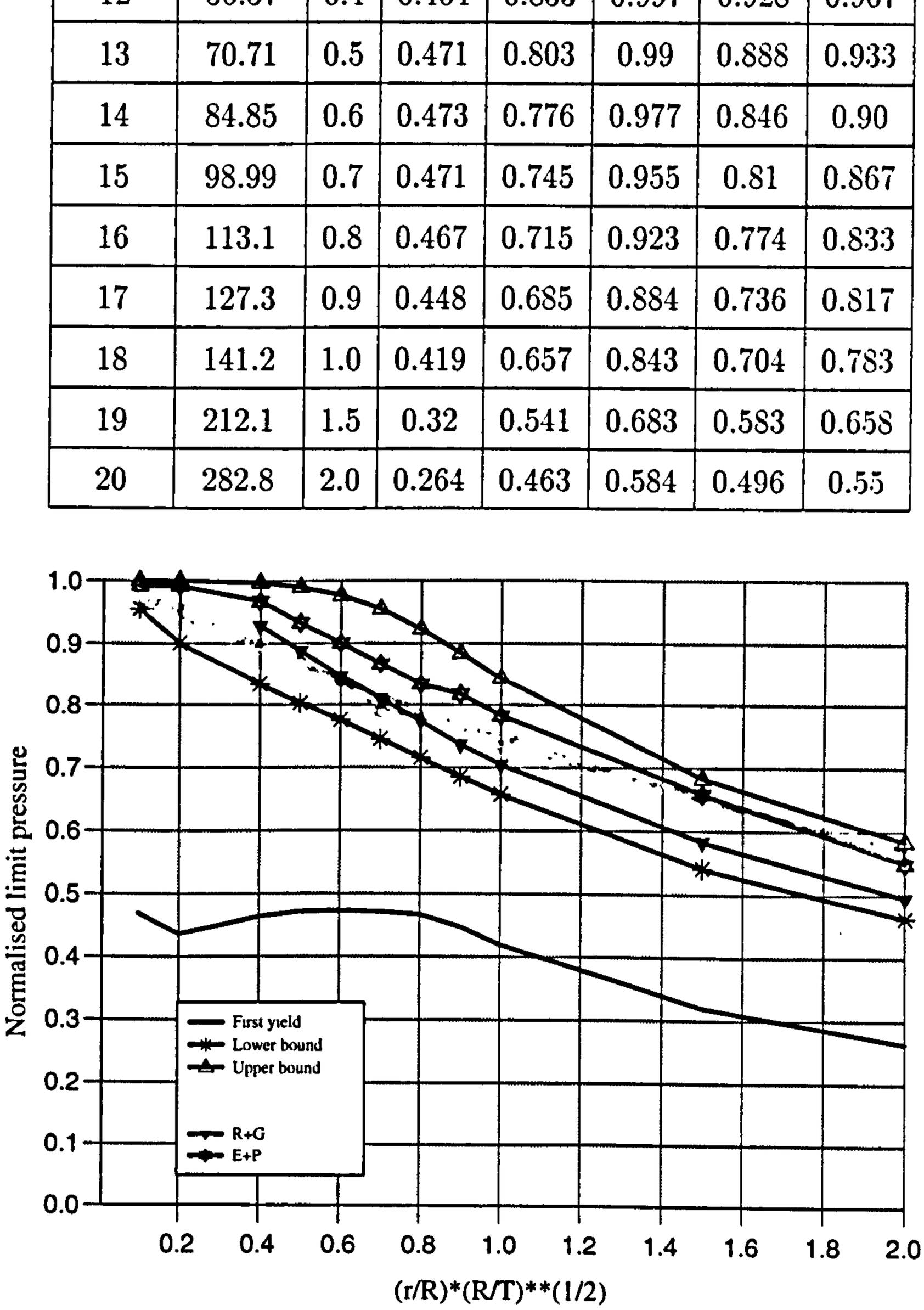

Figure 5.11: Normalised lower and upper bound limit pressure of nozzles, $T = 20mm$, $R/T = 50$

Table 5.6: *Normalised lower and upper bound limit pressure of nozzles,* $T = 40mm$, $R/T = 25$

Nozzle	$r(mm)$	ρ	$\bar{P}_y$	$\bar{P}_l$	$\bar{P}_u$	P_{R+G}	P_P
21	40	0.2	0.432	0.92	1.0	—	0.996
22	60	0.3	0.443	0.888	0.999	0.974	0.992
23	80	0.4	0.457	0.859	0.996	0.941	0.975
24	100	0.5	0.467	0.829	0.99	0.905	0.958
25	120	0.6	0.471	0.802	0.976	0.87	0.917
26	140	0.7	0.473	0.774	0.954	0.832	0.896
27	160	0.8	0.471	0.748	0.924	0.80	0.867
28	180	0.9	0.467	0.718	0.888	0.768	0.838
29	200	1.0	0.462	0.692	0.851	0.74	0.808
30	300	1.5	0.353	0.579	0.702	0.615	0.675
31	400	2.0	0.291	0.495	0.607	0.518	–

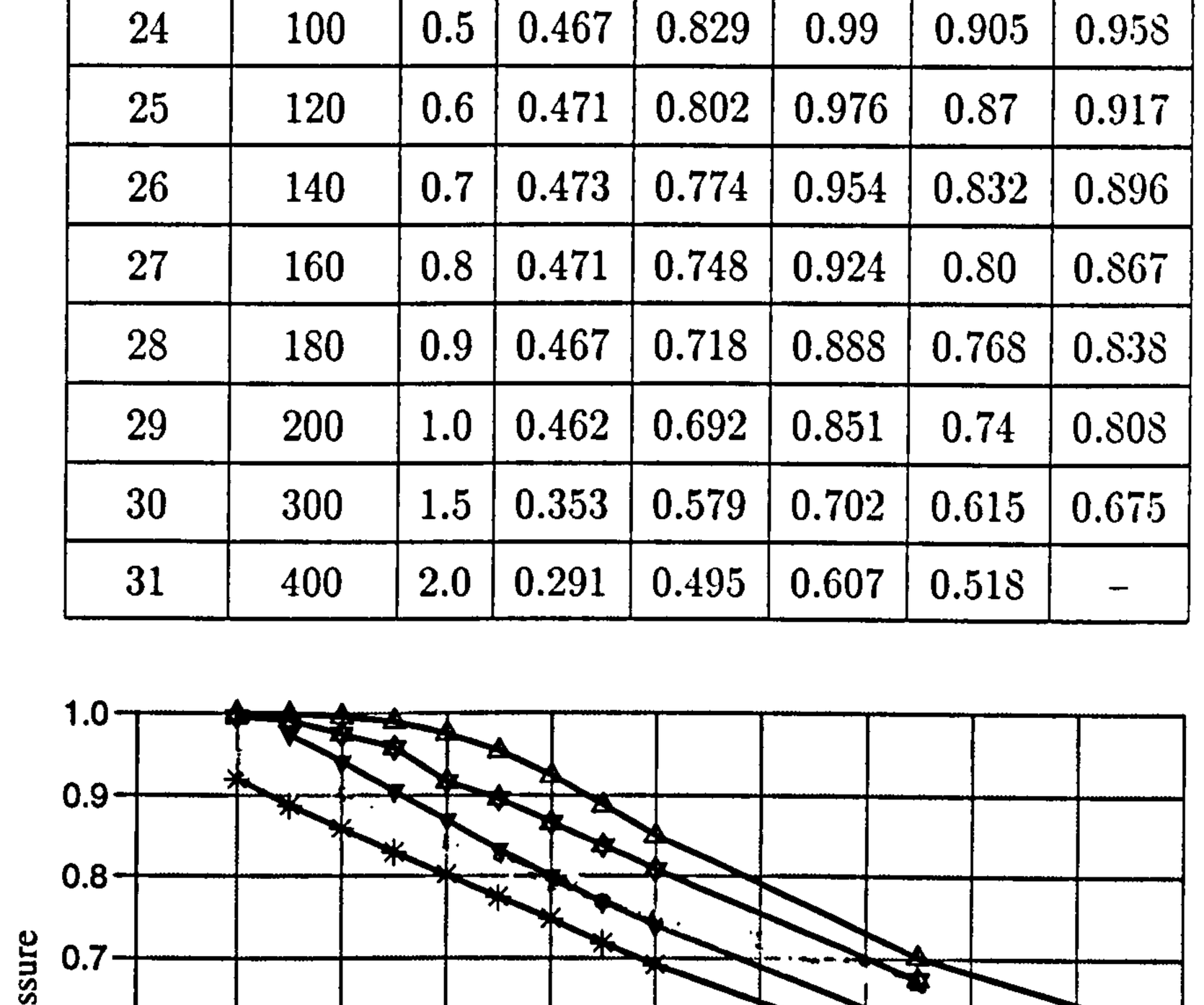

Figure 5.12: Normalised lower and upper bound limit pressure of nozzles, $T = 40mm$, $R/T = 25$

Table 5.7: *Normalised lower and upper bound limit pressure of nozzles.* $T = 100mm$, $R/T = 10$

Nozzle	$r(mm)$	ρ	$\bar{P}_y$	$\bar{P}_l$	$\bar{P}_u$	P_P
32	63.24	0.2	0.424	0.949	1.0	1.0
33	94.87	0.3	0.407	0.934	1.0	0.992
34	126.5	0.4	0.426	0.909	0.997	0.983
35	158.1	0.5	0.441	0.880	0.990	0.975
36	189.7	0.6	0.451	0.855	0.975	0.950
37	221.4	0.7	0.457	0.830	0.951	0.917
38	253.0	0.8	0.459	0.802	0.920	0.883
39	284.6	0.9	0.459	0.775	0.886	0.850
40	316.2	1.0	0.457	0.748	0.851	0.825
41	474.3	1.5	0.372	0.629	0.712	0.692
42	632.5	2.0	0.317	0.552	0.631	0.608

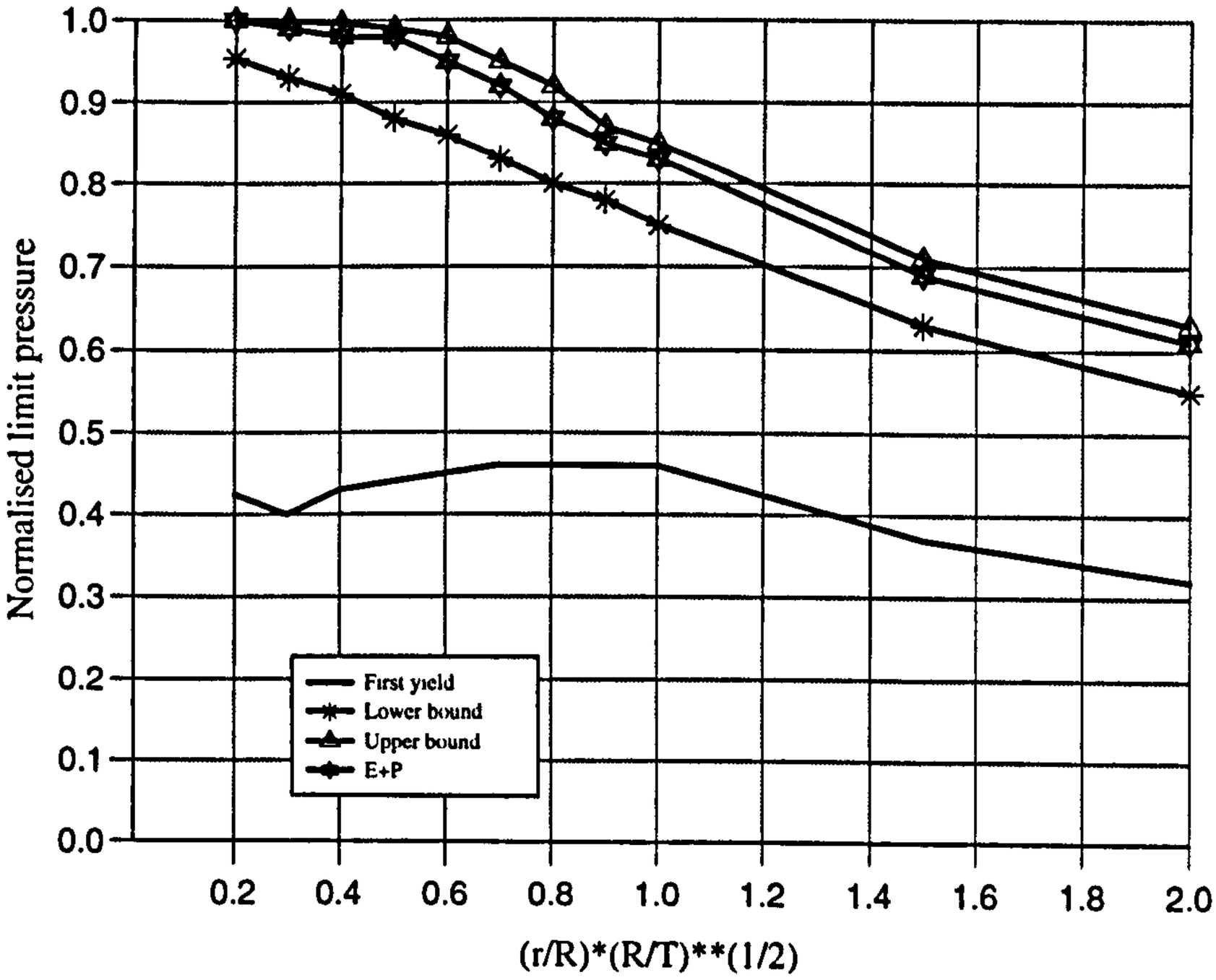

Figure 5.13: Normalised lower and upper bound limit pressure of nozzles. $T = 100mm$, $R/T = 10$

Table 5.8: *Normalised lower and upper bound limit pressure of nozzles.* $T = 120mm$, $R/T = 8.33$

Nozzle	$r(mm)$	ρ	$\bar{P}_y$	$\bar{P}_l$	$\bar{P}_u$	P_P
43	69.28	0.2	0.455	0.950	1.0	1.0
44	103.92	0.3	0.401	0.936	1.0	1.0
45	138 56	0.4	0.417	0.912	0.998	0.993
46	173.21	0.5	0.432	0.884	0.990	0.972
47	207.85	0.6	0.443	0.859	0.974	0.944
48	242.49	0.7	0.450	0.833	0.950	0.917
49	277.13	0.8	0.453	0.801	0.918	0.896
50	311.77	0.9	0.454	0.779	0.883	0.861
51	346.41	1.0	0.453	0.749	0.849	0.833
52	519.62	1.5	0.385	0.630	0.713	0.708
53	692.82	2.0	0.337	0.555	0.637	0.625

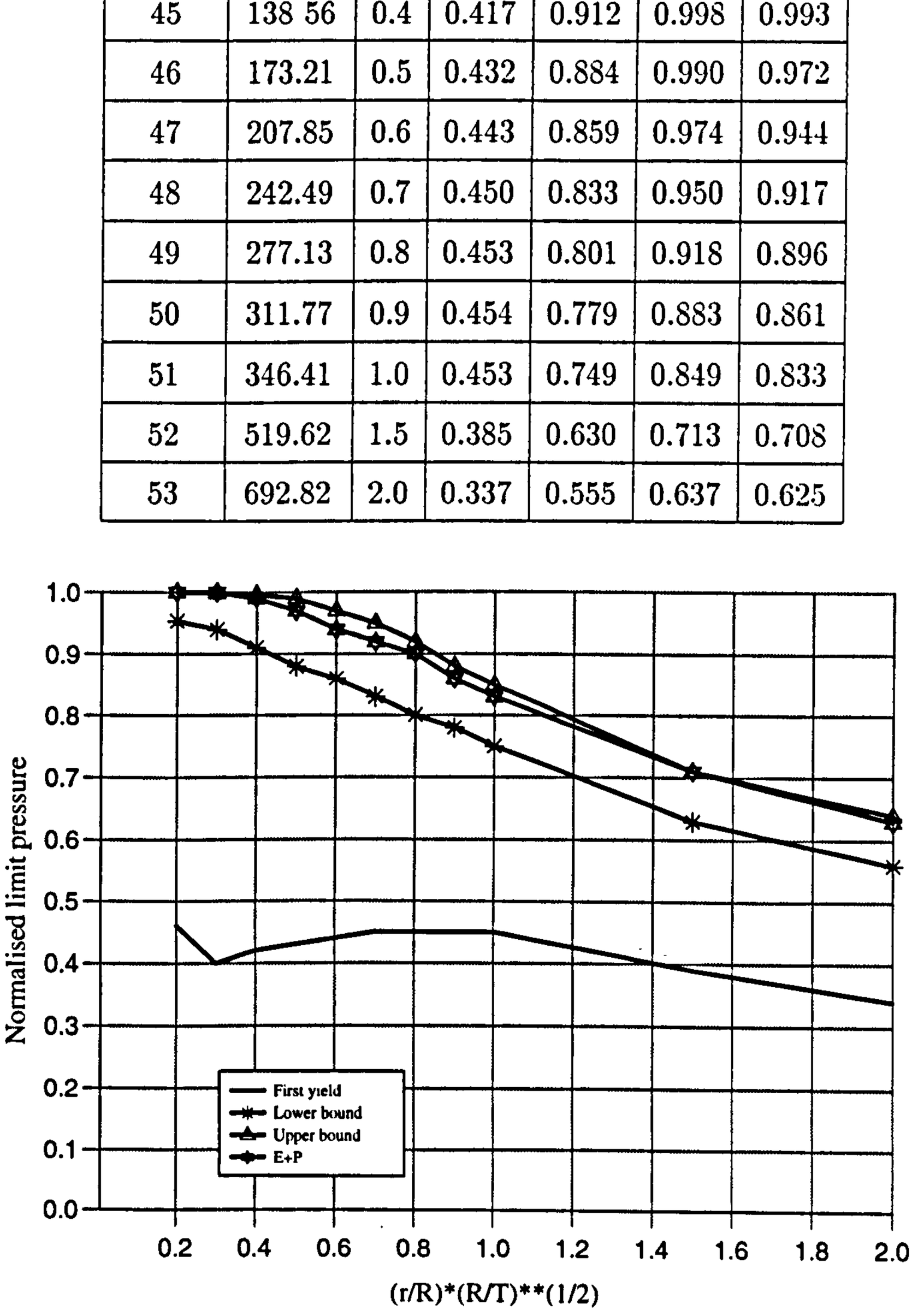

Figure 5.14: Normalised lower and upper bound limit pressure of nozzles. $T = 120mm$, $R/T = 8.33$

Table 5.9: *Normalised lower and upper bound limit pressure of nozzles.* $T = 140mm$, $R/T = 7.14$

Nozzle	$r(mm)$	ρ	$\bar{P}_y$	$\bar{P}_l$	$\bar{P}_u$	P_P
54	112.4	0.3	0.394	0.936	1.0	1.0
55	149.67	0.4	0.408	0.913	0.999	0.994
56	187.08	0.5	0.423	0.886	0.996	0.976
57	224.5	0.6	0.435	0.861	0.974	0.952
58	261.92	0.7	0.443	0.836	0.948	0.926
59	299.33	0.8	0.447	0.803	0.916	0.893
60	336.75	0.9	0.449	0.777	0.882	0.863
61	374.17	1.0	0.448	0.749	0.847	0.833
62	467.7	1.25	0.442	0.685	0.771	0.762
63	562.25	1.5	0.399	0.628	0.712	0.702
64	654.79	1.75	0.370	0.590	0.670	0.655

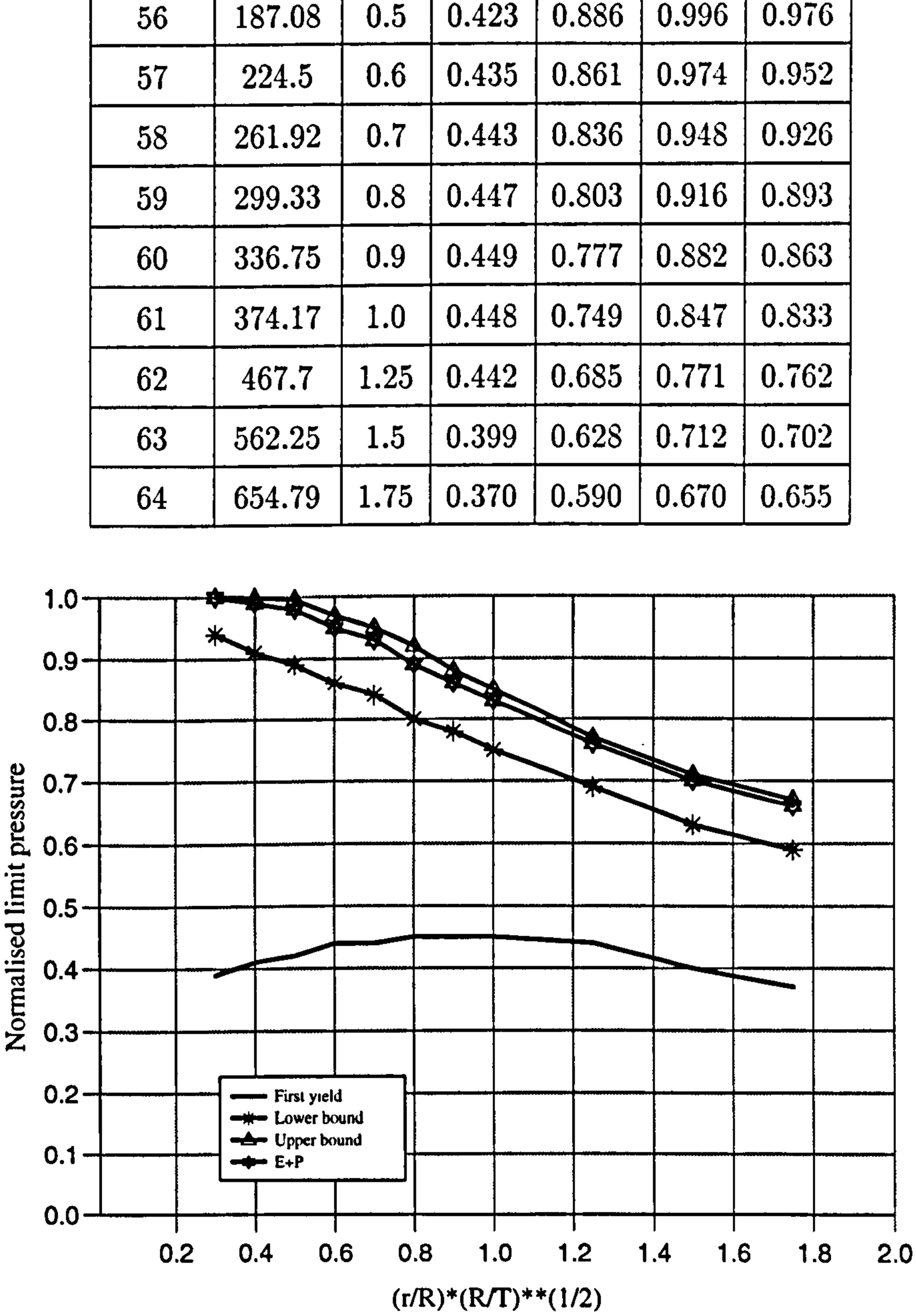

Figure 5.15: Normalised lower and upper bound limit pressure of nozzles. $T = 140mm$, $R/T = 7.14$

Table 5.10: *Normalised lower and upper bound limit pressure of nozzles.* $T = 160mm$, $R/T = 6.25$

Nozzle	$r(mm)$	ρ	$\bar{P}_y$	$\bar{P}_l$	$\bar{P}_u$	P_P
65	120	0.3	0.389	0.936	1.0	1.0
66	160	0.4	0.399	0.914	0.999	0.995
67	240	0.6	0.427	0.862	0.973	0.958
68	280	0.7	0.436	0.837	0.947	0.927
69	320	0.8	0.441	0.804	0.914	0.896
70	360	0.9	0.443	0.777	0.879	0.864
71	400	1.0	0.443	0.748	0.845	0.833
72	500	1.25	0.439	0.686	0.769	0.760
73	600	1.5	0.414	0.627	0.712	0.798
74	700	1.75	0.389	0.586	0.672	0.656

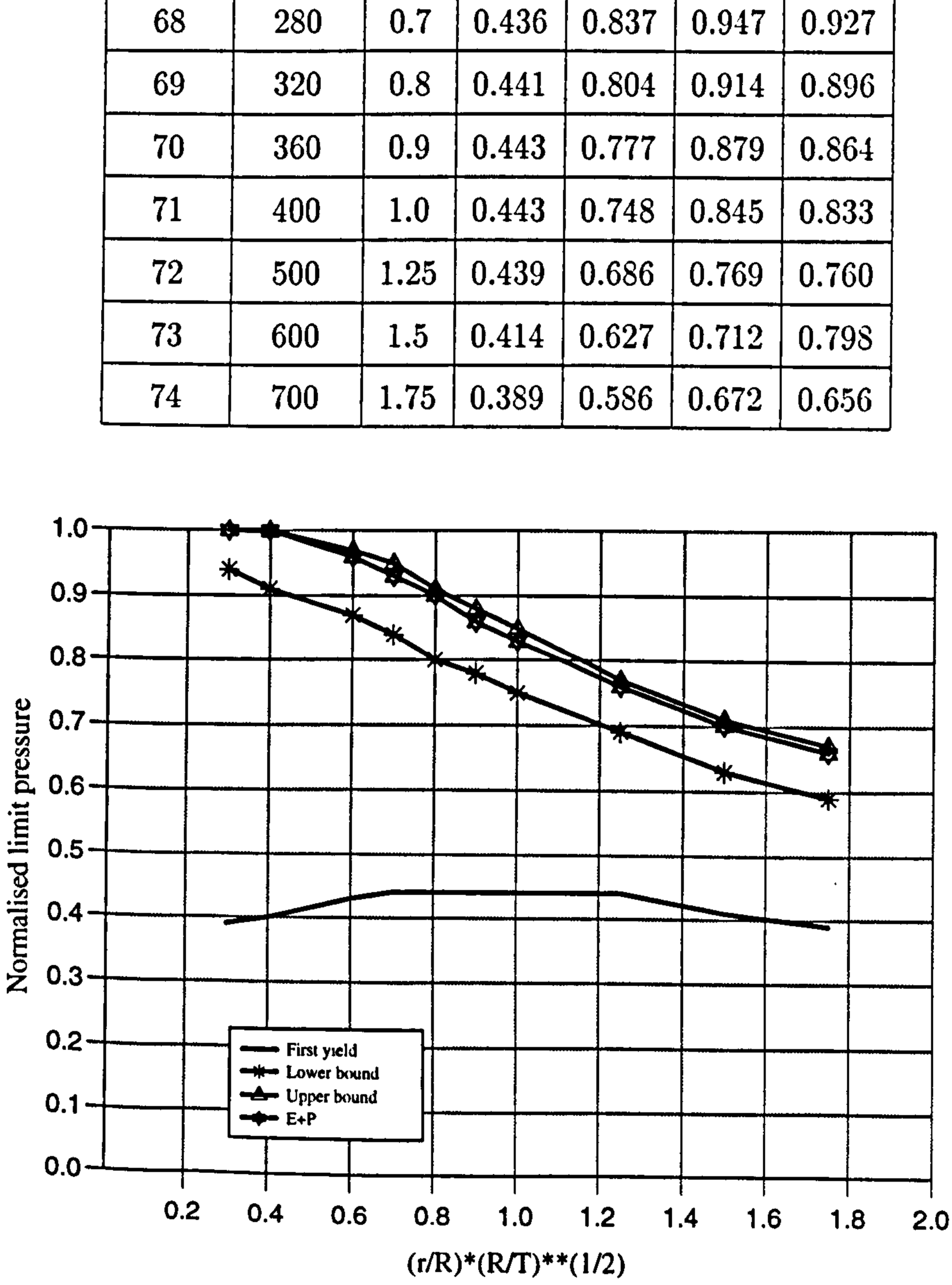

Figure 5.16: Normalised lower and upper bound limit pressure of nozzles. $T = 160mm$, $R/T = 6.25$

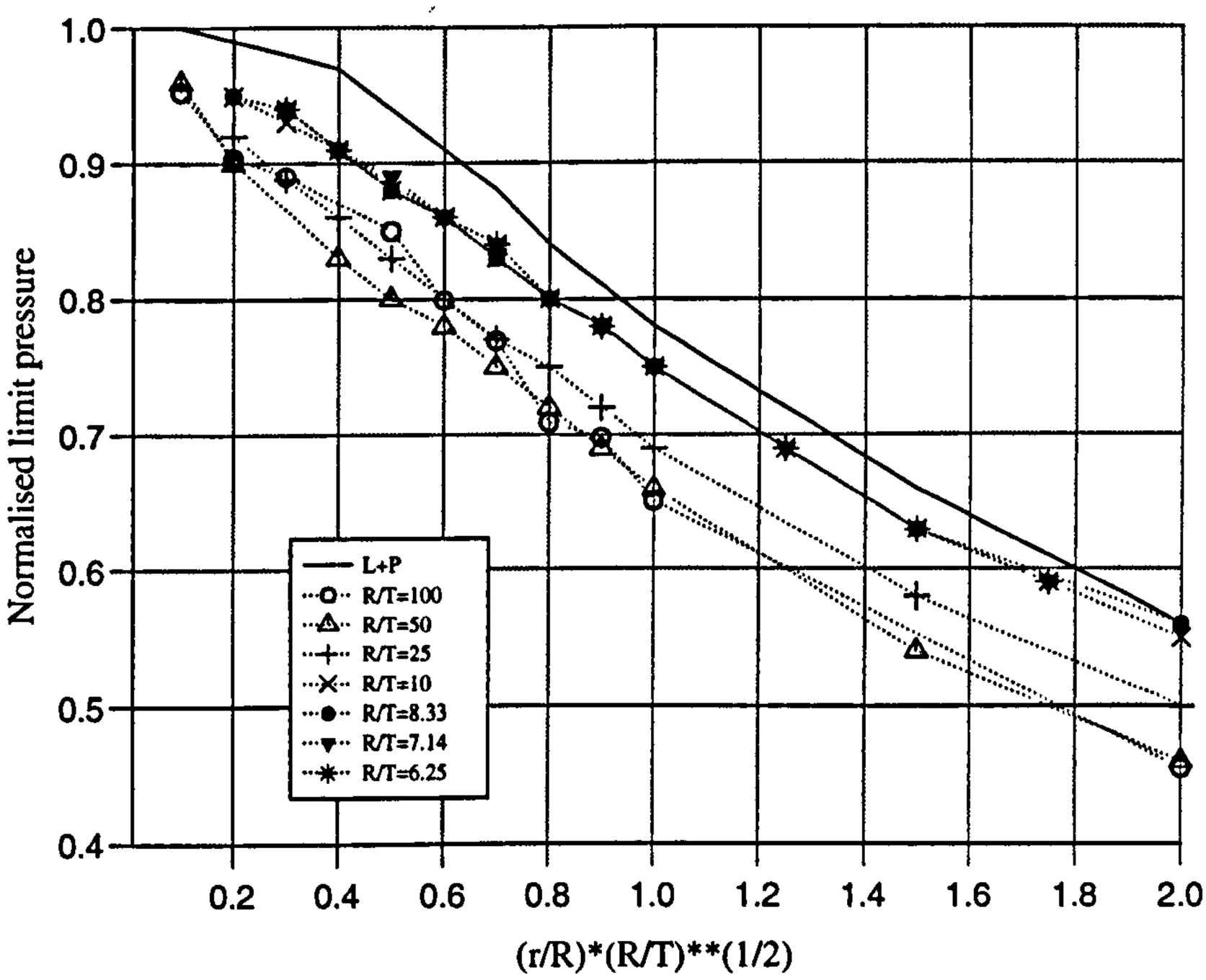

Figure 5.17: Normalised lower bound limit pressure of nozzles versus ρ, summary of results

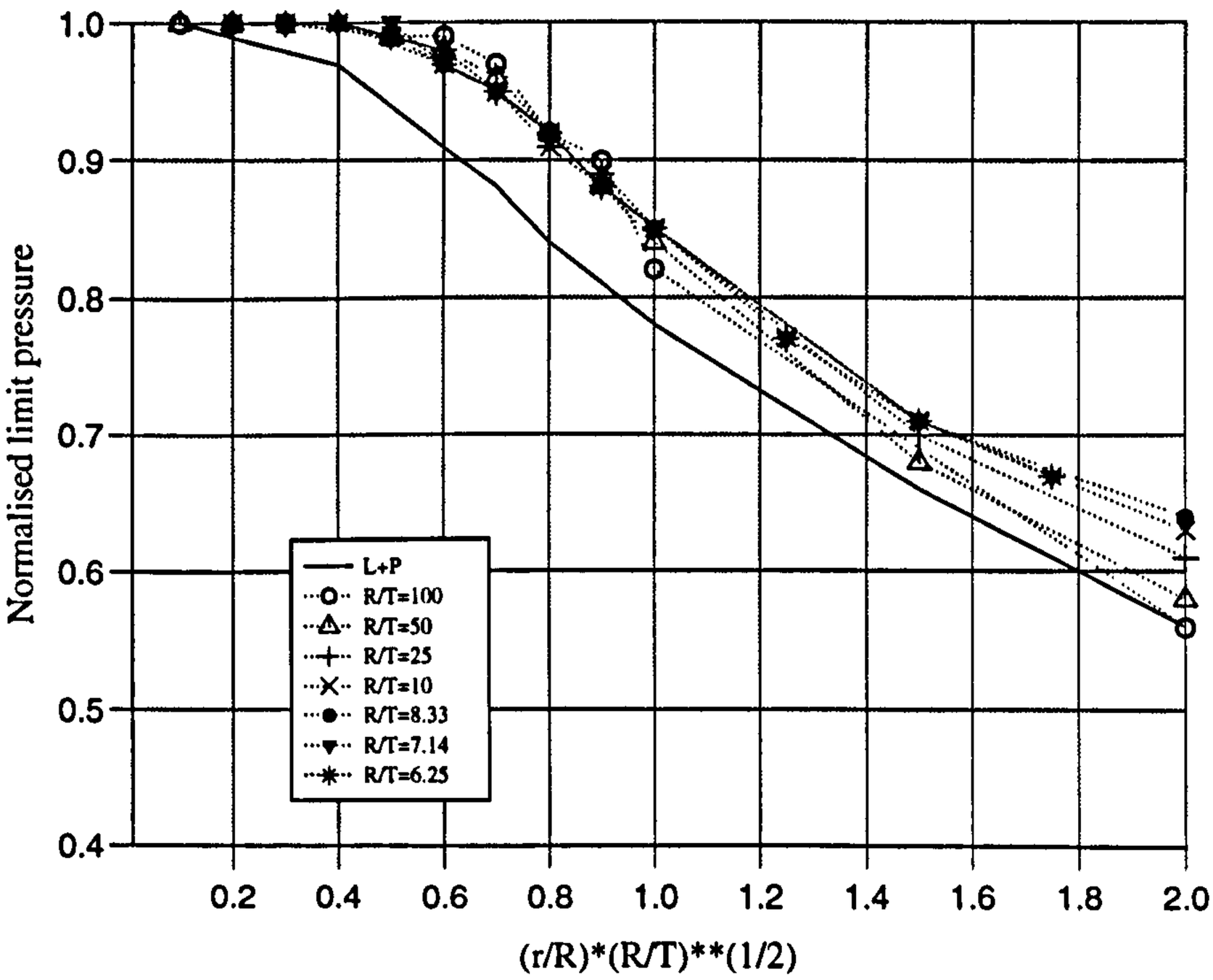

Figure 5.18: Normalised upper bound limit pressure of nozzles versus ρ, summary of results

CHAPTER 6

SHAKEDOWN ANALYSIS OF NOZZLES IN SPHERICAL PRESSURE VESSELS

6.1 Introduction

Currently design of pressure vessels allows plastic deformations to occur at discontinuities such as nozzle intersections. While it is possible to calculate the stress and strain distribution in the elastic-plastic range, the results of these calculations are of limited use because they are so dependent on residual stresses and loading history. Limit load and shakedown performance however are history independent and for that reason do provide practical guidance in making design decisions. If a structure is loaded statically, a knowledge of its limit load is usually sufficient. When the loading is cyclic shakedown performance becomes important because, by restricting the cyclic loading to the shakedown limit, the designer is assured that, after initial plastic deformation, further deformation is in the elastic range; the possibilities of incremental collapse or reversed plasticity are thus removed.

Limit pressures have already been obtained for the problem of radial nozzle intersecting a spherical pressure vessel in the previous Chapter. In this Chapter, lower and *new* upper bound shakedown pressures for the same problem will be estimated by the elastic compensation method.

6.2 A Brief Review of Shakedown Analysis of Nozzles in Spherical Pressure Vessel

Melan's lower bound shakedown theorem was first applied to the shakedown of pressure vessels by Leckie [1965]. Using only the elastic solution and Tresca yield criterion, he obtained lower bound shakedown factors for radial nozzles in

spheres under internal pressure. Later Leckie and Penny [1967] found the lower bound estimates of shakedown pressure, thrust and moment loadings for a nozzle/sphere intersection by using standard linear programming techniques. Their results have been presented in a useful graphical form. Findlay and Spence [1968] explained how shakedown loads could be obtained from a knowledge of the post-yield behaviour of pressure vessels. A simple graphical technique to estimate the shakedown loads for both cylinder/sphere and cylinder/cylinder intersections was suggested by Macfarlane and Findlay [1972], while the cyclic pressure tests were carried out on spherical pressure vessels with radial and oblique nozzles by Proctor and Flinders [1972]. The experiments demonstrate that the value of the cyclic pressure at which incremental straining occurs is close to the estimated shakedown pressure.

Recently Lu and Xue [1991] derived lower bound shakedown loads for axisymmetric shells by using the stress function method. In their paper a self-equilibrated stress obtained from the stress functions of thin shells is used for the static shakedown theorem as a residual stress. In combination with finite element method, a linear programming formulation of the shakedown analysis of axisymmetric shells is derived. Some examples of the plates and shells were given by them.

More recently, Mackenzie and Boyle [1993] have proposed a simple method of estimating shakedown loads for complex structures using the elastic compensation procedure. A similar technique has been presented independently by Carter and Ponter [1992].

6.3 Leckie and Penny's Method [1967]

It is worthwhile here recording the method used by Leckie and Penny [1967]. It uses more approximations than elastic compensation, and, in fact, is more elaborate as will be demonstrated below.

6.3.1 Assuptions and Definitions

It is well known for practical pressure vessels that the maximum stresses occur in the spherical portion at the point of intersection, although in some exceptional geometries, when the nozzle is very thin or the opening is large, maximum stresses can occur in the nozzle. In Leckie and Penny's [1967] paper, such exceptional cases were excluded and their investigation was confined to a study of stresses in the sphere. The material of the shell is assumed to be elastic perfectly plastic and to yield according to the Tresca yield criterion. Accordingly if the stresses at the surface are σ_ϕ in the meridional direction, σ_θ in the circumferential direction, and if the radial stress is neglected then the yield criteria are

$$|\sigma_\phi| \leq \sigma_y, \quad |\sigma_\theta| \leq \sigma_y, \quad |\sigma_\phi - \sigma_\theta| \leq \sigma_y \tag{6.1}$$

where σ_y is the yield stress obtained from a simple tension test.

6.3.2 The Elastic Solutions

Elastic solutions were already established, Penny and Leckie [1963]. for the the present geometries subjected to pressure, thrust and moment loadings. The solutions were obtained using the usual procedure of shell analysis of superimposing on to the membrane solution the effects of the edge forces which ensure compatibility of displacement of adjoining shells at their junction. In the case of the axisymmetric loadings of pressure and thrust the two-self-equilibrating edge forces are the horizontal force H and the moment M as shown in Figure 6.1.

6.3.3 The Shakedown Calculation for Pressure Loading

The method is based on Melan's theorem which states:

For a given load set **P**, *if any distribution of self-equilibrating residual stresses can be found which when taken together with elastically calculated stresses constitute a system of stresses within the yield limit (for the whole cycle) then* **P** *is a lower bound shakedown load set and the structure will shakedown.*

In the case of the shell structure under consideration, the local increases of stress are due to the edge forces H and M, and in order to counteract their effect residual self-equilibrating edge forces $\overline{H}$ and $\overline{M}$ in directions opposite to those of H and M were postulated. Within the shell itself, suitable stress systems in equilibrium with $\overline{H}$ and $\overline{M}$ are provided by the linear elastic theory.

For a geometry with given values of r/R, R/T and $t/T = (t/T)_1$, where r is the radius to mid-section of the nozzle, R the radius to mid-section of the shell, t the thickness of the nozzle and T the thickness of the sphere, the stresses at the junction (where they are most severe) given by Leckie and Penny [1967] were:

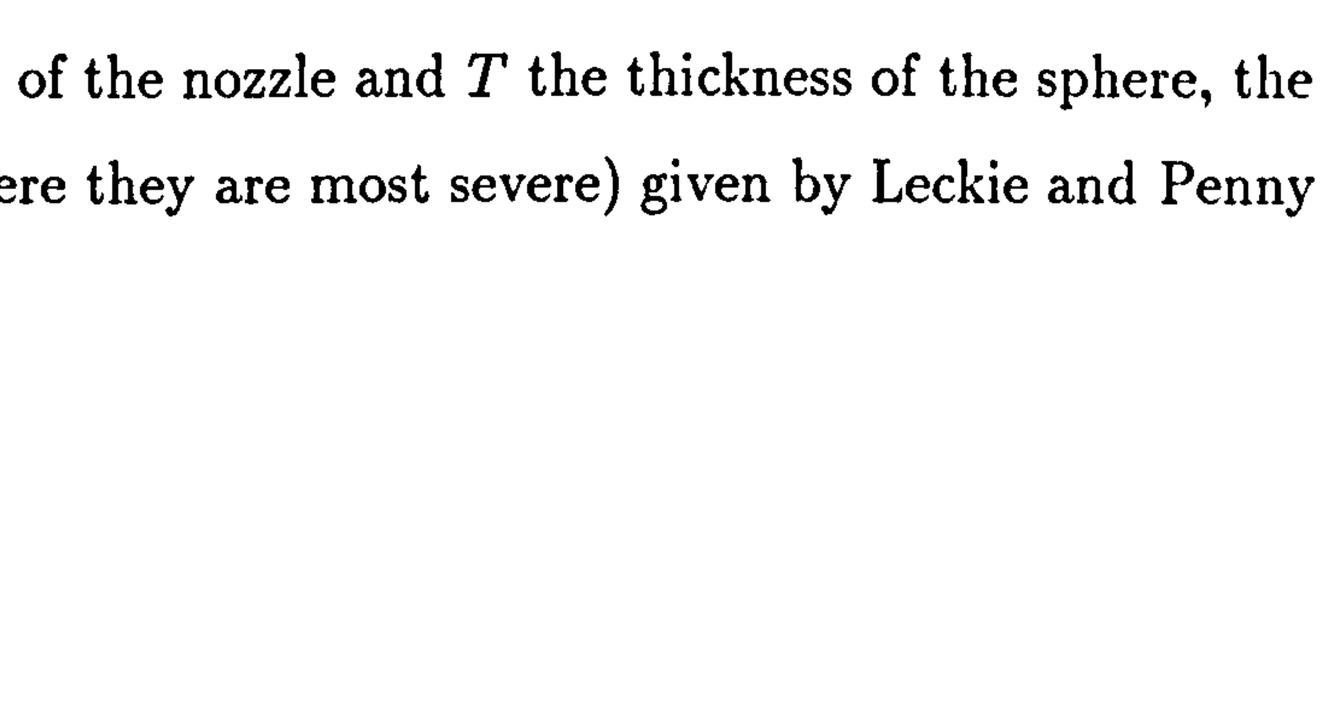

Figure 6.1: Edge forces for axisymmetric loading

	Inner surface	Outer surface
σ_ϕ/σ_y	$p_{11}\bar{p}$	$p_{12}\bar{p}$
σ_θ/σ_y	$p_{13}\bar{p}$	$p_{14}\bar{p}$

where

$$\bar{p} = \frac{pR}{2T\sigma_y}$$

The stresses caused by the edge forces (H_1, M_1) acting alone were found by subtracting the membrane stresses, yielding the following stresses:

	Inner surface	Outer surface
σ_ϕ/σ_y	$(p_{11}-1)\bar{p}$	$(p_{12}-1)\bar{p}$
σ_θ/σ_y	$(p_{13}-1)\bar{p}$	$(p_{14}-1)\bar{p}$

If residual values $\overline{H_1}$ and $\overline{M_1}$ were chosen such that $\overline{H_1} = (-\alpha/p)H_1$ and $\overline{M_1} = (-\alpha/p)M_1$ then the maximum residual stresses were:

	Inner surface	Outer surface
σ_ϕ/σ_y	$-(p_{11}-1)\alpha$	$-(p_{12}-1)\alpha$
σ_θ/σ_y	$-(p_{13}-1)\alpha$	$-(p_{14}-1)\alpha$

(6.2)

These stresses were referred to as the α residual stress group by Leckie and Penny [1967].

Leckie and Penny [1967] then derived a second set of residual stresses by using the results of the elastic calculation for the same values r/R, R/T but using a different value for $t/T = (t/T)_2$. This ensured that the edge forces H_2 and M_2 resulting from such calculations were in a proportion different from that of the H_1, M_1 edge forces. Proceeding as for the α residual stress group and assuming this time residual values of $\overline{H_2} = -(\beta/p)H_2$ and $\overline{M_2} = -(\beta/p)M_2$ then the stresses resulting from the β residual stress group were:

	Inner surface	Outer surface
σ_ϕ/σ_y	$-(p_{21}-1)\beta$	$-(p_{22}-1)\beta$
σ_θ/σ_y	$-(p_{23}-1)\beta$	$-(p_{24}-1)\beta$

(6.3)

Other stress residuals determined by Leckie and Penny [1967] in this way, by selecting another thickness ratio $(t/T)_3$ say, would simply be a linear combination of the previous two results since, at the level of the present calculations. the only unknowns were the residual horizontal force $\overline{H}$ and the residual moment $\overline{M}$.

Using the α and β groups as the assumed residual stresses the total elastic and residual stresses in the loaded state obtained by Leckie and Penny [1967] were:

	Inner surface	Outer surface
σ_ϕ/σ_y	$p_{11}\bar{p}-(p_{11}-1)\alpha-(p_{21}-1)\beta$	$p_{12}\bar{p}-(p_{12}-1)\alpha-(p_{22}-1)\beta$
σ_ϕ/σ_y	$p_{13}\bar{p}-(p_{13}-1)\alpha-(p_{23}-1)\beta$	$p_{14}\bar{p}-(p_{14}-1)\alpha-(p_{24}-1)\beta$

(6.4)

and in the unloaded state the stresses were given by the above stresses with $\bar{p}=0$.

The next step was to find the value of α and β which maximize the value of p according to the 12 limiting conditions

$$-1 \leq \frac{\sigma_\phi}{\sigma_y} \leq 1, \quad -1 \leq \frac{\sigma_\theta}{\sigma_y} \leq 1, \quad -1 \leq \frac{\sigma_\phi \sigma_\theta}{\sigma_y} \leq 1 \tag{6.5}$$

for the inside and outside surfaces and in the loaded and unloaded conditions.

This problem was resolved by Leckie and Penny [1967] using the 'standard form' of linear programming which is stated as follows:

Maximize $f = c_j x_j$ subject to the conditions

$$b_i^L \leq y_i = a_{ij} x_j \leq b_i^u$$

b_i^L and b_i^u are the lower and upper values of a fixed vector. In the present case

$$b_i^L = \{-1\ -1\ -1\ -1\ -1\ -1\ -1\ -1\ -1\ -1\ -1\ -1\}$$

$$b_i^u = \{1\ \ 1\ \ 1\ \ 1\ \ 1\ \ 1\ \ 1\ \ 1\ \ 1\ \ 1\ \ 1\ \ 1\}$$

$$a_{ij} = \begin{bmatrix} p_{11} & -(p_{11}-1) & -(p_{21}-1) \\ p_{13} & -(p_{13}-1) & -(p_{23}-1) \\ p_{11}-p_{13} & -(p_{11}-p_{13}) & -(p_{21}-p_{23}) \\ p_{12} & -(p_{12}-1) & -(p_{22}-1) \\ p_{14} & -(p_{14}-1) & -(p_{24}-1) \\ p_{12}-p_{14} & -(p_{12}-p_{14}) & -(p_{22}-p_{24}) \\ 0 & -(p_{11}-1) & -(p_{21}-1) \\ 0 & -(p_{13}-1) & -(p_{23}-1) \\ 0 & -(p_{11}-p_{13}) & -(p_{21}-p_{23}) \\ 0 & -(p_{12}-1) & -(p_{22}-1) \\ 0 & -(p_{14}-1) & -(p_{24}-1) \\ 0 & -(p_{12}-p_{14}) & -(p_{22}-p_{24}) \end{bmatrix} \tag{6.6}$$

$$x_j = \{\bar{p}\ \ \alpha\ \ \beta\},\ \ c_j = \{1\ \ 0\ \ 0\}$$

This process was performed on a computer for a large number of shell geometries for both flush and protruding nozzles by Leckie and Penny [1965]. Plotting the shakedown pressures on the basis of the geometric parameter $\rho = r/R\sqrt{R/T}$ yields the graphs shown in Figure 6.3 for the flush nozzles.

6.4 Shakedown Requirements in Pressure Vessel by Design Codes

It is worthwhile here reviewing the requirements of the pressure vessel design codes for shakedown since this rule will be compared to the elastic compensation results later. As will be seen the design rule for shakedown is very simple, and based only on a calculation of the elastic stresses.

The design by analysis rules included in Pressure Vessel Codes such as ASME *Boiler and Pressure Vessel (B&PV) Code* Section III and VIII (Division 2) [ASME. 1989] and the UK Code BS5500: *Specification for unfired fusion welded pressure vessels* [BSI, 1991] define criteria intended to preclude a number of failure mechanisms; gross plastic deformation, incremental collapse, buckling and fatigue. The specific problem is really that of incremental collapse, more commonly known as *ratchetting*. Ratchetting is associated with cyclic loading and describes a post-yield phenomenon in which the stress system reaches a cyclic state (after a few cycles of load) but plastic strain increases incrementally with each cycle. This is clearly undesirable and potential source of failure through plastic deformation. Ratchetting may be precluded by limiting the stress to the elastic range but this restrictive approach is unnecessary if *shakedown* of the structure can be assured. In the shakedown condition, a component which accumulates some plastic strain in the first (few) load cycles subsequently settles down to wholly elastic behaviour. with no further plastic strain as the load continues to cycle. Design for shakedown is clearly desirable, provided some limited plastic strain is tolerable in the first few cycles.

There are many ways of interpreting the various B&PV Code rules (both ASME and BSI), but it is important to understand them in the context of the Code failure criteria. Firstly all stresses calculated must satisfy the specified criteria which protect against fatigue. Once this limit has been achieved any localised *peak* stress can be ignored, and the remaining *primary plus secondary* stress must satisfy the shakedown criteria. Finally the *primary* stress (which could lead to gross plastic deformation) is identified and yield limited.

The ASME B&PV Code rules for design by analysis limit the primary stresses in various ways depending on the nature of the stress. Membrane stress is limited to about two thirds of yield while membrane plus bending stress is limited to yield; that is, no plastic strain is tolerable. Ignoring peak stresses, the remaining secondary stress is limited by the shakedown condition. The ASME B&PV Code

enforces shakedown in an approximate manner through the $3S_m$ secondary stress limit (where S_m is the allowable for primary membrane) which is approximately equivalent to twice yield. ASME VIII Division 2 Appendix 4 - 136.7 *Simplified Elastic-Plastic Analysis* states that the range of primary plus secondary membrane plus bending stress intensity, excluding thermal bending, must be less than $3S_m$. (Additional requirements are also imposed on fatigue calculations).

Two observations are important here. Firstly, the $3S_m$ limit for shakedown is *approximate* since it is assumed to be valid for all possible components and loads. This is contrary to detailed theoretical and experimental studies of the shakedown behaviour of many components [Leckie and Penny 1967, Proctor and Flinders 1968]. Secondly, *overall* shakedown is not achieved since the calculated peak stresses are not include. This distinction is interesting since it's design intent predates more modern studies on shakedown (for example by Toulios and White 1991).

Clearly, the present ASME rules for shakedown could be improved by allowing a direct check for shakedown, which is possible in the BSI rules. BS5500 Appendix A.3.1.2 *Incremental collapse*, states that 'The stress system imposed should shakedown to elastic action within the first few operating cycles'. To demonstrate conformance with this requirement 'a shakedown analysis (e.g. See **G.2.6**) should preferably be employed' (the specified alternative being elastic analysis and stress categorisation). The method of predicting shakedown loads used in Appendix G.2.6 *Spherical shells: shakedown loads for radial nozzles* is based on that used by Leckie and Penny [1967] to calculate shakedown loads for axisymmetric nozzles subject to pressure, thrust and moment loads.

6.5 Shakedown Loads by Elastic Compensation

The lower bound elastic compensation shakedown formulation was devised by Mackenzie and Boyle [1993]; a new upper bound shakedown formulation devised

by the Strathclyde Group will be presented in this section. Here a brief re-cap of the finite element implementation of the method is given. In fact the method is quite simple - the elastic compensation procedure is straightforward and does not rely on any major approximations or assumptions, it merely is a useful and powerful technique for generating suitable admissible strain fields for the upper bound theorem and residual stress fields for the lower bound theorem.

6.5.1 Lower Bound Shakedown Loads by Elastic Compensation

To begin with, it will be assumed that the load set is *proportional*, that is

$$P(t) = \mu[P_0 + f(t)\Delta P]$$

where P_0 and ΔP are assumed to be fixed, μ is variable *load factor* and $f(t)$ is a scalar function representing the variation over the cycle. Further it will be assumed that the function $f(t)$ takes the form shown in Figure 6.2. In this case the amplitude of the load set ΔP is applied then removed during the cycle around a constant set P_0.

For a proportional on/off load cycle Melan's theorem only needs to be checked twice during the cycle, at end-of-cycle ($t = T$)

$$|\sigma_r|_{max} \leq \sigma_y \tag{6.7}$$

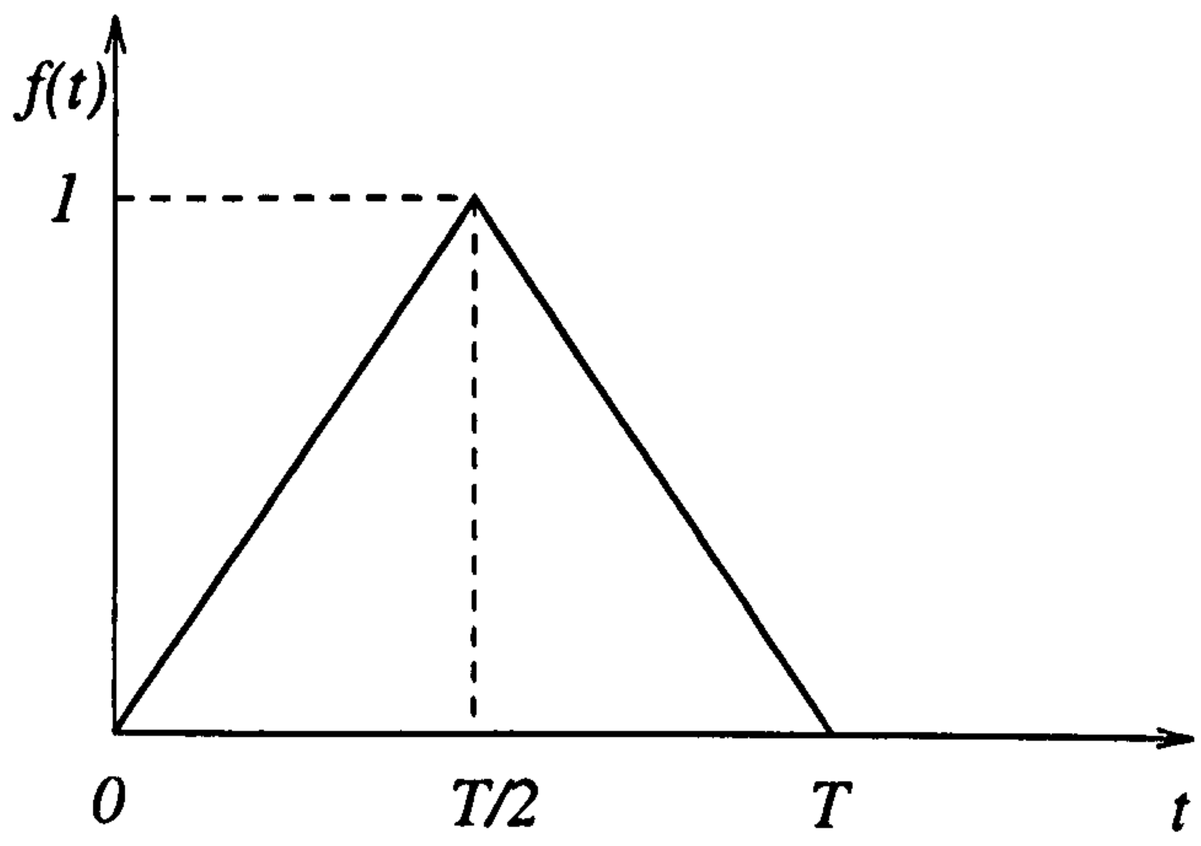

Figure 6.2: On/off load set variation

and at mid-cycle ($t = T/2$)

$$|\sigma_r + \sigma_e^\mu|_{max} \leq \sigma_y \tag{6.8}$$

It should be noted that in eqn. (6.8) the dependence on the load factor has been made explicit since σ_e^μ is defined as the elastic solution at mid-cycle when $f(t) = 1$.

This load set is fairly typical of many practical situations, particularly in pressure vessels - it serves mainly to introduce the use of the elastic compensation procedure in a simple and clear manner.

For the **lower bound** estimate, a specific residual stress field, denoted by σ_r^μ, is now constructed:

An initial linear elastic finite element analysis is performed for the nominal load set P_{nom} corresponding to a unit load factor $\mu = 1$ and $f(t) = 1$: this establishes a nominal elastic stress field σ_e^1. According to the elastic compensation procedure described in Chapter 3 this initial analysis forms *iteration zero* in a series of linear elastic analyses in which the elastic moduli of elements are systematically modified to redistribute the stress field in the structure. In each subsequent iteration, the modulus of *every element* in the model is modified according to an equation of the form:

$$E_i = E_{(i-1)} \frac{\sigma_0}{\sigma_{(i-1)}} \tag{6.9}$$

where subscript i is the iteration number, σ_n a nominal stress value and $\sigma_{(i-1)}$ the maximum (unaveraged) nodal equivalent stress associated with the element from the previous $(i-1)$th solution. The nodal stresses used from the finite element analysis should be unaveraged across elements (ie. not the usual averaged nodal data calculated for contouring) since the elastic modulus of adjacent elements will be different. The value chosen for σ_0 in eqn. (6.9) is somewhat arbitrary - usually equal to or two thirds of yield, it simply serves to adjust the elastic modulii during the analysis - it is the relative change in modulus which is important.

not its absolute value.. Care has to be taken, however, to ensure that the divisor of eqn. (6.9) does not approach zero as this could lead to numerical problems in the finite element solution.

Thus for the ith iteration corresponding to the nominal load set the redistributed stress field, σ_i^1, is obtained. The residual stress field, σ_{ri}^1, is now *defined* by the difference

$$\sigma_{ri}^1 = \sigma_i^1 - \sigma_e^1 \tag{6.10}$$

A lower bound shakedown load factor μ can now be constructed:

Since the elastic compensation procedure is based on linear elastic behaviour. the magnitude of the elastic, elastic compensation and residual stress fields for any value of the load factor must be proportional to the load factor.

$$\sigma_e^\mu = \mu\sigma_e^1, \quad \sigma_i^\mu = \mu\sigma_i^1, \quad \sigma_{ri}^\mu = \sigma_i^\mu - \sigma_e^\mu = \mu\sigma_{ri}^1 \tag{6.11}$$

Then, substituting eqns. (6.11) into the shakedown inequalities eqns. (6.7) and (6.8) gives

$$|\sigma_{ri}^\mu|_{max} = \mu|\sigma_{ri}^1|_{max} \leq \sigma_y \tag{6.12}$$

$$|\sigma_{ri}^\mu + \sigma_e^\mu|_{max} = \mu|\sigma_{ri}^1 + \sigma_e^1|_{max} \leq \sigma_y \tag{6.13}$$

respectively.

The optimal load factor can now be derived by applying the equality in eqns. (6.12) and (6.13). Either the maximum residual stress just reaches yield at end of cycle, so that from eqn. (6.12)

$$|\sigma_{ri}^\mu|_{max} = \mu|\sigma_{ri}^1|_{max} = \sigma_y$$

which can be rearranged as

$$\mu_{Ai} = \frac{\sigma_y}{|\sigma_{ri}^1|_{max}} = \frac{\sigma_y}{|\sigma_i^1 - \sigma_e^1|_{max}} \tag{6.14}$$

or the maximum residual plus elastic stress is at yield at mid-cycle, in which case

$$|\sigma_{ri}^\mu + \sigma_e^\mu|_{max} = \mu|\sigma_{ri}^1 + \sigma_e^1| = \sigma_y$$

and

$$\mu_{Bi} = \frac{\sigma_y}{|\sigma_{ri}^1 + \sigma_e^1|_{max}} = \frac{\sigma_y}{|\sigma_i^1|_{max}} \tag{6.15}$$

In eqns. (6.14) and (6.15) the denominations have also been expressed in terms of the elastic compensation stress, σ_i^1 using eqn. (6.10), since this, together with the corresponding elastic stress, σ_e^1, are usually available.

For the ith iteration the lower bound shakedown load factor μ_i is the *smaller* of the two calculated factors above:

$$\mu_i = \min(\mu_{Ai},\ \mu_{Bi}) \tag{6.16}$$

The elastic compensation procedure is run for several iterations (usually no more than ten elastic re-analyses are required) and the best lower bound shakedown load factor calculated using elastic compensation is the highest shakedown load factor μ_i obtained from the iteration sequence

$$\mu_{lower} = \max(\mu_i) \tag{6.17}$$

6.5.2 Upper Bound Shakedown Loads by Elastic Compensation

We now turn to the derivation of the **upper bound** load factor. An upper bound criterion for shakedown (usually referred to as kinematic shakedown) was presented by Koiter [1960]. It has been used extensively, together with Melan's theorem, in the estimation of shakedown loads; a useful survey has been given by Konig [1987]. However the major application has been to frame and plate structures, and although a few finite element techniques (using unconventional mathematical programming methods) have been proposed in the literature, there has been no generally applicable method for complex structures. This study will demonstrate a new upper bound method for the estimation of shakedown load using conventional linear elastic finite element analysis. As a consequence, the method is based on a novel interpretation of Koiter's theorem and makes use of the fundamental properties of solutions generated using the elastic compensation method.

Suppose that the load set acting on the structure is denoted by, $P_{(t)}$ (and can presented several simultaneous loads acting at the same time). The so-called *weak* form [Lubliner, 1990] of Koiter's upper bound shakedown theorem will be used:

(Koiter's Theorem) For a prescribed load set $P(t)$ cyclic with period T. if any kinematically admissible velocity v^* can be found such that

$$\int_0^T \left(\int_V f_P(t) \cdot v^* dV + \int_S T_P(t) \cdot v^* dS \right) dt \geq \int_0^T \int_V \dot{D}^* dV dt \qquad (6.18)$$

where $\dot{D}^*$ is the rate of plastic energy dissipation per unit volume corresponding to the strain rate $\dot{\epsilon}^*$ which is compatible with v^* and where $f_P(t)$ and $T_P(t)$ are the (idealised) body force and surface traction corresponding to the load set defined over the body V bounded by surface S, then shakedown has not taken place.

The rate of energy dissipation per unit volume for a perfectly plastic material with a Tresca criterion is given by

$$\dot{D}^* = \sigma_y |\dot{\epsilon}^*|_{max}$$

and for a von Mises criterion by

$$\dot{D}^* = \sigma_y \left[\frac{2}{3} (\dot{\epsilon}_1^{*2} + \dot{\epsilon}_2^{*2} + \dot{\epsilon}_3^{*2}) \right]^{1/2}$$

where $|\dot{\epsilon}^*| : i = 1, 2, 3$ are the principal strain rates for the kinematical admissible field and σ_y the yield stress.

It can be seen that the upper bound shakedown theorem requires the definition of a suitable kinematical admissible deformation for the component which satisfies inequality eqn. (6.18). By definition the load level for which this is verified will be an *upper bound* on the shakedown load (since it ensures non-shakedown).

The fact that the theorem requires velocities and strain rates is non-essential - it is only the compatible distribution which is required. It should also be noted that in the statement of the theorem given by eqn. (6.18) it is assumed that

homogeneous boundary conditions for the velocity are specified. However in the procedure which will be derived below, since the stress and strain fields used in the theorem have been derived through elastic compensation procedure for the *same* boundary value problem, this requirement is unnecessary in practice and is simply stated in this form for simplicity.

Each elastic compensation iteration, as well as providing a residual stress field, also gives a compatible displacement and strain field. Hence these can be used to define a kinematically determinate mode of deformation for the structure which can be applied to the upper bound theorem. However, this is achieved *indirectly*:

Due to the form of the proportional load set considered here, the velocity v^* and strain rate field $\dot{\epsilon}^*$ will be associated in the following with the compatible displacement and strain field at *mid-cycle* (ie when $f(t) = 1$) derived from elastic compensation.

In principle the elastic compensation procedure could be applied at any instant t during the load cycle and an elastic compensation stress field, corresponding to the load set P_t, derived. Let the instantaneous elastic compensation stress field for the ith iteration be denoted by $\sigma_i(t)$. *Since this stress field is in equilibrium with the applied load set it can be applied to the left hand side of Koiter's inequality, eqn. (6.18), using virtual work (Green's theorem)*:

$$\int_0^T \left(\int_V \sigma_i(t) \dot{\epsilon}^* dV \right) \geq \int_0^T \int_V \dot{D}^* dV dt \tag{6.19}$$

This substitution is a significant feature of the upper bound procedure derived here and leads to a simple upper bound analysis when combined with the elastic compensation analysis. It is more usual, for example in Koiter's proof of the theorem [1960] and in many practical analyses [Konig, 1987], to make this substitution with the *elastic* stress field.

Three further fundamental properties of the elastic compensation analysis can be used to simplify eqn. (6.19) further: (i) the strain field $\dot{\epsilon}^*$ is assumed constant. (ii) the load set is considered proportional and (iii) the elastic compensation stress

field is a linear elastic solution.

Firstly, with these properties the time integrals in eqn. (6.19) can be easily evaluated to give

$$U = \int_V \sigma_i^{\mu} \dot{\epsilon}^* dV \geq \int_V \dot{D}^* dV = D \tag{6.20}$$

where quantities U and D have been defined.

Secondly, the strain energy U from the (linear) elastic compensation analysis must very with the square of the load factor and the dissipation of internal energy D must be proportional to the load factor,

$$U = \mu^2 \int_V \sigma_i^1 \dot{\epsilon}^* dV = \mu^2 U_1 \tag{6.21}$$

$$D = \mu \int_V \dot{D}_1^* dV = \mu D_1 \tag{6.22}$$

where U_1 and D_1 are defined for the nominal load set P^d at mid-cycle (with load factor $\mu = 1$ and $f(t) = 1$). The quantities D_1 and U_1 are evaluated directly in the elastic compensation procedure.

The upper bound load factor in the load cycle for the ith elastic compensation analysis therefore occurs when equality is reached in eqn. (6.20)

$$\mu_i = \frac{D_1}{U_1} \tag{6.23}$$

Finally, the optimal upper bound from the sequence of the analysis is

$$\mu_{upper} = \min(\mu_i) \tag{6.24}$$

6.6 A Parameter Study

A parameter study is made here of pressurised nozzle/spherical vessels, as an extension of previous limit analyses in Chapter 5. Eighty four geometries, the same as those in Chapter 5, are investigated by the elastic compensation procedure, with the program *ANSYS*, using the eight noded isoparametric axisymmetric solid element PLANE82. A suite of macros, see Appendix II, have been developed in the *ANSYS* Parametric Design Language to automatically run through the elastic compensation procedure and evaluate both lower and upper bounds for shakedown analysis. The user then only needs to set up the initial elastic analysis and run the APDL macro. A maximum of 10 iterations were used in the elastic compensation analyses. The upper bound shakedown solutions calculated in the finite element analysis are approximate since energy and energy dissipation integrals are calculated by a summation based on element centroidal stress and strain data and element volume; since the summation is done over the whole finite element model the overall approximation error is small. More elaborate summation procedures could easily be devised but have so far been found to be unnecessary.

The model geometry, parameters and boundary conditions are the same as that in Chapter 5. An internal pressure is applied and cycled from zero up to maximum $P^d = \mu P_{nom}$ at mid-cycle and back to zero. A radial outward pressure P_r (equivalent to a capped nozzle pressure load) is required in the finite element model; this is evaluated as

$$P_r = \frac{P^d r_i^2}{r_o^2 - r_i^2} \tag{6.25}$$

where r_o is outside radius and r_i inside radius of the shell.

For all the models examined the modulus of elasticity is taken as $200E3.N/mm^2$ with Poisson's ratio 0.3. The yield stress of the material is taken as $300.N/mm^2$.

The lower and upper bound shakedown pressures, P_{ls} and P_{us}, were calculated

according to the equations (6.17) and (6.24) and normalised according to the equation:

$$\overline{p} = \frac{RP}{2T\sigma_y}$$

The normalised lower and upper bound shakedown pressures, $\overline{P}_{ls}$ and $\overline{P}_{us}$, with *two* dimensionalless geometry parameters ρ and $\mathbf{R/T}$ were plotted in Figures 6.3 to 6.11 and tabulated in Tables 6.1 to 6.8 respectively, where

$$\rho = \frac{r}{R}\sqrt{\frac{R}{T}}$$

introduced by Leckie and Penny [1967]. The shakedown pressures are compared with the elastically calculated load corresponding to the ASME B&PV Code (elastic) secondary stress limit, $3S_m$, and published results of Leckie and Penny [1967], $\overline{P}_{L+P}$.

6.7 Discussion of Results

Figures 6.3 to 6.10 show that the elastic compensation lower bound shakedown pressures $\overline{P}_{ls}$ are less than ASME B&PV $3S_m$ limit for all the nozzle configuration considered. The $\overline{P}_{ls}$ curves are similar in form to the $3S_m$ curves but the calculated lower bound shakedown pressure values are generally closer to the Leckie and Penny [1967] results, $\overline{P}_{L+P}$. $\overline{P}_{ls}$ and $\overline{P}_{L+P}$ are fairly similar for most values of ρ for the three higher R/T rations of 100, 50 and 25, however. $\overline{P}_{ls}$ is significantly greater than $\overline{P}_{L+P}$ for most of the ρ values in the nozzles of $R/T = 10,\ 8.33,\ 7.14$ and 6.25, except at $\rho = 0.3$ where the lower bound shakedown pressures calculated are much lower than $\overline{P}_{L+P}$. The $3S_m$ curves for these nozzles, i.e. $R/T = 10,\ 8.33,\ 7.14$ and 6.25, have fairly similar pattern as lower bound solutions in the region of $\rho = 1.0$ to 0.2.

As Leckie and Penny only considered variation of shakedown load with geometry parameter ρ, their results are constant for all the R/T ratios considered. However, both the elastic compensation pressures $\overline{P}_{ls}$, $\overline{P}_{us}$ and secondary stress

limit $3S_m$ vary with the R/T ratio, Figures 6.3 to 6.12. The results presented show that the Leckie and Penny's lower bound shakedown pressure $\overline{P}_{L+P}$ is lower than the secondary stress limit pressure $3S_m$ except for $R/T = 7.14,\ 6.25$. $\rho = 0.3$ in Figure 6.13.

It can be seen from the Tables 6.2 to 6.4 that for the three sets higher R/T ratios of 100, 50 and 25, the lowest shakedown factor is 1.498 with the model number 29 and the highest factor is 1.97 with the model number 10a. For the four sets lower R/T ratios of 10, 8.33, 7.14 and 6.25, however, the lowest shakedown factor is 1.506 with the model number 74, and the highest factor is 1.927 with the model number 32 as shown in Tables 6.5 to 6.8.

Figures 6.3 to 6.10 and 6.12 show that the elastic compensation upper bound solutions are 20 to 25 per cent higher than the results of Leckie and Penny [1967] with similar curve patterns for all models. Also, the obtained upper bound shakedown pressures are higher than the lower bound solutions. Comparing with $3S_m$ allowable pressures, it can be seen that for values of ρ greater than 0.7 the upper bound solutions are lower than $3S_m$, for ρ smaller than 0.7 the upper bound shakedown pressures are higher than $3S_m$. The greatest differences between obtained upper bound solutions and $3S_m$ allowable pressures lie in the regions of small diameter nozzles (where the use of the parameter ρ is questionable).

6.8 Concluding Comments

It could be concluded from the discussion above that the shakedown pressures vary not only with the geometry parameter ρ used to characterize nozzles by Leckie and Penny, but also with the radius to thickness ratio of the sphere. This additional parameter should be considered when deriving design curves for shakedown loads. The obtained results also suggest that the Leckie and Penny curves may not be conservative for all radius to thickness ratios.

The elastic compensation shakedown pressures for the R/T ratios of 10, 8.33, 7.14 and 6.25 are significantly greater than the Leckie and Penny values for most of the geometry range considered, suggesting that design to the BS5500 Code could be over-conservative if the Leckie and Penny curves are used. However, BS5500 simply requires that 'a shakedown analysis (e.g. See **G.2.6**) should preferably be employed' thus design based on the elastic compensation method would be acceptable.

The upper bound shakedown results would suggest that the $3S_m$ limits are not conservative, especially for the R/T ratios of 10, 8.33, 7.14 and 6.25 the $3S_m$ limits are much higher than the upper bound pressures for the values of ρ greater than 0.8. In the writer's experience (discussed in previous Chapters) the upper bound is usually more reliable since the lower bound is quite strict.

A method has been developed here which allows both upper and lower shakedown loads on pressure vessels to be estimated with useful accuracy. The method has been verified for the classic example of radial nozzle in aspherical pressure vessel and compared to the established solution of Leckie and Penny. The method can be easily easily extended to three dimensional geometry and other forms of load cycling.

6.9 References

American Society of Mechanical Engineers, (1989), *Boiler and Pressure Vessel Code*, New York, NY.

British Standards Institution, (1991), *BS 5500: British Standard Specification for Unfired Fusion Weled Pressure vessels.*

Carter, K.F. & Ponter, A.R.S., (1992), Calculation of limit loads and shakedown boundaries using the modified elastic modulus method, *Computational Plasticity, Fundamentals and Apllications*, Eds. Owen, Onate and Henton, Pineridge Press, Swansea, U.K., 1597-1608.

Findlay, G.E., and Spence, J., (1968), Applying the shakedown concept to pressure vessel design, *The Egineer*, **12**, July.

Hamilton, R., Boyle, J.T., Shi, J. and Mackenzie, D., (1995), A simple upper bound method for calculating approximate shakedown loads, *Trans ASME. J. Pressure Vessel Technology*, under review.

Koiter, W.T., (1960), *Progress in Solid Mechanics*, (ed. I. N. Sneddon and R. Hill), Vol. 1, North-Holland, Amsterdam.

König, J.A., (1987), *Shakedown of Elastic-Plastic Structures*, Elsevier, Amsterdam.

Leckie, F.A., (1965), Shakedown pressure for flush cylinder–sphere shell intersection, *J. Mech. Eng. Sci.*, **7**, 367–371.

Leckie, F.A., and Penny, R.K., (1967), Shakedown loads for radial nozzles in spherical pressure vessels, *Int. J. Solids and Structures*, **3**, 743–751.

Lu, M.W., Xue, W.M. and Chen, S.Z., (1991), Computational shakedown analysis of axi-symmetric shells: A lower bound solution. *Computational Mechanics*, Cheung, Lee & Leung (eds), Balkema, Rotterdam, 105–110.

Lubliner, J., (1990), *Plasticity Theory*, Macmillan Publishing Company. New York.

Macfarlane, W.A. and Findlay, G.E., (1972), A simple technique for calculating shakedown loads in pressure vessels, *Proc. Instn. Mech. Engrs.*, Vol. 186. 45–52.

Mackenzie, D., and Boyle, J.T., (1993), A simple method of estimating shakedown loads for complex structures, *PVP-Vol. 265, ASME*, 89-94.

Penny, P.K. and Leckie, F.A., (1963), Solutions for the stresses at nozzles in pressure vessels, *Bull. Weld Res. Coun.*, No. 90.

Proctor, E. and Flinders, R.F., (1968), Shakedown investigations on partial penetration welded nozzles in a spherical shell, *Nucl. Engrg. Des.*. 8. 171–185.

Table 6.1: *Normalised shakedown pressure of nozzles,* $r = 200mm$

Nozzle	$T(mm)$	ρ	$\overline{P}_y$	$\overline{P}_{ls}$	$\overline{P}_{us}$	$3S_m$	$\overline{P}_{L+P}$	P_{ls}/P_y
1	250.0	0.4	0.361	0.707	0.982	0.722	0.790	1.958
2	160.0	0.5	0.414	0.781	0.979	0.828	0.780	1.886
3	111.1	0.6	0.446	0.849	0.963	0.892	0.770	1.904
4	81.60	0.7	0.463	0.818	0.935	0.926	0.750	1.767
5	62.50	0.8	0.468	0.777	0.90	0.936	0.720	1.660
6	40.00	1.0	0.435	0.696	0.811	0.870	0.660	1.600
7	33.06	1.1	0.399	0.654	0.767	0.798	0.630	1.639
8	27.80	1.2	0.393	0.615	0.721	0.786	0.610	1.565
9	23.67	1.3	0.366	0.577	0.682	0.732	0.570	1.577

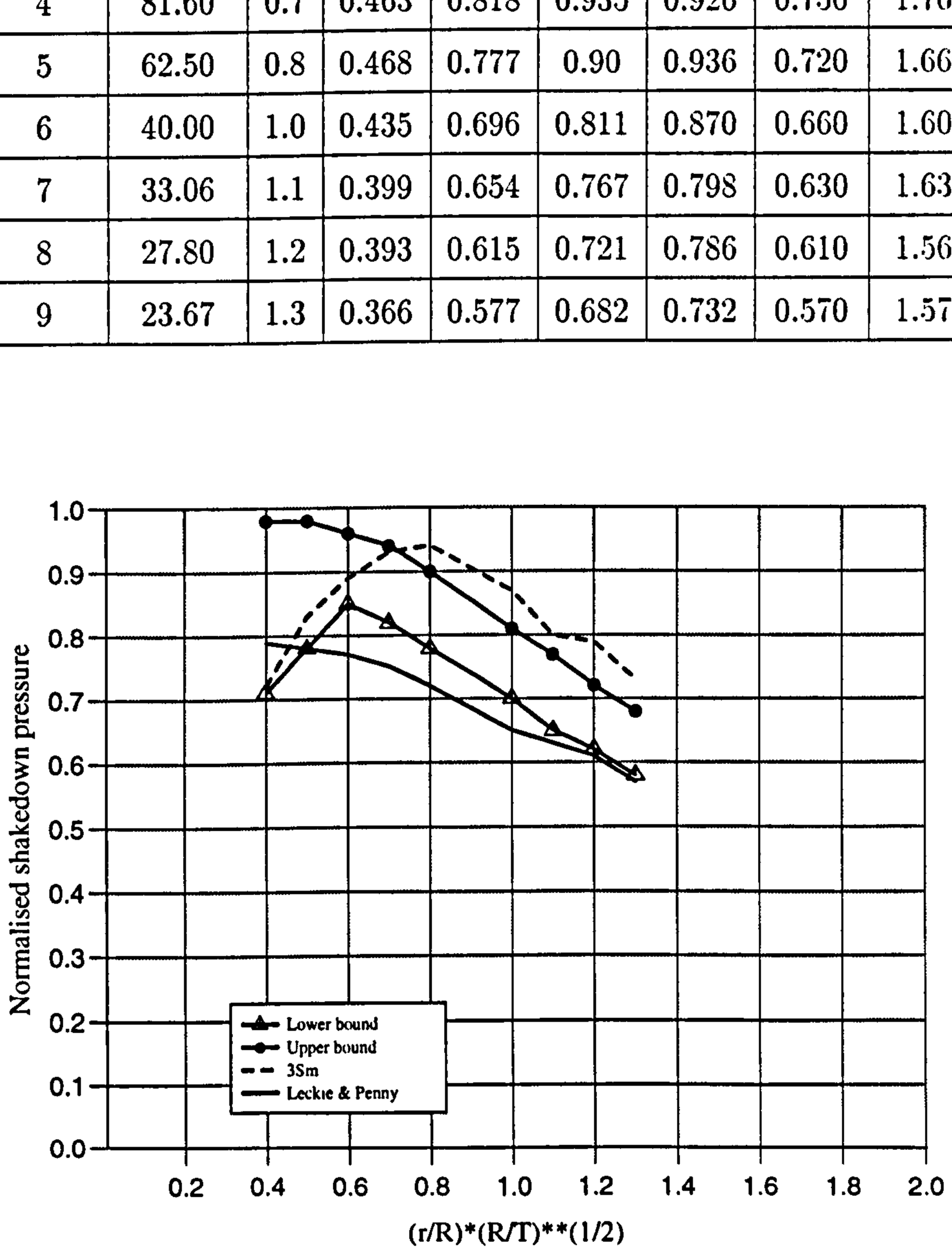

Figure 6.3: Normalised shakedown limit pressure of nozzles versus ρ. $r = 200mm$, $R = 1000mm$

Table 6.2: *Normalised shakedown pressure of nozzles,* $T = 10mm$, $R/T = 100$

Nozzle	$r(mm)$	ρ	$\overline{P}_y$	$\overline{P}_{ls}$	$\overline{P}_{us}$	$3S_m$	$\overline{P}_{L+P}$	P_s/P_y
10a	10	0.1	0.429	0.845	1.0	0.858	0.820	1.970
10b	20	0.2	0.442	0.857	1.0	0.884	0.805	1.939
10c	30	0.3	0.459	0.850	0.997	0.918	0.80	1.852
10d	40	0.4	0.467	0.849	0.993	0.934	0.790	1.818
10e	50	0.5	0.470	0.850	0.988	0.940	0.780	1.809
10f	60	0.6	0.469	0.799	0.962	0.938	0.770	1.704
10g	70	0.7	0.465	0.769	0.946	0.930	0.750	1.654
10h	80	0.8	0.459	0.709	0.917	0.918	0.720	1.545
10i	90	0.9	0.440	0.698	0.854	0.880	0.690	1.586
10j	100	1.0	0.412	0.651	0.804	0.824	0.660	1.580
10k	200	2.0	0.257	0.432	0.494	0.514	0.435	1.681
10l	300	3.0	0.183	0.312	—	0.366	0.340	1.705

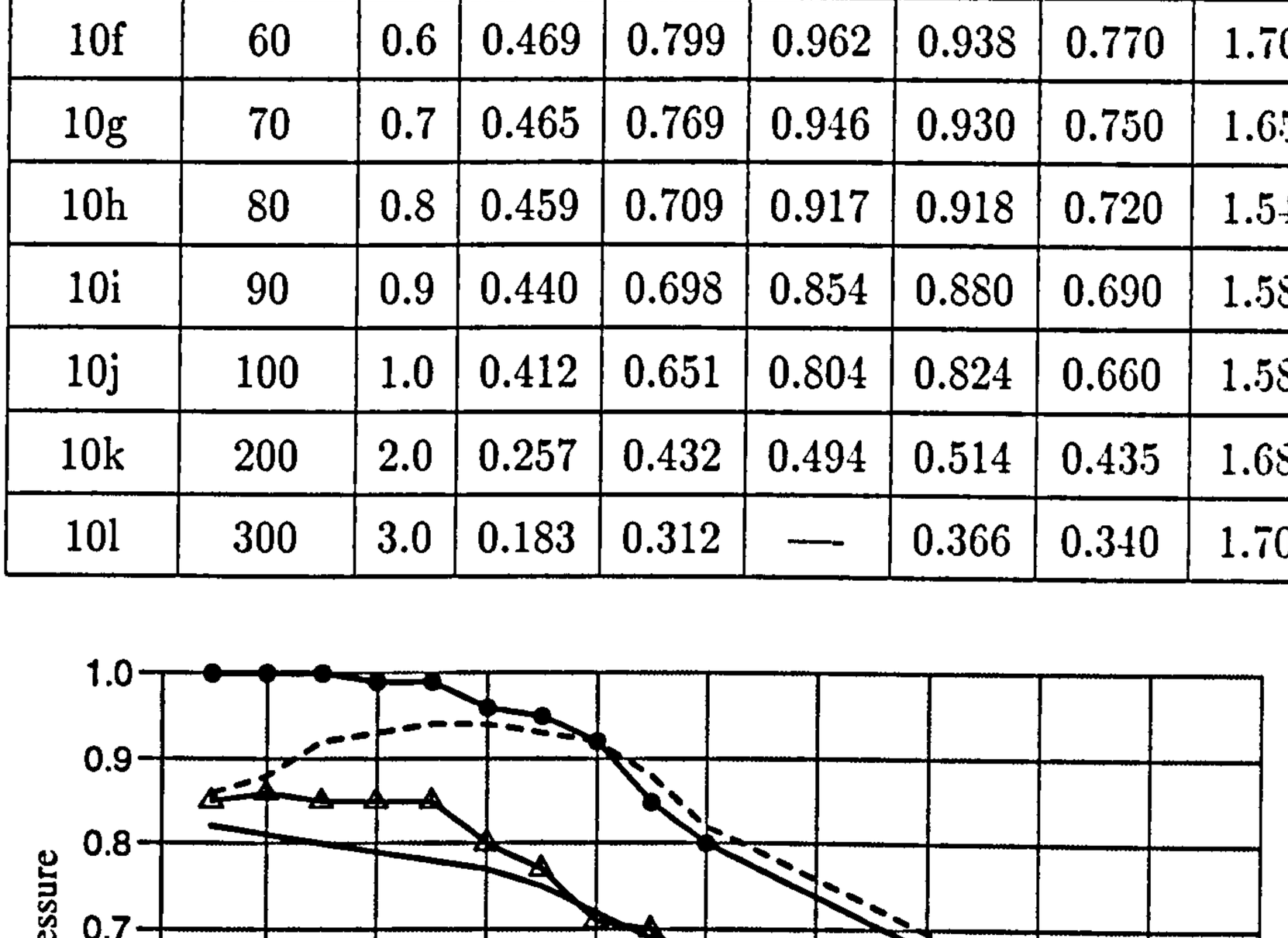

Figure 6.4: Normalised shakedown pressure of nozzles versus ρ. $T = 10mm$, $R/T = 100$

Table 6.3: *Normalised shakedown pressure of nozzles,* $T = 20mm$, $R/T = 50$

Nozzle	$r(mm)$	ρ	$\overline{P}_y$	$\overline{P}_{ls}$	$\overline{P}_{us}$	$3S_m$	$\overline{P}_{L+P}$	P_s/P_y
10	14.14	0.1	0.469	0.908	1.0	0.938	0.820	1.936
11	28.28	0.2	0.436	0.833	1.0	0.872	0.805	1.911
12	56.57	0.4	0.464	0.833	0.994	0.928	0.790	1.795
13	70.71	0.5	0.471	0.803	0.985	0.942	0.780	1.705
14	84.85	0.6	0.473	0.776	0.968	0.946	0.770	1.641
15	98.99	0.7	0.471	0.745	0.937	0.942	0.750	1.583
16	113.1	0.8	0.467	0.715	0.895	0.934	0.720	1.531
17	127.3	0.9	0.448	0.685	0.846	0.896	0.690	1.526
18	141.2	1.0	0.419	0.653	0.796	0.838	0.660	1.558
19	212.1	1.5	0.320	0.522	0.617	0.640	0.540	1.631
20	282.8	2.0	0.264	0.438	0.519	0.528	0.435	1.659

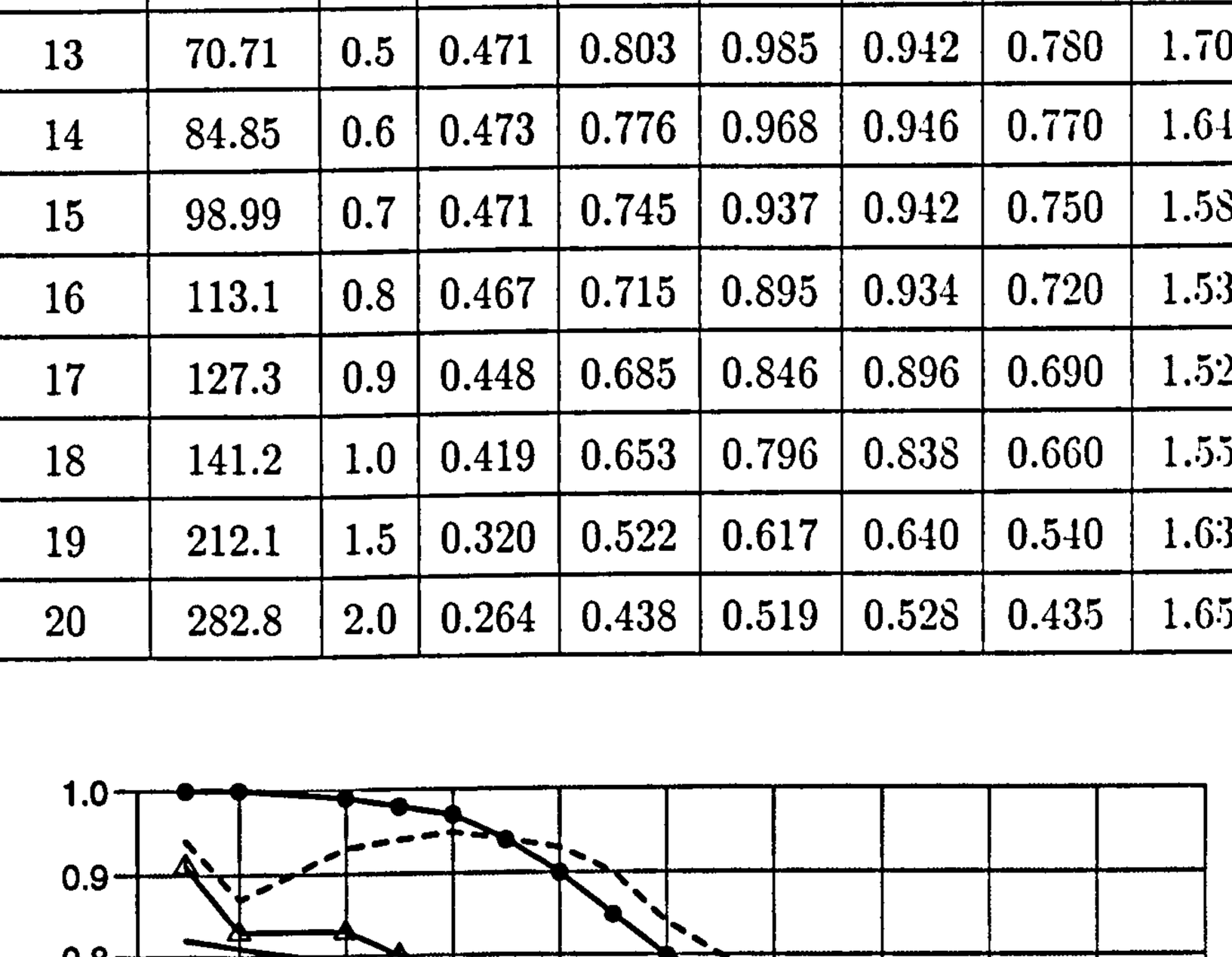

Figure 6.5: Normalised shakedown pressure of nozzles versus ρ. $T = 20mm$, $R/T = 50$

Table 6.4: *Normalised shakedown pressure of nozzles,* $T = 40mm$. $R/T = 25$

Nozzle	$r(mm)$	ρ	$\overline{P}_y$	$\overline{P}_{ls}$	$\overline{P}_{us}$	$3S_m$	$\overline{P}_{L+P}$	P_s/P_y
21	40	0.2	0.432	0.823	1.0	0.864	0.805	1.905
22	60	0.3	0.443	0.835	0.999	0.886	0.80	1.885
23	80	0.4	0.457	0.859	0.995	0.914	0.790	1.880
24	100	0.5	0.467	0.829	0.985	0.934	0.780	1.775
25	120	0.6	0.471	0.802	0.967	0.942	0.770	1.703
26	140	0.7	0.473	0.774	0.937	0.946	0.750	1.636
27	160	0.8	0.471	0.748	0.897	0.942	0.720	1.588
28	180	0.9	0.467	0.718	0.852	0.934	0.690	1.537
29	200	1.0	0.462	0.692	0.807	0.924	0.660	1.498
30	300	1.5	0.353	0.579	0.641	0.706	0.540	1.640
31	400	2.0	0.291	0.495	0.545	0.582	0.435	1.653

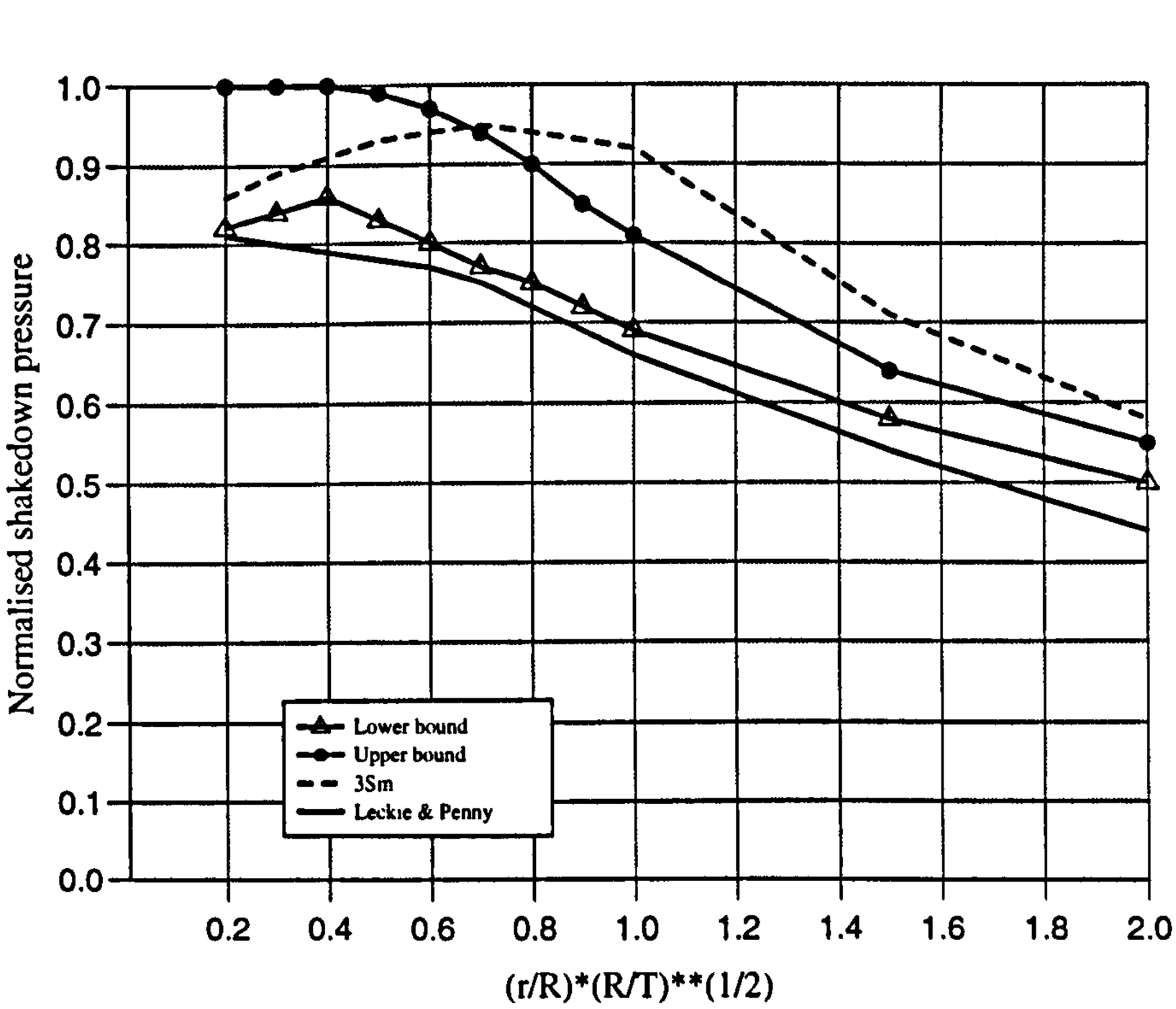

Figure 6.6: Normalised shakedown pressure of nozzles versus ρ. $T = 40mm$, $R/T = 25$

Table 6.5: *Normalised shakedown pressure of nozzles,* $T = 100mm$, $R/T = 10$

Nozzle	$r(mm)$	ρ	$\overline{P}_y$	$\overline{P}_{ls}$	$\overline{P}_{us}$	$3S_m$	$\overline{P}_{L+P}$	P_s/P_y
32	63.24	0.2	0.424	0.817	1.0	0.848	0.805	1.927
33	94.87	0.3	0.409	0.783	0.999	0.818	0.80	1.914
34	126.5	0.4	0.426	0.796	0.994	0.852	0.790	1.869
35	158.1	0.5	0.441	0.844	0.984	0.882	0.780	1.914
36	189.7	0.6	0.451	0.823	0.964	0.902	0.770	1.825
37	221.4	0.7	0.457	0.821	0.933	0.914	0.750	1.796
38	253.0	0.8	0.459	0.797	0.894	0.918	0.720	1.736
39	284.6	0.9	0.459	0.775	0.852	0.918	0.690	1.688
40	316.2	1.0	0.457	0.748	0.811	0.914	0.660	1.637
41	474.3	1.5	0.372	0.629	0.659	0.744	0.540	1.691
42	632.5	2.0	0.317	0.526	0.581	0.634	0.435	1.659

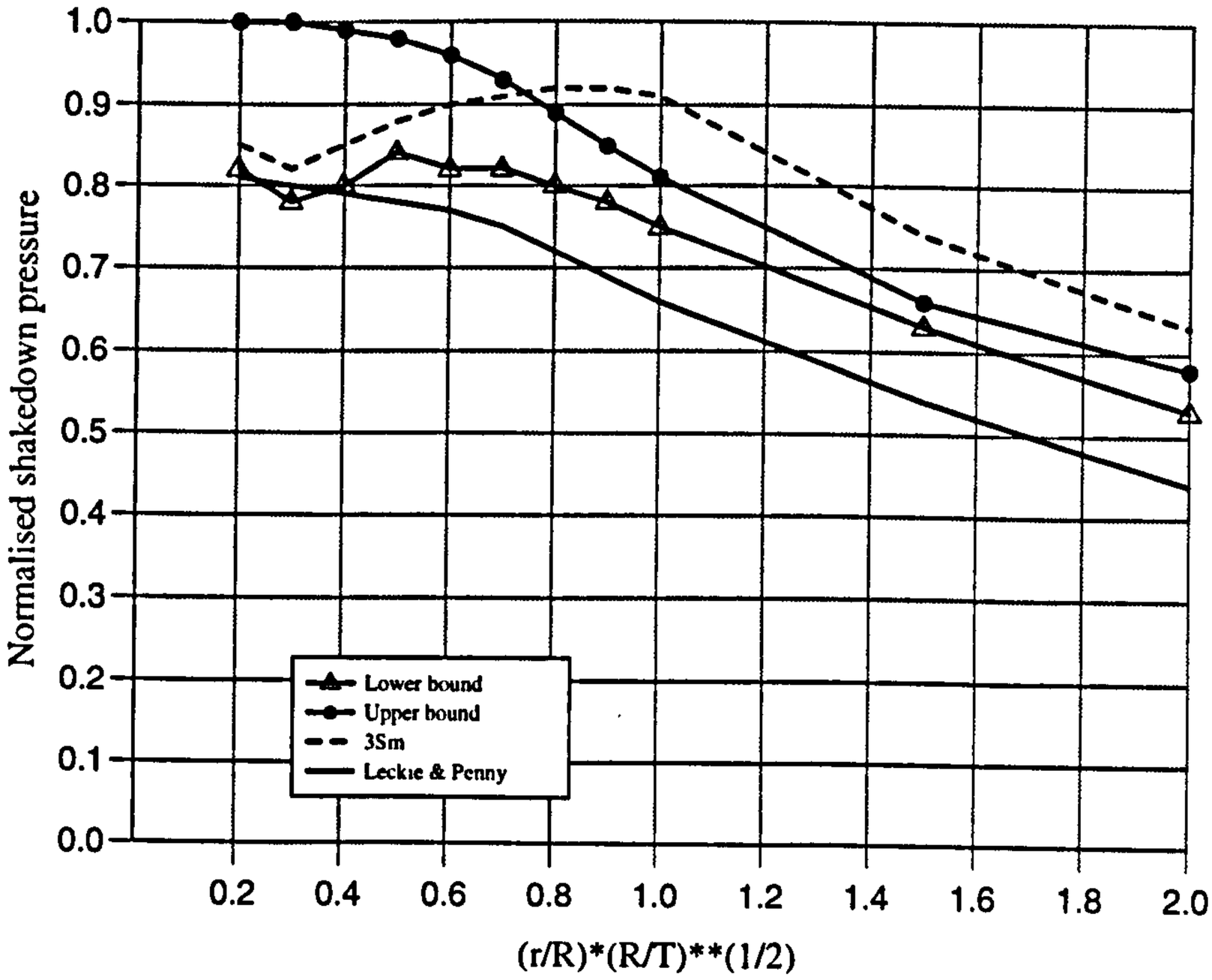

Figure 6.7: Normalised shakedown pressure of nozzles versus ρ. $T = 100mm$, $R/T = 10$

Table 6.6: *Normalised shakedown pressure of nozzles,* $T = 120mm$, $R/T = 8.33$

Nozzle	$r(mm)$	ρ	$\overline{P}_y$	$\overline{P}_{ls}$	$\overline{P}_{us}$	$3S_m$	$\overline{P}_{L+P}$	P_s/P_y
43	69.28	0.2	0.455	0.871	1.0	0.910	0.805	1.914
44	103.9	0.3	0.401	0.764	0.999	0.802	0.80	1.905
45	138.6	0.4	0.417	0.773	0.994	0.834	0.790	1.854
46	173.2	0.5	0.432	0.814	0.983	0.864	0.780	1.884
47	207.9	0.6	0.443	0.826	0.962	0.886	0.770	1.865
48	242.5	0.7	0.45	0.819	0.929	0.90	0.750	1.82
49	277.1	0.8	0.453	0.801	0.890	0.906	0.720	1.768
50	311.8	0.9	0.454	0.779	0.848	0.908	0.690	1.716
51	346.4	1.0	0.453	0.749	0.807	0.906	0.660	1.653
52	519.6	1.5	0.385	0.626	0.660	0.770	0.540	1.626
53	692.8	2.0	0.337	0.515	0.592	0.674	0.435	1.528

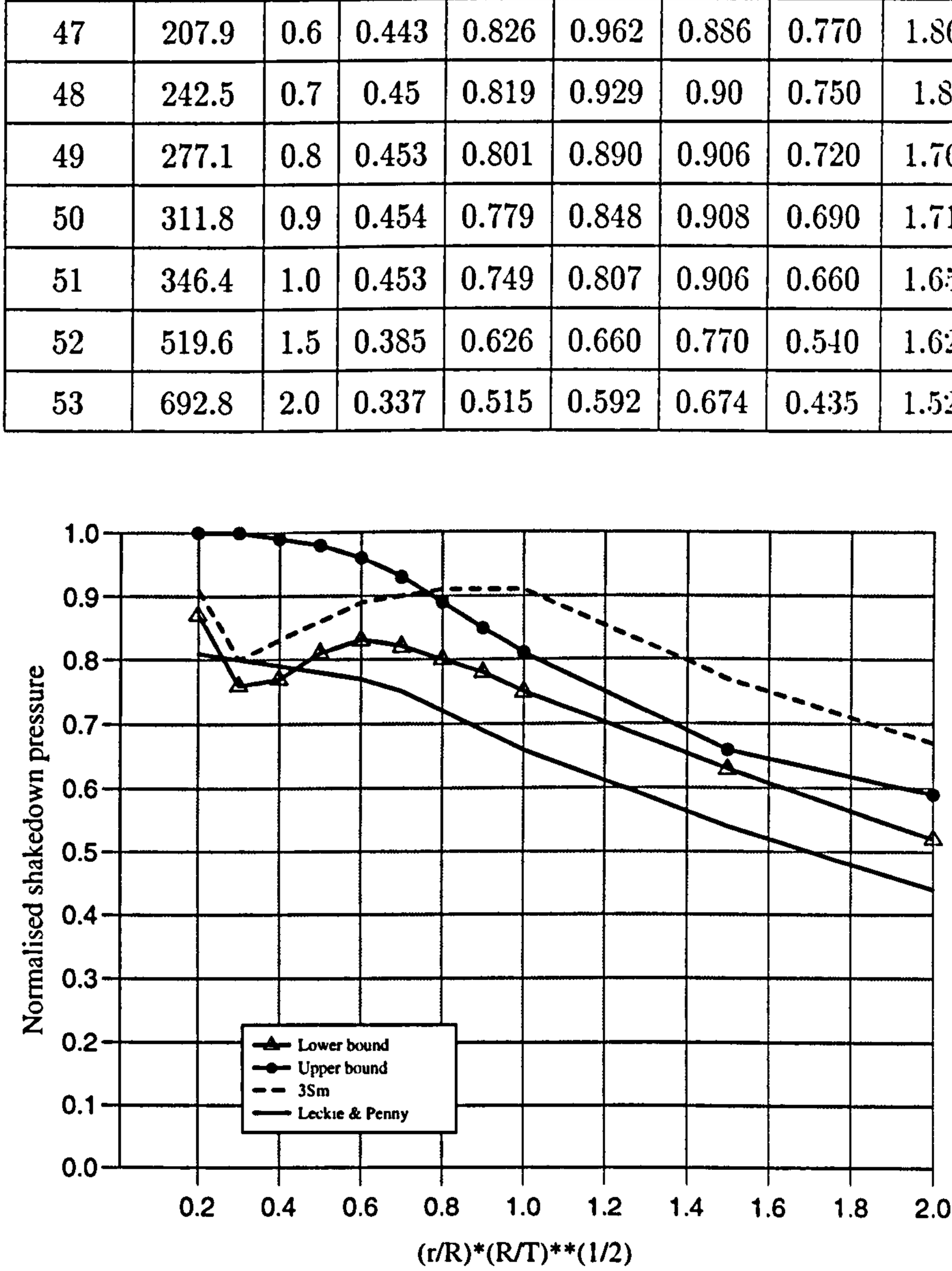

Figure 6.8: Normalised shakedown pressure of nozzles versus ρ. $T = 120mm$, $R/T = 8.33$

Table 6.7: *Normalised shakedown pressure of nozzles,* $T = 140mm$, $R/T = 7.14$

Nozzle	$r(mm)$	ρ	$\overline{P}_y$	$\overline{P}_{ls}$	$\overline{P}_{us}$	$3S_m$	$\overline{P}_{L+P}$	P_s/P_y
54	112.3	0.3	0.394	0.743	0.998	0.788	0.80	1.886
55	149.7	0.4	0.408	0.772	0.993	0.816	0.790	1.892
56	187.1	0.5	0.423	0.791	0.981	0.846	0.780	1.87
57	224.5	0.6	0.435	0.827	0.959	0.870	0.770	1.901
58	261.9	0.7	0.443	0.822	0.926	0.886	0.750	1.856
59	299.3	0.8	0.447	0.803	0.886	0.894	0.720	1.796
60	336.8	0.9	0.449	0.777	0.844	0.898	0.690	1.731
61	374.2	1.0	0.448	0.749	0.804	0.896	0.660	1.672
62	467.7	1.25	0.442	0.686	0.720	0.884	0.60	1.55
63	561.3	1.5	0.399	0.628	0.662	0.798	0.540	1.536
64	654.8	1.75	0.370	0.590	0.624	0.740	0.490	1.476

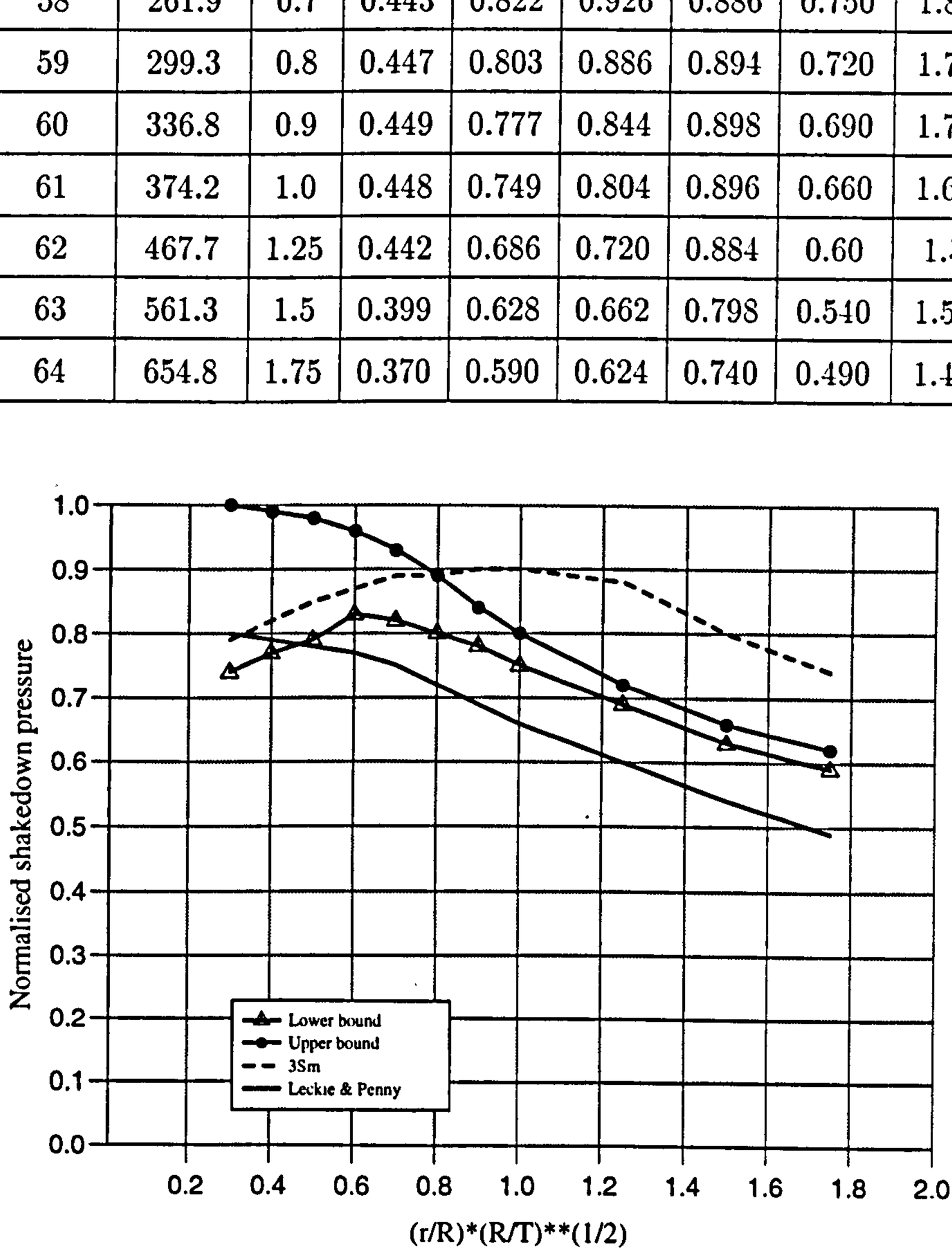

Figure 6.9: Normalised shakedown pressure of nozzles versus ρ. $T = 140mm$, $R/T = 7.14$

Table 6.8: *Normalised shakedown pressure of nozzles,* $T = 160mm$, $R/T = 6.25$

Nozzle	$r(mm)$	ρ	$\overline{P}_y$	$\overline{P}_{ls}$	$\overline{P}_{us}$	$3S_m$	$\overline{P}_{L+P}$	P_s/P_y
65	120	0.3	0.389	0.723	0.997	0.778	0.80	1.859
66	160	0.4	0.399	0.761	0.992	0.798	0.790	1.907
67	240	0.6	0.427	0.818	0.956	0.854	0.770	1.916
68	280	0.7	0.436	0.822	0.922	0.872	0.750	1.885
69	320	0.8	0.441	0.804	0.881	0.882	0.720	1.823
70	360	0.9	0.443	0.777	0.839	0.886	0.690	1.754
71	400	1.0	0.443	0.748	0.799	0.886	0.660	1.688
72	500	1.25	0.439	0.686	0.718	0.878	0.60	1.563
73	600	1.5	0.414	0.627	0.666	0.828	0.540	1.471
74	700	1.75	0.389	0.586	0.634	0.778	0.490	1.494

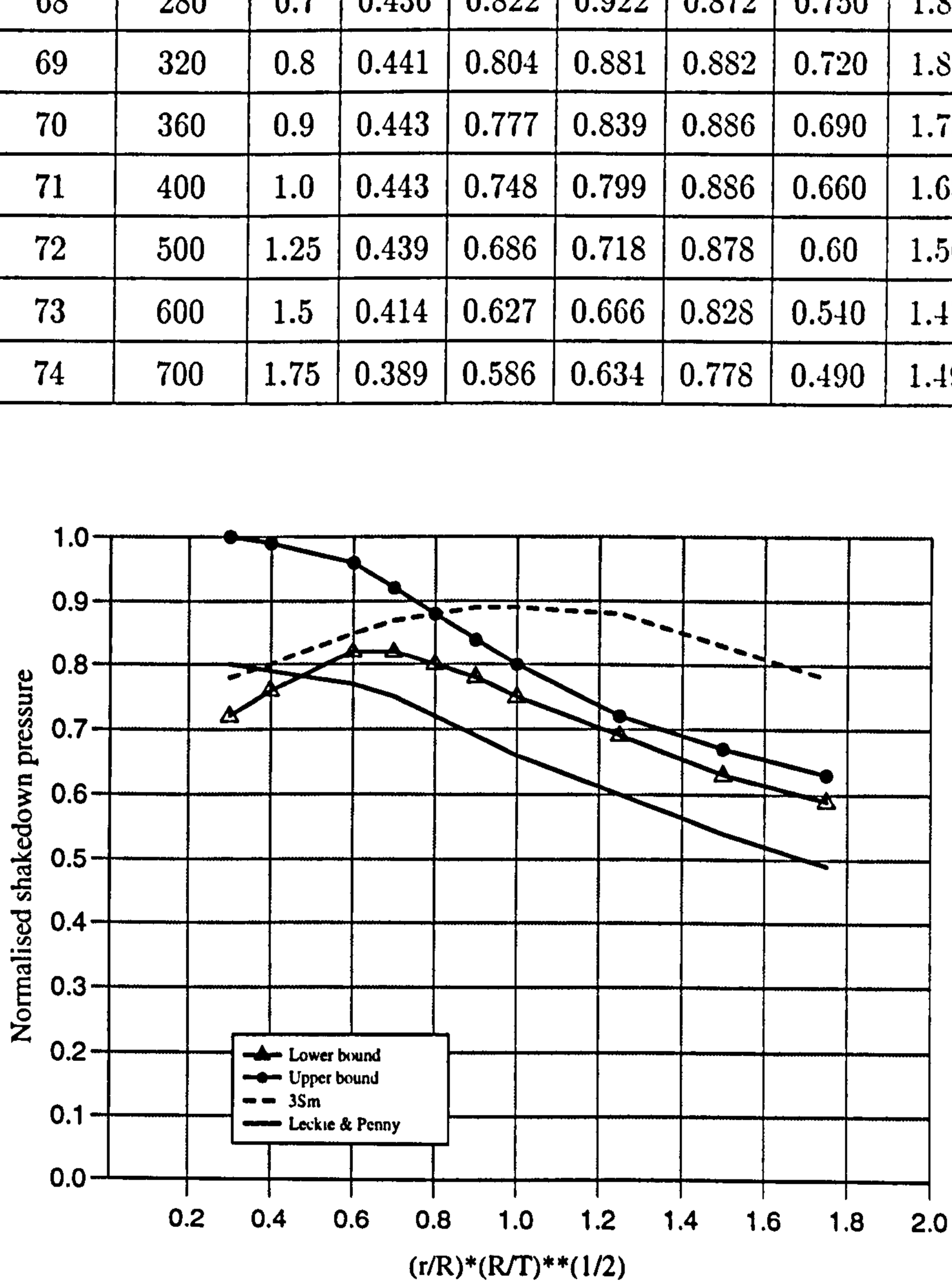

Figure 6.10: Normalised shakedown pressure of nozzles versus ρ. $T = 160mm$, $R/T = 6.25$

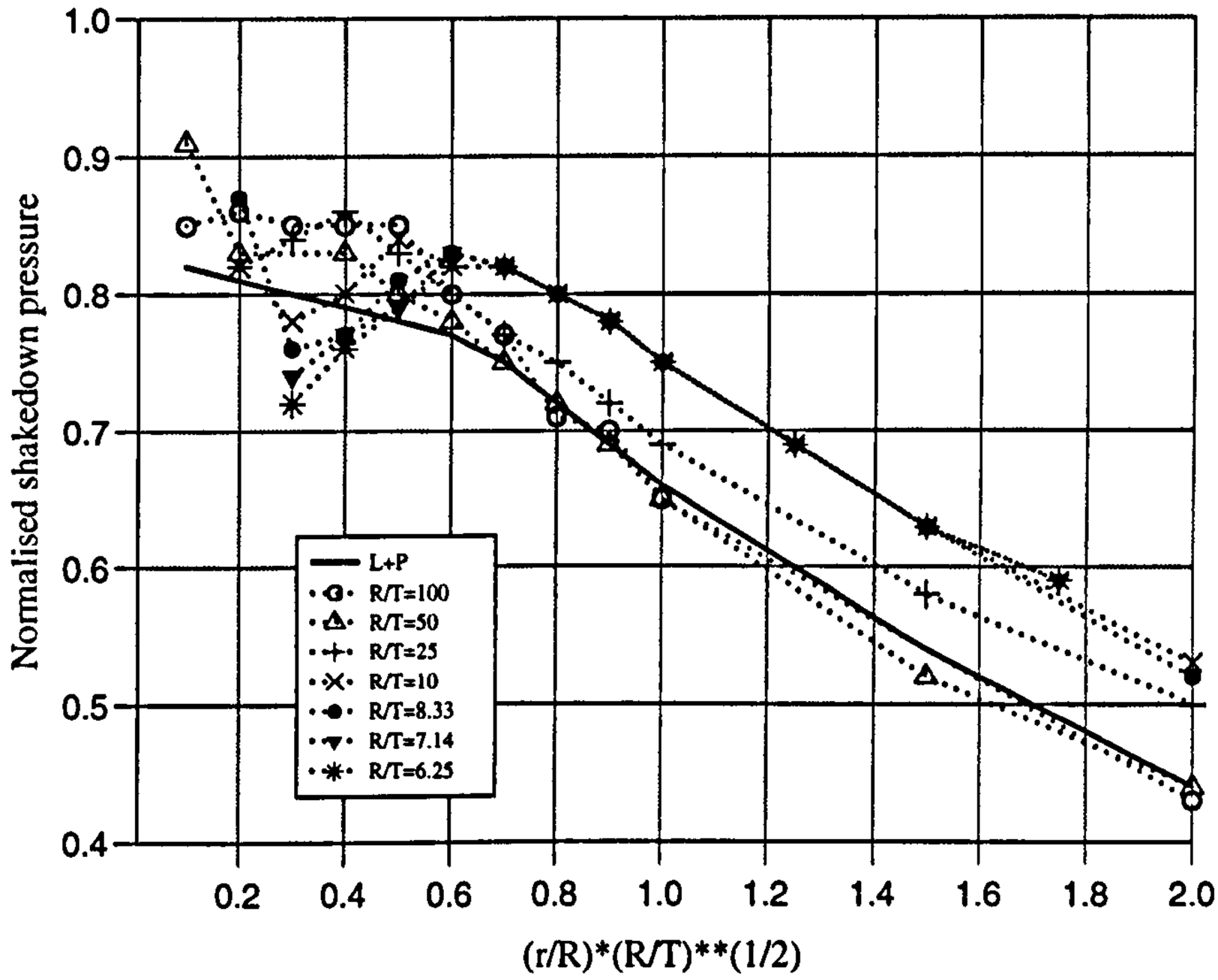

Figure 6.11: Normalised lower bound shakedown pressure of nozzles versus ρ. summary of results

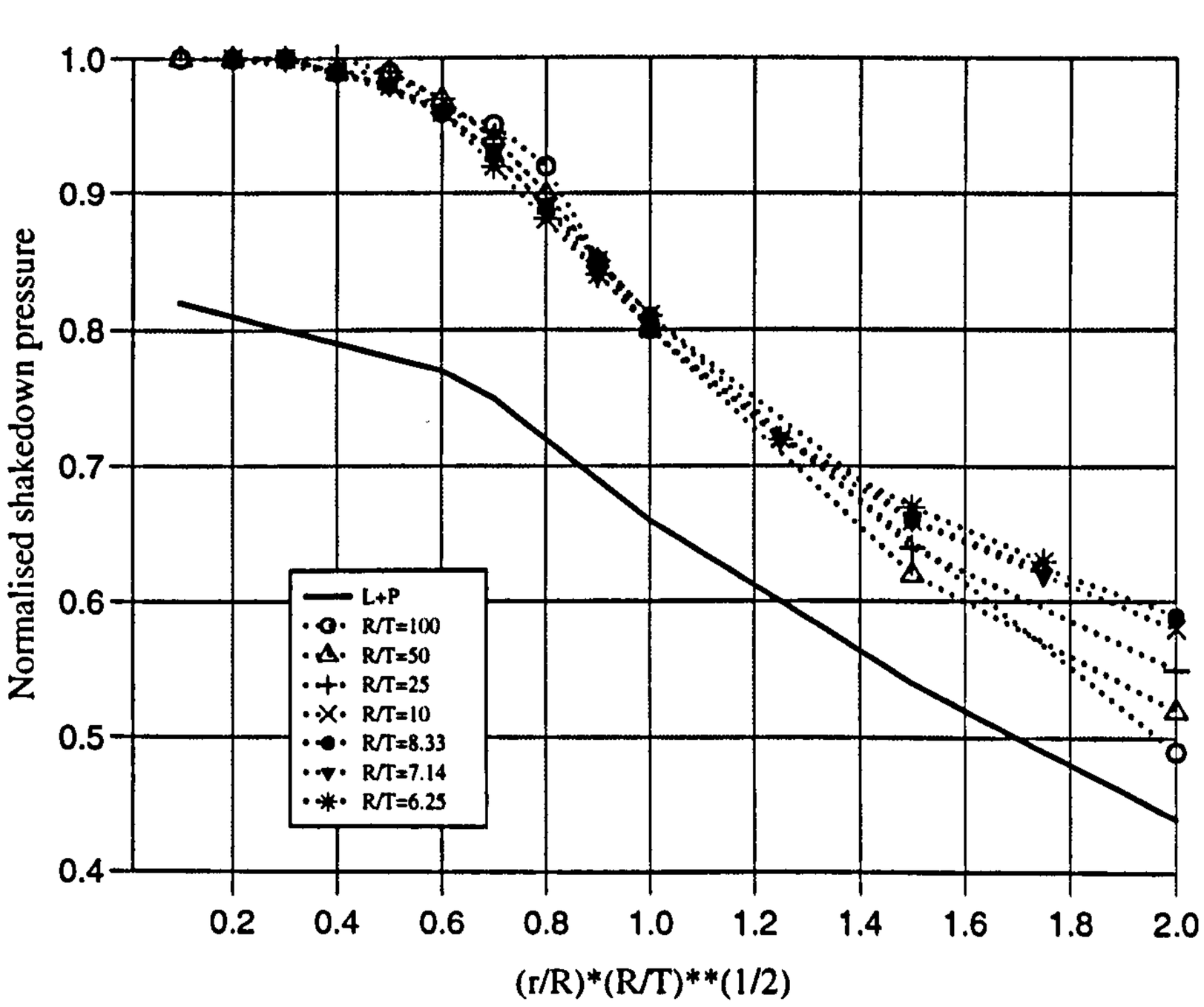

Figure 6.12: Normalised upper bound shakedown pressure of nozzles versus ρ. summary of results

CHAPTER 7

GENERALISED YIELD CRITERIA FOR STRUCTURAL ELEMENTS

7.1 Introduction

One of main the features of this thesis has been the extension of elastic compensation to include structural beam and shell elements. In Chapter 3 it was demonstrated that the use of solid elements led to unnecessarily excessive computations for simple frame problems, as expected.

The extension of elastic compensation to shell and beam analysis is achieved here through so-called generalised yield criteria. Generalised yield concepts have been used in limit analysis of beam and shell structures for a long time. There are many kinds of yield surfaces reported in the literature over the years. In this Chapter the generalised yield criteria for beams and thin shells will be reviewed at first and then finite element implementations for beam elements and shell elements using the elastic compensation will be derived.

7.2 Yield Criteria for Beams

The yield or limit surface concept has been used in inelastic frame analysis to describe the full plastification of thin sections under sectional forces (normal force, shear forces, bending moments, twisting or torsional moment and warping or bimoment). However, the complexity of the generalised yield surface is mainly due to the relatively large number of sectional force parameters used in the description of the yield surface. In addition, it is now well recognized that 'exact' representation of these yield conditions in terms of combined stress resultants, even for the simplest geometry of cross section, are not always available [Hodge 1959, Horne 1968]. Consequently, a wide variety of approximations have been

suggested in the literature. For example, considering the *planar* frame case, a common assumption in modeling the plastic behavior has been to assume that the cross section will yield due to bending moment alone, as in Jennings and Majid [1965], Vijakkhana *et al.* [1974], and Liapunov [1974]. The interaction between axial force and bending moment was considered by Korn and Galambos [1968], and Harung and Millar [1973] in establishing the yield surface of two-dimensional frames.

For circular sections, the relations between the plastic capacities of bending moment and torque was studied by Hill and Siebel [1951, 1953]. The interaction between plastic bending and twisting of I-sections with *warping restraint* was investigated by Boulton [1962], Dinno and Gill [1964], and Dinno and Merchant [1965], and was demonstrated to be significant.

A family of four-dimensional hyperplanar facets was used by Porter and Powell [1971] to approximate a five-dimensional yield surface for a pipe section subjected to internal pressure as well as other loadings. For C- and Z-sections, the yield surface equations were obtained by Gjelsvik [1981] and Doddazio *et al.* [1983], respectively, by neglecting the effect of uniform or St Venant torsion.

Yang and Fan [1988] presented the yield surface equations for I-section with nonuniform torsion using five stress resultants (i.e., normal force, two bending moments, warping moment and torsion). In this latter approach, a component yield surface will be formed for each of thin-walled plates, i.e., the flanges and web, of which the section in composed. Utilizing the stress resultant properties of the I-section, the component yield surfaces can be represented by families of two-dimensional curves. The advantage of this approach is the removal of large number of slope-discontinuous yield surface elements.

Several attempts have been also made for the *exact* derivation of the yield surface equations in special cases. For instance, *neglecting* the warping effect, Morris

and Fenves [1969] determined the yield surface for a number of doubly symmetric sections, in terms of an axial force, two bending moments, and a torque. Using the concept of superposition, Santathadaporn and Chen [1970], Chen and Atsuta [1977], and Zhou and Chen [1985] obtained exact yield surface for various cross-section subjected to axial force and biaxial moments.

In general, the yield surface can be represented by a single-equation surface or multi-faceted surface and also yield surfaces for some commonly used steel sections can be expressed in terms of the location of the central axis [Morris and Fenves 1969], [Santathadaporn and Chen 1970]. However, for a practical structural analysis, it is more convenient to approximate the yield surface by a single equation. Orbison *et al.* [1982] developed a yield surface equation for light- to medium-weight wide-flange sections. Al-Bermani and Kitipornchai [1990] derived yield surface equations for angle and circular hollow sections while Duan and Chen [1990] proposed a generalized four-parameter yield surface equation of this type for doubly symmetric sections (wide-flange, thin-walled circular tube. thin-walled box, rectangular and solid circular sections). This latter reference also included extensive comparisons of various proposed forms. For monosymmetric and asymmetric sections (channel, tee single- and double-angle sections). the yield surface equations were obtained by Kitipornchai *et al.* [1991]. Based on stress resultants approach, Gendy and Saleeb [1993] presented two approximated forms for yield surface equations, semi-quadratic and linear, as reasonable (upper and lower) bounds for two representative cases; i.e., rectangular and wide flange sections. The full plastification surface equation has been developed by Attalla *et al.* [1994] for H-shaped sections subjected to axial force and biaxial bending.

7.2.1 Generalised Yield Surface

Considering a slender beam subjected to axial force, F_x, two shearing forces. F_y and F_z, two bending moments, M_y and M_z, a warping moment. M_w and a torque, T_{sv}, Figure 7.1, (the warping moment is not shown since the nature of this

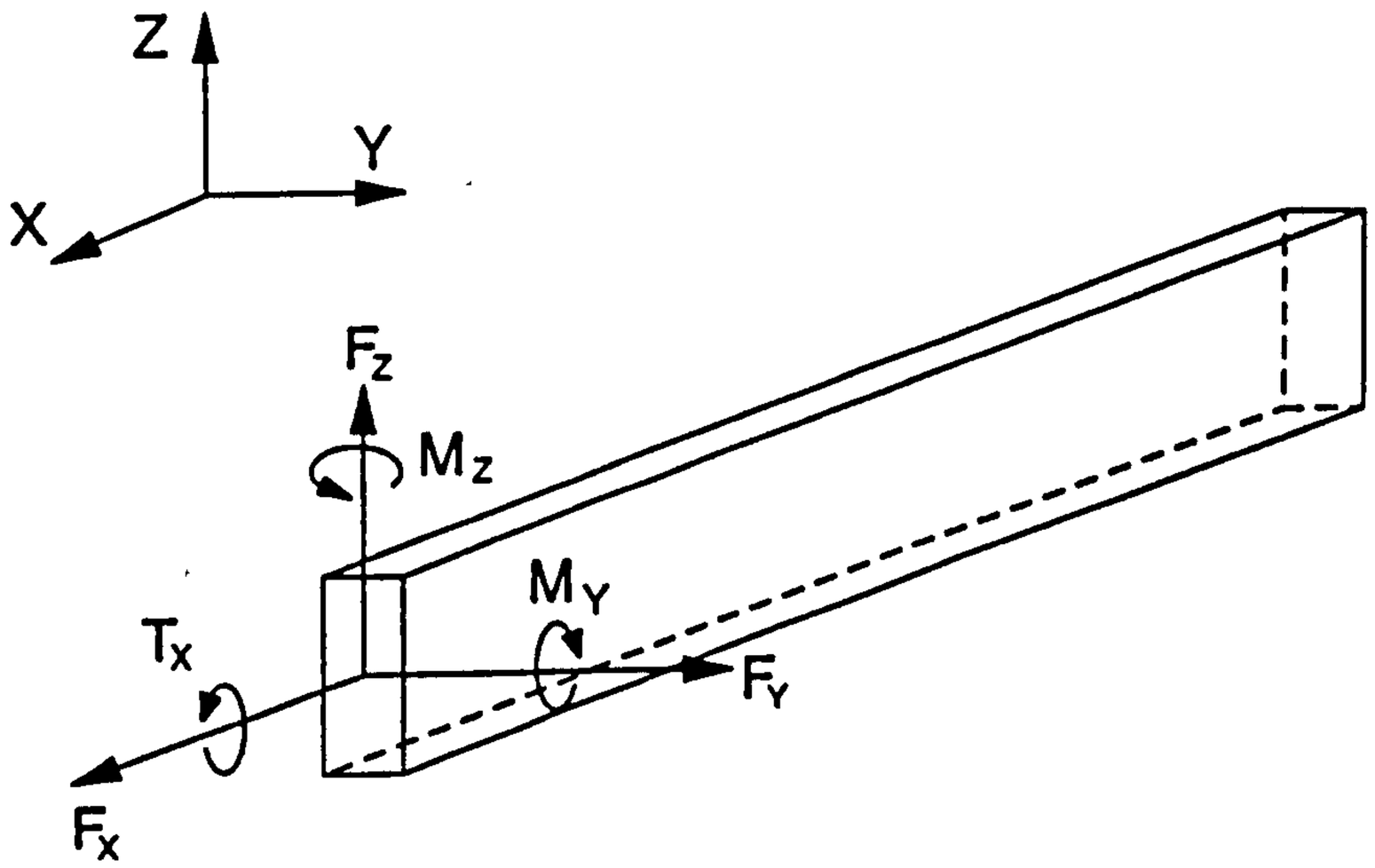

Figure 7.1: Beam element with applied forces and moments

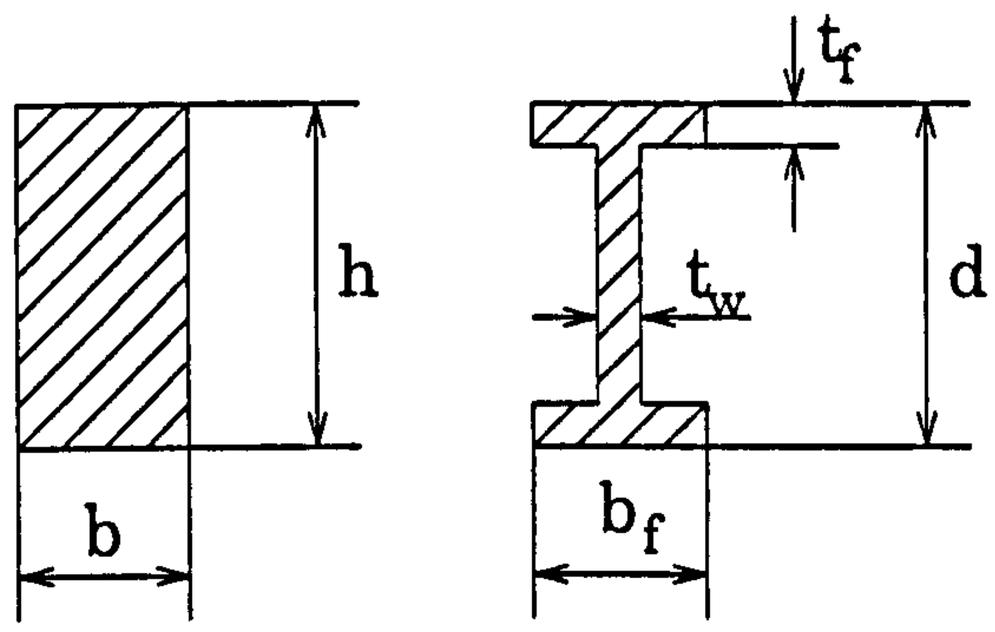

Figure 7.2: Rectangular and wide flange beam cross sections

moment is dependent on section properties). Two different shapes of cross section will be examined: a rectangular section and a wide flange section. Figure 7.2.

The generalised yield conditions are expressed in terms of the non-dimensional quantities

$$f_x = \frac{F_x}{F_{px}}, \quad f_y = \frac{F_y}{F_{py}}, \quad f_z = \frac{F_z}{F_{pz}}$$
$$m_y = \frac{M_y}{M_{py}}, \quad m_z = \frac{M_z}{M_{pz}}, \quad m_w = \frac{M_w}{M_{pw}}, \quad t_{sv} = \frac{T_{sv}}{T_{psv}} \qquad (7.1)$$

Where

F_{px} = full plastic axial force about $x-x$ principle axis

F_{py} = full plastic axial force about $y-y$ principle axis

F_{pz} = full plastic axial force about $z-z$ principle axis

M_{py} = full plastic bending moment about $y-y$ principle axis

M_{pz} = full plastic bending moment about $z-z$ principle axis

M_{pw} = full plastic warping moment

T_{psv} = full plastic torsion due to St Venant

For a rectangular section, Figure 7.2, the fully plastic moments are:

$$F_{px} = \sigma_y bh, \quad F_{py} = \tfrac{1}{\sqrt{3}}\sigma_y bh, \quad F_{pz} = \frac{1}{\sqrt{3}}\sigma_y bh$$

$$M_{py} = \frac{1}{4}\sigma_y hb^2, \quad M_{pz} = \tfrac{1}{4}\sigma_y bh^2, \quad T_{psv} = \frac{1}{2\sqrt{3}}\sigma_y b^2\left(h - \frac{b}{3}\right)$$

where σ_y is the yield stress, b is the width and h is the depth, as shown in Figure 7.2.

For a wide flange section:

$$F_{px} = \sigma_y A_f(2+\beta), \qquad F_{py} = \tfrac{2}{\sqrt{3}}\sigma_y A_f, \qquad F_{pz} = \frac{1}{\sqrt{3}}\sigma_y A_w$$

$$M_{py} = \frac{1}{2}\sigma_y A_f b_f, \quad M_{pz} = \sigma_y A_f d\left(1+\tfrac{\beta}{4}\right), \quad M_{pw} = \frac{1}{4}\sigma_y A_f b_f d$$

$$T_{psv} = \tfrac{1}{\sqrt{3}}\sigma_y A_f\left(t_f + \tfrac{\beta t_w}{4}\right)$$

with $\beta = A_w/A_f$, is the ratio of web area, A_w, to flange area, A_f. b_f the flange width, t_f the flange thickness, t_w the web thickness and d the depth of the section as shown in Figure 7.2.

7.2.2 Duan and Chen's Yield Criteria

The general shape of the yield surface proposed by Duan and Chen [1990] for a double symmetrical section under axial force and biaxial bending moments is

described by

$$m_y^{\alpha_y}(1-f_x^{\beta_z})^{\alpha_z}+m_z^{\alpha_z}(1-f_x^{\beta_y})^{\alpha_y}-(1-f_x^{\beta_y})^{\alpha_y}(1-f_x^{\beta_z})^{\alpha_z}=0 \qquad (7.2)$$

where the four parameter $\alpha_y, \alpha_z, \beta_y$ and β_z are dependent on the sectional shapes. area distribution, and axial forces. For example, for a rectangular section under biaxial loading, $\beta_y = \beta_z = 2$ and $\alpha_y = \alpha_z = 1.7 + 1.3 f_x$.

7.2.3 Gendy and Salleb's Yield Criteria

Based on work by Duan and Chen [1990], a simple and general yield surface for space frames subjected to axial force, two shearing forces, two bending moments. bimoment and torque was proposed by Gendy and Salleb [1993] for two different shapes of cross-sections, i.e., rectangular and wide flange sections, and under the perfectly plastic material assumption. Also two yield criteria were proposed: an upper bound, which is quite accurate, and a less accurate lower bound (based on linear iterpolation).

The *upper bound* of Gendy and Saleeb has a yield function, f_1, with quadratic form

$$f_1 = f_x^2 + f_y^2 + f_z^2 + \frac{1}{\lambda_y} m_y^2 + \frac{1}{\lambda_z} m_z^2 + m_w^2 + t_{sv}^2 - 1 = 0 \qquad (7.3)$$

where λ_y and λ_z depend on the shape of the cross-section as: rectangular cross-section

$$\lambda_y = \lambda_z = 1 - f_x^2 \qquad (7.4)$$

and wide flange cross-section

$$\lambda_y = 1 - f_x, \quad \lambda_z = 1 - 1.1 f_x^{7\beta} \qquad (7.5)$$

The *lower bound* yield function, f_2, has the linear form

$$f_2 = f_x + f_y + f_z + \frac{1}{\eta_y} m_y + \frac{1}{\eta_z} + m_z + m_w + t_{sv} - 1 = 0 \qquad (7.6)$$

where η_y and η_z are also two parameters dependent on the cross-section shapes: rectangular cross-section

$$\eta_y = \eta_z = 1 + f_x \tag{7.7}$$

and wide flange cross-section

$$\eta_y = 1 + 0.3 f_x^{0.75}, \quad \eta_z = 1 + (1.1 + \beta) f_x^{(1.1+0.4\beta)} \tag{7.8}$$

In the the following, the generalised yield criteria, eqns. (7.3) and (7.6), will be used in the form

$$\Pi_1 = (1 + f_1)\sigma_y, \quad \Pi_1 \leq \sigma_y \tag{7.9}$$

$$\Pi_2 = (1 + f_2)\sigma_y, \quad \Pi_2 \leq \sigma_y \tag{7.10}$$

Specifically only equation (7.10), the *lower bound* yield criteria will be used for the work in this study and the effects of warping are not considered.

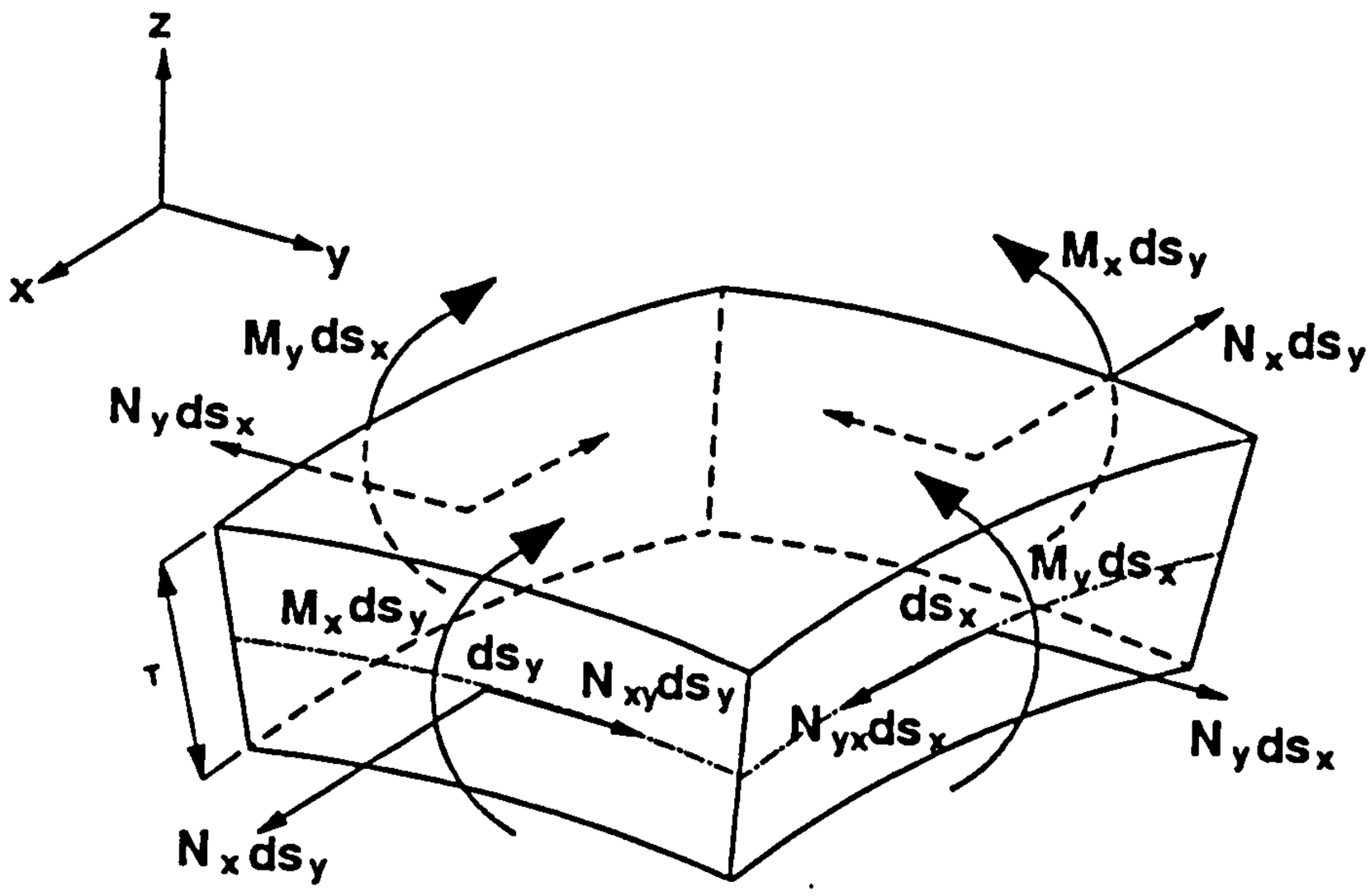

Figure 7.3: Stress resultants

7.3 Yield Criteria for Shells

In many previous studies of limit analysis problems on nozzle/sphere and nozzle/cylinder intersections, shell theories have been used. Therefore for these analyses, it is necessary to obtain the yield surfaces for the materials based on the shell variables. The equilibrium equations of thin shells are most conveniently written in terms of stress resultants as shown in Figure 7.3 and it is therefore also desirable to express the yield condition in terms of stress resultants. This was first examined by Ilyushin [1948] for the general thin shell obeying the von Mises yield criterion. The Kirchhoff-Love hypothesis of straight normals remaining straight and normal to the mid-surface was adopted. as was the assumption that the normal stress has negligible influence on the yield condition. In 1954 Onat and Prager [1954] derived the yield condition for a rotationally symmetric shell obeying the Tresca criterion. However, the resulting four-dimensional yield surface (with variables n_1, n_2, m_1 and m_2) is a function of three parameters p, q, r and so the yield condition is not expressed in terms only of the stress

resultants. However, it is possible in this case to eliminate p, q and r and to obtain a yield surface in terms of n_1, n_2, m_1 and m_2.

In 1961 Hodge [1961] derived a parametric representation of the yield surface for a rotationally symmetric shell with the von Mises criterion. Again there are three parameters p, q and r but this time it is not possible to eliminate them all. The approach of Hodge [1961] is different from Ilyushin [1948] where even for non-rotationally symmetric shells the quadratics of stress resultants are functions of only two parameters ζ and μ. However, the physical assumptions imply that these yield surfaces are equivalent and indeed p and q are evidently alternative parameters for ζ and μ in the rotationally symmetric case.

Ilyushin published his work in Russian [1948] and in French [1956], but an English version of his work was not available until it was translated by Crisfield [1974]. Various other approximations have been made to the exact Ilyushin surface and these have been discussed in some detail by Robinson [1971]. This work was discussed by Burgoyne [1979], and one of the alternative yield surfaces, that due to Ivanov [1967], has been used subsequently in numerical studies of plate and shell buckling problems by Crisfield [1979]. Ivanov uses a quadratic representation of yield surface in Q-space, as opposed to the linear representation of the approximate Ilyushin yield surface. Very recently Burgoyne and Brennan [1993] presented a reparametrization of the Ilyushin yield criterion for thin plates. These yield surfaces will be briefly introduced in the following subsection. More detailed reviews can be found in the books of Olszak & Sawczuk (1967), Save & Massonnet (1972) and Zyczkowski (1981).

7.3.1 Generalized Yield Condition

The principal stress resultants on an element of rotationally symmetric shell with rationally symmetric loading are N_1, N_1, M_1, M_2 as shown in Figure 7.1.

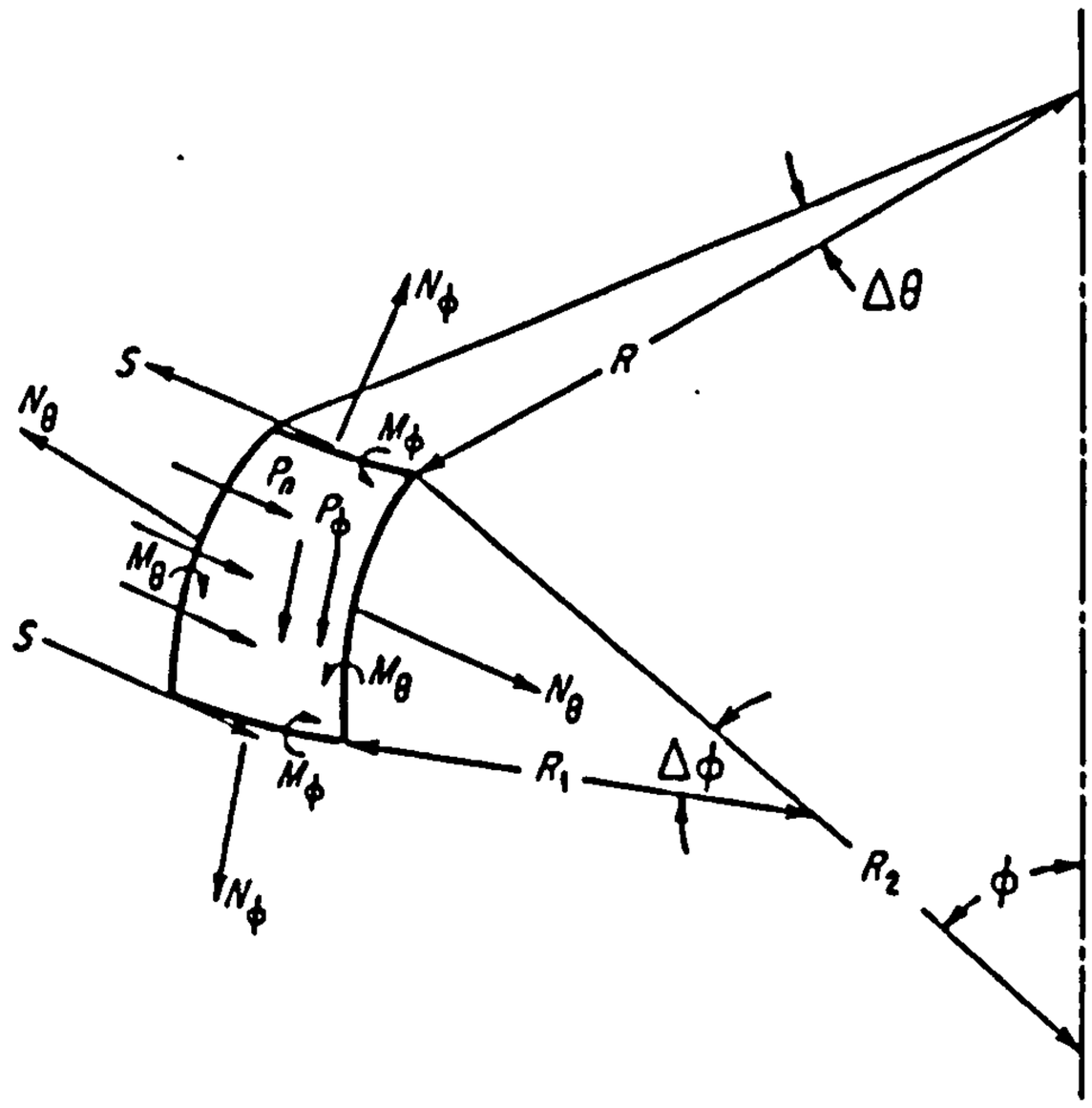

Figure 7.4: Shell element

The yield criterion may be written

$$f(N_1, N_2, M_1, M_2) = 1 \tag{7.11}$$

This expression for a rigid ideally plastic material means that for combinations of N_1, N_2, M_1, M_2 for which $f < 1$ the shell element is rigid. When $f = 1$, plastic flow takes place and f can never exceed unity.

7.3.2 Hodge [1954] Yield Surface for a Sandwich Shell (Tresca Material)

In 1954 Hodge derived a generalised yield surface for a sandwich shell using Tresca's yield criterion. A simplified outline of the process is described as follows:

Supposing an ideal sandwich shell is composed of two thin sheets. each of thickness T separated by a core of thickness $2H'$. which have a tensile yield stress σ'_y and are so thin that stress variation across each sheet can be neglected. and the core has sufficient stuffness to maintain the separation of the sheets but no tensile strength.

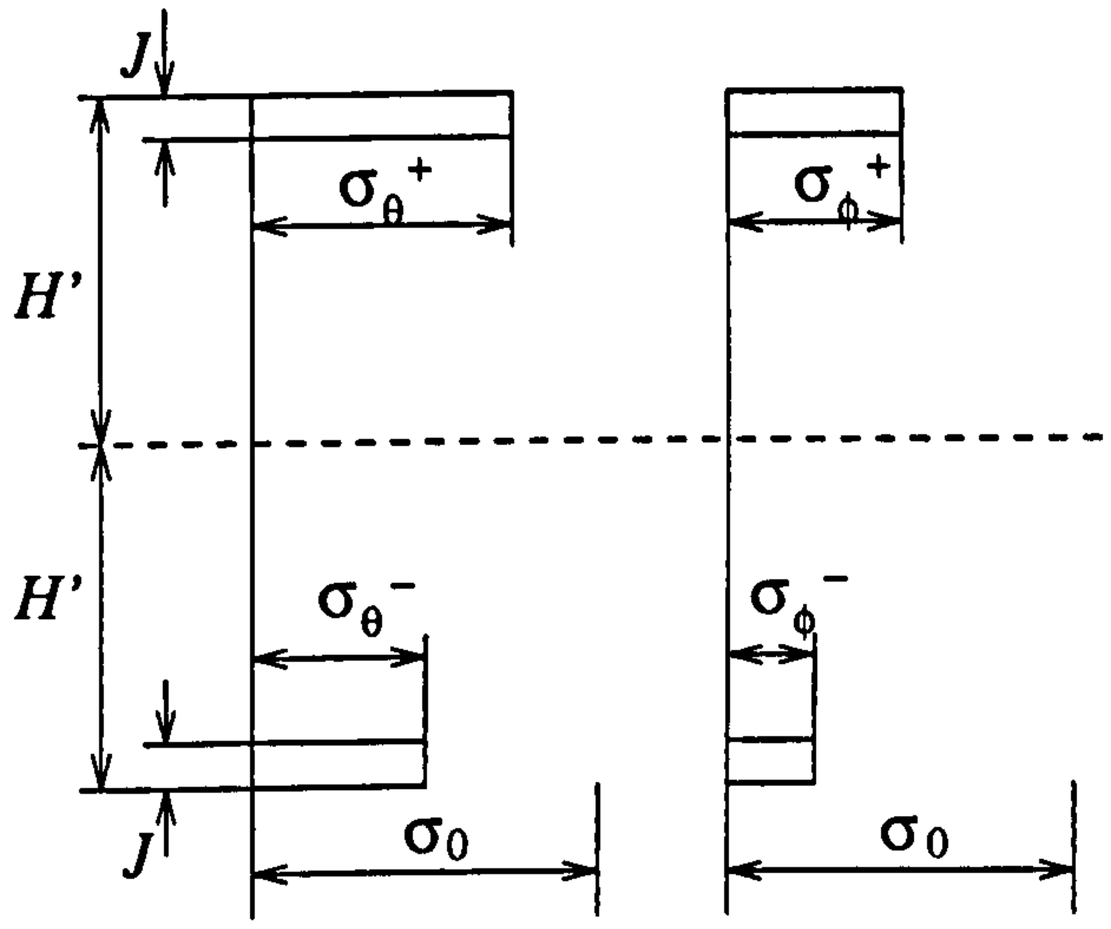

Figure 7.5: Stress distribution in ideal sandwich shell

Under these definitions,

$$N_0 = 2\sigma_y' T, \quad M_0 = 2\sigma_y' H' T \tag{7.12}$$

The corresponding values for a uniform shell of thickness $2H$ are

$$N_0 = 2\sigma_y H, \quad M_0 = \sigma_y H^2 \tag{7.13}$$

Therefore, the two shells will be equivalent if

$$\sigma_y' T = \sigma_y H, \quad H' = \frac{1}{2} H \tag{7.14}$$

Figure 7.5 shows the stress distribution at a typical point in the shell. Evidently the stress resultants are

$$N_1 = T(\sigma_1^+ + \sigma_1^-), \quad N_2 = T(\sigma_2^+ + \sigma_2^-)$$
$$M_1 = H'T(\sigma_1^- - \sigma_1^+), \quad M_2 = H'T(\sigma_2^- - \sigma_2^+) \tag{7.15}$$

In theory, and in most of the examples that follow, it is convenient to deal exclusively with dimensionless quantities. To this end we denote by N_0 the maximum direct stress which the shell can withstand in uniaxial tension and by M_0

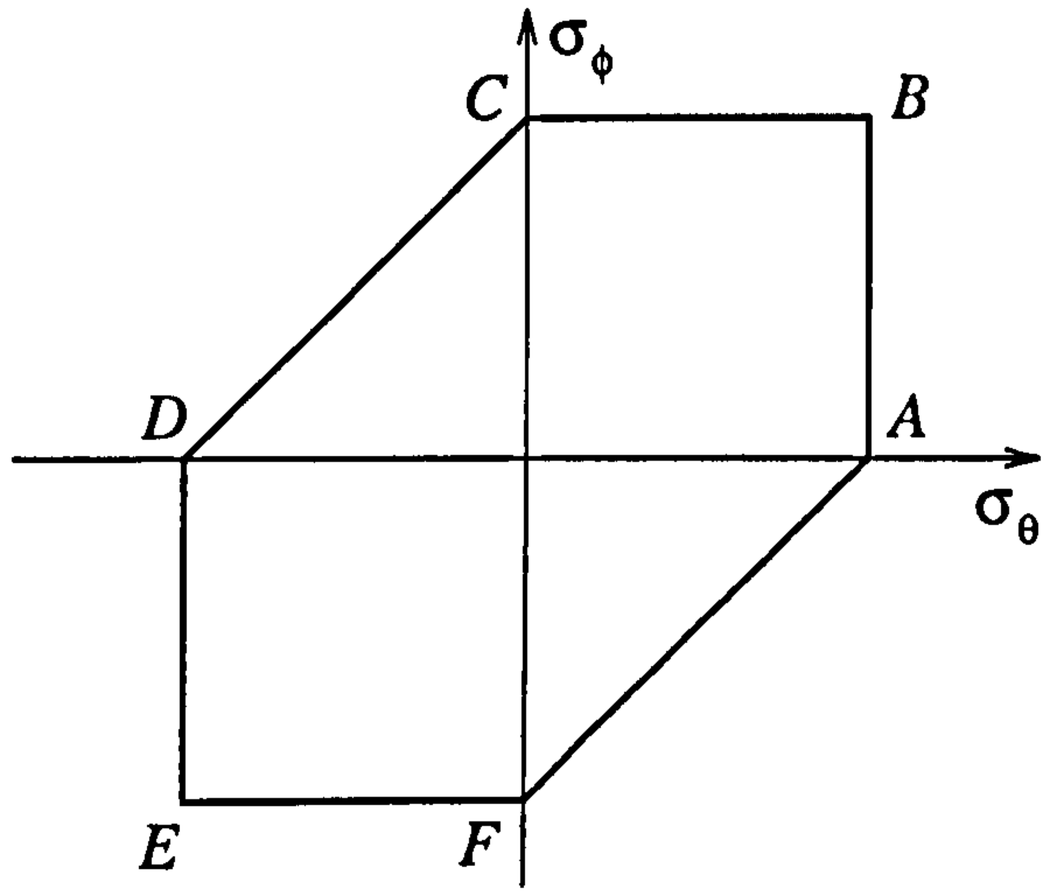

Figure 7.6: Tresca yield condition

the maximum uniaxial bending moment and define

$$n_1 = N_1/N_0, \qquad n_2 = N_2/N_0$$
$$m_1 = M_1/M_0, \qquad m_2 = M_2/M_0$$
$$\kappa_1 = (M_0/N_0)K_1, \quad \kappa_2 = (M_0/N_0)K_2 \tag{7.16}$$

where K_1 is the curvature in the circumferential direction and K_2 the curvature in the meridional direction.

Solving eqns. (7.16) for the stresses and introducing dimensionless stress resultants from eqns. (7.13) and (7.17) following forms are obtained

$$\sigma_1^+ = \sigma_y'(n_1 - m_1), \quad \sigma_2^+ = \sigma_y'(n_2 - m_2)$$
$$\sigma_1^- = \sigma_y'(n_1 + m_1), \quad \sigma_2^- = \sigma_y'(n_2 + m_2) \tag{7.17}$$

Tresca's yield condition states that the maximum shearing stress is less than half the tensile yield stress; hence

$$\max(|\sigma_1|, \quad |\sigma_2|, \quad |\sigma_1 - \sigma_2|) \leq \sigma_y' \tag{7.18}$$

The six inequalities implied by (7.18) must be satisfied by the stress in both the top and bottom sheets as given by eqns. (7.17). Therefore, the Tresca yield condition for the ideal sandwich shell consists of the twelve linear expressions listed

Table 7.1: *Tresca condition for sandwich shell [Hodge, 1960]*

Face	(σ_1, σ_2) Point		Stress Equation	Strain-Rate Vector
	Top	Bottom		
1	AB		$n_1 - m_1 = 1$	$\mu(1, 0, -1, 0)$
2	BC		$n_2 - m_2 = 1$	$\mu(0, 1, 0, -1)$
3	CD		$-n_1 + n_2 + m_1 - m_2 = 1$	$\mu(-1, 1, 1, -1)$
4	DE		$-n_1 + m_1 = 1$	$\mu(-1, 0, 1, 0)$
5	EF		$-n_2 + m_2 = 1$	$\mu(0, -1, 0, 1)$
6	FA		$n_1 - n_2 - m_1 + m_2 = 1$	$\mu(1, -1, -1, 1)$
7		AB	$n_1 + m_1 = 1$	$\mu(1, 0, 1, 0)$
8		BC	$n_2 + m_2 = 1$	$\mu(0, 1, 0, 1)$
9		CD	$-n_1 + n_2 - m_1 + m_2 = 1$	$\mu(-1, 1, -1, 1)$
0		DE	$-n_1 - m_1 = 1$	$\mu(-1, 0, -1, 0)$
α		EF	$-n_2 - m_2 = 1$	$\mu(0, -1, 0, -1)$
β		FA	$n_1 - n_2 + m_1 - m_2 = 1$	$\mu(1, -1, 1, -1)$

in Table 7.1. Since each of the faces of the resultant yield surface corresponds to one of the original Tresca yield conditions (Figure 7.6), a correspondence between physical stress point and stress-resultant point may be set up as indicated in Table 7.1.

The direction of the strain-rate vector is the same for all stress points on a given face; it is given by the gradient of the equation of the face as indicated in the last column of Table 7.1. At the intersection of two or more faces, it is evident that the resulting strain-rate vector may be any linear combination with positive coefficients of the strain-rate vectors for the corresponding sides.

7.3.3 Onat and Prager [1954] Yield Surface for a Uniform Shell (Tresca Material)

A generalised yield surface based on Tresca's condition for a uniform shell was first obtained by Onat and Prager [1954]. Here their method will be presented briefly.

The first step is to define the strain-rate vector in terms of a magnitude parameter ν and three direction parameters p, q and r. Thus

$$p = -\frac{\dot{e}_1}{4\dot{\kappa}_1}, \quad r = -\frac{\dot{e}_2}{4\dot{\kappa}_2}, \quad q = -\frac{1}{4}\frac{\dot{e}_1 + \dot{e}_2}{\dot{\kappa}_1 + \dot{\kappa}_2} \tag{7.19}$$

Therefore, the strain-rate vector is

$$\mathbf{q} = \nu[-4p(q-r), \quad -4r(p-q), \quad q-r, \quad p-q] \tag{7.20}$$

The stain rates in the material are now known in terms of p, q, and r since

$$\dot{\epsilon}_1 = \dot{e}_1 + 2\zeta\dot{\kappa}_1, \quad \dot{\epsilon}_2 = \dot{e}_2 + 2\zeta\dot{\kappa}_2 \tag{7.21}$$

ζ being the dimensionless coordinate in the thickness direction. Therefore, for any given p, q and r, $\dot{\epsilon}_1$ and $\dot{\epsilon}_2$ can be found for each ζ. The vector $(\dot{\epsilon}_1, \dot{\epsilon}_2)$ must be normal to the Tresca yield hexagon (Figure 7.6), hence the stresses are easily found. Finally, an integration yields the stress resultants in terms of the parameters p, q, and r. An ingenious graphical method is used in the paper of Onat and Prager [1954] to reduce the computations. The results are summarized in Table 7.2 which is subject to the following interpretations:

In all cases the upper or lower signs must be used consistently in a given line, the correct choice being that which makes $\mathbf{Q} \cdot \mathbf{q}$ positive.

If p, q and r are all distinct and all within the interval $(-\frac{1}{2}, \frac{1}{2})$, then the 'intermediate parameter' in Table 7.2 is the one of p, q, r which lies between the other two.

If p, q, and r are still distinct but one or more is greater than $\frac{1}{2}$, it must be replaced by $-\frac{1}{2}$.

Table 7.2: *Tresca condition for uniform shell [Hodge, 1960]*

Intermediate Parameter	Stress Resultants			
	n_1	n_2	m_1	m_2
p	$\mp(p+q)$	$\mp(p-r)$	$\pm 1 \mp 2(p^2+q^2)$	$\pm 2(r^2-q^2)$
q	$\mp(p+q)$	$\mp(q+r)$	$\pm 1 \mp 2(p^2+q^2)$	$\pm 1 \mp 2(q^2+r^2)$
r	$\mp(q-p)$	$\mp(q+r)$	$\pm 2(p^2+q^2)$	$\pm 1 \mp 2(q^2+r^2)$

If any of the parameters p, q or r become indeterminate as computed from eqns. (7.20), then the other two parameters must necessarily be equal. For example, if $\dot{e}_2 = \dot{\kappa}_2 = 0$, r is indeterminate and $p = q$. The appropriate yield surface is obtained when p is set equal to q in either of the first two lines of Table 7.2 and eliminated from those stresses which are independent of r. Thus, if $p = q$ the yield surface is

$$m_1 = \pm(1 - n_1^2) \tag{7.22}$$

Simmilarly, if $r = q$, either of the last two lines of Table 7.2 leads to

$$m_2 = \pm(1 - n_2^2) \tag{7.23}$$

Then, if $p = r$, the first or third lines show that

$$m_1 - m_2 = \pm[1 - (n_1 - n_2)^2] \tag{7.24}$$

Finally, if $p = q = r$, Table 7.2 can be used with the convention that the 'intermediate parameter' corresponds to the absolutely largest numerator of eqns. (7.19).

7.3.4 Hodge [1961] Yield Surface for Sandwich Shell (Mises Material)

Seven years later after his generalised yield surface for a sandwich shell was derived using Tresca's criterion, Hodge, in 1961, obtained a generalised yield condition for the same problem using von Mises's criterion [Hodge 1961]. This

formulation is very briefly presented as following:

In terms of principal stresses σ_1, σ_2, the Mises yield condition takes the form

$$\sigma_1^2 - \sigma_1\sigma_2 + \sigma_2^2 = (\sigma_y')^2 \tag{7.25}$$

Therefore, the desired yield condition is obtained by substituting eqns. (7.16) in eqn. (7.25). This leads to two nonlinear equations,

$$\begin{aligned} (n_1 + m_1)^2 - (n_1 + m_1)(n_2 + m_2) + (n_2 + m_2)^2 &\leq 1 \\ (n_1 - m_1)^2 - (n_1 - m_1)(n_2 - m_2) + (n_2 - m_2)^2 &\leq 1 \end{aligned} \tag{7.26}$$

For a point on the yield surface, the equality sign must hold in one equation of (7.26) and the inequality in the other. The strain-rate vectors corresponding to equality in (7.26), respectively, are

$$\begin{aligned} \mathbf{q} = \nu^{\pm}[&2(n_1 \pm m_1) - (n_2 \pm m_2), \\ &2(n_2 \pm m_2) - (n_1 \pm m_1), \\ &2(m_1 \pm n_1) - (m_2 \pm n_2), \\ &2(m_2 \pm n_2) - (m_1 \pm n_1)] \end{aligned} \tag{7.27}$$

If the equality sign holds in both parts of (7.26), the stress point is on the intersection of the two hypersurfaces; the strain-rate vector may be any linear combination with positive coefficients of the two vectors defined in (7.27).

7.3.5 Hodge [1961] Yield Surface for Uniform Shell (Mises Material)

Following his work for a sandwich shell, Hodge, at meantime, derived a generalised yield surface for a uniform shell using von Mises's yield criterion [Hodge 1961], but due to the complexity of the formulation this condition will not be presented here.

Table 7.3: *One-moment limited-interaction surface*

Face	Equation	Strain-rate Vector $(\dot{e}_1, \dot{e}_2, \dot{\kappa}_2)$
1	$n_1 = 1$	$\mu(1, 0, 0)$
2	$n_2 = 1$	$\mu(0, 1, 0)$
3	$-n_1 + n_2 = 1$	$\mu(-1, 1, 0)$
4	$-n_1 = 1$	$\mu(-1, 0, 0)$
5	$-n_2 = 1$	$\mu(0, -1, 0)$
6	$n_1 - n_2 = 1$	$\mu(1, -1, 0)$
7	$m_2 = 1$	$\mu(0, 0, 1)$
8	$-m_2 = 1$	$\mu(0, 0, -1)$

7.3.6 Other Approximate Yield Surfaces

Each of the generalised shell yield surfaces discussed above has been applied to a variety of problems, but inevitably because of the complexity involved the problems solved are not often of practical importance. Therefore, some attention has been given to the formulation of simpler approximate generalised yield surfaces since then.

7.3.6.1 One-Moment Limited-Interaction Surface

One such approximation has been proposed by Drucker and Shield [1959]. They argue that in most rotationally symmetric shell problems the moments are generally small compared with the direct stresses. Therefore, they ignored completely the hoop moment m_2. The longitudinal moment m_1 must be retained if boundary conditions are to be satisfied, but any interaction between it and the direct stresses is neglected. The resulting yield condition is defined by the eight planes listed in Table 7.3; it will be referred to as a one-moment limited-interaction surface.

Although the one-moment limited-interaction surface may lead to practically important results in problems for which its assumptions are reasonably valid, it is open to certain theoretical objections. In the first place, in order to eliminate m_1 from the problem, the equilibrium equations must be modified. Therefore, the theorems of limit analysis are no longer applicable. Further, it is not clear whether the arguments used to show that moments are unimportant in the case of static loading are equally valid under dynamic loads. Finally, even shells which are not shallow in the large may contain regions near the axis of symmetry where m_1 is locally important.

7.3.6.2 Two-Moment Limited-Interaction Surface

A modification of the one-moment limited-interaction surface which appears to eliminate some of its drawbacks while at the same time retaining much of its simplicity was proposed by Hodge [1960]. This surface, called the two-moment limited-interaction surface, is based on the premise that in most shell problems the moments and direct forces will not be of simultaneous importance so that yield relations between moment and force are of limited importance. However, the theory recognizes that either moment or direct force may dominate so that all resultants must be included. Thus, all interaction between force and force, or between moment and moment, is maintained, but all interactions between force and moment are neglected. The result is a linear surface in four dimensional space defined by the twelve planes listed in Table 7.4. Evidently, the twelve planes represent the six conditions on direct stresses in the absence of moments and the six conditions on moments in the absence of direct stresses.

Table 7.4: *Two-moment limited-interaction surface*

Face	Equation	Strain-rate Vector $(\dot{\epsilon}_1,\ \dot{\epsilon}_2,\ \dot{\kappa}_1,\ \dot{\kappa}_2)$
1	$n_1 = 1$	$\mu(1,\ 0,\ 0,\ 0)$
2	$n_2 = 1$	$\mu(0,\ 1,\ 0,\ 0)$
3	$-n_1 + n_2 = 1$	$\mu(-1,\ 1,\ 0,\ 0)$
4	$-n_1 = 1$	$\mu(-1,\ 0,\ 0,\ 0)$
5	$-n_2 = 1$	$\mu(0,\ -1,\ 0,\ 0)$
6	$n_1 - n_2 = 1$	$\mu(1,\ -1,\ 0,\ 0)$
7	$m_1 = 1$	$\mu(0,\ 0,\ 1,\ 0)$
8	$m_2 = 1$	$\mu(0,\ 0,\ 0,\ 1)$
9	$-m_1 + m_2 = 1$	$\mu(0,\ 0,\ -1,\ 1)$
0	$-m_1 = 1$	$\mu(0,\ 0,\ -1,\ 0)$
α	$-m_2 = 1$	$\mu(0,\ 0,\ 0,\ -1)$
β	$m_1 - m_2 = 1$	$\mu(0,\ 0,\ 1,\ -1)$

7.3.7 Iluyshin [1948] Yield Surface for a Uniform Shell (Mises Material)

The first investigation of yield conditions for shells was carried out by Ilyushin [1948]. He derived an exact form of the yield surface for a linear elastic, perfectly plastic isotropic material which obeys von Mises yield criterion.

The shell is assumed to be thin, so that z/R terms have been neglected in comparison with unity (z is thickness of shell and R is any radius of curvature). The shell material is assumed to be isotropic and does not strain harden. The non-dimensional stress resultants are defined:

$$n_{1,2} = \frac{1}{\sigma_y T}\int_{-T/2}^{T/2}\sigma_{1,2}dz \quad and \quad m_{1,2} = \frac{1}{\sigma_y T^2}\int_{-T/2}^{T/2}\sigma_{1,2}zdz \tag{7.28}$$

where

$\sigma_{1,2}$ – a stress component,

σ_y – yield stress of material in simple tension,

T – thickness of shell,

$n_{1,2}$ – dimensionless stress resultants acting on a shell element, $n = N/\sigma_y T$,

$m_{1,2}$ – dimensionless bending moments acting on a shell element, $m = 4M/\sigma_y T^2$.

The material is assumed to obey von Mises' yield criterion:

$$f = \frac{(\sigma_1^2 - \sigma_1\sigma_2 + \sigma_2^2 + 3\sigma_{12}^2)}{\sigma_y^2} = 1 \tag{7.29}$$

It will then be convenient to define quadratic stress intensities Q_t, Q_m and Q_{tm} as:

$$\begin{aligned} Q_t &= n_1^2 + n_2^2 - n_1 n_2 + 3n_{12}^2 \\ Q_m &= m_1^2 + m_2^2 - m_1 m_2 + 3m_{12}^2 \\ Q_{tm} &= n_1 m_1 - \frac{1}{2} n_1 m_2 - \frac{1}{2} n_2 m_1 + n_2 m_2 + 3n_{12} m_{12} \end{aligned} \tag{7.30}$$

Corresponding to the quadratic stress intensities, quadratic strain intensities can also be defined:

$$\begin{aligned} P_\epsilon &= \epsilon_1^2 + \epsilon_2^2 - \epsilon_1\epsilon_2 + \epsilon_{12}^2 \\ P_\kappa &= \kappa_1^2 + \kappa_2^2 - \kappa_1\kappa_2 + \kappa_{12}^2 \\ P_{\epsilon\kappa} &= = \kappa_1(\epsilon_1 + \frac{1}{2}\epsilon_2) + \kappa_2(\epsilon_2 + \frac{1}{2}\epsilon_1) + \kappa_{12}\epsilon_{12} \end{aligned} \tag{7.31}$$

where

ϵ_1, ϵ_2, ϵ_{12} – strain components,

κ_1, κ_2, κ_{12} – dimensionless curvature components.

There are six stress resultants for any element of the shell, n_1, n_2, n_{12}, m_1, m_2 and m_{12}, so the yield surface will be a function of five parameters. By considering the three non-dimensional quadratic stress intensities, Q_t, Q_m and Q_{tm}, the surface can be reduced to a surface in a 3-dimensional space, and can thus be represented by two independent parameters. Ilyushin [1948] represented the

surface in terms of two non-dimensional parameters ζ and μ. The derivation can be found in Crisfield's paper [1974a], and the resulting equations summarized as:

$$Q_t = \frac{1}{\Delta_1^2}(\mu^2\psi^2 + 2^2)$$

$$Q_{tm} = \frac{2}{\Delta_1^3}(\mu^2\Delta\psi^2 + \Delta 2^2 + \mu^2 2\psi + 2\chi)$$

$$Q_m = \frac{4}{\Delta_1^4}[\mu^2\psi^2(\mu^2+\Delta^2)+2^2(4\mu 2+\Delta^2)+2\mu^2\Delta 2\psi-2\mu^2\psi\chi+2\Delta 2\chi+\chi^2] \quad (7.32)$$

where

$$2 = \zeta - 1,$$

$$\psi = |\log_e \frac{[1+\sqrt{(1-\mu^2)}]}{\mu} \pm log_e \frac{[\zeta+\sqrt{(\zeta^2-\mu^2)}]}{\mu}|,$$

$$\chi = |\sqrt{(1-\mu^2)} \pm \zeta\sqrt{(\zeta^2-\mu^2)}|,$$

$$\Delta_1 = \sqrt{(1-\mu^2)} \pm \sqrt{(\zeta^2-\mu^2)},$$

$$\Delta = \frac{\sqrt{(1-\zeta^2)}}{\Delta_1},$$

subject to the conditions that

$$0 \leq \mu \leq 1$$

$$\mu \leq \zeta \leq 1 \quad (7.33)$$

(Note that Ilyushin actually used (λ) instead of (ζ) written here; this has been changed to avoid confusion with the plastic strain rate multiplier which is conventionally also represented by λ). Either the plus sign is taken throughout or the minus sign throughout. This formulation results in a negative Q_{tm} but it is shown that by using a different range of ζ and μ we obtain the reflexion of the above surface about $Q_{tm} = 0$. Since only $|Q_{tm}|$ will be considered, this additional part yields nothing new.

Ilyushin then goes on to give several particular cases where this relation can be expressed directly in terms of Q_t, Q_m and Q_{tm}:

(i) $P_\epsilon > 0$, $P_\kappa = 0$, for which the yield surface is $Q_m = 0$, $Q_t = 1$.

(ii) $P_\kappa > 0$, $P_\epsilon = 0$, for which $Q_m = 1$, $Q_t = 0$,

(iii) $P_\epsilon > 0$, $P_\kappa > 0$, $P_{\epsilon,\kappa} = 0$. With this latter case $\zeta = 1$ and therefore $Q_{tm} = 0$. The other two quadratic forms Q_t and Q_m are expressed in terms of μ

but it is shown that for all values of μ

$$1 \leq Q_t + Q_m \leq 1.096$$

Therefore a first approximation to the yield surface is, for all ζ and μ,

$$Y_1 = Q_t + Q_m = 1 \tag{7.34}$$

(iii) contains (i) and (ii) as limiting cases.

Letting a vector $\mathbf{a} = (2n_1 - n_2,\ \sqrt{3n_2},\ 2\sqrt{3n_{12}})$ and $\mathbf{b} = (2m_1 - m_2.\ \sqrt{3m_2}.\ 2\sqrt{3m_{12}})$ and applying the Schwarz inequality

$$|\mathbf{a}| \cdot |\mathbf{b}| \geq |\mathbf{a} \cdot \mathbf{b}|$$

yields

$$Q_t Q_m \geq Q_{tm}^2$$

which occurs only when $n_1/m_1 = n_2/m_2 = n_{12}/m_{12}$, the yield condition becomes

$$Y_2 = Q_m = (1 - Q_t)^2 \tag{7.35}$$

In this case the parameter $\mu = 0$ and $0 \leq Q_t \leq 1$. The maximum value of $|Q_{tm}|$ occurs when

$$Q_m = \frac{4}{9},\ \ Q_t = \frac{1}{3},\ \ \text{and}\ \ |Q_{tm}| = \frac{2}{9}\sqrt{3}$$

This lies on the planes

$$Y_3 = Q_t + Q_m + |Q_{tm}|/\sqrt{3} = 1 \tag{7.36}$$

7.3.8 Iluyshin [1948] Yield Surface for a Sandwich Shell (Mises Material)

Now consider the von Mises sandwich shell yield criterion. In this approximation the uniform shell is replaced by a sandwich one in which a central

core carries the shear stresses q_1 and q_2 and the outer layers carry stresses $(n_1+m_1,\ n_2+m_2,\ n_{12}+m_{12})$ and $(n_1-m_1,\ n_2-m_2,\ n_{12}-m_{12})$ respectively. For details see Nakamura [1963]. Therefore, we have two yield criteria:

$$(n_1 \pm m_1)^2 + (n_2 \pm m_2)^2 - (n_1 \pm m_1)(n_2 \pm m_2) + 3(n_{12} \pm m_{12}) \leq 1$$

where the plus sign is used throughout for one face and the minus sign for the other. Thus

$$Y_4 = Q_t + Q_m + 2|Q_{tm}| = 1 \tag{7.37}$$

If yielding occurs on one face only, the normality rule gives

$$\kappa_1 = \pm\epsilon_1,\quad \kappa_2 = \pm\epsilon_2,\quad \kappa_{12} = \pm\epsilon_{12}$$

On the other hand,

(i) if $P_\epsilon > 0,\ P_\kappa = 0$, yielding occurs on both faces and we get $Q_t = 1,\ Q_m = 0$.

(ii) if $P_\kappa > 0,\ P_\epsilon = 0$, yielding occurs on both faces and $Q_m = 1,\ Q_t = 0$.

(iii) if $P_\kappa > 0,\ P_\epsilon > 0,\ P_{\epsilon\kappa} = 0$, then again yielding occurs on both faces and so:

$$Q_t + Q_m + 2Q_{tm} = 1$$

$$Q_t + Q_m - 2Q_{tm} = 1$$

Hence

$$Q_{tm} = 0 \ \text{ and } \ Q_t + Q_m = 1$$

Thus for restrictions (i), (ii) and (iii) the sandwich shell condition and Ilyushin's condition are equivalent.

7.3.9 Rozenblyum [1954] Yield Surface for a Uniform Shell (Mises Material)

Rozenblyum [1954] proposed another alternative yield surface by assuming a linear stress distribution across the shell thickness and postulating the yield

condition as an average. The resulting yield surface is

$$Q_t + \frac{3}{4}Q_m = 1 \tag{7.38}$$

It can immediately be seen that this is very similar to equation (7.34). It is indicated by Robinson [1971] that equation (7.38) is not a very good approximation.

7.3.10 Ivanov [1967] Yield Surface for a Uniform Shell (Mises Material)

The approximate yield surfaces so far considered have been linear in the variables Q_t, Q_m and Q_{tm} with the exception of equation (7.35), which was $Q_m = (1 - Q_t)^2$. The equation (7.36) is very close to the optimum linear approximation but by introducing more complicated expressions it is possible to get closer bounds. This has been done by Ivanov [1967]. He presents two approximations:

$$Y_5 = Q_t + \frac{1}{2}Q_m + \sqrt{\frac{1}{4}Q_m^2 + Q_{tm}^2} = 1 \tag{7.39}$$

$$Y_6 = Q_t + \frac{1}{2}Q_m + \sqrt{\frac{1}{4}Q_m^2 + Q_{tm}^2} - \frac{1/4(Q_tQ_m - Q_{tm}^2)}{Q_t + 0.48Q_m} = 1 \tag{7.40}$$

Ivanov's surfaces overcome many of the difficulties associated with the approximate Ilyushin yield surface; it has no discontinuities except one in slope at $Q_t = 1$ where the exact surface also has a slope discontinuity, and equation (7.40) always lies within 1% of the exact surface.

All these approximations discussed in this subsection have been reviewed by Robinson [1971] who concludes that Ilyushin's original approximation eqn. (7.36) is the best of linear (in Q_t, Q_m, Q_{tm} space) surfaces. He also shows that the maximum error by using eqn. (7.36) is about 6 per cent on the safe side and 3.5 per cent on the unsafe side.

7.3.11 Robinson [1988] Yield Surface for Axi-Symmetric Thin Cylinder (Mises Material)

Assuming the transverse shear stresses can be neglected and that the shell material obeys the von Mises yield criterion, a simple yield surface, for axi-symmetric thin cylinders loaded axi-symmetrically, was obtained by Robinson [1988] by making the assumption $M_2 = \frac{1}{2}M_1$, where M_2 is the hoop bending moment and M_1 the axial bending moment. The proposed yield surface is

$$n_1^1 + n_2^2 - n_1 n_2 + \frac{3}{4}m_1^2 + \frac{\sqrt{3}}{4}|n_1 m_1| = 1 \qquad (7.41)$$

Robinson [1988] concludes that for the yield surface equation (7.36) the effect of equation (7.41) is to produce an answer which is conservative by at most 2.5 per cent, and in practice probably much less and also indicates that this conclusion will still be valid if transverse shear force is included in the yield surface.

7.3.12 The Effect of Transverse Shear Stresses on The Yield Surface

All the yield surfaces mentioned so far have neglected the influence of transverse shear stresses on the yield function. The effect of transverse shear stresses on the yield surface has been considered in the works of Shopio [1961], Haybl and Sherborne [1972] and Robinson [1973]. The detailed yield surface formulations can be found in Robinson's paper [1973].

It was proposed by Robinson [1971] that the dimensionless transverse shear stress resultants can be included in Q_t which would then equal $n_1^2 + n_2^2 - n_1 n_2 + 3n_{12}^2 + 3q_1^2 + 3q_2^2$ because in most cases q_1 and q_2 are less than 0.1 in magnitude and hence the transverse shear terms would be less than 0.06. In his latter paper, Robinson [1973] proved this suggestion. Then the approximate yield surfaces can obtained by replacing Q_t in the yield functions Y_1, Y_2, Y_3, Y_4, Y_5 and Y_6 by $Q_t + Q_q$ where $Q_q = 3q_1^2 + 3q_2^2$. It is found that [Robinson 1973] the resulting bounds are very little different.

A new function has been suggested by Robinson [1973]:

$$Y_7' = Q_t + Q_q + \frac{1}{2}Q_m + \sqrt{\frac{1}{4}Q_m^2 + Q_{tm}^2} - 0.24\sqrt{Q_q|Q_{tm}|} - \frac{1/4[(Q_t + Q_q)Q_m - Q_{tm}^2]}{Q_t + Q_q + 0.48Q_m} \tag{7.42}$$

which is accurate to within about plus or minus 2 per cent in all cases.

From these studies it can be concluded that the transverse shear stress resultants have negligible effect on the yield condition in most thin shell applications.

7.3.13 Other Subsequent Yield Surfaces

In 1974 Crisfield [1974b] proposed a modified form of Ilyushin's yield surface. This modification makes the yield criterion more suitable for use in the collapse analysis of thin steel plates and shells under buckling loads. Again in 1979 Criisfield [1979] proposed a modified form of Ivanov's yield surface for the analysis of imperfect thin steel plates subject to unaxial compression.

An alternative theory of elastic-plastic behaviour of shells has been proposed by Bieniek and Funaro [1976], who recognized that the subsequent yield surface translates in the hyperspace of moments. Very recently, Burgoyne and Brennan [1993] presented a reparametrization of the Ilyushin yield criterion for thin plates which produces a simpler (though still exact) form which is suitable for use in practical formulations.

7.4 Finite Element Implementation by Elastic Compensation

7.4.1 Beam Element Implementation

As described in the Chapter 3, elastic compensation analysis is a technique which uses conventional elastic finite element analysis to simulate plastic failure mechanisms in complex structures. An initial elastic analysis, corresponding to an isotropic homogeneous material, is first carried out. Following this a sequence

of linear elastic analysis are performed such that the stress field in the current. say ith analysis, is used to modify the elastic modulus of each element for the next, $(i+1)$th analysis, according to the simple ratio

$$E^e_{(i+1)} = E^e_i \frac{\sigma_n}{\sigma^e_i} \tag{7.43}$$

where E^e_i is current value of Young's modulus in element e, $E^e_{(i+1)}$ is the new value for the next analysis. From eqn. (7.43) the elastic moduli are modified according to the ratio of a nominal stress value, σ_n, to the maximum nodal equivalent stress associated with element e, σ^e_i. Using this simple procedure high stressed elements have their modulus reduced while low stressed elements have their's increased.

Each analysis in the sequence is carried out for some nominal load set, P_n: the values used for the nominal stress and load set are not important - stress used in eqn. (7.43) should be the unaveraged value, since the elastic moduli of adjacent elements are different it would be incorrect to average across elements.

The resulting redistributed stress and strain fields can be used with the bounding theorems of plasticity to estimate safe load factors. For example for a single load:

The lower bound limit load elastic compensation procedure carries out the analysis sequence for the nominal load set until the maximum stress in the whole finite element model, σ_{max} can be reduced no further using eqn. (7.43). Then, invoking the lower bound limit load theorem and using the fact that each elastic compensation analysis must give stresses proportional to the applied load (since the material behaviour is linear elastic in elastic compensation), a lower bound limit load can be constructed as

$$P_L = P_n \frac{\sigma_y}{\sigma_{max}} \tag{7.44}$$

In the above, from eqns. (7.43) and (7.44), the elastic compensation procedure is described for two-dimensional plane or three dimensional solid finite element models. However it is now shown how the method can be extended to lower bound limit analysis for slender beams using a generalised yield criterion, specif-

ically the approximate forms of Gendy and Saleeb [1993], eqns. (7.3) and (7.6).

By an obvious extension of eqns. (7.43) and (7.44), for a frame composed of slender beams, if either the Gengy and Saleeb generalised beam yield criteria are used with the nominal stress σ_n, rather than the actual yield stress, then eqn. (7.43) may be written to modify the elastic modulus of a beam element ϵ as

$$E^e_{(i+1)} = E^e_i \frac{\sigma_n}{\Pi^e_i} \tag{7.45}$$

where Π^e_i is the appropriate yield function from eqn. (7.9) or (7.10) evaluated for the (unaveraged) nodal stress resultants in element e. As in the above, the elastic compensation procedure carries out several re-analyses for the nominal load set but now until the maximum **yield function** in the beam model, Π_{max} can be reduced no further. then the lower bound limit load is

$$P_L = P_n \frac{\sigma_y}{\Pi_{max}} \tag{7.46}$$

7.4.2 Shell Element Implementation

Until now, the elastic compensation procedure has been used with two-dimensional plane or three dimensional [Nadarajah 1993] solid finite element models and beam element implementation. In this subsection the method is extended to a shell element based on a generalised yield criterion. Here both Ilyushin and Ivanov yield surfaces will be used.

It is more convenient to define stress function Q_N, Q_M and Q_{NM} as:

$$\begin{aligned} Q_N &= N_1^2 + N_2^2 - N_1 N_2 + 3N_{12} \\ Q_M &= M_1^2 + M_2^2 - M_1 M_2 + 3M_{12} \\ Q_{NM} &= N_1 M_1 - \frac{1}{2} N_1 M_2 - \frac{1}{2} N_2 M_1 + N_2 M_2 + 3N_{12} M_{12} \end{aligned} \tag{7.47}$$

However Ilyushin's approximate yield surface eqn. (7.36) can be rewritten as:

$$\Pi^2_{IL} = Q_N + Q_M + \frac{|Q_{NM}|}{\sqrt{3}} = \sigma_y^2 \tag{7.48}$$

and Ivanov's yield surface eqn. (7.40) can be rewritten as:

$$\Pi_{IV}^2 = Q_N + \frac{Q_M}{2} + \sqrt{\left[\frac{Q_M^2}{4} + Q_{NM}^2\right]} + \frac{1}{4}\left[\frac{Q_N Q_M - Q_{NM}^2}{Q_N + 0.48 Q_M}\right] = \sigma_y^2 \qquad (7.49)$$

By an obvious extension of eqns. (7.43) and (7.44), for a shell finite element model, if either the Ilyushin, eqn. (7.48), or Ivanov, eqn. (7.49) generalised yield surfaces are used with the nominal stress σ_n, rather than the actual yield stress. then eqn. (7.43) may be rewritten to modify the elastic modulus of a shell element as

$$E_i = E_{(i-1)} \frac{\sigma_n}{\Pi_{(i-1)}} \qquad (7.50)$$

where $\Pi_{(i-1)}$ is the yield function, eqn. (7.48) or (7.49), evaluated for the (unaveraged) nodal stress resultants in each element. As in the above, the elastic compensation procedure carries out several re-analyses now according to eqn. (7.50) until the maximum *yield function* in the shell model, Π_{max}, for the nominal load set, can be reduced no further, then the lower bound limit load is

$$P_L = P_n \frac{\sigma_y}{\Pi_{max}} \qquad (7.51)$$

7.5 Discussion

The extention of elastic compensation method based generalised yield criteria and the finite element implementations of beam and shell elements using the extended elastic compensation procedure have been demonstrated in this Chapter. In following two Chapters, we will use the proposed procedure to analyse beam and shell structures.

7.6 References

Al-Bermani, F. and Kitipornchai, S., (1990), Elasto-plastic large deformation analysis of thin-walled structures. *Engng Struct***12**(1), 28-36.

Attalla, M.R., Deierlein, G.G. and McGuire, W., (1994), Spread of plasticity: Quasi-plastic-hinge approach. *J. Struct Engng.***120**(8), 2451–2473.

Bieniek, M.P. and Funaro, J.R., (1976), *Elasto-Plastic Behavior of Plates and Shells*, Techn. Rep. DNA 3954T, Defence Nuclear Agency. Weidlinger Associates, New York.

Boulton, N.S., (1962), Plastic twisting and bending of I-beam in which the warping is restricted. *Int. J. Mech. Sci.***4**, 491–502.

Burgoyne, C. J., (1979), Discussion on Friez, P. A., Elasto-plastic buckling in short thin-walled beams and columns, *Proc. Instn Civ. Engrs*, **65**. 857-874: Discussion 67, 559-560.

Burgoyne, C. J. and Brennan, M. G., (1993), Exact Ilyushin yield surface. *Int. J. Solids Structures* Vol. 30, No. 8, 1113-1131.

Chen, W.F. and Atsuta, T., (1977), *Theory of Beam Columns*, Vol. 2, *Space Behavior and Design*, pp. 195–269. McGraw-Hill, New York.

Crisfiled, M. A., (1974a), *Some approximations in non-linear analysis of rectangular plates using finite elements*, Transport and Road Research Lab. Report 51 UC.

Crisfiled, M. A., (1974b), *On an Approximate Yield Criterion for Thin Steel Shells*, Transport and Road Research Laboratory, TRRL Report LR658.

Crisfield, M. A., (1979), *Ivanov's yield criterion for thin plates and shells using finite elements*, Transport and Road Research Lab Report 919.

Daddazio, R.P., Bieniek, M.P. and DiMaggio, F.L., (1983), Yield surface for thin bars with warping restraint. *J. Engng Mech. Div, ASCE* **109**. 450–465.

Dinno, K.S. and Gill, S.S., (1964), The plastic torsion I-sections with warping restraint. *Int. J. Mech. Sci.***6**, 27–43.

Dinno, K.S. and Merchant, W., (1965), A procedure for calculating the plastic collapse of I-sections under bending and torsion. *Struct. Engineer***43**. 219–221.

Doddazio, R.P., Bieniek, M.P. and DiMaggio, F.L., (1983), Yield surface for thin bars with warping restraint. *J. Engng Mech. Div, ASCE* **109**. 450–465.

Drucker , D.C., and Shield, R.T., (1959), Limit analysis of symmetrically loaded thin shells of revolution, *Trans. ASME*, Vol.81, Ser. E, 61–68.

Duan, L. and Chen, W.F., (1990, A yield surface equation for doubly symmetrical sections. *Engng Struct,* **12**(2), 114–119.

Ellyin, F., and Sherbourne, A.N., (1965), Limit analysis of axisymmetric intersecting shells of revolution, *Nucl. Struct. Engng.*, **2**, 86.

Gendy, A.S. and Saleeb, A.F., 1993), Generalized yield surface representations in the elasto-plastic three-dimensional analysis of frames. *Computers & Structures* Vol. 49, No. 2, 351–362.

Gill, S.S., (1970), *The Stress Analysis of Pressure Vessles & Pressure Vessle Componemts*, Pergamon.

Gjelsvik, A., (1981), *The Theory of Thin Walled Bars.* John Wiley & Sons, New York.

Harung, H.S. and Millar, M.A., (1973), General failure analysis of skeletal plane frames. *J. Struct. Div., ASCE* **99** 1051–1076.

Hodge, P.G. Jr., (1954), The rigid-plastic analysis of symmetrically loaded cylindrical shells, *J. Appl. Mech.* **21**, 336–342.

Hodge, P.G. Jr, (1959), *Plastic Analysis of Structures.* McGraw-Hill. New York.

Hodge, P.G. Jr., (1960), Yield conditions for rotationally symmetricshells under axisymmetric loading, *J. Appl. Mech.* **27**, 323–331.

Hodge, P.G. Jr., (1961), The Mises yield condition for rotationally symmetric shells, *Q. Appl. Math.* **18**, 305–311.

Hodge, P.G. Jr., (1963), *Limit Analysis of Rotationally Symmetric Plates and Shells*, Prentice Hall (Englewood Cliffs, N. Y.).

Horne, M.R., (1968), The Stability of Elastic Plastic Structures Mechanics, Vol. 2. North-Holland, Amsterdam.

Ilyushin, A. A., (1948), *Plasticity* (in Russian), Gostekhizda, Moscow and *Plasticite* (in French), Eyrolles, Paris (1956).

Ivanov, G. V., (1967), Aproximating the final relationship between the forces and the moments of the shells under the Mises plasticity condition (in Russian). em Inzhenernyi Zhurnal Mekhanika Tverdogo Tela, No. 6, 74-75.

Jennings, A. and Majid, K., (1965), An elastic-plastic analysis by computer for framed structures loaded up to collapse. *Struct. Engineer* **43**, 407–412.

Kitipornchai, S., Zhu, K., Xiang, Y. and Al-Bermani, F., (1991), Single-equation yield surfaces for monosymmetric and asymmetric sections. *Engng Struct.* **13**, 366–370.

Korn, A. and Galambos, T.V., (1968), Behaviour of elasto-plastic frames. *J. Struct. Div., ASCE*, 1119–1142.

Liapunov, S., (1974), Ultimate strength of multistory steel rigid frames. *J. Struct. Div., ASCE* **100**, 1643–1655.

Morris, G.A. and Fenves, S.J., (1969), Approximate yield surface equations. *J. Engng Mech. Div., ASCE* **95**, 947–954.

Olszak, W. and Sawczuk, A., (1967), *Inelastic Behaviour in Shells*. Noordhoff. Groningen.

Onat, E.T. and Prager, W., (1954), Limit analysis of shells of revolution; *Proc. Royal Netherlands Academy of Science*, Vol. 57, 534–548.

Orbison, J.G., McGuire, W. and Abel, J.F., (1982), Yield surface applications in nonlinear steel frame analysis. *Comput. Meth. Apll. Mech. Engng* **33**. 557–573.

Porter, F.L. and Powell, G.H., (1971), Static and dynamic analysis of inelastic frame structures. *Report No. EERC 71-3*, Earthquake Engineering Research Center. Univ. of California. Berkeley, Calif.

Robinson, M., (1971), A comparison of yield surface for thin shells, *Int. J. Mech. Sci.* **13**, 345-354.

Robinson, M., (1973), The effect of transverse shear stresses on the yield surface for thin shells, *Int. J. Solids Structures*, Vol. 9, 819–828.

Robinson, M., (1988), The yield surface for axi-symmetric thin cylinder. *Int. J. Mech. Sci.*, Vol. 30, No. 12, 959–962.

Rozenblyum, V. I., (1954), *Prikl Mat Mekh.* **18**, 289.

Santathadaporn, S. and Chen, W.F., (1970), Interaction curves for sections under combined biaxial bending and axial force. *WRC Bulletin*. No. 148. New Youk.

Save, M.A. and Massonnet, C.E., (1972), *Plastic Analysis and Design of Plates. Shells and Disks*, North-Holland, Amsterdam.

Shapiro, G.S., (1961), On yield surfaces for ideally plastic shells. *Problems of Continuum Mechanica*, Philadelphia, 414.

Vijakkhana, C., Nishino, F. and Lee, S.L., (1974), Inelastic stability of unbraced building frames. *J. Struct. Div., ASCE*, **100**, 645–667.

Yang, Y. B. and Fan, H.T., (1988), Yield surface modeling of I-sections with nonuniform torsion. *J. Engng Mech. Div., ASCE*, **114**, 953–972.

Zhou, S.P. and Chen, W.F., (1985), Design criteria for box columns under biaxial loading. *J. Struct. Engng*, **111**, 2643–2658.

Zyczkowski, M., (1981), *Combined Loadings in the Theory of Plasticity*. PWN. Warsaw.

CHAPTER 8

GENERALISED LIMIT ANALYSIS OF BEAMS AND FRAMES

8.1 Introduction

In Chapter 3 limit analysis of frames was carried out using a solid finite element model. In Chapter 7 the elastic compensation method based on Gendy and Salleb's generalised yield criterion has been developed. In this chapter, a number of beams and frames will be analysed to obtain limit loads using this method. The results calculated using the elastic compensation procedure will be compared with those obtained by plastic theory.

8.2 Limit Solutions for Simple Structures by Plastic Theory

Limit loads for a number of beams and frames has been obtained by many researchers based on the simple plastic theorems, such as Neal [1956, 1977]. Baker and Heyman [1969, 1971] and Chakrabarty [1987]. In this section, some simple limit solutions will be presented for completeness, again to emphasise the relative simplicity of elastic compensation by comparison.

The plastic methods can be applied to beams and frames of any material. provided that the members behave reasonably closely in accordance with the plastic hinge assumption. This means that whenever the bending moment reaches a critical value a plastic hinge formes and can undergo extensive rotation while the bending moment remains sensibly constant.

The plastic hinge hypothesis forms the basis of the calculation of *plastic collapse* loads. When a frame structure is subjected to steadily increasing loads. the formation of the first plastic hinge does not in general cause plastic collapse.

Further increase of the loads can usually be carried, and other plastic hinges form successively until finally there are enough hinges to permit a mechanism motion. Plastic collapse then occurs. This process has been examined for a number of simple structures by many researchers in the past years. In this section, three simple examples will be presented. For completeness, again to emphasise the relative simplicity of elastic compensation by comparision.

8.2.1 Simply Supported Beam

The first structure to be considered is a simply supported beam of uniform cross section, which has a span L and is subjected to a central concentrated load P, as shown in Figure 8.1(a). The bending moment diagram for this beam is shown in Figure 8.1(b), the maximum sagging bending moment at the centre of the beam being $PL/4$. Since the beam is statically determinate, the form of this diagram is independent of the properties of the beam, and in particular of the assumed (M, κ) relation, where M is bending moment and κ the curvature of the beam.

If P is increased steadily from zero, the beam at first behaves elastically. Eventually the central bending moment reaches the value M_P, and a plastic hinge forms beneath the load. The beam then continues to deflect at constant load as the plastic hinge rotates, and so fails by plastic collapse. The plastic collapse load P_c is determined by equating the magnitude of the central bending moment to the plastic moment, giving

$$\begin{aligned} \frac{1}{4}P_cL &= M_P \\ P_c &= \frac{4M_P}{L} \end{aligned} \tag{8.1}$$

Since bending moments at other cross sections are less than M_P, the beam remains elastic everywhere except at the central cross section. The constancy of the load, and therefore of the bending moments during plastic collapse, implies constancy of the curvatures. The increase of deflection during collapse is therefore

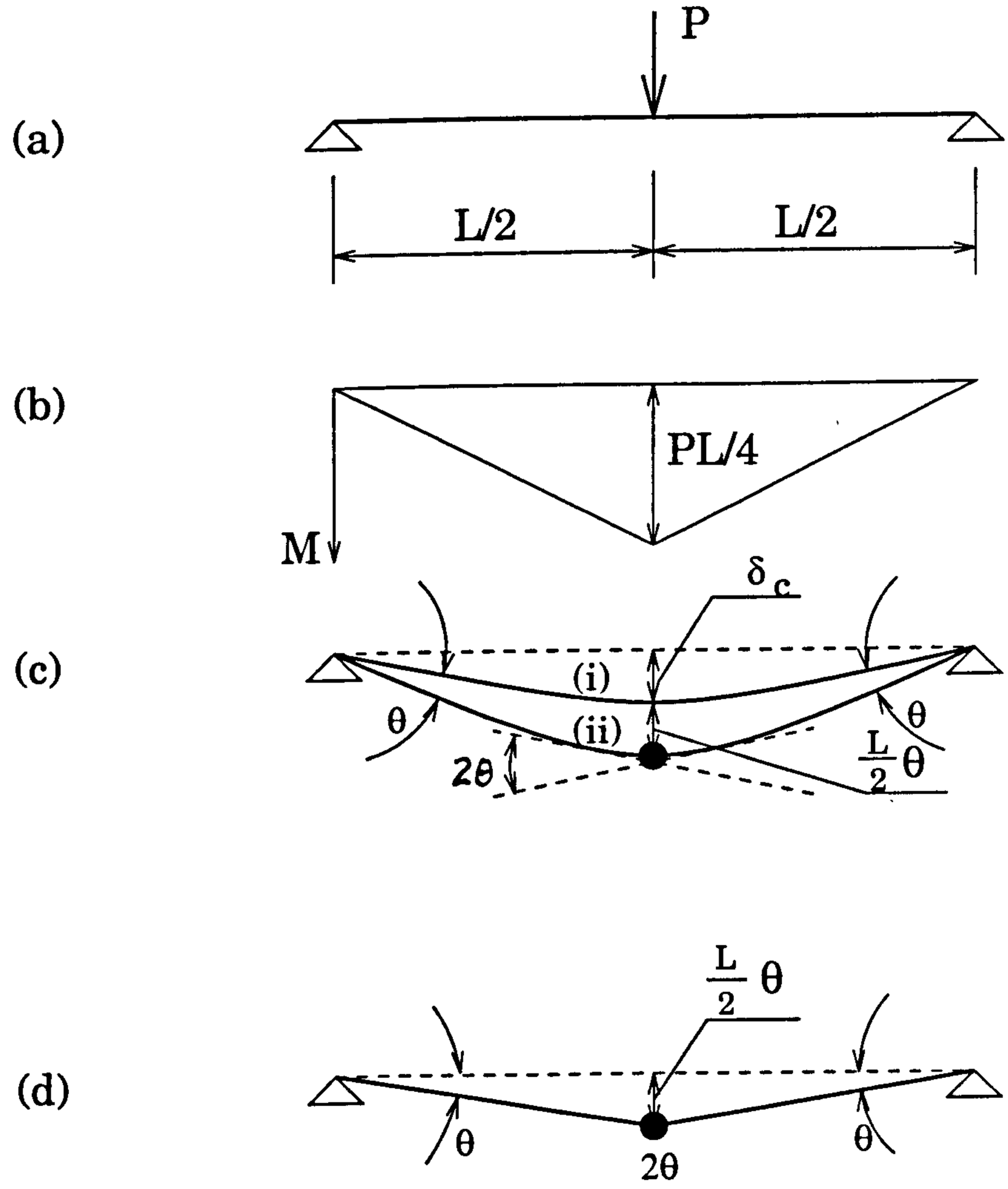

Figure 8.1: Simply supported beam with central concentrated load

due solely to the rotation at the central plastic hinge. This effect is illustrated in Figure 8.1(c) and (d). Curve (i) in Figure 8.1(c) is the deflected form of the beam just as the collapse load P_c is attained, but before any rotation has occurred at the central plastic hinge. Curve (ii) is the deflected form of the beam after the central hinge has undergone rotation through an arbitrary angle 2θ. The curved shape of each half of the beam is the same in case (ii) as in case (i). Figure 8.1(d) shows the changes of deflection which have occurred during plastic collapse, obtained as the difference between the deflections in case (ii) and case (i); each half of the beam is straight in this figure. These changes of deflection are thus due solely to the rotation at the plastic hinge. Figure 8.1(d) represents the collapse mechanism for this simple case.

The elastic central deflection δ of the beam is $PL^3/48EI$. As the collapse load is attained the central deflection δ_c at the point of collapse is therefore given by

$$\delta_c = \frac{P_c L^3}{48EI} = \frac{M_P L^3}{12EI}$$

making use of eqn. (8.1). The behaviour of the beam can now be summarized on a diagram relating the load P to the central deflection δ. This load-deflection relation as Ocb in Figure 8.2. Oc is the behaviour in the elastic range. and cb represents plastic collapse under constant load, the increase of deflection from c to b being $L\theta/2$, as in the mechanism of Figure 8.1(d).

The hinge rotation and therefore the additional deflection developed during plastic collapse in indefinite. However, if very large deflections occurred. the change in geometry of the structure would affect the conditions of equilibrium. for example by enabling the load to be supported partly by direct tension in the two halves of the beam. The simple plastic theory does not concern itself with such effects; it predicts the loads at which large deflections are imminent. as at the point c in Figure 8.2.

The broken curve commencing at a in Figure 8.2 shows qualitatively the effect of taking into account the difference between the yield moment M_y and the plastic

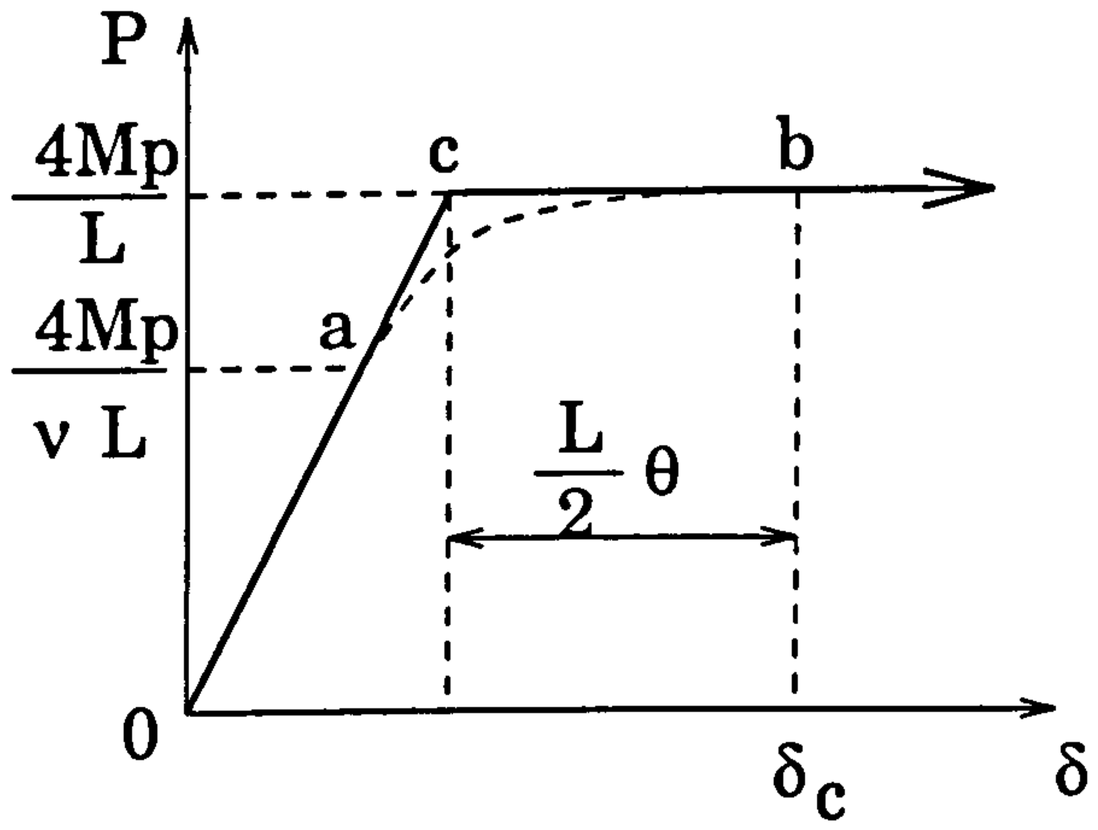

Figure 8.2: Load-deflection relation for simply supported beam

moment M_P. Elastic behaviour would cease at the yield load P_y when the central bending moment was M_y, where

$$P_y = \frac{4M_y}{L} = \frac{4M_P}{\nu L} = \frac{P_c}{\nu}$$

ν being the shape factor. Plastic collapse would still occur at the same value of P as before, but greater deflections would be developed before collapse.

For this simple example the ratio of the collapse load P_c to the yield load P_y is equal to ν, the shape factor. The ratio of P_c to P_y is aways ν for any statically determinate structure, in which the greatest bending moment is proportional to the load and occurs at the same position regardless of the value of the load. Yield occurs when this greatest bending moment is equal to M_y, and collapse occurs when it is equal to M_P, for the introduction of a single hinge is always sufficient to reduce a statically determinate structure to a mechanism. It follows that the ratio of P_c to P_y is the same as the ratio of M_P to M_y, which by definition is the shape factor ν.

Equation (8.1) shows how the plastic collapse load was calculated by equating the maximum bending moment to the plastic moment. This is a statical procedure but the collapse load can also be found by a kinematical procedure. During collapse there is no change in elastic strain energy stored in beam. since the

bending moment distribution remains unaltered. The work done by loads during a small motion of the collapse mechanism is therefore equal to the work absorbed in the plastic hinge, since the motion is quasi-statical. In the mechanism motion of Figure 8.1(d) the load P_c moves through a distance $L\theta/2$ and so does work $P_cL\theta/2$. The rotation at the plastic hinge is 2θ, so that the work adsorbed in the hinge is $2M_P\theta$. It follows that

$$\frac{1}{2}P_cL\theta = 2M_P\theta$$

$$P_c = \frac{4M_P}{L}$$

which agrees with eqn. (8.1).

8.2.2 Fixed-Ended Beam

The behaviour of a fixed-ended beam of uniform cross section and length L, carrying a uniformly distributed load P, will now be considered. In what follows a consistent sign convention will be used for bending moments, curvatures and hinge rotations. Positive bending moments are those which cause tensile stresses in the fibres adjacent to the broken line in Figure 8.3(a), and positive curvatures and hinge rotations correspond to tensile strain in the same fibres.

The bending moment diagram has the parabolic form shown schematically in Figure 8.3(b); a statical analysis gives the equilibrium equation

$$M_2 - M_1 = \frac{PL}{8} \tag{8.2}$$

The beam has one statical indeterminacy or redundancy; the separate values of M_1 and M_2 cannot be found from equilibrium alone.

The state of deformation depicted in Figure 8.3(c) forms the basic of the subsequent calculations. Here the beam has developed a slope – o_1 at entire span is presumed to be behaving elastically. An elastic analysis (by. for example.

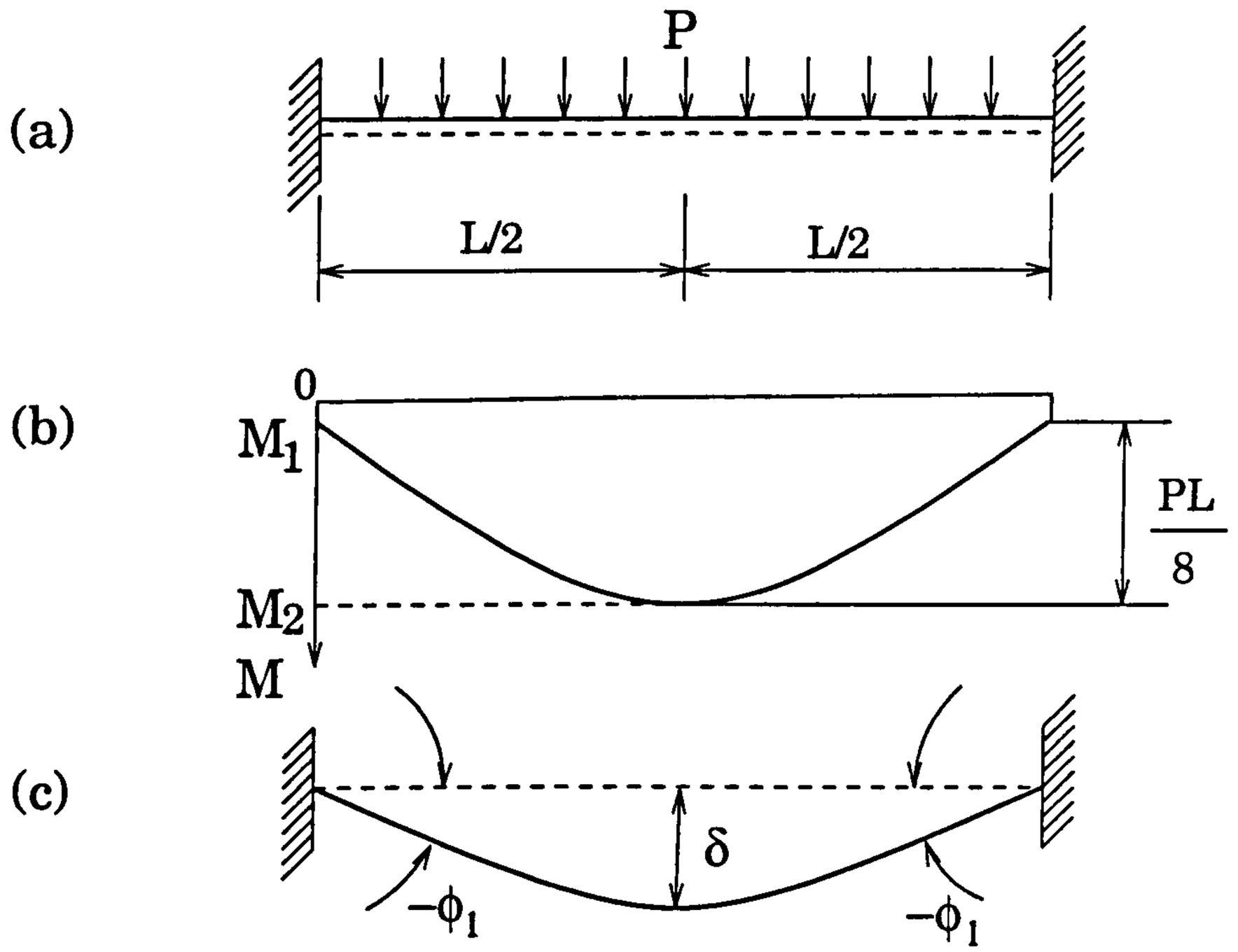

Figure 8.3: Fixed-ended beam with uniformly distributed load

elementary beam theory) gives the following compatibility equation:

$$M_1 = -\frac{1}{12}PL - \frac{2EI\phi_1}{L} \tag{8.3}$$

and it can also be shown that

$$\delta = \frac{PL^3}{384EI} - \frac{1}{4}L\phi_1 \tag{8.4}$$

If P is increased steadily from zero the behaviour is at first wholly elastic. so that $\phi_1 = 0$. Equations (8.2), (8.3) and (8.4) then solve to give the elastic solution

$$M_1 = -\frac{1}{12}PL$$
$$M_2 = \frac{1}{24}PL$$
$$\delta = \frac{PL^3}{384EI}$$

Elastic behaviour ceases when $M_1 = -M_P$, so that plastic hinges form at each end of the beam. The yield load P_y is therefore given by

$$-\frac{1}{12}P_yL = -M_P$$

Table 8.1: *Fixed-ended beam: proportional loading*

$\frac{\Delta PL}{M_P}$	$\frac{PL}{M_P}$	$\frac{M_1}{M_P}$	$\frac{M_2}{M_P}$	$\frac{\phi_1 EI}{M_P L}$	$\frac{\delta EI}{M_P L^2}$
	12	-1	0.5	0	1/32
4		0	0.5	-1/6	5/96
	16	-1	1	-1/6	1/12

$$P_y = \frac{12M_P}{L} \tag{8.5}$$

At this value of the load, the state of the beam is as given in the first line of Table 8.1. Figure 8.4(a) shows the deflected form of the beam at the load P_y, and Figure 8.4(b) shows the corresponding bending moment diagram. If P increases from P_y to $P_y + \Delta P$, the plastic hinge at each end of the beam will undergo rotation while M_1 remains constant at the value $-M_P$. All changes occurring in this 'step' will be denoted by the prefix Δ. Figure 8.4(c) shows the corresponding deflected form of the beam during this step, which is characterized by

$$M_1 = -M_P, \quad \Delta M_1 = 0, \quad \Delta\phi_1 < 0.$$

Equations (8.2), (8.3) and (8.4) become

$$\Delta M_2 = \frac{\Delta PL}{8} \tag{8.6}$$

$$0 = -\frac{1}{12}\Delta PL - \frac{2EI\Delta\phi_1}{L} \tag{8.7}$$

$$\Delta\delta = \frac{\Delta PL^3}{384EI} - \frac{1}{4}L\Delta\phi_1 \tag{8.8}$$

Since ΔM_1 is zero, there is only one unknown bending moment increment ΔM_2, whose value is obtained immediately from the equilibrium equation (8.6). The beam is therefore statically determinate in this step. However, there is now a new geometrical unknown $\Delta\phi_1$. This is found from the compatibility equation (8.7) to be

$$\Delta\phi_1 = -\frac{\Delta PL^2}{24EI} \tag{8.9}$$

Substituting in eqn. (8.8)

$$\Delta\delta = \frac{5\Delta PL^3}{384EI} \tag{8.10}$$

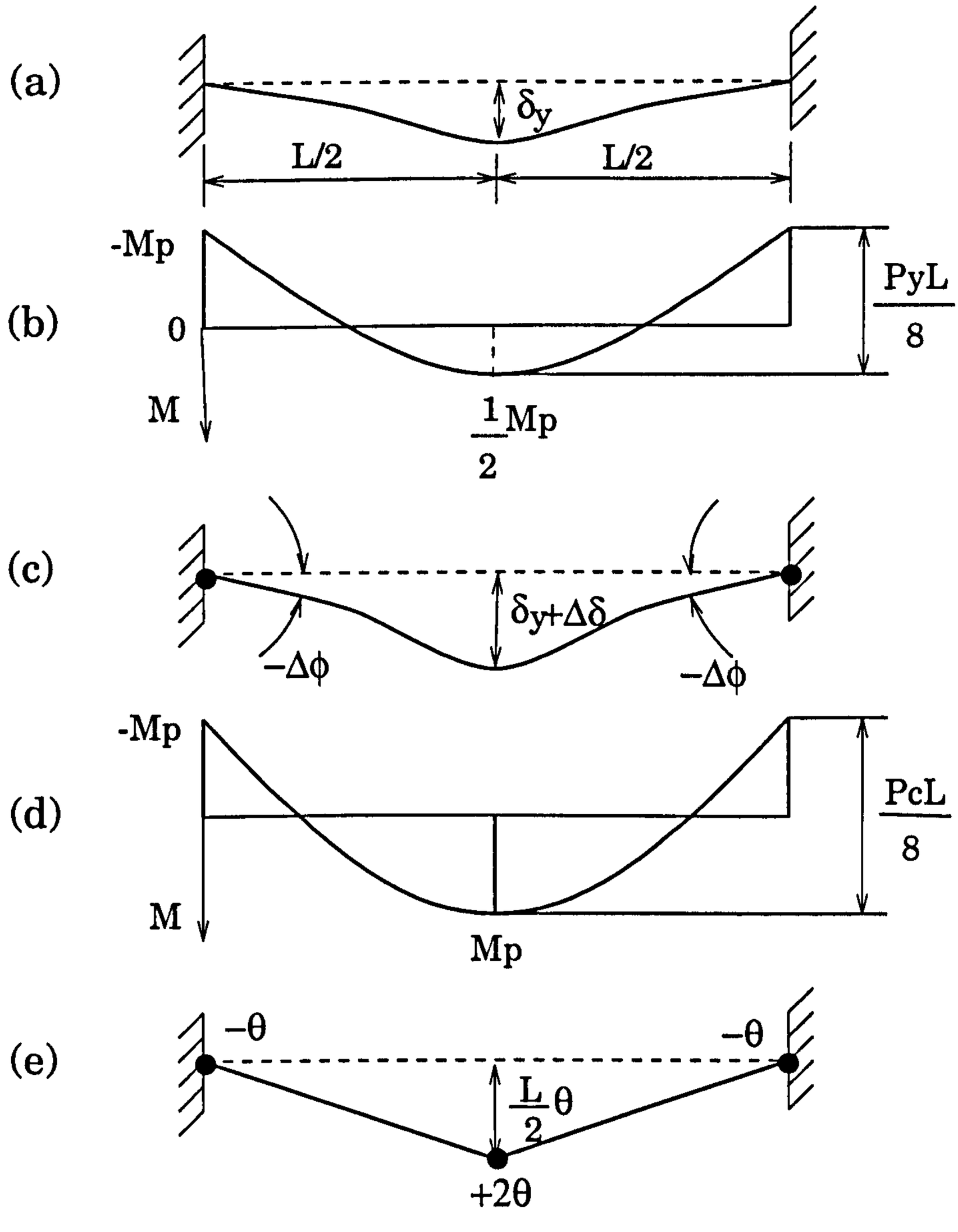

Figure 8.4: Behaviour of fixed-ended beam above yield load

Equations (8.6), (8.9) and (8.10) show that the incremental relations between ΔP, ΔM_2, $\Delta\phi_1$ and $\Delta\delta$ are those for a simple supported beam. This is because the conditions $\Delta M_1 = 0$, $\Delta\phi_1 \neq 0$ correspond to simply supported end conditions.

At the beginning of this step the value of M_2 is $0.5M_P$, as shown in Table 8.1. As ΔP increases, M_2 increases in accordance with eqn. (8.6) until it reaches the value M_P. The bending moment distribution is then as shown in Figure 8.4(d). The corresponding value of ΔP is given by

$$0.5M_P + \frac{\Delta PL}{8} = M_P$$

$$\Delta P = \frac{4M_P}{L}$$

From eqns. (8.9) and (8.10) the corresponding values of $\Delta\phi_1$ and $\Delta\delta$ are

$$\Delta\phi_1 = -\frac{M_PL}{6EI}$$

$$\Delta\delta = \frac{5M_PL^2}{96EI}$$

These incremental values are entered in the second line of Table 8.1, and the third line shows the resulting situation at the end of the step, with $P = 12M_P/L + 4M_P/L = 16M_P/L$.

When P has this value, a plastic hinge forms at the mid-point, and the beam then collapses, the collapse mechanism being as shown in Figure 8.4(e). The collapse load P_c is

$$P_c = 16M_P/L \tag{8.11}$$

When $P = P_c$, but before the central plastic hinge has begun to rotate, the beam is said to be at the *point of collapse*. The conditions at the point of collapse are those given in the last line of Table 8.1. The hinge rotations $-\theta$ at each end of the beam which are shown in the collapse mechanism of Figure 8.4(e) are additional to the rotations $-M_PL/6EI$ which have already developed at the point of collapse.

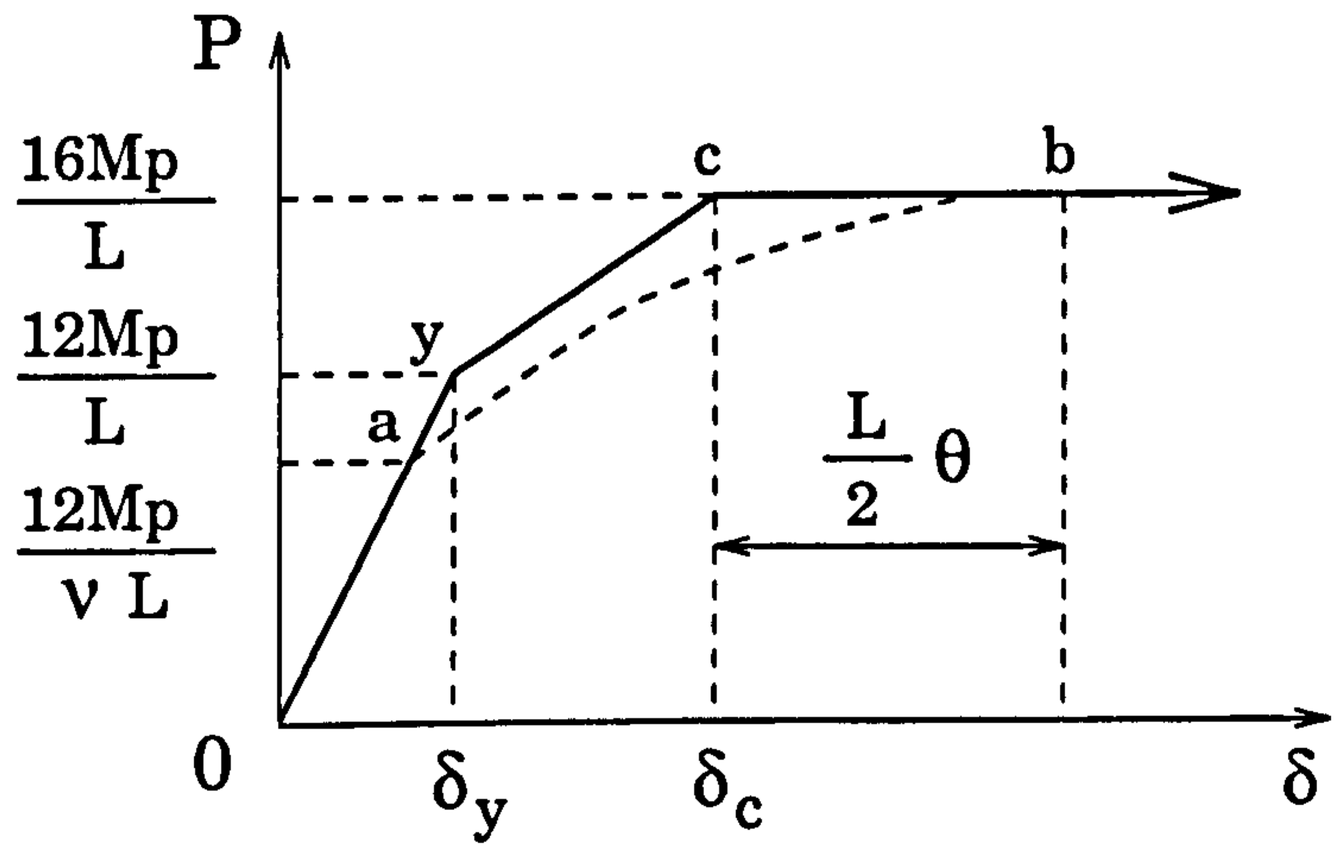

Figure 8.5: Load-deflection relation for fixed-ended beam

The load-deflection relation is shown in Figure 8.5, in which Oy represents the elastic behaviour up to P_y, yc represents the elastic-plastic step and cb represents plastic collapse by the mechanism of Figure 8.4(e). The broken curve commencing at a shows schematically the type of relation which would be obtained if the yield moment M_y was less than M_P.

This load-deflection relation is typical for a beam or frame with one redundancy. When the first plastic hinge forms at the yield load (in this case a symmetrical pair of hinges), the structure is rendered statically determinate for further increases of the load, and the plastic hinge rotations which then occur cause a reduction in the slope of the load-deflection relation. Collapse does not occur until a further plastic hinge forms, thus reducing the structure to a mechanism. In general a finite increase in the load above the yield value will be required to bring the bending moment at the final plastic hinge position up to the plastic moment.

The behaviour of the fixed-ended beam is thus fundamentally different from the behaviour of the simply supported beam, for which the load-deflection relation was shown in Figure 8.2. In that case the formation of a single plastic hinge caused collapse, and the ratio of the collapse load P_c to the yield load P_y was the

shape factor ν. However, for the fixed-ended beam just considered the yield load P_y is $12M_P/\nu L$, while the collapse load P_c is $16M_P/L$, so that the ratio of P_c to P_y is $4\nu/3$. The greater margin between the yield and collapse loads for the fixed-ended beam is consequence of the single redundancy which exists in this case.

It can be seen by inspection that there is only one possible collapse mechanism for the fixed-ended beam, this being the symmetrical mechanism of Figure 8.4(e). This enables the plastic collapse load to be calculated directly by either a statical or a kinematical procedure.

The statical procedure consists simply of sketching the bending moment diagram at collapse, as in Figure 8.4(d). It is seen that

$$\frac{P_c L}{8} = 2M_P$$

$$P_c = \frac{16M_P}{L}$$

The kinematical procedure is based on the collapse mechanism of Figure 8.4(e). Since the central deflection is $L\theta/2$, the average vertical displacement of the uniformly distributed load P_c if $L\theta/4$, so that the work done by the load during this mechanism motion is $P_c L\theta/4$. At each plastic hinge the work absorbed must be positive, and is the product of M_P and the magnitude of the hinge rotation. Equating the work done to the work absorbed,

$$\frac{1}{4}P_c L\theta = M_P(\theta) + M_P(2\theta) + M_P(\theta) = 4M_P\theta$$

$$P_c = \frac{16M_P}{L}$$

8.2.3 Interaction Diagram of a Portal Frame

The last example to be considered is the rectangular portal frame whose dimensions and loading are shown in Figure 8.6(a). All the members of this frame

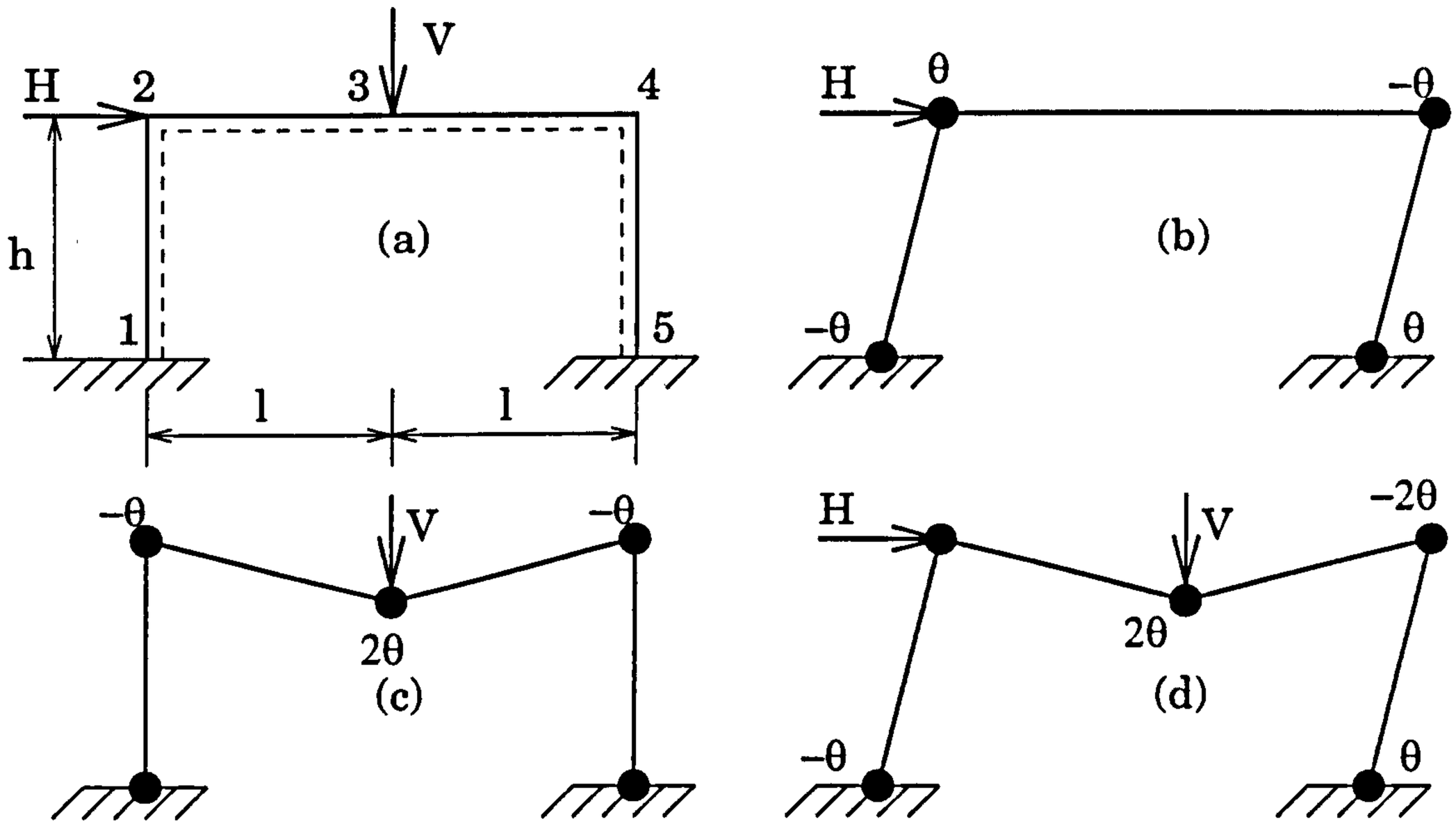

Figure 8.6: Plastic collapse of a portal frame

are uniform with flexural rigidity EI and plastic moment M_P. The joints at sections 2 and 4 are rigid, and the columns are rigidly built-in at their bases 1 and 5. The sign convention for bending moment, curvature and hinge rotation is again that positive value correspond to tensile stresses or strains in the fibers adjacent to the broken line.

Within each of the four segments of the frame which are straight and free from external load, namely 12, 23, 34 and 45, the shear force must be constant. The bending moment must therefore vary linearly along each of these segments. The values of the bending moments M_1, M_2, M_3, M_4 and M_5 at the five numbered cross sections therefore specify the bending moment distribution throughout the frame. Moreover, since the bending moment cannot exceed M_P in magnitude at any cross section, it follows that plastic hinges can only occur at the ends of these segments. Thus, the only possible locations of plastic hinges are the five numbered sections.

The frame has three redundancies, for if a cut were made at any section, and

the shear force, axial force and bending moment were specified at this section, it would become statically determinate. It follows that there must be two equations of equilibrium connecting the five bending moments. For the determination of the bending moments which occur when the frame is wholly elastic there must therefore be three equations of compatibility. For situations in which some plastic hinges have developed, it is still possible to develop three approximate equations of compatibility, and the two equations of equilibrium will still apply.

There are three possible mechanisms, shown in Figure 8.6(b) to (d), each representing a virtual displacement pattern defined by a hinge rotation θ. In the panel mechanism (b), the horizontal load H moves through a distance $h\theta$ producing a virtual work of amount $Hh\theta$. Equating this to the virtual work absorbed at the hinges, we have

$$M_1(-\theta) + M_2(\theta) + M_4(-\theta) + M_5(\theta) = hH\theta$$

or

$$-M_1 + M_2 - M_4 + M_5 = Hh \tag{8.12}$$

In the beam mechanism (c), the vertical load V does work of amount $Vl\theta$, while no work is done by horizontal load H. The principle of virtual work gives

$$M_2(-\theta) + M_3(2\theta) + M_4(-\theta) = Vl\theta$$

or

$$-M_2 + 2M_3 - M_4 = Vl \tag{8.13}$$

The combined panel and beam mechanism (d) involves virtual works $Hh\theta$ and $Vl\theta$ done by the horizontal and vertical loads respectively, and the work equation becomes

$$M_1(-\theta) + M_3(2\theta) + M_4(-2\theta) + M_5(\theta) = Hh\theta + Vl\theta$$

or

$$-M_1 + 2M_3 - 2M_4 + M_5 = Hh + Vl \tag{8.11}$$

Since eqn. (8.14) may be obtained by adding together (8.12) and (8.13), only two of these equations are independent. This is a consequence of the fact that the frame has three redundancies and five unknown critical moments.

We are concerned here with only positive values of H and V. If the frame actually collapses in the mode of Figure 8.6(b), the magnitude of the bending moment at each of the four plastic hinges must be equal to M_P. Since the sign of the bending moment must be the same as that corresponding hinge rotation. $M_1 = -M_P$, $M_2 = M_P$, $M_4 = -M_P$, and $M_5 = M_P$ for this mode of collapse. The bending moment distribution, which is linear in each segment of the frame (the shearing force bending moment), will be statically admissible if $-M_P \leq M_3 \leq M_P$. Equations (8.12) and (8.13) therefore furnish

$$Hh = 4M_P, \quad 0 \leq Vl \leq 2M_P \tag{8.15}$$

When the mechanism of Figure 8.6(c) represents the actual mode of collapse, it is necessary to set $M_1 = -M_P$, $M_3 = M_P$, and $M_4 = -M_P$ in equations (8.12) and (8.13). Using the restrictions $-M_P \leq M_1 \leq M_P$ and $M_P \leq M_5 \leq M_P$ required by the condition of static admissibility, we have

$$Vl = 4M_P, \quad 0 \leq Hh \leq 2M_P \tag{8.16}$$

Finally, regarding the mechanism of Figure 8.6(d) as actual for the state of collapse, and setting $M_1 = -M_P$, $M_3 = M_P$, $M_4 = -M_P$ and $M_5 = M_P$ in eqns (8.12) and (8.13), relationship between H and V under the restriction $-M_P \leq M_2 \leq M_P$ is obtained as

$$Hh + Vl = 6M_P, \quad 2M_P \leq Hh \leq 4M_P \tag{8.17}$$

The relationship between H and V producing plastic collapse is shown graphically in Figure 8.7, the mode of collapse associated with each linear segment of the diagram being as indicated. Such a diagram, known as an *interaction diagram*, is always a convex locus enclosing the origin. Any combination of H and V represented by a point inside the diagram constitutes a safe state of external loading.

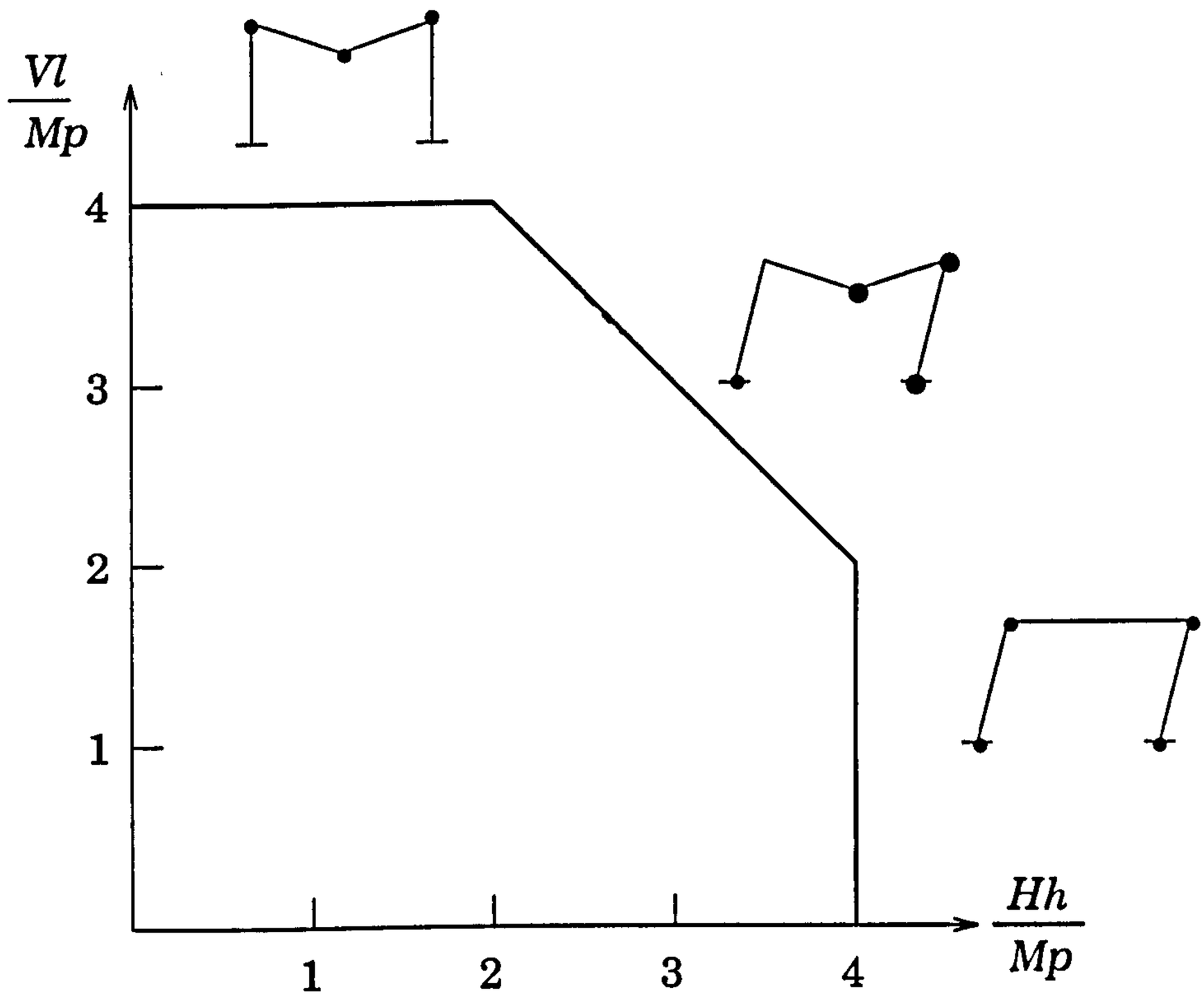

Figure 8.7: Interaction diagram for plastic collapse of a fixed-base rectangular portal frame

The collapse equation corresponding to any assumed mechanism of collapse may be directly obtained by a kinematical analysis in which the work done by the external loads is equal to the work absorbed at the plastic hinges. Since plastic work is always positive, the sign convention may be dispensed with in writing down the work equation, from which an upper bound can be derived.

8.3 Limit Analysis by Generalised Yield Criterion

The limit behaviour of beams and frames have been described briefly in the previous section based on the simple plastic theorems. In this section the same problems will be carried out using the Gendy and Saleeb's *lower bound* yield criterion, eqn (7.3).

Nine examples will be analyzed: seven have been taken from the literature (Gandy and Saleeb [1993], Baker and Heyman [1971]) for comparison and include three standard beam benchmark problems, three two-dimensional frames with proportional loading and one three dimensional frame. In addition to these, two two-dimensional frames with combined load (Lubliner [1990] and Konig [1987]) are also examined. In all models the effects of warping are not considered. The lower bound limit loads were calculated using eqn. (7.64).

The finite element software *ANSYS* (1994) is used here. The element types used throughout are either a two noded beam element (*ANSYS* MEAM3) for two dimensional problems or a two noded three dimensional beam element (*ANSYS* BEAM4) for the space frame. A macro has been written in the *ANSYS* Parametric Design Language (APDL), see Appendix II, to carry out the elastic compensation analysis automatically. The user thus only needs to set up the initial elastic analysis and then call the APDL macro, which takes over the solution sequence and terminates with the best calculated lower bound limit state. The frame finite element models required are not conventional. Each frame member needs to be modeled with several beam elements in order to correctly simulate

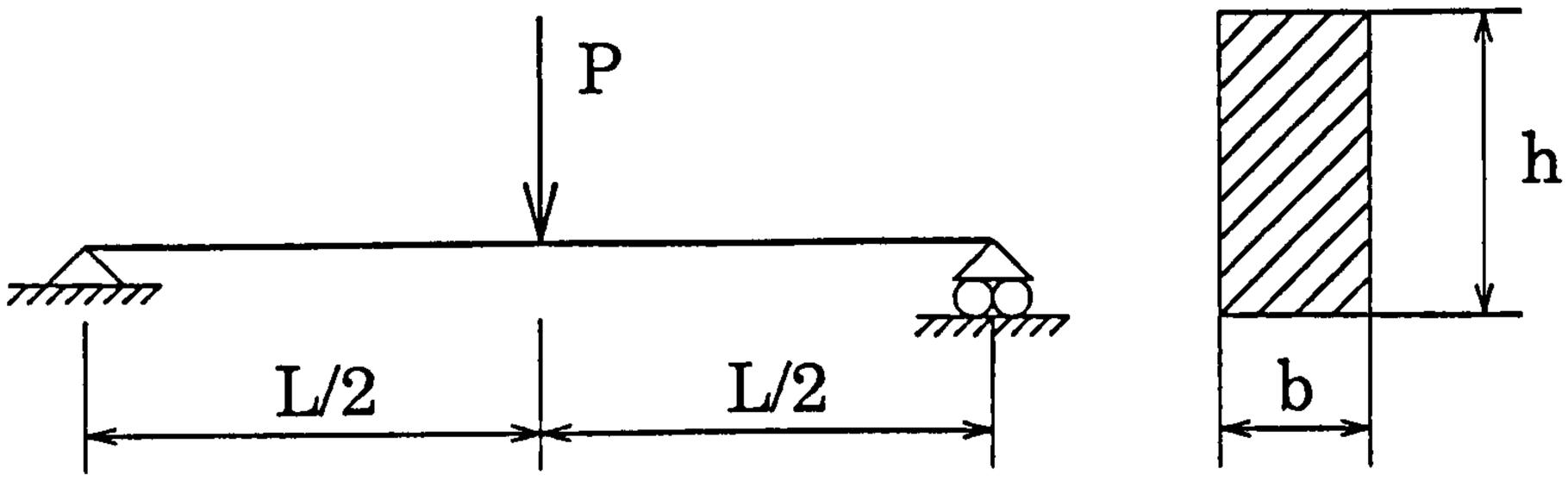

Figure 8.8: Simple supported beam

the collapse mechanism. For example in the problems considered here typically fifty elements were used in each member.

In practice, for large frame problems some mesh refinement would be required in the vicinity of the simulated collapse mechanisms to obtain a good lower bound. This is not particularly difficult in modern finite element analysis systems. A fairly simple procedure to efficiently implement elastic compensation can be derived: an initial analysis sequence be run to establish critical regions - the finite element model in these regions would be refined and the sequence re-run, and so on. Frame members which do not contain critical regions would not require refinement. Again this would be fairly straightforward using an APDL macro. This procedure was not found necessary in the current problem since only test examples are examined.

1. *A simple supported beam*

The first example is a beam of a rectangular cross-section simple supported at each ends and subjected to a concentrated load at the middle of the beam as shown in Fig. 8.8, where $L = 6000mm$. $b = 59.5mm$. $h = 120mm$ and $\sigma_y = 210N/mm^2$. A total of 100 elements were meshed in the finite element model. The lower bound limit load calculated is 60 KN and the plastic collapse load eqn. (8.1), $P_c = 4M_p/L$, is 63 KN. where M_p is the fully plastic moment

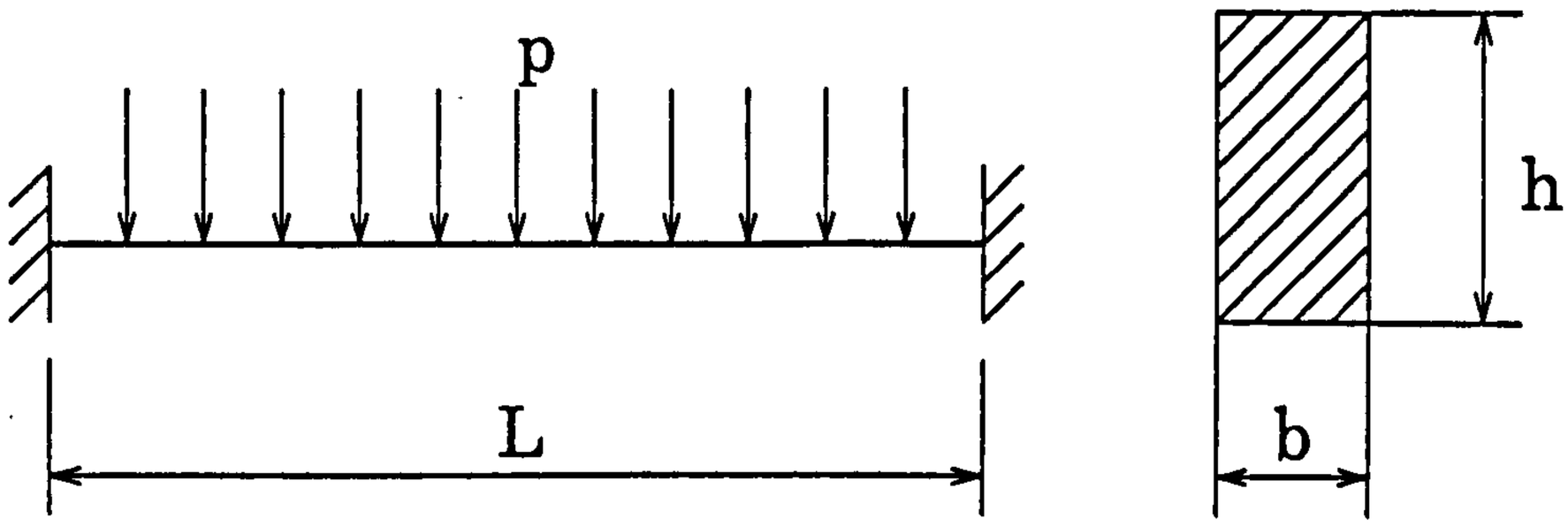

Figure 8.9: Fixed-ended beam carrying a uniformly distributed load

and L is the length of the beam. Evidently, the solution using the elastic compensation method is a good estimate of the limit load.

2. *A fixed-ended beam carrying a uniformly distributed load*

The second example is a fixed-ended beam with a rectangular cross-section and a uniformly distributed load as shown in Fig. 8.9, where $L = 1000mm$. $b = 30mm$, $h = 100mm$ and $\sigma_y = 210N/mm^2$. In the finite element mesh. 100 elements were developed. The lower bound limit load calculated using elastic compensation is 231.7 KN which can be compare with the exact plastic collapse load 252 KN obtained by the equation (8.11), $P_c = 16M_p/L$.

3. *A clamped end beam problem*

The third example is a beam of a rectangular cross-section clamped at both ends and subjected to a concentrated load as shown in Fig. 8.10. where $L = 1000mm, b = 30mm$, $h = 100mm$ and $\sigma_y = 210N/mm^2$. The element numbers meshed in this problem were 100. The lower bound limit load calculated using elastic compensation is 78.6 KN and the limit load obtained by Gendy and Saleeb is 80 KN. Evidently, the solution using the elastic compensation method is good agreement with the theoretical result.

4. *A two-bay frame problem*

The fourth example is a two-bay frame with geometry and loading as shown

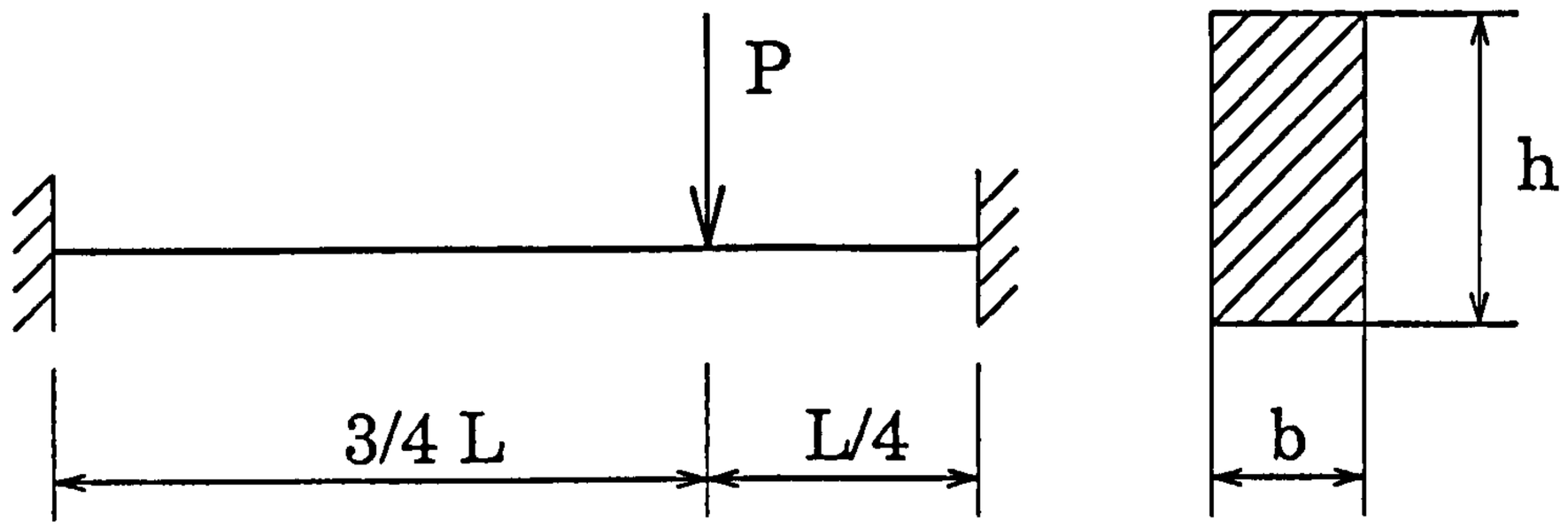

Figure 8.10: Clamped end beam

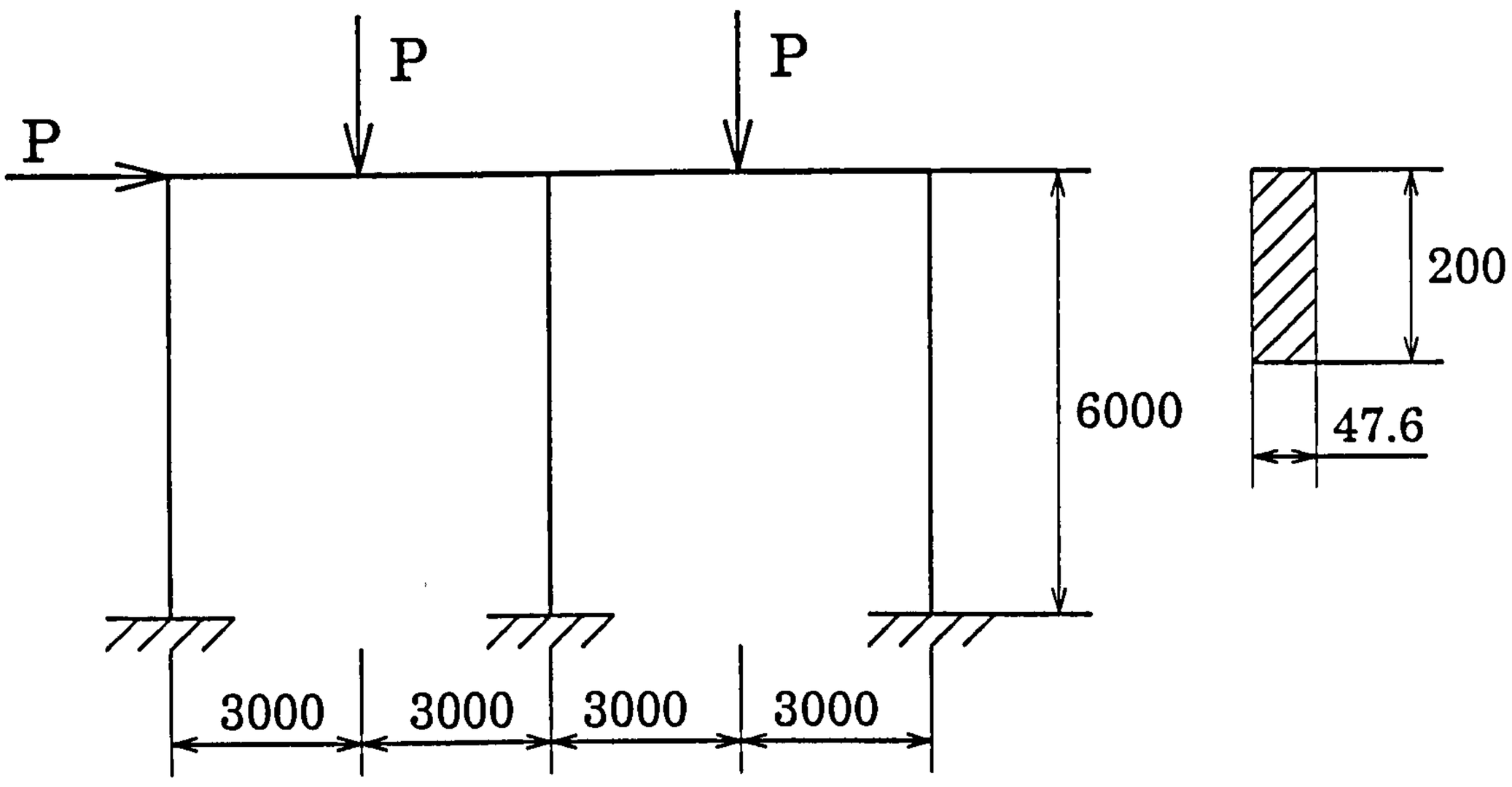

Figure 8.11: Two-bay frame

in Fig. 8.11. The lower bound limit load calculated using elastic compensation is found to be 86.5 KN while the 'exact' solution of classical limit analysis given by Baker and Heyman [1971] is 91 KN.

5. *A one-bay, two-story frame problem*

In Fig. 8.12. the geometric and material data for one-bay, two-story frame are given. The lower bound limit load obtained by the elastic compensation method is 38.7 KN which can again be compared with the result of 40KN from Baker and Heyman [1971].

6. *A two-bay, two-story frame problem*

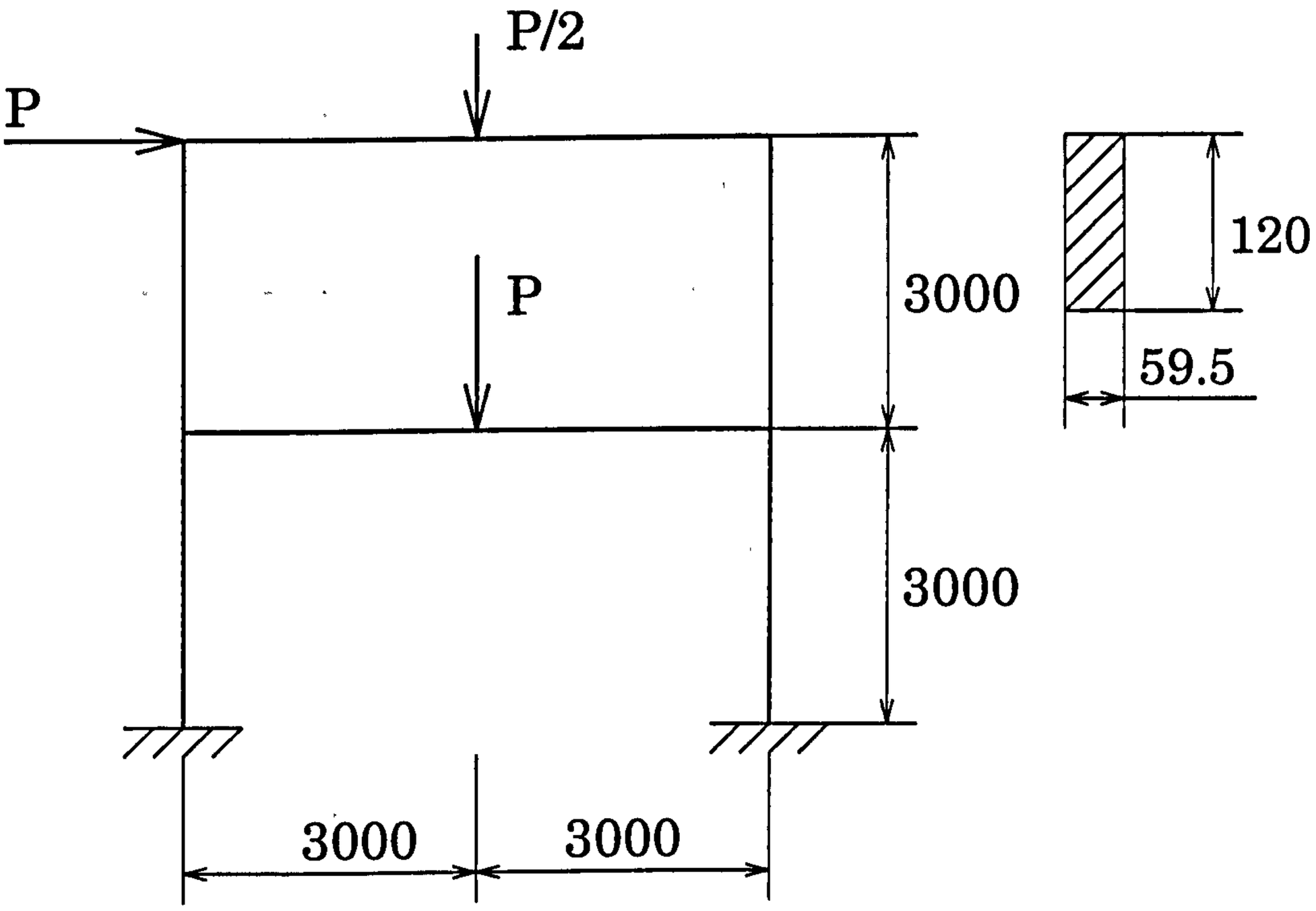

Figure 8.12: One-bay, two-story frame

A two-bay, two-story frame with geometry and loading as shown in Fig. 8.13. The material data are taken from the previous example. The lower bound limit load from elastic compensation is 40.4 KN which can be compared to the result of 45 KN [Gendy and Saleeb 1993].

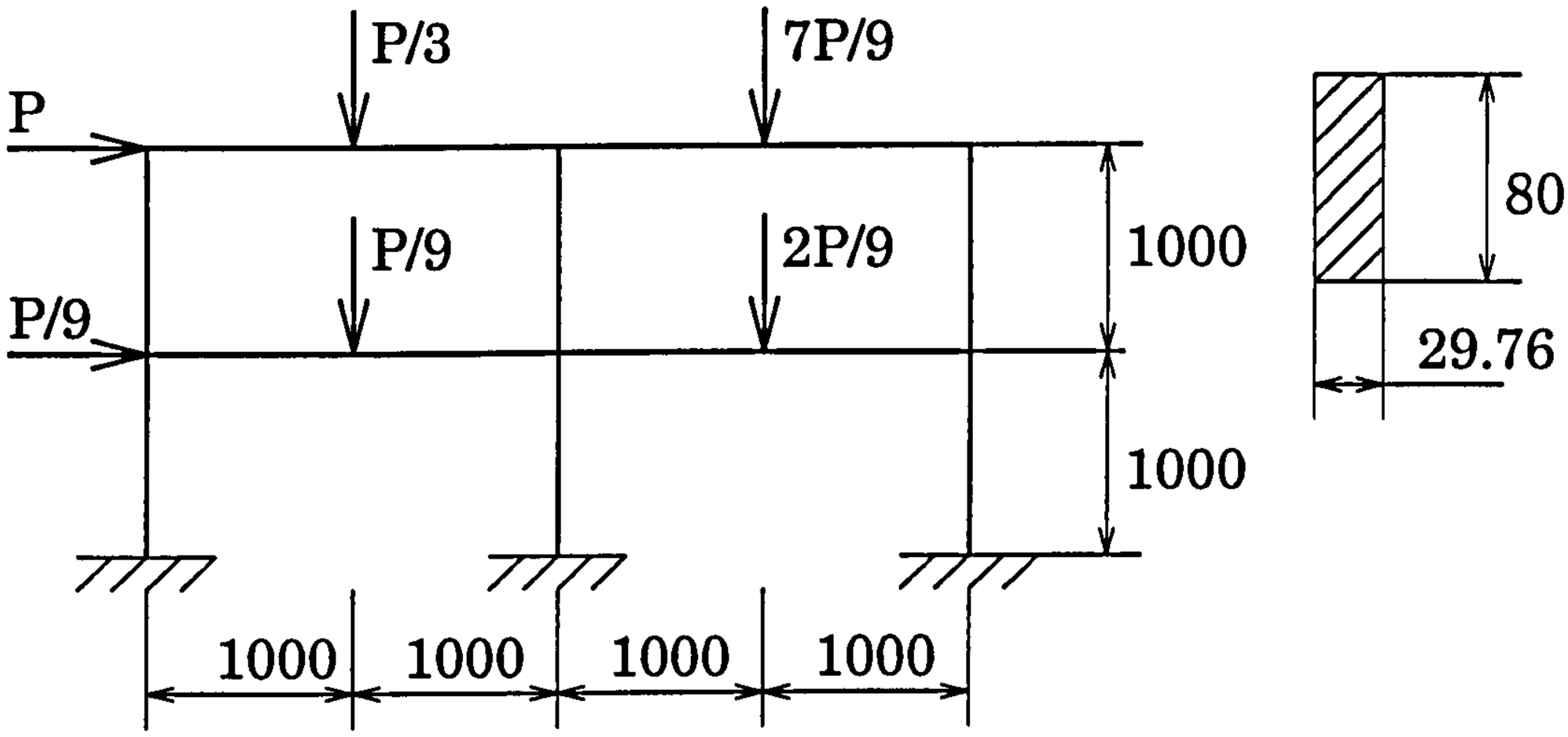

Figure 8.13: Two-bay, two-story frame

7. *A space frame problem*

A space frame shown in Fig. 8.14. from Gengy and Saleeb [1993]. The columns and beams are made of $W10 \times 60$ and $W18 \times 60$ sections, respectively. Each member is of length $L = 144$ in. (3.7 m). The material properties are: $E =$ 30,000 ksi (206.7 GPa); $G = 11,500$ ksi (79.2 GPa); and $\sigma_y = 34$ ksi (234 MPa). Gendy and Saleeb also quote results from two other sources, (Marino [1970]. Yang and Fan [1988]); the load deflection curves reported in Gendy and Saleeb [1993] are reproduced in Figure 8.15. and the limit load obtained by the elastic compensation method is superimposed.

8. *One-bay, one-story frame under combined load*

A one-bay, one story frame subject to combined loads is shown in Figure 8.16. taken from Lubliner [1990]. An interaction diagram can be constructed from elastic compensation; the result is shown in Figure 8.17 together with the solutions from Lubliner and Chapter 3 (M_P is plastic moment of frame).

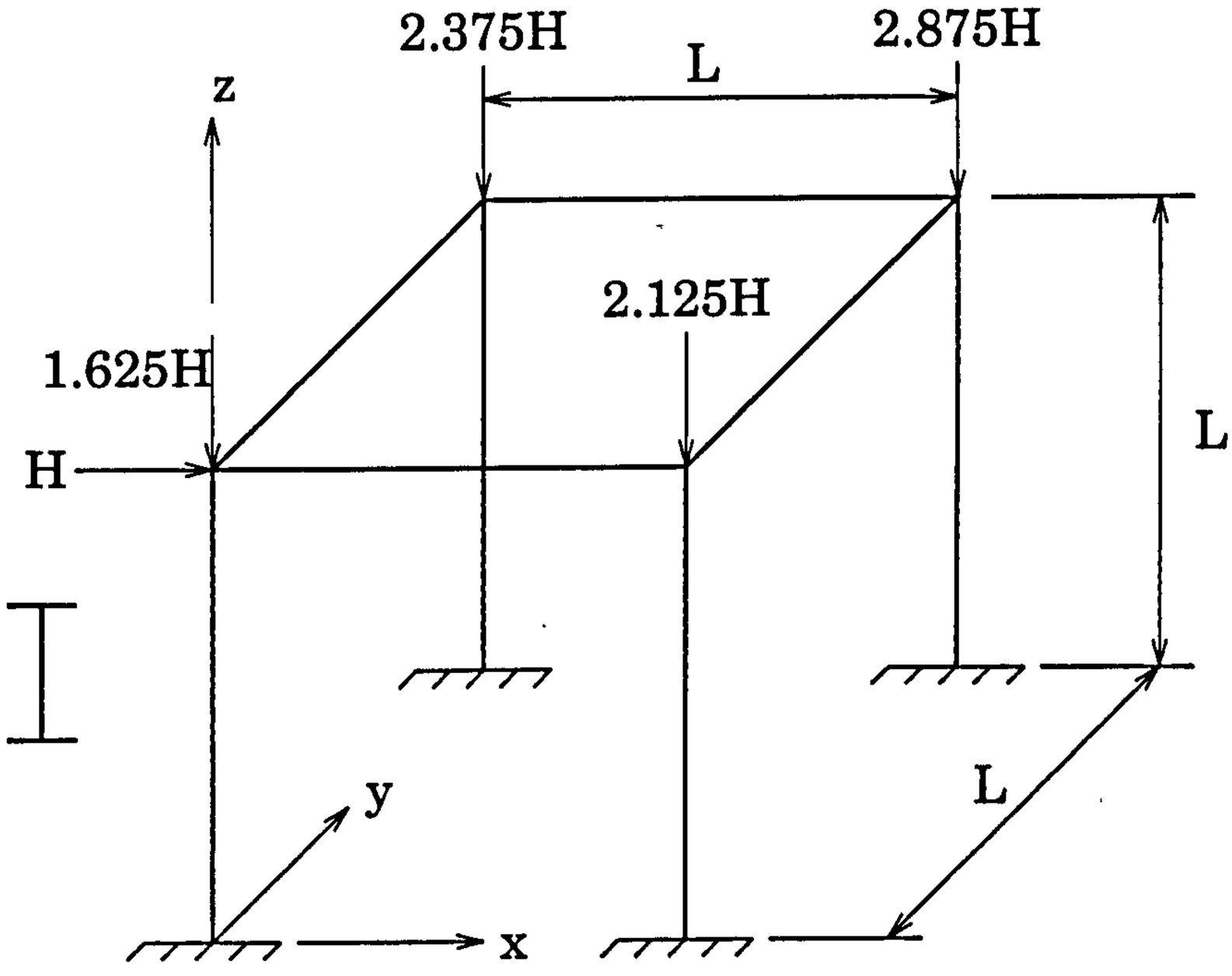

Figure 8.14: Three-dimensional frame with wide-flange cross-section

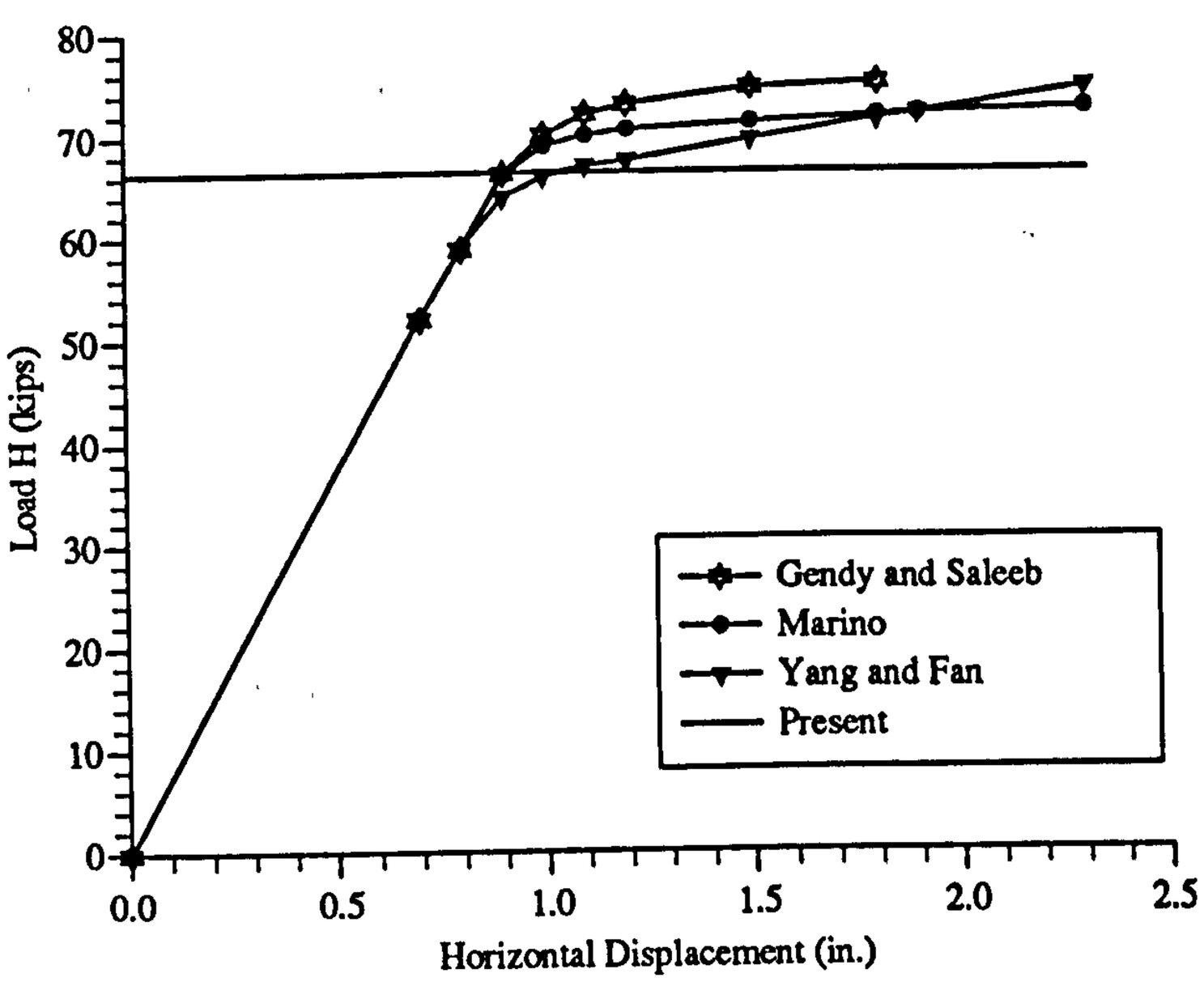

Figure 8.15: Horizontal displacement at the loaded point of a three-dimensional frame with wide-flange cross-section

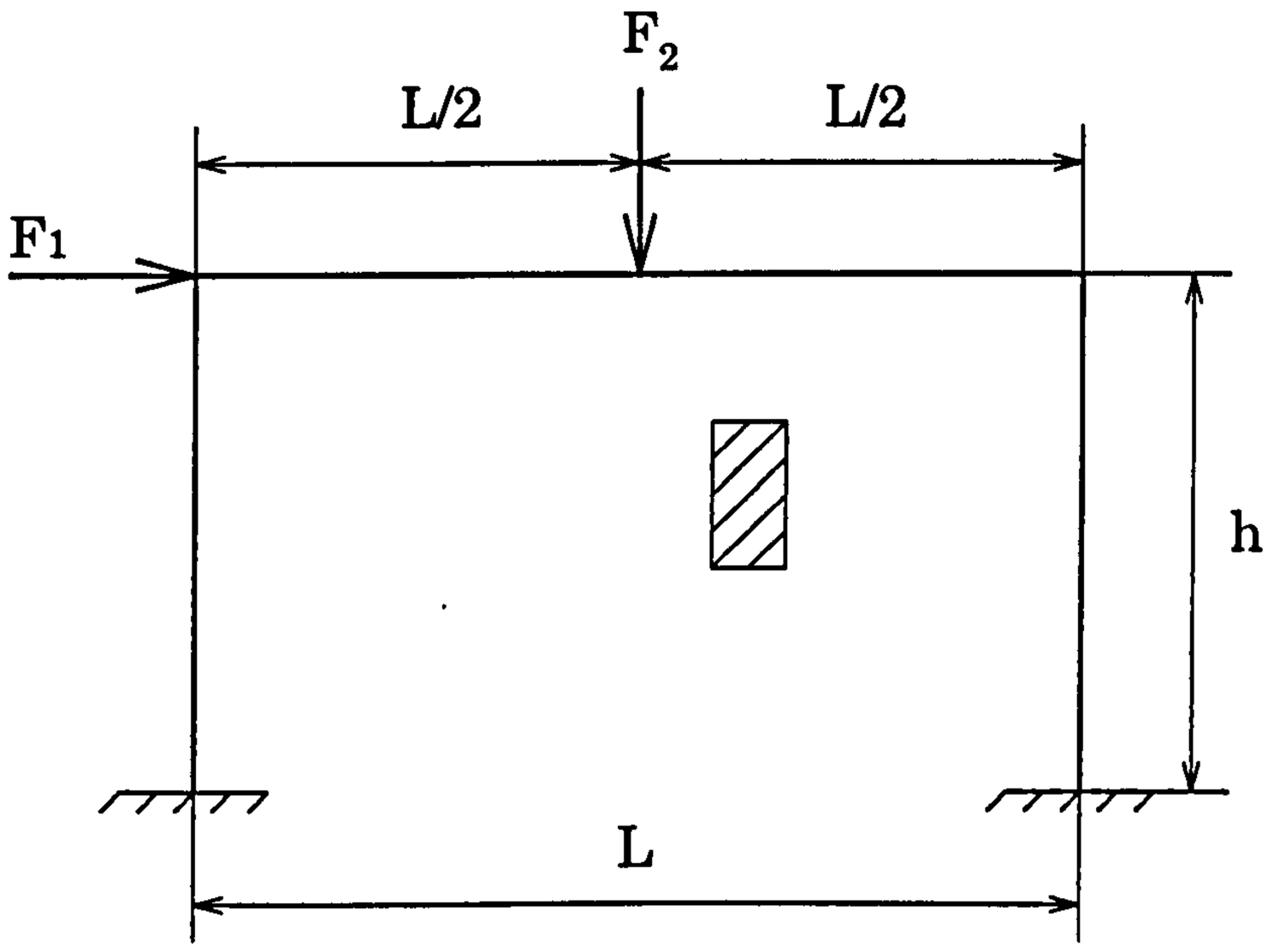

Figure 8.16: One-bay, one-story frame

9. *One-bay, two-story frame under combined load*

Finally a one-bay, two-story frame is shown in Figure 8.18 taken from König [1987]. The beam-to-column stiffness ratio is $2\sqrt{2}$ and the ratio of plastic moments in beams and columns is 2 : 1, and the ratios of h/L are: 1/4, 1/2, 1 and 2. Limit load interaction diagrams are compared with the results obtained in Chapter 3 using solid element model and those of König [1987] in Figures 8.19 to 8.22. In these, $p = \overline{P}l/M_P$, $w = \overline{H}l/M_P$, p is normalized vertical load , w is normalized horizontal load, $\overline{P}$ is vertical loads calculated from the analysis. $\overline{H}$ is horizontal loads calculated from analysis and M_P is plastic moment of frame.

8.4 Shakedown Analysis by Elastic Compensation

To find the shakedown load, various methods have been developed. One of these is based on mathemetical programming [Maier *et al.* 1982, 1986] [König 1987]. But the computing time required by this method increases exponentially as structures become larger and larger thus making this method impractical for the analysis of real structures. In this study, the shakedown load can be obtained by the elastic compensation method.

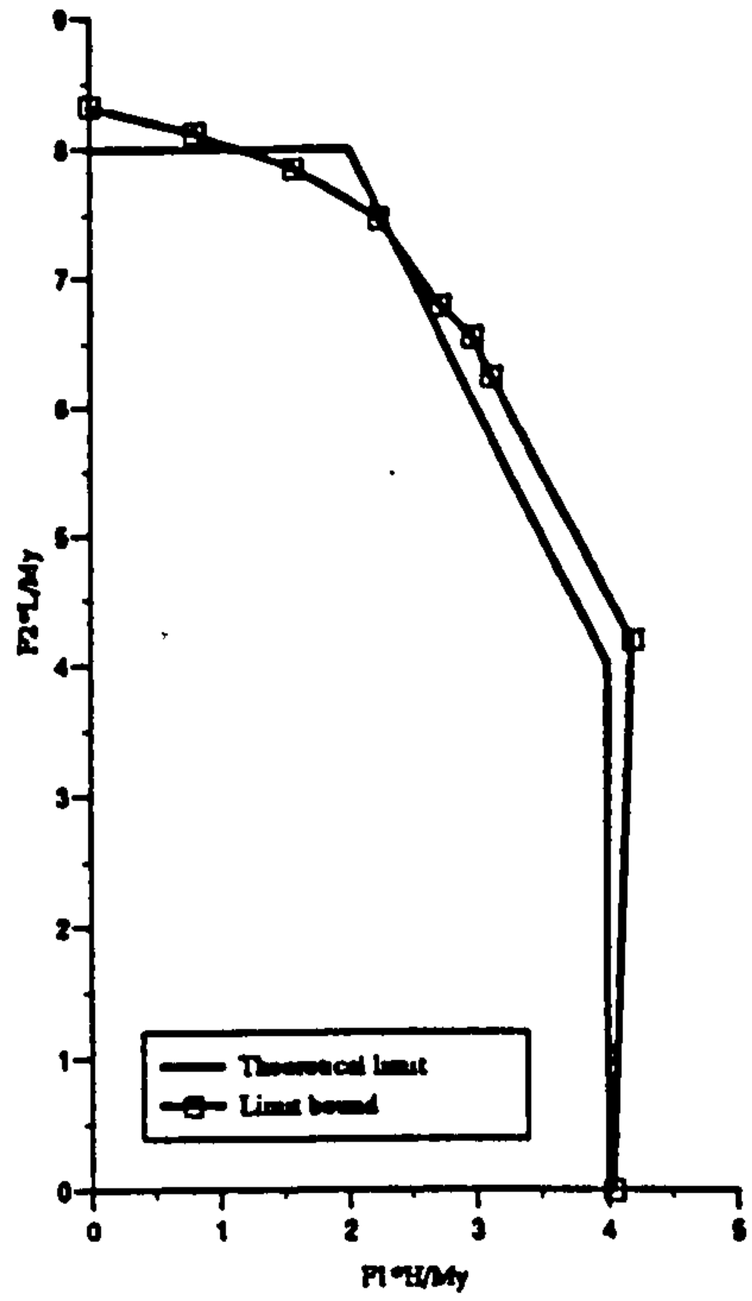

Figure 8.17: Results of one-bay, one-story frame

According to the *statical shakedown theorem*, a framed structure will shake down under a set of loads varying between prescribed limits if

$$M_r: \quad |M_r|_{max} \leq M_P \tag{8.18}$$

exists and satisfies the condition:

$$|M_r + M_e|_{max} \leq M_P \tag{8.19}$$

Since the conditions of the shakedown theorem include those of the lower bound theorem of plastic collapse, the limiting load for shakedown cannot exceed the load corresponding to static collapse:

$$P_s \leq P_L \tag{8.20}$$

It is known from previous Chapter that if either the Gengy and Saleeb [1993] generalised beam yield criteria are used with the nominal stress σ_n, rather than

the actual yield stress, then the elastic modulus of a beam element e may be written as

$$E^e_{(i+1)} = E^e_i \frac{\sigma_n}{\Pi^e_i}$$

where Π^e_i is the appropriate yield function from eqn. (7.9) or (7.10) evaluated for the (unaveraged) nodal stress resultants in element e. As in the above, the elastic compensation procedure carries out several re-analyses for the nominal load set but not until the maximum **yield function** in the beam model, Π_{max} can be reduced no further. Then the lower bound limit load is

$$P_L = P_n \frac{\sigma_y}{\Pi_{max}}$$

The redistributed moment calculated by the elastic compensation procedure for each iteration is designated as a possible shakedown moment M_{si}: that is, the moment in the component under full load after shakedown has occurred. This moment is taken to be the sum of the initial elastic moment M_e and a residual moment M_{ri} (for iteration i):

$$M_{si} = M_e + M_{ri} \tag{8.21}$$

Thus, the residual moment M_r is defined implicity in the elastic compensation procedure, such that:

$$M_{ri} = M_{si} - M_e \tag{8.22}$$

Shakedown criterion (8.18) may therefore be rewritten as:

$$|M_{si} - M_e| \leq M_P \tag{8.23}$$

As the elastic compensation procedure is linear, the magnitude of the moment is proportional to the applied load set. Therefore

$$\frac{P}{P^d} = \frac{M}{M^d} \tag{8.24}$$

Where P^d and M^d are a nominal applied load set and resulting moment respectively. The elastic and shakedown moments can therefore be written:

$$M_e = M^d_e \frac{P}{P^d} \tag{8.25}$$

$$M_{si} = M_{si}^{d} \frac{P}{P^{d}} \tag{8.26}$$

Substituting expressions (8.25), (8.26) into (8.23) and invoking shakedown criterion (8.18) gives:

$$|M_{ri}| = |M_{si}^{d} - M_{e}^{d}|_{max} \frac{P}{P^{d}} \leq M_{P} \tag{8.27}$$

Similarly, criterion (8.19) gives:

$$|M_{si}|_{max} = |M_{si}^{d}| \frac{P}{P^{d}} \leq M_{P} \tag{8.28}$$

At shakedown, either the residual moment is at full plastic:

$$|M_{ri}|_{max} = |M_{si}^{d} - M_{e}^{d}|_{max} \frac{P_{1i}}{P^{d}} = M_{P} \tag{8.29}$$

with the maximum shakedown moment less than or equal to full plastic, or the maximum shakedown moment is at full plastic:

$$|M_{si}|_{max} = |M_{si}^{d}|_{max} \frac{P_{2i}}{P^{d}} = M_{P} \tag{8.30}$$

with the maximum residual moment less than or equal to full plastic. Equation (8.29) gives a shakedown load P_{1i} for iteration i, such that

$$P_{1i} = P^{d} \frac{M_{P}}{|M_{si}^{d} - M_{e}^{d}|_{max}} \tag{8.31}$$

and equation (8.30) gives a shakedown load P_{2i} for iteration i, such that

$$P_{2i} = P^{d} \frac{M_{P}}{|M_{si}^{d}|_{max}} \tag{8.32}$$

The lower bound shakedown load P_{si} calculated for iteration i is the smaller of the three calculated loads P_{1i}, P_{2i} and P_{L} that is;

$$P_{si} = min(P_{1i},\ P_{2i},\ P_{L}) \tag{8.33}$$

Two two-dimensional frames with combined load analysed by the plastic theory will also examined by the proposed method and using Gendy and Saleed's (1993) lower bound yield criteria eqn. (7.10). For the fixed-base rectangular portal frame shown in Figure 8.23, the lower bound shakedown loads calculated are shown in Figure 8.24 together with those of calculated by the plastic theory. For

the two-story frame shown in Figure 8.25, the all results are shown in Figure 8.26.

8.5 Concluding Comments

It is known from previous sections that the limit loads obtained by the elastic compensation method based on generalised yield criteria are in good agreement with the theoretical results. It can be seen from the Figure 8.24 and 8.26 that the lower bound shakedown loads calculated by the elastic compensation method are very close to the theoretical solution.

In this chapter, the lower bound limit and shakedown loads of 2-D and 3-D beam and frame structures were obtained by the elastic compensation method. The calculated lower bound limit loads obtained by the proposed method are found to be quite accurate. The elastic compensation method can therefore be used to estimate the limit loads of complex structures for design purposes without resource to complex inelastic analysis.

8.6 References

ANSYS User's Manual, (1994), Swanson Analysis System, Inc.

Baker, J.F. and Heyman, J., (1969), *Plastic Analysis of Frames*, Cambridge.

Baker, J. and Heyman, J., (1971), *Plastic Design of Frames*, Vols I and II. Cambridge University Press.

Baker, J.F., Horne, M.R. and Heyman, J., (1956), *The Steel Skeleton*. Vol. 2. Cambridge.

Beedle, L.S., (1958), *Plastic Design of Steel Frames*, Wiley (New York)

Chakrabarty, J., (1987), *Theory of Plasticity*, McGraw-Hill Book Co., Singapore.

Charnes, A., and Greenberg, H.J., (1951), Plastic collapse and linear programming, Abstract No,506, *American Mathemetical Society*, Providence. R.I.

Charnes, A., Lemke, C.E., and Zienkiewicz, O.C., (1959), Virtual work, linear programming and plastic limit analysis, *Proc., Royal Society of London.* Ser. A, **251**, 110–116.

Cohn, M.Z., Ghosh, S.K., and Parimi, S.R., (1972), Unified approach to theory of plastic structures, *J. Eng. Mech. Div.***98**, 1133–1158.

Daddazio, R.P., Bieniek, M.P. and DiMaggio, F.L., (1983), Yield surface for thin bars with warping restraint. *J. Engng Mech. Div, ASCE* **109**. 450–465.

Dorn, W.S., and Greenberg, H.J., (1957), Linear programming and plastic limit analysis of structure, *Quarterly of Appl. Math.*, **15** (2), 155–167.

Fenves, S..J., and Gonzales, C.A., (1971), Network topological formulation of analysis and design of rigid plastic framed structures, *Int. J. Numberical Methods in Engrg.*, **3**, 425–441.

Gavarini, C., (1966), Fundemental plastic analysis theorems and duality in linear programming, *Ingegneria Civile* **18**.

Gendy, A.S. and Saleeb, A.F., 1993), Generalized yield surface representations in the elasto-plastic three-dimensional analysis of frames. *Computers & Structures* Vol. 49, No. 2, 351–362.

Heyman, J., (1952), Plastic analysis and design of steel framed structures, Preliminary Publication, *4th Congress, International Association for Bridge and Structural Engineering*, Cambridge / London.

Heyman, J., (1957), *Plastic Design of Portal Frames*, Cambridge.

Hodge, P.G. Jr, (1959), *Plastic Analysis of Structures.* McGraw-Hill, New York.

Horne, M.R., (1954), A moment-distribution method for the analysis and design of structures by plastic theory, *proc., Institution of Civil Engineers*, part 3. Vol. 3, 51.

Horne, M.R., (1968), The Stability of Elastic Plastic Structures Mechanics. Vol. 2. North-Holland, Amsterdam.

Horne, M.R., (1971), *The Plastic Theory of Structures*, Nelson.

König, J.A., (1987), *Shakedown of Elastic-Plastic Structures*, PWN–Polish Scientific Publishers, Warsaw and Elsevier, Amsterdam.

Lubliner, J. , (1990), *Plasticity Theory*, Macmillan Publishing Company, New York.

Mackenzie, D., and Boyle, J.T., (1993), A method of estimating limit loads by iterative elastic analysis. I–Simple examples. *Int. J. Pres. Ves. & Piping.* Vol. 53, No.1, 77–95.

Mackenzie, D., Shi, J., Nadarajah, C., and Boyle, J.T., (1992). An iterative elastic analysis procedure for estimating lower bound limit loads. *PVP-Vol. 230, ASME*, 129–134.

Mackenzie, D., Nadarajah, C., Shi, J., and Boyle, J.T., (1993). Simple bounds on limit loads by elastic finite element analysis. *J. Pres. Ves. Technology.* Vol.115, 27–31.

Mackenzie, D., Shi, J. and Boyle, J. T., (1994), Finite element modeling for limit analysis by the elastic compensation method. *Computer & Structures.* Vol. 51, No. 4, 403–410.

Maier, G. and Munro, J., (1982), Mathematical programming application to engineering plastic analysis. *Appl. Mech. Rev.* **35**, 1631–1643.

Maier, G. and Lioyd, D., (1986), Update to 'Mathematical programming application to engineering plastic analysis'. *ASME Appl. Mech. Update.* 377–383.

Marino, S., (1970), *Analysis of Space Frames*, thesis presented to Lehigh Univ., Bethlehem, Pa., in partial fulfillment of the requirements for the degree of Doctor of Philosophy.

Munro, J. and Smith, D.L., (1972), Linear programming duality in plastic analysis and synthesis. In: *International Symposium on Computer-Aided Structural Design*, Coventry.

Neal, B.G., (1956), *The Plastic Methods of Structural Analysis*, Chapman and Hall (London).

Neal, B.G., (1977), *The Plastic Methods of Structural Analysis*, Third Edition. Chapman and Hall (London).

Neal, B.G. and Symonds, P.S., (1950/1951), The calculation of collapse loads for framed structures, *Proc. I.C.E.*, **35**, 21.

Neal, B.G. and Symonds, P.S., (1952), The rapid calculation of plastic collapse loads for a framed structure, *Proc. I.C.E.*, **1** (3), 58.

Tin-Loi, F., (1995), Plastic limit analysis of plane frames and grids using GAMS. *Computers & Structures*, **54**(1), 15–25.

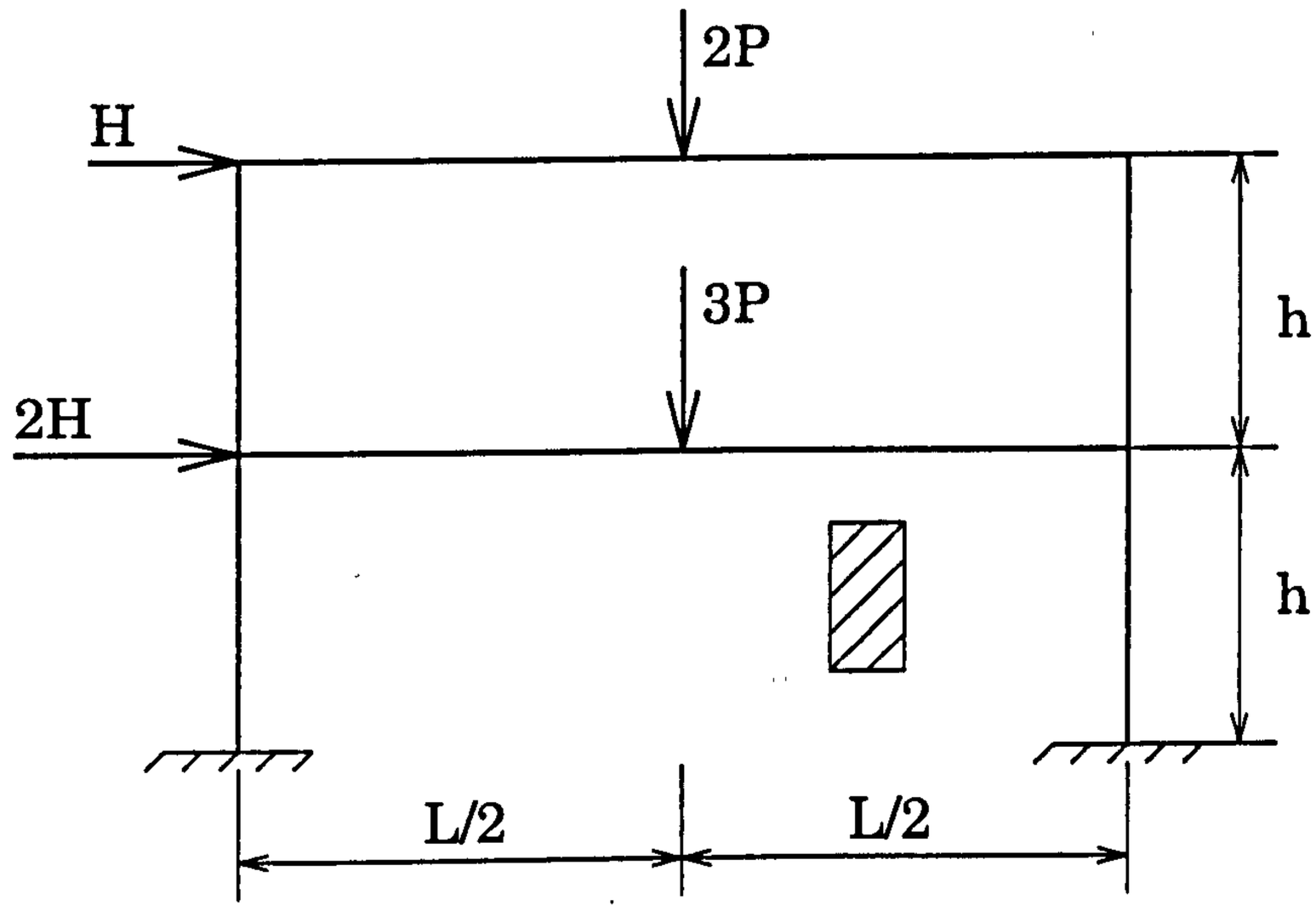

Figure 8.18: One-bay, two-story frame

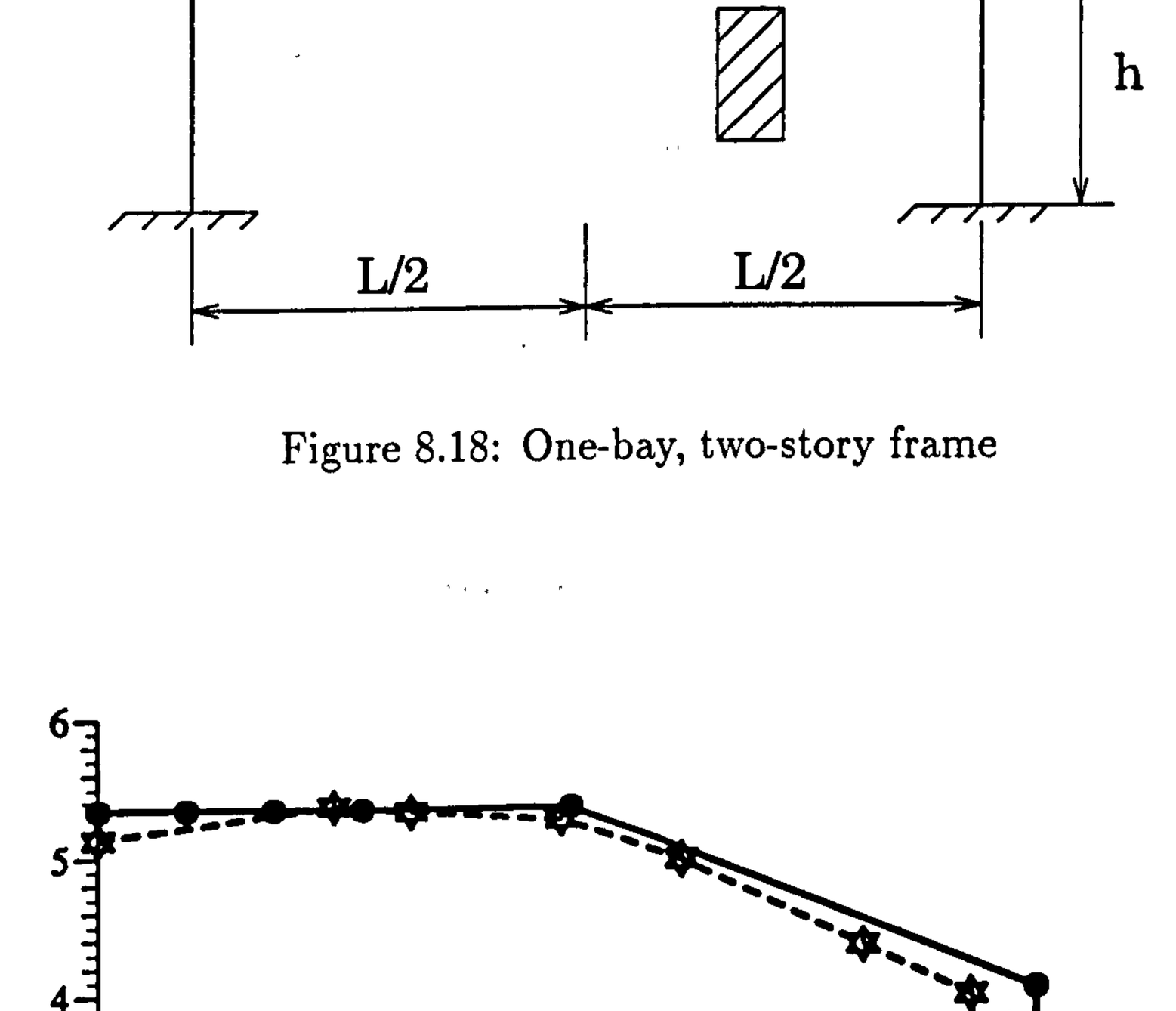

Figure 8.19: Results of one-bay, two-story frame, $h/L = 1/4$

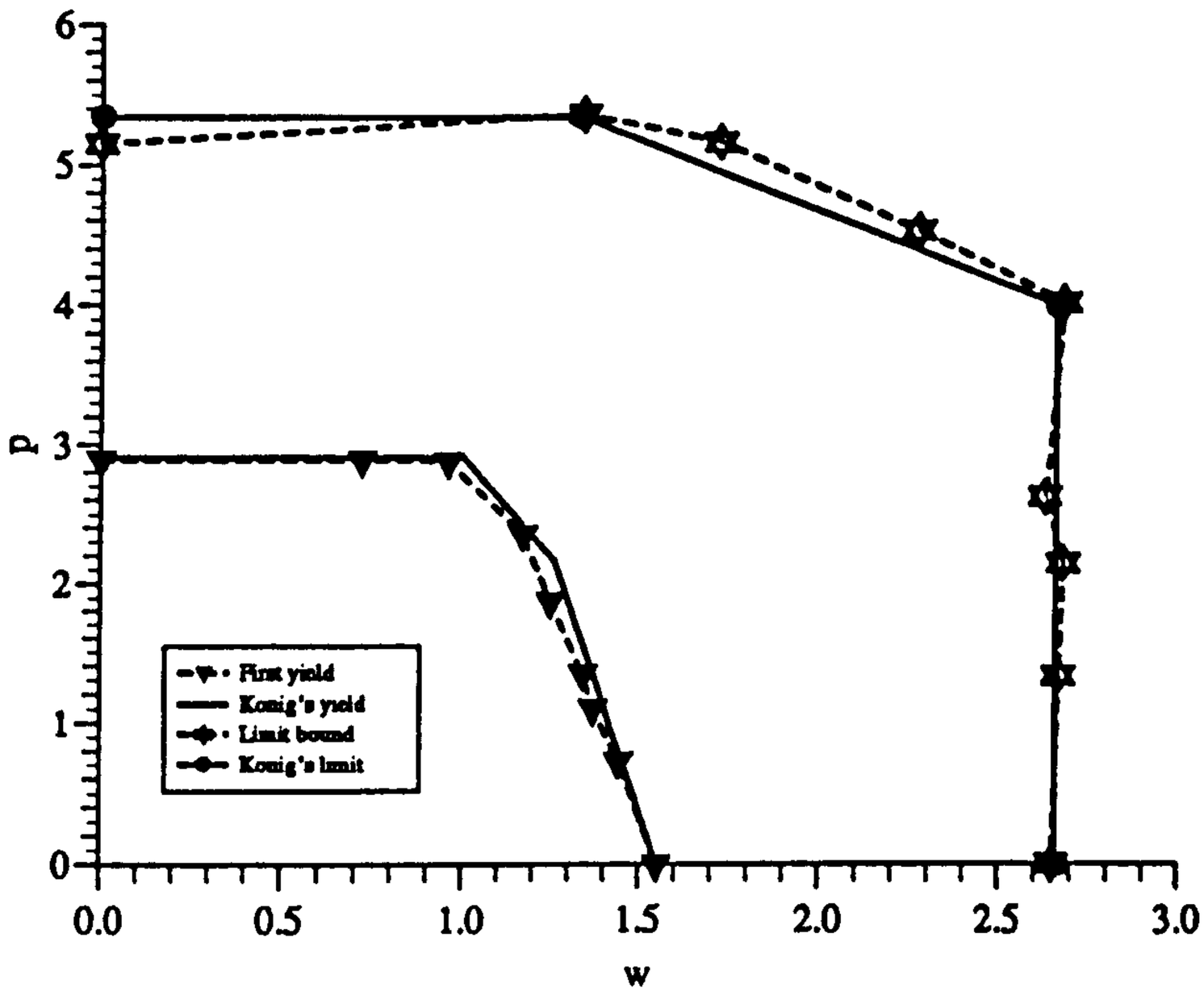

Figure 8.20: Results of one-bay, two-story frame, $h/L = 1/2$

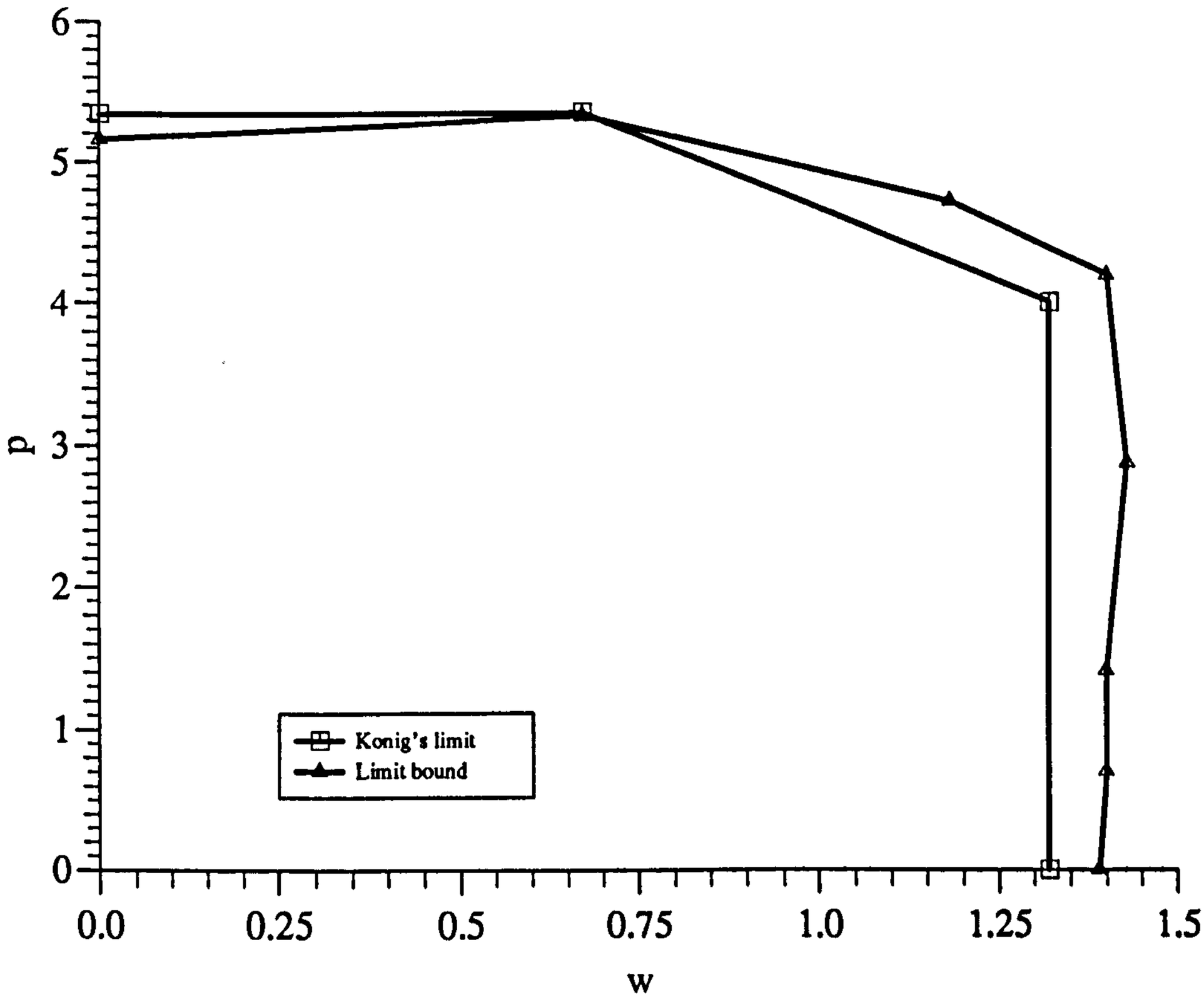

Figure 8.21: Results of one-bay, two-story frame, $h/L = 1$

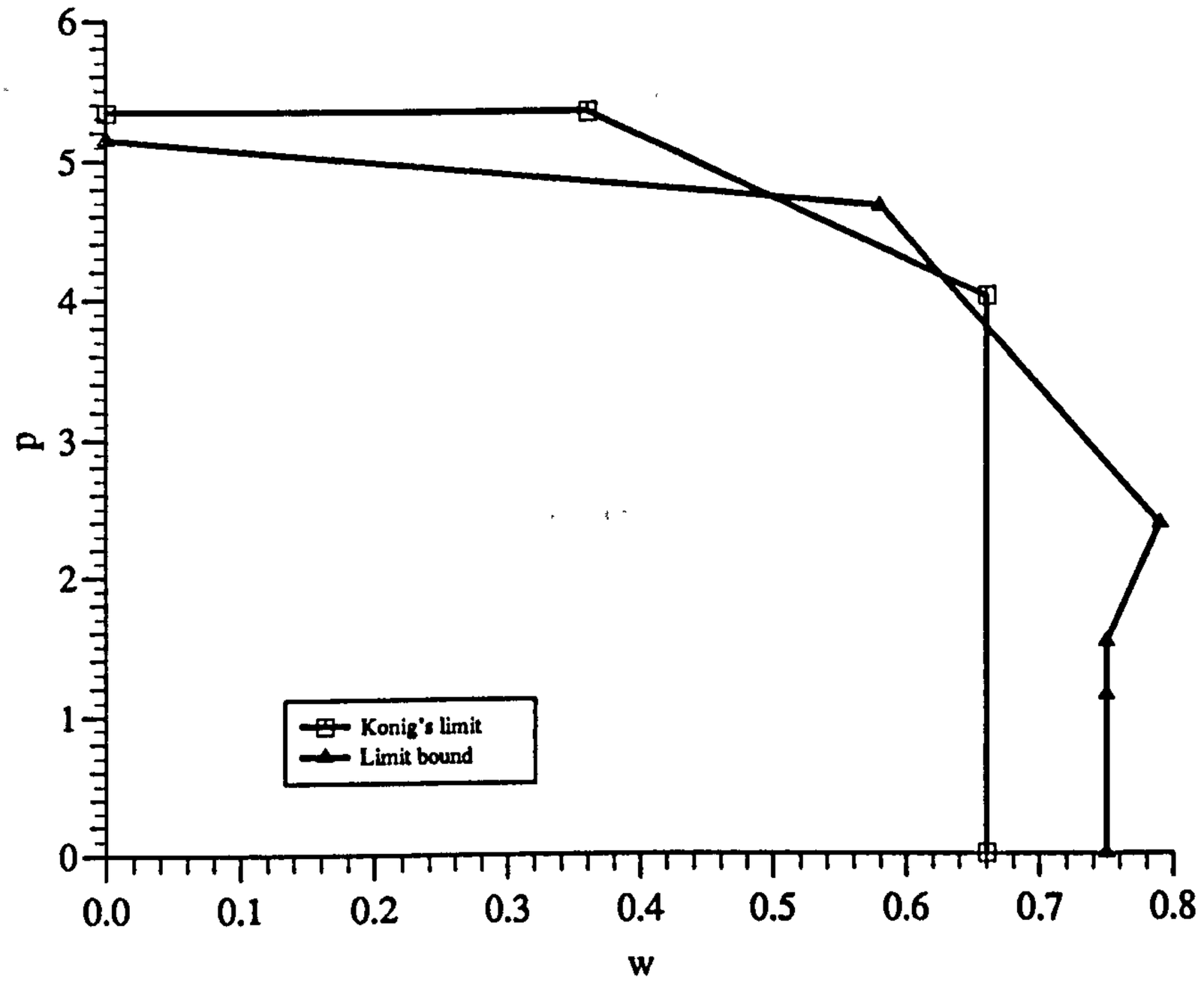

Figure 8.22: Results of one-bay, two-story frame, $h/L = 2$

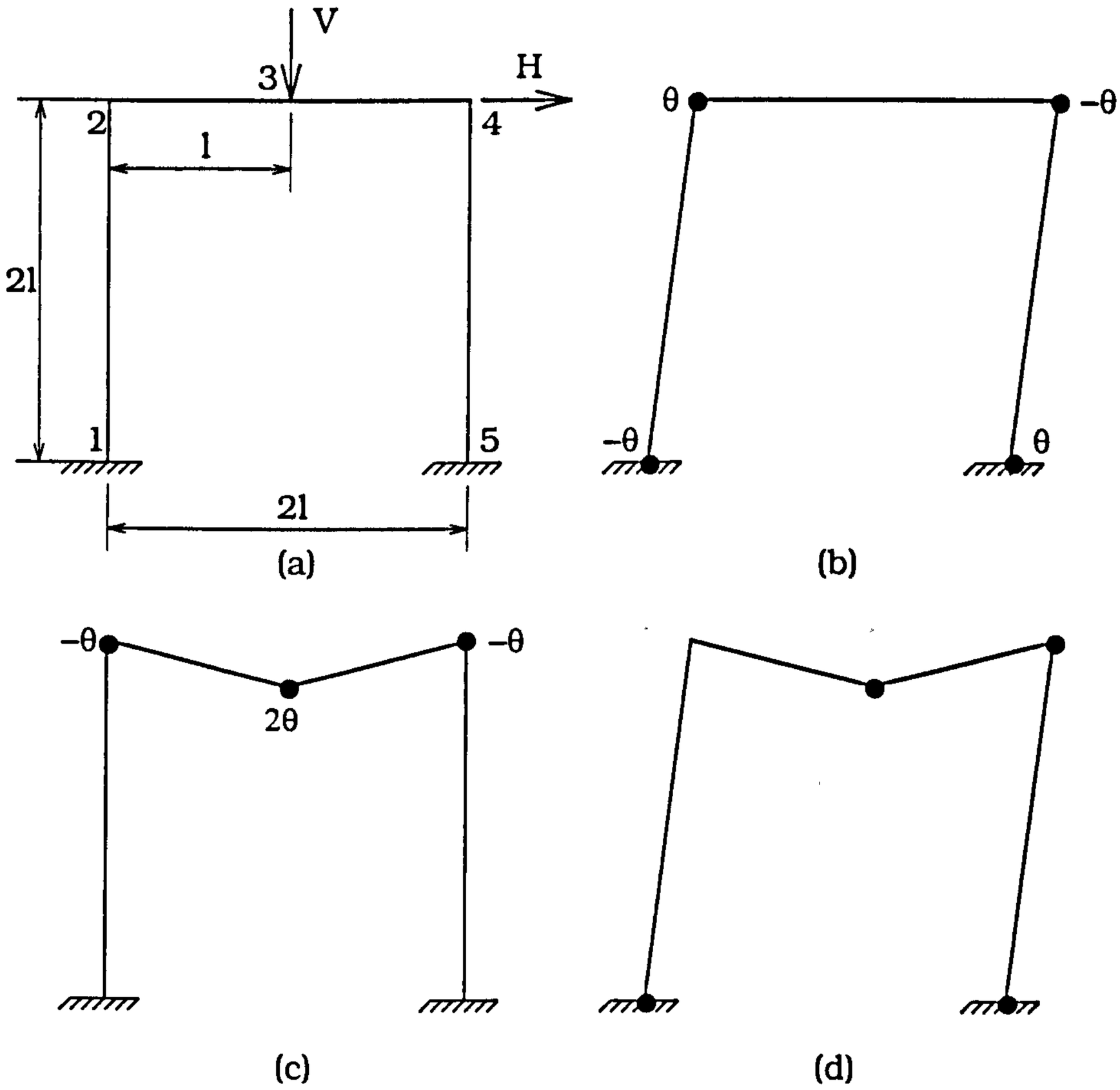

Figure 8.23: Incremental collapse of a portal frame under variable repeated loads

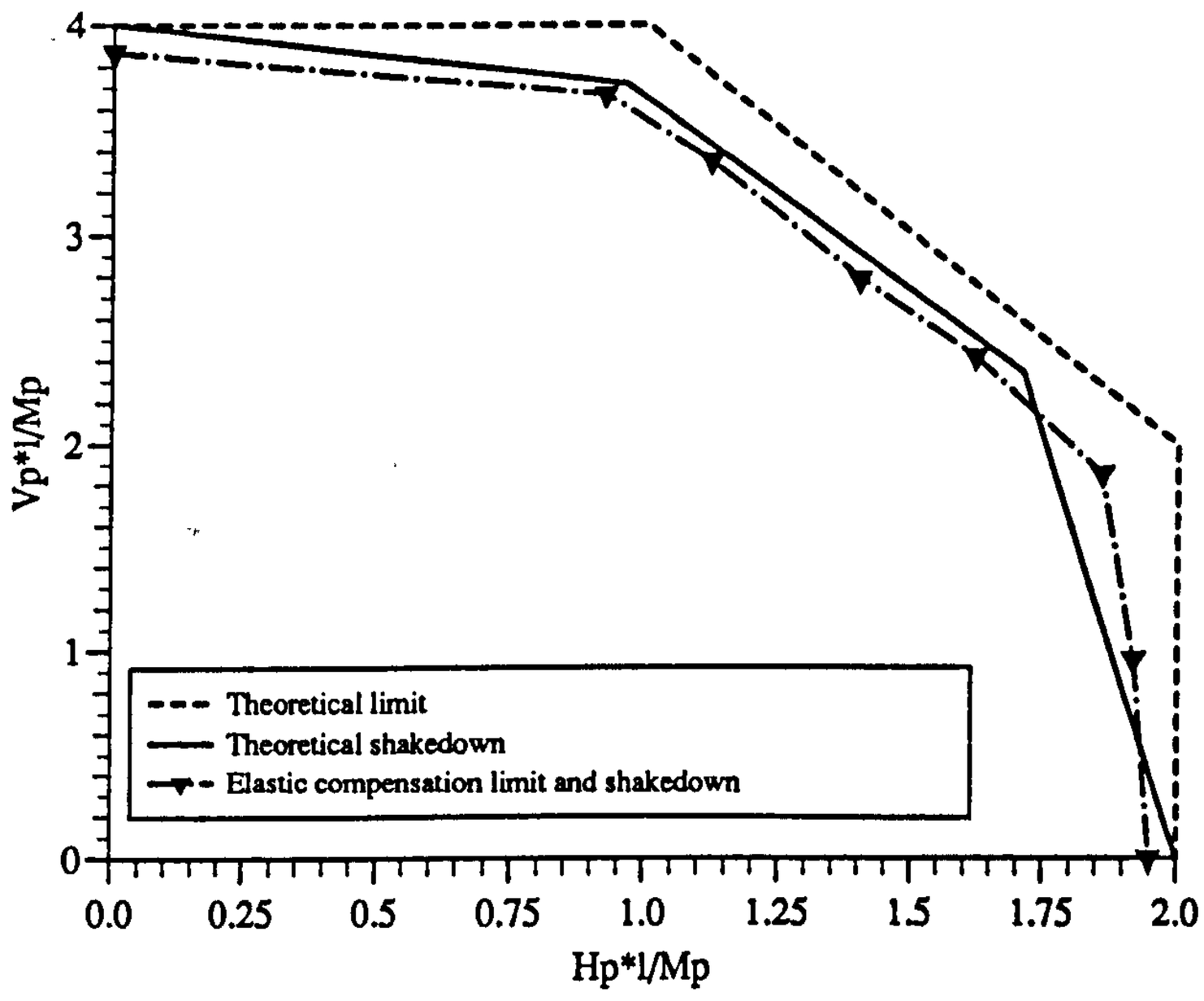

Figure 8.24: Interaction diagrams for a fixed-base portal frame under static and cyclic loading

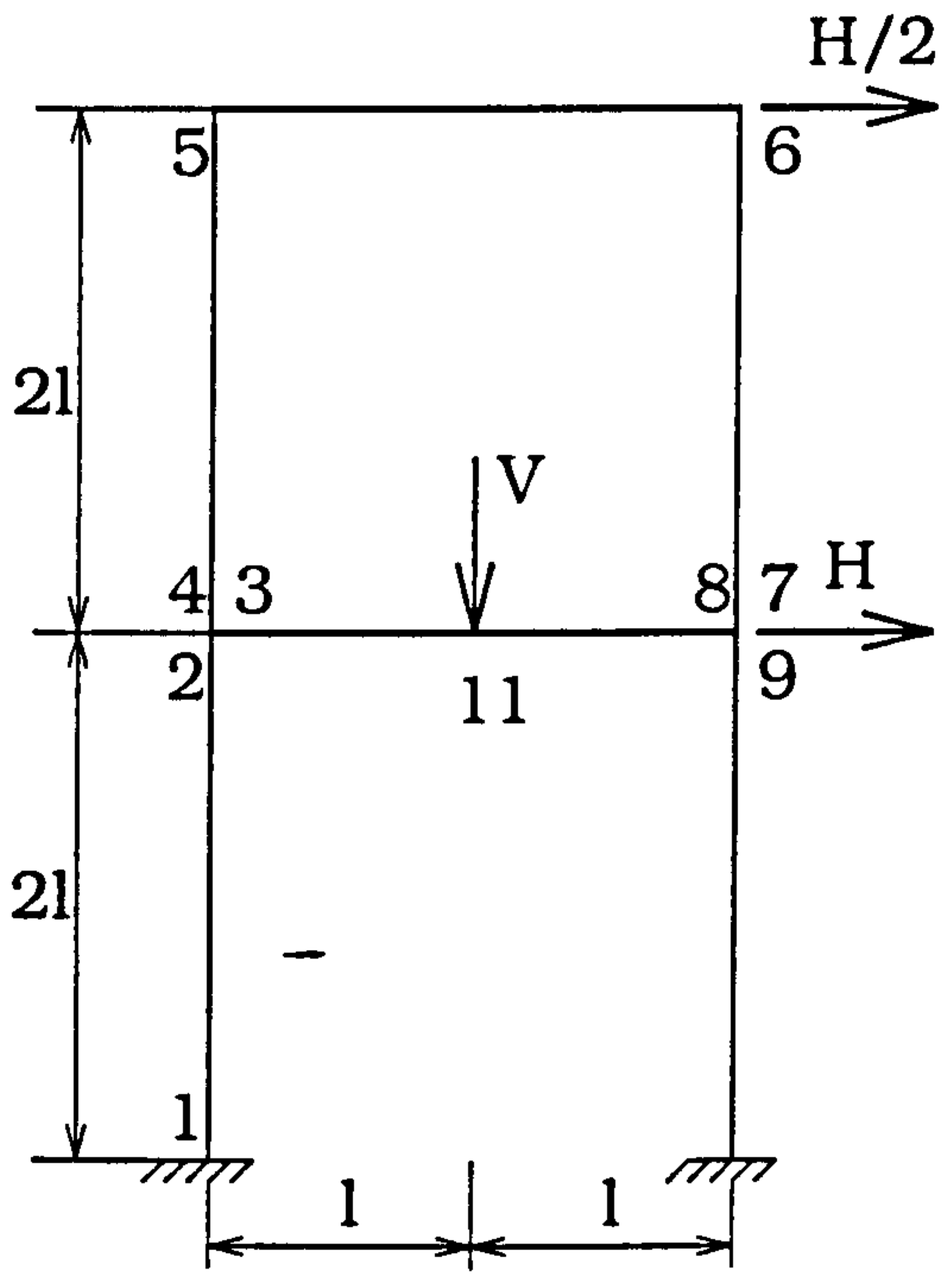

Figure 8.25: A two-story frame with possible collapse mechanisms

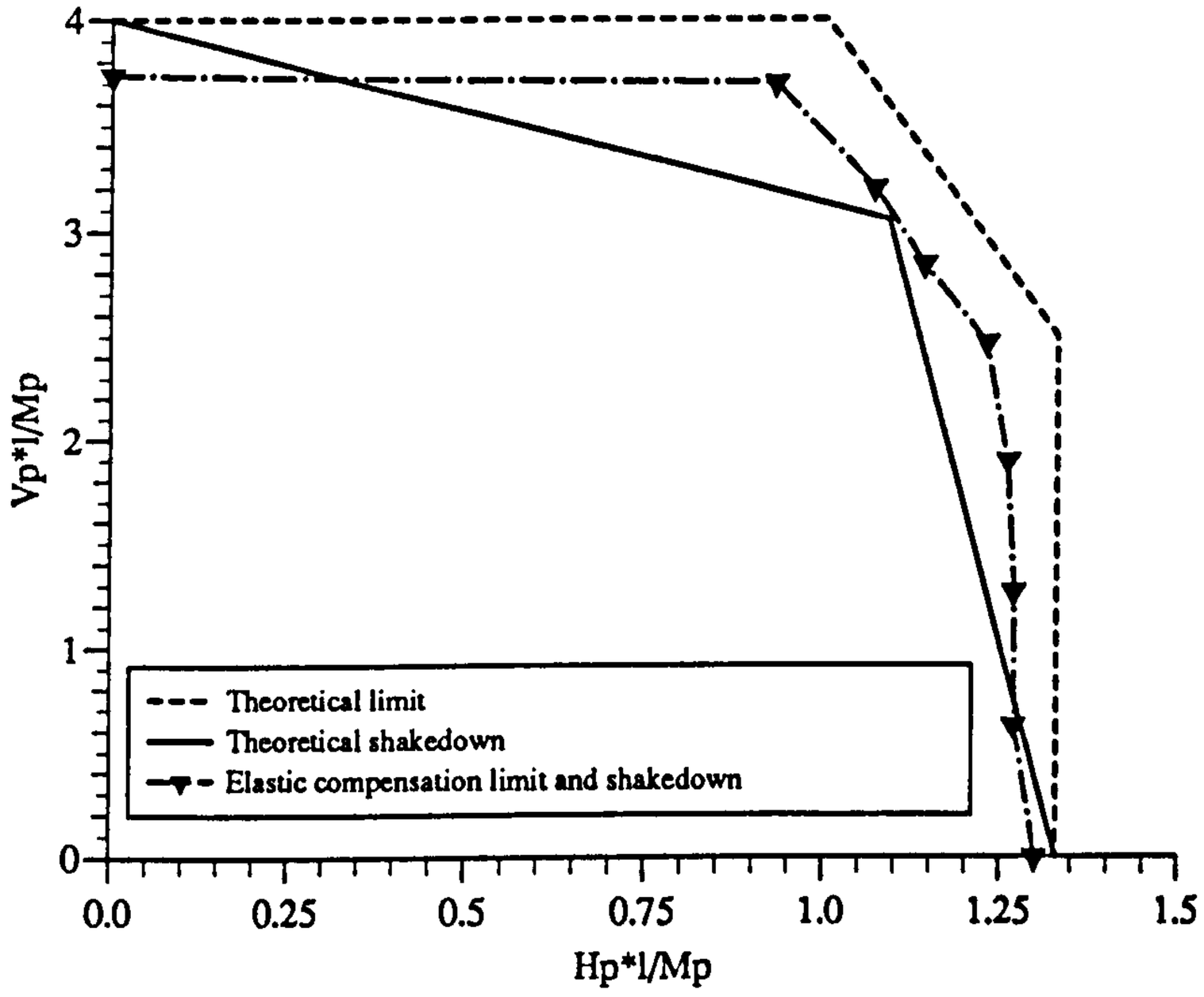

Figure 8.26: Interaction diagrams for a two-story rectangular frame

CHAPTER 9

GENERALISED LIMIT ANALYSIS OF NOZZLES IN SHELLS

9.1 Introduction

In Chapter 5 limit analysis of the nozzle problem was presented. In Chapter 7. the elastic compensation procedure based on Ilyushin's and Ivanov's generalised yield criterion has been developed. In this Chapter, a parametric study of the limit loads for nozzles in spherical and also for cylindrical pressure vessels will be carried out respectively, using this method and compared to the previous results.

9.2 Generalised Limit Analysis of Nozzles in Spherical Shells

9.2.1 Model Geometry

Thirty one pressuried axisymmetric nozzle/sphere models with fixed sphere radius, sphere thickness and nozzle thickness ($t/T = 1$) are investigated in such a way that the ratios R/T and t/T are held constant. The nozzle/spherical shell geometries are shown in Figure 9.1. Here the dimensionless geometry parameter ρ: $\rho = \frac{r}{R}(\frac{R}{T})^{\frac{1}{2}}$ is used as same as that in the paper of Leckie and Payne [1965]. In Figure 9.1, r is the radius to mid-section of the nozzle, R the radius to mid-section of the shell, t the thickness of the nozzle and T the thickness of the sphere. P is the internal pressure and P_r the radial outward pressure as shown.

The shell radius R is fixed at $R = 1000$ and three wall thickness are examined ($T = 10,\ 20$ and $40mm$) giving three groups of models with constant shell radius to thickness ratio of $R/T = 100,\ 50$ and 25. In this way, the variation in limit load with **two** dimensionless geometry parameters ρ and R/T was investigated. For all the models examined the modulus of elasticity is taken as $200E3.N/mm^2$ with Poisson's ratio 0.3. The yield stress of the material is taken as $300.N/mm^2$.

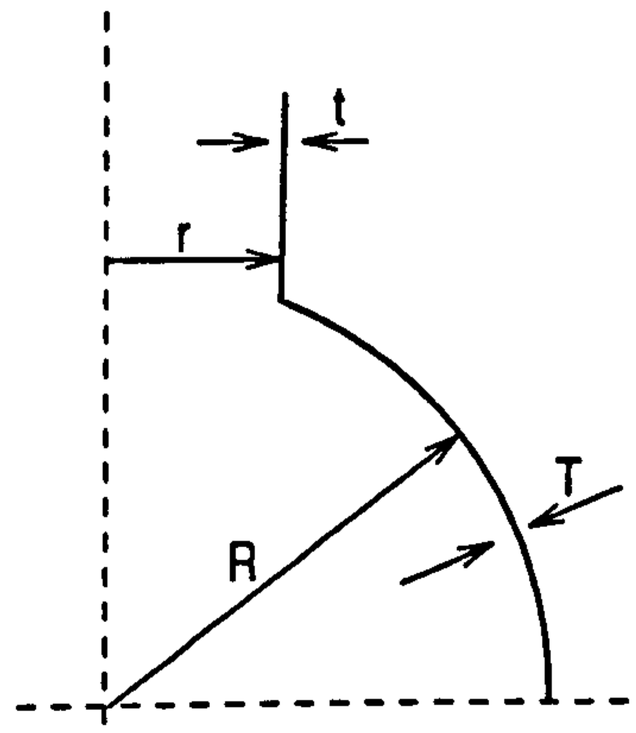

Figure 9.1: **The geometry of axisymmetric nozzle in spherical shell**

9.2.2 Finite Element Model

Finite element models were created in *ANSYS* using two noded axisymmetric structural shell element SHELL51. The models were restrained in the meridional direction, but allowed to move radially, at a distance sufficiently far removed from the nozzle. Internal pressure P and radial nozzle pressure P_r equivalent to an capped nozzle pressure load,

$$P_r = \frac{Pr_i^2}{r_o^2 - r_i^2}$$

where r_o is outside radius and r_i inside radius of the shell, were applied. The model finite element mesh for model 10j is shown in Figure 9.2. The model loadings and boundary conditions are the same as that of solid element model in Chapter 5.

9.2.3 Limit Loads of Nozzles in Spherical Shells

The calculated elastic compensation limit pressures, P_{IL} and P_{IV}, obtained using Ilyushin's and Ivanov's yield functions, eqn (7.48) and eqn (7.49) respectively, are normalized according to the equation:

$$\overline{P} = \frac{R}{2T\sigma_y}P$$

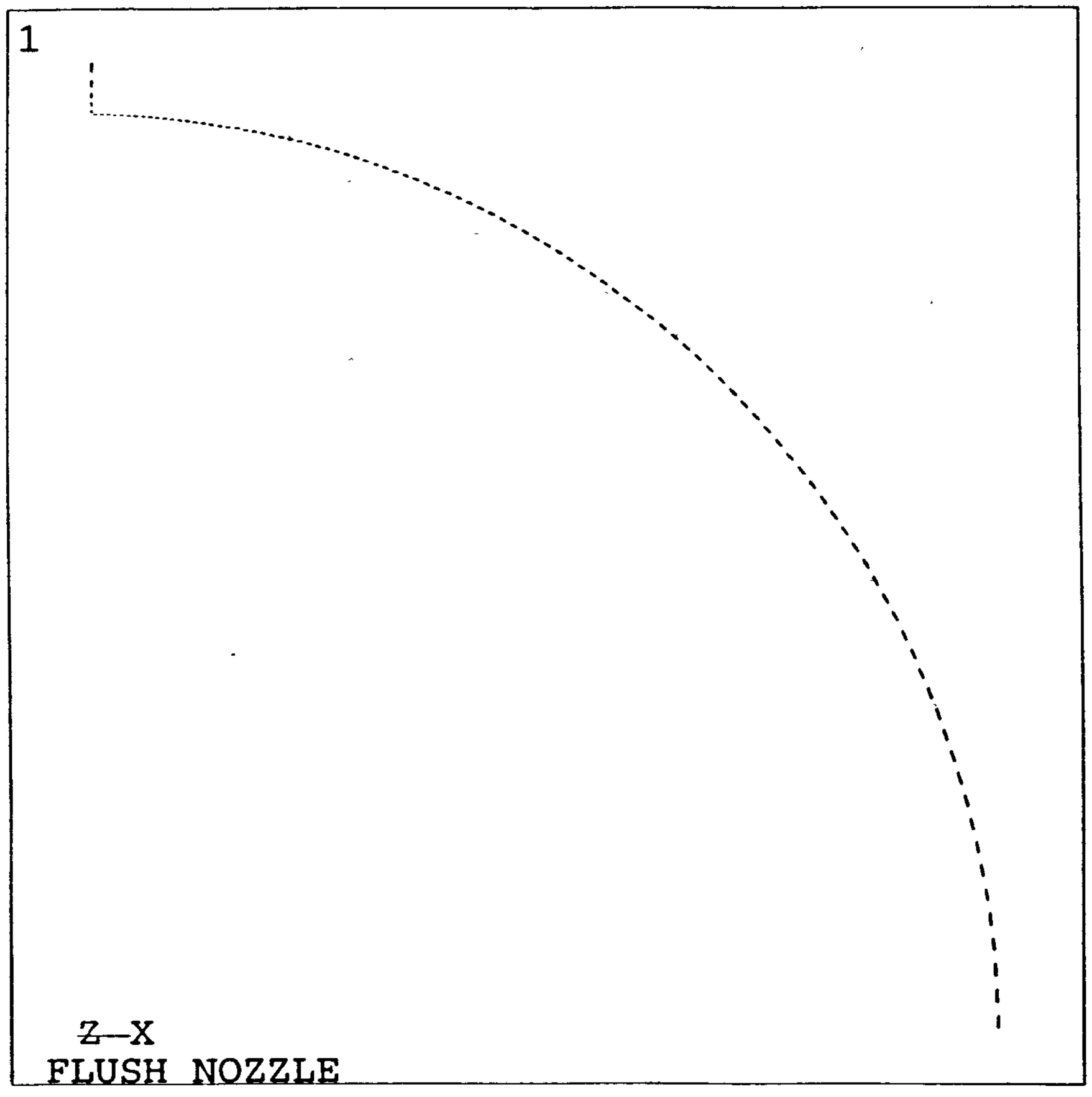

Figure 9.2: Shell finite element mesh for nozzle/spherical intersection

These are compared in Tables 9.1-9.3 and Figures 9.3-9.5 with elastic-perfectly plastic finite analysis, $\overline{P_p}$, with the previous solutions in Chapter 5 – the first yield pressure, $\overline{P_y}$, the lower and upper bound limit pressures, $\overline{P_l}$ and $\overline{P_u}$ – and the Robinson and Gill [1973] lower bound limit solution $\overline{P_{R+G}}$.

9.2.4 Discussion of Results

The results show that there is no real distinction between the results using Ilyushin or Ivanov yield function. It can be seen from Figures 9.3 to 9.5 that the limit pressures calculated lie closer to the previous lower bound solution (Chapter 5) for lower values of ρ and closer to the upper bound for higher values, but, in Figures 9.3 to 9.5, shows a different slope to the results derived here using Ilyushin or Ivanov's approximate yield function. The Robinson and Gill [1973] solution is also bounded by the previous solutions (Chapter 5). In fact Robinson and Gill [1973] also used Ilyushin's approximate shell yield function, but used optimisation techniques applied to the lower bound limit load theorem but these were based on approximate polynomial representations for the shell stresses and would not be expected to reflect the actual stress system close to collapse.

9.2.5 Concluding Comments

Comparing the results of the parametric study with results from literature and incremental elastic-plastic analysis (with an elastic-perfectly plastic material model) indicates that the elastic compensation method is a robust method for bounding limit loads without recourse to complex incremental elastic-plastic analysis. The results of the study also indicate that whilst the lower bound limit load is a function of the dimensionless geometry parameter ρ used by Leckie *et al*, it cannot be fully characterised by this single parameter. The spread in the results for the lower and upper bound limit pressure for the various R/T ratios indicates that this parameter also has an influence.

It has been shown here that efficient estimates of lower bound limit loads in axisymmetric nozzle in spherical shells and other axisymmetric shell structures, such as torispherical and conical ends and a skirted vessel [Boyle, Hamilton, Shi and Mackenzie, 1995], can be obtained using approximate shell-type yield functions. While detailed elasto-plastic finite element analyses of axisymmetric shell structures can be easily derived, the approach suggested here only requires a few elastic analyses and would be a more economic way of generating either the large number of results required to take in a more complete parameter survey or a quick estimate of plastic collapse loads in complex ring stiffened vessels. The next step would be to extend this approach to more complex three dimensional pressure vessel geometries.

Table 9.1: *Normalised lower and upper bound limit pressure of nozzles.* $T = 10mm$, $R/T = 100$

Nozzle	$r(mm)$	ρ	$\bar{P}_y$	$\bar{P}_l$	$\bar{P}_u$	$\bar{P}_{IL}$	$\bar{P}_{IV}$	P_{R+G}	P_P
10a	10	0.1	0.429	0.953	1.0	0.992	0.984	—	0.992
10b	20	0.2	0.442	0.904	1.0	0.966	0.96	—	0.992
10c	30	0.3	0.459	0.885	1.0	0.925	0.918	—	0.975
10e	50	0.5	0.47	0.85	0.993	0.91	0.899	0.876	0.958
10f	60	0.6	0.469	0.799	0.993	0.831	0.834	0.836	0.917
10g	70	0.7	0.465	0.769	0.968	0.804	0.813	0.80	0.883
10h	80	0.8	0.459	0.709	0.918	0.773	0.781	0.744	0.85
10i	90	0.9	0.44	0.698	0.901	0.74	0.75	0.71	0.817
10j	100	1.0	0.412	0.651	0.817	0.714	0.725	0.68	0.792
10k	200	2.0	0.257	0.455	0.561	0.523	0.539	0.472	0.542

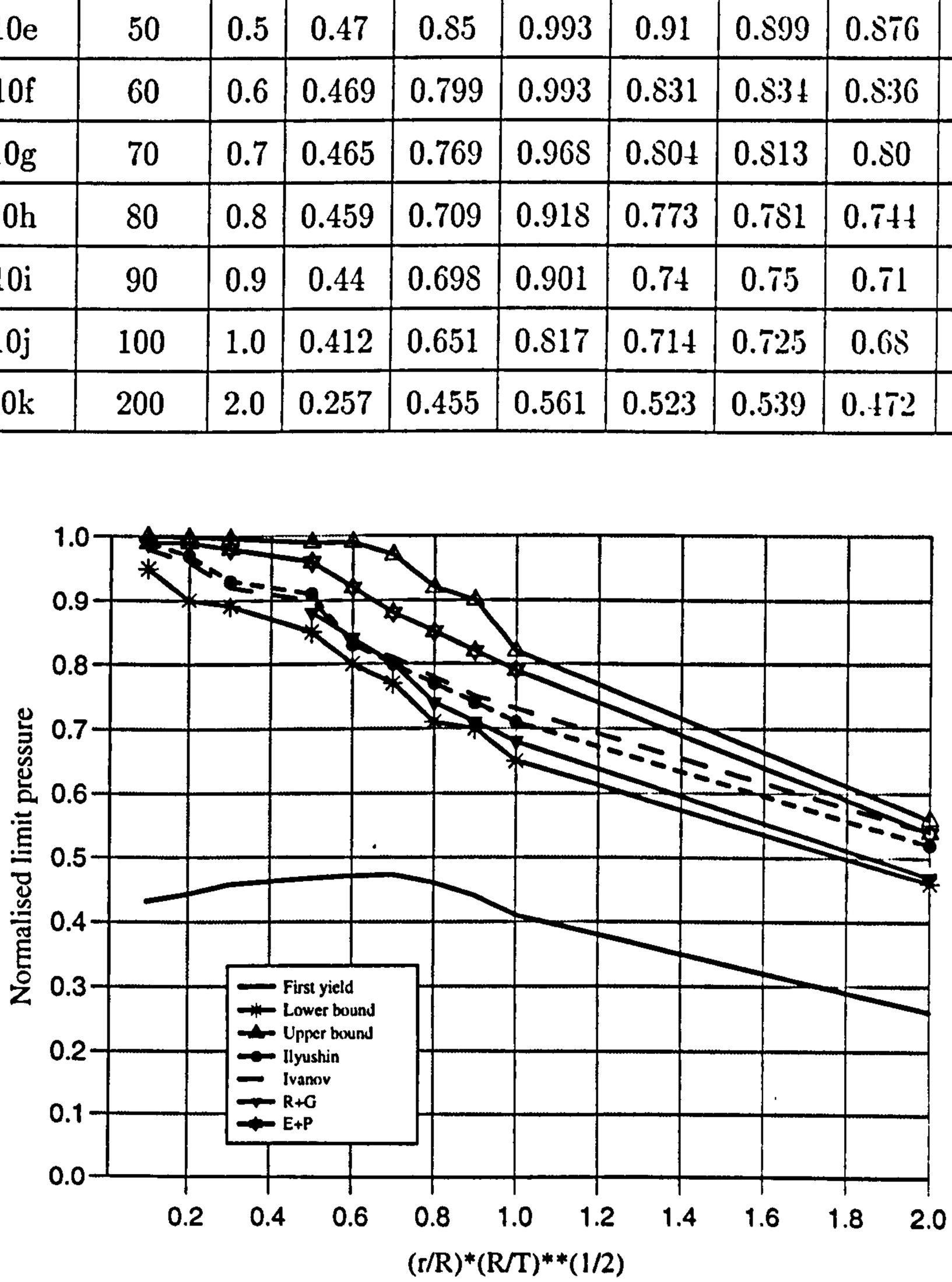

Figure 9.3: Normalised lower and upper bound limit pressure of nozzles. $T = 10mm$, $R/T = 100$

Table 9.2: *Normalised lower and upper bound limit pressure of nozzles.* $T = 20mm$, $R/T = 50$

Nozzle	$r(mm)$	ρ	$\bar{P}_y$	$\bar{P}_l$	$\bar{P}_u$	$\bar{P}_{IL}$	$\bar{P}_{IV}$	P_{R+G}	P_P
10	14.14	0.1	0.469	0.955	1.0	0.97	0.963	—	0.992
11	28.28	0.2	0.436	0.9	1.0	0.952	0.944	—	0.992
12	56.57	0.4	0.464	0.833	0.997	0.896	0.893	0.928	0.967
13	70.71	0.5	0.471	0.803	0.99	0.868	0.866	0.888	0.933
14	84.85	0.6	0.473	0.776	0.977	0.84	0.838	0.846	0.90
15	98.99	0.7	0.471	0.745	0.955	0.791	0.815	0.81	0.867
16	113.1	0.8	0.467	0.715	0.923	0.783	0.792	0.774	0.833
17	127.3	0.9	0.448	0.685	0.884	0.756	0.767	0.736	0.817
18	141.2	1.0	0.419	0.657	0.843	0.732	0.747	0.704	0.783
19	212.1	1.5	0.32	0.541	0.683	0.657	0.649	0.583	0.658
20	282.8	2.0	0.264	0.463	0.584	0.56	0.573	0.496	0.55

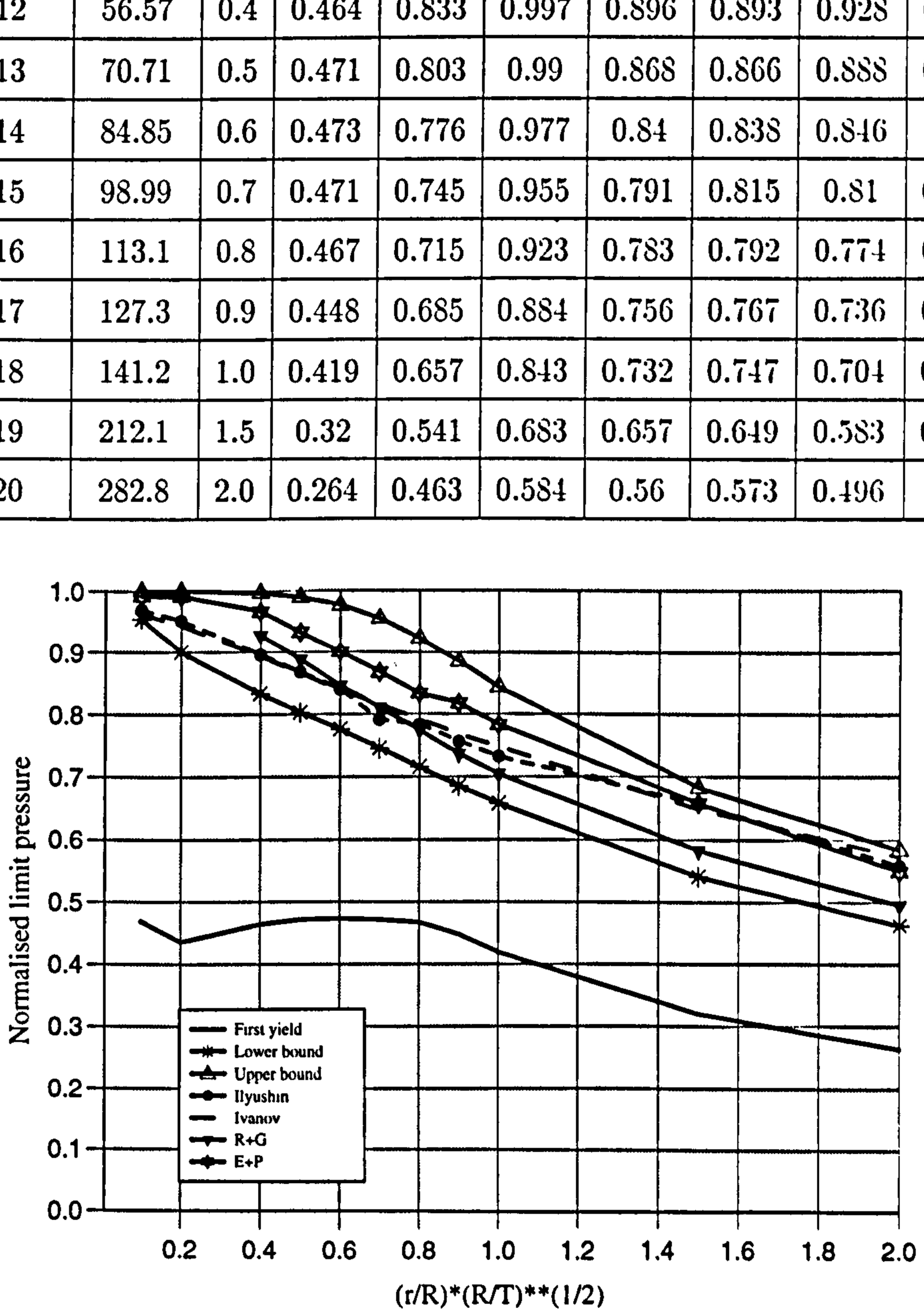

Figure 9.4: Normalised lower and upper bound limit pressure of nozzles. $T = 20mm$, $R/T = 50$

Table 9.3: *Normalised lower and upper bound limit pressure of nozzles.* $T = 40mm$, $R/T = 25$

Nozzle	$r(mm)$	ρ	$\bar{P}_y$	$\bar{P}_l$	$\bar{P}_u$	$\bar{P}_{IL}$	$\bar{P}_{IV}$	P_{R+G}	P_P
21	40	0.2	0.432	0.92	1.0	0.947	0.928	—	0.996
22	60	0.3	0.443	0.888	0.999	0.927	0.919	0.974	0.992
23	80	0.4	0.457	0.859	0.996	0.90	0.895	0.941	0.975
24	100	0.5	0.467	0.829	0.99	0.871	0.873	0.905	0.958
25	120	0.6	0.471	0.802	0.976	0.843	0.848	0.87	0.917
26	140	0.7	0.473	0.774	0.954	0.817	0.825	0.832	0.896
27	160	0.8	0.471	0.748	0.924	0.792	0.803	0.80	0.867
28	180	0.9	0.467	0.718	0.888	0.769	0.781	0.768	0.838
29	200	1.0	0.462	0.692	0.851	0.749	0.762	0.74	0.808
30	300	1.5	0.353	0.579	0.702	0.663	0.676	0.615	0.675
31	400	2.0	0.291	0.495	0.607	–	–	0.518	–

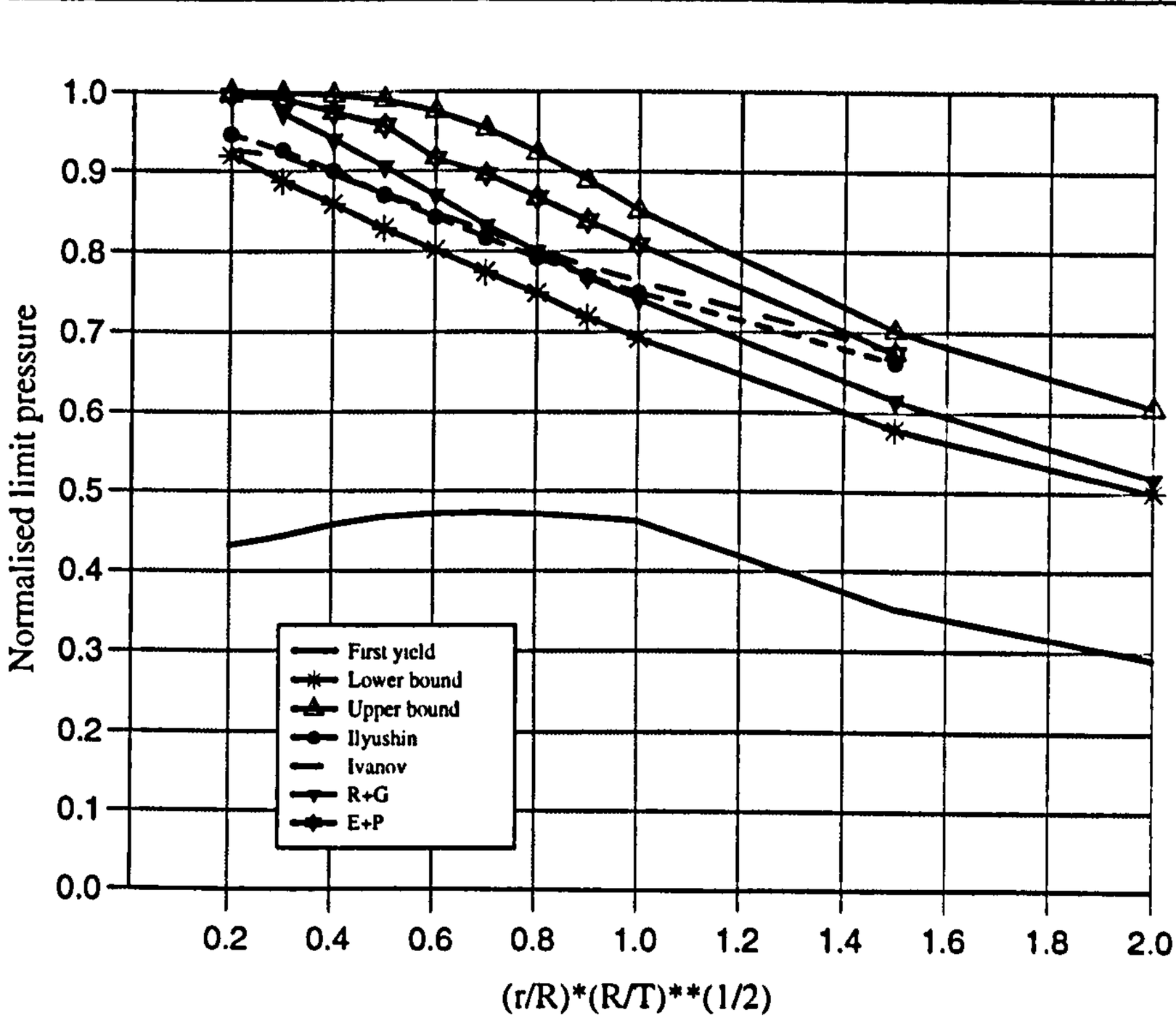

Figure 9.5: Normalised lower and upper bound limit pressure of nozzles. $T = 40mm$, $R/T = 25$

9.3 Generalised Limit Analysis of Nozzles in Cylinder Shells Under Internal Pressure

9.3.1 Brief Review of Limit Analysis of Nozzles in Cylinder Shells Under Internal Pressure

Lower Bound Limit Analysis

The problem of two intersecting cylindrical shells under internal pressure is a common situation in the pressure vessel industry. Because of the lack of rotational symmetry the problem of the limit analysis of a branch in a cylindrical vessel is much more difficulty than the case of a spherical vessel, but there are a number of attempts at theoretical solutions. The first appears to be due to Goodall [1967] who obtained some lower bound solutions for the small radius radial nozzle using the shallow shell equations and the approximate Tresca two-moment limited interaction yield surface. The assumed stress field was very simple, as a result of which it was not possible to get strict equilibrium of forces and moments at the intersection.

Lower bound results using Y_1 eqn. (7.34) have been presented by Ellyin and Turkkan [1971]. Although using non-linear programming and von Mises yield criterion, their method of handing the intersection equilibrium equations is quite different and, in addition, their assumed stress distribution has a fixed number of terms in the series expansion. Moreover, there appears to be an inconsistency in the analysis concerning the equilibrium across the zones employed. Different pressures have been used in each zone whereas a lower bound stress field should be in equilibrium with the same pressure everywhere. Results were given for a large number of parameters but unfortunately there seems to be errors in the analysis [Robinson 1978] and so the results will not be true lower bounds.

Erbatur [1972] did a general lower bound analysis valid for oblique nozzles also, but, because of limitations imposed by computer store, the results obtained

were not very satisfactory. In 1975 Robinson [1975] using **thin shell** theory with series expansion for the stress resultants and using Ilyushin's approximate yield surface (Y_3), eqn. (7.36), obtained a lower bound limit presure. The coefficients in the series were optimised using a non-linear programming technique. However it was reported that occasionally the program failed to converge at values of ($r/R \leq 0.5$), and the results obtained for large nozzles ($r/R > 0.8$) were lower than lower bounds available at that present time.

In 1976 Biron *et al.* [1976] attempted a lower bound formulation using Ilyushin's approximated yield surface (Y_1), eqn. (7.34), and dividing the structure into segments. Within the segments the stress resultans are approximate by a finite series, the coefficients of which are optimised. It was found out by Biron that strict satisfaction of the continuity equation at the junction of the nozzle and cylinder was not possible, hence a tolerance B_i necessary for a satisfactory solution was introduced. It was pointed out by the author that there was some difficulty in deciding the value of B_i necessary for satisfactory solution. Hence this method does not seem to give a satisfactory solution.

Srinivasaiah and Schroeder [1977] in 1977 found a lower bound limit pressure of cylinder/cylinder intersection based on three dimensional stress fields expanded in series at every point of the shell and of the intersection. The equations they obtained were solved using a computer so as to obtain the limit pressure which did not voilate yield condition. The von Mises yield condition was used throughout the volume of the branch and cylinder. However, it was found that the limit pressure tended to fluctuate as the number of the collocation sections were increased and at the same time high residuals were found at a few collocation points, which rendered the lower bounds to be low for design if diameter ratios of the cylinders were smaller than 0.5.

In Robinson's paper [1977] a non-linear programming approach and the Ilyushin's yield surface Y_3, eqn. (7.36), have been used. Then a parametric study for a lower

bound limit pressure for the case of a flush nozzle in cylindrical vessel under internal pressure has been carried out by Robinson [1978]. A lower bound solution for various parameters of cylinder to cylinder intersection was obtained by using both shallow and deep shell theories. The results he obtained were used to plot various graphs. For these graphs, the higher of the **shallow** of **deep shell** results was taken. These graphs are useful for finding the lower bound limit pressure for various parameters of nozzle/cylinder intersection. Finally he made comparisons between theoretical and experimental results for certain parameters. It was pointed out that experimental results would be subjected to a great deal of uncertainty for many resons: (i) the effect of anisotropy and strain hardening of material used and consequently difficulty in defining yield stress, (ii) differing amount of weld material at the intersection of the two shells, (iii) local defects due to geometry inaccuracies or inhomogeneties. In addition to these there is a major uncertainty because of the number of ways in which **plastic load** could be estimated as mentioned earlier.

Upper Bound Limit Analysis

Upper bounds for radial nozzles in the range $r/R \leq 0.5$ were obtained by Cloud and Rodabaugh [1968] but their results are not true upper bounds as several terms were omitted from the equations. They assumed the two-moment limited interaction yield surface. However, because of the neglect of several terms and some approximations made, this method can be regarded as giving only a rough estimate, but it has the advantage that values can be obtained from a formula.

Schroeder and Rangeranjan [1969] developed an upper bound analysis valid for radial nozzles with $r/R > 0.4$, and using Ilyushin's first yield surface Y_1, eqn. (7.34). The equation was solved using a computer which did the numerical integration and minimisation to obtain the upper bound limit pressure. The upper bound solution when compared with experimental results showed that it was about 20% higher. In this analysis the assumed velocity field had some degree of

freedom so that is was possible to gradually lower the upper bound by allowing a more general velocity field. Hence the bounds were improved still further by Schroeder [1971], Schroeder and Roy[1971] for the entire range of (r/R). It was found that the new analysis gave an upper bound solution which was lower than the solution obtained by Schroeder and Rangeranjan [1969].

Experimental Investigation

Some experimental work on the behaviour of branches in cylindrical vessels beyond the elastic limit has been reported by a number of researchers. such as Rose [1965], Winkler *et al.* [1965], Cottam and Gill [1966], Clare and Gill [1966]. Rodabaugh and Cloud [1968], Calladine and Goodall [1969], Ellyin [1976] [1977] and Schroeder *et al* [1977].

Since the late 1970's very few more detailed analyses for limit pressure have been published and more emphasis has been placed on deriving specific results for particular geometries either through testing or detailed elasto-plastic finite element analysis. Very recently a detailed study, using the elastic compensation method, of cylinder-cylinder intersections under internal pressure and in-plane moment loading by Nadarajah [1993] and Nadarajah *et al.* [1995] has shown that fairly detailed three dimensional finite element modeling is required to obtain acceptable bounds. This is computationally expensive (but still much less than detailed elasto-plastic analysis Nadarajah *et al.* [1995]). A simpler approach would thus be preferable. In last section a simple but effective technique for the calculation of lower bound limit loads for axisymmetric thin shells was demonstrated. The key feature of that study is the use of approximate yield criteria for thin shells. In this section this approach is extended to general shell structures and demonstrated for the pressurised cylinder-cylinder intersection problem through a detailed parameter survey. The finite element modeling and analysis time which may be required is greatly reduced.

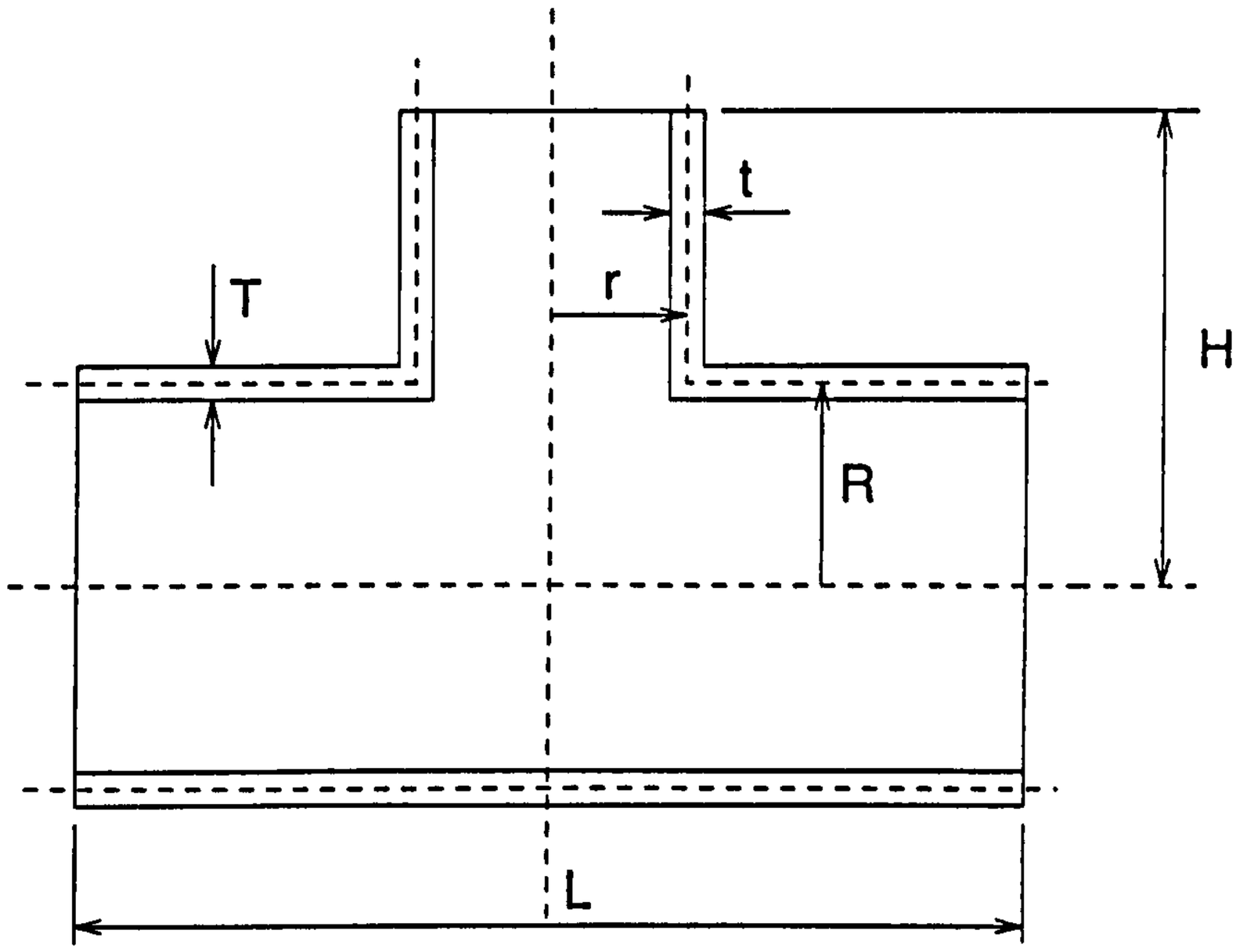

Figure 9.6: Cylinder/cylinder geometry

9.3.2 Model Geometry

The basic geometry and notation are given in Figure 9.6: the main cylinder has mean radius R and thickness T while the 'nozzle' has mean radius r and thickness t. The length of the cylinder is denoted by L; the height of the nozzle from the axis of the main cylinder is denoted by H.

A series of twenty seven models are developed corresponding to three different ratios of cylinder radius to thickness, $(R/T) = 50, 100$ and 200. For each of these models three different ratios of nozzle to cylinder radius are considered. $(r/R) = 0.1,\ 0.2,\ 0.4$, and three different ratios of nozzle to cylinder thickness. $(t/T) = 1,\ 0.5, 0.25$. These are summarised in Table 9.4. The geometric parameters, $R,\ L$ and H were constant for each model with values $R = 500$mm. $L = 2000$mm and $H = 700$mm.

9.3.3 Finite Element Model

The finite element model is developed using 8-node structural shell element SHELL93 in *ANSYS* [1994]. In all the finite element models, a quarter of the nozzle and cylinder was modeled with an internal pressure and a total of 245 elements; typical models are shown in Figure 9.7. The mesh used is characteristic of thin shell finite element models used for nozzle problems and will be demonstrated to give useful results for limit loads in comparison with previous solutions. However it should be noted that in general some mesh refinement would be required in the vicinity of the simulated collapse mechanisms to obtain a good lower bound. This is not particularly difficulty in modern finite element analysis systems: it is suggested here, for elastic compensation, that an initial analysis sequence be run to establish critical regions - the mesh in these regions would be refined and the sequence re-run, and so on. This procedure was not found necessary in the current problem. In addition, since shell elements only are required on a meshed doubly curved surface such mesh refinement is straightforward - this is *not* the case if brick elements are used in a full three dimensional model Nadarajah [1993] and Nadarajah *et al.* [1995]!

Symmetric boundary conditions were imposed on the two planes of symmetry. At the ends of the nozzle and the cylinder axial pressure was also applied. A constraint in the circumferential direction was also placed on the end of the cylinder. The loads and boundary conditions applied here are the same as Nadarajah [1993], given in Figure 9.8, and are thus adopted for comparison purposes. Similarly, the (initial) elastic modulus and Poisson's ratio were taken as 200E3 N/mm^2 and 0.3 respectively with nominal yield stress of material was taken as 300 N/mm^2.

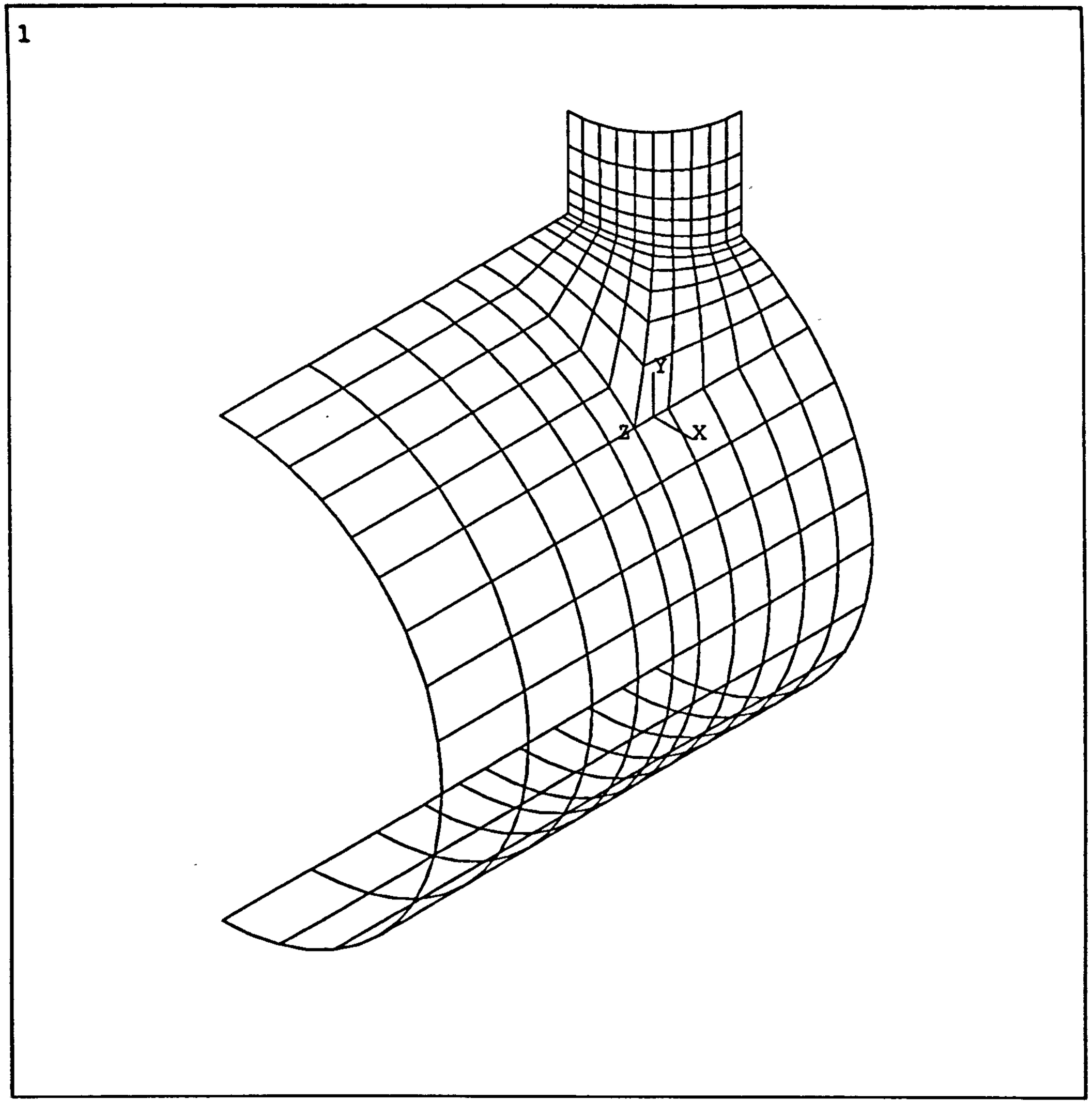

Figure 9.7: Finite element mesh of cylinder/cylinder intersection

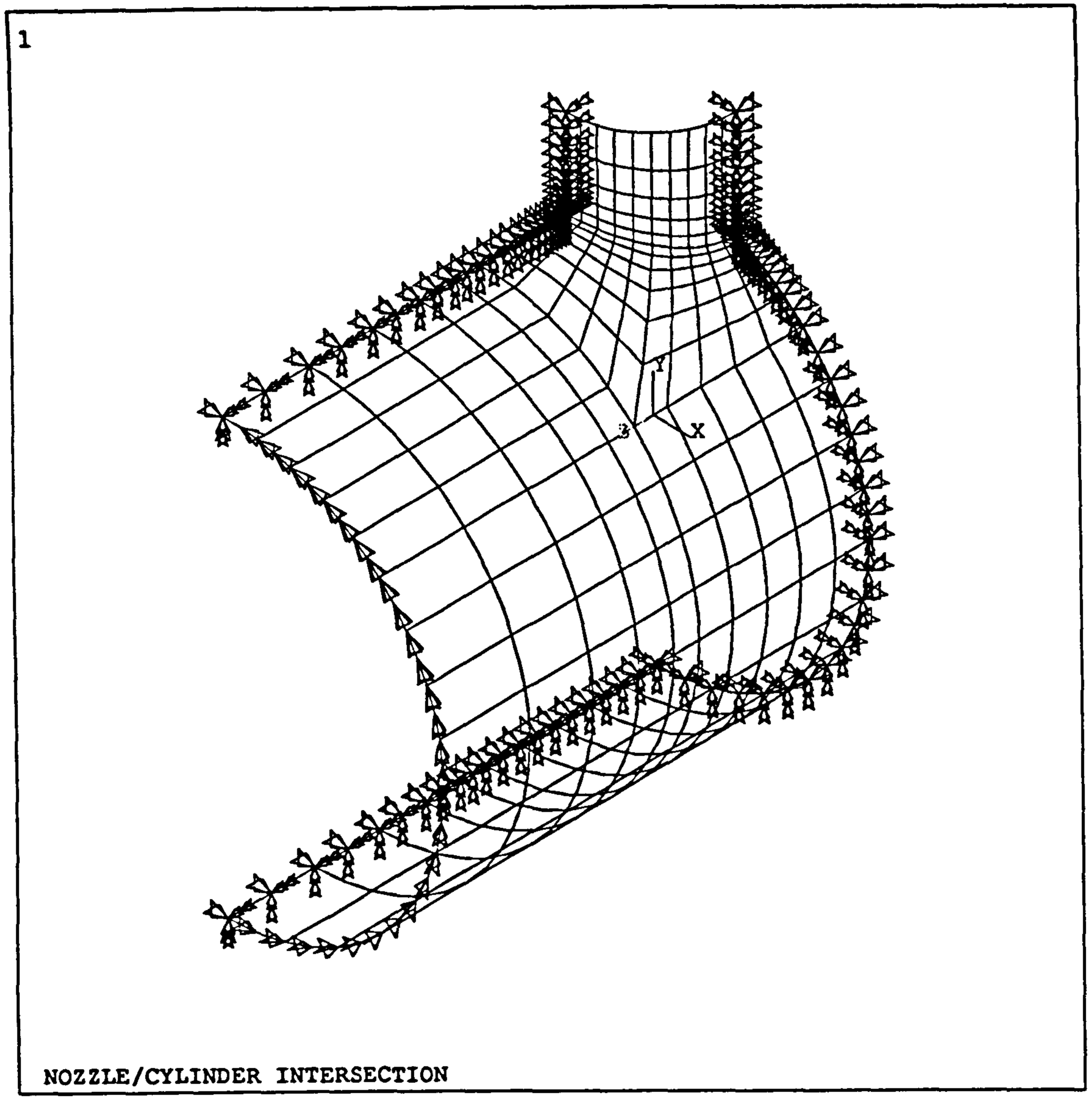

Figure 9.8: Boundary conditions of cylinder/cylinder intersection

9.3.4 Discussion of Results

The elastic compensation was performed automatically through an ANSYS Design Parametric Language (ADPL) macro which is the same as previous section. Up to six iterations are performed for each model and the modulus is corrected using the equation (7.50). Then the elastic compensation limit pressures for Ilyushin's, P_{IL}, and Ivanov's, P_{IV}, generalised yield criteria were obtained using eqn. (7.51). To assist in a comparison with previously published results. pressures are normalised according to the equation:

$$\overline{P} = \frac{R}{2T\sigma_y} P$$

The normalised limit pressures, $\overline{P}_{IL}$ and $\overline{P}_{IV}$, obtained by the elastic compensation procedure are summarised in Table 9.4 and shown in Figures 9.9 to 9.11 for $R/T = 50$, Figures 9.12 to 9.14 for $R/T = 100$, Figures 9.15 to 9.17 for $R/T = 200$.

These results are compared to the lower, $\overline{P}_l$, and upper, $\overline{P}_u$, bound limit pressures and extrapolated results from detailed elasto-plastic analysis, $\overline{P}_P$. These results are taken from Nadarajah *et al.* [1995]: 8-node isoparametric solid elements (SOLID45 of *ANSYS*) were used for elastic compensation lower bound and upper bound limit analyses and up to 14 iterations were required, the elasto-plastic analyses were carried out using 4-node shell elements (SHELL43 of ANSYS). Also shown are Robinson's [1978] lower bound limit pressure, $\overline{P}_R$ which was derived using Ilyushin's generalised yield criteria and a nonlinear programming technique.

It can be seen from the Table 9.4 that the normalised limit pressures, $\overline{P}_{IL}$ and $\overline{P}_{IV}$, obtained by the elastic compensation procedure, based on Ilyushin or Ivanov's equation respectively are generally higher than the results obtained from Robinson [1978] and Nadarajah *et al.* [1995]. More significantly, the new shell lower bound estimate is very close to the elasto-plastic shell analysis. Also, the results obtained from Ilyushin and Ivannov's criteria are comparable (and in

Table 9.4: *Normalised limit pressures for the cylinder-cylinder intersections*

R/T	t/T	r/R	$\bar{P}_R$	$\bar{P}_P$	$\bar{P}_L$	$\bar{P}_U$	$\bar{P}_{IL}$	$\bar{P}_{IV}$
50	1.0	0.1	0.931	0.92	0.82	1.0	0.85	0.83
50	0.5	0.1	0.827	0.81	0.74	0.93	0.82	0.82
50	0.25	0.1	0.770	—	0.66	—	0.71	0.71
50	1.0	0.2	0.666	0.75	0.61	0.87	0.70	0.70
50	0.5	0.2	0.526	0.64	0.51	0.74	0.61	0.60
50	0.25	0.2	0.479	—	0.42	—	0.60	0.59
50	1.0	0.4	0.401	0.47	0.37	0.52	0.51	0.51
50	0.5	0.4	0.283	0.36	0.26	0.40	0.41	0.42
50	0.25	0.4	0.234	—	0.21	—	0.35	0.36
100	1.0	0.1	0.850	0.87	0.74	1.0	0.82	0.81
100	0.5	0.1	0.715	0.77	0.64	0.87	0.69	0.70
100	0.25	0.1	0.671	—	0.55	—	0.62	0.61
100	1.0	0.2	0.550	0.62	0.49	0.74	0.64	0.64
100	0.5	0.2	0.425	0.50	0.39	0.60	0.59	0.59
100	0.25	0.2	0.381	—	0.32	—	0.46	0.47
100	1.0	0.4	0.259	0.37	0.28	0.42	0.41	0.41
100	0.5	0.4	0.161	0.25	0.18	0.30	0.34	0.33
100	0.25	0.4	0.138	—	0.14	—	0.23	0.21
200	1.0	0.1	0.691	0.79	0.69	0.87	0.78	0.78
200	0.5	0.1	0.556	0.64	0.52	0.66	0.58	0.59
200	0.25	0.1	0.513	—	0.44	—	0.45	0.47
200	1.0	0.2	0.418	0.55	0.38	0.61	0.52	0.53
200	0.5	0.2	0.327	0.41	0.30	0.48	0.44	0.45
200	0.25	0.2	0.286	—	0.20	—	0.25	0.26
200	1.0	0.4	0.201	0.29	0.19	0.33	0.32	0.32
200	0.5	0.4	0.131	0.18	0.13	0.22	0.22	0.23
200	0.25	0.4	0.117	—	0.09	—	0.11	0.11

fact only results based on Iiyushin's function. $\overline{P}_{IL}$, are used in Figures 9.9 to 9.17.

9.3.5 Concluding Comments

This section describes a simple technique for the estimation of lower bound limit loads using conventional plastic *shell* analysis and the elastic compensation method. This new technique has been applied to the problem of estimating limit pressures in cylinder/cylinder intersections and compared to more detailed solid finite element lower and upper bound analysis, to elasto-plastic shell finite element analysis, and to previous solutions from the literature.

It can be concluded that the new simpler elastic compensation method for thin shell finite element analysis can be used to give practical (lower bound) limit loads. Since the new method is based on thin shell analysis considerable benefits over full three dimensional analysis are feasible and the technique has much potential for future application.

9.4 References

ASME Boiler and Pressure Vessel Code, (1974), Section III, Division 1. Par. 1430, Appendix II.

ASME Boiler and Pressure Vessel Code, (1975), Section III, Division 1. Par. 1430, 1975 Winter Addendum.

ASME Boiler and Pressure Vessel Code, (1977), Section VIII, Division 2. Appendix 4, Par. 4-136.3 and Appendix 6, Par. 6-153.

Biron, A., & Courchesene, A., (1976), On limit analysis of cylinder-cylinder intersections subjected to internal pressure, *Nuclear Engineering and Design*. Vol. 36, No. 1, Jan., 66-80.

Boyle, J.T., Hamilton, R., Shi, J. and Mackenzie, D., (1996), A simple method of calculating limit loads for axisymmetric thin shells, *Trans ASME. J. Pressure Vessel Technology*, under review.

Clare, K.D. and Gill, S.S., (1966), Effect of vessel diameter/thickness ratio on the behaviour beyond the elastic limit of flush nozzles in cylindrical pressure vessels: experimental investigation, *J. Mech. Engrg. Sci.*, Vol. 8, No. 1. 357–362.

Calladine, C.R. and Goodall, I.W., (1969), Plastic behaviour of thin cylindrical pressure vessels with circular cut outs and radial branches, *J. Mech. Eng. Sci.*, **11**, No. 4, 351–363.

Cloud, R. L., & Rodabaugh, E. C., (1968), Approximate analysis of the plastic limit pressure of nozzles in cylindrical shells, *J. Engrg. for Power. Trans. ASME, Ser. A*,(**2**), 171-176.

Cottam, W.J. and Gill, S.S., (1966), Experimental investigation of the behaviour beyond the elastic limit of flush nozzles in cylindrical pressure vessels. *J. Mech. Engrg. Sci.*, Vol. 8, No. 3. 330–350.

Dinno, L.S., and Gill, S.S., (1965a), The limit analysis of a pressure vessel consisting of the junction of a cylindrical and spherical shell. *Int. J. Mech. Sci.*, **7**, 21–42.

Dinno, L.S., and Gill, S.S., (1965b), Experimental investigation into plastic behaviour of flush nozzles in spherical pressure vessels, *Int. J. Mech. Sci.*, **7**, 817.

Drucker , D.C., and Shield, R.T., (1959), Limit analysis of symmetrically loaded thin shells of revolution, *Trans. ASME*, Vol.81, Ser. E, 61–68.

Ellyin, F., (1976), Experimental investigation of limit loads of nozzles in cylindrical vessels, *WRC Bulletin*, No. 219, September.

Ellyin, F., (1977), An experimental study of elasto-plastic response of branch-pipe connections subjected to internal pressure, external couple and combined loadings, *WRC Bulletin 230*, September.

Ellyin, F., and Sherbourne, A.N., (1965a), Limit analysis of axisymmetric intersecting shells of revolution, *Nucl. Struct. Engng.*, **2**, 86.

Ellyin, F., and Sherbourne, A.N., (1965b), The collapse of cylinder/sphere intersection pressure vessel, *Nucl. Struct. Engng.*, **2**, 169–180.

Ellyin, F. & Turkkan, N., (1971), Lower bound to limit pressure of nozzle-to-cylindrical shell attachment, *ASME Paper 71-PVP-38*. 1971.

Erbatur, F., *Limit Analysis of Cylinder-Cylinder Intersections*. PhD Thesis. University of Manchester, 1972.

Gerdeen, J.C., (1982), *Limit Analysis and Plasticity*, Pressure Vessel and Piping Design Technology, A decade of progress, ASME.

Gill, S.S., (1964), The limit pressure for a flush cylindrical nozzle in spherical pressure vessel, *Int. J. Mech. Sci.*, **6**, 105–115.

Gill, S.S., (1970), *The Stress Analysis of Pressure Vessels & Pressure Vessel Componemts*, Pergamon.

Goodall, I. W., *On the Design of Intersections in Pressure Vessels*. PhD Thesis. Cambridge University, 1967.

Kulkarni, A. K., Neale, K. W., & Ellyin, F., (1975), Consistent theories for intersecting shells, *Nuclear Engineering and Design*, Vol. 35, 377-385.

Leckie, F.A. and Payne, D.J., (1965-1966), Some observations on the design of spherical pressure vessels with flush cylindrical nozzles, *Proc. Inst. Mech. Engineers*, Vol. 180, Part I, No. 20, 497–501.

Nadarajah, C., (1993), *A Design Study of Nozzles and Attachments in Pressure Vessels*, Doctoral Thesis, University of Strathclyde, Glasgow.

Nadarajah, C., Mackenzie, D., and Boyle, J.T., (1995), Approximate limit and shakedown analysis of nozzle-cylinder intersections under internal pressure and in-plane moment loading, *Int. J. Pres. Ves. Piping*, under review.

Robinson, M., (1975), Lower bound limit pressure of a flush radial cylindrical branch in a cylindrical pressure vessel, Paper G1/6. Transaction of the 3rd International Conference on Structural Mechanics in Reactor Technology. London, September.

Robinson, M., (1977), A lower bound to the limit pressure of a flush radial cylindrical branch in a cylindrical pressure vessel, in *Developments in Stress Analysis for Pressuried Components*, Ed. R. W. Nichols, Apllied Science Publishers, London, Chap. 8.

Robinson, M., (1978), Lower-bound limit pressure for the cylinder-cylinder intersection: A parametric survey, *Journal of Pressure Vessel Technology*, Vol. 100, 65-73.

Robinson, M., and Gill, S. S., (1973), Limit analysis of flush radial and oblique cylindrical nozzles in spherical pressure vessels. Part 1: A parametric survey of results, *Int. J. of Pressure Vessel and Piping*, Vol. 1, No. 3, July, 199-231.

Rodabaugh, , E.C. and Cloud, R.L., (1968), Assessment of the plastic strength of pressure vessel nozzles, ASME Paper 68, PVP8. *Journal of Engineering for Industry.*

Rose, R.T., (1965), Stress analysis on nozzles in thin walled cylindrical pressure vessels, *British Welding J.*, **12**, No. 2.

Save, M.A., (1972), Experimental verification of plastic limit analysis of torispherical and toriconical heads, *Pressure Vessels and Piping: Design and Analysis*, Vol. 1, ASME, New York, 382–416.

Save, M.A. and Massonnet, C.E., (1972), *Plastic Analysis and Design of Plates, Shells and Disks*, North-Holland, Amsterdam.

Schroeder, J., (1971), Upper bounds to limit pressures of branch-pipe lateral connections. Part II: Bounds for branch/pipe diameter ratios larger than 0.7, ASME Paper No. 71-PVP-44.

Schroeder, J., & Rangerajan, P. (1969), Upper bounds to limit pressures of branch-pipe tee connections, *Proceedings of First International Conference on Pressure Vessel Technology*, Delft, Netherlands, Part 1, 272-292.

Schroeder, J., and Roy, B.K., (1971), Upper bounds to limit pressures of branch-pipe lateral connections. Part II: Bounds for branch/pipe diameter ratios smaller than 0.7, ASME Paper No. 71-PVP-43.

Schroeder, J., Srinivasaiah, K.R. and Graham, P., (1977), Analysis of test data on branch-pipe connections exposed to internal pressure and/or external couples, *WRC Bulletin*, No. 200, September.

Shapiro, G.S., (1961), On yield surfaces for ideally plastic shells, *Problems of Continuum Mechanica*, Philadelphia, 414.

Srinivasaiah, K.R., & Schroeder, J., (1977), Lower bounds to limit pressures of a tee-intersection od cylindrical shells based on a three-dimensional stress field, *Nuclear Engineering and Design*, Vol. 41, No. 2, Apr., 265-280.

Winkler, E.J., Lowenberg, A.L. and Pickett, A.G., (1965). Experimental investigation of plastic collapse of pressure vessel models, Southwest Research Institute, San Antonio, Tex., September 15.

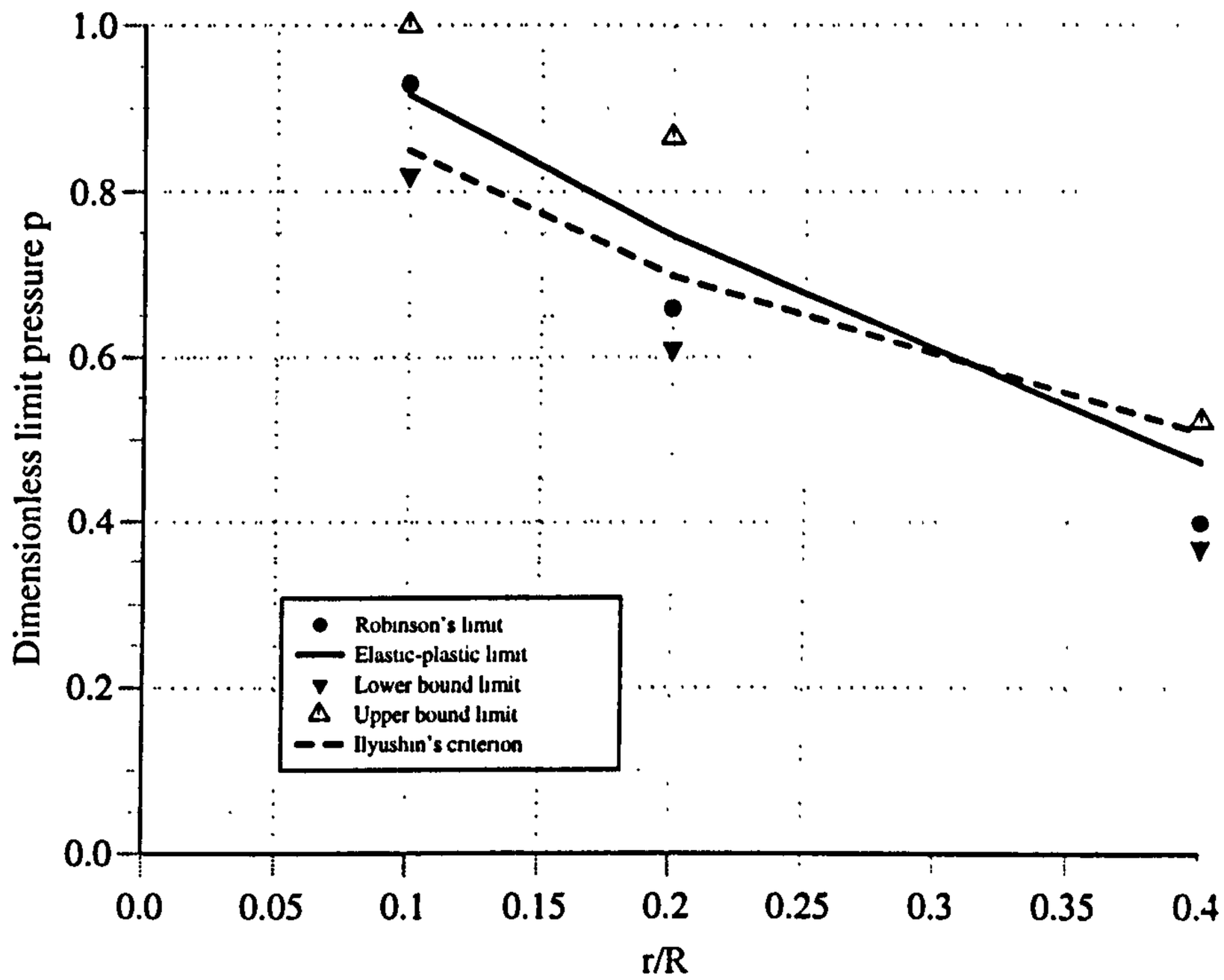

Figure 9.9: Normalised limit pressures of nozzles versus r/R, ($t/T = 1$, $R/T = 50$)

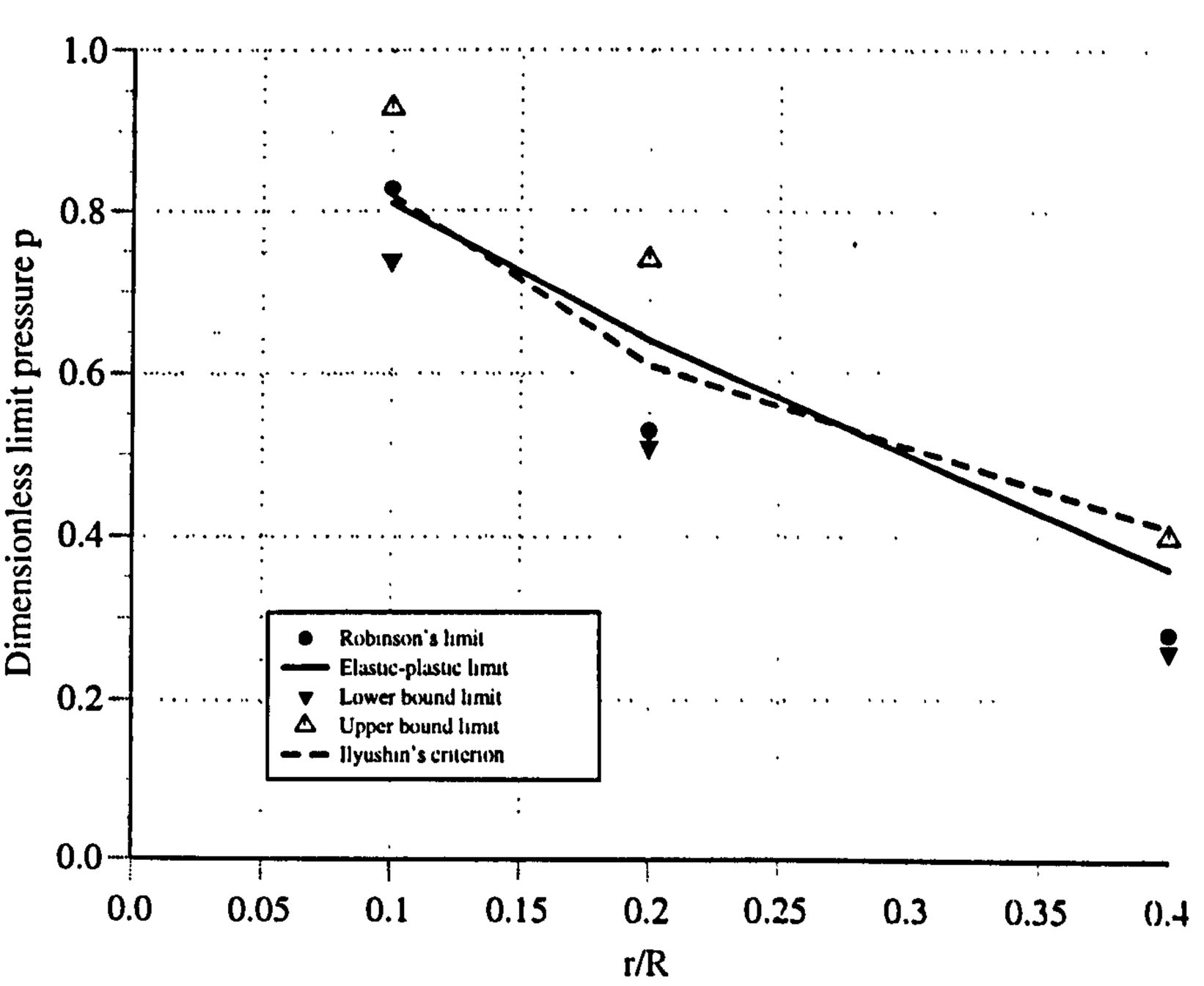

Figure 9.10: Normalised limit pressures of nozzles versus r/R, ($t/T = 0.5$, $R/T = 50$)

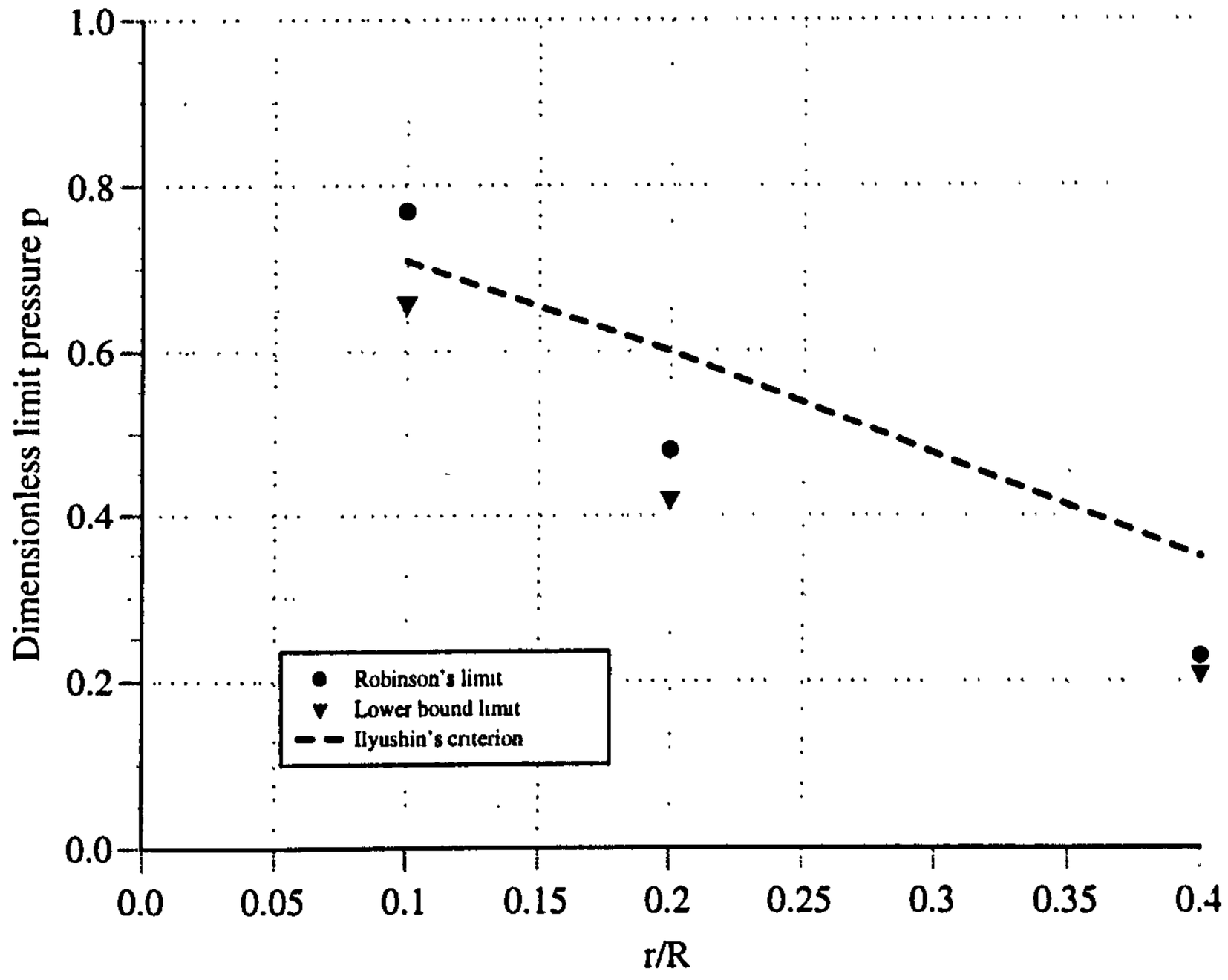

Figure 9.11: Normalised limit pressures of nozzles versus r/R. ($t/T = 0.25$, $R/T = 50$)

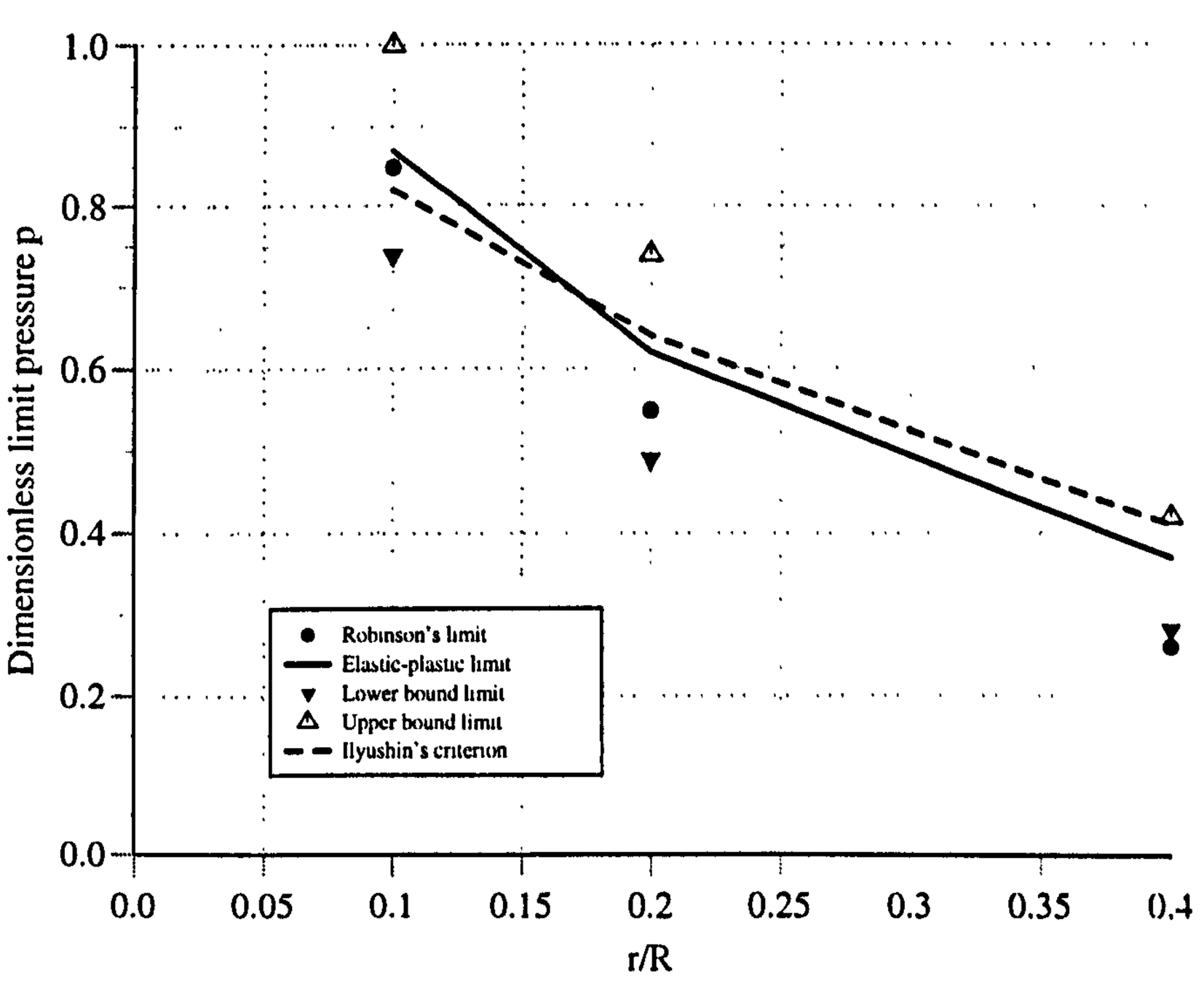

Figure 9.12: Normalised limit pressures of nozzles versus r/R. ($t/T = 1$. $R/T = 100$)

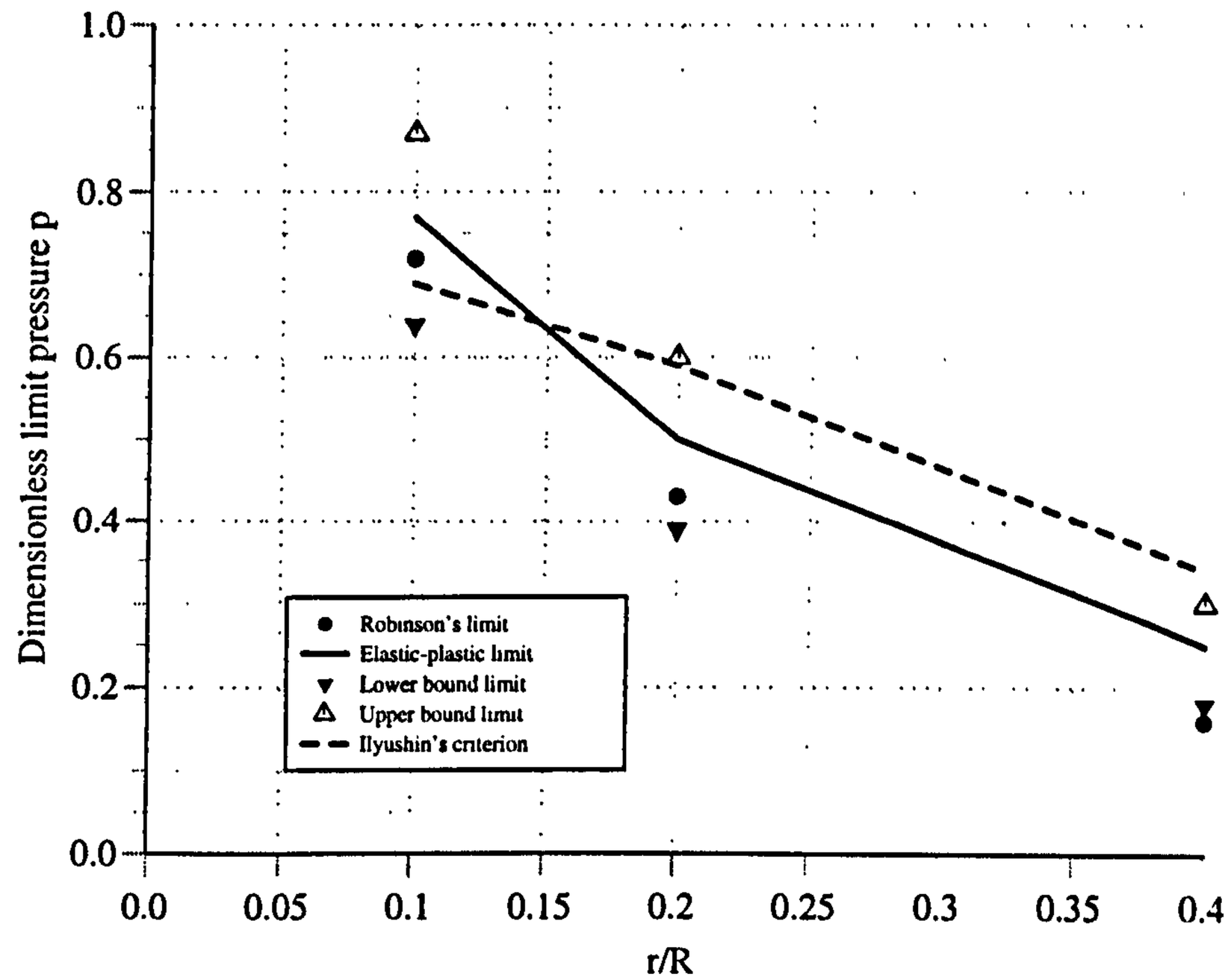

Figure 9.13: Normalised limit pressures of nozzles versus r/R, ($t/T = 0.5$, $R/T = 100$)

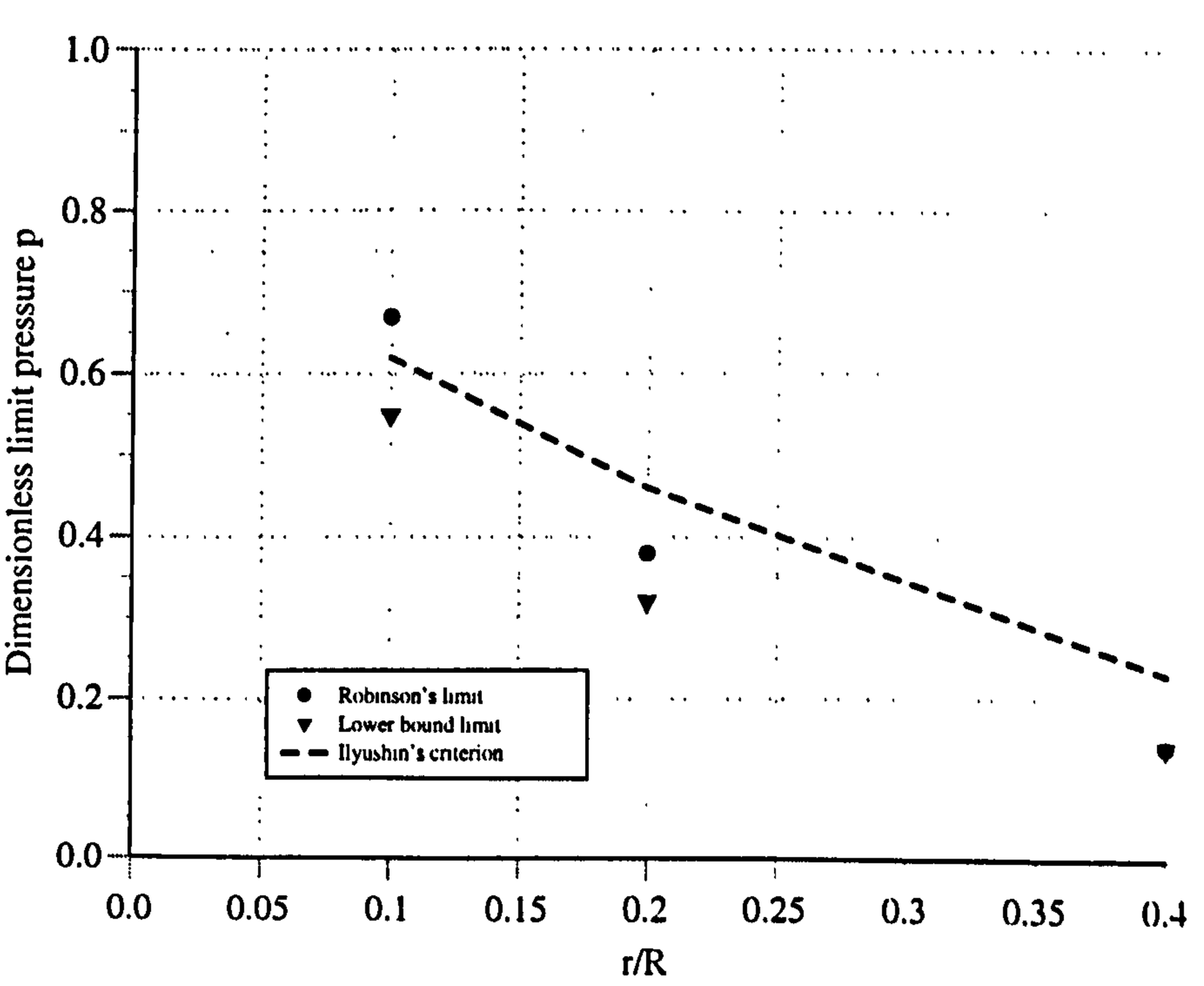

Figure 9.14: Normalised limit pressures of nozzles versus r/R, ($t/T = 0.25$, $R/T = 100$)

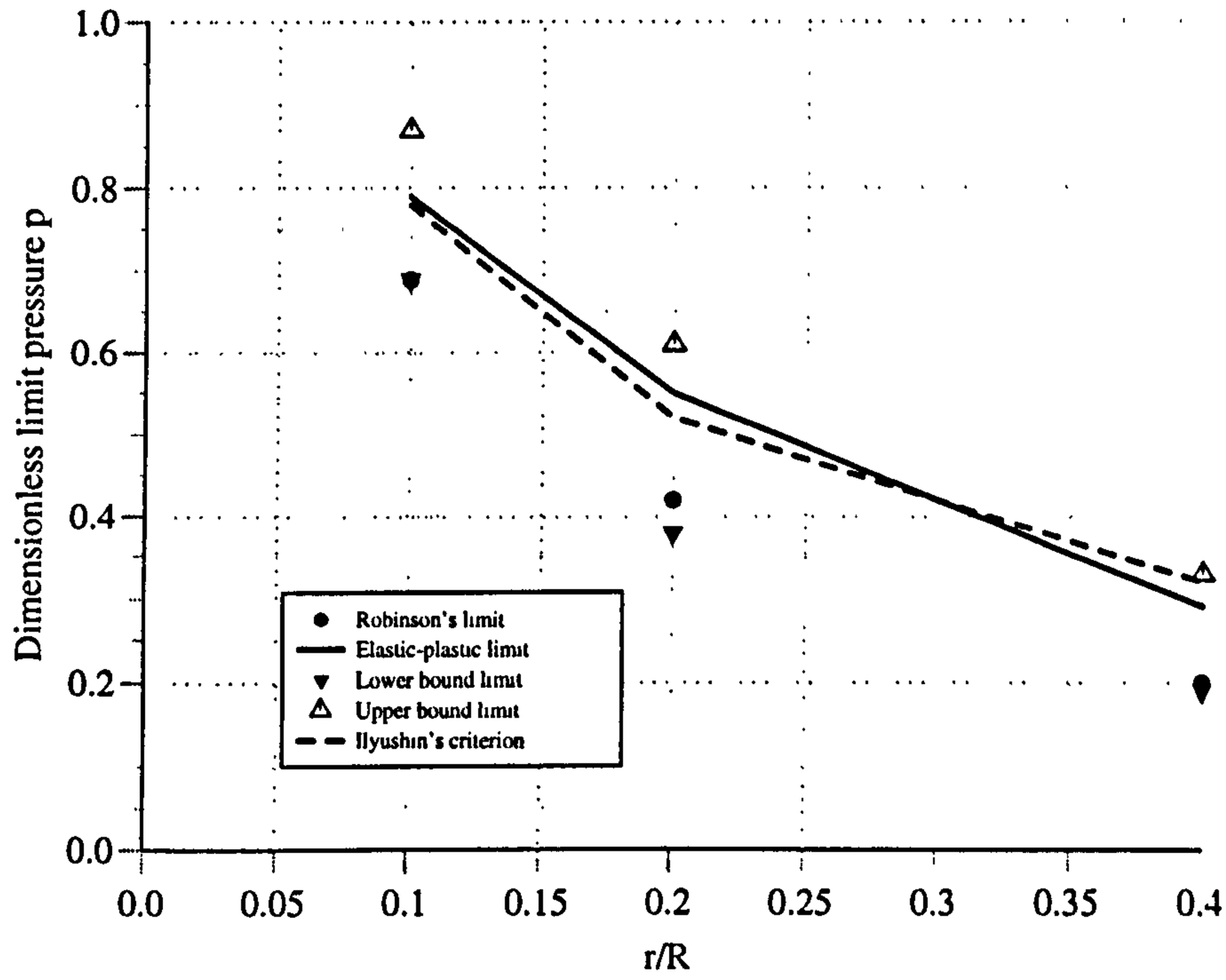

Figure 9.15: Normalised limit pressures of nozzles versus r/R, ($t/T = 1.$ $R/T = 200$)

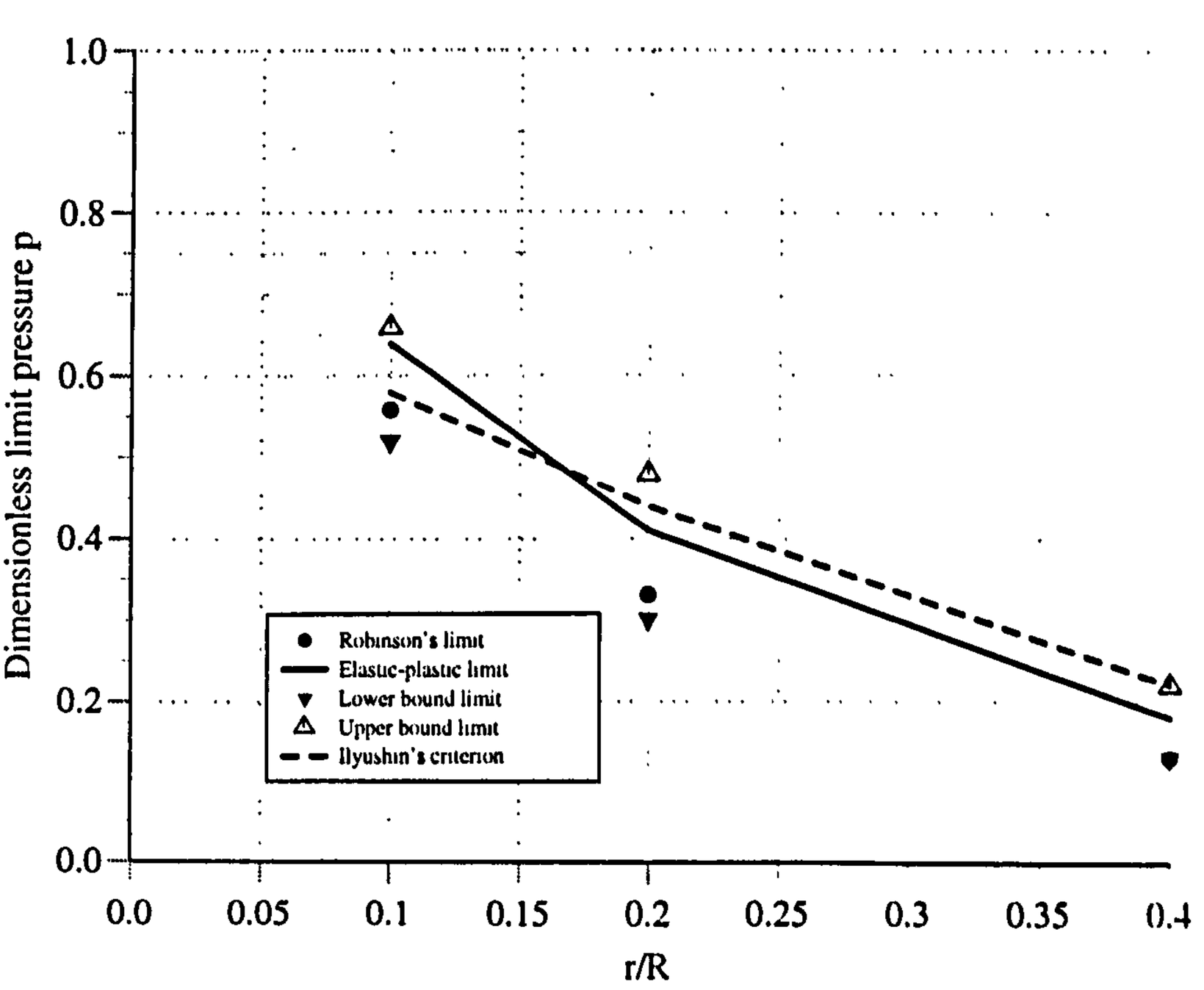

Figure 9.16: Normalised limit pressures of nozzles versus r/R. ($t/T = 0.5$. $R/T = 200$)

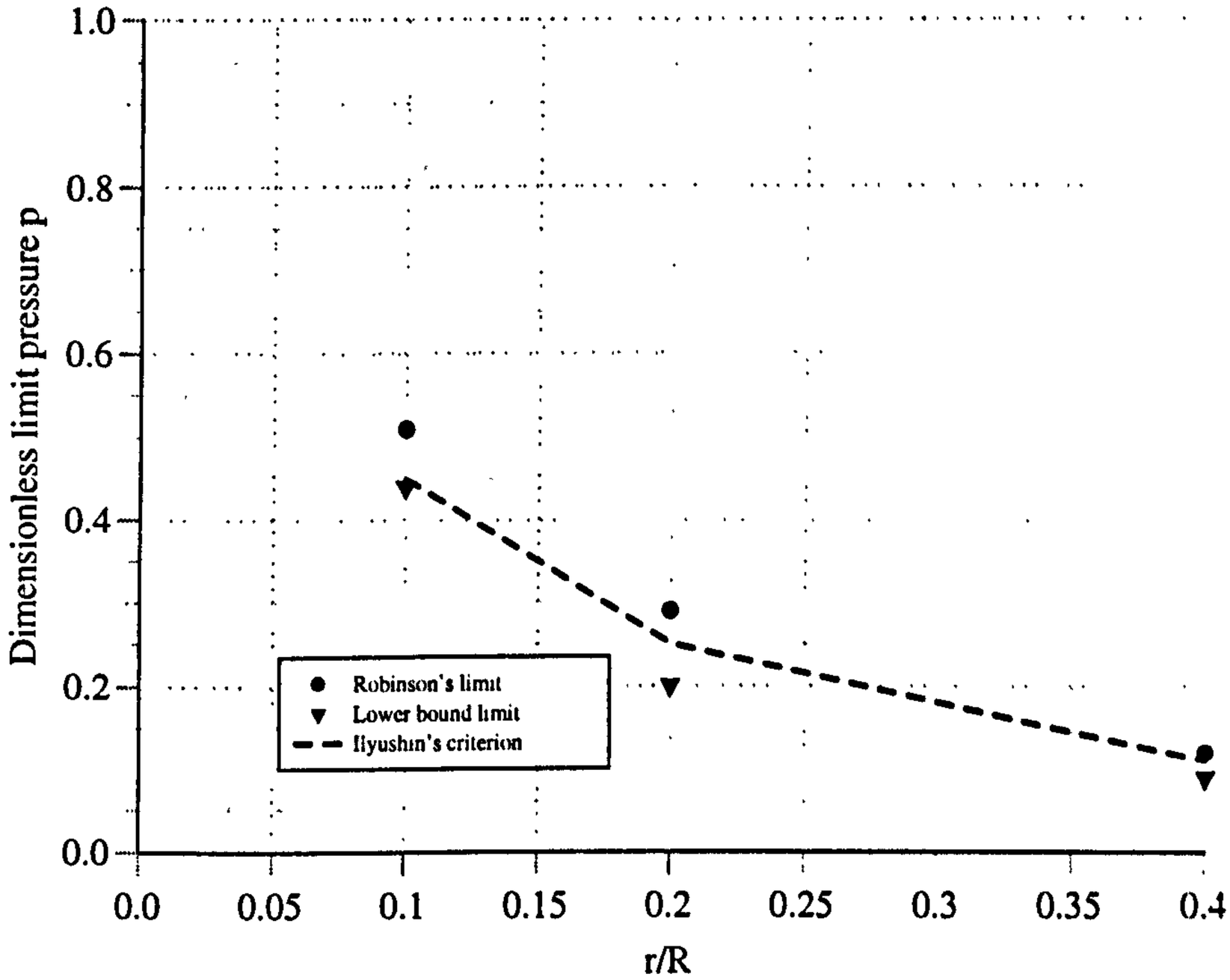

Figure 9.17: Normalised limit pressures of nozzles versus r/R. ($t/T = 0.25$, $R/T = 200$)

CHAPTER 10

CONCLUSIONS

10.1 Introduction

The development of a new, simple finite element method is presented which can greatly simplify limit and shakedown analysis of a range of complex structures. It is attractive to stress analysts and designers. This development has been achieved in this study using the novel **elastic compensation** method which has been developed by the Strathclyde Research Group and in this thesis.

The method of elastic compensation has been shown in this study to give accurate bounds on plastic limit loads for a range of complex geometries **using elastic finite element analysis only**, such as thick cylinders and nozzle/sphere intersections under internal pressure and plates with a central hole subjected to multiple loading conditions. The method has been further developed based on the use of **generalised yield surface** of structural components (beams and shells) in plasticity for limit analysis of **large** complex structures, such as thin-walled structures and frames. The extension of elastic compensation to **shakedown** has also been investigated. This new procedure has been shown to provide both lower and upper bounds to shakedown for a single load and interaction diagrams for multiple loading. The shakedown procedure has been verified on a range of structural problems. The algorithms required to carry out elastic compensation have been formalised as a set of macros in the *ANSYS* Parametric Design Language [1993]. The detailed findings from the study are summarised in the following Section.

10.2 Detailed Findings

10.2.1 Elastic Compensation Using Solid Elements

The eight noded isoparametric solid element PLANE82 in *ANSYS* was used in the elastic compensation analysis for calculating lower and upper bound limit loads and shakedown limits for a range of structures, such as pressurised cylinders, one-bay, one-story and one-bay, two story frames subjected to multiple loading in Chapter 3, plates with a central hole subjected to multiple loading conditions in Chapter 4 and nozzle/sphere intersections under internal pressure in Chapter 5. It was found that the limit load bounds obtained are generally within 10% of each other; further the bounds could be improved with increasing mesh density in the regions of the failure mechanism [Mackenzie, Shi and Boyle, 1994] and the upper bound is generally closer to the elasto-plastic solution.

10.2.2 Elastic Compensation Using Beam Elements

As one aim of this project, the elastic compensation method has been further developed based on the use of generalised yield criteria of structural components (beams and shells) in plasticity for limit analysis of large complex thin-walled structures in this study.

Both two noded beam elements BEAM3 and BEAM4 in ANSYS were used in the elastic compensation limit analysis of a number of 2-D and 3-D beam and frame structures using generalised yield criteria, respectively. The calculated lower bound limit loads obtained for a single load and interaction diagrams for multiple loading are very accurate, and the computing time is significantly reduced.

10.2.3 Elastic Compensation Using Shell Elements

The two noded axisymmetric structural shell element SHELL51 and eight noded structural shell element SHELL93 were used in the elastic compensation limit analyses of nozzles in spherical and cylindrical shells under internal pressure based on Ilyushin's and Ivanov's generalised yield criteria, respectively. It was found that the limit pressures calculated lie closer to the previous lower bound solution (solid element) for lower values of a dimensionless geometry parameter ρ: $\rho = \frac{r}{R}(\frac{R}{T})^{\frac{1}{2}}$ and closer to the upper bound for higher values, and very importantly the computing time is significantly reduced compared to the solid element for the same problem.

10.2.4 Limit Loads of Nozzles in Spherical Vessels

Limit load bounds for eighty four nozzles in spherical pressure vessels have been obtained in Chapter 5 by using eight noded isoparametric solid element PLANE82 in *ANSYS*. The results obtained have been shown to give accurate bounds on limit loads for the geometries comparing to the results from literature [Leckie and Penny, 1965], [Robinson and Gill, 1973] and new elasto-plastic analysis (with an elastic-perfectly plastic material model). It was found that the lower bound limit load is a function of a dimensionless geometry parameter ρ proposed by Leckie *et al*, but it cannot be fully characterised by this single parameter. The spread in the results for the lower and upper bound limit pressure for the various radius to thickness ratios indicates that this parameter also has an influence.

It has also been shown that efficient estimates of lower bound limit loads in axisymmetric nozzle in spherical shells, Chapter 9, and other axisymmetric shell structures, such as torispherical and conical ends and a skirted vessel [Boyle *et al*, 1995], can be obtained using approximate shell-type yield functions. While detailed elasto-plastic finite element analyses of axisymmetric shell structures can be easily derived, the approach suggested here only requires a few elastic analy-

ses and would be a more economic way of generating either the large number of results required to take in a more complete parameter survey or a quick estimate of plastic collapse loads in complex ring stiffened vessels.

10.2.5 Limit Loads of Nozzles in Cylindrical Vessels

A series of twenty seven nozzles in cylindrical shells under internal pressure have also been carried out in Chapter 9. The obtained results were compared with the lower and upper bound limit pressures and detailed elasto-plastic analysis previously obtained by Nadarajah *et al.* [1995], and also compared to Robinson's [1978] lower bound limit pressure, which was derived using Ilyushin's generalised yield criteria and a nonlinear programming technique. It was shown that the obtained results were generally higher than the results obtained from Robinson [1978] and Nadarajah *et al.* [1995]. More significantly, the new lower bound estimate is very close to the elasto-plastic shell analysis. Since the new method is based on thin shell analysis considerable benefits over full three dimensional analysis are feasible and the technique has much potential for future application.

10.2.6 Shakedown Loads of Nozzles in Spherical Vessels

The extension of elastic compensation to **shakedown** has been verified for both lower and upper bounds to shakedown loads for the nozzle/sphere geometry under internal pressure.

The lower and upper bound shakedown limits for eighty four nozzles in spherical pressure vessels have been carried out in Chapter 6. The results show that the elastic compensation lower bound shakedown pressures are less than ASME B&PV Code $3S_m$ limit for all the nozzle configuration considered. The shakedown curves are similar in form to the $3S_m$ curves but the calculated lower bound shakedown pressure values are generally closer to the Leckie and Penny [1967] results.

As Leckie and Penny only considered variation of shakedown load with the geometry parameter ρ, their results are constant for all the radius to thickness ratios considered. However, both the elastic compensation pressures and secondary stress limit $3S_m$ vary with the radius to thickness ratio. The results also show that the Leckie and Penny's lower bound shakedown pressure is lower than the secondary stress limit pressure $3S_m$ except for radius to thickness ratios $R/T = 7.14,\ 6.25,\ \rho = 0.3$. The detailed discussion can be found in Chapter 6.

The results also show that the elastic compensation upper bound solutions are 20 to 25 per cent higher than the results of Leckie and Penny [1967] with similar patterns for all models. Comparing with $3S_m$ allowable pressures. it can be seen that for values of ρ greater than 0.7 the upper bound solutions are lower than $3S_m$, for ρ smaller than 0.7 the upper bound shakedown pressures are higher than $3S_m$. The greatest differences between obtained upper bound solutions and $3S_m$ allowable pressures lie in the regions of small diameter nozzles (where the use of the parameter ρ is questionable).

It can be concluded for nozzles in spherical pressure vessels that the shakedown pressures vary not only with the geometry parameter ρ used to characterize nozzles by Leckie and Penny, but also with the radius to thickness ratio of the sphere. This additional parameter should be considered when deriving design curves for shakedown loads. The obtained results also suggest that the Leckie and Penny curves may not be conservative for all radius to thickness ratios.

The elastic compensation shakedown pressures for the R/T ratios of 10. 8.33. 7.14 and 6.25 are significantly greater than the Leckie and Penny values for most of the geometry range considered, suggesting that design to the BS 5500 Code [1994] could be over-conservative if the Leckie and Penny curves are used. However, BS 5500 simply requires that 'a shakedown analysis (e.g. See **G.2.6**) should preferably be employed' thus design based on the elastic compensation method

would be acceptable.

The upper bound shakedown results would suggest that the 3.5_m limits are not conservative, especially for the R/T ratios of 10, 8.33, 7.14 and 6.25 the 3.5_m limits are much higher than the upper bound pressures for the values of ρ greater than 0.8. In the writer's experience the upper bound is usually more reliable since the lower bound is quite strict.

10.2.7 Limit and Shakedown Loads of Frames Under Multiple Loading

Limit and shakedown analyses of a number of 2-D and 3-D beam and frame structures using generalised yield criteria have been carried out in Chapter 8. The calculated lower bound limit loads obtained for a single load and interaction diagrams for multiple loading are accurate as compared to known solutions in the literature. It is seen from this study that the limit loads and shakedown limits obtained are good agreement with the theoretical results. The elastic compensation method can therefore be used to estimate the limit and shakedown loads of complex structures for design purposes without resource to complex inelastic analysis.

10.2.8 Application of Design by Analysis

The ability to estimate plastic collapse mechanisms, through limit and shakedown analysis, of complex shell and frame structures has significant potential outwith the mechanical engineering field to the design of large **civil and building structures.** The techniques developed here offer considerable advantages over existing methods since conventional elastic finite element analysis can be used.

In the **pressure vessel industry** there is still considerable interest in the research of Strathclyde Group. The elastic compensation method has been rec-

ommended in the recent ASME **White Paper** [Pastor et al, 1994] on pressure vessel design by analysis. The White Paper arose from requests from the US pressure vessel industry to address well known deficiencies in design by analysis based on elastic analysis. The recommendations of an ASME/PVP/PVRC Committee, set up to investigate these requests, concluded that the future lay in inelastic analysis and estimation of plastic failure mechanisms and highlighted the advantages of elastic compensation.

10.3 Recommendations for Further Work

Finally, in concluding the entire study and its findings, the suggestions are recommended for further work:

Since the elastic compensation based on the generalised yield criteria is a newly developed technique, the effectiveness of the method for different meshes especially for three dimensional models should be examined. A parametric study on the limit loads for nozzles in cylindrical shells under in-plane moment of the nozzle should also examined. The results obtained from this method can then be compared with that of available in literature to check the accuracy.

So far the elastic compensation method has been used to obtain lower and upper bound limit loads and shakedown limits of structures without any cracks. it is possible that the method can be used to obtain limit loads of **cracked structures** and **composite structures.**

Further, it is possible that the elastic compensation method can be extented to estimated **stability in brittle-plastic structures** (such as concrete or rock). And it is also possible that the method can be used in structural **shape optimisation.** At present some of these work are being carried out in the Strathclyde Research Group.

10.4 References

American Society of Mechanical Engineers, (1995), *ASME Boiler and Pressure Vessel Code.*

Boyle, J.T., Hamilton, R., Shi, J. and Mackenzie, D., (1996), A simple method of calculating limit loads for axisymmetric thin shells, *Trans ASME. J. Pressure Vessel Technology*, under review.

British Standards Institute, (1994), *BS 5500: Specification for unfired Fusion Welded Pressure Vessels*, London.

Leckie, F.A. and Payne, D.J., (1965-1966), Some observations on the design of spherical pressure vessels with flush cylindrical nozzles, *Proc. Inst. Mech. Engineers*, Vol. 180, Part I, No. 20, 497–501.

Leckie, F.A., and Penny, R.K., (1967), Shakedown loads for radial nozzles in spherical pressure vessels, *Int. J. Solids and Structures*, **3**, 743–751.

Mackenzie, D., Shi, J. and Boyle, J. T., (1994), Finite element modeling for limit analysis by the elastic compensation method.*Computer & Structures*. Vol. 51, No. 4, 403–410.

Nadarajah, C., Mackenzie, D., and Boyle, J.T., (1995), Approximate limit and shakedown analysis of nozzle-cylinder intersections under internal pressure and in-plane moment loading, *Int. J. Pres. Ves. Piping*, under review.

Robinson, M., (1978), Lower-bound limit pressure for the cylinder-cylinder intersection: A parametric survey, *Journal of Pressure Vessel Technology*. Vol. 100, 65-73.

Robinson, M., and Gill, S. S., (1973), Limit analysis of flush radial and oblique cylindrical nozzles in spherical pressure vessels. Part 1: A parametric survey of results, *Int. J. of Pressure Vessel and Piping*, Vol. 1, No. 3, July, 199-231.

Pastor, T.P., et al, (1994), White paper on ASME Code Primary Limits in "Stress Classification for ASME B & PV Code Primary Stress Limits" Vol DA-06A, ASME Press Vess and Piping Conf, Minneapolis, 1994.

Swanson Analysis System, (1993), ANSYS User Manuals Vol. I-IV.

APPENDIX I

PUBLISHED PAPERS

1. **Shi, J.**, Mackenzie, D., and Boyle, J.T., (1993), A method of estimating limit loads by iterative elastic analysis. III–Torispherical heads under internal pressure. *Int. J. Pres. Ves. & Piping*, Vol. 53, No.1, 121– 142.

2. Mackenzie, D., **Shi, J.**, Nadarajah, C., and Boyle, J.T., (1992). An iterative elastic analysis procedure for estimating lower bound limit loads, *ASME PVP-Vol. 230*, 129–134.

3. Mackenzie, D., Nadarajah, C., **Shi, J.**, and Boyle, J.T., (1993). Simple bounds on limit loads by elastic finite element analysis, *J. Pres. Ves. Technology*. Vol.115. 27–31.

4. Mackenzie, D., **Shi, J.** and Boyle, J. T., (1994), Finite element modeling for limit analysis by the elastic compensation method, *Computer & Structures*. Vol. 51. No. 4, 403–410.

5. Hamilton, R. , **Shi, J.** , Mackenzie, D., and Boyle, J.T., (1994). Approximate limit analysis of pressurized axisymmetric nozzles: A parameter study. *ASME PVP-Vol. 277*, 121–126.

6. Mackenzie, D., Hamilton, R., Boyle, J.T. and **Shi, J.**, (1995). Secondary stress and shakedown in axisymmetric nozzles, *ASME PVP-Vol. 313-1*. 409–413.

Int. J. Pres. Ves. & Piping 53 (1993) 121–142

A Method of Estimating Limit Loads by Iterative Elastic Analysis. III—Torispherical Heads Under Internal Pressure

Jinhua Shi,* D. Mackenzie & J. T. Boyle

Department of Mechanical Engineering, University of Strathclyde, Glasgow, Scotland, UK, G1 1XJ

(Received 24 December 1991; accepted 5 January 1992)

ABSTRACT

A simple method of estimating limit loads using a sequence of elastic finite element analyses and the lower bound theorem, termed elastic compensation, is demonstrated on the problem of the estimation of the limit behaviour of torispherical pressure vessel heads. Two possible techniques of elastic compensation are discussed, one which has general application and one possibly specific to heads. The results are compared to a series of detailed elastic-plastic finite element analyses and to classical solutions.

1 INTRODUCTION

In order to overcome problems with stress categorisation in design by analysis, and to allow the use of design based on limit analysis, the authors[1] have proposed a simple technique, based on repeated finite element analysis with successive modifications to the elastic modulus, which can be used to develop suitable stress fields for the lower bound theorem. This technique—which is referred to here as elastic compensation—has been shown to give accurate results for simple problems, and for selected generic pressure vessel problems.[2] This procedure is not new, but now has been shown to provide a systematic

* Visiting Scholar, Hebei Electric Power Survey & Design Institute, Shijiazhuang, Hebei, People's Republic of China.

Int. J. Pres. Ves. & Piping 0308–0161/92/$05·00

procedure which can be used to estimate limit loads reliably using routine elastic analysis.

The aim of the present paper is to demonstrate the applicability of the method of elastic compensation for the classic problem of a pressurised torispherical head. Two different interpretations of the procedure—one quite general to any pressure vessel component, the other verified here for heads—are discussed. The results are compared with detailed elastic plastic analysis and with existing solutions.

2 PLASTIC BEHAVIOUR OF TORISPHERICAL HEADS

The literature on the structural behaviour of torispherical heads is well established. Three early papers on plastic collapse mechanisms were published by Drucker and Shield[3–5] in the late 1950s. In these papers, a limit analysis of torispherical and toriconical heads as shells of revolution using a simplified yield surface for a Tresca material was developed. This led to a simple approximate formula for the limit pressure:

$$P_D = \left(0{\cdot}33 + 5{\cdot}5\frac{r}{D}\right)\frac{t}{L} + 28\left(1 - 2{\cdot}2\frac{r}{D}\right)\left(\frac{t}{L}\right)^2 - 0{\cdot}0006 \qquad (1)$$

where the dimensions for a torispherical end are given in Fig. 1. This formula, for thin heads, is implicit in most pressure vessel design rules usually combined with the 'Formdehngrenze' method[6] for thicker heads.

Many studies followed the pioneering work of Drucker and Shield: for example, Biron and Charleux[7] and Taylor and Robinson,[8] using

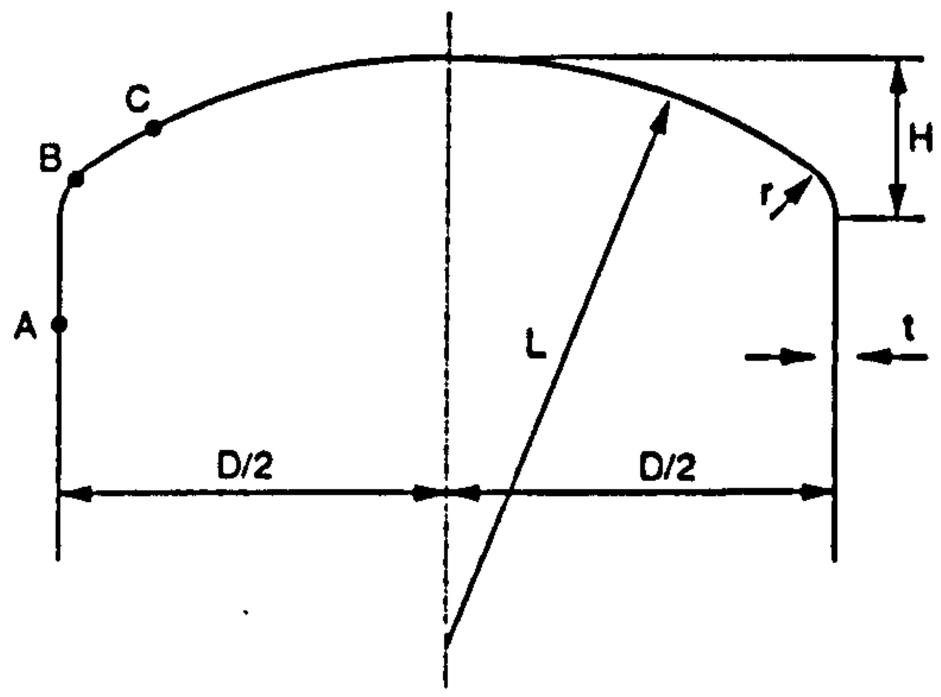

Fig. 1. Torispherical head geometry.

various thin shell yield criteria, developed more detailed limit analyses while Crisp[9] and Simonen and Hunter[10] used elasto-plastic analysis, this latter paper also took into account the effect of change of geometry on the behaviour of ellipsoidal and torispherical heads. Calladine[11] presented a novel and interesting analysis of the limit pressure of torispherical ends leading to a further simple formula which gave results similar to Shield and Drucker. Experimental work in the plastic deformation of torispherical heads has been reported by Save,[12] Findlay *et al.*[13] and Kirk and Gill[14] among others. A summary has been given by Gerdeen.[15]

The general pattern of behaviour of torispherical ends under internal pressure is thus well understood. As pressure builds up, it tends to force the spherical cap outwards along the axis and the meridional membrane tensions pull the toroidal knuckle inwards towards the axis.

For thin walled heads, if the torus wall is thick enough to avoid buckling but thin compared with the radius of the knuckle, and the material does not work-harden, a plastic hinge circle will form at B, Fig. 1, to permit the central region of the knuckle to compress in the circumferential direction and bend inwards. A hinge circle will form at C in the spherical cap and the third hinge circle A usually forms in the cylinder. The entire knuckle region between A and C is plastic since inward motion of appreciable extent coincides with plastic contraction of the circumference. The deformation pattern is shown in Fig. 2.

For thicker vessels, the first hinge circle may form in the cylinder or in the spherical region. This can be seen in the following.

In order to determine the elasto-plastic behaviour and limit pressure in representative torispherical heads, four geometries are employed,

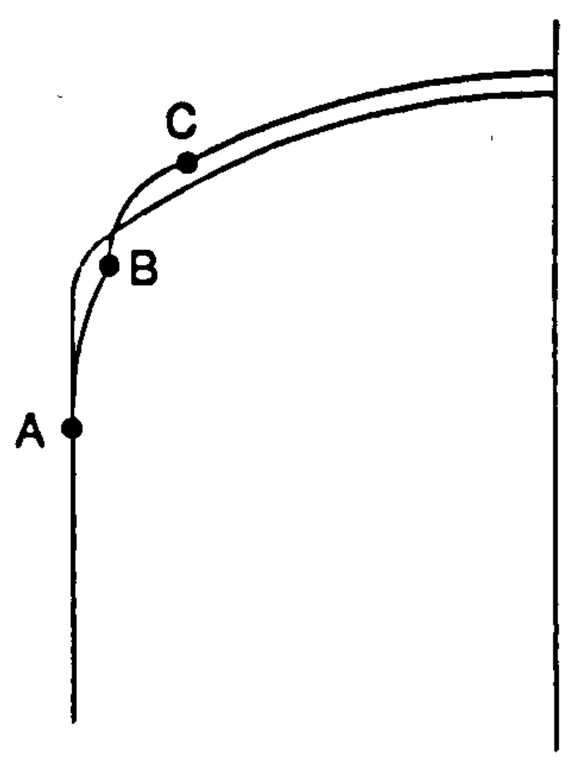

Fig. 2. Torispherical head deformation mechanism.

TABLE 1
Head Shape Parameters and Dimensions

Head No.	*t/D*	*h/D*	*r/D*	*R/D*	*D (in)*	*t (in)*
31	0·015	0·151	0·092	1·541	37·00	0·555
32	0·015	0·207	0·070	0·813	37·00	0·555
4	0·050	0·250	0·125	0·750	37·00	1·85
26	0·050	0·207	0·125	1·021	37·00	1·85

taken from Townley *et al.*;[16,17] Table 1 gives the detailed dimensions of the models. The models are analysed independently here using the finite element analysis system ANSYS. The elasto-plastic analysis undertaken here includes large deformation effects. The post yield behaviour is based on a Von Mises criterion, and a perfectly-plastic material is assumed initially. The material properties are taken from Townley *et al.* as: Young's modulus 29E06 psi, Poisson's ratio 0·29, and yield stress 30 300 psi.

Although the collapse mechanism is known, the sequence of hinge formation with increasing pressure depends on the geometry. For Head No. 31, the three hinge mechanisms form almost simultaneously at a pressure of about 410 psi; further slight increases in pressure bring the head close to collapse. In the case of Head No. 32, the first hinge forms in the knuckle region at a pressure of 520 psi, followed by the second hinge in the spherical cap at a pressure of 600 psi, and finally at a pressure of 636 psi, the third hinge forms in the cylinder—the pressure can be increased further to about 685 psi before the head is close to collapse as the hinge circles spread. In Head No. 4, the first hinge mechanism forms in the cylinder at a pressure of 3050 psi, the second in the spherical cap at 3275 psi and the third in the knuckle at 3425 psi which is close to collapse. For Head No. 26 the first hinge forms in the spherical cap at 2600 psi, the second in the knuckle at 2750 psi and the third in the cylinder at 2860 psi again close to collapse.

Representative plots of these detailed elasto-plastic analyses are given in Figs 3–6 showing pressure versus equivalent strain at the most highly stressed point. From this a simple criterion for plastic collapse has been proposed by Townley, who defined the excessive deformation pressure as that required to produce an equivalent plastic strain of 1%. In the case of torispherical heads, this definition leads to a slightly lower value of pressure for plastic collapse, but the differences are not of practical significance. It should be noted that this definition corresponds closely to the pressure values when three hinge circles form

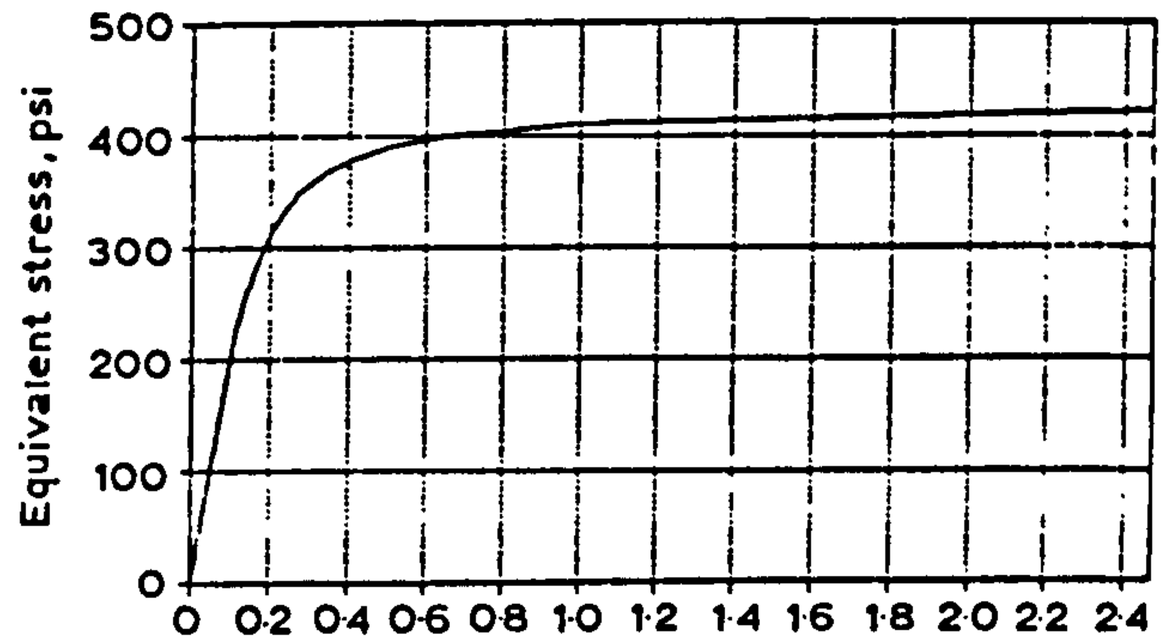

Fig. 3. Elasto-plastic analysis of Head 31.

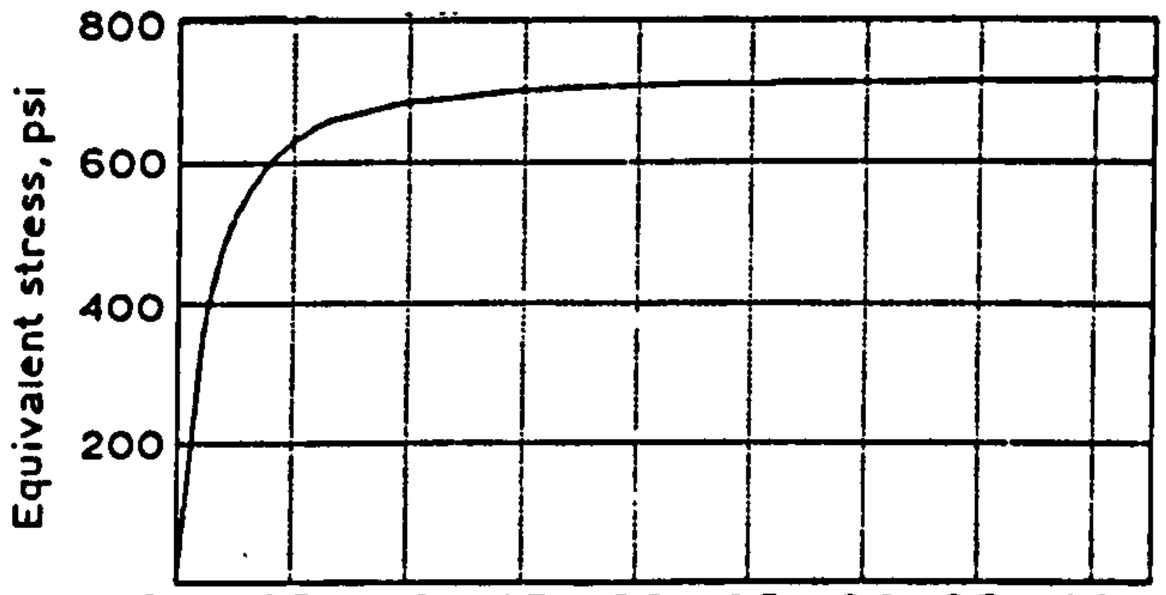

Fig. 4. Elasto-plastic analysis of Head 32.

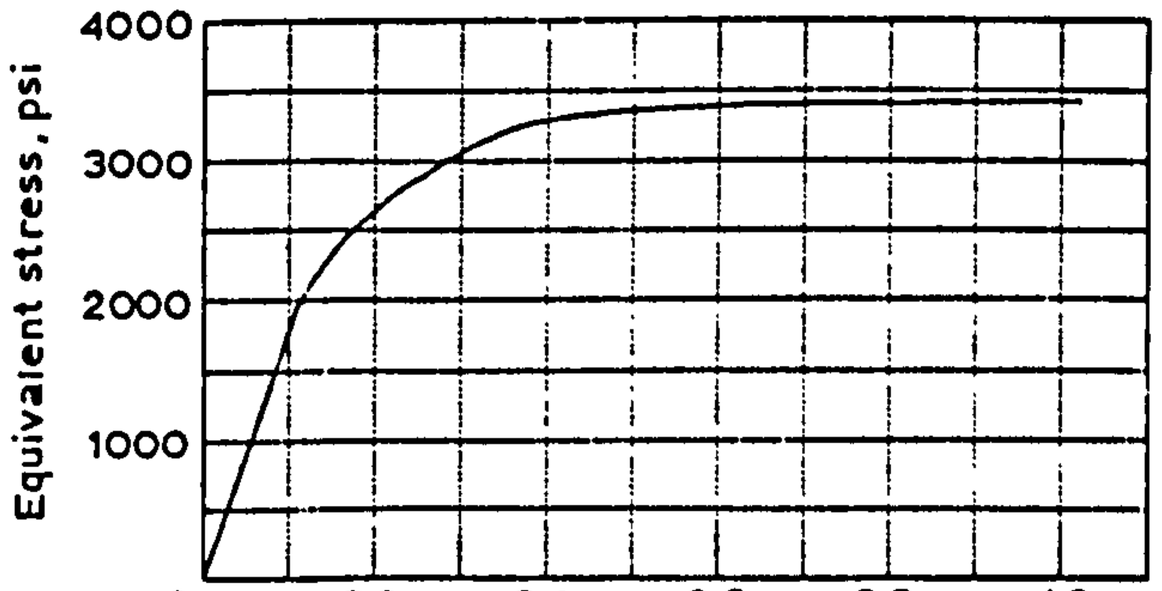

Fig. 5. Elasto-plastic analysis of Head 4.

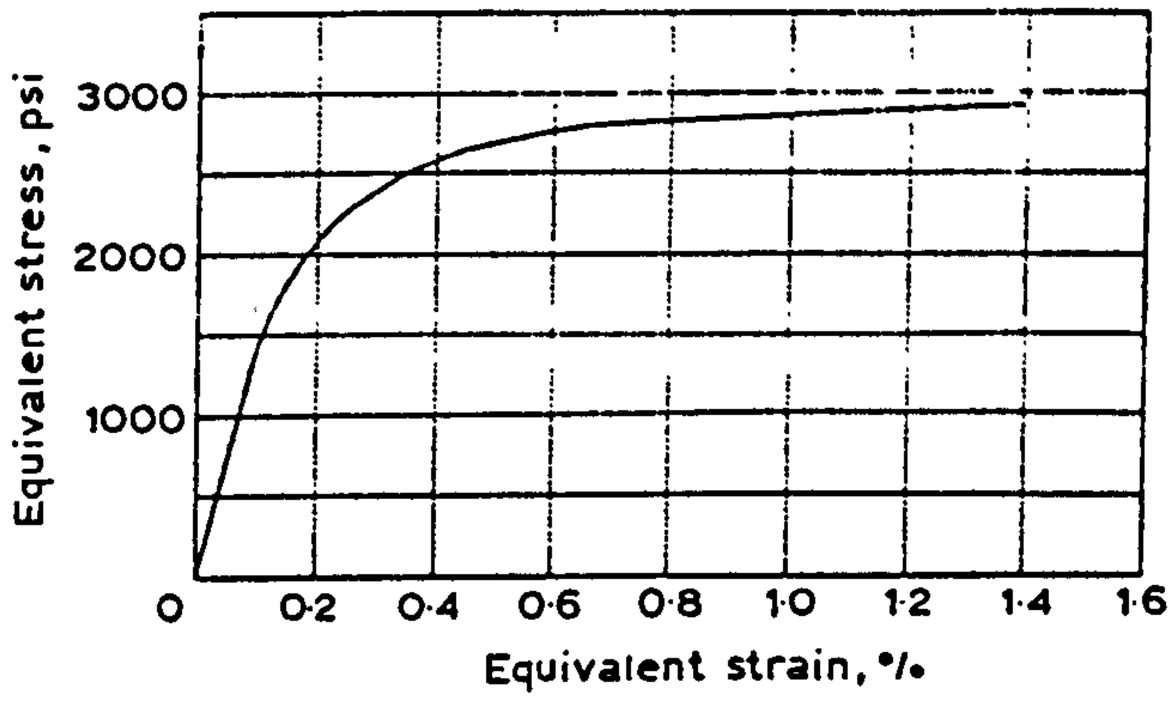

Fig. 6. Elasto-plastic analysis of Head 26.

in the present analyses which could be taken as the definition of the onset of collapse.

3 ESTIMATION OF LIMIT LOADS BY ELASTIC COMPENSATION

These analyses can be taken as the basis for a demonstration of the elastic compensation procedure. Here the general method described by the authors[1] will be examined first, followed by a modification which gives improved results for the present problem.

3.1 A simple lower bound

The basis of this method of estimating limit loads by elastic finite element analysis is the lower bound theorem. The aim is to generate the best admissible stress field, corresponding to the highest load such that derived stresses are in equilibrium and do not violate the yield condition. For a given load, the admissible stress field is derived by a sequence of elastic calculations where the elastic moduli of selected regions are modified to bring local stresses below yield—this is referred to as elastic compensation. The problem is then to determine the best load value, that is the highest which can be used, with as few as possible load steps.

The simplest method is to set an arbitrary load level (perhaps the design load P_D so that the initial elastic analysis can be used in a conventional design by analysis) and to carry through the sequence of elastic calculations such that the elastic modulus in each element is

modified according to

$$E_i = E_{i-1}\frac{\sigma_n}{\sigma_{i-1}} \tag{2}$$

for the ith iteration, where σ_{i-1} is the maximum unaveraged nodal equivalent in the element from the previous finite element solution. The value of σ_n is somewhat arbitrary, since the solution will later be scaled, but is usually taken as half or two-thirds yield. This is not critical. After several iterations the maximum stress in the model generally exhibits a net decrease until a near limit value, σ_R, after the Rth iteration is reached. This provides an admissible stress field for the given load. Since the solution is linear elastic the best lower bound estimate of the limit load, P_L, can be found through proportionality

$$P_L = P_D\frac{\sigma_y}{\sigma_R}$$

which corresponds to the highest load such that the final compensated stress in the elastic reduction procedure, σ_R, just reaches yield. This procedure can of course be extended to combined loading in several ways.

This procedure can be carried out automatically, with no user intervention. The results—referred to as Method 1—are shown in Table 4 (below) compared to the results of the detailed elasto-plastic analyses with the criterion of a 1% equivalent strain limit. These are discussed later.

3.2 An improved procedure

The above basic procedure can be modified in a number of ways to give improved results. These improvements usually require more analyses. One possibility, discussed in the context of flush nozzles, is in a companion paper.[2] A further variation is given here in which an improved result can be obtained by a single sequence of analyses for a given load level and a simple formula.

The basis for this modification is the general elastic reduced modulus procedure[1,2] used by several authors. In this a load level above that for the first yield is set and the elastic moduli of only those elements above yield are reduced according to the rule $E(\sigma_y/\sigma_e)$ where σ_e is the calculated (von Mises) effective stress for each of the selected elements. This procedure is repeated until the compensated elastically calculated stress is below yield. This final stress field could be used as an admissible stress, with the given load level a lower bound on the limit

load. The load is increased and the reduction procedure repeated. Eventually further load increases will not allow compensated stresses to be brought below yield and thus the best lower bound can be determined. This of course requires several analyses at each load level, as mentioned previously, but does give results very close to the limit load found from detailed elasto-plastic analysis.

However this can be considerably simplified if it is observed that the reduced modulus procedure, at loads close to the limit load, gives similar predictions of the strain level, specifically near collapse at about 1% strain. This is shown for Head No. 32 in Fig. 7. Based on this observation and an examination of a range of analysis results the following simplified procedure, which only requires analysis at one load level, has been devised. This is presented here as an alternative interpretation of the elastic compensation results:

- Perform an elastic analysis with the load condition P about 50–80% above that for first yield, P_y.
- Perform the reduced modulus analyses as described before.
- Finally estimate the limit pressure using the following approximate relation for the most highly stressed element:

$$\frac{P_L}{P} = (\varepsilon_L/\varepsilon_r)^{1/2 \cdot 4F} \tag{3}$$

where P_L is the limit pressure, ε_L is the equivalent limit strain and ε_r is the elastic strain from the reduced modulus procedure with

$$F = \frac{E\varepsilon_r}{\sigma_y} \tag{4}$$

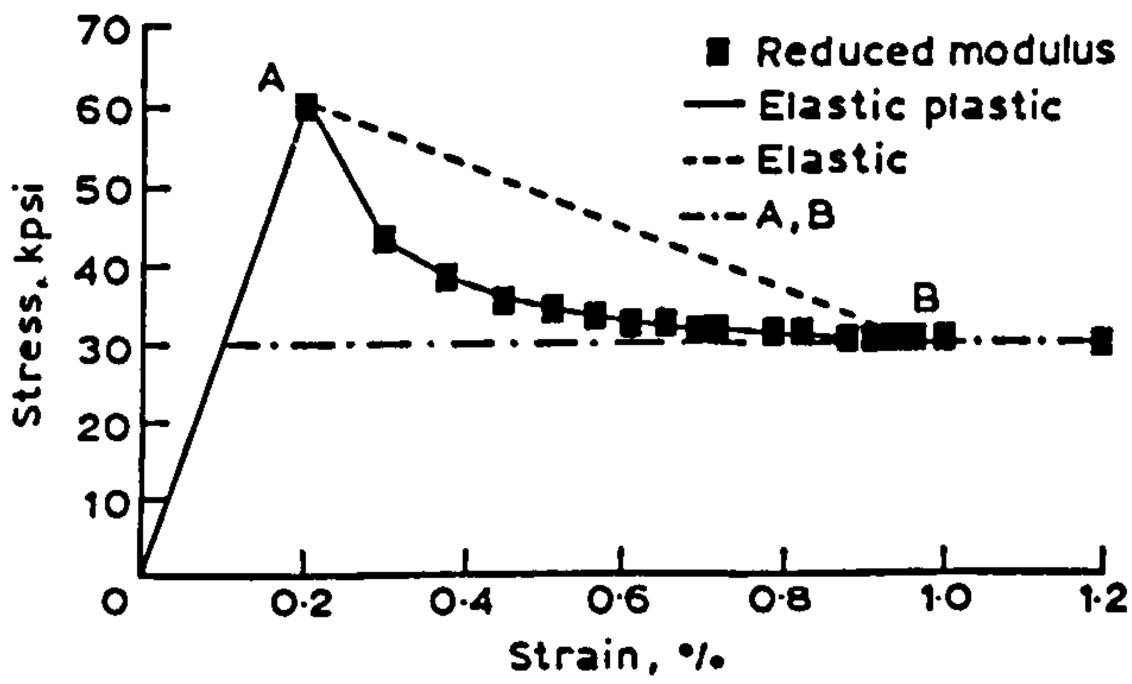

Fig. 7. Results for elasto-plastic, elastic and elastic compensation analyses for Head 32.

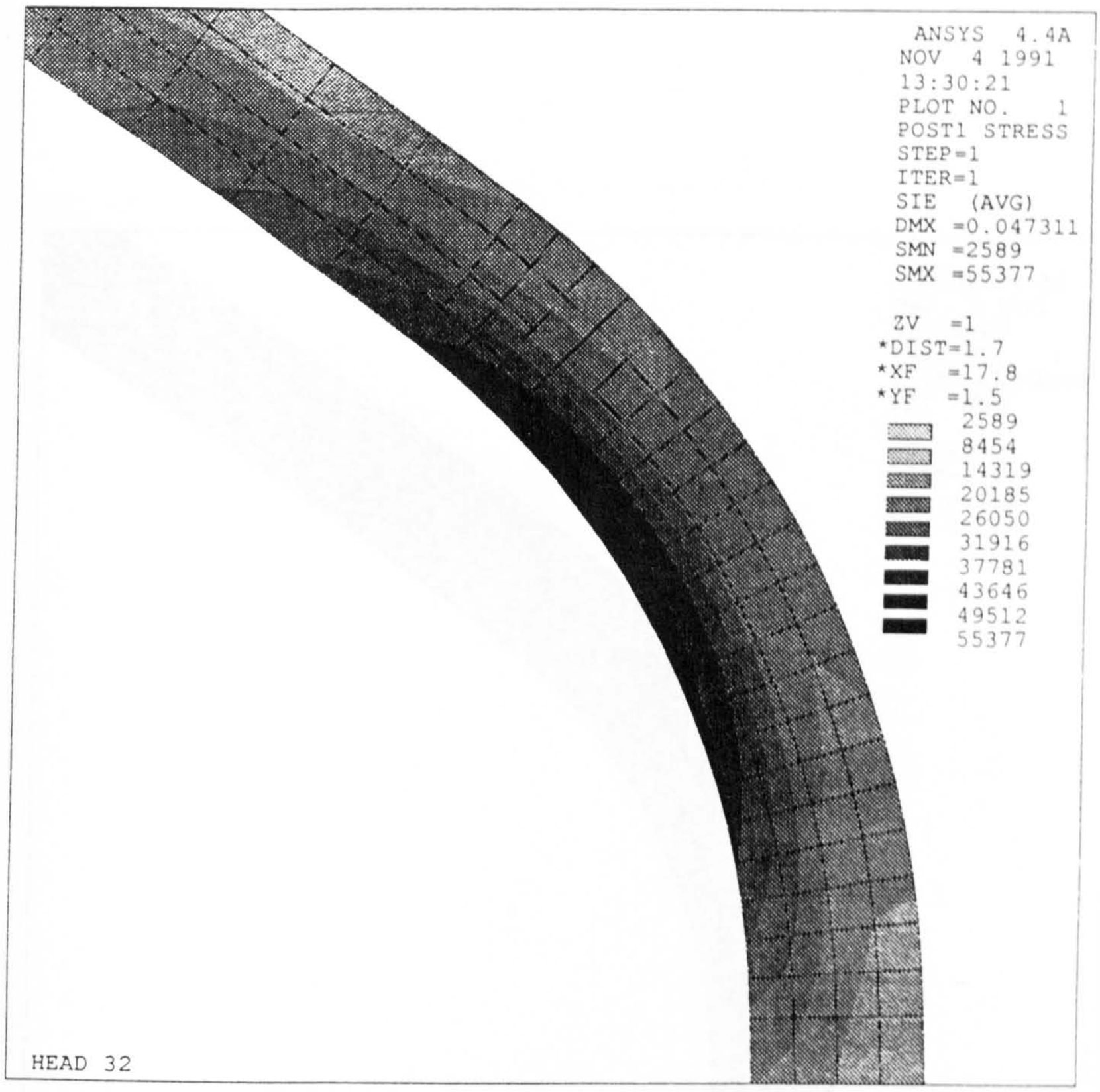

Fig. 8. Equivalent stress contour plot from initial elastic analysis of Head 32.

TABLE 2
Head 32 Modulus Reduction

Iteration No.	σ_{max} (*psi*)	E_r (*psi*)
—	55 377	290 000 00
1	40 969	158 675 30
3	34 568	970 726 9
5	32 459	773 828 6
7	31 419	686 882 1
9	30 902	645 025 9

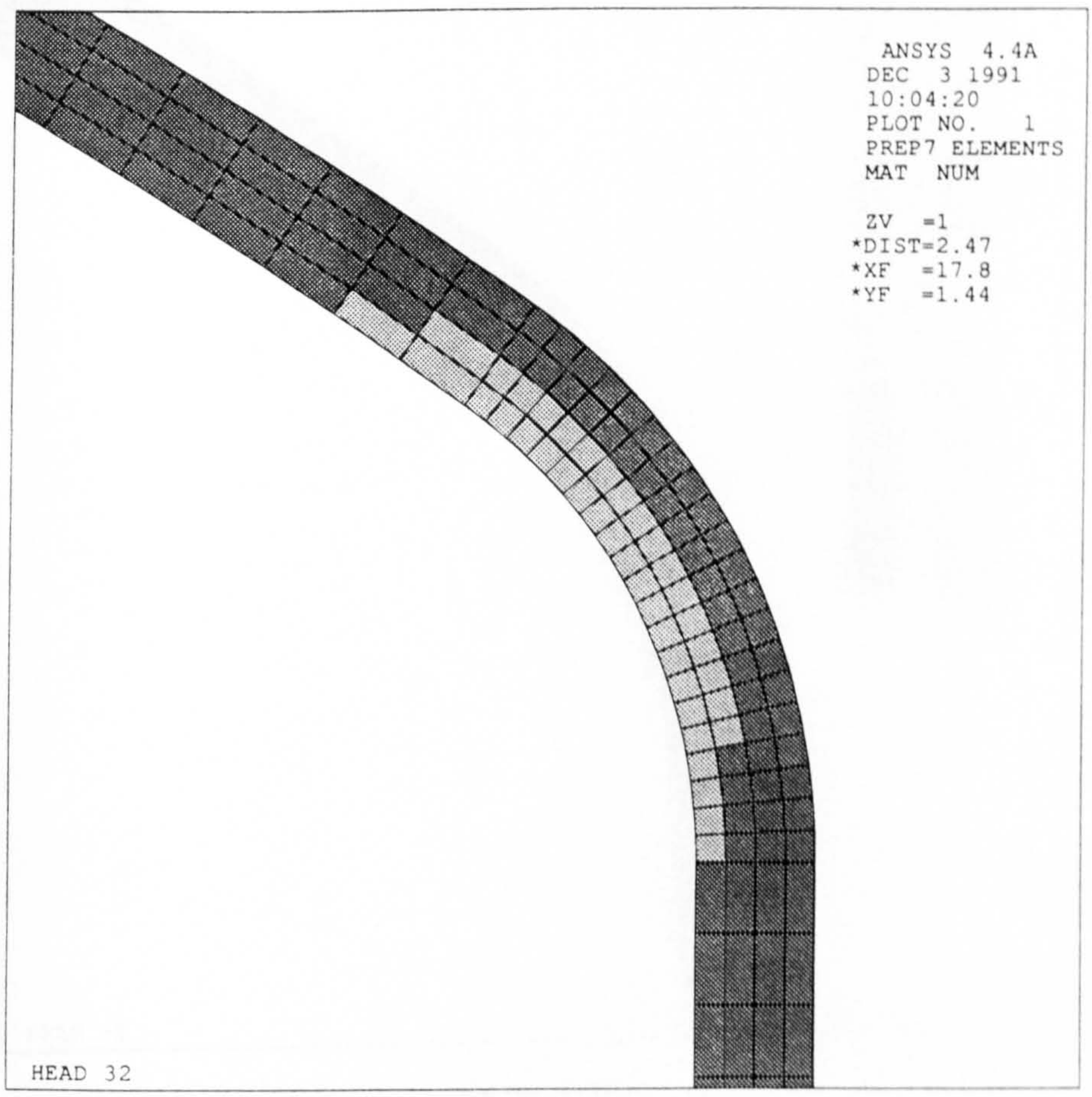

Fig. 9. Modified elements and stress contour plot: first iteration.

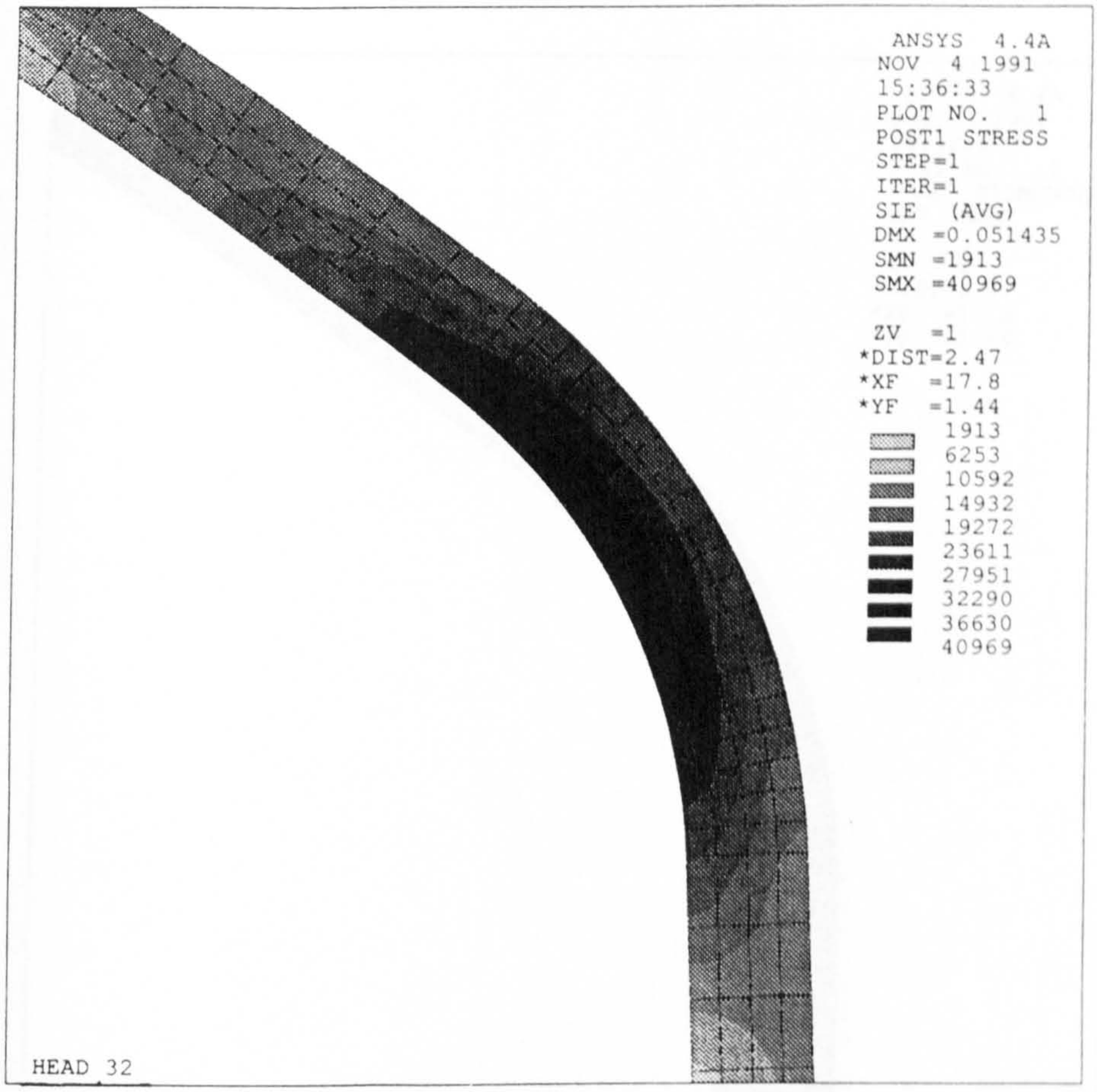
ANSYS 4.4A
NOV 4 1991
15:36:33
PLOT NO. 1
POST1 STRESS
STEP=1
ITER=1
SIE (AVG)
DMX =0.051435
SMN =1913
SMX =40969
ZV =1
*DIST=2.47
*XF =17.8
*YF =1.44
1913
6253
10592
14932
19272
23611
27951
32290
36630
40969
HEAD 32

Fig. 9—*contd.*

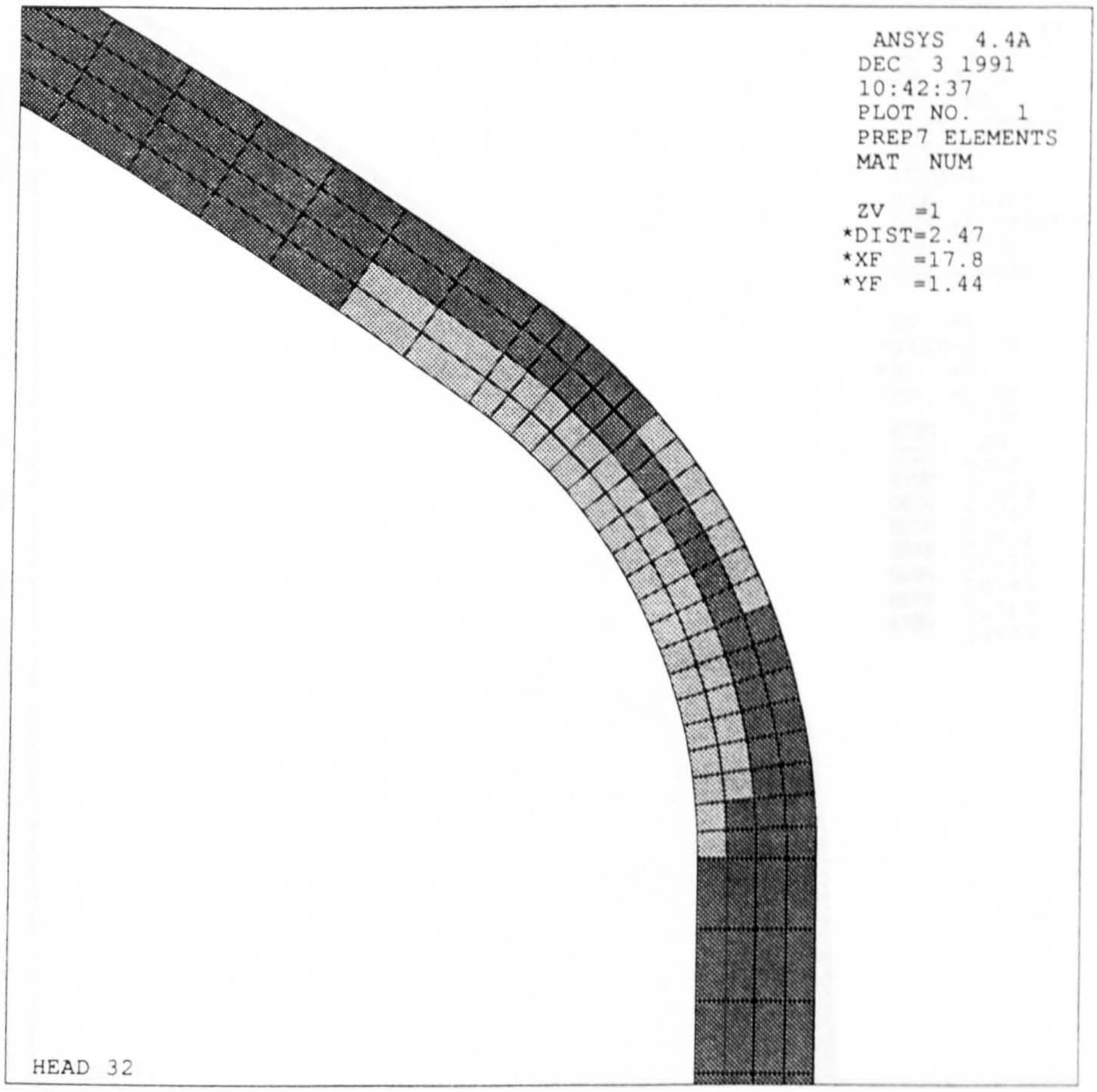

Fig. 10. Modified elements and stress contour plot: second iteration.

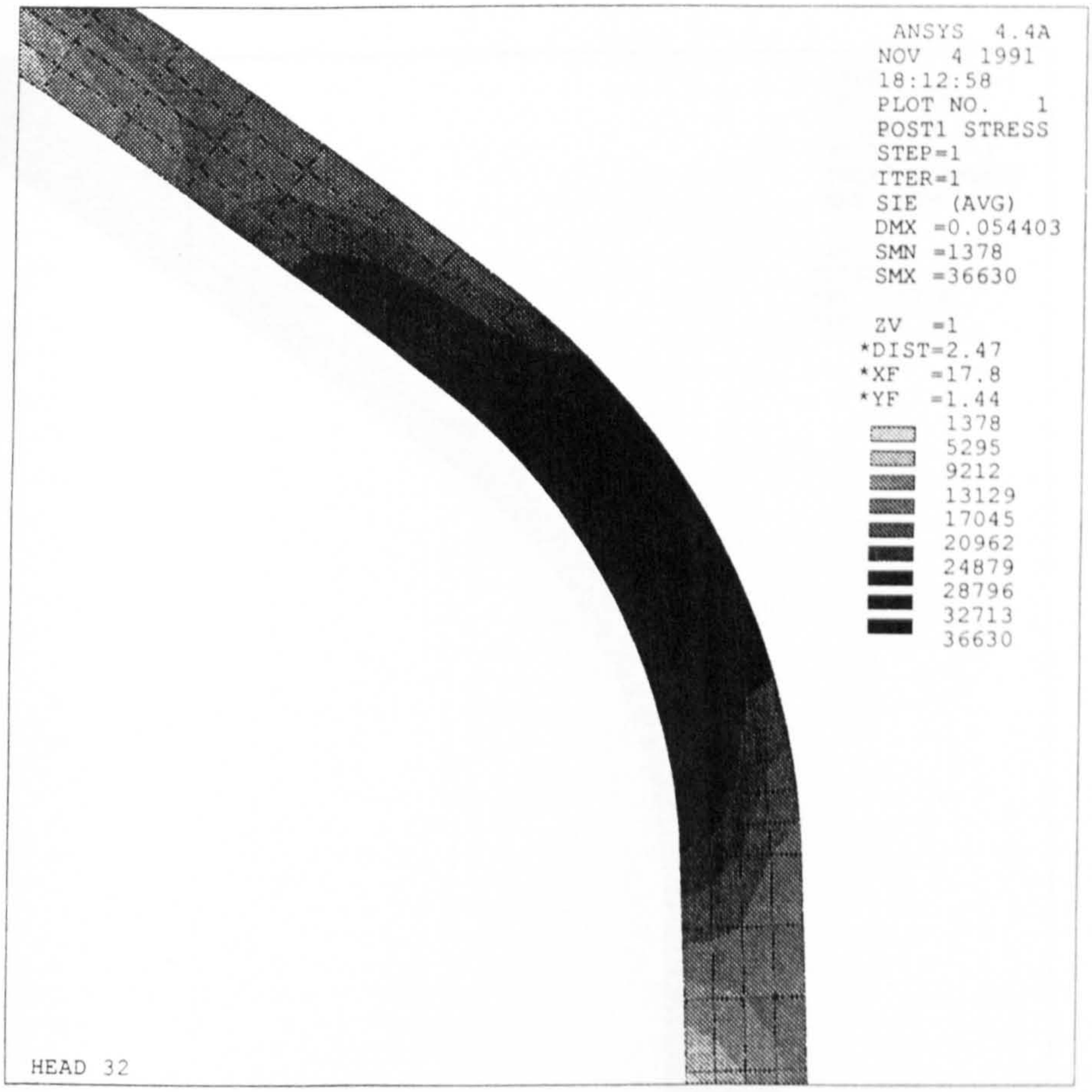
ANSYS 4.4A
NOV 4 1991
18:12:58
PLOT NO. 1
POST1 STRESS
STEP=1
ITER=1
SIE (AVG)
DMX =0.054403
SMN =1378
SMX =36630
ZV =1
*DIST=2.47
*XF =17.8
*YF =1.44
1378
5295
9212
13129
17045
20962
24879
28796
32713
36630
HEAD 32

Fig. 10—*contd.*

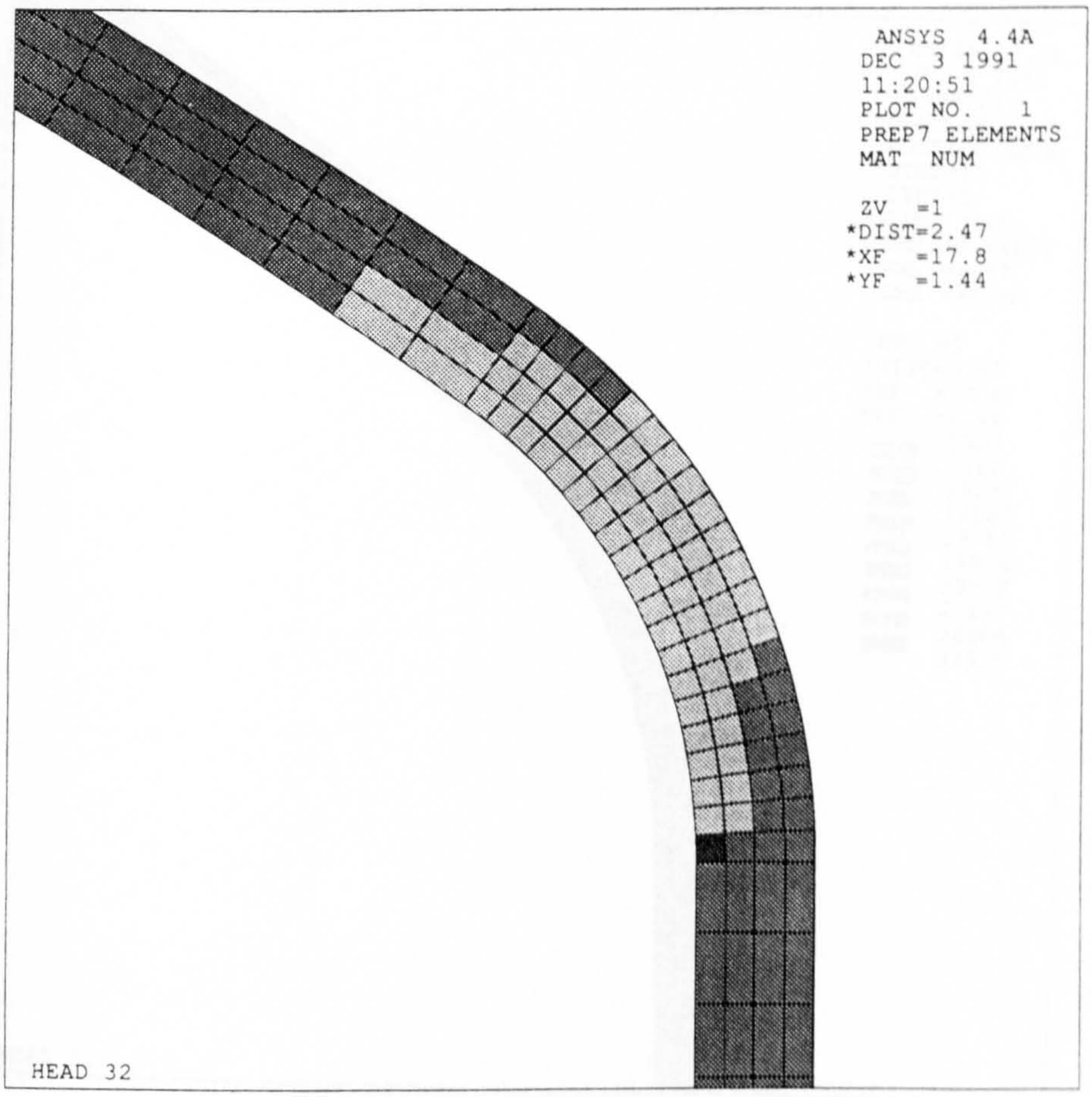

Fig. 11. Modified elements and stress contour plot: third iteration.

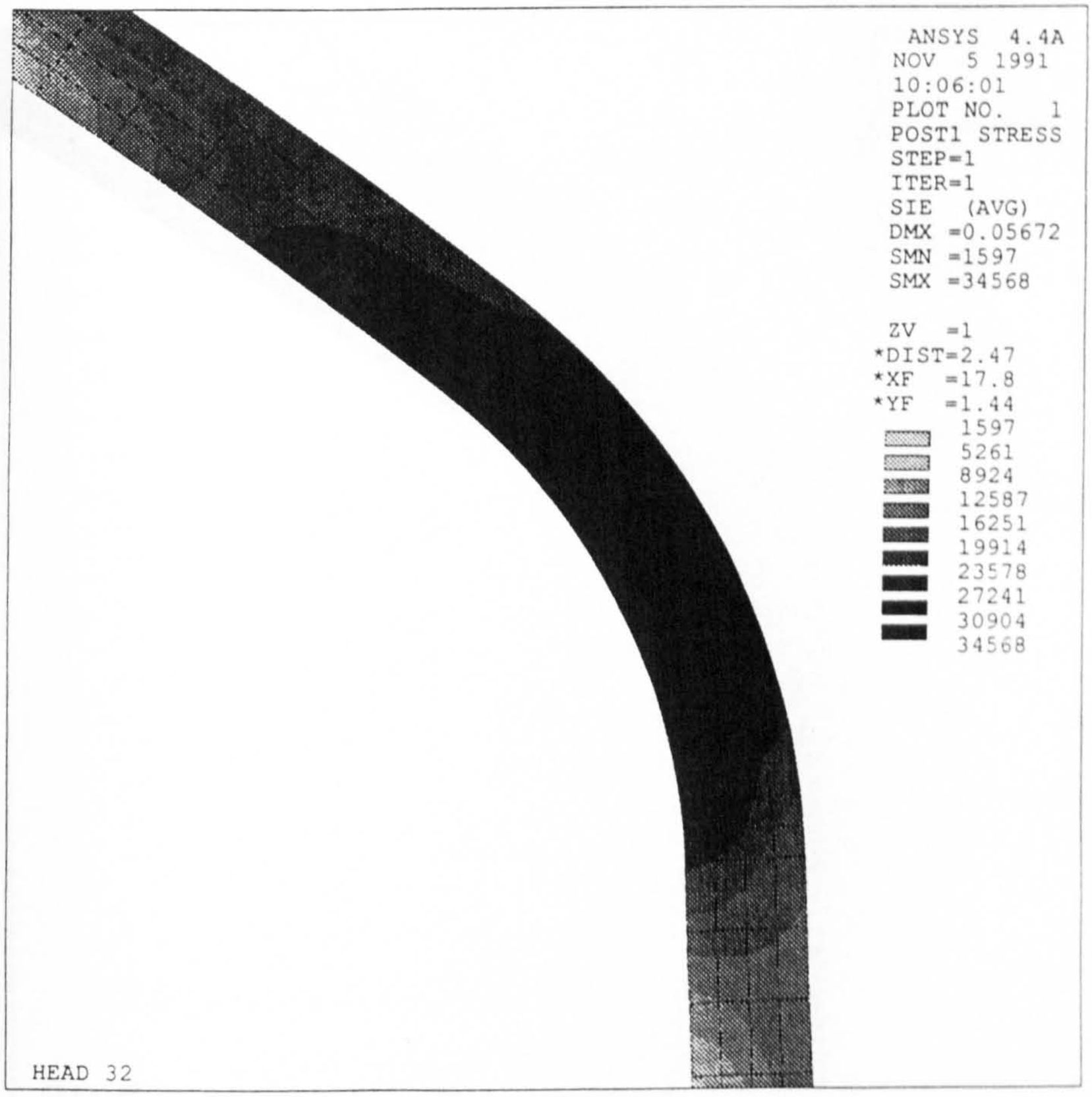
ANSYS 4.4A
NOV 5 1991
10:06:01
PLOT NO. 1
POST1 STRESS
STEP=1
ITER=1
SIE (AVG)
DMX =0.05672
SMN =1597
SMX =34568
ZV =1
*DIST=2.47
*XF =17.8
*YF =1.44
1597
5261
8924
12587
16251
19914
23578
27241
30904
34568
HEAD 32

Fig. 11—*contd.*

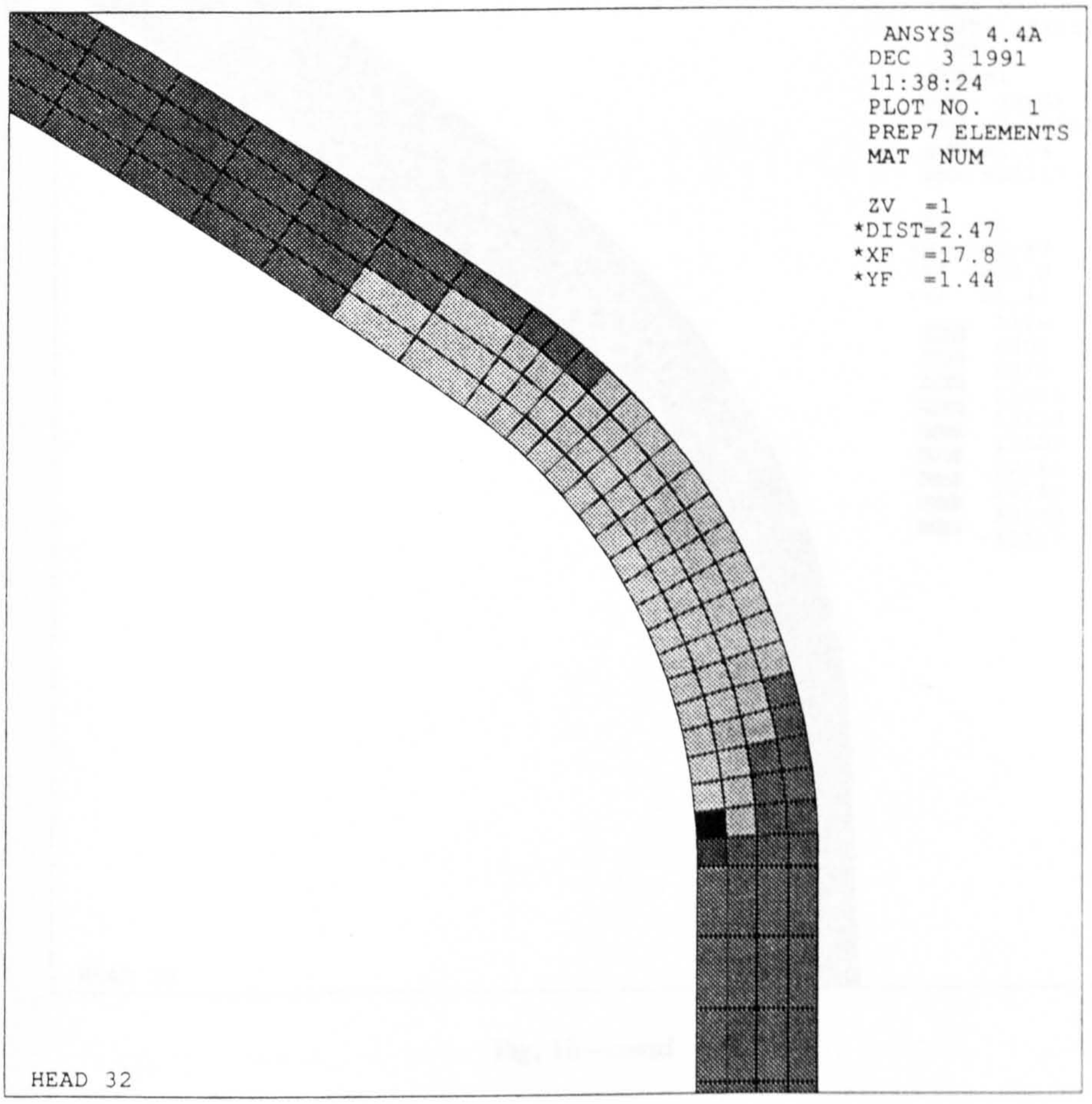

Fig. 12. Modified elements and stress contour plot: fourth iteration.

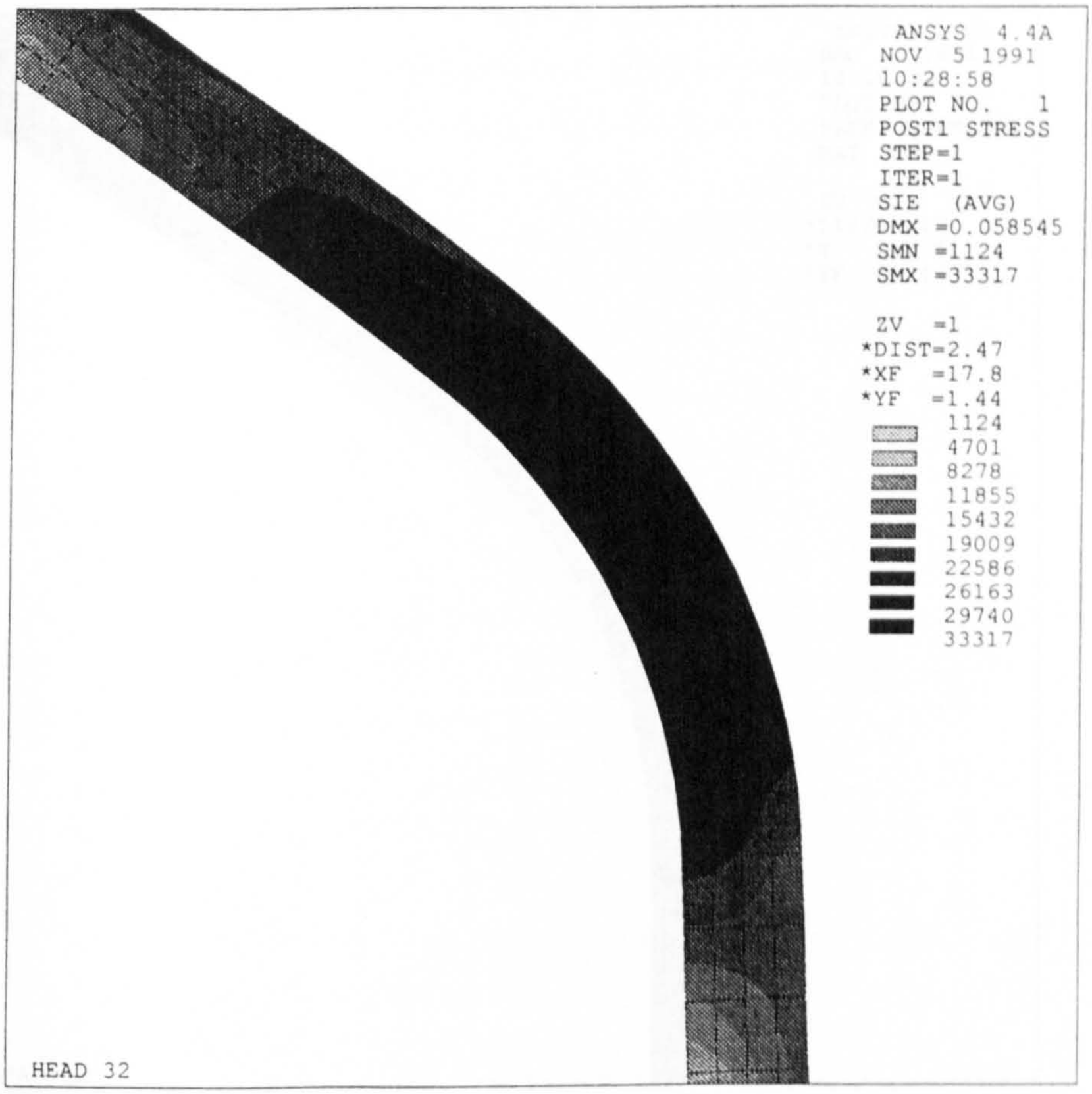
ANSYS 4.4A
NOV 5 1991
10:28:58
PLOT NO. 1
POST1 STRESS
STEP=1
ITER=1
SIE (AVG)
DMX =0.058545
SMN =1124
SMX =33317
ZV =1
*DIST=2.47
*XF =17.8
*YF =1.44
1124
4701
8278
11855
15432
19009
22586
26163
29740
33317
HEAD 32

Fig. 12—*contd.*

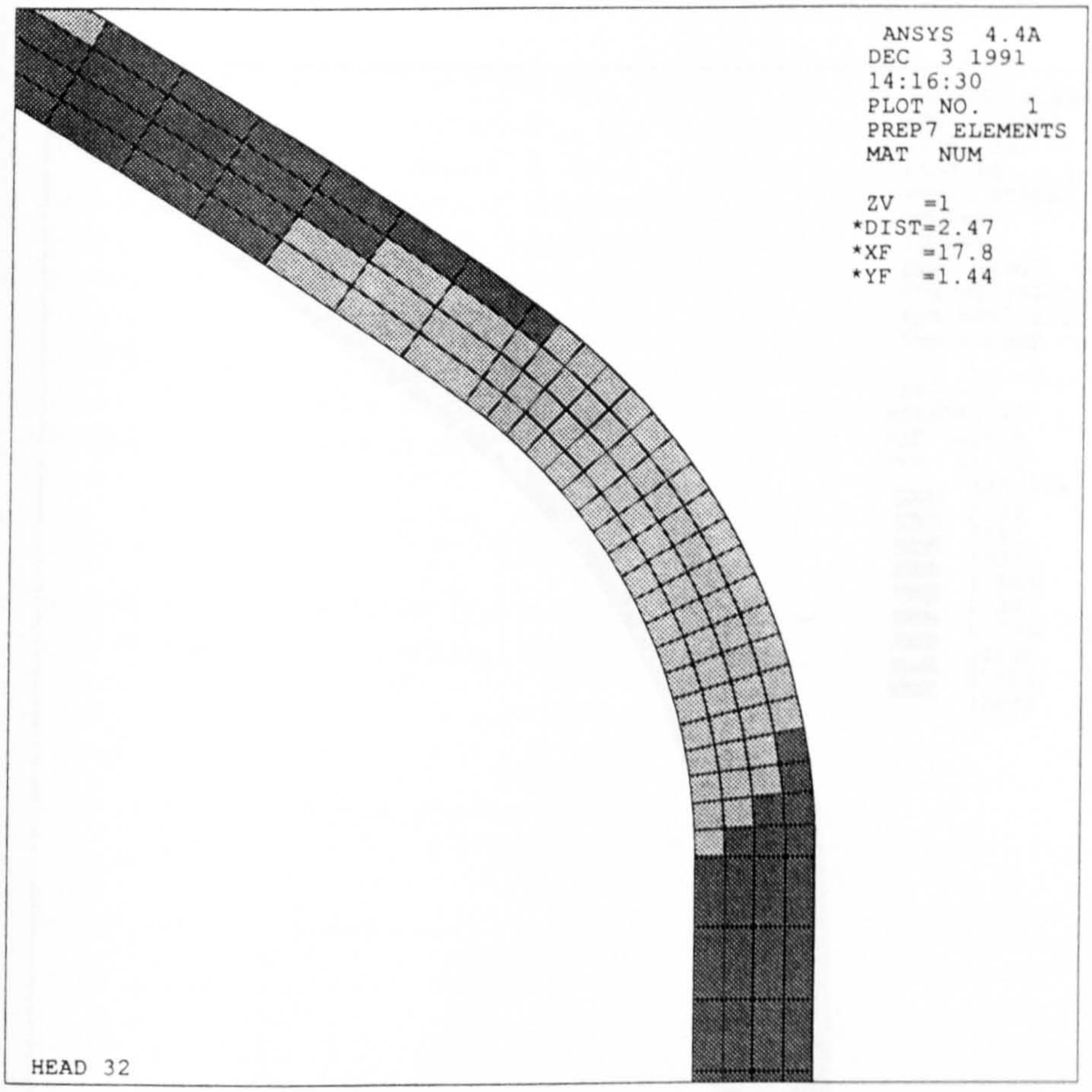

Fig. 13. Modified elements and stress contour plot: ninth iteration.

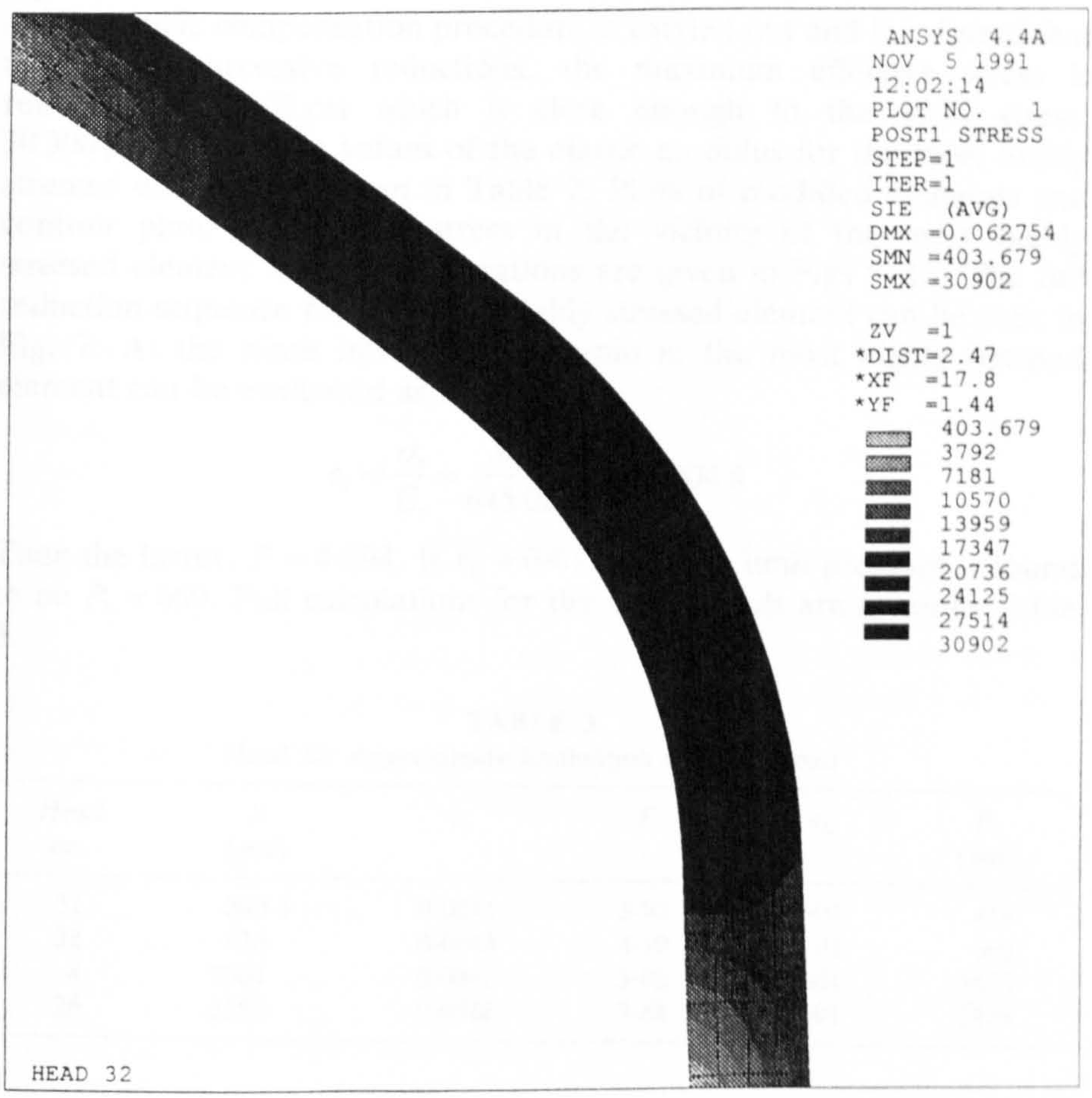
ANSYS 4.4A
NOV 5 1991
12:02:14
PLOT NO. 1
POST1 STRESS
STEP=1
ITER=1
SIE (AVG)
DMX =0.062754
SMN =403.679
SMX =30902
ZV =1
*DIST=2.47
*XF =17.8
*YF =1.44
403.679
3792
7181
10570
13959
17347
20736
24125
27514
30902
HEAD 32

Fig. 13—*contd.*

The factor of 2·4 in eqn (3) is relatively insensitive to the chosen load level. By way of example, this procedure is given in detail for Head No. 32. The applied pressure is set at 626 psi. Details of the initial finite element model are shown in Fig. 8 together with a contour plot of equivalent stress.

The elastic compensation procedure is carried out and it is found that after nine successive reductions, the maximum effective stress is reduced to 30 902 psi which is close enough to the yield stress, 30 300 psi. Successive values of the elastic modulus for the most highly stressed element are given in Table 2. Plots of modified elements and contour plots of effective stress in the vicinity of the most highly stressed element for several iterations are given in Figs 9–13. The full reduction sequence for the most highly stressed element can be seen in Fig. 7. At the ninth iteration, the strain in the most highly stressed element can be evaluated as,

$$\varepsilon_r = \frac{\sigma_r}{E_r} = \frac{30\,902}{645\,025\,9} = 0{\cdot}004\,8$$

Then the factor, $F = 4{\cdot}594$. If $\varepsilon_L = 0{\cdot}01$, then the limit pressure is found to be $P_L = 669$. Full calculations for the other heads are given in Table 3.

TABLE 3
Head 32: Approximate Evaluation of Limit Load

Head no.	*P (psi)*	ε_r	*F*	ε_L	P_L *(psi)*
31	380·5	0·0041	3·92	0·01	418
32	626	0·0048	4·59	0·01	669
4	3304	0·0041	3·92	0·01	3633
26	2550	0·0038	3·64	0·01	2848

4 DISCUSSION

The approximate limit pressures for the four heads found using this simple procedure, labelled as Method 2, together with those of Method 1 and the detailed elasto-plastic analysis are given in Table 4. The results from Drucker and Shield's formula for thin heads are also shown. From this it can be seen that both methods give good agreement with elasto-plastic analysis. Method 1 givens systematic lower bounds, but only 80% of that estimated by elasto-plastic analysis in some cases.

TABLE 4
Comparison of Estimated Limit Pressures

Head No.	*Elasto-plastic (psi)*	*Method* 1 *(psi)*	*Method* 2 *(psi)*	*Eqn.* (*1*) *(psi)*
31	417	344	418	293
32	685	568	669	626
4	3425	3262	3633	4789
26	2890	2381	2848	3307

The error of Method 2 is 6% at most but on the high side (although still probably safe given the strain criterion). Among the four heads, only Head No. 32 conformed well with Drucker and Shield's formula. For thicker walled heads, this paper's method gives better results than that of Drucker and Shield (as expected).

ACKNOWLEDGEMENTS

This research has been funded in part by a grant from the UK Science & Engineering Research Council. Use of the ANSYS software through an educational license from Swanson Analysis Systems is also acknowledged.

REFERENCES

1. Mackenzie, D. & Boyle, J. T., A method of estimating limit loads by iterative elastic analysis I—Simple examples. *Int. J. Pres. Ves. & Piping*, **53** (1993) 77–95.
2. Nadarajah, C., Mackenzie, D. & Boyle, J. T., A method of estimating limit loads by iterative elastic analysis II—Nozzle sphere intersections with internal pressure and radial load. *Int. J. Pres. Ves. & Piping*, **53** (1993) 97–119.
3. Shield, R. T. & Drucker, D. C., Limit strength of thin-walled pressure vessels with an ASME Standard Torispherical Head. *Proc. Third US Natn. Cong. Appl. Mech.*, ASME, 1958, pp. 665–72.
4. Drucker, D. C. & Shield, R. T., Limit analysis symmetrically loaded shells of revolution. *J. Appl. Mech.*, **26** (1959) 61.
5 Shield, R. T. & Drucker, D. C., Design of thin-walled torispherical and toriconical pressure-vessel heads. *J. Appl. Mech.*, **28** (1961) 292.
6. Mitchell, S. E., The 'Formdehngrenze' design method and its influence on current specifications for dished ends of boilers and pressure vessels. NEL Report No. 171, 1964.
7. Biron, A. & Charleux, G., *Int. J. Mech. Sci.*, **14** (1972) 25.
8. Taylor, T. E. & Robinson, M., UMIST, Internal Report, 1971.

9. Crisp, R. J., A computer survey of the behaviour of torispherical drumheads under internal pressure. *Nucl. Engng Design*, **11** (1970) 457.
10. Simonen, F. A. & Hunter, D. T., Elastic-plastic deformation in pressure vessel heads. WRC Bulletin No. 163, 1971.
11. Calladine, C. R., *First Int. Conf. on Pressure Vessel Technology*, Delft (1969).
12. Save, M., Experimental verification of plastic limit analysis of torispherical and toriconical heads. *Pressure Vessels and Piping: Design and Analysis, Vol. 1.* ASME, 1972, pp. 382–416.
13. Findlay, G. E., Moffat, D. G. & Stanley, P., Torispherical drumheads: a limit-pressure and shakedown investigation. *J. Strain Anal.*, **6** (1971) 147.
14. Kirk, A. & Gill, S. S., The failure of torispherical ends of pressure vessels due to instability and plastic deformation—an experimental investigation, *Int. J. Mech. Sci.*, **17** (1975) 525.
15. Gerdeen, J. C., A critical evaluation of plastic behaviour data and a united definition of plastic loads for pressure components. WRC Bulletin, 254, 1979.
16. Townley, C. H. A., Findlay, G. E., Goodman, A. M. & Stanley, P., Elastic-plastic computation as a basis for design charts for torispherical pressure vessel ends, *Proc. Instn Mech. Engrs*, **185** (1971) 63/71.
17. Townley, C. H. A., The design of pressure vessel details. *Engineer, Lond.*, **227** (1968) 438.

PVP-Vol. 230, Stress Classification, Robust Methods,
and Elevated Temperature Design
ASME 1992

AN ITERATIVE ELASTIC ANALYSIS PROCEDURE FOR ESTIMATING LOWER BOUND LIMIT LOADS

D. Mackenzie, J. Shi,* C. Nadarajah, and J. T. Boyle
Department of Mechanical Engineering
University of Strathclyde
Glasgow, Scotland

ABSTRACT

A simple method for estimating lower bound limit loads by an iterative elastic analysis procedure called *the elastic compensation method* is discussed. The method aims to establish an admissible stress field for the lower bound limit load theorem and is quite general. Several sample analyses of pressurised components are presented and calculated limit loads compared with solutions from the literature. It is concluded that the method is suitable for calculating limit loads for design purposes.

INTRODUCTION.

In recent paper, Kalnins and Updike[1] considered the role of limit and elastic-plastic analyses in pressure vessel design and concluded that:

> "... an elastic analysis may not provide an effective way for calculating an allowable pressure that prevents gross distortion with a specific margin of safety. Unless a plastic analysis is also performed, there is no way of assessing the margin of safety provided by elastic analysis..."

Traditionally, such a plastic (or limit) analysis requires inelastic analysis of the component, however, work on stress categorisation by *reduced modulus analysis* has indicated that it is often possible to gauge the effect of local inelasticity in pressurised components by an *iterative elastic finite element analysis* procedure in which local elastic material properties are systematically modified in order to simulate inelastic behaviour[2][3][4][5][6][7]. In this paper, a simple systematic procedure for estimating lower bound limit loads by iterative elastic analysis, referred to as the *method of elastic compensation*, is presented. The procedure is one of several investigated by the writers as part of a research project into stress categorisation in pressure vessel design funded by the UK Science and Engineering Research Council[8][9][10].

The estimation of limit loads by performing iterative elastic finite element analysis and invoking the lower bound limit load theorem was proposed by Marriott in ref. 3. The lower bound limit load theorem may be stated as follows:

> If a statically admissible stress field in which the stress nowhere exceeds the yield exists for a given component under a given loading system, the loading is a lower bound limit load.

The statically admissible stress field may be any linear elastic solution for the given component geometry and loading. Applying the lower bound theorem to a linear elastic solution based on isotropic homogeneous material properties gives a lower bound corresponding to the initial yield load for the component which, in general, will be a poor approximation to the actual collapse load. Marriott, however, proposed that lower bound limit loads can be obtained "to any desired degree of accuracy" by applying reduced modulus procedures in an iterative elastic finite element analysis which causes the initially calculated (isotropic) stresses to redistribute to lower values. If an elastic solution which satisfies the lower bound theorem can be established for a component subject to given load, that load is a lower bound on the limit load of the component.

An alternative method for estimating limit loads by an iterative elastic procedure has been proposed by Seshadri and Fernando. The *GLOSS r-node method*[11] uses two elastic analyses to determine points or *r-nodes* (related to *skeletal points* in reference stress techniques for creep analysis) at which the stresses are essentially statically determinate. The r-node method has been shown to give good estimates of limit loads for a number of components but, at present, has the apparent disadvantage of requiring manual intervention in the procedure. Problems may arise in determining, and indeed interpreting, what is meant by r-nodes in non-axisymmetric 3-D structures.

The procedure discussed here, the elastic compensation method, is based on the earlier work of Marriott and Seshadri.

THE ELASTIC COMPENSATION METHOD.

Initially, an elastic finite element analysis of the component is performed for the specified design loading, P_d. The results of this homogeneous isotropic elastic analysis can be used in a standard *design by analysis*, but in addition is used as *iteration zero* in a series of linear elastic analyses in which the modulii of elements are changed in order to redistribute the stress in the component. In each subsequent iteration, the modulus of each element is modified according to an equation of the form:

$$E_i = E_{(i-1)} \frac{\sigma_e}{(\sigma_{(i-1)})} \qquad (1)$$

where subscript i is the iteration number, σ_e a nominal stress value

*Visiting Scholar, Hebei Electric Power Survey and Design Institute
Shijiazhuang, Hebei, People's Republic of China

and $\sigma_{(i-1)}$ the maximum (unaveraged) nodal equivalent stress associated with the element from the previous solution. This procedure is similar to that used in the GLOSS r-node method, and differs slightly from Marriott's procedure in which *only* elements with stress intensity S greater than the code allowable Sm have their modulii reduced according to the expression:

$$E_i = E_{(i-1)}\frac{Sm}{S}$$

The value of σ_r in (1) is somewhat arbitrary - usually half or two thirds yield - and has not been found to be critical in the example problems considered below. Some care has to be taken, however, to ensure that the nodal stress in the divisor of (1) does not approach zero as, for example, could happen at the mid-surface of components subject to pure bending. This would lead to elements of excessively high stiffness in the model and possible numerical problems in the finite element solution.

Plotting the maximum stress in the model against iteration number results in a graph of the form shown in Figure 1. The procedure may cause the maximum stress to increase or decrease between iterations but it is generally found that over a number of iterations there is a net decrease in maximum stress with respect to the initial solution.

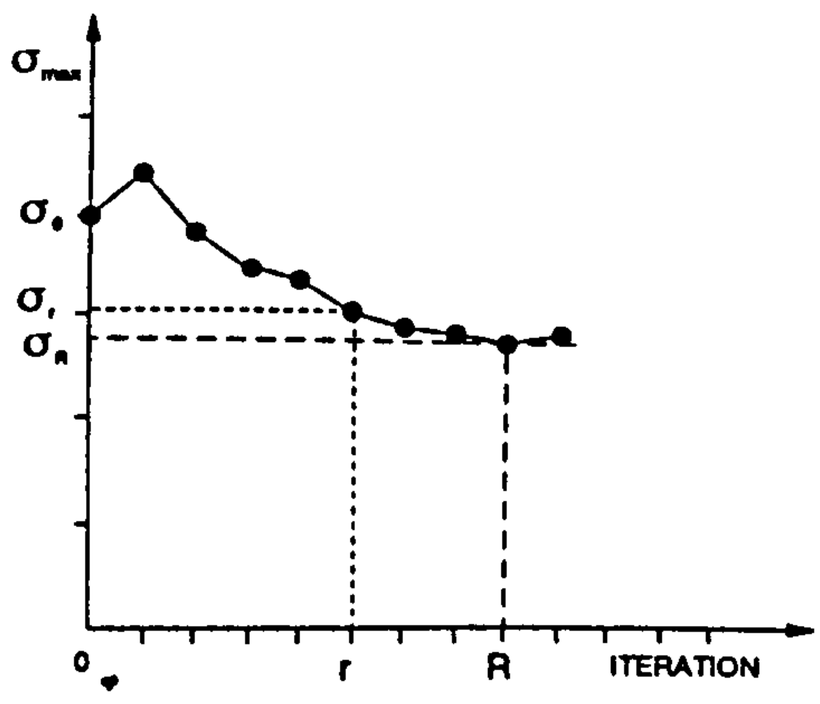

Figure 1. Maximum stress for each iteration.

The initial solution is a homogeneous isotropic linear elastic solution. The subsequent solutions are inhomogeneous and anisotropic but are still linear elastic and hence the component stress is proportional to the applied load. These solutions can be used to define lower bound limit loads for the component by invoking the lower bound theorem:

Consider an arbitrary solution, iteration r, as illustrated in Figure 1. For the given load P_d, the maximum stress given by iteration r is σ_r, where σ_r may be greater or less than the yield stress. As the solution is linear, the load P_l to give a maximum stress of σ_Y in the solution can be calculated from the proportionality of the solution; that is,

$$\frac{P_l}{P_d} = \frac{\sigma_Y}{\sigma_r}$$

Hence

$$P_l = P_d\frac{\sigma_Y}{\sigma_r}$$

The above solution meets the requirements of the lower bound limit load theorem in that it is statically admissible and the maximum stress does not exceed yield. Thus load P_l is a lower bound limit load for the component.

Limit loads can be evaluated for any iteration in the above manner, however, the *best* lower bound limit load is given by considering the solution in which the maximum stress has the lowest value, say iteration R, in which the maximum stress is σ_R. This solution gives a lower bound limit load

$$P_L = P_d\frac{\sigma_Y}{\sigma_R}$$

where P_L is the best estimate of limit load given by the above procedure.

SAMPLE ANALYSES.

Five problems illustrating the use of the elastic compensation method are presented below. All the analyses were performed using the ANSYS finite element program.

3.1 Beam under combined bending and tension.

The first example is that of a beam of unit depth and thickness under combined tension and bending, as illustrated in Figure 2.

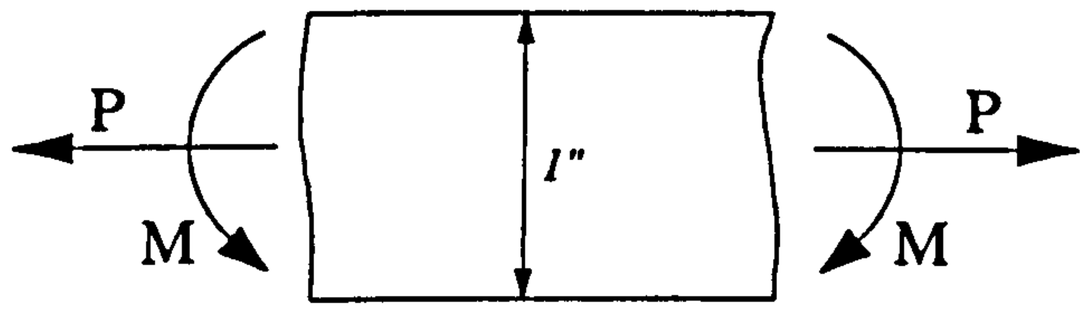

Figure 2. Beam under combined loading

The beam material has Young's modulus $E = 29E6$ psi and yield stress $\sigma_Y = 30E3$ psi. The theoretical collapse load of a cantilever beam under direct force P and moment M is given by the expression:

$$\frac{M}{M_Y} = \frac{3}{2}\left[1 - \left(\frac{P}{P_Y}\right)^2\right]$$

where, if d is the depth of the beam:

$$P_Y = \sigma_Y d \quad \text{and} \quad M_Y = \frac{\sigma_Y d^2}{6}$$

Three finite element models of the beam with 6, 12 and 24 linear quadrilateral plane stress elements through the depth were created and up to 8 iterations based on the equation:

$$E_i = E_{(i-1)}\frac{20E3}{\sigma_{(i-1)max}}$$

were performed for each model. The elastic compensation results are compared with the exact solution and GLOSS r-node results with a mesh of 25 elements through depth (from ref. 11) in Figure 3.

Clearly, the finer the mesh the better the estimated limit load. However, it is found that finer meshes may require greater numbers of iterations than course meshes to give a good solution. A typical plot of maximum model stress against iteration is shown in Figure 4. This illustrates that although a 16 element mesh eventually gives a better estimate of limit load than 6 or 12 element meshes, the initial stress reduction is poor in comparison with the courser meshes.

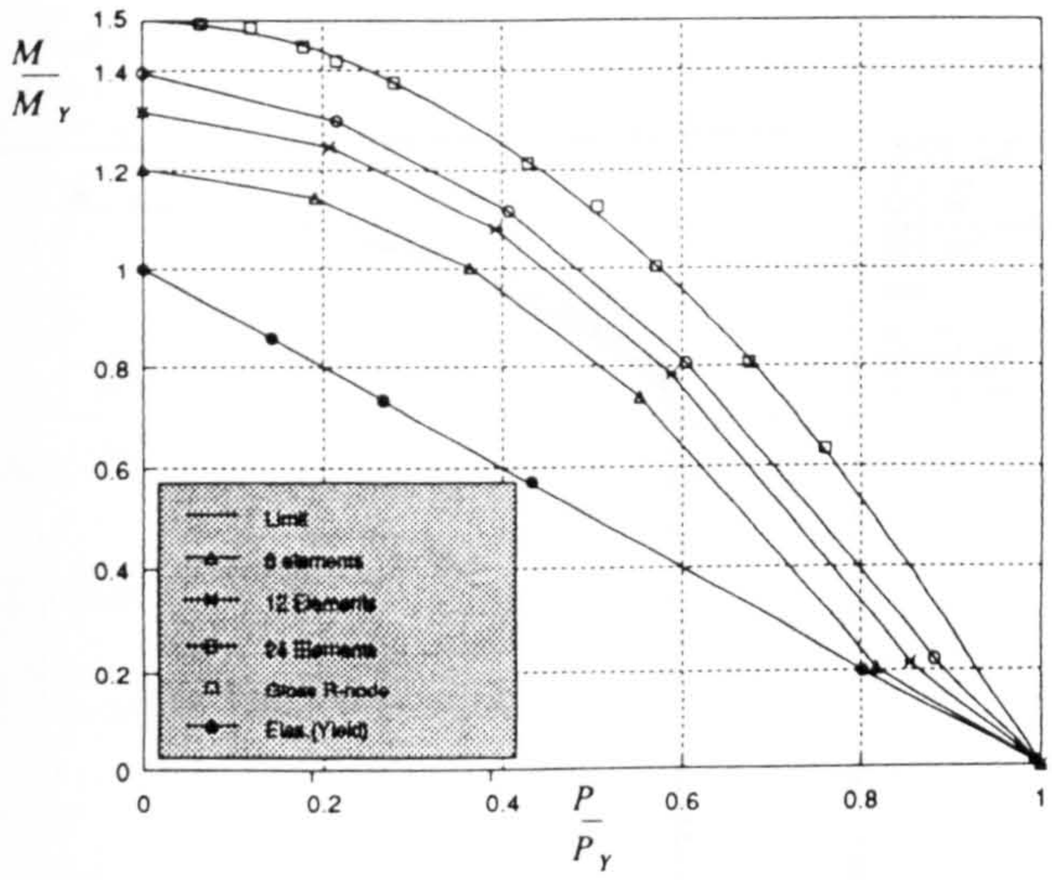

Figure 3. Lower bound limit load by iterative elastic analysis.

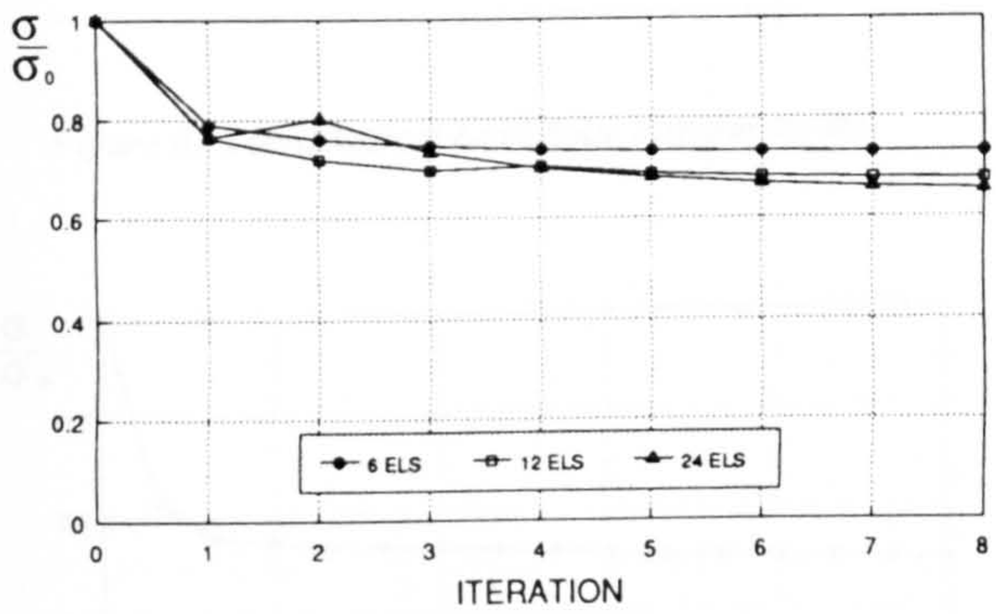

Figure 4. Maximum model stress for each iteration.

3.2 Thick Cylinder.

Three thick cylinders under plain strain conditions as were investigated. The material properties used were:

$E = 200E3\ N/mm^2 \quad \nu = 0.3 \quad \sigma_Y = 300\ N/mm^2$

The theoretical limit pressure of a thick cylinder subject to internal pressure based on the Von Mises yield criterion is given by the equation:

$$P_L = \frac{2}{\sqrt{3}}\sigma_Y \ln\left(\frac{r_o}{r_i}\right)$$

where r_o is the outer radius and r_i the inner radius of the cylinder. The dimensions of the cylinders investigated here are given in Table 1.

MODEL	r_i (mm)	r_o (mm)
1	20	30
2	20	40
3	20	50

Table 1. Thick cylinder dimensions.

Two models were created for each cylinder geometry, with meshes of 7 and 15 linear isoparametric axisymmetric solid elements through thickness, and 8 elastic compensation iterations were performed for each model. The lower bound limit pressures given by the elastic compensation method and the theoretical limit loads are compared in Tables 2 and 3.

MODEL	LIMIT PRESSURE N/mm^2		
	7 ELS.	15 ELS	THEO.
1	125.4	128.7	140.5
2	212.2	222.4	240.1
3	274.7	292.3	317.4

Table 2. Elastic compensation and theoretical limit pressures.

MODEL	$\left(\frac{P_{L(7els)}}{P_{L(theo)}}\right)\%$	$\left(\frac{P_{L(15els)}}{P_{L(theo)}}\right)\%$
1	89.2	91.6
2	88.4	92.6
3	86.6	92.1

Table 3. Comparison of elastic compensation and theoretical limit loads.

3.3 Torispherical End.

The third example is a torispherical end, as illustrated in Figure 5:

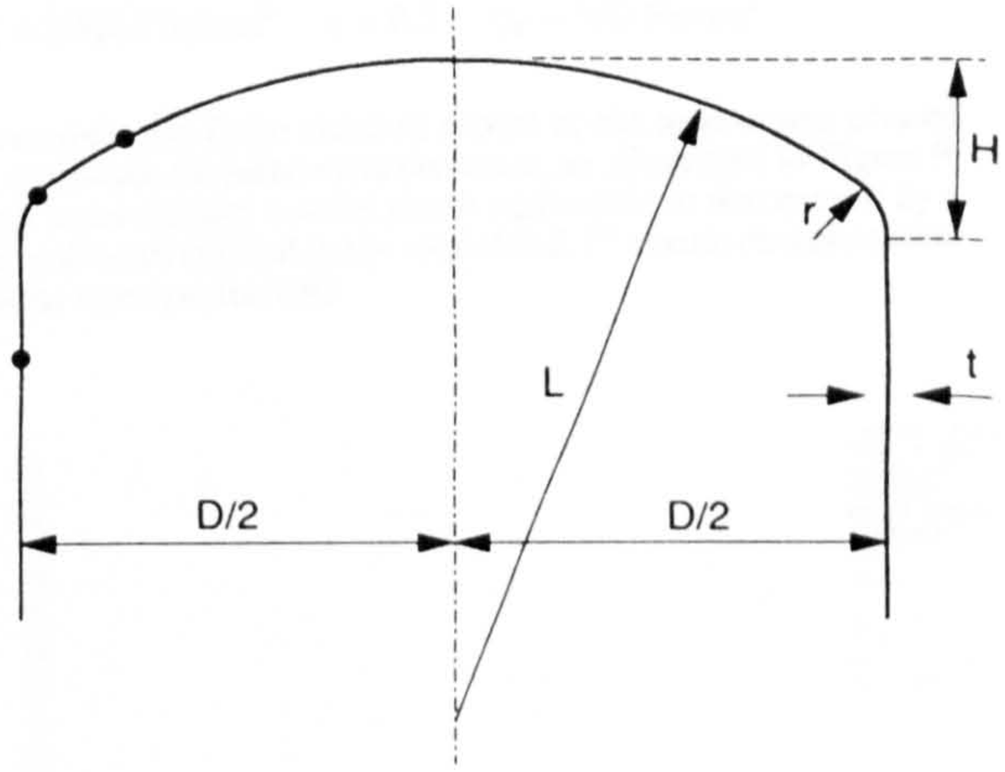

Figure 5. Torispherical end.

where

$D = 37\,in. \quad \frac{t}{D} = 0.015 \quad \frac{h}{D} = 0.207 \quad \frac{r}{D} = 0.07 \quad \text{and} \quad \frac{L}{D} = 0.813$

The material properties were:

$E = 29E6\ psi \quad \sigma_Y = 30300\ psi \quad \nu = 0.29$

An axisymmetric finite element model of the head with four linear quadrilateral isoparametric solid elements through thickness, as shown in Figure 6, was created and 15 elastic compensation iterations performed. The maximum stress is plotted against iteration in Figure 7.

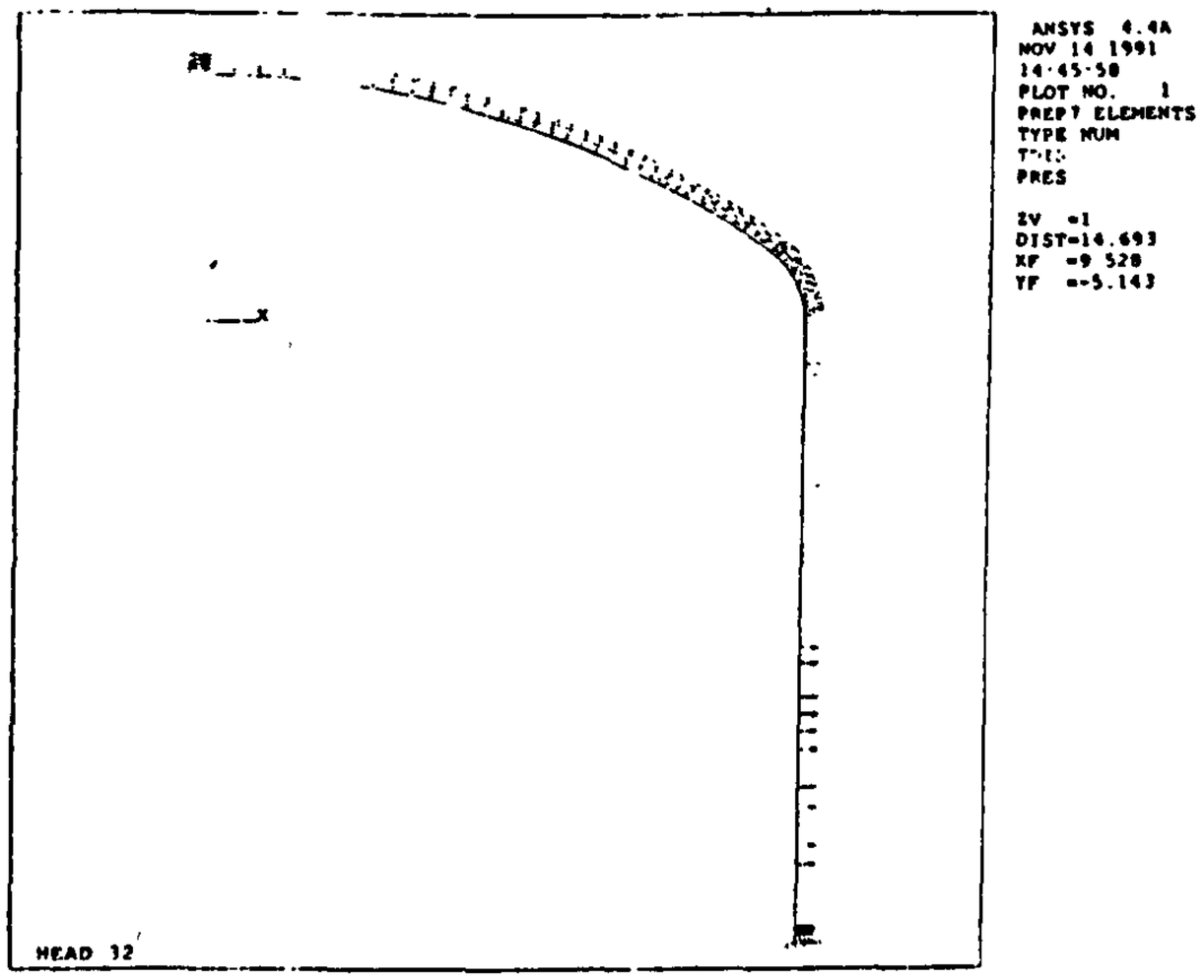

Figure 6. Torispherical head finite element model.

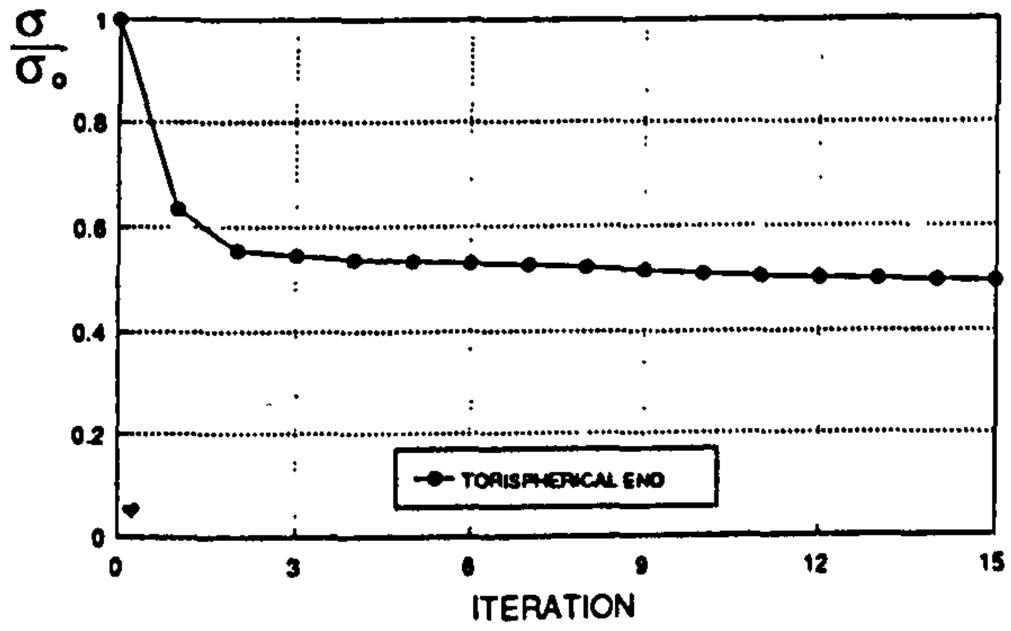

Figure 7. Maximum stress per iteration.

The elastic compensation (EC) lower bound limit load limit load is compared with an inelastically calculated limit load, (the pressure at 1% equivalent strain), and the lower bound limit load given by the Shield & Drucker expression[12]:

$$P_D = \left(0.33 + 5.5\frac{r}{D}\right)\frac{t}{L} + 28\left(1 - 2.2\frac{r}{D}\right)\left(\frac{t}{L}\right)^2 - 0.0006$$

in Table 4.

EC	P_D	INELAS.	$\left(\frac{EC}{P_D}\right)\%$	$\left(\frac{EC}{INELAS}\right)\%$
568 psi	626 psi	685 psi	90.7	82.9

Table 4. Comparison of elastic compensation, inelastic and Shield & Drucker limit pressure.

3.4 Nozzle in Spherical Shell

The fourth example is a nozzle in a spherical shell, illustrated in Figure 8, under internal pressure and radial nozzle load.

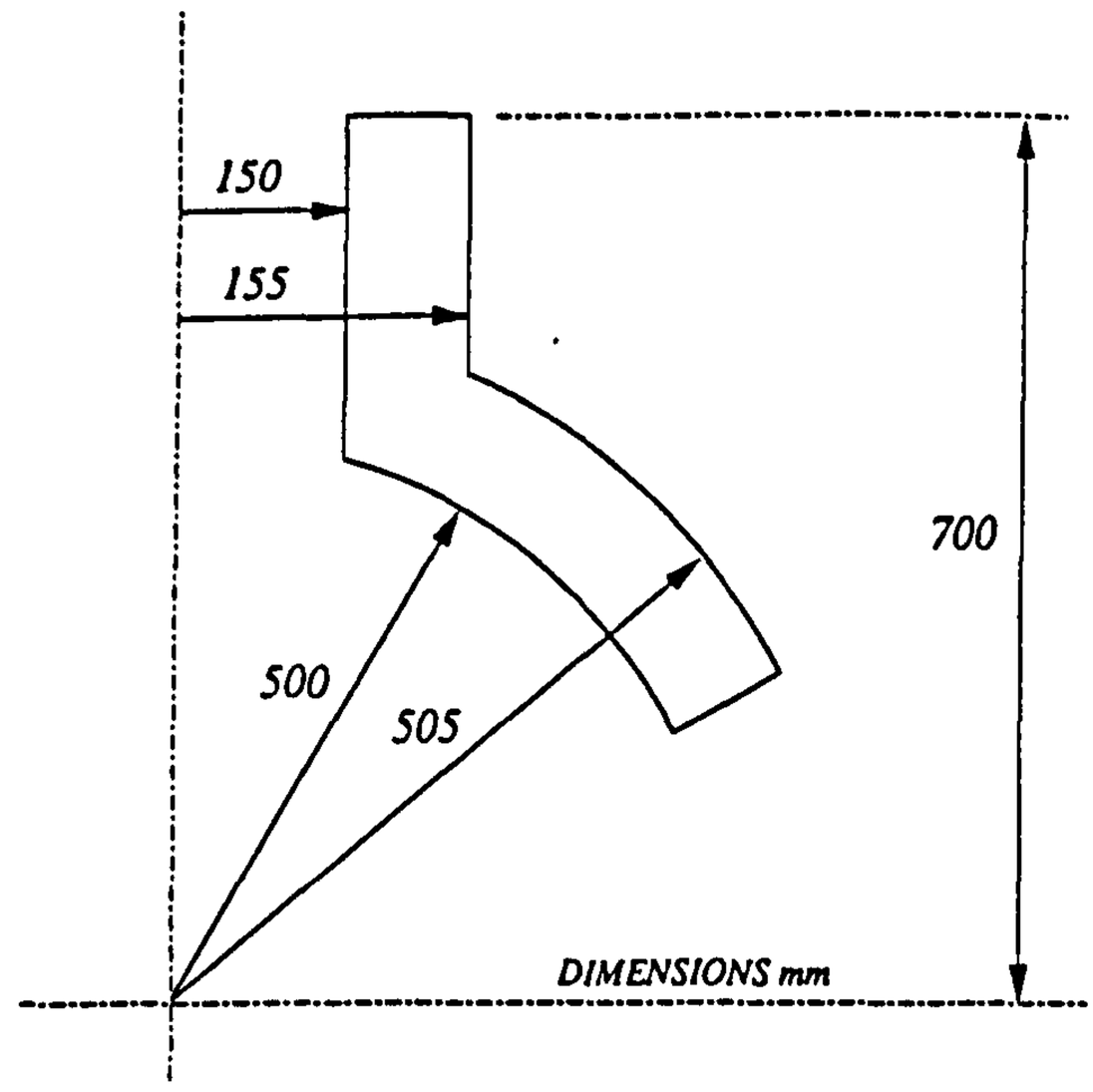

Figure 8. Nozzle geometry.

The material properties used were:

$E = 200E3\ N/mm^2 \quad \nu = 0.3 \quad \sigma_Y = 300\ N/mm^2$

An axisymmetric finite element model of the nozzle was created using quadratic isoparametric elements, as illustrated in Figure 9. Internal pressure and a radial thrust equivalent to that caused by a closed end were applied to the model and 15 elastic compensation iterations were performed.

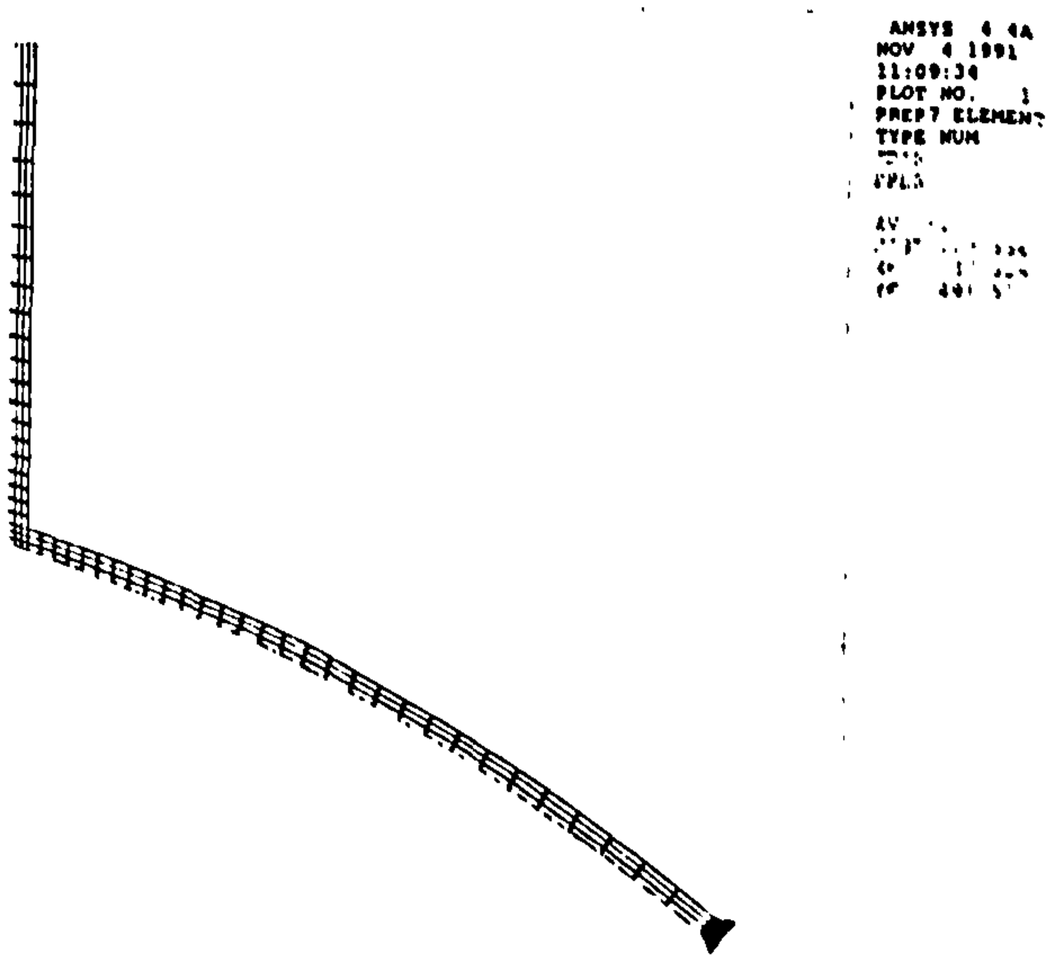

Figure 9. Nozzle finite element model.

The lower bound limit pressure calculated by the elastic compensation procedure (EC) is compared with Robinson's non-linear programming lower bound (ROB) in Table 5.

EC	ROB	$\left(\frac{EC}{ROB}\right)\%$
2.09 N/mm²	2.15 N/mm²	97.2

Table 5. Comparison of elastic compensation and Robinson limit pressure for nozzle intersection.

3.5 Toriconical end.

The final example is a toriconical end, as illustrated in Figure 10, under internal pressure.

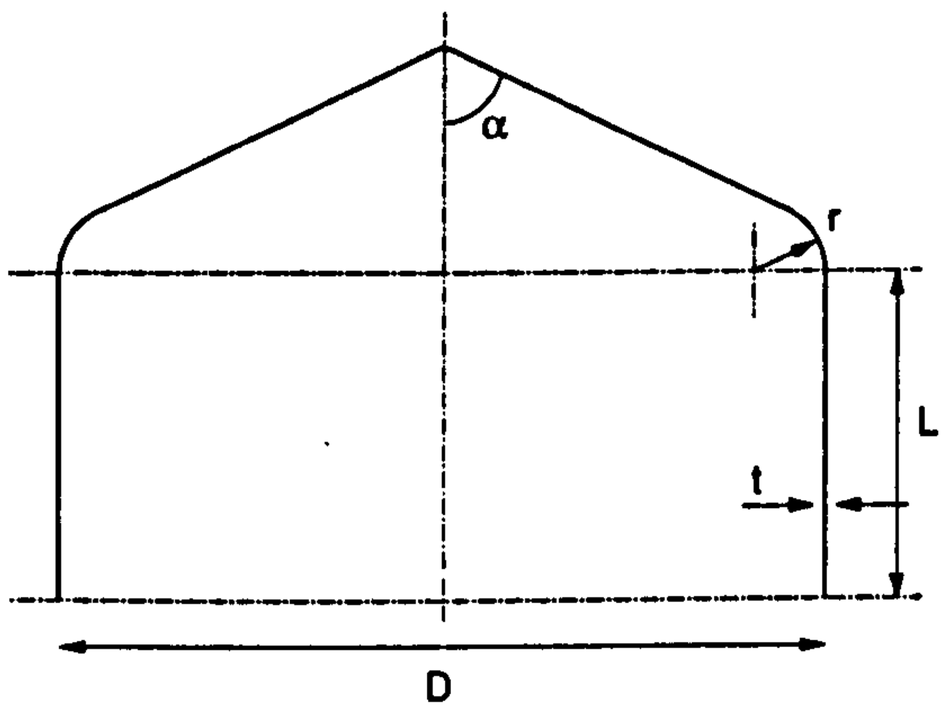

$$D = 1000mm \qquad \frac{r}{D} = 0.06 \qquad \alpha = 45°$$

Figure 10. Toriconical end.

The material properties are:

$$E = 200E3\ N/mm^2 \qquad \nu = 0.3 \qquad \sigma_y = 300\ N/mm^2$$

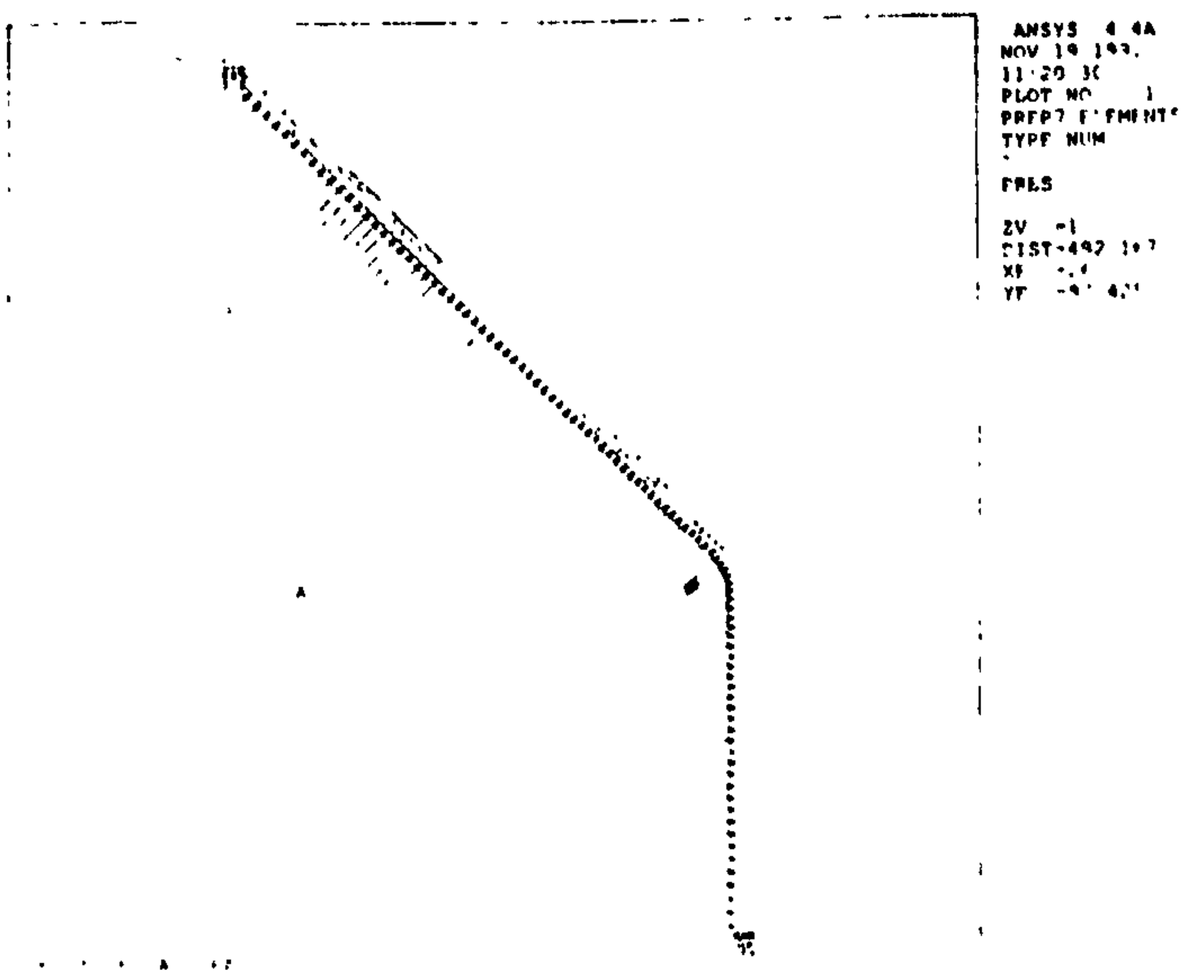

Figure 11. Toriconical head model 1 finite element model.

Two axisymmetric finite element models of linear isoparametric solid elements were created: Model 1, with 3 elements through thickness and Model 2 with 6 elements through thickness. Model 1 is shown in Figure 11.

The elastic compensation procedure, with up to 15 iterations, was applied to both models. A plot of maximum equivalent stress per iteration for model 1 is shown in Figure 12.

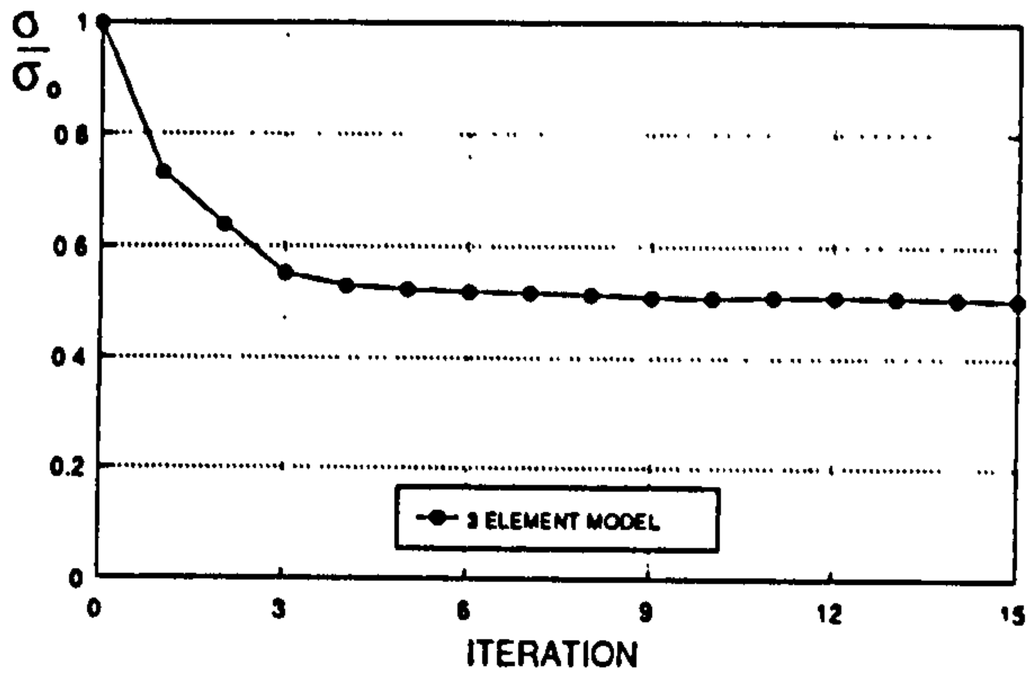

Figure 12. Model 1 maximum stress per iteration.

The estimated lower bound limit pressures given by the elastic compensation analyses (MOD1 and MOD2) are compared with the Gerdeen & Hutula theoretical plastic limit load[13],(G&H) in Table 6.

MOD1	MOD2	G&H	$\left(\frac{MOD1}{G\&H}\right)\%$	$\left(\frac{MOD2}{G\&H}\right)\%$
9.77	10.25	12.02	81.3	85.3

Table 6. Comparison of elastic compensation and Gerdeen & Hutula limit load.

DISCUSSION.

The sample analyses presented above illustrate the use of the elastic compensation method in determining lower bound limit loads for design purposes. Clearly, the accuracy of the method depends to some extent on the particular component geometry, loading and finite element model, however, the advantage of the proposed method is that it is general and can be used to obtain approximate *conservative* limit loads with minimal intervention on the part of the designer. It is fairly simple to write model preprocessing and postprocessing programs to perform the procedure automatically and, in addition, it would be fairly simple for commercial software vendors to incorporate such routines in their products: for example, using *macros* in ANSYS.

Alternative approaches to calculating limit loads by iterative analysis, such as the r-node method, may give more accurate values for limit load for specific components but such procedures require greater user input: for example, determining the location of r-nodes etc. At first sight the computing cost of performing the iterative elastic compensation method may seem expensive but it must be emphasised that the cost of performing say eight elastic analyses of a component is almost insignificant in comparison with a non-linear elasto-plastic analysis of the same component using suitable load steps and convergence criteria to obtain good approximate limit loads, particularly for 3-D structures.

It is expected that further work will allow "fine-tuning" of the elastic compensation method in order enhance the accuracy of the solution for given generic components, however, the procedure given above has been shown to be robust (in all of the examples considered thus far) and can be used to establish lower bound limit loads for design purposes without recourse to complex inelastic analysis or extensive manual intervention.

ACKNOWLEDGEMENT

This research has been funded by a grant from the UK Science & Engineering Research Council. Use of the ANSYS software through an educational license is also acknowledged.

References

1. Kalnins A & Updike P "Role of plastic limit and elastic-plastic analyses in design," ASME PVP-Vol. 210-2, pp135-142, San Diego, (1991).

2. Dhalla A K, "Verification of an elastic procedure to estimate follow-up". ASME PVP, Vol. 86, New York (1984), pp81-96.

3. Marriott D L, "Evaluation of Deformation or load control of stresses under inelastic conditions using elastic finite element stress analysis". Proc. ASME PVP Conf., Vol 136, Pittsburgh (1988).

4. Boyle J T & Mackenzie D, "An investigation of a simple procedure for stress categorisation". Proc. ASME PVP Conf., Vol. 210-2, San Diego, (1991), pp161-165.

5. Seshadri R & Kizhatil R K, "Inelastic analyses of pressure components using the "GLOSS" diagram". Proc. ASME PVP, Vol. 186, Nashville, pp105-113, (1990).

6. Mackenzie D & Boyle J T, "On stress categorisation by the reduced modulus method". Under review, ASME j. Pres. Ves. Tech.

7. Mackenzie D & Boyle J T, "Assessment of classification procedures for finite element stresses". To be presented at Int. Conf. on Pres. Ves. Tech., Dusseldorf, June 1992.

8. Mackenzie D & Boyle J T, "A method of estimating limit loads by iterative elastic analysis I - simple examples," Submitted for publication.

9. Nadarajah C, Mackenzie D & Boyle J T, "A method of estimating limit loads by iterative elastic analysis II - nozzle sphere intersections with internal pressure and radial load," Submitted for publication.

10. Shi J, Mackenzie D & Boyle J T, "A method of estimating limit loads by iterative elastic analysis III - torispherical heads," Submitted for publication.

11. Seshadri R & Fernando C P D, "Limit loads of mechanical components and structures using the GLOSS R-Node method". ASME PVP, Vol. 210-2, San Diego, (1991), pp125-134.

12. Shield R T & Drucker D C, "Design of thin-walled torispherical and toriconical pressure-vessel heads," J. App. Mech. 28, 292 (1961).

13. Gerdeen J C & Hutula D N, "Summary report on plastic limit analysis of hemispherical and toriconical head pressure vessels," WRC Bulletin 163.

D. Mackenzie

C. Nadarajah

J. Shi

J. T. Boyle

Department of Mechanical Engineering.
University of Strathclyde.
Glasgow, Scotland, U.K.

Simple Bounds on Limit Loads by Elastic Finite Element Analysis

A method for bounding limit loads by an iterative elastic continuum finite element analysis procedure, referred to as the elastic compensation method, is proposed. A number of sample problems are considered, based on both exact solutions and finite element analysis, and it is concluded that the method may be used to obtain limit-load bounds for pressure vessel design by analysis applications with useful accuracy.

1 Introduction

In current practice, pressure vessel design by analysis is most commonly based on elastic finite element analysis and the rules defined in Codes such as the ASME Boiler and Pressure Vessel Code Sections III and VIII (Division 2) [1] and BS5500 [2]. This approach gives rise to two significant problems in the design: elastic analysis is used to assess possible inelastic failure mechanisms and the design by analysis rules are essentially based on shell theory. These problems introduce the concept of *stress categories* into the design procedure: the designer performs the analysis and partitions the calculated stresses into *peak*, *primary* and *secondary* stress categories, each of which is associated with distinct failure mechanisms, (fatigue, gross distortion and ratcheting, respectively) and subject to different limiting values. Code guidelines are given for categorization of stresses at particular locations arising from specific loading; however, these guidelines are often based on shell theory concepts such as membrane and bending stresses which are not directly applicable to 2-D and 3-D solid finite element results. A number of categorization techniques (such as stress linearization [3] and reduced modulus categorization methods [4]) have been proposed to aid the designer in appropriate categorization of stress; however, to date, no satisfactory solution has been found [5, 6] and stress categorization remains problematic.

The foregoing problems essentially arise from current practice: the Code rules in fact allow the designer to circumvent categorization problems by performing *plastic* or *limit* analyses of the component which, unlike elastic analysis, take account of stress redistribution upon yield. (Indeed, it has recently been argued that plastic analysis should be the preferred method for assessing failure modes associated with gross distortion due to a single application of pressure [7].) Plastic and limit analysis can be performed using nonlinear finite element programs; however, nonlinear finite element analysis is intrinsically more difficult to perform than elastic analysis: material models must be defined, the iterative solution procedure must be suitably controlled, and much greater computing resources are required. In order to make the transition from elastic to inelastic or limit-load-based design for real structures, simplified analysis methods are required.

One simplified method for calculating lower-bound limit loads by iterative elastic finite element analysis has previously been presented (see references [8–11]). The *elastic compensation method* was developed from the reduced modulus stress categorization method [12], in which the effects of material inelasticity are simulated by repeated elastic analyses in which the elasticity modulus of the component is systematically reduced at regions of high stress. Marriott proposed that this method could be extended to limit analysis by using modulus reduction techniques in conjunction with the *lower-bound limit-load theorem* [13]. An alternative method of calculating limit loads by repeated elastic analysis has been proposed by Seshadri et al. [14]. In the GLOSS r-node method, statically determinate stresses at locations referred to as r-nodes are identified by iterative elastic analysis in which regions of high stress have their modulus reduced, while regions of low stress have theirs increased. The stresses at the r-node locations are insensitive to the assumed material model and considered to be reference stresses similar to creep reference stresses [15].

The object of the elastic compensation method as defined in references [8–11] is to establish a stress field suitable for substitution into the lower-bound theorem by systematically modifying the local elastic modulus in a finite element model so as to cause the stress to redistribute. Initially a conventional elastic finite element analysis is performed for an arbitrary load set, P_1. This initial homogeneous isotropic solution is taken as iteration zero in a series of linear elastic analyses, in which the elastic modulus of each element is modified according to an expression of the form

$$E_i = E_{(i-1)} \frac{\sigma_n}{(\sigma_{(i-1)})}$$

where subscript i is the iteration number, σ_n a nominal stress value, and $\sigma_{(i-1)}$ the maximum (unaveraged) nodal equivalent stress associated with the element calculated in the previous iteration. This iterative procedure redistributes the stress in the component and over a number of iterations the net effect is

Contributed by the Pressure Vessels and Piping Division for publication in the JOURNAL OF PRESSURE VESSEL TECHNOLOGY. Manuscript received by the PVP Division, June 29, 1992; revised manuscript received November 18, 1992. Associate Technical Editor: M. Moktarian.

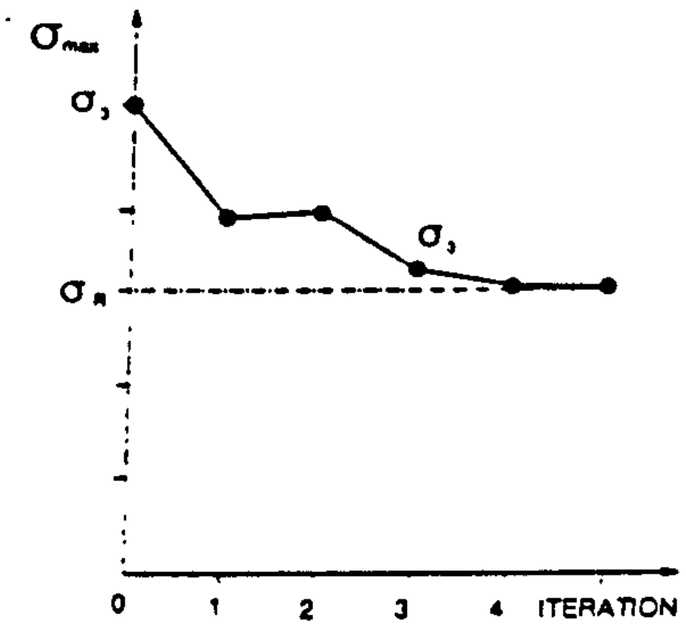

Fig. 1 Maximum stress for each iteration

to decrease the maximum stress in the model as illustrated in Fig. 1.

A lower-bound limit load can then be calculated by invoking the lower-bound limit-load theorem, which states that if a statically admissable stress field in which the stress nowhere exceeds yield exists for a given component under given loading, the loading is a lower bound on the limit load. The elastic compensation solution meets the first requirement of the lower-bound theorem in that it is statically admissible (subject to the usual finite element approximations). As the iteration solutions are linear elastic, the stress magnitude is proportional to the applied load. A lower-bound limit load can therefore be established by calculating the load required to give a maximum (unaveraged) nodal stress equal to the nominal yield strength σ_Y from proportionality. Considering the iteration giving the lowest value of maximum nodal stress σ_R

$$P_L = P_1 \frac{\sigma_Y}{\sigma_R}$$

where P_L is the best estimate of limit load given by the foregoing procedure. The applied load set P_1 is not restricted to single loads and may represent multiple forces, moments, pressures, etc., in the manner of proportional loading in conventional limit analysis. This paper extends the foregoing method to allow calculation of limit-load bounds by considering the upper-bound limit-load theorem.

2 Upper-Bound Limit Loads

The upper-bound limit-load theorem states that if, for a given load set, the rate of dissipation of internal energy in a body is equal to the rate at which external forces do work in any postulated mechanism of deformation, the applied load set will be equal to or greater than the plastic collapse load [16]. Mathematically, a complete plastic collapse solution requires definition of P and σ, an equilibrium set of loads and stresses respectively, and $\dot{\epsilon}$ and $\dot{u}$, a geometrically compatible set of displacement and strain increments, respectively. An upper-bound solution requires only a *partial* or *incomplete* plastic collapse solution to be defined; specifically, $\dot{u}^*$ and ϵ^*, representing any compatible sets of displacement and strain increments, respectively, which define a geometrically possible mode of deformation. The asterisk notation therefore denotes a solution which is incomplete in the sense that the stress field is not defined. Applying virtual work to the problem, it can be shown [16]

$$\Sigma P\dot{u}^* \le \int_V \dot{D}^* dV \qquad (1)$$

where $\dot{D}^*$ is the increment of dissipation of energy per unit volume calculated for the incomplete solution. The increment of energy dissipation per unit volume for a Tresca perfectly plastic material is given by the expression

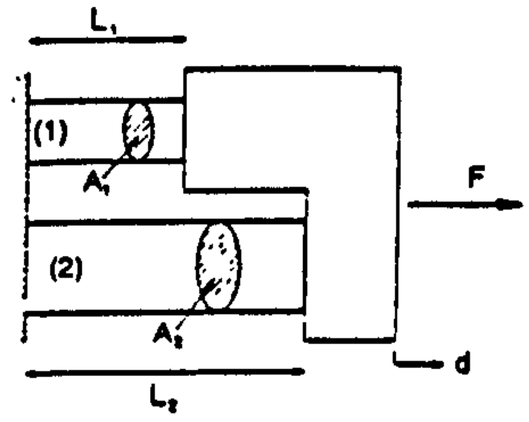

Fig. 2 Two-bar structure

$$\dot{D}^* = \sigma_Y |\dot{\epsilon}^*|_{max}$$

where $|\dot{\epsilon}^*|$ is the greatest principal strain rate magnitude. In the case of a Mises perfectly plastic material, the more complex expression

$$\dot{D}^* = \sigma_Y \sqrt{\frac{2}{3}(\dot{\epsilon}_1^{*2} + \dot{\epsilon}_2^{*2} + \dot{\epsilon}_3^{*2})}$$

is valid, where $|\dot{\epsilon}_i^*|: i = 1, 2, 3$ are the principal strain rates.

The upper-bound theorem requires the definition of a geometrically possible mode of deformation for the component: essentially, compatible sets of displacement and strain increments must be defined. This is done automatically when the elastic compensation iteration procedure is applied to a finite element model. The elastic compensation procedure results in an anisotropic inhomogeneous linear elastic solution, the compatible displacement and strain fields of which can be used to define a geometrically possible mode of deformation of the structure.

An upper-bound limit load for a structure can be obtained by substituting the elastic compensation displacement increment field $\dot{u}^*$ and strain increment field $\dot{\epsilon}^*$ into the upper-bound theorem as expressed in Eq. (1). However, this approach can lead to practical problems as calculating the work term can be laborious if corresponding load and displacement vectors are not directly accessible in the finite element program, (pressure loads on nonplanar surfaces present particular problems). In practice, it is more convenient to take advantage of the linear elastic nature of the elastic compensation solution: as the solution is elastic, the *external work done* must equal the *elastic strain energy* of the structure; thus

$$\Sigma P\dot{u}^* = \int_V \sigma\dot{\epsilon}^* dV$$

where σ is the elastically calculated stress, and $\dot{\epsilon}^*$ the elastically calculated strain increment. Thus, the upper-bound theorem inequality may be written

$$\int_V \sigma\dot{\epsilon}^* dV \le \int_V \dot{D}^* dV \qquad (2)$$

Example 1: Two-Bar Structure. The limit load of a simple two-bar structure as illustrated in Fig. 2 was considered in reference [8], where it was shown that the limit load given by the elastic compensation method was identical to the exact limit load, given by the expression

$$\frac{F_L}{F_Y} = \frac{L_2(A_1 + A_2)}{A_1L_2 + A_2L_1}$$

where F_L and F_Y represent limit load and yield load, respectively. The same result is found if the elastic compensation solution is substituted into the upper-bound limit-load theorem as given in the foregoing. The elastic stress in each bar may be evaluated simply as

$$\sigma_1 = \frac{FE_1L_2}{A_1E_1L_2 + A_2E_2L_1} \quad \sigma_2 = \frac{FE_2L_1}{A_1E_1L_2 + A_2E_2L_1}$$

$$\frac{\sigma_1}{\sigma_2} = \frac{E_1L_2}{E_2L_1}$$

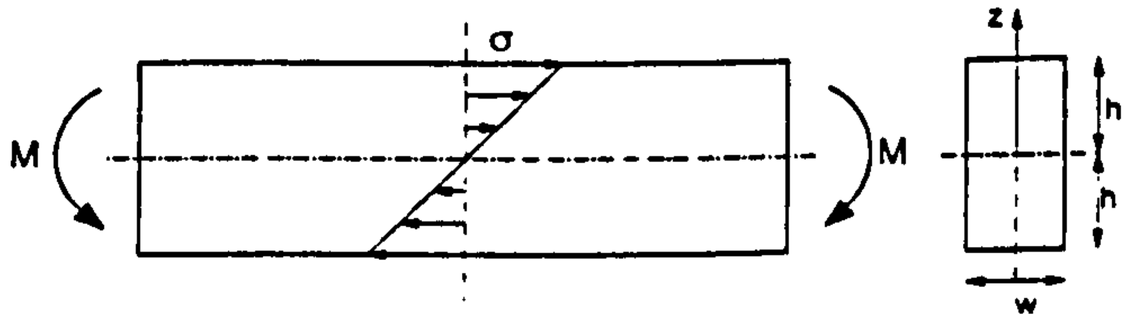

Fig. 3 Beam under pure bending

where initially $E_1 = E_2 = E_o$. Assuming bar 2 to be longer than bar 1, first yield will occur in bar 1 when $F = F_Y$

$$\sigma_1 = \frac{F_Y L_2}{A_1 L_2 + A_2 L_1} = \sigma_Y$$

Using *elastic compensation*, the elastic modulii in the bars are corrected based on the results of the initial elastic analysis according to the expression

$$E_m = E_o \frac{S}{\sigma}$$

where E_m is the modified modulus, E_o is the original modulus, σ the elastically calculated stress in the bar, and S an arbitrarily chosen value of stress. Substituting the expression for corrected modulus into the bar stress equations gives

$$\sigma_1 = \frac{F}{A_1 + A_2} \quad \sigma_2 = \frac{F}{A_1 + A_2}$$

that is, $\sigma_1 = \sigma_2$. Applying the upper-bound theorem to the elastic compensation analysis gives

$$\int_V \sigma \epsilon dV = \int_V \sigma_Y \epsilon dV$$

which simplifies to

$$\sum_{i=1}^{2} \sigma_i \epsilon_i V_i = \sum_{i=1}^{2} \sigma_Y \epsilon_i V_i \Rightarrow \sigma_1 = \sigma_2 = \sigma_Y \simeq \frac{F_L}{A_1 + A_2}$$

for the simple bar structure. Substituting the expressions for σ_1, σ_2 and σ_Y into the foregoing gives

$$\frac{F_L}{F_Y} = \frac{L_2(A_1 + A_2)}{A_1 L_2 + A_2 L_1}$$

which agrees with the exact solution.

Example 2: Beam Under Pure Bending. The limit load of a rectangular beam under a pure bending moment as illustrated in Fig. 3 was considered in reference [8], where it was shown that the limit load given by the elastic compensation method was identical to the exact limit load

$$M_L = \frac{3}{2} M_Y$$

The same result is found if the elastic compensation solution is substituted into the upper-bound limit-load theorem as given in the foregoing. Applying the elastic compensation procedure to the beam results in the following strain and stress distributions [8]:

$$\epsilon_{(z)} = \kappa z = \frac{2}{3} \frac{M^2 z}{E_o \alpha M_Y I}$$

$$\sigma_{(z)} = E_{(z)} \epsilon_{(z)} = \frac{2}{3} \frac{Mh}{I}$$

where E_o is the initial elastic modulus, M_Y the moment at first yield, and α an arbitrary constant such that $0 < \alpha < 1$. Considering symmetry, applying the upper-bound theorem gives

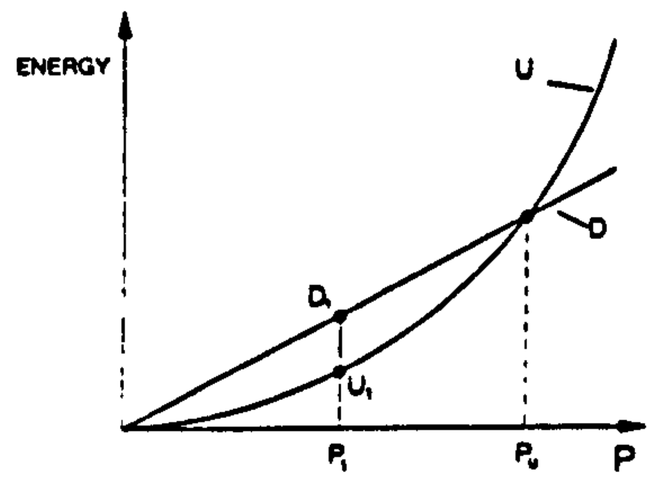

Fig. 4 Plot of strain energy and energy dissipation against applied external load

$$2 \int_0^h \sigma \epsilon dz = 2\sigma_Y \int_0^h \epsilon dz$$

or

$$\frac{4}{9} \frac{M^3 h^3}{E_o \alpha M_Y I^2} = \frac{2}{3} \sigma_Y \frac{M^2 h^2}{E_o \alpha M_Y I}$$

which simplified and rearranged yields the exact limit load

$$M_L = \frac{3}{2} M_Y$$

3 Upper-Bound Limit Loads by FEA

In a linear elastic analysis, the upper-bound theorem may be expressed by inequality (2)

$$\int_V \sigma \dot{\epsilon}^* dv \leq \int_V \dot{D}^* dV$$

or

$$U \leq D$$

The strain energy U of a linear elastic body varies with the applied load set squared. The dissipation of internal energy D varies directly with the applied load set. Thus,

$$U = \int_V \sigma \dot{\epsilon}^* dv = AP^2 \tag{3a}$$

$$D = \int_V \dot{D}^* dV = BP \tag{3b}$$

Plotting strain energy and energy dissipation against applied external load gives curves of the form shown in Fig. 4.

When the strain energy and energy dissipation curves intersect, the load is an upper bound on the limit load. The intersection can be calculated by performing an analysis for an arbitrary load set P_1 and evaluating the corresponding strain energy U_1 and energy dissipation D_1. Substituting the calculated values into Eqs. (3*a*) and (3*b*) gives

$$A = \frac{U_1}{P_1^2} \quad B = \frac{D_1}{P_1}$$

and the strain energy and energy dissipation may be expressed as

$$U = \frac{U_1}{P_1^2} P^2 \quad D = \frac{D_1}{P_1} P$$

The applied load set P is an upper-bound limit P_u load when $U = D$; that is,

$$\frac{U_1}{P_1^2} P_u^2 = \frac{D_1}{P_1} P_u$$

and, hence, the upper-bound limit load is given by the expression

Fig. 5 Beam under combined loading

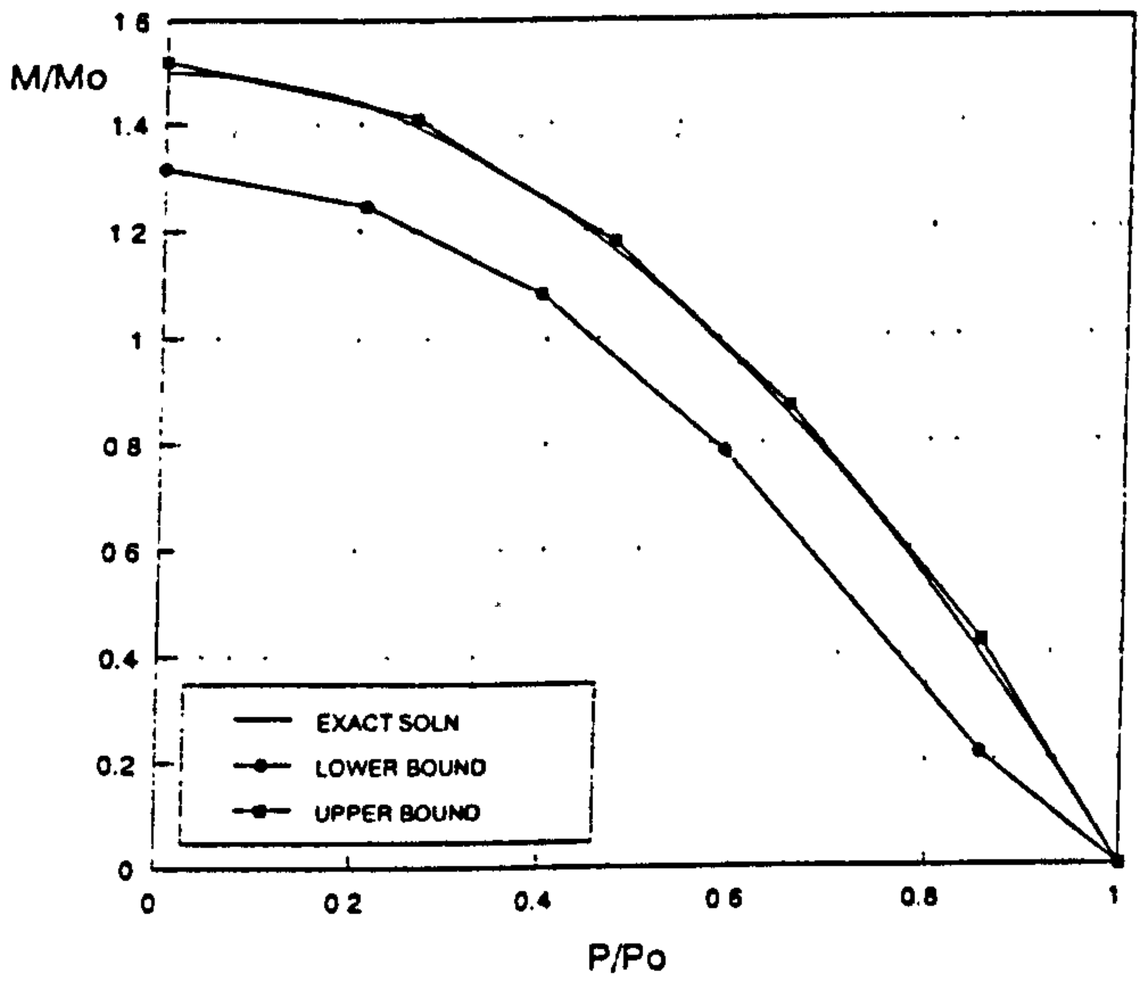

Fig. 6 Beam under combined loading limit-load bounds by iterative elastic analysis

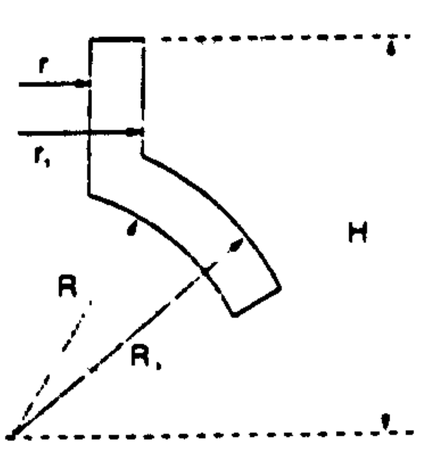

Fig. 7 Nozzle/sphere intersection

$$P_u = \frac{D_1}{U_1} P_1$$

4 FEA Examples

In this section a number of example problems are investigated by finite element analysis using the program ANSYS [17]. The upper-bound solutions calculated in the finite element analysis are approximate as the strain energy and energy dissipation integrals are calculated approximately by a summation based on element centroidal data and volume. Nonlinear elastic-plastic finite element analysis, used for comparison purposes, is based on an elastic-perfectly plastic material model.

Beam Under Bending and Tension. As an example of the foregoing, consider a beam of unit width and depth under combined direct and bending loading, as illustrated in Fig. 5. The theoretical collapse load of a cantilever beam of unit width under direct force P and moment M is given by the expression

$$\frac{M}{M_Y} = \frac{3}{2}\left[1 - \left(\frac{P}{P_Y}\right)^2\right]$$

where, for a beam of depth d, $P_Y = \sigma_Y d$ and $M_Y = \sigma_Y d^2/6$.

In the finite element model, 12 linear quadrilateral plane stress elements were taken through the depth of the beam. Up to 8 iterations were performed for each model and the modulus correction equation used throughout was

$$E_i = E_{(i-1)} \frac{20E3}{\sigma_{(i-1)\max}}$$

where $\sigma_{(i-1)\max}$ is the maximum (unaveraged) nodal stress calculated in the previous analysis. The bounded limit surface given by the elastic compensation procedure is compared with the exact solution in Fig. 6.

Nozzle/Sphere Intersection. Limit-load bounds were calculated for six thin nozzle/sphere intersections. The models were created from higher order (quadratic) axisymmetric elements with three or four elements through wall thickness. The modulus correction equation used was

$$E_i = E_{(i-1)} \frac{200}{\sigma_{(i-1)\max}}$$

where $\sigma_{(i-1)\max}$ is the maximum (unaveraged) nodal stress calculated in the previous analysis.

Series A intersections, defined in Table 1 and Fig. 7, were subjected to internal pressure loading only. Lower and upper-bound limit loads obtained by the elastic compensation procedure are compared with elastic-perfectly plastic finite element analysis, and the lower-bound results of Robinson and Gill [18] in Table 2. Series B intersections, defined in Table 3 and Fig. 7 were subject to radial downward load on the nozzle only.

Lower and upper-bound limit loads obtained by the elastic compensation procedure are compared with elastic-perfectly plastic finite element analysis and with rigid-perfectly plastic analysis upper and lower-bound solutions in which the nozzle was considered to be a rigid boss [19] in Table 4.

Torispherical Head. Limit-load bounds were calculated for four torispherical heads as defined in Fig. 8 and Table 5.

Table 1 Series A nozzle dimensions

NOZZLE	r_i (mm)	r_o (mm)	R_i (mm)	R_o (mm)	H (mm)
A1	150	155	500	505	600
A2	100	120	500	520	600
A3	250	255	500	520	460
A4	250	260	500	510	550

Table 2 Series A limit pressures (N/mm^2)

NOZZLE	Lower Bound	E-P	Upper Bound	Robinson & Gill [9]
A1	2.09	2.34	2 8	2.15
A2	15 9	17 8	18 4	16
A3	5 87	—	6 4	6 48
A4	4 08	—	4 86	4 4

Table 3 Series B nozzle dimensions

NOZZLE	r_i (mm)	r_o (mm)	R_i (mm)	R_o (mm)	H (mm)
B1	150	155	500	505	600
B2	100	120	500	520	600

Table 4 Series B limit pressures (N/mm^2)

Specimen	Lower Bound	E-P	Upper Bound	Lower Bound [19]	Upper Bound [19]
B1	47.5	57.5	63.7	33.71	37.46
B2	104.2	117	142.5	170	233.3

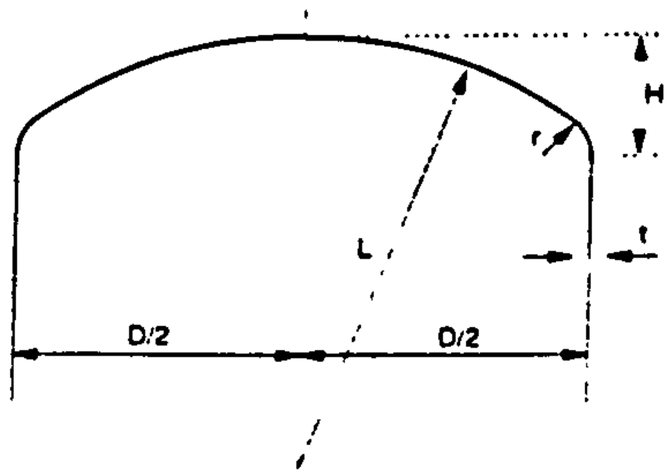

Fig. 8 Torispherical head geometry

Finite element models were created in ANSYS using a uniform mesh with six higher order (quadratic) quadrilateral axisymmetric elements through wall thickness. The modulus correction equation used was

$$E_i = E_{(i-1)} \frac{209}{\sigma_{(i-1)\max}}$$

where $\sigma_{(i-1)\max}$ is the maximum (unaveraged) nodal stress calculated in the previous analysis. The calculated limit-load bounds are compared with the elastic-plastic calculated limit loads (pressure at 1 percent equivalent strain) in Table 6.

5 Discussion and Conclusion

In general, the elastic compensation limit loads calculated in the foregoing sample analyses are found to be of useful accuracy, particularly in the case of the upper-bound loads, which are very close to the inelastically calculated limit load. However, it should be noted that the calculated upper-bound limit loads may not be true upper bounds as the energy integrals calculated in the sample analyses are **approximate** values, based on centroidal stresses and strains. Elements which integrate the energy terms by Gaussian quadrature are currently being developed by a colleague of the writers and it may be that the true upper-bound loads are higher.

The proposed method has several features convenient to the design engineer: it can be implemented automatically in standard linear elastic commerical finite element programs (thus, minimal manual intervention is required) and, unlike nonlinear methods, detailed inelastic material models, loading histories and nonlinear iteration/convergence controls are not required. However, investigation of the procedure is at an early stage and further work is required to examine the effects of mesh density, etc., on the accuracy of the solution [20].

Acknowledgments

This research was funded by the UK Science and Engineering Research Council. Mr. C. Nadarajah is funded by ICI plc. Use of the ANSYS software through an educational license from Swanson Analysis is also acknowledged.

Table 5 Head shape parameters and dimensions

HEAD	t/D	h/D	r/D	R/D	D (mm)	t (mm)
HD31	0.015	0.151	0.092	1.541	940	14
HD32	0.015	0.207	0.070	0.813	940	14
HD4	0.050	0.250	0.125	0.750	940	47
HD26	0.050	0.207	0.125	1.021	940	47

Table 6 Torispherical end limit pressures (N/mm^2)

Head	Lower Bound	Elastic-Plastic	Upper Bound
HD31	2.32	2.88	2.96
HD32	3.71	4.72	5.02
HD26	16.12	19.93	20.75
HD4	21.66	23.61	24.33

References

1 American Society of Mechanical Engineers, ASME Boiler and Pressure Vessel Code, 1989.

2 British Standards Institution, "BS5500: Specification for Unfired Fusion Welded Pressure Vessels," 1991.

3 Kroenke, W. C., "Classification of Finite Element Stresses According to ASME Section III Stress Categories," *Proceedings, 94th ASME Winter Annual Meeting*, 1973.

4 Dhalla, A. K., "A Simplified Procedure to Classify Stresses for Elevated Temperature Service," *Proceedings*, ASME-PVP, Vol. 120, San Diego, Calif., 1987, pp. 177-188.

5 Hechmer, J. L., and Hollinger, G. L., "Three-Dimensional Stress Criteria," ASME PVP, Vol. 210-2, San Diego, 1991, pp. 181-191.

6 Mackenzie, D., and Boyle, J. T., "On Stress Categorization by Reduced Modulus Analysis," ASME JOURNAL OF PRESSURE VESSEL TECHNOLOGY, submitted for publication.

7 Kalnins, A., and Updike, D. P., "Role of Plastic Limit and Elastic-Plastic Analyses in Design," ASME PVP, Vol. 210-2, San Diego, 1991, pp. 135-142.

8 Mackenzie, D., and Boyle, J. T., "A Method of Estimating Limit Loads by Iterative Elastic Analysis. I—Simple Examples," *International Journal of Pressure Vessels and Piping*, Vol. 53, No. 1, 1993, pp. 77-95.

9 Nadarajah, C., Mackenzie, D., and Boyle, J. T., "A Method of Estimating Limit Loads by Iterative Elastic Analysis. II—Nozzle Sphere Intersections With Internal Pressure and Radial Load," *International Journal of Pressure Vessels and Piping*, Vol. 53, No. 1, 1993, pp. 97-119.

10 Shi, J., Mackenzie, D., and Boyle, J. T., "A Method of Estimating Limit Loads by Iterative Elastic Analysis. II—Torispherical Heads Under Internal Pressure," *International Journal of Pressure Vessels and Piping*, Vol. 53, No. 1, 1993, pp. 121-142.

11 Mackenzie, D., Shi, J., Nadarajah, C., and Boyle, J. T., "An Iterative Elastic Analysis Procedure for Estimating Lower-Bound Limit Loads," *Proceedings*, ASME PVP, New Orleans, La., 1992.

12 Jones, G. L., and Dhalla, A. K., "Classification of Clamp Induced Stresses in Thin-Walled Pipe," *Proceedings*, ASME PVP-Vol. 81, New York, N.Y., 1981.

13 Marriott, D. L., "Evaluation of Deformation or Load Control of Stresses Under Inelastic Conditions Using Elastic Finite Element Stress Analysis," *Proceedings*, ASME PVP-Vol. 136, Pittsburgh, Pa., 1988.

14 Seshadri, R., and Fernando, C. P. D., "Limit Loads of Mechanical Components and Structures Using the GLOSS R-Node Method," ASME PVP-Vol. 210-2, San Diego, Calif., 1991, pp. 125-134.

15 Boyle, J. T., and Spence, J., *Stress Analysis for Creep*, Butterworths, 1983.

16 Calladine, C. R., *Plasticity for Engineers*, Ellis Horwood Ltd., Chichester, 1985.

17 DeSalvo, G. J., and Gorman, R. W., *ANSYS User's Manual*, Swanson Analysis Systems Inc., USA.

18 Robinson, M., and Gill, S. S., "Limit Analysis of Flush Radial and Oblique Cylindrical Nozzles in Spherical Pressure Vessels. Part I: A Parametric Survey of Results," *International Journal of Pressure Vessel and Piping*, Vol. 1, No. 3, July 1973, pp. 199-231.

19 Palusamy, S., "Limit Pressure of Spherical Shells Subjected to External Axial Force," *Nuclear Engineering Design*, Vol. 16, 1971, pp. 13-23.

20 Mackenzie, D., Shi, J., and Boyle, J. T., "Finite Element Modelling for Limit Analysis by the Elastic Compensation Method," *Computers & Structures*, under review.

Pergamon

Computers & Structures Vol. 51, No. 4, pp. 403–410, 1994

0045-7949/94 $7.00 + 0.00

FINITE ELEMENT MODELLING FOR LIMIT ANALYSIS BY THE ELASTIC COMPENSATION METHOD

D. MACKENZIE,† J. SHI and J. T. BOYLE
Department of Mechanical Engineering, University of Strathclyde, Glasgow, U.K.

(*Received* 20 *November* 1992)

Abstract—The elastic compensation method is a continuum finite element based method for calculating lower bound limit loads by iterative elastic analysis. This paper considers the effects the finite element mesh density, element order and the iterative elastic procedure itself have on the calculated limit loads for a number of sample problems. It is found that the calculated value of lower bound limit load improves with mesh density and higher element order. It is noted that in practice designers are often restricted to working with fairly course meshes (due to computational considerations) and a method for calculating approximate limit loads using fairly coarse meshes is proposed.

1. INTRODUCTION

Structural limit loads can be calculated by a number of analysis techniques, the state of the art being incremental finite element analysis by specialist non-linear programs such as ABAQUS. However, calculation of limit loads by detailed inelastic analysis can be difficult and expensive: material models must be defined, appropriate load step and iteration controls applied and greater computing resources are required than for a comparable elastic analysis. In practice, limit analysis for design considerations is often performed using simplified methods, most commonly based on limit load *bounding theorems*. The bounding theorem approach has several advantages over elastic–plastic analysis: the solution is path independent, detailed material models are not required (the material is implicitly assumed to be rigid–perfectly plastic or elastic–perfectly plastic) and the solution procedure is linear (that is, non-iterative). The disadvantage of simple methods based on bounding theorems is that they cannot be used for detailed calculations of plastic deformation: they address structural strength, not stiffness.

One area in which calculation of limit loads is of great interest is pressure vessel design (where gross plastic collapse is a possible failure mechanism) [1]. Recently, simple finite element based methods for calculating lower bound and approximate limit loads of pressurised components (modelled by continuum finite elements) have been proposed by Marriot [2] and Seshadri and Fernando [3] respectively. Both of these methods are based on iterative *elastic* analysis. In Marriott's method, the elastic moduli of highly loaded elements are systematically reduced in an iterative elastic analysis procedure so as to cause the stress to redistribute. If, after redistribution, the maximum stress in the model is less than the yield, the applied load satisfies the lower bound limit load theorem:

> If a statically admissible stress field in which the stress nowhere exceeds the yield exists for a given component under a given loading system, the loading is a lower bound limit load.

In Seshadri's method, the GLOSS r-node method, iterative elastic analysis is used to identify the location of *statically determinate* stresses in the component; that is, stresses which are effectively insensitive to the assumed material model. These positions are defined as redistribution-nodes, or r-nodes, and r-node stresses treated in a similar manner to reference stresses in the analysis of creep [4]. The r-node method is used to calculate approximate limit loads for components based on the assumption that plastic collapse will not occur provided the r-node stresses are less than yield. The present writers combined aspects of both the above methods in a third simplified method which seeks to obtain lower bound limit loads by iterative elastic (continuum) finite element analysis [5–7]. The elastic compensation method can be used to define lower bound limit loads for any structure modelled by *continuum* finite elements: that is, 2-D and 3-D solid elasticity elements. The basic procedure is described in the next section.

2. THE ELASTIC COMPENSATION METHOD

Initially, a finite element model is created (using 2-D or 3-D continuum elements) and a *nominal load* set P_d (generally comprising of a number of different types of load such as point forces, pressure, etc.), applied. A linear elastic finite element analysis is then

† Author to whom correspondence should be addressed.

performed and the linear elastic stress field obtained. This solution forms iteration zero in a series of linear elastic analyses of the model. After each iteration, the elastic modulus of each element in the model is modified according to the equation:

$$E_i = E_{(i-1)} \frac{\sigma_n}{(\sigma_{(i-1)})}, \qquad (1)$$

where subscript i is the present iteration number, σ_n a nominal stress value and $\sigma_{(i-1)}$ the maximum (unaveraged) nodal *equivalent stress* associated with the element from the previous solution. It must be ensured that the nodal stress in the divisor of the *compensation equation* (1) does not approach zero as, for example, could happen at the mid-surface of components exhibiting beam or shell type behaviour when subject to pure bending. This would lead to elements of excessively high stiffness in the model and possible numerical problems in the finite element solution.

Plotting the maximum stress in the model against iteration number results in a graph of the form shown in Fig. 1. Modifying the modulus of elasticity of the elements causes the stress to redistribute between iterations. In some cases the redistribution may cause the maximum stress in the model to increase between iterations but it is generally found that over a number of iterations there is a net decrease in maximum stress with respect to the initial solution.

The stress fields obtained for each iteration meet the lower bound limit load theorem requirement of statical admissibility (within the usual limitations of the finite element procedure) but the maximum stress may or may not violate the requirement that it should not exceed yield, depending on the magnitude of the applied load set P_d. The best value for lower bound limit load possible for a given stress distribution is one in which the maximum stress is yield. The value of the applied load giving such a maximum stress can be calculated from simple proportionality. As the iterative analyses are linear elastic, the magnitude of the maximum stress in the model is proportional to the applied load. For an arbitrary iteration, say r in

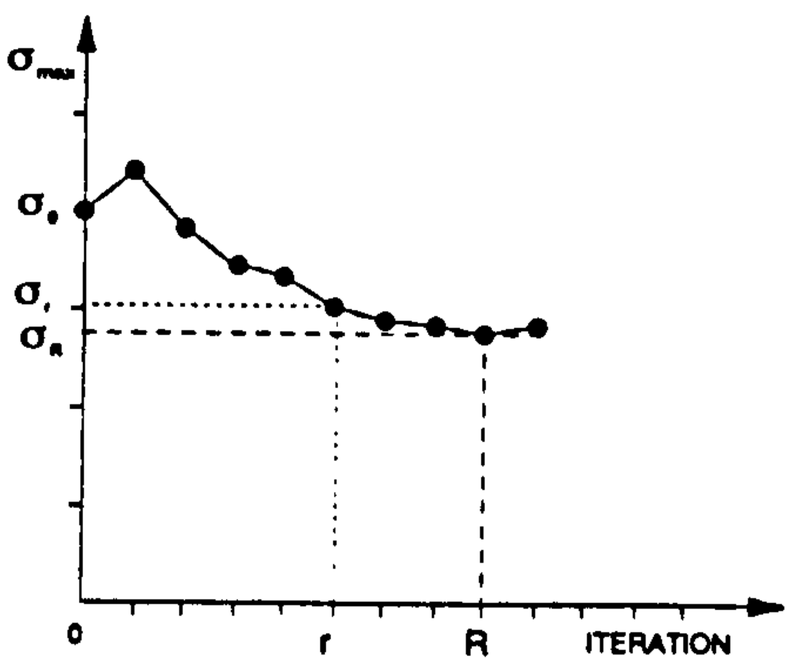

Fig. 1. Maximum stress for each iteration.

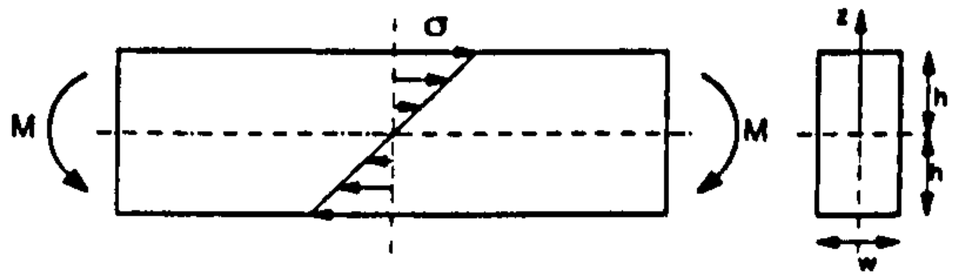

Fig. 2. Beam under pure bending.

Fig. 1, the applied load set P_d gives a maximum stress of σ_r, (which may be greater or less than yield). Thus the load set P_1 to give a maximum stress of σ_Y in the model is simply:

$$P_1 = P_d \frac{\sigma_Y}{\sigma_r}.$$

Load set P_1 is a lower bound limit load set for the component comprising of individual loads in the same proportion as they occur in the applied load set P_d. The best lower bound limit load is given by considering the solution in which the maximum stress has the lowest value, say iteration R, in which the maximum stress is σ_R. This solution gives a lower bound limit load:

$$P_L = P_d \frac{\sigma_Y}{\sigma_R},$$

where load set P_L is the best estimate of limit load given by the above procedure.

A number of limit analyses using the elastic compensation procedure have been presented in references [5–7], where it was shown that the method could be used to calculate useful lower bound limit loads in pressure vessel design. The object of this paper is to examine the effect of aspects of *finite element modelling* on the accuracy of the solution.

3. BASIC CONSIDERATIONS

Mesh density has an intrinsic and significant effect on the accuracy of limit loads given by the elastic compensation method. This can be demonstrated by considering the limit behaviour of a beam under pure bending. A closed form elastic compensation solution for the limit load of a rectangular beam under pure bending, as illustrated in Fig. 2, was presented in reference [5], where the calculated limit load was shown to agree *exactly* with the elastic-perfectly plastic solution: that is,

$$\frac{M_L}{M_Y} = 1.5,$$

where M_L is the limit moment and M_Y the moment at first yield of the beam.

In a continuum finite element analysis of such a beam, it must be discretized into a number of elements through depth. Consider a beam with six elements through depth, as shown in Fig. 3. An initial

homogeneous elastic solution based on Engineers Theory of Beam Bending gives a stress field in which the axial stress varies with z according to:

$$\sigma_{(z)} = \frac{Mz}{I}.$$

The elastic modulus of each element in the beam is modified by substituting stresses calculated in the initial solution, iteration 0, into the compensation equation:

$$E_1 = E_0 \frac{\sigma_n}{\sigma_0}$$

where σ_0 is the maximum stress calculated within the domain of the element in iteration 0. Considering symmetry, one half of the beam need be considered; elements 1–3 in Fig. 3. Applying the compensation equation gives:

$$E_{(z)} = E_1 = E_0 \frac{\sigma_n}{\sigma_{1_{max}}} \quad \text{for} \quad 0 \leqslant z \leqslant \frac{h}{3}$$

$$E_{(z)} = E_2 = E_0 \frac{\sigma_n}{\sigma_{2_{max}}} \quad \text{for} \quad \frac{h}{3} \leqslant z \leqslant \frac{2h}{3}$$

$$E_{(z)} = E_3 = E_0 \frac{\sigma_n}{\sigma_{3_{max}}} \quad \text{for} \quad \frac{2h}{3} \leqslant z \leqslant h.$$

This procedure effectively results in an inhomogeneous or composite beam model, the elastic modulus being constant in each element. Applying equilibrium to a section through the beam, noting the symmetric stress distribution, gives:

$$M = 2w \int_0^h \sigma_{(z)} z \, dz,$$

where w is the width of the beam. Assuming uniaxial stress and the plane sections remain plane:

$$\sigma = E_{(z)} \epsilon \qquad \epsilon = \kappa z$$

the beam moment–curvature equation becomes:

$$M = 2w \int_0^h E_{(z)} \kappa z^2 \, dz = \kappa I_1$$

$$I_1 = 2w \int_0^h E_{(z)} z^2 \, dz.$$

Substituting for $E_{(z)}$ in I_1 gives:

$$I_1 = 2w \left[E_1 \int_0^{h/3} z^2 \, dz + E_2 \int_{h/3}^{2h/3} z^2 \, dz + E_3 \int_{2h/3}^{h} z^2 \, dz \right]$$

$$= \frac{I}{27} [E_1 + 7E_2 + 19E_3].$$

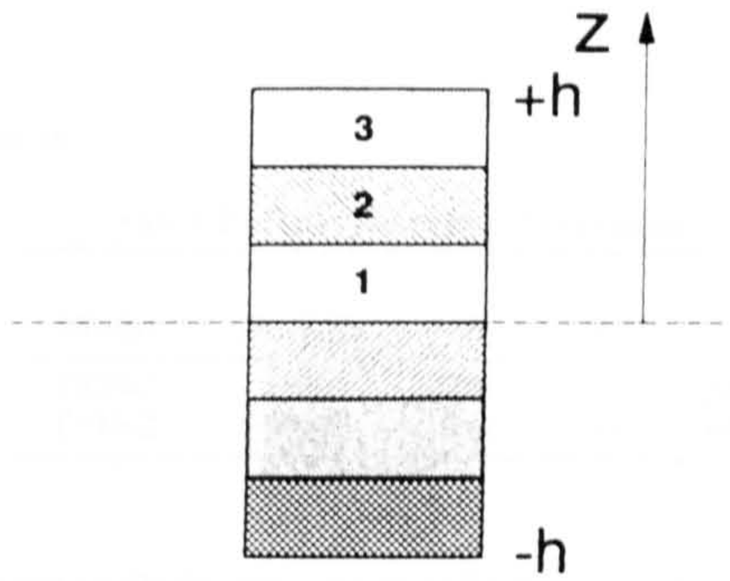

Fig. 3. Discretized beam.

From strain displacement:

$$\epsilon_{(z)} = \kappa z = \frac{Mz}{I_1} = \frac{27Mz}{I(E_1 + 7E_2 + 19E_3)} = Cz.$$

Substituting the maximum elastic stress in each element into the compensation equation and rearranging, it is found that:

$$E_1 = 3E_3 \quad \text{and} \quad E_2 = \tfrac{3}{2}E_1.$$

Therefore

$$C = \frac{27M}{I(E_1 + 7E_2 + 19E_3)} = \frac{54}{65} \frac{M}{E_3 I}.$$

From the stress–strain relationship $\sigma = E_{(z)}\epsilon$, the stress field is defined piecewise across the depth by the equations:

$$\sigma_{1(z)} = E_1 Cz \quad \text{for} \quad 0 \leqslant z \leqslant \frac{h}{3}$$

$$\sigma_{2(z)} = E_2 Cz \quad \text{for} \quad \frac{h}{3} \leqslant z \leqslant \frac{2h}{3}$$

$$\sigma_{3(z)} = E_3 Cz \quad \text{for} \quad \frac{2h}{3} \leqslant z \leqslant h.$$

Thus the stress field given by the elastic compensation procedure is *discontinuous*, as illustrated in Fig. 4, with maximum stress:

$$\sigma_m = \frac{54}{65} \frac{Mh}{I}.$$

A lower bound on the limit load is given by calculating the moment resulting in a maximum stress of yield in the beam. It is simple to show that this occurs when $M = M_L$, where:

$$\frac{M_L}{M_Y} = \frac{65}{54} = 1.2,$$

a reduction of 20% in the calculated limit load in comparison with the continuously varying elastic compensation solution.

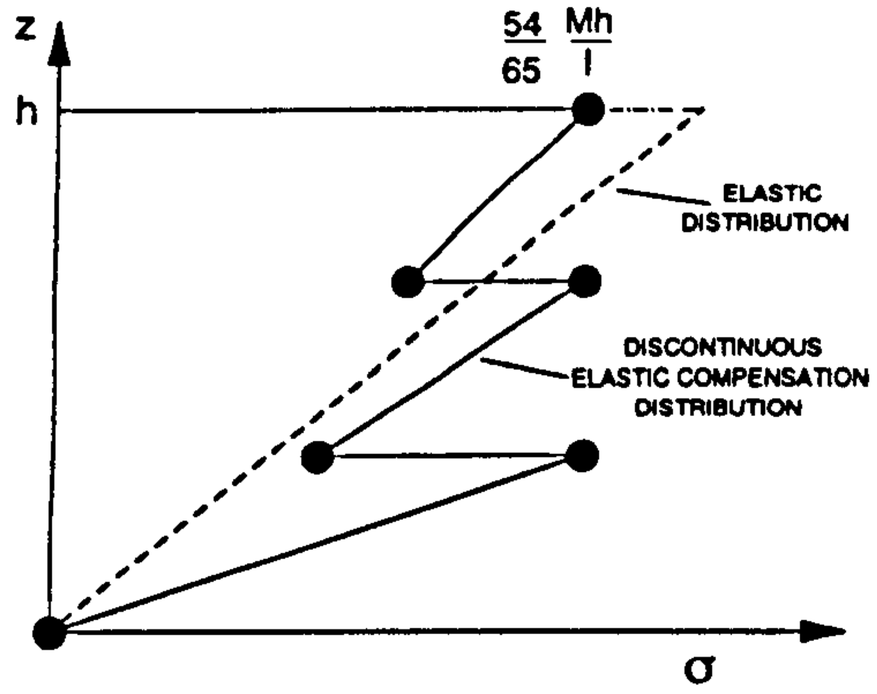

Fig. 4. Discontinuous stress distribution given by elastic compensation.

This simple problem highlights three important features of the elastic compensation procedure:

- Discretization *per se* introduces conservative error to the limit load calculation.
- In general, the modulus compensation procedure leads to *discontinuous* stress fields and care must be taken to ensure that lower bound limit load calculations are based on *unaveraged* stresses. Many commercial programs average stress results to give a smooth stress distribution by default. Smoothed stress fields may violate the lower bound theorem requirement for a statically admissible stress field, as smoothing algorithms do not take account of equilibrium. Smoothed stress fields may be used to give *approximate* limit loads but to obtain *true* lower bound limit loads unaveraged stresses must be used.
- The value of σ_n used in the compensation equation (1) has little effect on the solution and can be arbitrarily chosen (this has been verified in analyses of other sample problems in which values of half yield, two thirds yield, and yield gave almost identical solutions).

4. MODELLING CONSIDERATIONS: EXAMPLE PROBLEMS

In order to investigate the effect of a number of modelling parameters on the elastic compensation solution, a number of finite element analysis sample problems are considered: four torispherical pressure vessel heads, as defined in Fig. 5 and Table 1, and two toriconical heads, as defined in Fig. 6 and Table 2, all subject to internal pressure. Finite element analysis was performed using the commercial finite element program ANSYS. The elastic compensation procedure was performed automatically by defining ANSYS ADPL *macros*. Two types of ANSYS element were used; the four-node axisymmetric solid element STIF42 (linear with added shape functions) and the eight node axisymmetric solid element STIF82 (higher order, quadratic). Finite element models of TOR1 and CON1 (with three elements through thickness) are shown in Figs 7 and 8.

Table 1. Torispherical end dimensions

Model	D (in)	$\frac{t}{D}$	$\frac{h}{D}$	$\frac{r}{D}$	$\frac{L}{D}$
TOR1	37	0.015	0.207	0.07	0.813
TOR2	37	0.05	0.207	0.125	1.021
TOR3	37	0.07	0.207	0.07	0.813
TOR4	37	0.14	0.207	0.07	0.813

Table 2. Toriconical end dimensions

Model	D (mm)	$\frac{r}{D}$	α	t
CON1	1000	0.06	45	20
CON2	1000	0.06	75	40

4.1. *Mesh density and element order*

In any infinite element analysis, the user must define the element type and the mesh density for the model. Both these factors effect the accuracy of a conventional finite element solution and, from the simple example above, the discretization procedure is expected to effect the elastic compensation results. The effect of element order and mesh density on

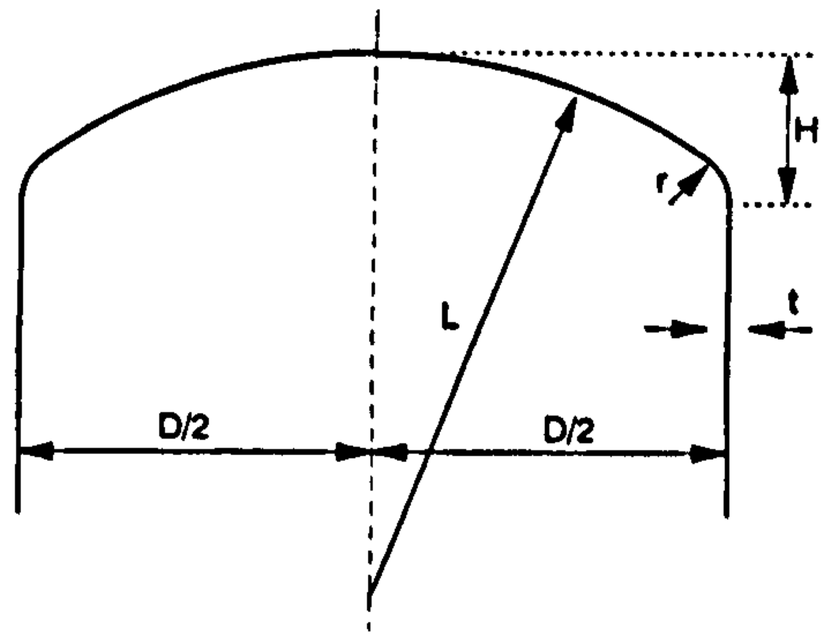

Fig. 5. Torispherical end (E = 29E6 (psi); σ_Y = 30,300 psi; ν = 0.29).

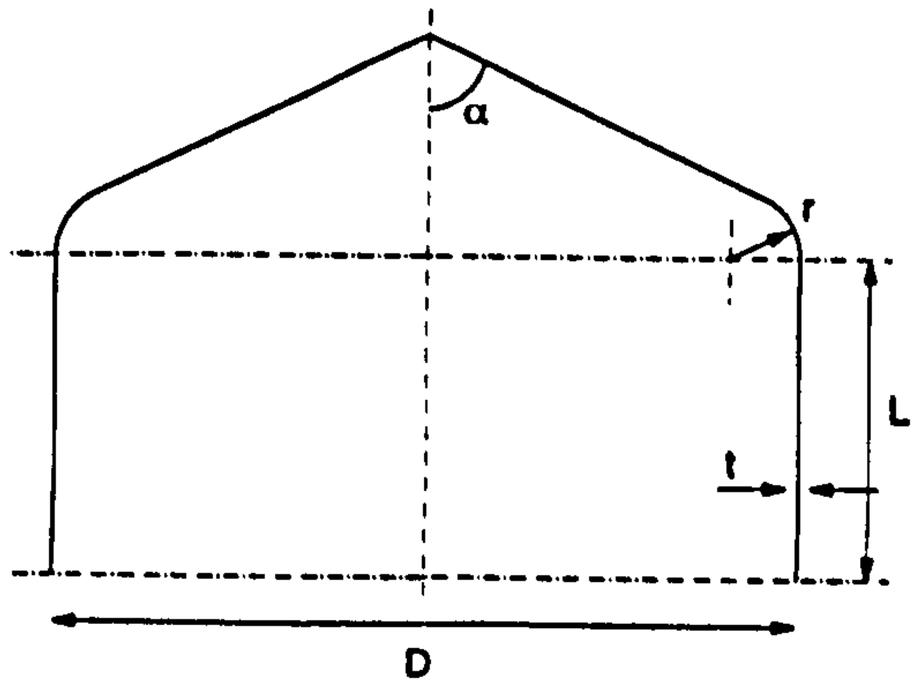

Fig. 6. Toriconical end (E = 200E3 N/mm²; ν = 0.3; σ_Y = 300 N/mm²).

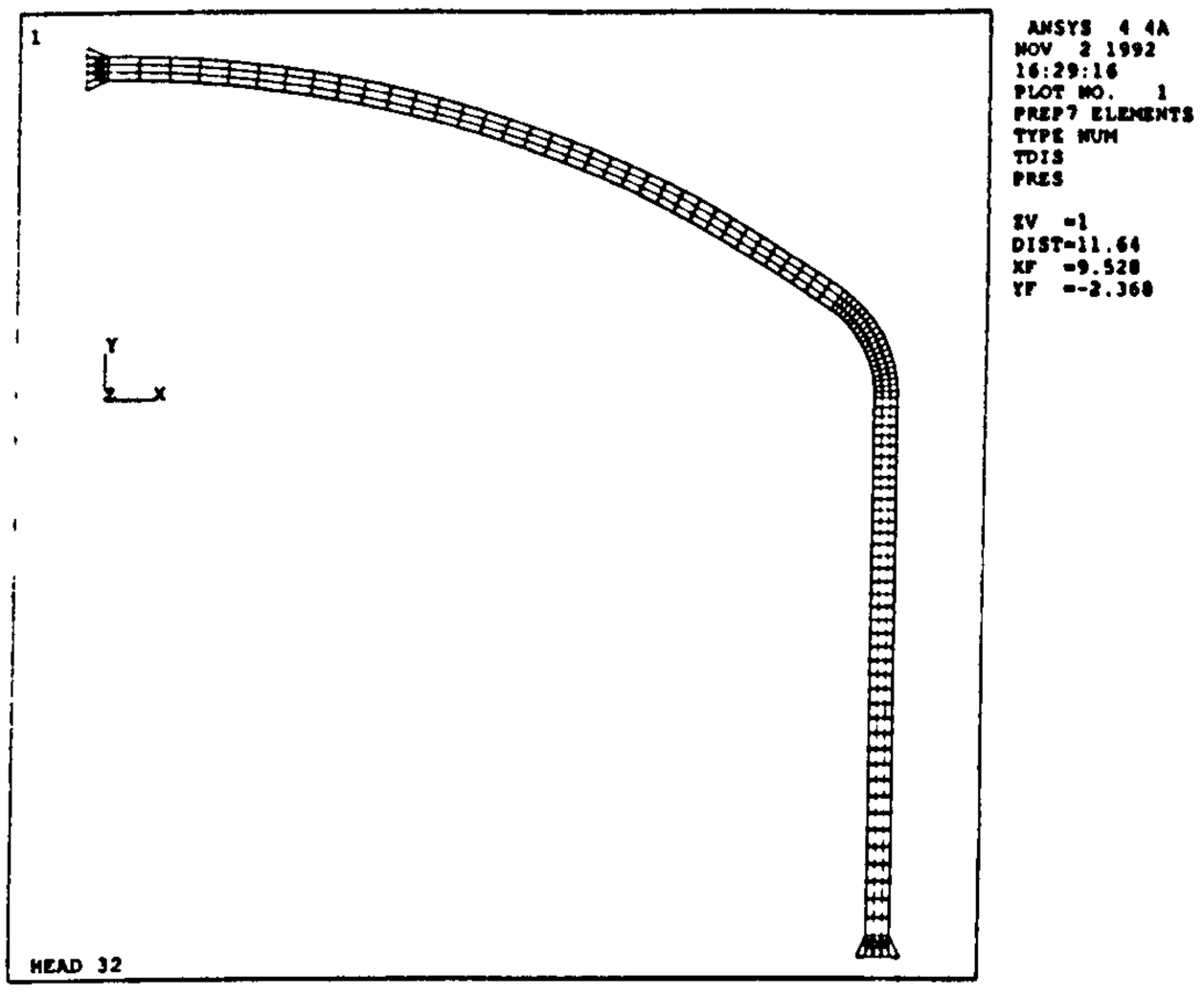

Fig. 7. TOR1 finite element model: three elements through thickness.

TOR1 and CON1 maximum stress values in the initial elastic analysis is illustrated in Figs 9 and 10, where the maximum von Mises stress $\bar{\sigma}$, normalized with respect to the maximum von Mises stress calculated for the finest STIF82 mesh, is plotted against both the *number of elements* and *number of nodes* through thickness for up to 10 uniform elements through the wall thickness.

4.2. *Variation in maximum stress with iteration*

The maximum normalized von Mises stress per iteration for models TOR1 and CON1 is plotted against iteration number for a number of mesh densities, (indicated by the number of elements through wall thickness), in Figs 11 and 12. Clearly, the effect of the elastic compensation procedure is to cause a net reduction in stress over a number of iterations, although an increase may occur between iterations in some cases. The case of stress increasing between iterations is seen more clearly in a similar plot for TOR2, as shown in Fig. 13.

4.3. *Variation of calculated limit load with mesh density*

The variation is calculated limit load with mesh density (nodes through wall) for TOR1 and CON1

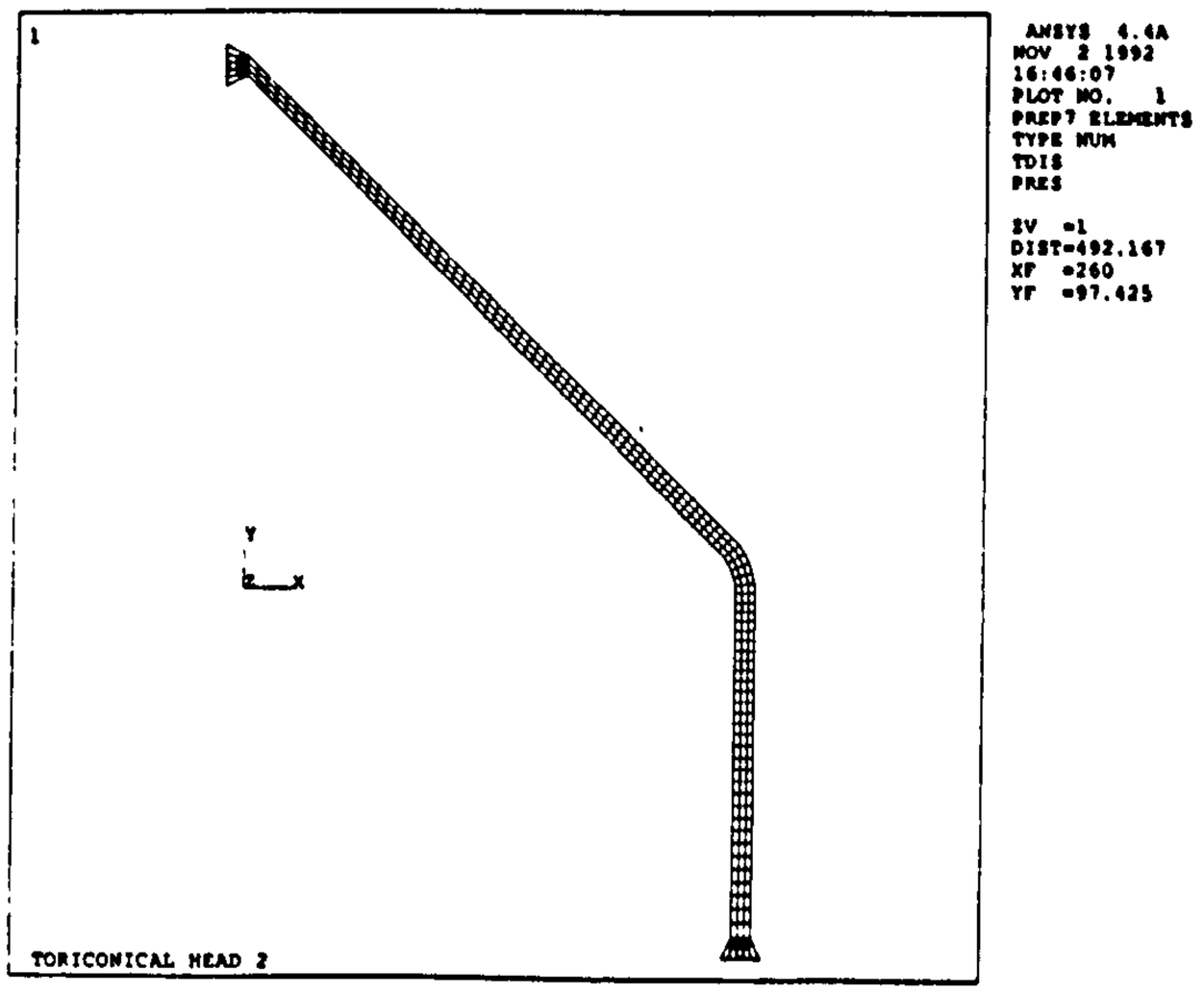

Fig. 8. CON1 finite element model: three elements through thickness.

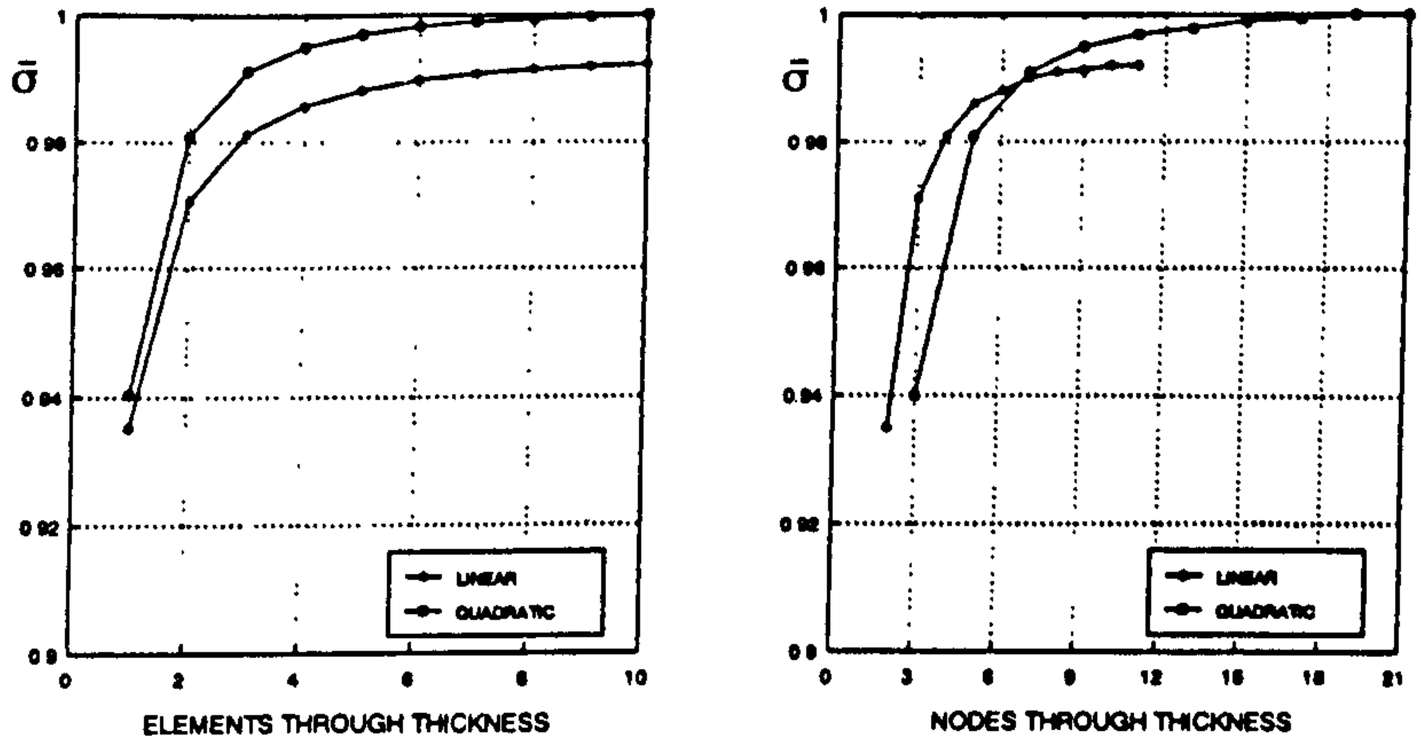

Fig. 9. TOR1 maximum normalized stress.

(iteration 8) is shown in Figs 14 and 15. The limit load for each mesh has been normalized with respect to the yield load calculated from the initial elastic analysis for *that mesh*. Both the mesh density and element order effects the calculated value of the limit load: finer meshes and higher order shape functions give better lower bound limit loads.

4.4. *Comparison with elastic–plastic analysis*

Lower bound limit loads calculated by the elastic compensation method, P_{ec}, are compared with limit loads calculated by elastic–perfectly plastic analysis, P_{ep}, in Table 3. The limit criteria for inelastic analysis was taken to be load at 1% total strain. The results shown are higher order (STIF82) meshes.

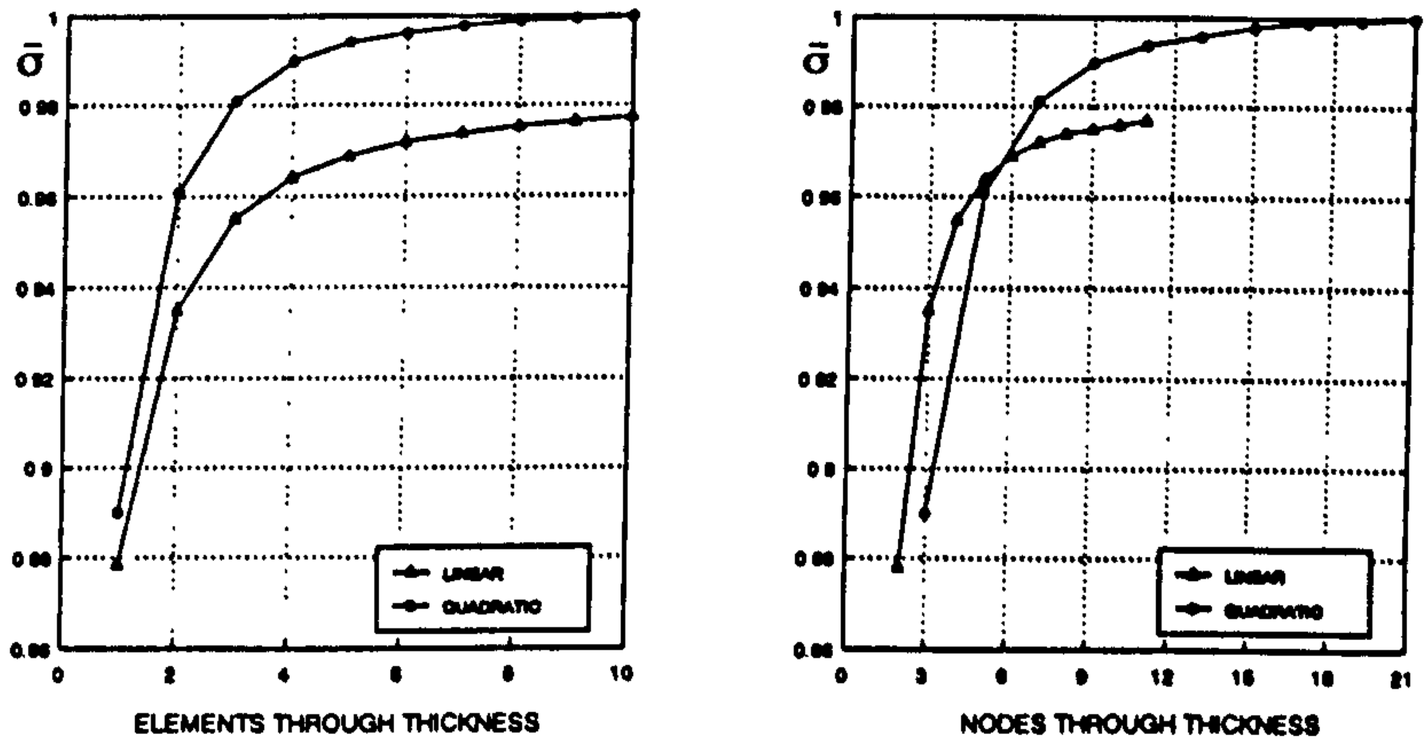

Fig. 10. CON1 maximum normalized stress.

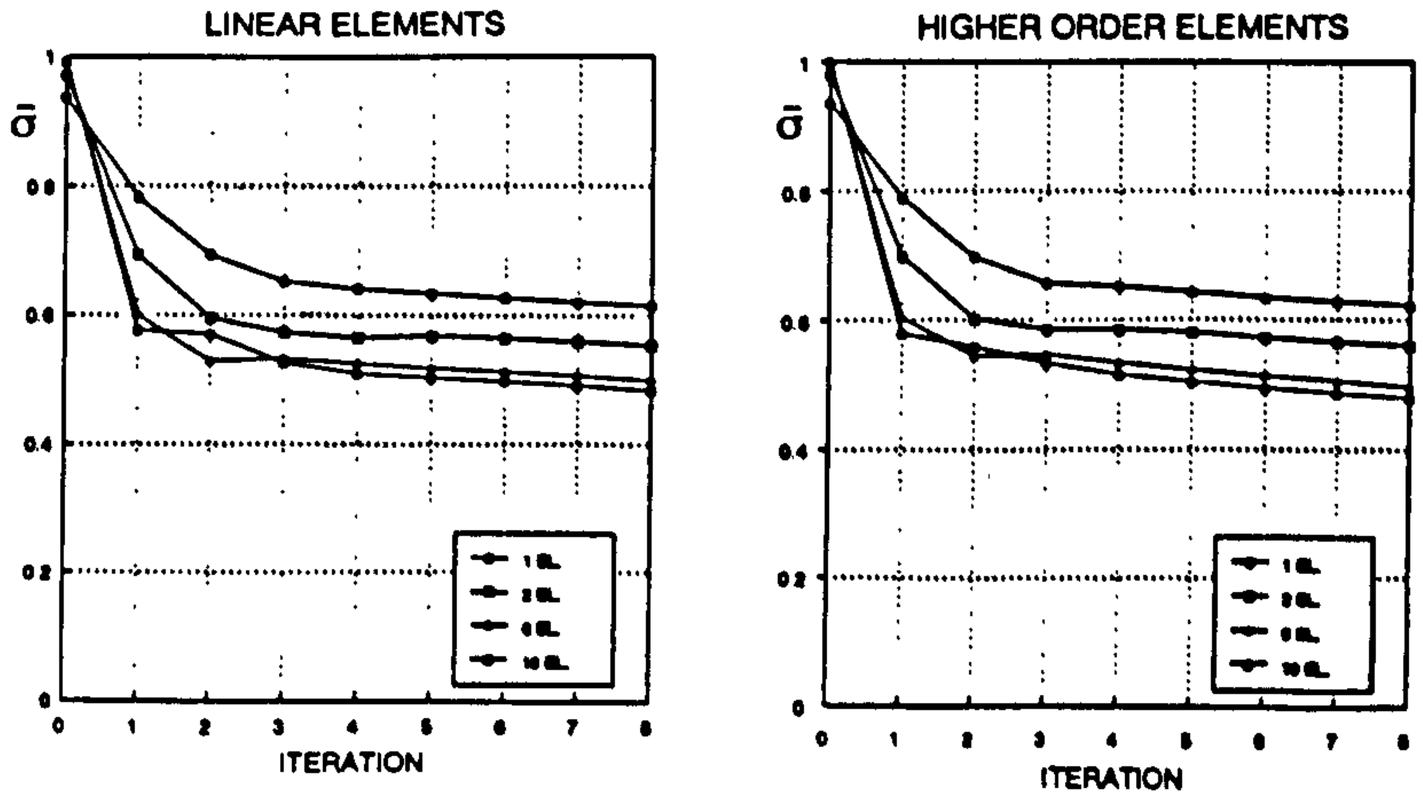

Fig. 11. TOR1 maximum normalized stress per iteration.

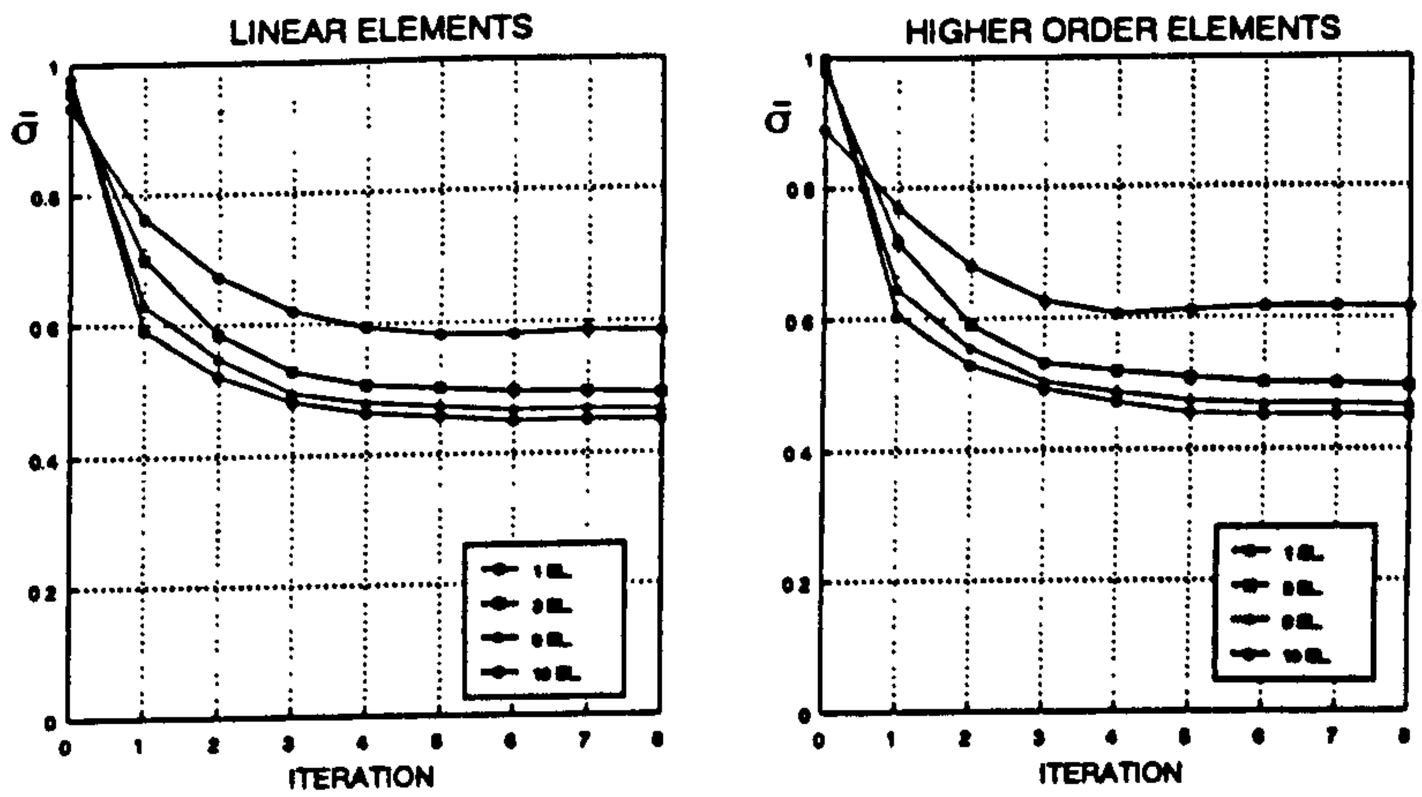

Fig. 12. CON1 maximum normalized stress per iteration.

Table 3. Comparison of elastic compensation and elastic–plastic analysis lower bound limit loads

Component	$\frac{P_{ec}}{P_{ep}}$
TOR1	0.84
TOR2	0.84
TOR3	0.80
TOR4	0.85
CON1	0.89
CON2	0.86

4.5. *Approximate limit loads by elastic compensation*

It was stated above that many commercial programs automatically average stress results to give a smooth stress field which may not satisfy criteria of the lower bound theorem and that only *unaveraged* stresses should be used if a lower bound limit load is required. However, smoothed stresses can be used to calculate *approximate* limit loads for components which *may* be closer to the actual limit load than a lower bound calculated by corresponding unaveraged results. The effect of using averaged stresses in the elastic compensation method is illustrated in Table 4 for the four torispherical heads: TOR1 with four elements through thickness and TOR2 and TOR4 with 10 elements through thickness and TOR3 with six elements through thickness. P_L and P_a are the lower bound and approximate limit loads respectively.

5. DISCUSSION AND CONCLUSIONS

The sample problems considered above highlight several important aspects of finite element modelling for limit analysis by the elastic compensation method. In the examples presented, the method gives values

Table 4. Lower bound and approximate limit loads

Component	$\frac{P_L}{P_{ep}}$	$\frac{P_a}{P_{ep}}$
TOR1	0.78	0.80
TOR2	0.84	0.90
TOR3	0.80	0.89
TOR4	0.85	0.89

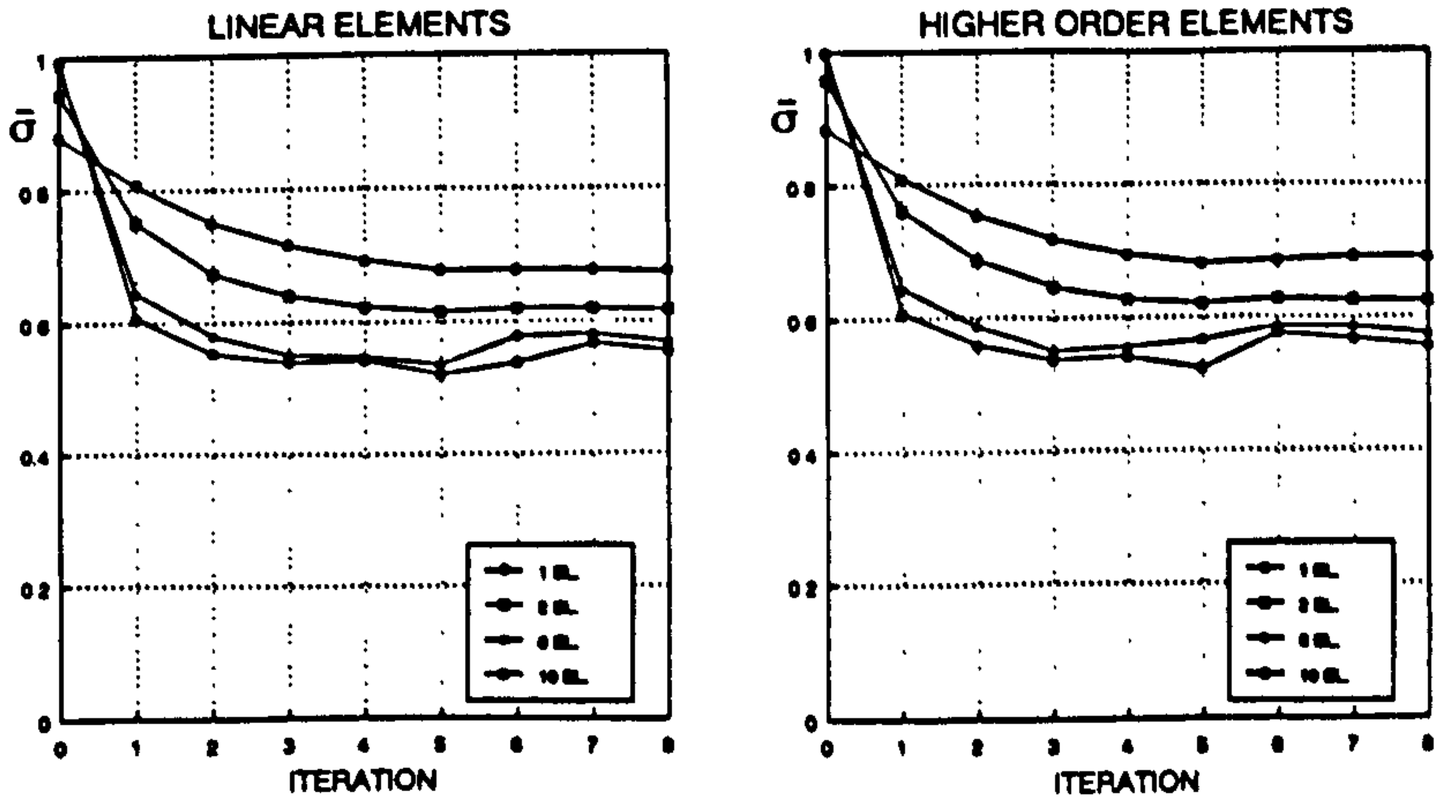

Fig. 13. TOR2 maximum normalized stress per iteration.

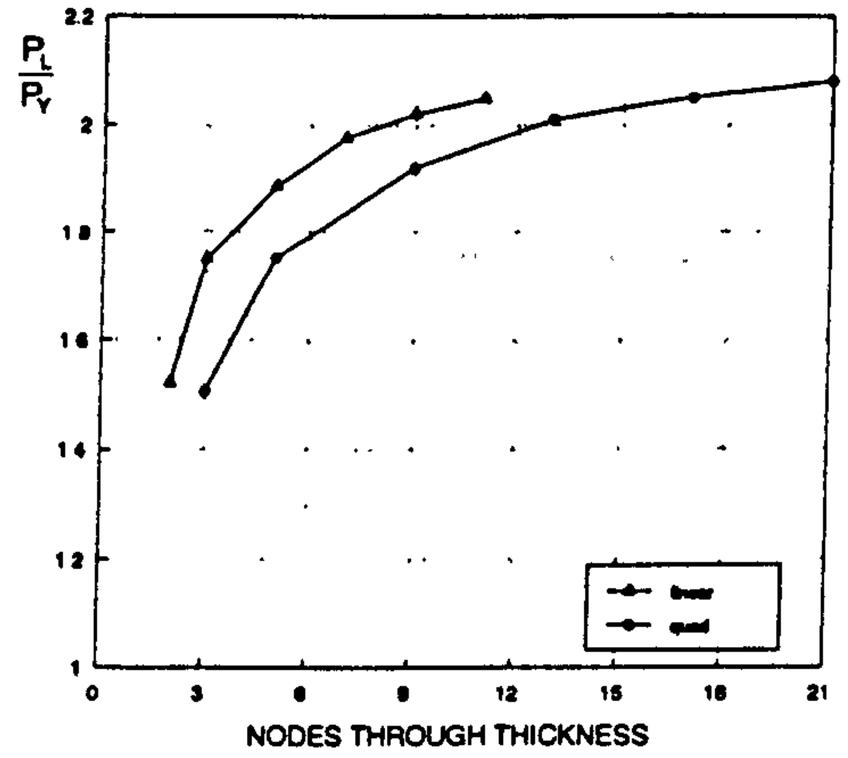

Fig. 14. TOR1 lower bound limit load (iteration 8).

of lower bound limit load within 11% to 20% of loads calculated by elastic–plastic analysis, however, the accuracy of the method is significantly effected by mesh density and element order. The best results are given by high density high order meshes but, in practice, computing and perhaps software limitations may restrict the model to a more modest size and some compromise between accuracy and expediency must be made. Approximate limit loads can be calculated by substituting averaged or smoothed stress fields into the lower bound theorem. Such stress fields may violate the lower bound theorem but they do appear to give good approximate solutions using even fairly course meshes. The use of the smoothed stress field approach may be particularly useful in 3-D continuum analysis, where practical computing and software restrictions limit the permissible mesh density: for example, in pressure vessel applications models commonly have two or three elements through thickness.

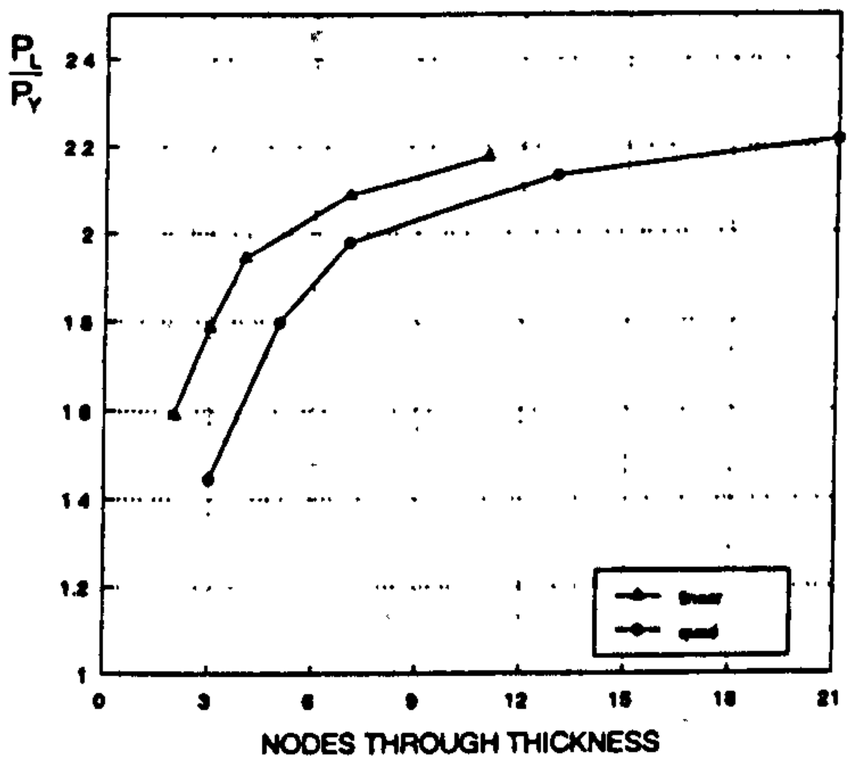

Fig. 15. CON1 lower bound limit load (iteration 8).

REFERENCES

1. J. C. Gerdeen, A critical evaluation of plastic behaviour data and a united definition of plastic loads for pressure components. WRC Bulletin 254 (1979).
2. D. L. Marriott, Evaluation of deformation or load control of stresses under inelastic conditions using elastic finite element stress analysis. *Proc. ASME PVP Conf.* Vol. 136. Pittsburgh, PA (1988).
3. R. Seshadri and C. P. D. Fernando, Limit loads of mechanical components and structures using the GLOSS R-Node method. *ASME PVP*, Vol. 210-2. San Diego, CA, pp. 125–134 (1991).
4. J. T. Boyle and J. Spence, *Stress Analysis for Creep*. Butterworths, London (1983).
5. D. Mackenzie and J. T. Boyle, A method of estimating limit loads by iterative elastic analysis. I—Simple examples. *Int. J. Pres. Ves. Piping* **53**, 77–95 (1993).
6. C. Nadarajah, D. Mackenzie and J. T. Boyle, A method of estimating limit loads by iterative elastic analysis. II—Nozzle sphere intersections with internal pressure and radial load. *Int. J. Pres. Ves. Piping* **53**, 97–119 (1993).
7. J. Shi, D. Mackenzie and J. T. Boyle, A method of estimating limit loads by iterative elastic analysis. III—Torispherical heads under internal pressure. *Int. J. Pres. Ves. Piping* **53**, 97–119 (1993).

PVP-Vol. 277, Recertification and Stress Classification Issu
ASME 19

APPROXIMATE LIMIT ANALYSIS OF PRESSURISED AXISYMMETRIC EQUAL THICKNESS NOZZLES: A PARAMETER STUDY

R Hamilton, J Shi, D Mackenzie and J T Boyle
Department of Mechanical Engineering
University of Strathclyde
Glasgow, Scotland

ABSTRACT

A parametric study of limit loads for pressurised axisymmetric nozzle/sphere intersections with equal nozzle/shell thickness is presented. Lower and upper bound limit loads are calculated by the elastic compensation method and results are found to be consistent with alternative analyses from the literature.

INTRODUCTION

Limit analysis of axisymmetric nozzles under internal pressure has received considerable attention in the literature. In the 1960s, Gill[1], Dinno et al[2] and Ellyin et al[3] used approximate shell type circumscribing yield surfaces to develop lower and upper bound limit pressures according to principles discussed by Drucker and Shield[4,5], for a flush cylindrical nozzle in a spherical pressure vessel. Leckie and Payne[6] replotting Gill's results for limit pressure against a single dimensionless nozzle geometry parameter ρ for various nozzle to shell thickness ratios, where

$$\rho = \frac{r}{R}\left(\frac{R}{T}\right)^{\frac{1}{2}}$$

and r is the nozzle radius, R the sphere radius, and T the thickness of the sphere, as illustrated in Figure 1.

Gill[7] has also presented summarised results in a similar form. Robinson and Gill[8] proposed an improved solution to the problem in the early 1970s, using linear programming techniques based on approximate shell type yield criterion of Ilyushin[9]. Thus the majority of published results for the limit pressure of nozzle/sphere intersections have assumed thin shell theory and usually an approximate yield criterion; results have proved reliable within the limitations related to the thin shell assumptions. Limited elas-to-plastic finite element solutions and experimental results for specific geometries can be found in the literature; these have mostly confirmed the approximate limit pressures. A more complete review of the topic is presented in reference[10].

In this paper a parametric study of axisymmetric nozzle/spherical shell models with equal nozzle/shell thickness is presented. Lower and upper bound limit pressures are obtained for 74 nozzle geometries using the elastic compensation method, which is defined in detail in references[11,12,13]. The elastic compensation method is an iterative elastic analysis procedure in which the elastic moduli of individual elements are weighted to produce stress, strain and displacement fields suitable for application of the lower and upper bound limit load theorems. A similar technique has been presented by Carter & Ponter[14]. Plots of upper and lower bound limit pressure versus the nozzle geometry parameter ρ and R/T ratio are presented and compared with results from the literature and to new elasto-plastic analyses.

PARAMETER STUDY OF AXISYMMETRIC NOZZLE IN SPHERICAL SHELL

The model geometry parameters are shown in Figure 1. A fillet of radius f=t/2 at the nozzle/sphere intersection is modelled in order to counter the problem of singularities at re-entrant corners in elasticity theory. The internal pressure is P and the radial outward pressure P_r, as shown. For the first stage of the study the radius ratio was constant at R/r= 5 (R=1000, r=200mm), with thickness T=t varied from 250mm to 23.67mm over 9 models, (this naturally leads to some rather curious nozzle geometries). The detailed geometric parameters are shown in Table 1.

The modulus of elasticity was 200E3N/mm^2, Poisson's ratio 0.3 and yield stress 300N/mm^2 throughout. Results are based on the Von Mises yield criterion. Finite element analysis was performed using the program ANSYS, with the eight noded isoparametric axisymmetric solid element STIF82 used throughout. Cut surface boundary conditions allowing radial expansion but precluding meridional displacement were applied at a distance sufficiently far removed from the nozzle for the effect of the constraint to be negligible. A typical finite element mesh is shown in Figure 2. Internal pressure P and radial nozzle pressure P_r (equivalent to an capped nozzle pressure load) were applied, where

$$P_r = \frac{P r_i^2}{r_o^2 - r_i^2}$$

Calculated lower and upper bound limit load pressures, P_l and P_u respectively, are normalised according to the expression

$$\overline{P} = \frac{R}{2T\sigma_y} P_l$$

Normalised lower and upper bound limit pressures, $\overline{P}_l$ and $\overline{P}_u$ respectively, and normalised pressure to first yield $\overline{P}_y$ for models 1 to 9 are given in Table 2 and plotted against the nozzle geometry parameter ρ in Figure 3, (a maximum of 10 elastic compensation iterations were used in the analyses). Lower bound limit loads by Leckie and Payne[7] are also given in Table 2 and Figure 3.

Following this initial study, a series of models with set sphere radius, sphere thickness and nozzle thickness (t/T=1) was investigated such that **R/T and t/T was constant.** Nozzle radius r was varied to give a range of values for ρ. R was set at R=1000 and six wall thicknesses examined (T=20,40,100,120,140,160) giving six groups of models with constant shell radius to thickness ratio of R/T=50, 25, 10, 8.33, 7.14 and 6.25. In this way, the variation in limit load with *two* dimensionless geometry parameters ρ and R/T was investigated.

The results of the elastic compensation analyses are compared with Robinson and Gill[8] for the thinner shells and with new elasto-plastic analysis (with an elastic-perfectly plastic material model) for thicker nozzles, R/T<=10, where there does not appear to be any comparable results available in the literature (due to the limitations of shell theory). The results are presented in Tables 3-6 and Figures 4-7 for R/T=50, 25, 10, 6.25 (results for R/T=8.33 and 7.14 have been omitted for brevity) and summarised and compared with the results of Leckie and Payne[6] in Figures 8 and 9.

DISCUSSION AND CONCLUSIONS

Comparing the results of the parametric study with results from the literature and incremental elastic-plastic analysis (with an elastic-perfectly plastic material model) indicates that the elastic compensation method is a robust method for bounding limit loads without recourse to complex incremental elastic-plastic analysis. The results of the study also indicate that whilst the lower bound limit load is a function of the dimensionless geometry parameter ρ used by Leckie *et al*, it cannot be fully characterised by this single parameter. The spread in the results for the lower and upper bound limit pressure for the various R/T ratios indicates that this parameter also has an influence.

ACKNOWLEDGEMENTS

This research was funded by the UK Science & Engineering Research Council. Use of the ANSYS software through an educational license from Swanson Analysis is also acknowledged.

REFERENCES

1 Gill SS, The limit pressure for a flush cylindrical nozzle in spherical pressure vessel. Int J.Mech Sci, 1964, Vol 6, pp 105-115

2 Dinno L S and Gill S S, The limit analysis of a pressure vessel consisting of the junction of a cylindrical and spherical shell, Int.J.Mech Sci,1965, Vol 7,pp21-42

3 Ellyin F & Sherbourne A N, The collapse of cylinder/sphere intersecting pressure vessel, Nuclear Structural Engineering, Vol 2, pp 169-180 (1965)

4 Drucker D C & Shield R T, J.Applied Mechanics,26-61 (1959)

5 Shield R T & Drucker D C, 3rd U.S National Congress of Applied Mechanics, June 1958, pp665

6 Leckie F A, and Payne D J, "Some Observations on the Design of Spherical Pressure Vessels with Flush Cylindrical Nozzles", Proc. Inst. Mech. Engineers, 1965-1966, 180, part I, No. 20, pp 497-512.

7 Gill S S: "The Stress Analysis of Pressure Vessels & Pressure Vessel Components" Pergamon, 1970

8 Robinson M & Gill S S, Limit analysis of flush radial and oblique cylindrical nozzles in spherical pressure vessels. Part I: A parametric survey of results, International Journal of Pressure Vessel and Piping, Vol 1, No3 July 1973, pp199-231

9 Ilyushin A A, Plasticity (in Russian), Gostekhizda, Moscow (1948) and Plasticite (in French), Eyrolles, Paris (1956)

10 C Nadarajah, D Mackenzie & J T Boyle, "A simple method of estimating limit loads by iterative elastic analysis II - Nozzle sphere intersections under internal pressure and radial load," Int. J. Pres. Vess. & Piping, Vol. 53, 97-120,1993

11 D Mackenzie & J T Boyle et al, "A simple method of estimating limit loads by iterative elastic analysis I, II & III" Int. J. Pres. Vess & Piping, Vol.53, 77-142, 1993

12 D Mackenzie, J Shi, C Nadarajah & J T Boyle, "An iterative elastic analysis procedure for estimating lower bound limit loads," Proc. ASME PVP, New Orleans, 1992.

13 Mackenzie D, Nadarajah C, Shi j & Boyle J T, "Simple bounds on limit loads by elastic finite element analysis," Trans. ASME J. Pres. Ves. Tech., Vol 115, No. 1, (1993), pp27-31.

14 K F Carter & A R S Ponter "Calculation of Limit Loads and Shakedown Boundaries using the Modified Elastic Modulus Method", In: Computational Plasticity, Fundamentals and Applications, Eds. Owen, Onate and Henton, Pineridge Press, Swansea, U.K., 1992, pp 1597-1608.

FIGURES AND TABLES

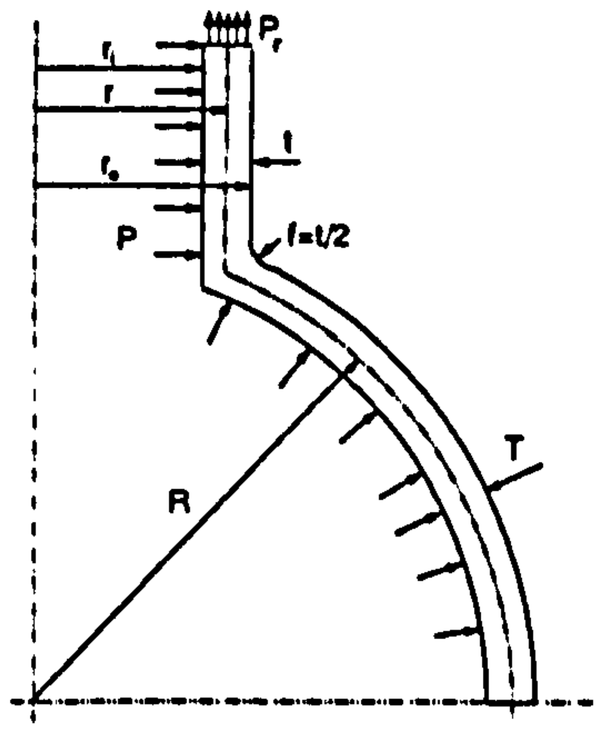

FIGURE 1. GEOMETRY DETAILS FOR AXISYMMETRIC NOZZLE IN SPHERICAL SHELL.

TABLE 1 NOZZLE MODEL GEOMETRY, r=200mm, R=1000mm

Noz.	1	2	3	4	5	6	7	8	9
R (mm)	1000	1000	1000	1000	1000	1000	1000	1000	1000
r (mm)	200	200	200	200	200	200	200	200	200
T (mm)	250	160	111.1	81.6	62.5	40	33.06	27.8	23.67
R/T	4	6.25	9	12.25	16	25	30.25	36	42.2
ρ	0.4	0.5	0.6	0.7	0.8	1.0	1.1	1.2	1.3

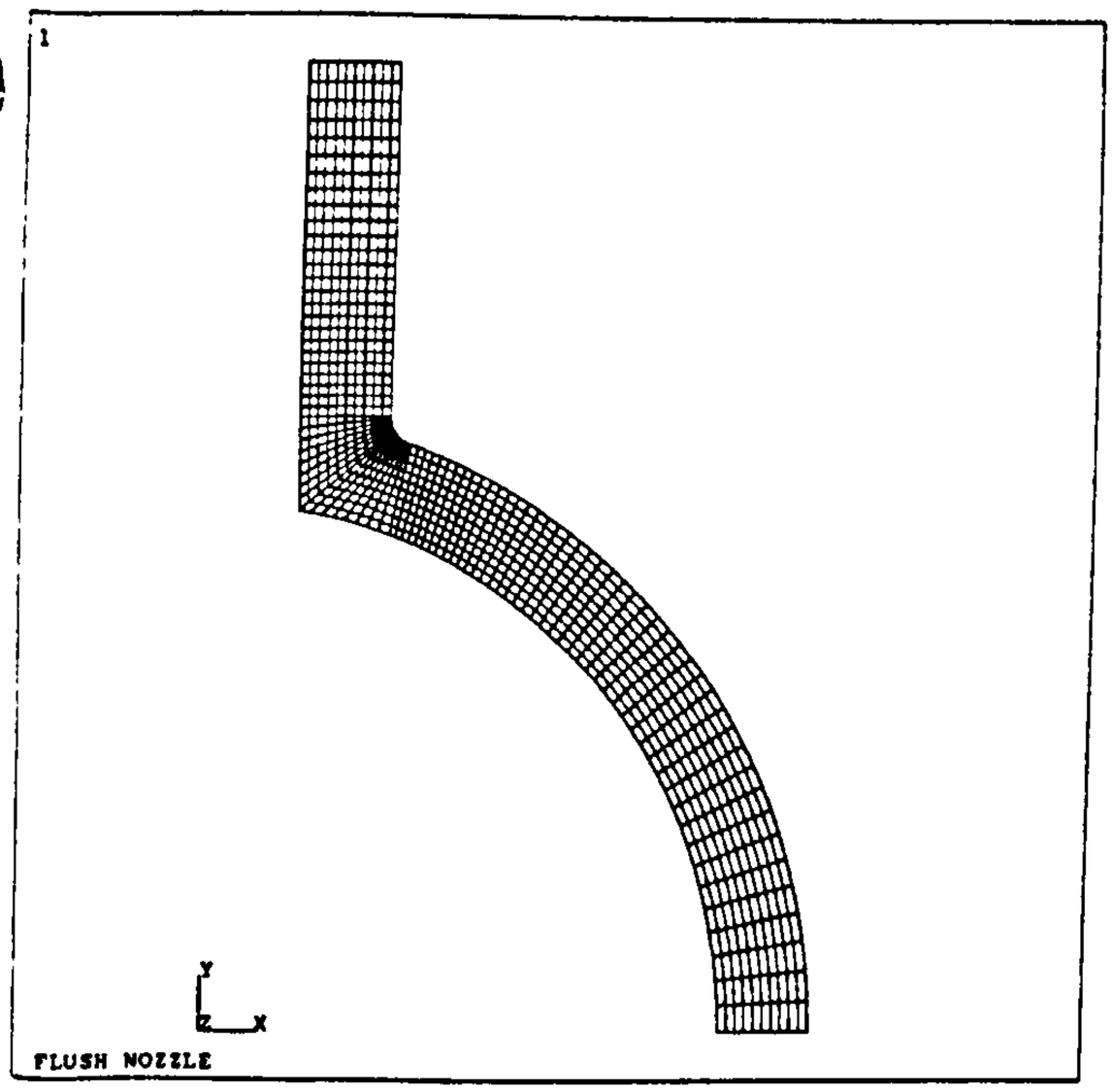

FIGURE 2. TYPICAL FINITE ELEMENT MESH FOR NOZZLE/SPHERE INTERSECTION.

TABLE 2 NORMALISED LOWER BOUND LIMIT PRESSURE OF NOZZLES , r=200mm, R=1000mm.

Nozzle	T(mm)	ρ	$\bar{P}_y$	$\bar{P}_i$	$\bar{P}_u$	L+P[13]
1	250	0.4	0.361	0.923	1.000	0.969
2	160	0.5	0.414	0.898	0.990	0.944
3	111.1	0.6	0.446	0.862	0.974	0.911
4	81.6	0.7	0.463	0.818	0.952	0.876
5	62.5	0.8	0.468	0.777	0.923	0.841
6	40	1.0	0.435	0.696	0.850	0.775
7	33.06	1.1	0.399	0.659	0.812	0.747
8	27.8	1.2	0.393	0.615	0.770	0.725
9	23.67	1.3	0.366	0.577	0.741	0.700

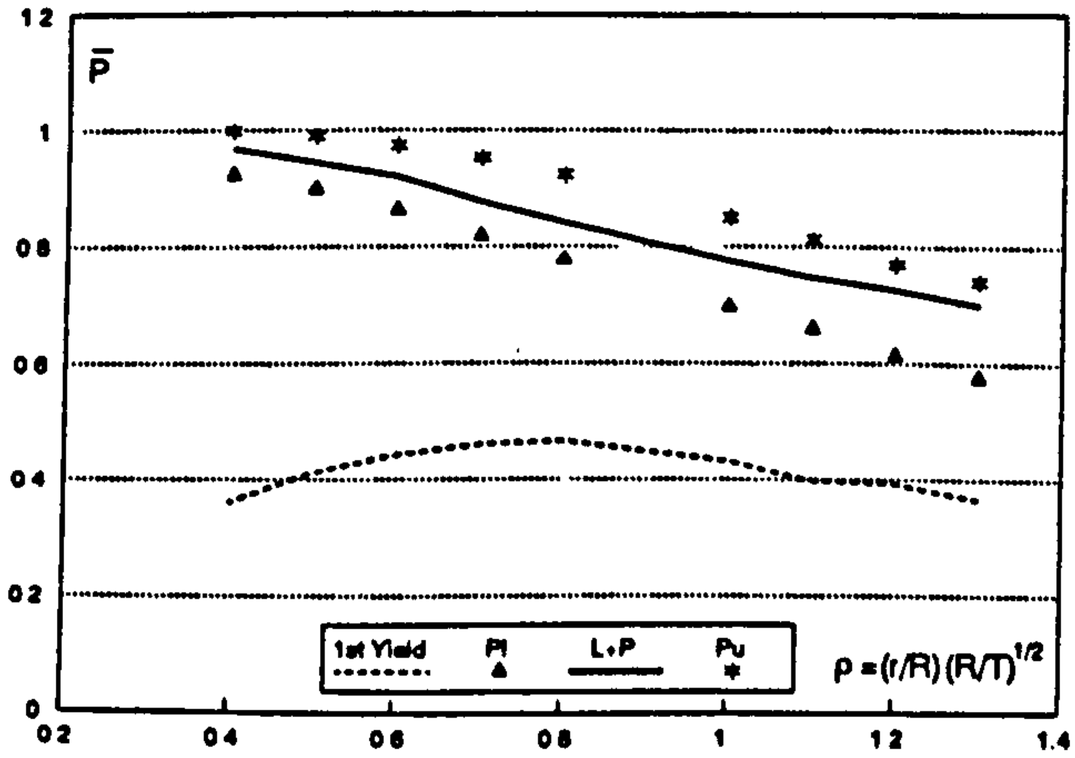

FIGURE 3. NORMALISED LOWER BOUND LIMIT PRESSURE OF NOZZLES VERSUS ρ, r=200mm, R=1000mm

TABLE 3 NORMALISED LOWER BOUND LIMIT PRESSURE OF NOZZLES , T=20MM, R/T=50

Nozzle	r(mm)	ρ	$\bar{P}_s$	$\bar{P}_i$	$\bar{P}_u$	R+G''
10	14.14	0.1	0.469	0.955	1.0	-
11	28.28	0.2	0.436	0.90	1.0	-
12	56.57	0.4	0.464	0.833	0.997	0.928
13	70.71	0.5	0.471	0.803	0.99	0.888
14	84.85	0.6	0.473	0.776	0.977	0.846
15	98.99	0.7	0.471	0.745	0.955	0.810
16	113.1	0.8	0.467	0.715	0.923	0.774
17	127.3	0.9	0.448	0.685	0.884	0.736
18	141.2	1.0	0.419	0.657	0.843	0.704
19	212.1	1.5	0.32	0.541	0.683	0.583
20	282.8	2.0	0.264	0.463	0.584	0.496

TABLE 4 NORMALISED LOWER BOUND LIMIT PRESSURE OF NOZZLES , T=40mm, R/T=25

Nozzle	r(mm)	ρ	$\bar{P}_s$	$\bar{P}_i$	$\bar{P}_u$	R+G''
21	40	0.2	0.432	0.920	1.0	-
22	60	0.3	0.443	0.888	0.999	0.974
23	80	0.4	0.457	0.859	0.996	0.941
24	100	0.5	0.467	0.829	0.990	0.905
25	120	0.6	0.471	0.802	0.976	0.870
26	140	0.7	0.473	0.774	0.954	0.832
27	160	0.8	0.471	0.748	0.924	0.800
28	180	0.9	0.467	0.718	0.888	0.768
29	200	1.0	0.462	0.692	0.851	0.740
30	300	1.5	0.353	0.579	0.702	0.615
31	400	2.0	0.291	0.495	0.607	0.518

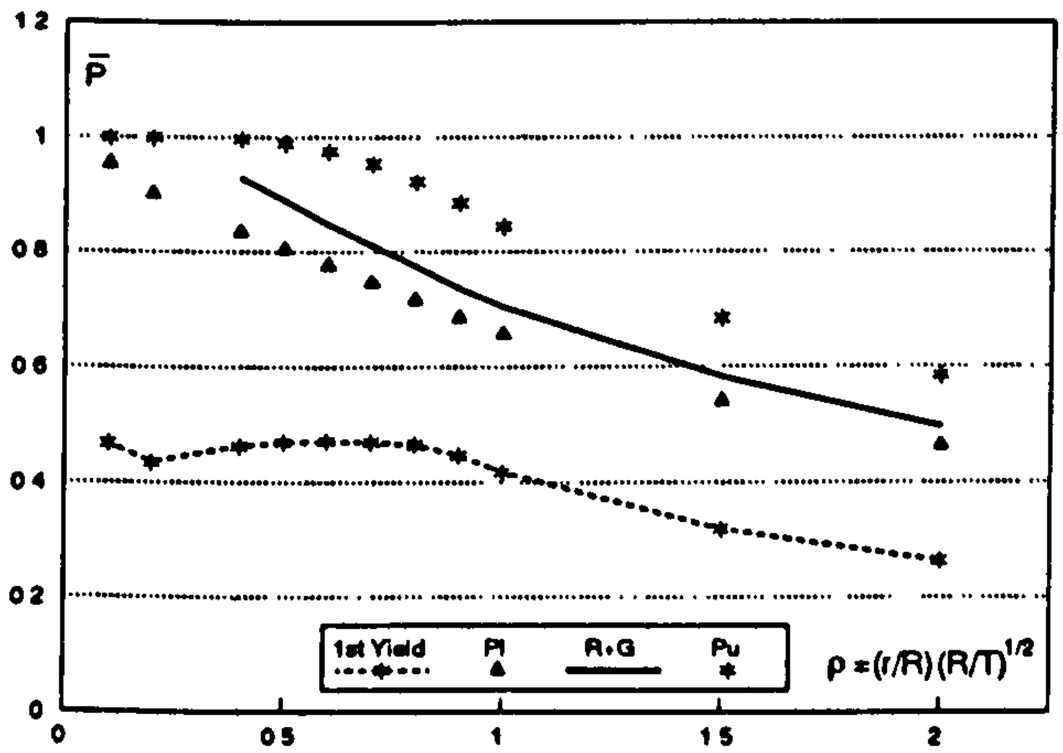

FIGURE 4. NORMALISED LOWER BOUND LIMIT PRESSURE OF NOZZLES VERSUS ρ, T=20mm, R/T=50

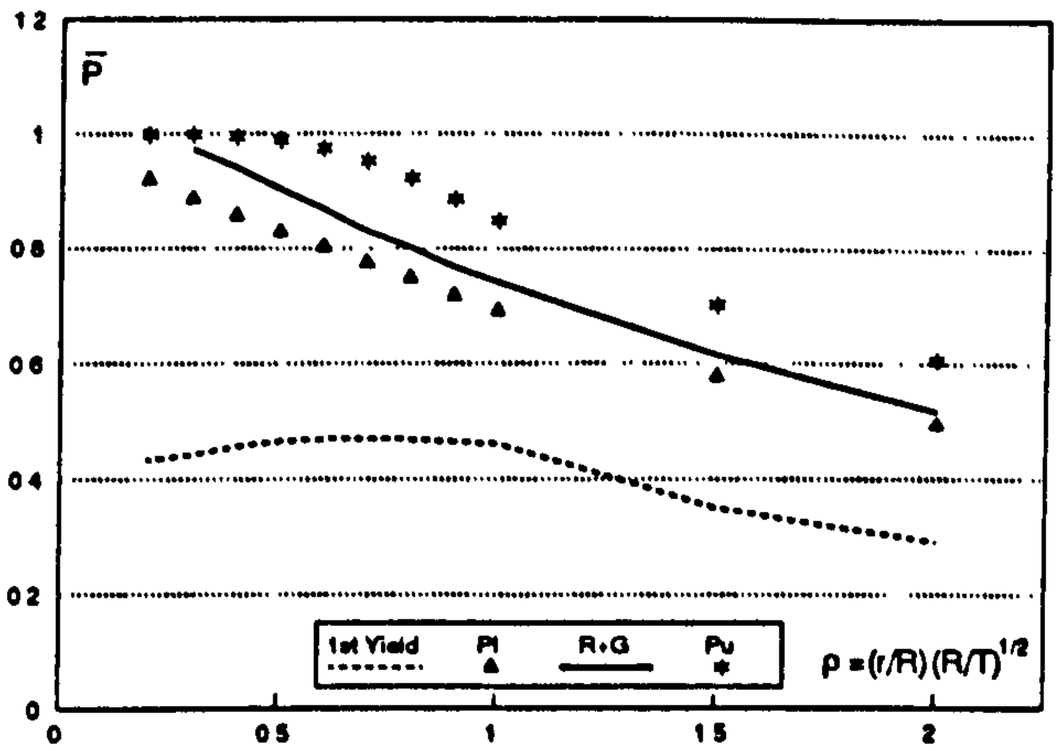

FIGURE 5. NORMALISED LOWER BOUND LIMIT PRESSURE OF NOZZLES VERSUS ρ, T=40mm, R/T=25

TABLE 5 NORMALISED LOWER BOUND LIMIT PRESSURE OF NOZZLES , T=100mm, R/T=10

Nozzle	r(mm)	ρ	$\overline{P}_s$	$\overline{P}_i$	$\overline{P}_u$	E/P
32	63.24	0.2	0.424	0.949	1.0	1.0
33	94.87	0.3	0.407	0.934	1.0	-
34	126.5	0.4	0.426	0.909	0.997	0.983
35	158.1	0.5	0.441	0.88	0.990	-
36	189.7	0.6	0.451	0.855	0.975	0.933
37	221.4	0.7	0.457	0.83	0.951	-
38	253.0	0.8	0.459	0.802	0.920	0.883
39	284.6	0.9	0.459	0.775	0.886	-
40	316.2	1.0	0.457	0.748	0.851	0.817
41	474.3	1.5	0.372	0.629	0.712	-
42	632.5	2.0	0.317	0.552	0.631	0.608

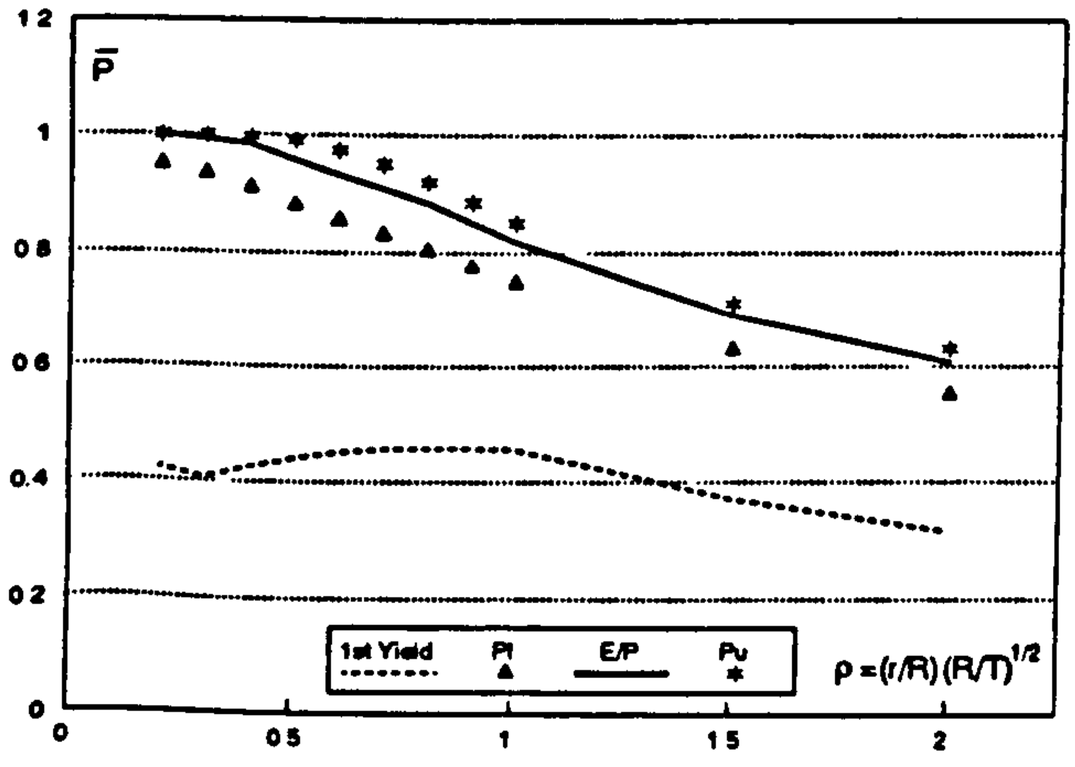

FIGURE 6. NORMALISED LOWER BOUND LIMIT PRESSURE OF NOZZLES VERSUS ρ, T=100mm, R/T=10

TABLE 6 NORMALISED LOWER BOUND LIMIT PRESSURE OF NOZZLES , T=160mm, R/T=6.25

Nozzle	r(mm)	ρ	$\overline{P}_s$	$\overline{P}_i$	$\overline{P}_u$	E/P
65	120	0.3	0.389	0.936	1.0	1.0
66	160	0.4	0.399	0.914	0.999	-
67	240	0.6	0.427	0.862	0.973	0.948
68	280	0.7	0.436	0.837	0.947	-
69	320	0.8	0.441	0.804	0.914	0.885
70	360	0.9	0.443	0.777	0.879	-
71	400	1.0	0.443	0.748	0.845	0.823
72	500	1.25	0.439	0.686	0.769	-
73	600	1.5	0.414	0.627	0.712	0.687
74	700	1.75	0.389	0.586	0.672	0.646

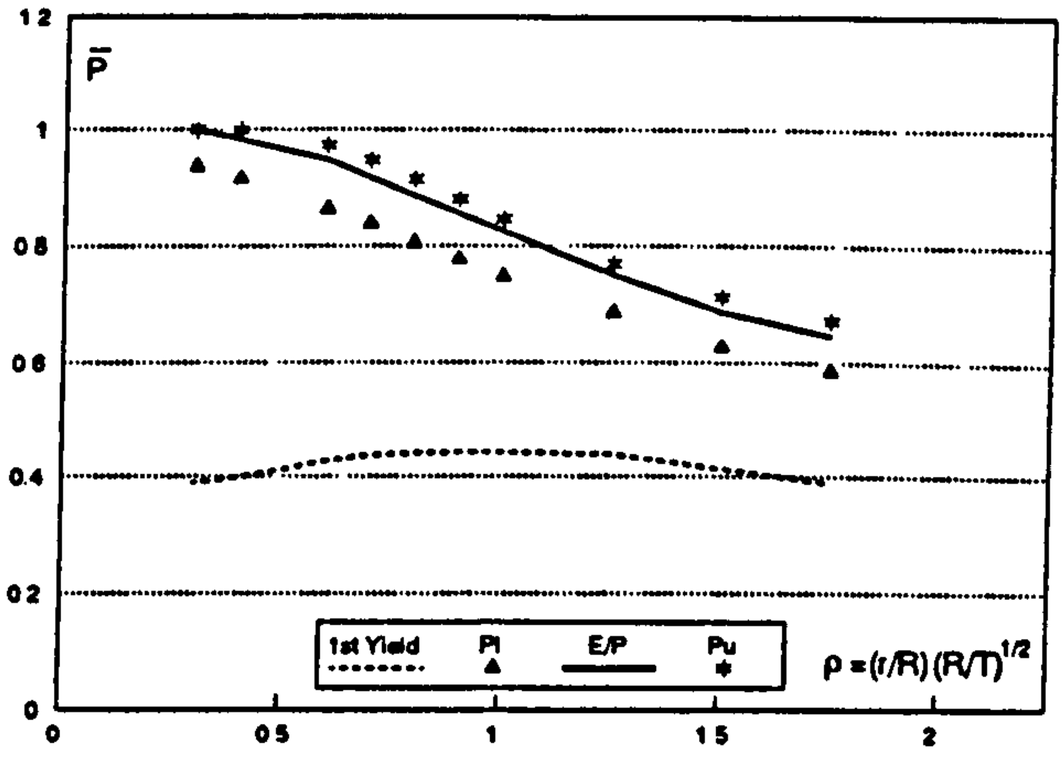

FIGURE 7. NORMALISED LOWER BOUND LIMIT PRESSURE OF NOZZLES VERSUS ρ, T=160mm, R/T=6.25

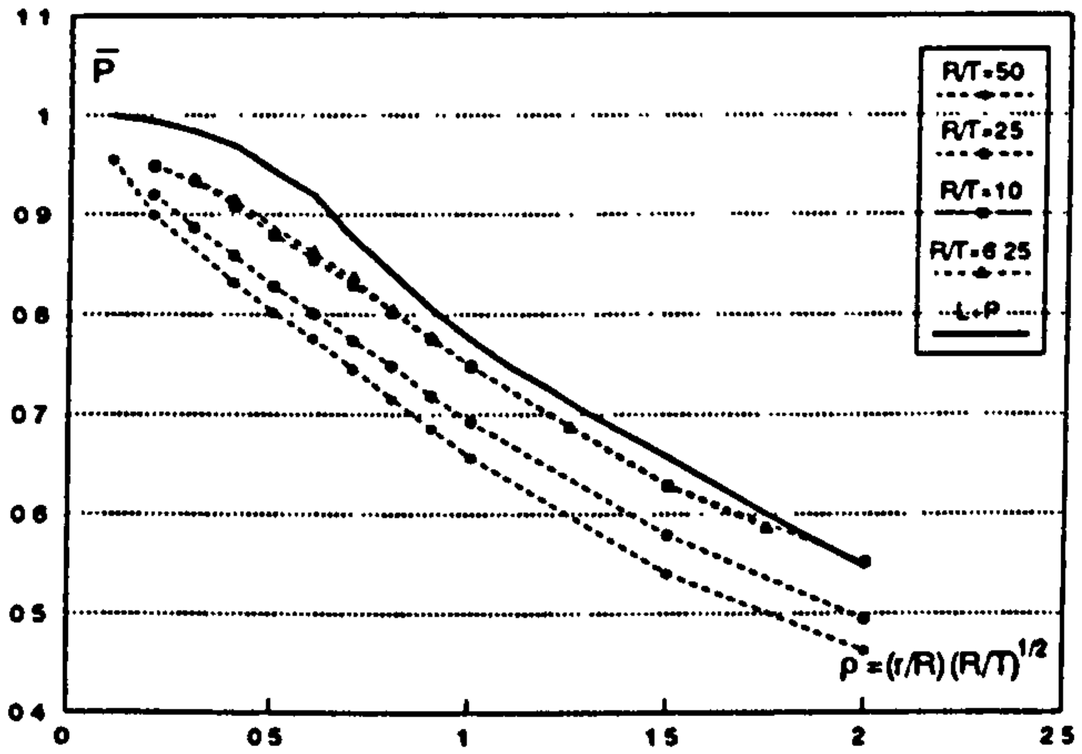

FIGURE 8. NORMALISED LOWER BOUND LIMIT PRESSURE OF NOZZLES VERSUS ρ, SUMMARY OF RESULTS

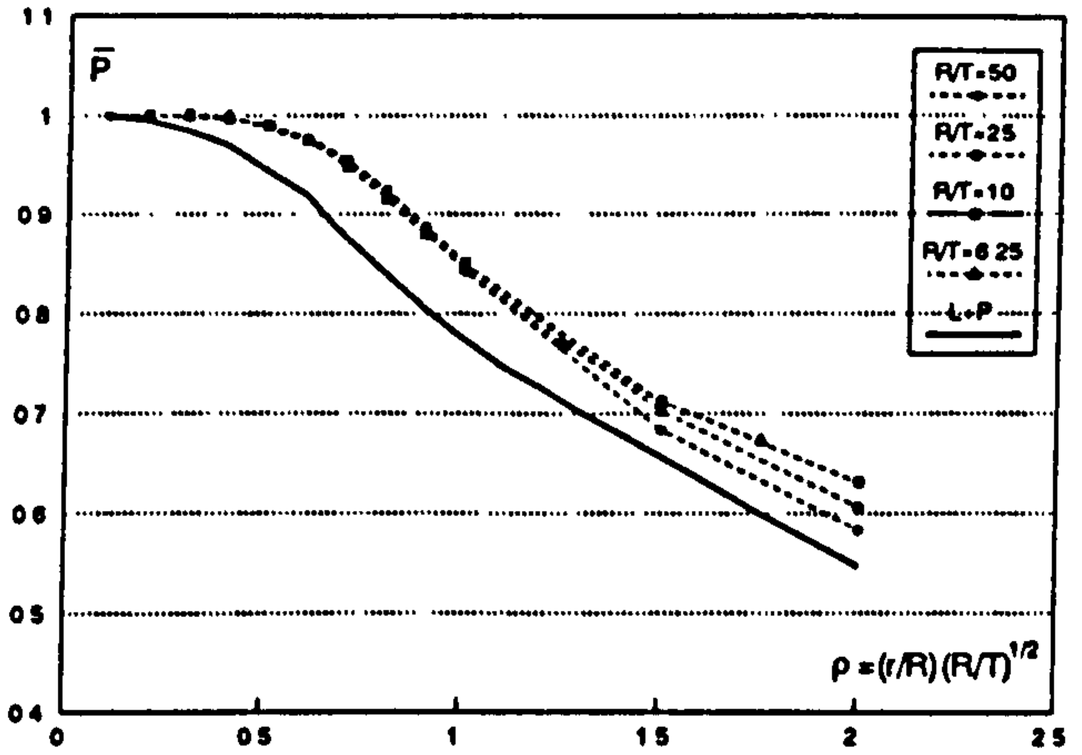

FIGURE 9. NORMALISED UPPER BOUND LIMIT PRESSURE OF NOZZLES VERSUS ρ, SUMMARY OF RESULTS

PVP-Vol. 313-1, International Pressure Vessels and Piping
Codes and Standards: Volume 1 — Current Applications
ASME 1995

SECONDARY STRESS AND SHAKEDOWN IN AXISYMMETPIC NOZZLES

D Mackenzie, JT Boyle, R Hamilton, J Shi
Department of Mechanical Engineering
University of Strathclyde
Glasgow, Scotland

ABSTRACT

An investigation of the shakedown behaviour of equal-thickness axisymmetric nozzles in spheres is presented. The elastic compensation method is used to obtain shakedown loads for a range of nozzle configurations. The calculated shakedown pressures are compared with shakedown curves from the literature and the ASME B&PV Code Section VIII Division 2 primary plus secondary stress requirements.

INTRODUCTION

The design by analysis rules included in Pressure Vessel Codes such as ASME *Boiler and Pressure Vessel (B&PV) Code* Sections III and VIII (Division 2) (ASME, 1989) and the UK Code BS5500: *Unfired fusion welded pressure vessels* (BSI, 1991) define criteria to preclude a number of failure mechanisms; gross plastic deformation, incremental collapse, buckling and fatigue. This paper examines the specific problem of incremental collapse, more commonly known as *ratchetting*. Ratchetting is associated with cyclic loading and describes a post-yield phenomenon in which the stress system reaches a cyclic state (after a few cycles of load) but plastic strain increases incrementally with each cycle. This is clearly undesirable and a potential source of failure through plastic deformation.

Ratchetting may be precluded by limiting the stress to the elastic range but this restrictive approach is unnecessary if *shakedown* of the structure can be assured. In the shakedown condition, a component which accumulates some plastic strain in the first (few) load cycles subsequently settles down to wholly elastic behaviour with no further plastic strain as the load continues to cycle. Design for shakedown is clearly desirable, provided some limited plastic strain is tolerable in the first few cycles.

The B&PV Code rules for design based on elastic analysis may be interpreted in the context of the Code failure criteria as follows:

- All elastically calculated stresses must satisfy the specified fatigue criteria.
- The primary plus secondary stress must satisfy the shakedown criterion.
- The primary stress must satisfy the gross plastic deformation criterion.

Code stress limits are defined in terms of the (primary membrane) allowable stress S_m, which is approximately equivalent to two thirds yield. The ASME B&PV Code (Section VIII Division 2 Appendix 4 - 134) shakedown criterion requires the primary plus secondary stress intensity, derived from the highest value at any point across the thickness of a section (neglecting peak), to be limited to $3S_m$: that is, the elastically calculated stress range is limited to less than twice yield (ASME, 1969). This criterion seeks to ensure *overall* (or plastic) shakedown, in which the structural response is controlled by a dominant elastic core (Toulios & White 1991). Local plastic action due to peak stress is assumed to be constrained by the surrounding elastic region and peak stress can therefore be neglected in the shakedown analysis.

The $3S_m$ limit for shakedown is applied to all possible components for all possible loads, however, experimental and theoretical studies of the shakedown behaviour of many components have suggested that ratchetting may occur for cyclic stress ranges below the $2\sigma_y$ limit. Proctor & Strong (1968) have reported experimental shakedown loads for nozzles in spheres at less than the $2\sigma_y$ range and Leckie & Penny (1967) report similar results for analysis based on Melan's lower bound theorem and thin shell theory.

In BS5500, a direct check for shakedown is possible: Appendix A.3.1.2 *Incremental collapse*, states that "The stress system imposed should shakedown to elastic action within the first few operating cycles". To demonstrate conformance with this requirement "a shakedown analysis (e.g. See **G.2.6**) should preferably be employed" (the specified alternative being elastic analysis and stress categorisation). The method of predicting shakedown loads used in Appendix G.2.6 *Spherical shells: shakedown loads for radial nozzles* is based on that used by Leckie

& Penny (1967) to calculate shakedown loads for axisymmetric nozzles subject to pressure, thrust and moment loads. The Leckie and Penny method is based on Melan's theorem:

For a given load set P, if any distribution of self-equilibriating residual stresses can be found which when taken together with elastically calculated stresses constitute a system of stresses within the yield limit (for the whole cycle) then P is a lower bound shakedown load set and the structure will shake down.

Leckie and Penny used elastic thin shell solutions for a variety of nozzle loading configurations to obtain shakedown loads curves for a wide range of nozzle geometries (although the assumptions inherent in the thin shell theory used may restrict the accuracy of solutions for thick vessels).

Since the work of Penny and Leckie, several alternative methods for calculating shakedown loads using various finite element formulations have been proposed. Ideally, an incremental elastic-plastic analysis can be run for a number of cycles and strain accumulation examined to determine if shakedown occurs for a particular loading. This approach is time consuming and only determines whether or not shakedown occurs for the considered load: trial and error must be used to establish the highest shakedown load. Belytschko (1972) and Corradi & Zavelani (1974) applied linear programming techniques directly to the shakedown theorems but this computationally intensive approach has only been applied to simple two dimensional structures. However, Mackenzie & Boyle (1993) proposed a simpler method for calculating lower bound shakedown loads based on iterative elastic finite element analysis and Melan's lower bound shakedown load theorem. The method uses the *elastic compensation method* (previously proposed for limit analysis (Mackenzie *et al*, 1993)) to obtain elastic and residual stress fields suitable for substitution into Melan's lower bound limit load theorem. In many respects, the method is an extension of Penny and Leckie's shell analysis approach to 2-D and 3-D solid finite element analysis.

The advantage of adopting bounding theorems for calculating shakedown loads is that they only require incomplete plasticity solutions. Melan's theorem states that a structure will shakedown for a given load if an acceptable residual stress system can be identified. The specified residual stress field need not be the actual residual stress system in the real structure. In addition, compatibility requirements and constitutive relations need not be considered. The elastic compensation approach proposed by Mackenzie and Boyle requires much less computing effort than alternative finite element shakedown analysis procedures and can be applied to 2-D and 3-D solid finite element models. In this paper, shakedown loads given by the elastic compensation method are compared with those given by Penny and Leckie and the twice yield load criterion used in Code elastic analysis.

LOWER BOUND SHAKEDOWN LOADS BY ELASTIC COMPENSATION

The lower bound elastic compensation shakedown formulation has previously been described by Mackenzie and Boyle (1993). Here a brief re-cap of the finite element implementation of the method is given. It is assumed here that the applied load is cycled from zero up to a specified value then back down to zero. The aim is to find the maximum allowable load for shakedown to occur; this will be the shakedown load. The following notation is used:

σ_r is a residual stress field

σ_e the elastic stress field

σ_Y the material yield stress

In the elastic compensation method, an initial linear elastic finite element analysis is performed for a nominal design loading P^d to establish the elastic stress field σ_e. This analysis forms iteration zero in a series of linear elastic analyses in which the moduli of elements are systematically modified to redistribute the stress in the component. In each subsequent iteration, the modulus of each element is modified according to the equation:

$$E_i = E_{(i-1)} \frac{\sigma_n}{(\sigma_{(i-1)})} \qquad (1)$$

where subscript i is the iteration number, σ_n a nominal stress value and $\sigma_{(i-1)}$ the maximum (unaveraged) nodal *equivalent stress* associated with the element from the previous solution. The value chosen for σ_n in (1) is somewhat arbitrary - usually half or two thirds yield.

The redistributed stress field calculated for each iteration is designated as a possible *shakedown* stress field σ_{s_i}: that is, the stress field in the component under full load after shakedown has occurred. This stress field is taken to be the sum of the initial elastic stress field σ_e and a residual stress field σ_{r_i} (for iteration i):

$$\sigma_{s_i} = \sigma_e + \sigma_{r_i} \qquad (2)$$

Thus, the residual stress field σ_r is defined implicitly in the elastic compensation procedure, such that:

$$\sigma_{r_i} = \sigma_{s_i} - \sigma_e \qquad (3)$$

Since the load is cycled from zero to a specified value, *two* conditions for shakedown must be considered since the residual stress must itself be within the yield limit (when the zero load condition is reached during the cycle) to satisfy Melan's theorem. The two conditions are expressed as pressures P_{1_i} and P_{2_i} for each iteration i, where

$$P_{1_i} = P^d \frac{\sigma_Y}{|\sigma'_{s_i} - \sigma'_e|_{max}} \qquad (4a)$$

$$P_{2_i} = P^d \frac{\sigma_Y}{|\sigma'_{s_i}|_{max}} \qquad (4b)$$

The lower bound shakedown load P_{S_i} calculated for iteration i is the **smaller** of the two calculated loads P_{1_i} and P_{2_i}, that is:

$$P_{S_i} = \min(P_{1_i}, P_{2_i}) \qquad (5)$$

The best lower bound shakedown load is the highest iteration shakedown load P_{S_i}:

$$P_S = \max(P_{S_i}) \qquad (6)$$

SHAKEDOWN LOADS FOR AXISYMMETRIC NOZZLES

The axisymmetric model geometry and various parameters are shown in Figure 1. A fillet of radius f=t/3 is included at the outside of the intersection to avoid a re-entrant corner singularity in the solution. The internal pressure is P^d and the radial outward pressure P_r (equivalent to an capped nozzle pressure load) were applied, where

$$P_s = \frac{P^d r_i^2}{r_o^2 - r_i^2} \qquad (7)$$

The modulus of elasticity was 200E3N/mm^2, Poisson's ratio 0.3 and yield stress 300N/mm^2. The von Mises yield criterion was assumed. Finite element analysis was performed using the program ANSYS (Swanson Analysis Systems, Inc., 1993), using the eight noded isoparametric axisymmetric solid element PLANE82. Cut surface boundary conditions allowing radial expansion but precluding meridional displacement were applied at a distance sufficiently far removed from the nozzle for the effect of the constraint to be negligible. A typical finite element mesh is shown in Figure 2.

Shakedown pressures P_{L1} and P_{L2} were calculated according to the equations (4a) and (4b) and normalized according to the equation:

$$\overline{P} = \frac{R}{2T\sigma_y} P \qquad (8)$$

The variation in shakedown load with *two* dimensionless geometry parameters ρ and R/T was investigated, where

$$\rho = \frac{r}{R}\left(\frac{R}{T}\right)^{\frac{1}{2}}$$

Three series of models were examined, within which the sphere radius (R) and wall thicknesses (t=T) were held constant and nozzle radius r varied to give a range of values for geometry parameter ρ. R was set at 1000mm throughout, and three wall thicknesses examined - 10mm, 20mm and 100mm - giving three groups of models with constant shell radius to thickness ratio of R/T=100, 50 and 10 respectively.

Normalised lower bound shakedown pressures calculated by the elastic compensation method, $\overline{P}_s$, are plotted against the nozzle geometry parameter ρ in Figures 3 to 5 for R/T ratios of 100, 50 and 10 respectively. A maximum of 10 iterations were used in the elastic compensation analyses. The normalized shakedown pressures are compared with published results of Leckie and Penny (1967) $\overline{P}_{LP}$, and the load corresponding to an elastic stress range of $3S_m$ ($2\sigma_y$), $\overline{P}_{3S_m}$. For simplicity, $\overline{P}_{3S_m}$ is based on the total elastic stress; that is, primary plus secondary plus peak stress are included in the considered elastic stresses. This assumption is conservative with respect to the ASME (overall) $3S_m$ shakedown criterion, which considers only primary plus secondary stress, and corresponds to a criterion for *strict* shakedown.

As Leckie & Penny only considered variation of shakedown load with geometry parameter ρ, their results are constant for all the R/T ratios considered. However, it has been found that both $\overline{P}_s$ and $\overline{P}_{3S_m}$ vary with the R/T ratio. The results presented show that the Leckie & Penny shakedown pressure $\overline{P}_{LP}$ is lower than the secondary stress limit pressure $\overline{P}_{3S_m}$ except for high R/T and ρ values (large diameter nozzles) in Figure 3.

The elastic compensation shakedown pressures $\overline{P}_s$ are less than $\overline{P}_{3S_m}$ for all the nozzle configurations considered. The $\overline{P}_s$ curves are similar in form to the $\overline{P}_{3S_m}$ curves but the calculated shakedown pressure values are generally closer to the Penny & Leckie results. $\overline{P}_s$ and $\overline{P}_{LP}$ are fairly similar for most values of ρ for the two higher R/T ratios of 100 and 50, however, $\overline{P}_s$ is significantly greater than $\overline{P}_{LP}$ for most of the ρ values in the R/T=10 nozzle.

DISCUSSION AND CONCLUSIONS

Figures 3 to 5 show that elastic compensation method lower bound shakedown pressures are consistently lower than the pressure corresponding to an elastic stress range of $3S_m$, the shakedown criterion implicit in the ASME B&PV Code. As the method is a lower bound, these results do not by themselves demonstrate unconservatism in the Code shakedown limit but they do support experimental results suggesting that ratchetting can occur at loads lower than predicted by the $3S_m$ criterion. (The writers are currently developing an upper bound elastic compensation shakedown procedure which will be useful in determining whether or not the Code secondary stress limit is conservative).

Figures 3 to 5 also suggest that the shakedown pressure varies not only with the single geometry parameter ρ used to characterize nozzles by Leckie & Penny, but also with the radius to thickness ratio of the vessel. This additional geometry parameter should be considered when deriving design curves for shakedown loads. For this reason, the lower bound curves of Leckie & Penny may not be conservative for geometries (radius to thickness ratios) satisfying the specified geometry parameter ρ, (although it is noted that the curves compare results based on two different types of analysis - shell analysis and 2-D solid finite element analysis - and in that respect the Figures do not compare like with like).

The elastic compensation shakedown pressures for the R/T ratio of 10 are significantly greater than the Leckie and Penny values for most of the geometry range considered, suggesting that design to the BS5500 Code could be over-conservative if the Leckie and Penny curves are used. However, BS5500 simply requires that "a shakedown analysis .... should preferably be employed" thus design based on the elastic compensation method would be acceptable.

The technique used in this paper provides a simple method for calculating shakedown loads in pressure vessels. This has been demonstrated for the example case of nozzles in spherical shells under internal pressure. This particular problem was chosen as data is available in the literature for comparison purposes: in practice, the allowable load for this type of component is usually controlled by the gross plastic collapse failure criterion and Code minimum thickness/reinforcement requirements. However, the elastic compensation method can be applied to more complex three dimensional geometry, under combined loading (and other forms of load cycle) in which the shakedown criterion may be more critical.

ACKNOWLEDGEMENT

This research has been funded by a grant from the UK EPSRC. Use of the ANSYS software through an educational license is also acknowledged.

REFERENCES

American Society of Mechanical Engineers (1989), Boiler and Pressure Vessel Code.

ASME, (1969), Criteria of the ASME Boiler and Pressure Vessel Code for Design by Analysis in Sections III and VIII, Division 2, The American Society of Mechanical Engineers, New York, NY.

Belytschko T (1972), "Plane stress shakedown analysis by finite elements," Int. J. Mech. Sci., Vol 14, pp619-625.

British Standards Institution (1991), BS5500: Specification for unfired fusion welded pressure vessels.

Corradi L and Zavelani A (1974), "A linear programming approach to shakedown analysis of structures," Comput. Methods Mech. Eng., Vol 3, pp37-53.

Leckie F A and Penny R K (1967), "Shakedown Loads for Radial Nozzles in Spherical Pressure Vessels," Int. J. Solids Structures, Vol. 3, pp743-755.

Mackenzie D & Boyle J T (1993) "A Simple Method of Estimating Shakedown Loads for Complex Structures," ASME PVP Vol -265, Denver.

Mackenzie D, Nadarajah C, Shi J & Boyle JT (1993), "Simple bounds on Limit Lopads by Elastic Finite Element Analysis," J. Pres. Ves. Tech., Vol 115, No. 1, pp27-31.

Proctor E and Strong J T (1972), "Pressure tests on flush cylinder-cylinder intersections. Elastic and elastic/plastic behaviour," CEGB, Research Dept., Report RD/B/N2244

Swanson Analysis Systems, Inc. (1993), "ANSYS User's Manual for Revision 5.0A, SASI, PO Box 65, Johnson Road, Houston PA 15342-0065.

Toulious M & White P S (1991), "Simplified design methods by shakedown and an alogonthm for IE", Applied Solid Mechanics-4, pp162-177, Elsevier Science Publishers.

FIGURES

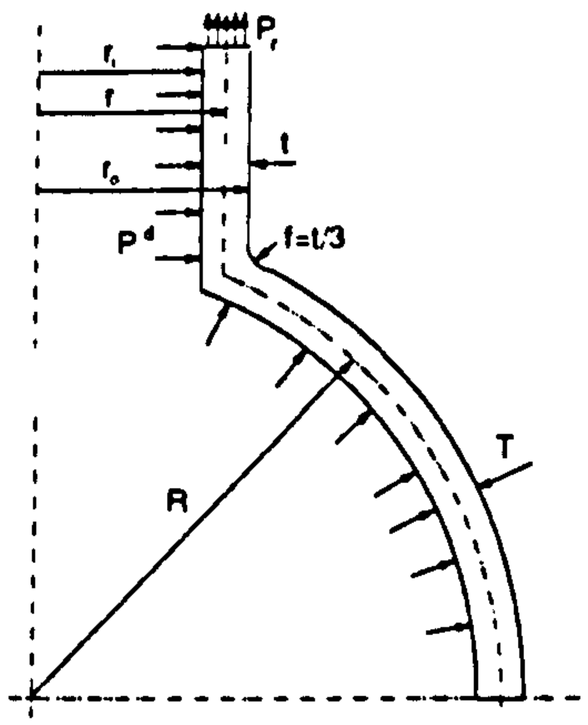

FIGURE 1. GEOMETRY DETAILS FOR AXISYMMETRIC NOZZLE IN SPHERICAL SHELL.

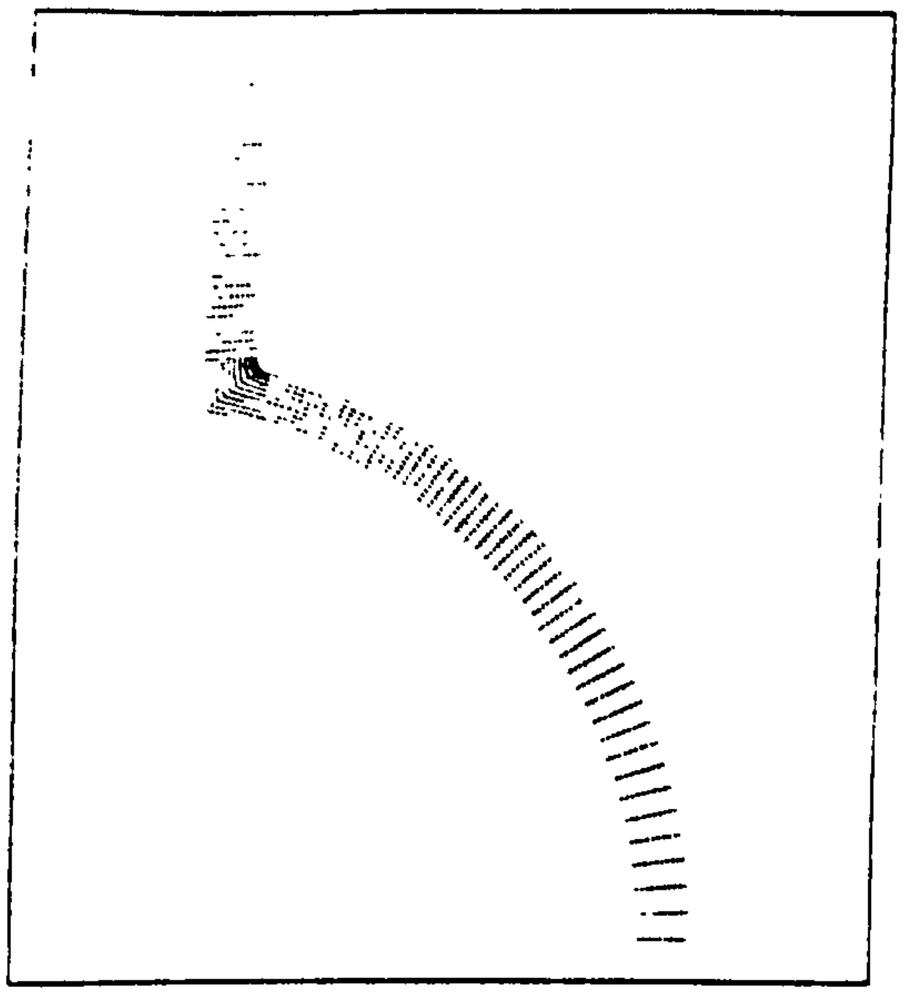

FIGURE 2. TYPICAL FINITE ELEMENT MESH FOR NOZZLE/SPHERE INTERSECTION.

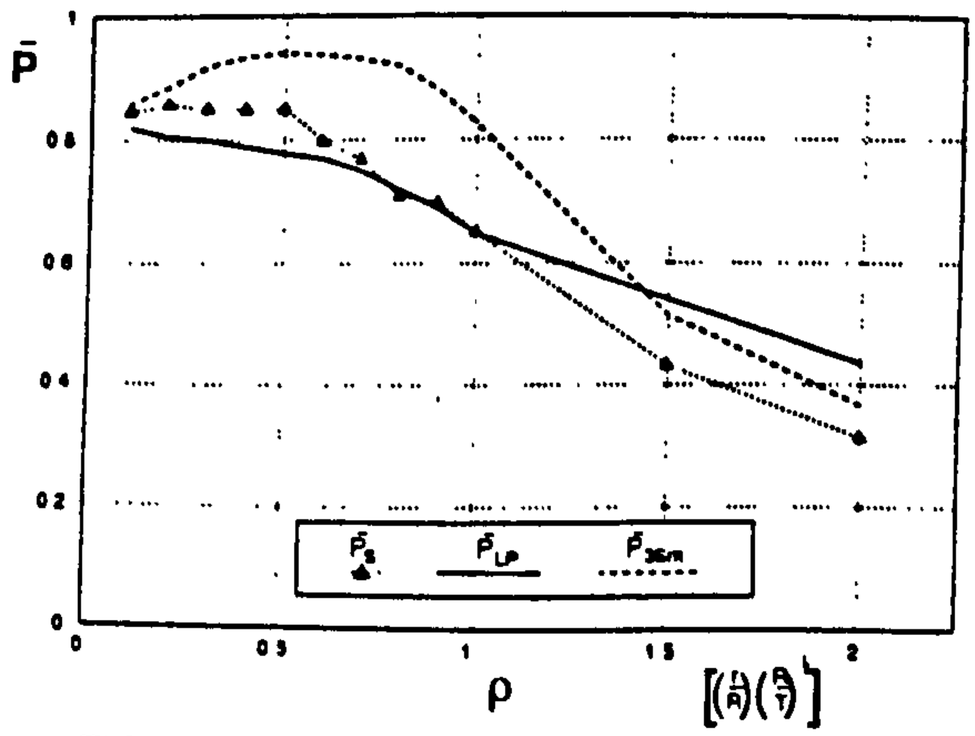

FIGURE 3. NORMALISED LOWER BOUND SHAKEDOWN PRESSURE OF NOZZLES VERSUS ρ, T=10mm, *R/T*=100

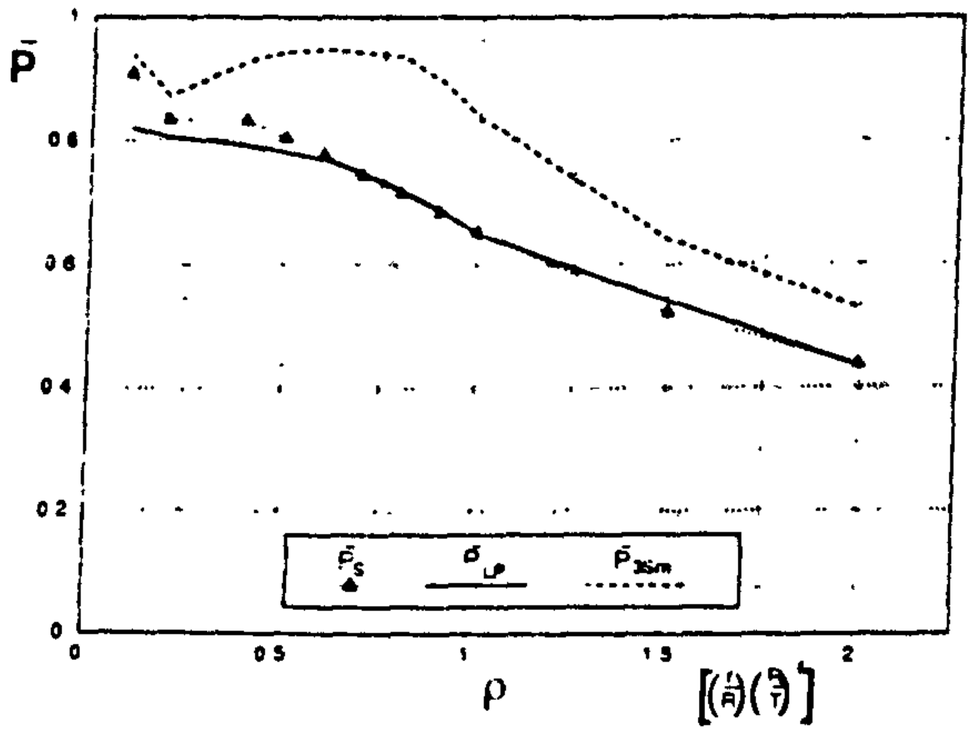

FIGURE 4 NORMALISED LOWER BOUND SHAKEDOWN PRESSURE OF NOZZLES VERSUS ρ, T=20mm, *R/T*=50

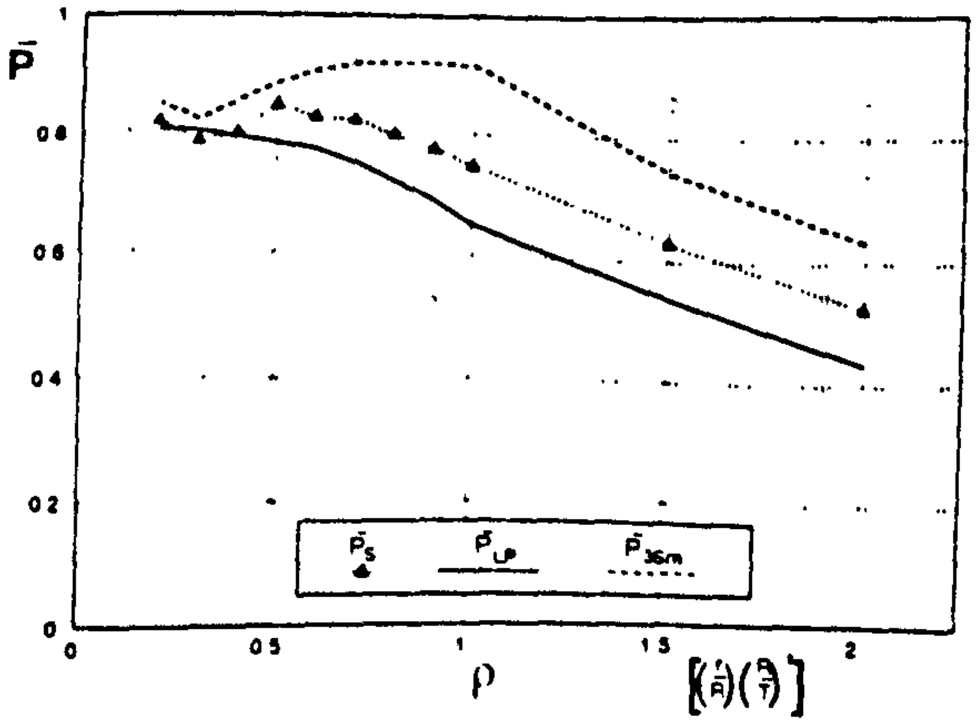

FIGURE 5. NORMALISED LOWER BOUND SHAKEDOWN PRESSURE OF NOZZLES VERSUS ρ, T=100mm, *R/T*=10

APPENDIX II

MACROS FOR THE ELASTIC COMPENSATION METHOD

AII.1 MACROS FOR SOLID ELEMENTS

MAC5

```
/com ******** ELASTIC COMPENSATION METHOD *********
/com
/com            LOWER BOUND LIMIT LOAD
/com                    AND
/com           SHAKEDOWN LOAD BATCH FILE
/com
/com       INPUT FILE               = model.log
/com       GRAPHICS RESULTS FILE    = res.f33
/com       TEXT RESULTS FILE        = record
/com       NO. ITERATIONS           = 10
/com       YIELD STRESS             = 300N/mm2
/com       ADDITIONAL FILES         = emodi,ext3,
/com                                   post,text.
/com
/com       VON MISES YIELD CRITERIA
/com       PLANE82 2D 8-NODE SOLID and
/com         SOLID45 3D 8-NODE SOLID
/com
/com  ***********************************************
/com
/com   define arrays for storage
/com
*dim,shake,,10
*dim,resid,,10
*dim,comp,,10
*dim,itemp,,10
/com
/com  ***********************************************
/com
/com  ITERATION 0: ELASTIC SOLUTION
/com
/nopr
/inp,model,log
/post1
set
/com
/com  WRITE ELASTIC SOLUTION TO A LOAD CASE FILE
/com              FOR SHAKEDOWN CALCS.
/com
lcwrite,1
/com
/inp,post
/com  ***********************************************
/com
/com  PLOT ELASTIC RESULTS TO FILE=res.f33
/com
/title, ITERATION 0: ELASTIC STRESS FIELD
/show,res,f33
```

```
/windo,1,-0.8,0.8,-0.8,0.8
/gline,1,-1
/cont,1,5
/dscale,1,1
plnsol,s,eqv
/com  get max stress from last plot into parm. elas
*get,elas,plnsol,,max
reset
/com
/com  ***********************************************
/com
/com   READ STRESS AND CALCULATE NEW MODULUS FOR EACH
/com   ELEMENT WRITE NEW MODULUS VALUES TO FILE=PREPMOD
/com
/com /inp,ecor
i=0.0
/inp,emodi
/com  ***********************************************
/com
/com   PERFORM MODULUS MODIFICATION FOR EACH
/com       ITERATION USING A DO LOOP
/com
iters=10
/com
*do,I,1,iters,1
    *status,I
    /com  ***********************************************
    /com
    /com   READ IN PREPMOD FILE TO CHANGE
    /com   MODULUS OF EACH ELEMENT AND SOLVE
    /com
    /com    /inp,modi
    /com
    /prep7                      * Re-enter preprocessor
    /nopr
    /com  resume and keep current parameters
    parsav,all
    resume                      * Resume last model
    parres,new
    *use,PREPMOD                * Use command file
    save
    finish
    /solve
    solve
    fini
    /post1
    /com  ***********************************************
    /com
    /com   PLOT SHAKEDOWN AND RESIDUAL
    /com   RESULTS TO FILE=res.f33
    /com
    /inp,post
    /inp,ext3
    /com  ***********************************************
    /com
    /com   READ STRESS AND CALCULATE NEW MODULUS FOR EACH ELEMENT
    /com   WRITE NEW MODULUS VALUES TO FILE=PREPMOD
    /com
    /inp,emodi
    /com
    /com  ***********************************************
    /com
```

```
    /com  WRITE RESULTS OUT TO TEXT FILE: record
    /com   CALCULATE LIMIT LOAD AND SHAKEDOWN
    /com            LOAD MULTIPLIERS
    /inp,text
    /com
    /com  ****************************************************
/com
*enddo
/com
/com end do loop
/com
exit
```

EMODI

```
SET                                          * Read results file
ETABLE,VMI,NMISC,5
ETABLE,VMJ,NMISC,10
ETABLE,VMK,NMISC,15
ETABLE,VML,NMISC,20
ETABLE,VMM,NMISC,25
ETABLE,VMN,NMISC,30
ETABLE,VMO,NMISC,35
ETABLE,VMP,NMISC,40
SM=300                                       * Define SM as max stress: ie yield
NU=0.3                                       * Define first run Poisson ratio
/NOPR
*GET,EMAX,ELEM,,NUM,MAX                      * Get max element number as EMAX
/COM
*CFOPEN,PREPMOD                              * Open command file PREPMOD
ENUM=1                                       * For first element do:
:LB1
*GET,EVMI,VMI,ENUM
*GET,EVMJ,VMJ,ENUM
*GET,EVMK,VMK,ENUM
*GET,EVML,VML,ENUM
*GET,EVMM,VMM,ENUM
*GET,EVMN,VMN,ENUM
*GET,EVMO,VMO,ENUM
*GET,EVMP,VMP,ENUM
! MNUM=ENUM+10 old command                  * Material number
! this command allows different
! materials to be used(upto 10)
*GET,MNUM,ELEM,ENUM,ATTR,MAT                 * Material number
*GET,EXVAL,EX,MNUM
SMAX=EVMI
*IF,EVMJ,LE,SMAX,:SK1
SMAX=EVMJ
:SK1
*IF,EVMK,LE,SMAX,:SK2
SMAX=EVMK
:SK2
*IF,EVML,LE,SMAX,:SK3
SMAX=EVML
:SK3
*IF,EVMM,LE,SMAX,:SK4
SMAX=EVMM
:SK4
*IF,EVMN,LE,SMAX,:SK5
```

```
SMAX=EVMN
:SK5
*IF,EVMO,LE,SMAX,:SK6
SMAX=EVMO
:SK6
*IF,EVMP,LE,SMAX,:SK7
SMAX=EVMP
:SK7
SF=SM/SMAX                          * Evaluate reduction factor
ER=EXVAL*SF                         * Define new elastic stiffness
*IF,I,GT,0.0,:KK1                   * check for elastic solution
MNUM=ENUM+10
:KK1
*CFWRITE,MP,EX,MNUM,ER              * Write to commands to PREPMOD
*CFWRITE,MAT,MNUM
*CFWRITE,EMOD,ENUM
:LB2
ENUM=ENUM+1                         * Next element
*IF,ENUM,LE,EMAX,:LB1
*CFCLOS                             * Close command file
FINISH
```

EXT3

```
LCDEF,2
LCFACT,2,-1
LCASE,2
/WINDO,1,-0.8,0.8,-0.8,0.8
/TITLE, SHAKEDOWN STRESS FIELD
/GLINE,1,-1
/CONT,1,5
/DSCALE,1,1
PLNSOL,S,EQV
LCFILE,1
LCASE,1
LCOPER,ADD,2
/WINDO,1,-0.8,0.8,-0.8,0.8
/TITLE, RESIDUAL STRESS FIELD
/GLINE,1,-1
/CONT,1,5
/DSCALE,1,1
PLNSOL,S,EQV
/COM  ***********************************************
/COM  Get max stress from last plot into
/COM  parm rsmax and array shake
/COM  ***********************************************
*GET,RSMAX,PLNSOL,,MAX
RESID(I)=RSMAX
```

POST

```
ETABLE,VMI,NMISC,5
ETABLE,VMJ,NMISC,10
ETABLE,VMK,NMISC,15
ETABLE,VML,NMISC,20
ETABLE,VMM,NMISC,25
```

```
ETABLE,VMN,NMISC,30
ETABLE,VMO,NMISC,35
ETABLE,VMP,NMISC,40
```

TEST

```
/COM
/COM  Get max between shake and resid arrays
/COM    for shakedown calculation
/COM
*VOPER,COMP(1),SHAKE(1),MAX,RESID(1)
/COM
/COM  Open file for output of results
/COM
*CFOPEN,RECORD
*VWRITE,ELAS
(/,"   Elastic =",f8.2,//)
*VWRITE,
("    Iteration    Shakedown   Residual      Comp",//)
ITEMP(I)=I
*VWRITE,ITEMP(1),SHAKE(1),RESID(1),COMP(1)
(4f12.2,/)
/COM
/COM  Calculate limit load and shakedown load multipliers
/COM
/COM  Get min value in each of the shake and comp arrays
/COM  for shakedown and limit calculations
/COM
*VSCFUN,SHMAX,MIN,SHAKE(1)
LMULT=SM/SHMAX
*VWRITE,LMULT,SHMAX
(//,"   Limit multiplier     =",f8.3,f8.2,/)
*VSCFUN,CMAX,MIN,COMP(1)
SMULT=SM/CMAX
*VWRITE,SMULT,CMAS
("   Shakedown multiplier =",f8.3,f8.2,/)
*VWRITE,SM
("   Yield Stress (N/mm2) =",f8.2)
/COM
/COM
*CFCLOSE,RECORD
```

TRIAL1

```
/POST1
RESUME
SET
ETABLE,PRS1,S,1
ETABLE,PRS2,S,2
ETABLE,PRS3,S,3
LCDEF,2
LCFACT,2,-1
LCASE,2
LCFILE,1
LCASE,1
LCOPER,ADD,2
```

*ELEMENT PRINCIPAL STRESS

```
*GET,EMAX,ELEM,,NUM,MAX
*CFOPEN,eqsts
T=0
ENUM=1
:LB1
*GET,SP1,PRS1,ENUM
*GET,SP2,PRS2,ENUM
*GET,SP3,PRS3,ENUM
A=ABS((SP1-SP2))**2
B=ABS((SP2-SP3))**2
C=ABS((SP3-SP1))**2
D=(A+B+C)
T=SQTR(D)/SQRT(2)
*CFWRIT,F,T
ENUM=ENUM+1
*IF,ENUM.LE,EMAX,:LB1
*CFCLOSE
FINISH
```

TRIAL2

```
/POST1
RESUME
SET,1,1
ETABLE,EQVS,S,EQV                    *Equivalent stress
ETABLE,EVL,VOLU                      *Element volume
ETABLE,EQVSN,EPEL,EQV                *Elastic equivalent strain
*SET,YS,300                          *Define YS as yield stress
*GET,EMAX,ELEM,,NUM,MAX              *Get max element number as EMAX
*CFOPEN,eqstn                        *Open equivalent strain file
T=0
A=0
SN=0
ENUM=1
:LB1
*GET,ES,EQVS,ENUM
*GET,V,EVL,ENUM
*GET,ESN,EQVSN,ENUM
K=V*ESN
*CFWRITE,EN,K
Q=V*ESN*ES
W=V*ESN*YS
T=T+Q
A=A+W
SN=SN+K
ENUM=ENUM+1
*IF,ENUM,LE,EMAX,:LB1
*CFCLOSE
*CFOPEN,energy
*CFWRITE,D,A
*CFWRITE,U,T
*CFWRITE,N,SN
*CFCLOSE
FINI
```

AII.2 MACROS FOR SHELL ELEMENTS

BATCH93

```
/BATCH,list  ! Optional command (to run in batch mode)
/com     *** ELASTIC COMPENSATION METHOD ***
/com  GENERAL YIELD SURFACE LOAD BATCH FILE FOR SHELL 93
/com  ------------------------------------------------
/com
/com  INPUT FILE = model.log
/com  GRAPHICS RESULTS FILE = res.f33
/com
/com  CREATE MODEL IN PREP7: READ IN model.log
/com
/inp,model93,log
/com  SOLVE - ITERATION 0
/inp,model93,solu
/post1
set
/com  WRITE ELESTIC SOLUTION TO A LOAD CASE FILE FOR SHAKEDOWN CALCS.
lcwrite,1,eresu   ! Write current load case to jobname.l1
/inp,post93
/title, ITERATION 0: ELASTIC STRESS FIELD
/show,res,f33
/windo,1,-0.8,0.8,-0.8,0.8
shell,top
plnsol,s,eqv
shell,bot
plnsol,s,eqv
/page,,,6000
/output,elastic
pretab
/output
reset
/com   WRITE 'PREPMOD'
/inp,ecor93
/sys,cp YSURF YSURF0
/com   MODIFY PREP7
/com
/com                    ITERATION 1
/com
/inp,modi
/inp,model93,solu
/post1
csys,1
/inp,post93
/inp,ext93
reset
/inp,emodi93
/sys,cp YSURF YSURF1
/com
/com                    ITERATION 2
/com
/inp,modi
/inp,model93,solu
/post1
csys,1
/inp,post93
/inp,ext93
```

```
reset
/inp,emodi93
/sys,cp YSURF YSURF2
/com
/com                    ITERATION 3
/com
/inp,modi
/inp,model93,solu
/post1
csys,1
/inp,post93
/inp,ext93
reset
/inp,emodi93
/sys,cp YSURF YSURF3
/com
/com                    ITERATION 4
/com
/inp,modi
/inp,model93,solu
/post1
csys,1
/inp,post93
/inp,ext93
reset
/inp,emodi93
/sys,cp YSURF YSURF4
/com
/com                    ITERATION 5
/com
/inp,modi
/inp,model93,solu
/post1
csys,1
/inp,post93
/inp,ext93
reset
/inp,emodi93
/sys,cp YSURF YSURF5
/com
EXIT
```

ECOR93

```
SET                                     * Read results file
ETABLE,NTX,SMISC,1
ETABLE,NTY,SMISC,2
ETABLE,NTXY,SMISC,3
ETABLE,MMX,SMISC,4
ETABLE,MMY,SMISC,5
ETABLE,MMXY,SMISC,6
SM=300                                  * Define SM as max stress: ie yield
E=200e6                                 * Define first run elastic modulus
NU=0.3                                  * Define first run Poisson ratio
T1=5                                    * Nozzle thickness
T2=10                                   * Cylnder thickness
CMAX=6                                  * Max column number
/NOPR
*GET,EMAX,ELEM,,NUM,MAX                 * Get max element number as EMAX
```

```
*CFOPEN,MAXENO                          * Open file to store max el no
*CFWRITE,R,EMAX
*CFCLOS
/COM
*CFOPEN,PREPMOD                         * Open command file PREPMO
ENUM=1                                  * For first element do:
:LB1
T=T1
/INP,ilyushin                           * Ilyushin yield surface
MNUM=ENUM+10                             * Material number
ER=E
ER=E/SQRT(W)                                 * Define new elastic stiffness
*CFWRITE,MP,EX,MNUM,ER                  * Write to commands to PREPMOD
*CFWRITE,MAT,MNUM
*CFWRITE,EMOD,ENUM
:LB2
ENUM=ENUM+1                             * Next element
*IF,ENUM,LE,50,:LB1
:LB3
T=T2
/INP,ilyushin
MNUM=ENUM+10                            * Material number
ER=E
ER=E/SQRT(W)                            * Define new elastic stiffness
*CFWRITE,MP,EX,MNUM,ER                  * Write to commands to PREPMOD
*CFWRITE,MAT,MNUM
*CFWRITE,EMOD,ENUM
:LB4
ENUM=ENUM+1
*IF,ENUM,LE,EMAX,:LB3
*CFCLOS                                  * Close command file
*CFOPEN,YSURF                           * Open command file YSURF
ENUM=1                                  * For first element do:
:LB5
T=T1
/INP,ilyushin
*CFWRITE,ys,w
:LB6
ENUM=ENUM+1                              * Next element
*IF,ENUM,LE,200,:LB5
:LB7
T=T2
/INP,ilyushin
*CFWRITE,ys,w
:LB8
ENUM=ENUM+1                              * Next element
*IF,ENUM,LE,EMAX,:LB7
*CFCLOS
/GOPR
/COM   ***** FIRST ITERATION ELEMENT MODULUS CORRECTION COMPLETE *****
FINISH
```

EMODI93

```
SET                                     * Read results file
ETABLE,NTX,SMISC,1
ETABLE,NTY,SMISC,2
ETABLE,NTXY,SMISC,3
ETABLE,MMX,SMISC,4
```

```
ETABLE,MMY,SMISC,5
ETABLE,MMXY,SMISC,6
SM=300                                  * Define SM as max stress: ie yield
NU=0.3                                  * Define first run Poisson ratio
T1=5                                    * Nozzle thickness
T2=10                                   * Cylnder thickness
CMAX=6                                  * Max column number
/NOPR
*GET,EMAX,ELEM,,NUM,MAX                 * Get max element number as EMAX
*CFOPEN,MAXENO                          * Open file to store max el no
*CFWRITE,R,EMAX
*CFCLOS
/COM
*CFOPEN,PREPMOD                         * Open command file PREPMO
ENUM=1                                  * For first element do:
:LB1
T=T1
/INP,ilyushin
MNUM=ENUM+10                             * Material number
*GET,EXVAL,EX,MNUM
ER=EXVAL/SQRT(W)                         * Define new elastic stiffness
*CFWRITE,MP,EX,MNUM,ER                   * Write to commands to PREPMOD
*CFWRITE,MAT,MNUM
*CFWRITE,EMOD,ENUM
:LB2
ENUM=ENUM+1                              * Next element
*IF,ENUM,LE,200,:LB1
:LB3
T=T2
/INP,ilyushin
MNUM=ENUM+10                             * Material number
*GET,EXVAL,EX,MNUM
ER=EXVAL/SQRT(W)                         * Define new elastic stiffness
*CFWRITE,MP,EX,MNUM,ER                   * Write to commands to PREPMOD
*CFWRITE,MAT,MNUM
*CFWRITE,EMOD,ENUM
:LB4
ENUM=ENUM+1
*IF,ENUM,LE,EMAX,:LB3
*CFCLOS                                  * Close command file
*CFOPEN,YSURF                           * Open command file YSURF
ENUM=1                                  * For first element do:
:LB5
T=T1
/INP,ilyushin
*CFWRITE,ys,w
:LB6
ENUM=ENUM+1                              * Next element
*IF,ENUM,LE,50,:LB5
:LB7
T=T2
/INP,ilyushin
*CFWRITE,ys,w
:LB8
ENUM=ENUM+1                                     * Next element
*IF,ENUM,LE,EMAX,:LB7
*CFCLOS
/GOPR
/COM   ***** FIRST ITERATION ELEMENT MODULUS CORRECTION COMPLETE *****
FINISH
```

EXT93

```
LCDEF,2
LCFACT,2,-1
LCASE,2
/WINDO,1,-0.8,0.8,-0.8,0.8
/TITLE, SHAKEDOWN STRESS FIELD
SHELL,TOP
PLNSOL,S,EQV
SHELL,BOT
PLNSOL,S,EQV
/PAGE,,,6000
/OUTPUT,results
PRETAB
/OUTPUT
LCFILE,1,ERESU
LCASE,1
LCOPER,ADD,2
/WINDO,1,-0.8,0.8,-0.8,0.8
/TITLE, RESIDUAL STRESS FIELD
SHELL,TOP
PLNSOL,S,EQV
SHELL,BOT
PLNSOL,S,EQV
```

ILYUSHIN

```
/COM  ILYUSHIN YIELD SURFACE MACRO
CNUM=1                                  * For first column do:
*GET,ENTX,ETAB,CNUM,ELEM,ENUM
CNUM=2                                  * For second column
*GET,ENTY,ETAB,CNUM,ELEM,ENUM
CNUM=3                                  * For third column
*GET,ENXY,ETAB,CNUM,ELEM,ENUM
CNUM=4                                  * For fourth column
*GET,EMMX,ETAB,CNUM,ELEM,ENUM
CNUM=5                                  * For fifth column
*GET,EMMY,ETAB,CNUM,ELEM,ENUM
CNUM=6                                  * For sixth column
*GET,EMXY,ETAB,CNUM,ELEM,ENUM
A=SM*T
B=SM*T*T
N1=ENTX/A
N2=ENTY/A
N12=ENXY/A
M1=4*EMMX/B
M2=4*EMMY/B
M12=4*EMXY/B
C=N1*N1
D=N2*N2
F=N1*N2
G=3*N12*N12
H=M1*M1
I=M2*M2
J=M1*M2
K=3*M12*M12
O=N1*M1
PQ=0.5*N1*M2
```

```
Q=0.5*N2*M1
R=N2*M2
U=3*N12*M12
QT=C+D-F+G
QM=H+I-J+K
QTM=O-PQ-Q+R+U
V=ABS(QTM)/3**0.5
W=QT+QM+V
```

IVANOV

```
/COM  IVANOV YIELD SURFACE MACRO
CNUM=1                                  * For first column do:
*GET,ENTX,ETAB,CNUM,ELEM,ENUM
CNUM=2                                  * For second column
*GET,ENTY,ETAB,CNUM,ELEM,ENUM
CNUM=3                                  * For third column
*GET,ENXY,ETAB,CNUM,ELEM,ENUM
CNUM=4                                  * For fourth column
*GET,EMMX,ETAB,CNUM,ELEM,ENUM
CNUM=5                                  * For fifth column
*GET,EMMY,ETAB,CNUM,ELEM,ENUM
CNUM=6                                  * For sixth column
*GET,EMXY,ETAB,CNUM,ELEM,ENUM
A=SM*T
B=SM*T*T
N1=ENTX/A
N2=ENTY/A
N12=ENXY/A
M1=4*EMMX/B
M2=4*EMMY/B
M12=4*EMXY/B
C=N1*N1
D=N2*N2
F=N1*N2
G=3*N12*N12
H=M1*M1
I=M2*M2
J=M1*M2
K=3*M12*M12
O=N1*M1
PQ=0.5*N1*M2
Q=0.5*N2*M1
R=N2*M2
U=3*N12*M12
QT=C+D-F+G
QM=H+I-J+K
QTM=O-PQ-Q+R+U
V1=0.25*(QT*QM-QTM**2)
V2=QT+0.48*QM
V3=V1/V2
V4=0.25*QM*QM+QTM*QTM
V5=V4**0.5
W=QT+0.5*QM-V3+V5
```

POST93

```
SET                                          * Read results file
ETABLE,SVTI,NMISC,5
ETABLE,SVTJ,NMISC,15
ETABLE,SVTK,NMISC,25
ETABLE,SVTL,NMISC,35
ETABLE,SVBI,NMISC,10
ETABLE,SVBJ,NMISC,20
ETABLE,SVBK,NMISC,30
ETABLE,SVBL,NMISC,40
```

APPENDIX III

ANSYS FINITE ELEMENT LIBRARY

BEAM3 2-D Elastic Beam

BEAM3 is a uniaxial element with tension, compression, and bending capabilities. The element has three degrees of freedom at each node: translations in the nodal x and y directions and rotation about the nodal z-axis.

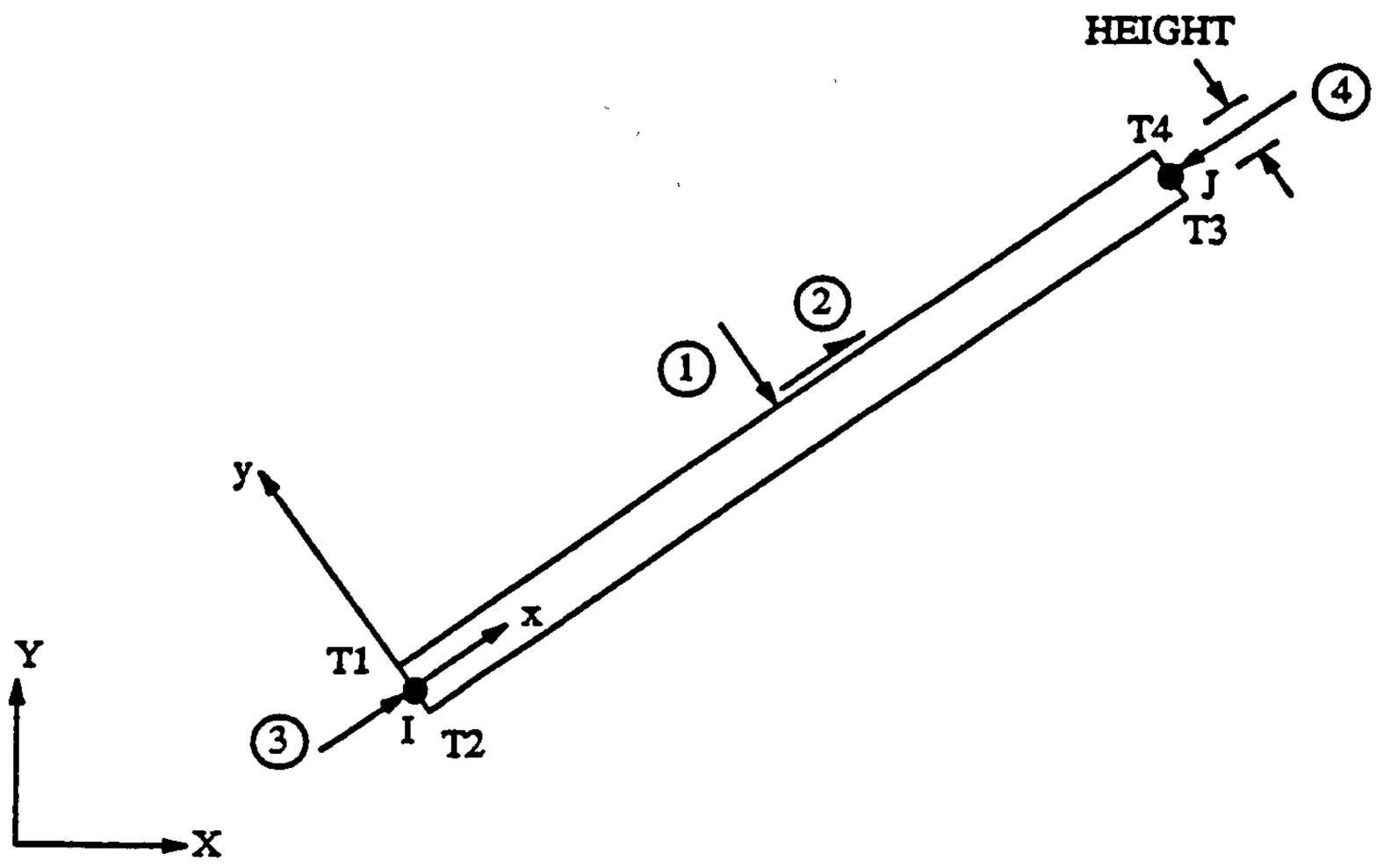

BEAM3 2–D Elastic Beam

BEAM4 3-D Elastic Beam

Beam4 is a uniaxial element with tension, compression, torsion and bending capabilities. The element has six degrees of freedom at each node: translations in the nodal x, y and z directions and rotations about the nodal x, y, and z axes.

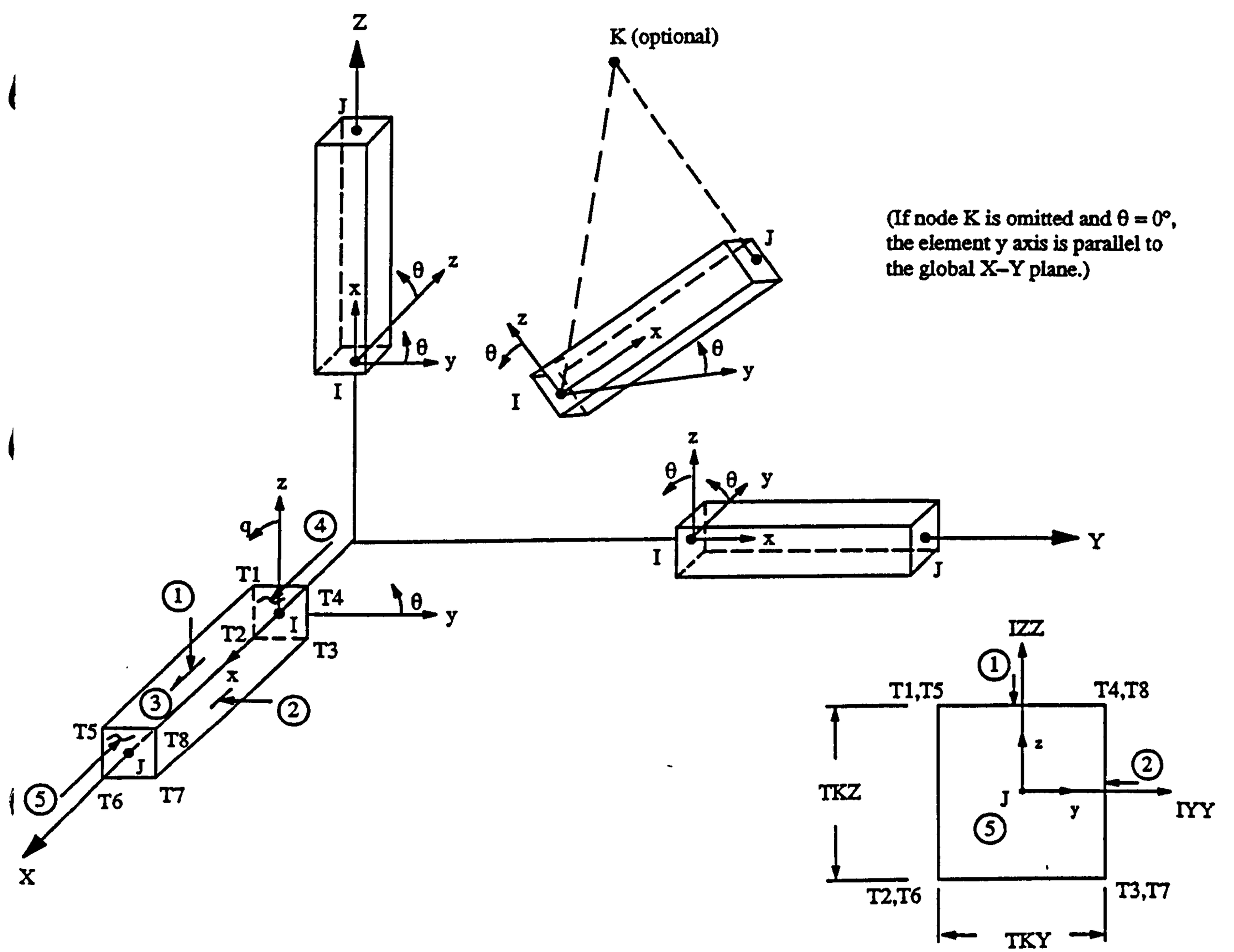

(If node K is omitted and θ = 0°, the element y axis is parallel to the global X–Y plane.)

BEAM4 3–D Elastic Beam

PLANE82 2-D 8-Node Structural Solid

PLANE82 is a higher order version of the two-dimensional, four-node element (PLANE42). It provides more accurate results for mixed (quadrlateral-triangular) automatic meshes and can tolerate irregular shapes without as much loss of accuracy. The 8-node elements have compatible displacement shapes and are well suited to model curved boundaries.

The 8-node element is defined by eight nodes having two degrees of freedom at each node: translations in the nodal x and y directions. The element may be used as a plane element or as an axisymmetric element. The element has plasticity, creep, swelling, stress stiffening, large deflection and large strain capabilities.

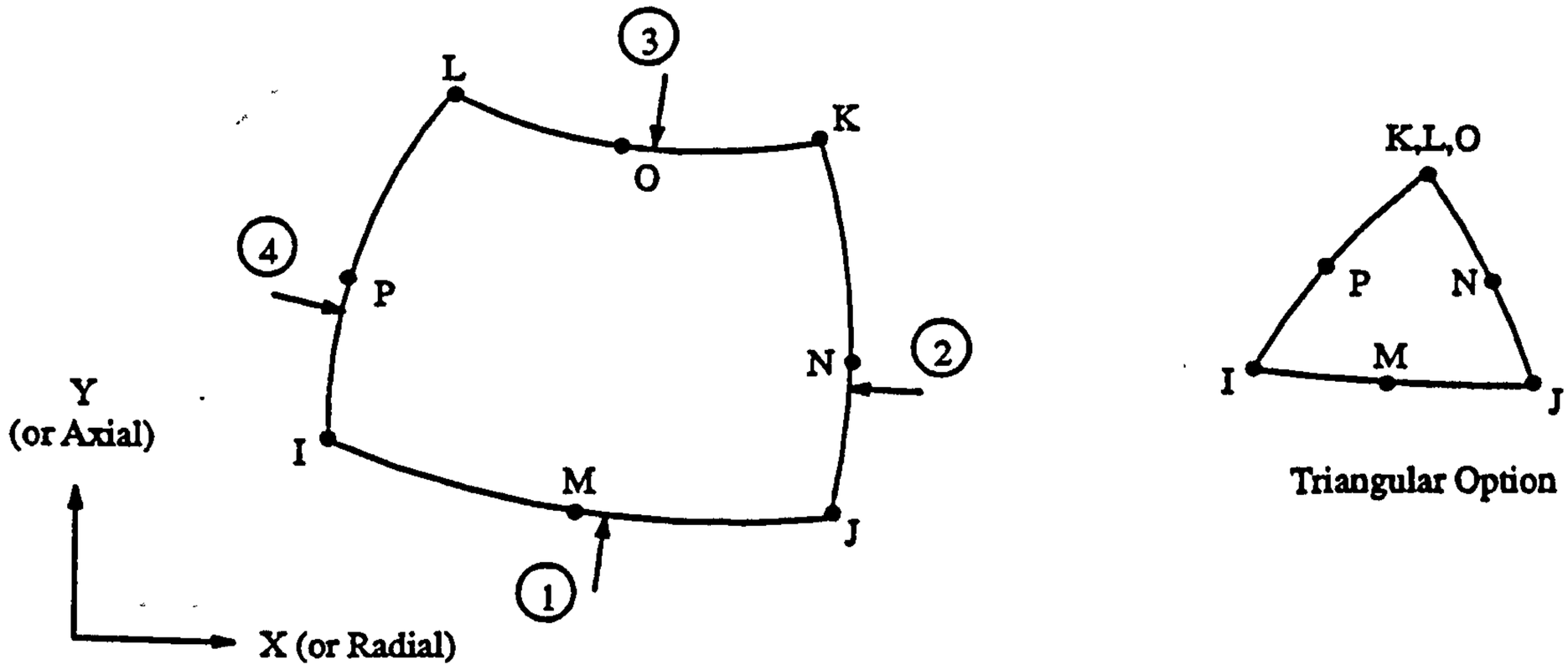

PLANE82 2–D 8–Node Structural Solid

SHELL43 Plastic Shell

SHELL43 is well suited to model nonlinear, flat or warped, thin to moderately-thick shell structures. The element has six degrees of freedom at each node: translations in the nodal x, y and z directions and rotations about the nodal x, y, and z axes. The deformation shapes are linear in both in-plane directions. For the out-of-plane motion, it uses a mixed interpolation of tensorial components. The element has plasticity, creep, stress stiffening, large deflection and large strain capabilities.

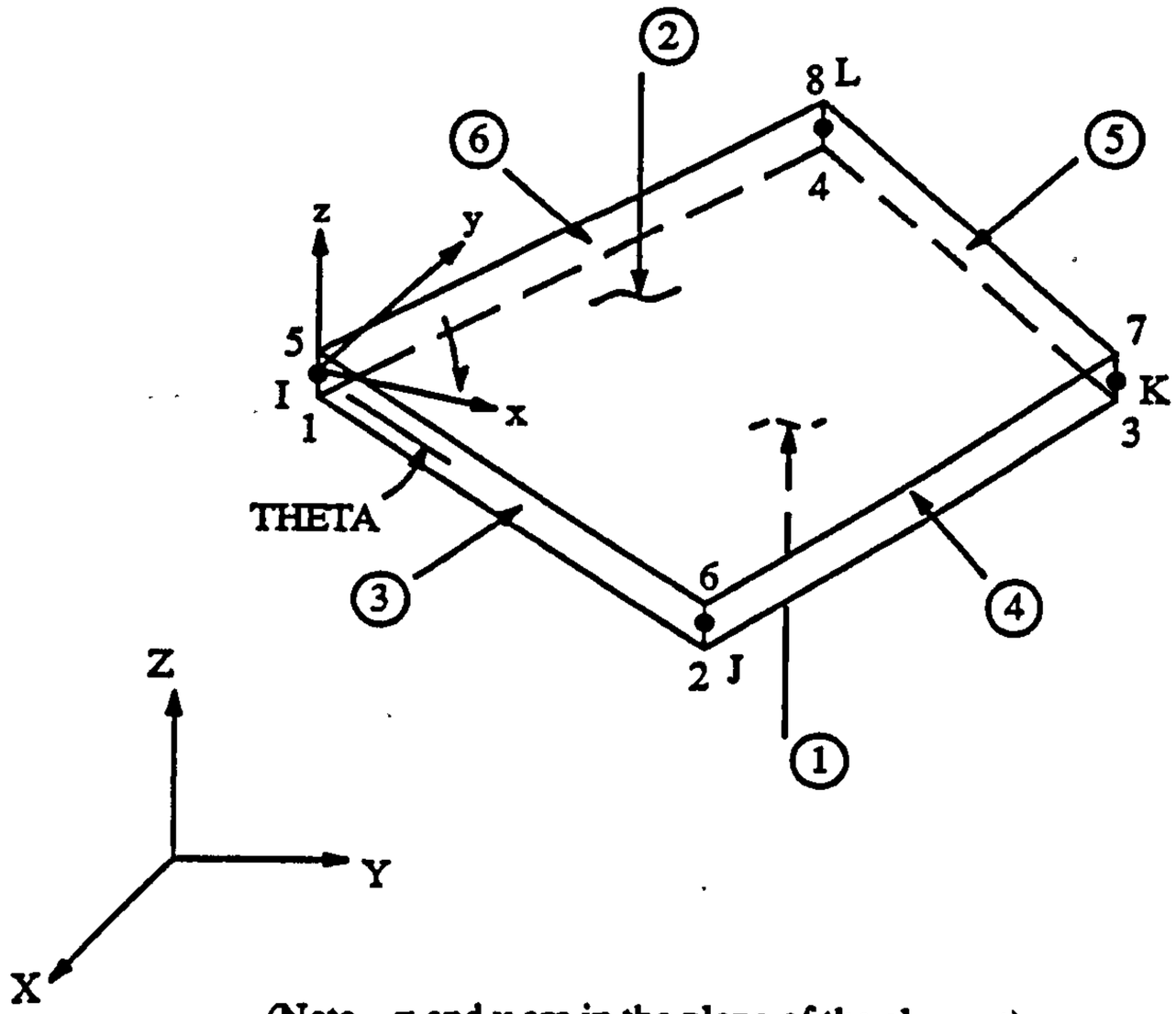

(Note – x and y are in the plane of the element)

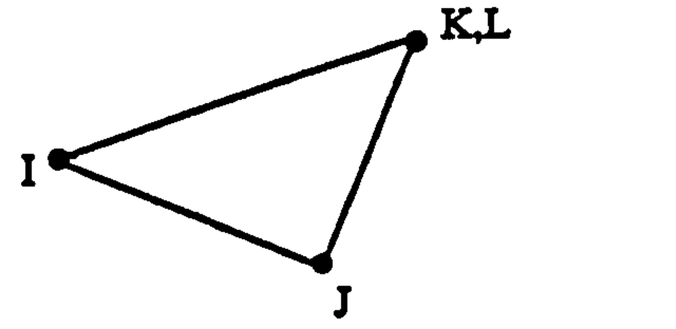

(Triangular Option – not recommended)

SHELL43 Plastic Shell

SHELL51 Axisymmetric Structural Shell

SHELL51 has four degrees of freedom at each node: translations in the nodal x, y, and z directions and a rotation about the nodal z axis. Extreme orientations of the conical shell element result in a cylindrical shell element or an annular disc element. The shell element may have a linearly varying thickness. The element has plasticity, creep, swelling, stress stiffening, large deflection, and torsion capability.

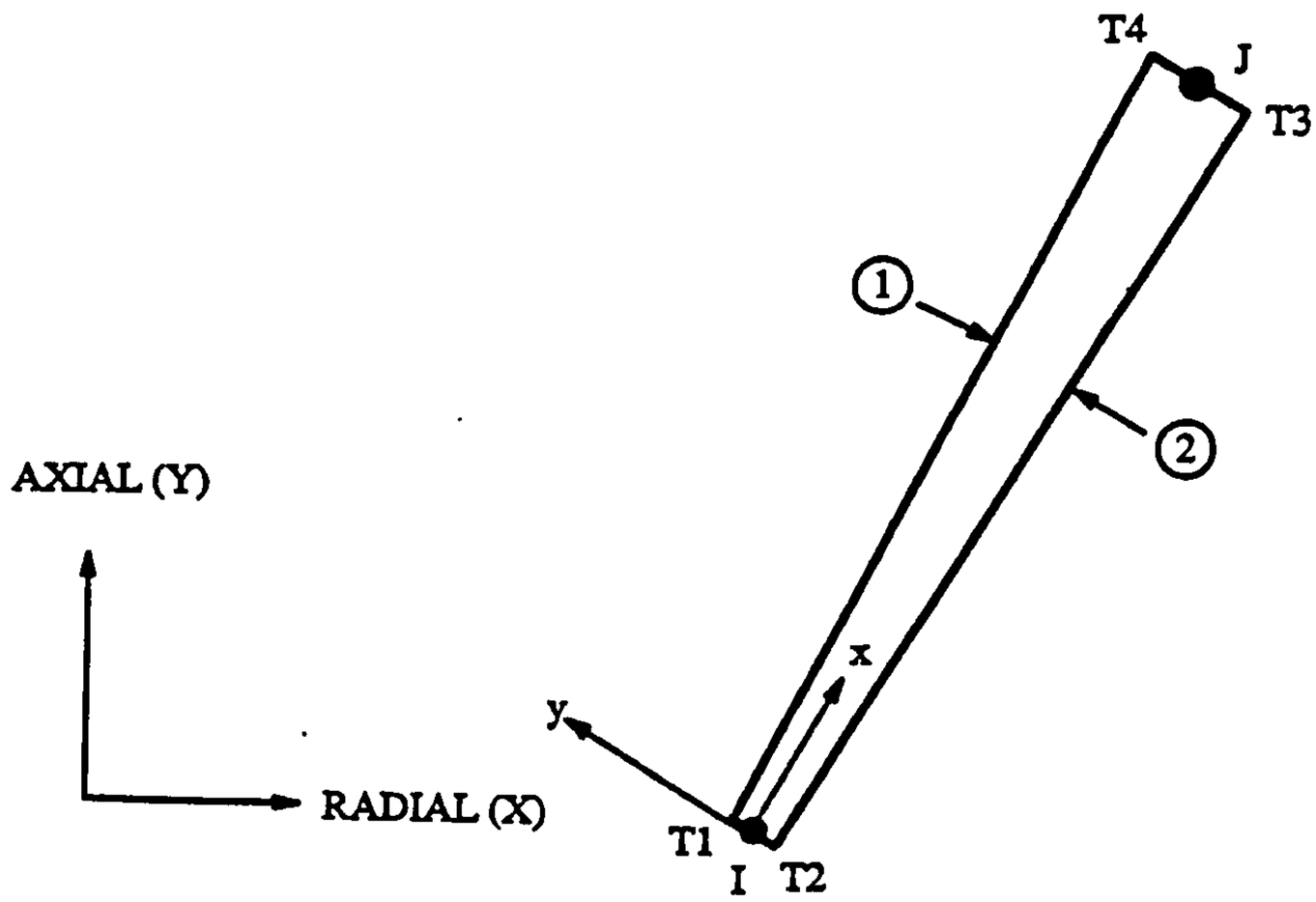

SHELL51 Axisymmetric Structural Shell

SHELL93 8-Node Structural Shell

SHELL93 is particularly well suited to model curved shells. The element has six degrees of freedom at each node: translations in the nodal x, y, and z directions and a rotation about the nodal x, y, and z axes. The deformation shapes are quadratic in both in-plane directions. The element has plasticity, stress stiffening, large deflection, and large strain capabilities.

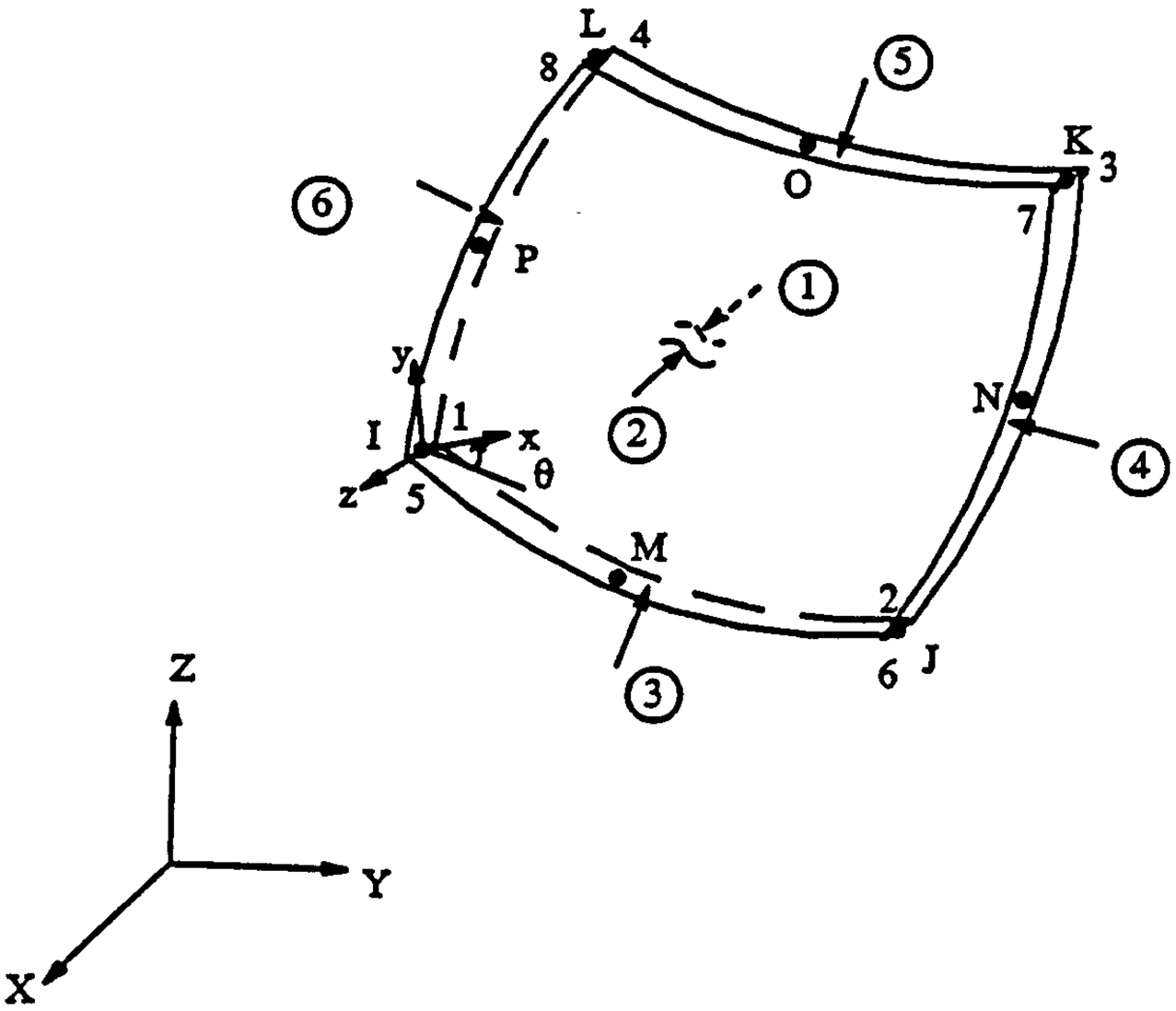

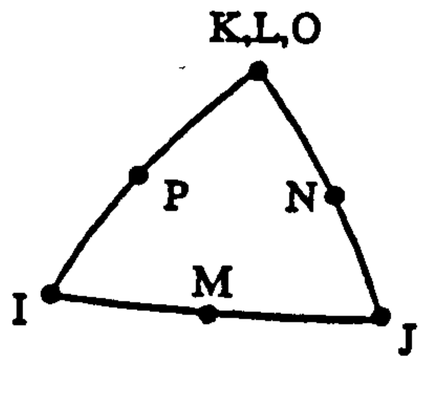

Triangular Option

SHELL93 8–Node Structural Shell

SOLID45 3-D Structural Solid

SOLID45 is used for the three-dimensional modelling of solid structures. The element is defined by eight nodes having three degrees of freedom at each node: translations in the nodal x, y, and z directions. The element has plasticity, creep, swelling, stress stiffening, large deflection and large strain capabilities.

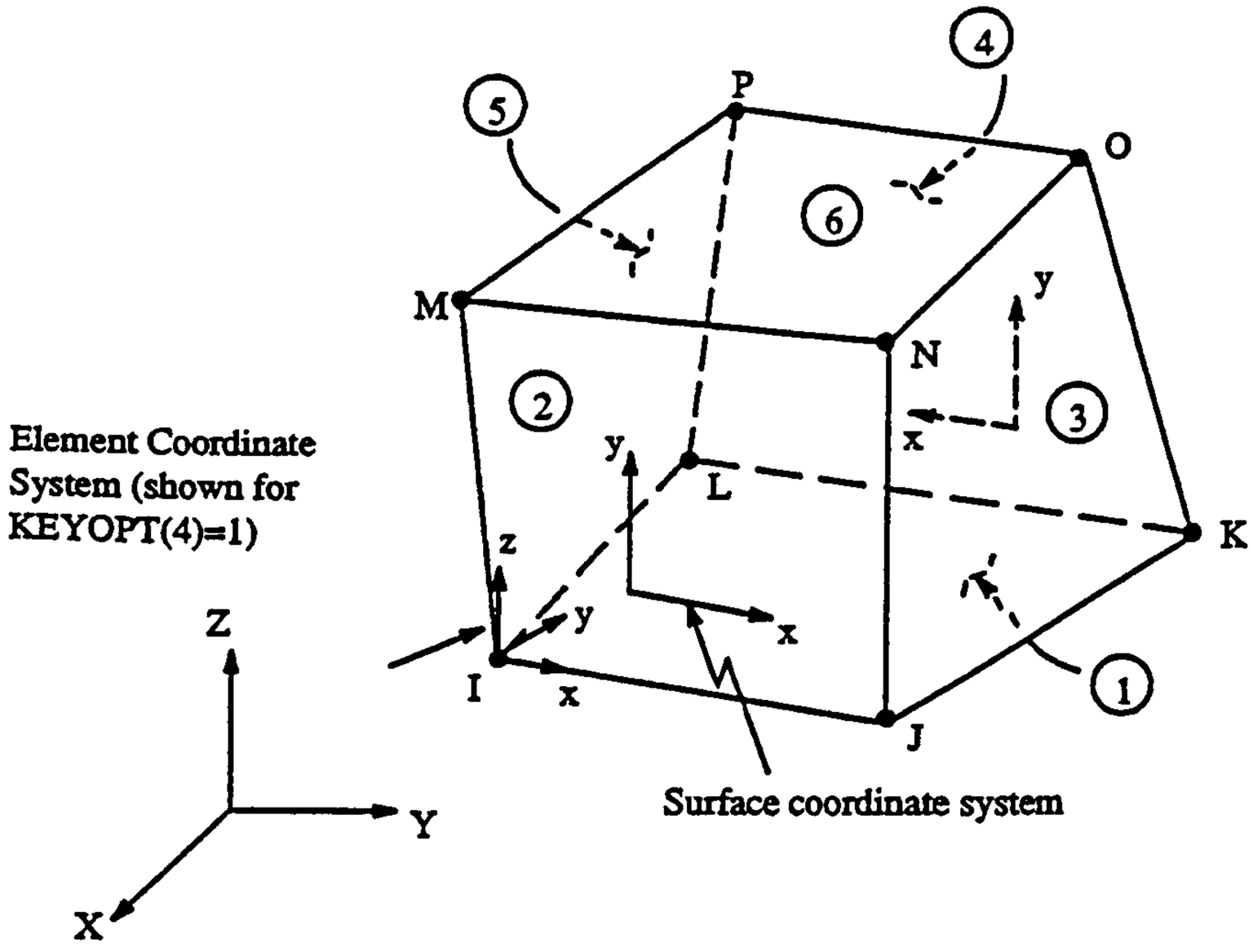

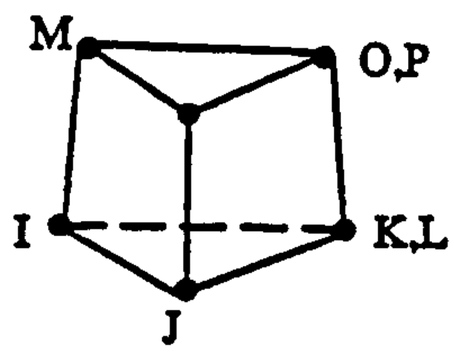

(Prism option)

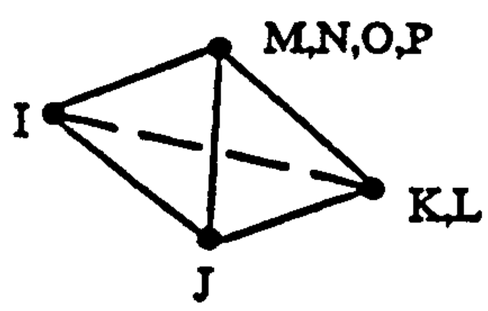

(Tetrahedral Option – not recommended)

SOLID45 3–D Structural Solid